THE UNIVERSITY OF QUEENSLAND

AUSTRALIA

IDENTIFICATION OF POTENTIAL MEDIATORS OF OXIDATIVE DAMAGE AND TARGETS FOR NOVEL TREATMENTS FOR CHRONIC KIDNEY DISEASE

David Machin Small

Bachelor of Science (Biomedical) Hons I

A thesis submitted for the degree of Doctor of Philosophy at

The University of Queensland in 2014

School of Medicine

ABSTRACT

Chronic kidney disease (CKD) is a common and serious problem causing a significant burden to healthcare systems and, most importantly, the affected individual. Despite this, few successful treatments exist for CKD. Understanding the pathophysiological features that are common to chronic kidney pathologies is vital to identify targets for treatment. Oxidative stress has been implicated in all chronic diseases, acting via highly conserved pathways of disease progression. However, evidence to date shows limited benefit of antioxidants as therapies for CKD patients, suggesting a need to better identify the pathways that are stimulated.

This thesis focuses on the role of oxidative stress, the regulation of mitochondrial homeostasis, the action of antioxidant compounds, and the disruption of oxidant signalling networks in chronic kidney pathologies (reviewed in **Chapter 1**). The aims of this project were to: (1) to use an *in vitro* model of oxidative stress-induced kidney injury to determine how a failure in balance between oxidative stress and oxidant control causes the cellular characteristics of CKD, then to determine whether exogenous antioxidants can prevent and restore renal cell bioenergetics and reduce cell injury; (2) to use an *in vivo* model of oxidative stress-induced kidney injury with molecular and metabolic imaging to measure potential biomarkers identified in Aim 1, in association with changes in kidney structure and function, and determine whether treatment with an antioxidant therapy modulates kidney disease pathology; and (3) to explore the links between biomarkers of oxidative stress and clinical characteristics of CKD in patients to determine whether a lifestyle intervention in conjunction with standard nephrology care improve systemic oxidative stress and whether this influences kidney function. The renal specific *in vitro*, *in vivo*, and clinical models and the methods used are explained in **Chapter 2**.

Chapter 3 reports the separate and cumulative effects of oxidative stress, mitochondrial dysfunction and cell senescence in promoting loss of renal cells in an *in vitro* model of kidney disease. The results demonstrate that oxidative stress and cell senescence cause mitochondrial destabilization and kidney tubular epithelial cell loss. This may contribute to the development of cellular and tissue atrophy seen in CKD.

Chapter 4 further defines the role of mitochondrial alterations as a consequence of a specifically-impaired oxidant signalling regulatory mechanism, namely, peroxisome proliferator-activated receptor-gamma (PPARγ)-regulated mitochondrial biogenesis. Oxidative stress promoted mitochondrial destabilisation in kidney proximal tubular epithelial cells, in association with

increased PPARγ *Serine 112* phosphorylation. Despite their positive effects in other tissues, PPARγ agonists failed to protect proximal tubular epithelial (PTE) cells, and appear to be detrimental to kidney PTE cell health when oxidative stress induces the cell damage.

Chapter 5 examined mediators of oxidative stress in an *in vivo* model of acute to chronic kidney injury progression, in a spatial and temporal manner via intravital multiphoton microscopy (MPM) in the mouse kidney. Fluorescence lifetime imaging microscopy (FLIM) coupled MPM identified significant and dynamic metabolic substrate utilisation by kidney tubular cells promoting oxidative stress in progressive CKD. Mitochondrial dysfunction is persistent in structurally-normal tubules of the chronically-damaged kidney, potentially enhancing free radical production in a progressive manner.

Chapter 6 examined the influence of antioxidants in reducing oxidative stress-induced kidney damage using *in vitro* and *in vivo* models. *In vitro* studies revealed that NAC was superior in reducing oxidative stress-induced PTE cell apoptosis, compared to Coenzyme Q_{10}, alpha(α)-tocopherol or trolox. *In vivo* studies utilised 4-6 week old C57Bl6 mice on a 5% NAC diet that underwent bilateral ischaemia-reperfusion injury (20 min). Intravital MPM, histopathology, and protein analysis revealed that NAC protects against early kidney damage, but enhances the progression of chronic kidney pathology by eliminating redox-sensitive endogenous cytoprotective signalling. FLIM of cortex and medulla highlight mitochondrial dysfunction and the negative effects of NAC. This does not support general antioxidants for the treatment of CKD.

Chapter 7 examined systemic biomarkers of oxidative stress in stage 3-4 CKD patients. 136 patients from the LANDMARK-III cohort underwent standard nephrology care with or without an exercise and lifestyle intervention. Clinical tests and oxidative stress biomarkers (plasma isoprostanes, glutathione peroxidase, total antioxidant capacity) were taken at baseline and at 12 months. No significant differences were identified over 12-months in systemic oxidative stress markers, or eGFR. The results highlight the biological variability of systemic oxidative stress biomarkers in CKD patients.

In summary (**Chapter 8**), this thesis presents oxidative stress as a common and unifying concept of pathophysiological change in chronic kidney pathology at a cellular level. Oxidative stress actively promotes cell death and cell cycle arrest in PTE cells whilst enhancing the secretion of pro-fibrotic factors to increase tubulointerstitial fibrosis. Correcting this process requires are targeted approach,

however is increasingly difficult given the complexity of the cellular, physiological, and systemic responses to oxidative stress.

DECLARATION BY AUTHOR

This thesis is composed of my original work, and contains no material previously published or written by another person except where due reference has been made in the text. I have clearly stated the contribution by others to jointly-authored works that I have included in my thesis.

I have clearly stated the contribution of others to my thesis as a whole, including statistical assistance, survey design, data analysis, significant technical procedures, professional editorial advice, and any other original research work used or reported in my thesis. The content of my thesis is the result of work I have carried out since the commencement of my research higher degree candidature and does not include a substantial part of work that has been submitted to qualify for the award of any other degree or diploma in any university or other tertiary institution. I have clearly stated which parts of my thesis, if any, have been submitted to qualify for another award.

I acknowledge that an electronic copy of my thesis must be lodged with the University Library and, subject to the General Award Rules of The University of Queensland, immediately made available for research and study in accordance with the *Copyright Act 1968*.

I acknowledge that copyright of all material contained in my thesis resides with the copyright holder(s) of that material. Where appropriate I have obtained copyright permission from the copyright holder to reproduce material in this thesis.

PUBLICATIONS DURING CANDIDATURE

Peer reviewed publications

Small DM, Morais C, Coombes JS, Bennett NC, Johnson DW, Gobe GC. 2014. Oxidative Stress-Induced Alterations in PPARgamma and Associated Mitochondrial Destabilisation Contribute to Kidney Cell Apoptosis. *Am J Physiol Renal Physiol*. **307**: 814-822.

Diwan V, **Small DM**, Kauter KB, Gobe GC, Brown L. 2014. Gender differences in adenine-induced chronic kidney disease and cardiovascular complications in rats. *Am J Physiol Renal Physiol*. **307**: 1169-1178.

Peternelji TT, Marsh SA, Morais C, **Small DM**, Dalbo VJ, Tucker PS, Coombes JS. 2014. O-GlcNAc protein modification in C2C12 myoblasts exposed to oxidative stress indicates parallels with endogenous antioxidant defense. *Biochem Cell Biol*. **93**: 1-11.

Beetham KS, Howden EJ, **Small DM**, Briskey DR, Rossi M, Isbel N, Coombes JS. 2014. Oxidative stress contributes to muscle atrophy in chronic kidney disease patients. *Redox Rep*. doi: 10.1179/1351000214Y.0000000014.

Hornos Carneiro MF, Morais C, **Small DM**, Vesey DA, Barbosa F, Jr., Gobe GC. 2014. Thimerosal induces apoptotic and fibrotic changes to kidney epithelial cells in vitro. *Environ Toxicol*. doi: 10.1002/tox.22012.

Small DM, Sanchez WY, Roy S, Hickey MJ, Gobe GC. 2014. Multiphoton fluorescence microscopy of the live kidney in health and disease. *J Biomed Opt* **19**: 020901.

Morais C, **Small DM**, Vesey DA, Martin J, Johnson DW, Gobe GC. 2014. Fibronectin and transforming growth factor beta contribute to erythropoietin resistance and maladaptive cardiac hypertrophy. *Biochem Biophys Res Commun* **444**: 332-337.

Small DM, Bennett NC, Roy S, Gabrielli BG, Johnson DW, Gobe GC. 2012. Oxidative stress and cell senescence combine to cause maximal renal tubular epithelial cell dysfunction and loss in an in vitro model of kidney disease. *Nephron Exp Nephrol* **122**: 123-130.

Small DM, Gobe GC. 2012. Cytochrome c: potential as a noninvasive biomarker of drug-induced acute kidney injury. *Expert Opin Drug Metab Toxicol* **8**: 655-664.

Small DM, Coombes JS, Bennett N, Johnson DW, Gobe GC. 2012. Oxidative stress, anti-oxidant therapies and chronic kidney disease. *Nephrology (Carlton)* **17**: 311-321.

Book Chapters

Small DM, Gobe GC. 2013. Oxidative Stress and Antioxidant Therapy in Chronic Kidney and Cardiovascular Disease. Oxidative Stress and Chronic Degenerative Diseases – a Role for Antioxidants. Dr. Jose Antonio Morales-Gonzalez (Ed.) InTech Croatia. ISBN: 978-953-51-1123-8.

Conference Abstracts

Small DM, Sanchez WY, Roy SF, Morais C, Johnson DW, Gobe GC. November 2014. *Acute Kidney Injury Progresses to Chronic Kidney Disease via Persistent Metabolic Alterations and Oxidative Stress*. American Society of Nephrology Kidney Week 2014. Oral Presentation.

Small DM, Sanchez WY, Roy S, Morais C, Johnson DW, Gobe GC. August 2014. *N-Acetyl-Cysteine Enhances Chronic Kidney Pathology Following Acute Kidney Injury*. Modern Views on Kidney Function: The Legacy of Homer Smith. "The Kidney in Health and Disease Research Theme Meeting". Oral Presentation.

Small DM, Sanchez WY, Roy S, Morais C, Johnson DW, Gobe GC. August 2014. *Progression to Chronic Kidney Disease After Acute Kidney Injury Involves Prolonged Oxidative Stress and Persistent Tubular Metabolic Alterations.* 50th Annual Scientific Meeting of the Australian and New Zealand Society of Nephrology. Oral Presentation for the Basic Science Award.

Small DM, Sanchez WY, Roy S, Morais C, Johnson DW, Gobe GC. May 2014. *Acute Kidney Injury Induced Metabolic Alterations and Oxidative Stress in Kidney Tubules that Promote Progression to Chronic Kidney Disease*. Australian Society for Medical Research Postgraduate Student Conference 2014. Poster Presentation - first prize.

Small DM, Morais C, Johnson DW, Gobe GC. October 2013. *Peroxisome Proliferator Activated Receptor Gamma (γ) Activation Does Not Protect Human Kidney Proximal Tubular Epithelial Cells against Oxidative Stress.* American Society of Nephrology Kidney Week 2013. Oral presentation.

Small DM, Sanchez WY, Roy S, Johnson DW, Gobe GC. October 2013. *Intravital Multiphoton Microscopy can Visualize Oxidative Damage and Tubulointerstitial Fibrosis after Kidney Ischemia-Reperfusion Injury*. American Society of Nephrology Kidney Week 2013. Poster presentation.

Shahzad M, **Small DM**, Morais C, Wojcikowski K, Gobe GC. October 2013. *Protection Against H_2O_2-induced cell death by Angelica sinensis and Astragalas membranaceus in HK2 Human Kidney cells.* American Society of Nephrology Kidney Week 2013. Poster Presentation.

Small DM, Morais C, Johnson DW, Gobe GC. September 2013. *Peroxisome Proliferator Activated Receptor-γ Activation Does Not Protect Human Kidney Proximal Tubular Cells against Oxidative Stress*. 49th Annual Scientific Meeting of the Australian and New Zealand Society of Nephrology. Nephrology (Carlton). 18 suppl. 1. 148. Oral Presentation.

Small DM, Sanchez WY, Roy S, Johnson DW, Gobe GC. July 2013. *Intravital Multiphoton Microscopy can Visualize Oxidative Damage and Tubulointerstitial Fibrosis after Kidney Ischemia-Reperfusion Injury*. Translational Research Institute Inaugural Annual Poster Symposium. Poster presentation.

Small DM, Morais C, Johnson DW, Gobe GC. July 2013. *Human Kidney Proximal Tubular Epithelial Cells are not Protected Against Oxidative Stress by PPARγ Agonists.* Translational Research Institute Inaugural Annual Poster Symposium. Finalist for oral presentation.

Small DM, Morais C, Johnson DW, Gobe GC. June 2013. *Human Kidney Proximal Tubular Epithelial Cells are not Protected against Oxidative Stress by Peroxisome Proliferator Activated Receptor Gamma (PPARγ) Agonists.* Princess Alexandra Hospital Health Symposium. Poster presentation.

Small DM, Bennett NC, Coombes JS, Johnson DW, Gobe GC. May 2013. *Mitochondrial Homeostasis is Impeded by Degradation and Autophagy in Oxidative Stress Induced Renal Cell Injury*. 50th European Renal Association – European Dialysis Transplantation Association Conference. Poster presentation.

Small DM, Bennett NC, Coombes JS, Johnson DW, Gobe GC. August 2012. *Altered Mitochondrial Homeostasis, p62 And PPARγ and α Contribute To Oxidative Stress-Induced Kidney Injury.* American Society of Nephrology Kidney Week 2012. Poster presentation.

Small DM, Bennett NC, Coombes JS, Johnson DW, Gobe GC. August 2012. Discipline of Medicine, Discipline of Surgery – Inaugural Research Symposium, The University of Queensland. *Altered Mitochondrial Homeostasis, p62 And PPARγ and α Contribute To Oxidative Stress-Induced Kidney Injury.* Oral presentation.

Small DM, Royet Y, Gobe GC. August 2012. *N-Acetyl-Cysteine Attenuates Oxidative Stress-Induced Apoptosis in Kidney Proximal Tubular Epithelial Cells.* Translational Nephrology: From Mechanisms to Therapeutics. "The Kidney in Health and Disease Research Theme Meeting". Oral presentation.

Small DM, Bennett NC, Coombes JS, Johnson DW, Gobe GC. August 2012. *Oxidative Stress-Induced Alterations in Mitochondrial Homeostasis In Human Proximal Tubular Epithelial Cells.* 48th Annual Scientific Meeting of the Australian and New Zealand Society of Nephrology. Nephrology (Carlton). 17 suppl. 2. 229. Oral Presentation.

Small DM, Bennett NC, Roy S, Gabielli B, Gobe GC. September 2011. *Dysfunctional Mitochondria Contribute to the Loss of Renal Mass in Oxidative Stress-Induced Chronic Kidney Disease.* Princess Alexandra Hospital Health Symposium. Poster presentation.

Small DM, Bennett NC, Roy S, Gabrielli B, Gobe GC. August 2011. *Oxidative Stress, Cell Senescence, and Dysfunctional Mitochondria Combine to Contribute to Renal Cell Loss in the Ageing Kidney.* Discipline of Medicine Inaugural Research Symposium, The University of Queensland. Oral presentation.

Small DM, Bennett NC, Roy S, Gobe GC. July 2011. *Dysfunctional Mitochondria Contribute to the Loss of Renal Mass in Oxidative Stress-Induced Chronic Kidney Disease.* 48th European Renal Association – European Dialysis Transplantation Association Conference. Poster presentation.

Small DM, Bennett NC, Roy S, Gabrielli B, Gobe GC. April 2011. *Oxidative Stress And Cell Senescence Synergistically Contribute To Renal Cell Aging Via Dysfunctional Mitochondria.* International Society of Nephrology - World Congress of Nephrology. Poster presentation.

Small DM, Bennett NC, Crane D, Gobe GC. September 2010. *Oxidative Stress, Cellular Apoptosis and Senescence of the Ageing Kidney: Role of the Mitochondria.* 46th Annual Scientific Meeting of the Australian and New Zealand Society of Nephrology. Nephrology (Carlton). 15 suppl. 4. 91. Oral presentation.

PUBLICATIONS INCLUDED IN THIS THESIS

Small DM, Coombes JS, Bennett N, Johnson DW, Gobe GC. 2012. Oxidative stress, antioxidant therapies and chronic kidney disease. *Nephrology (Carlton)* **17**: 311-321 – incorporated as Chapter 1

Contributor	Statement of contribution
David M Small (Candidate)	Wrote and edited the paper (80%)
Jeff S Coombes	Edited the paper (10%)
Nigel C Bennett	Edited the paper (5%)
David W Johnson	Edited the paper (5%)
Glenda C Gobe	Wrote and edited the paper (20%)

Small DM, Bennett NC, Roy S, Gabrielli BG, Johnson DW, Gobe GC. 2012. Oxidative stress and cell senescence combine to cause maximal renal tubular epithelial cell dysfunction and loss in an in vitro model of kidney disease. *Nephron Exp Nephrol* **122**: 123-130 – incorporated as Chapter 3.

Contributor	Statement of contribution
David M Small (Candidate)	Designed experiments (55%) Performed the experiments (85%) Wrote the paper (70%)
Nigel C Bennett	Designed experiments (5%) Wrote and edited paper (5%)
Sandrine Roy	Performed the experiments (5%)
Brian G Gabrielli	Designed experiments (5%) Wrote and edited paper (5%)
David W Johnson	Designed experiments (5%) Wrote and edited paper (5%)
Glenda C Gobe	Designed experiments (30%)

	Performed experiments (10%) Wrote and edited paper (15%)

Small DM, Morais C, Coombes JS, Bennett NC, Johnson DW, Gobe GC. 2014. Oxidative Stress-Induced Alterations in PPARgamma and Associated Mitochondrial Destabilisation Contribute to Kidney Cell Apoptosis. *Am J Physiol Renal Physiol*. **307**: 814-822. – incorporated as Chapter 4.

Contributor	Statement of contribution
David M Small (Candidate)	Designed experiments (50%) Performed the experiments (95%) Analysed the results (80%) Wrote and edited the paper (70%)
Christudas Morais	Designed experiments (5%) Performed the experiments (5%) Edited the paper (5%)
Jeff S Coombes	Designed experiments (5%) Edited the paper (5%)
Nigel C Bennett	Designed experiments (5%) Edited the paper (5%)
David W Johnson	Designed experiments (5%) Edited the paper (5%)
Glenda C Gobe	Designed experiments (30%) Analysed the results (20%) Wrote and edited the paper (30%)

CONTRIBUTIONS BY OTHERS TO THE THESIS

Due recognition acknowledging contributions made to this thesis has been made throughout the thesis document and within the Acknowledgements section. Two major contributions are Dr David Briskey, who contributed to non-routine technical work in this thesis by performing the plasma F_2-isoprostanes assay as outlined in Chapter 7; and Mr Clay Winterford who contributed to non-routine technical work in this thesis by performing and providing assistance with immunohistochemistry for relevant research chapters.

STATEMENT OF PARTS OF THE THESIS SUBMITTED TO QUALIFY FOR THE AWARD OF ANOTHER DEGREE

Part of Chapter 3 was submitted for BSc (Biomedical) Honours, The University of Queensland, 2010, a degree awarded 19 December 2010. After commencing my PhD, more work was added to the basic results from this research chapter.

ACKNOWLEDGEMENTS

I would first and foremost like to thank my principal supervisor Associate Professor Glenda Gobe. Your mentorship, enthusiasm, and patience over the past years have been something I will never forget. Who would have thought that by taking a small undergraduate research project in your lab would lead to honours and a PhD. Not only have you provided me with the foundation to perform scientific research, but also how to approach any challenging situation in my future career. You have taught me that anything can be achieved through three common attributes - persistence, determination, and hard work. Sincerely, thank you.

I would like to thank my associate supervisors for their continual support. To be able to work with such inspiring people is a true privilege. I thank Dr Nigel Bennett for his patience, help in answering all of my annoying questions, and teaching me the practicalities of lab research, especially during the early days. Dr Christudas Morais, for his wealth of experience and frank, challenging questions, especially, "what does that mean?" Professor Jeff Coombes, for teaching me that research is not all about cells or animals. Professor David Johnson, for his clinical insight and forever quick email replies. The passion for what you all do does not go unnoticed.

I would like to thank all members of the CKDR lab past and present, in particular, Dr David Vesey for always taking the time to discuss a result. Also, Dr Vishal Diwan, Dr Miko Yamada and Dr Catherine Cheung, thank you for your immense support. The recent additions of Dr Michael Keng Lim Ng and Robert Ellis have also brought many enthusiastic conversations and a much needed coffee break here and there.

I would like to thank Dr Sandrine Roy of the Diamantina Institute microscopy facility. The past years would have been significantly more difficult if it was not for your immense enthusiasm and indispensable help with microscopy. Thank you to Dr Anne Bernard for making statistics sounds effortless. Thank you to Dr Robyn Webb, Dr Rick Webb and Dr Kathryn Green for the challenging support of electron microscopy. Thank you to Dr David Briskey for your tireless efforts with the isoprostanes assay. Thank you to Clay Winterford from the QIMR Histology facility – your wealth of histology knowledge and has made life easier.

This PhD project would not have been possible without financial support and a living scholarship provided by The University of Queensland and the National Health and Medical Research Council.

Travel funding to attend national and international conferences has primarily been provided by The Australian and New Zealand Society of Nephrology and Glenda.

Not only did the move to the Translational Research Institute bring great facilities, it also brought new colleagues and lasting friendships - a big thank you to Kevin Fagan and Victoria Gadd for easing the pressure of what can be a stressful time!

I would like to thank all of my family and friends for your support and encouragement. Especially, I would like to thank my beautiful partner Anna - thank you for always being there to take my mind off things, making me laugh, and realise that there is more to life than work.

Finally, I thank my family - Mum, Dad and Jaime. You have always supported me no matter what I have decided to do. Despite this PhD consuming my life over the past years, your unconditional love and support will be forever appreciated.

David Small

KEYWORDS

kidney, oxidative stress, mitochondria, proximal tubule, reactive oxygen species, intravital microscopy

AUSTRALIAN AND NEW ZEALAND STANDARD RESEARCH CLASSIFICATIONS (ANZSRC)

ANZSRC code: 110312, Nephrology and Urology, 50%
ANZSRC code: 111699, Medical Physiology not elsewhere classified, 25%
ANZSRC code: 060103 Cell Development, Proliferation and Death, 25%

FIELDS OF RESEARCH (FOR) CLASSIFICATION

FoR code: 1116, Medical Physiology, 50%
FoR code: 0601, Biochemistry and Cell Biology, 50%

TABLE OF CONTENTS

LIST OF FIGURES

CHAPTER 1

CHAPTER 2

CHAPTER 3

CHAPTER 4

LIST OF TABLES

ABBREVIATIONS

All abbreviations are listed in alphabetical order

ºC	Degrees Celsius
3D	Three-dimensional
8-OHdG	8-hydroxy-2'-deoxyguanosine
21d-IR	21 days post ischaemia-reperfusion
α_1	Amplitude coefficient of relative short lifetime
α_2	Amplitude coefficient of relative long lifetime
α_1/α_2	Redox ratio
$ABTS^+$	2,2'-azinobis(3-ethylbenzothiazoline 6-sulfonate)
ACEi	Angiotensin-converting enzyme inhibitors
ADP	Adenosine dinucleotide phosphate
AGE	Advanced glycation end products
AKI	Acute kidney injury
AMP	Adenosine mononucleotide phosphate
AMPK	Adenosine monophosphate-activated protein kinase
ANOVA	Analysis of variance
AOPP	Advanced oxidation protein products
Apaf1	Apoptotic peptidase activating factor-1
API	Apigenin
API+H	Combined apigenin and hydrogen peroxide treatment
ARE	Antioxidant response element
ATCC	American Type Cell Collection
αTOC	Alpha-tocopherol
ATP	Adenosine triphosphate
AU	Arbitrary units
Bardoxolone	Bardoxolone methyl
Bax	Bcl-2-associated x protein
BCA	Bicinchoninic
Bcl-2	B-cell lymphoma-2
Bcl-X_L	Bcl-x long isoform
BHT	Butylated hydroxytoluene
Blotto	Skim milk in TBST (see TBST)

BMI	Body mass index
BP	Blood pressure
BSA	Bovine serum albumin
Ca^{2+}	Calcium ion
CAT	Catalase
CDK	Cyclin-dependent kinase
CKII	Caseine kinase 2
CKD	Chronic kidney disease
CO_3^-	Carboxyl anion
CoQ_{10}	Coenzyme Q 10
CREB	cAMP response element-binding
CRP	C-reactive protein
CVD	Cardiovascular disease
Cyt C	Cytochrome C
DAB	Diaminobenzidine 2-hydrochloride
DAPI	4',6-diamidino-2-phenylindole
Δ12-mo	Change over 12-months
dH_2O	Distilled water
DHA	Docosahexanoic acid
DHE	Dihydroethidium
DMEM	Dubecco's modified Eagle's medium
DMSO	Dimethylsulfoxide
DNA	Deoxyribose nucleic acid
EDTA	Ethylenediaminetetraacetic acid
eGFR	Estimated glomerular filtration rate
EPA	Eicosapentanoic acid
EPR	Electron paramagnetic resonance
ERK	Extracellular regulated kinase
ESKD	End stage kidney disease
ESR	Electron spin resonance
ETC	Electron transport chain
EtOH	Ethanol
FAD+	Flavin adenine dinucleotide (oxidised)
$FADH_2$	Flavin adenine dinucleotide (reduced)
FasL	Fas ligand

FBS	Fetal bovine serum
FGF	Fibroblast growth factor
FLIM	Fluorescence lifetime imaging microscopy
FoxO	Forkhead proteins
FRET	Fluorescence resonance energy transfer
FSG	Fish skin gelatin
GAPDH	Glyceraldehyde 3-phosphate dehydrogenase
GC-MS	Gas chromatography-tandem mass spectroscopy
GCN5	General control of amino-acid synthesis 5
GGT	γ-glutamyl transpeptidase
GLUT4	Glucose transporter type 4
GPX	Glutathione peroxidase
Grx	Glutaredoxins
GST	Glutathione-S-transferase
h	Hour
H&E	Haematoxylin and eosin
Hb	Haemoglobin
HbA1c	Haemoglobin A1c
H_2O	Water
H_2O_2	Hydrogen peroxide
HBS	Hanks buffered solution
HDL	High density lipoprotein
HK-2	Human kidney-2 cells
HO-1	Heme oxygenase-1
HOCl	Hypochlorous acid
HOMA	Homeostasis model assessment
HPLC	High performance liquid chromatography
HPV	Human papilloma virus
HRP	Horseradish peroxidase
ICC	Immunocytochemistry
IF	Immunofluorescence
IHC	Immunohistochemistry
IκB	Inhibitor of nuclear factor-beta
IL-1	Interleukin-1
IL-1β	Interleukin-1 beta

IL-6	Interleukin-6
IMM	Inner mitochondrial membrane
IR	Ischaemia-reperfusion
IsoP	F_2-Isoprostanes
iv	Intravenous
JNK	c-Jun N-terminal kinase
Keap1	Kelch-like ECH-associated protein 1
LC3β	Microtubule-associated protein 1A/1B light chain 3-beta
LDL	Low density lipoprotein
λEm	Emission wavelength
LDH	Lactate dehydrogenase
Log_e	Natural logarithm
MAPK	Mitogen-activated protein kinases
MCP-1	Monocyte chemoattractant protein-1
MDA	Malondialdehyde
MDRD	Modified diet in renal disease eGFR equation
MitoQ	Mitoubiquinone mesylate (10-(6'-ubiquinonyl)-decyltriphenylphosphonium)
MitoVit E	Mitochondrial targeted-vitamin E
MMP	Mitochondrial membrane potential
MnSOD	Manganese superoxide dismutase
mRNA	Messenger ribose nucleic acid
mtDNA	Mitochondrial DNA
MPM	Multiphoton microscopy
MTT	3-(4,5-dimethylthiazol-2-yl)-2,5-diphenyltetrazolium bromide
NAC	N-acetyl cysteine
NaCl	Sodium chloride
NAD+	Nicotinic adenine dinucleotide (oxidised)
NADH	Nicotinic adenine dinucleotide (reduced)
NADP+	Nicotinic adenine dinucleotide phosphate (oxidised)
NADPH	Nicotinic adenine dinucleotide phosphate (reduced)
NAD(P)H	NADH and NADPH
NaF	Sodium fluoride
Nampt	Nicotinamide phosphoribosyltransferase
NaOH	Sodium Hydroxide
NF-κB	Nuclear-factor-κ B

NQO1	NAD(P)H:quinone oxidoreductase
$NO^{\bullet}$	Nitric oxide
NO_2	Nitrogen dioxide
NOS	Nitric oxide synthase
Nrf2	Nuclear receptor erythroid response factor 2
O_2	Molecular oxygen
$O_2^{\bullet-}$	Superoxide anion
$OH^{\bullet}$	Hydroxide anion
$ONOO^-$	Peroxynitrite
p62	Protein 62 (also called sequestome 1 – SQSTM1)
Park2	Parkin 2
PBS	Phosphate buffered saline
PCNA	Proliferating cell nuclear antigen
PDGF	Platelet derived growth factor
PGC-1α	Peroxisome proliferator receptor gamma coactivator 1 alpha
PGC-1β	Peroxisome proliferator receptor gamma coactivator 1 beta
PF	Paraformaldehyde
PINK1	Phosphate and tensin homology-induced kinase 1
Piog	Pioglitazone
PKCβ	Protein kinase C beta
PPARα	Peroxisome proliferator activated receptor – alpha
PPARβ/δ	Peroxisome proliferator activated receptor – beta/delta
PPARγ	Peroxisome proliferator activated receptor – gamma
PPARγ-1	Peroxisome proliferator activated receptor – gamma 1
PPARγ-2	Peroxisome proliferator activated receptor – gamma 2
PPARs	Peroxisome proliferator activated receptors
p-PPARγ	Phosphorylated (Ser112) peroxisome proliferator activated receptor gamma
Prx	Peroxyredoxins
PTE	Proximal tubular epithelial
PTP	Permeability transition pore
PVD	Peripheral vascular disease
PVDF	Polyvinylidene difluoride
QC	Quality control
RAAS	Renin-angiotensin-aldosterone-system
RIPA	Radioimmunoprecipitation assay

RNS	Reactive nitrogen species
$R\text{-}O^{\cdot}$	Peroxyl
R-OOH	Organic peroxides
ROS	Reactive oxygen species
Rosi	Rosiglitazone
rpm	Rotations per minute
RT	Room temperature
SA-β-gal	Senescence-associated beta galactosidase
SBHA	Sodium butyrate
SD	Standard deviation
SDS	Sodium-dodecyl-sulfate
SDS-PAGE	Sodium-dodecyl-sulphate polyacrylamide gel electrophoresis
SEM	Standard error of the mean
Ser36	Serine 36
Ser112	Serine 112
Sirt1	Sirtuin 1
Sirt3	Sirtuin 3
Sirt4	Sirtuin 4
SOD	Superoxide dismutase
TAC	Total antioxidant capacity
TBARS	Thiobarbituric acid reactive substance
TBS	Tris-buffered saline
TBST	Tris buffered saline with Tween-20
TCSPC	Time-corrected single-photon counting
TdT	Terminal deoxynucleotidyl transferase
TEM	Transmission electron microscopy
TGF-β1	Transforming growth factor beta 1
Tlx	Trolox
τ_1	Short lifetime
τ_2	Long lifetime
τ_m	Average weighted lifetime
TMRM	Tetramethyl rhodamine methyl ester
TNFα	Tumour necrosis factor-alpha
TRI	Translational research institute
Trog	Troglitazone

Trx	Thioredoxins
TZD	Thiazolidinediones
UV	Ultraviolet
Vit E	Vitamin E
WR	Working reagent

CHAPTER 1

Literature Review, Hypotheses and Aims

This thesis is presented as a literature review (Chapter 1) followed by a chapter detailing general materials and methods (Chapter 2), five original research sections that have, in some cases, been published (Chapters 3-7) and a general discussion of the results (Chapter 8). Copies of the published review articles relevant to this thesis and original research publications can be found in Appendices A. The review articles contribute to, and were updated, for Chapter 1.

1.1 GENERAL INTRODUCTION

Chronic disease is an increasingly important concern to health systems worldwide. Kidney disease is no exception to this, with increasing incidence and prevalence of chronic kidney disease (CKD) in developed and developing nations (Saran *et al.*, 2010). The population prevalence of CKD exceeds 10 % in most countries and is more than 50 % in high-risk subpopulations (Hallan *et al.*, 2012; Levey and Coresh, 2012; Matsushita *et al.*, 2012; Eckardt *et al.*, 2013). Recent evidence from the Australian population shows that 1 in 10 adults has CKD (ABS, 2013) while 1 in 3 is at increased risk of developing CKD throughout their life (KHA, 2014). The insidious nature of CKD is evident in that less than 10 % of people with CKD are aware they have symptoms of CKD (ABS, 2012; Radhakrishnan *et al.*, 2014). Most importantly, since 2000 there has been a dramatic increase in the prevalence of end stage kidney disease (ESKD) suggesting that current therapies that target progressive CKD have limited impact (White and Chadban, 2014). The identification of therapeutics that target particular mechanisms or molecular pathways is hindered by the disparate aetiology of CKD. A growing body of evidence demonstrates that the kidneys are not only target organs of many diseases but also can initiate a systemic pathophysiological process owing to their complex functions and effects on body homeostasis. Even with no other overt pathology such as hypertension or diabetes, age *per se* is a major risk factor for development of CKD (Radhakrishnan *et al.*, 2014), further adding to the health burden in our increasingly ageing population. Research investigating the development and progression of CKD is increasingly necessary.

CKD is primarily defined by a reduction in glomerular filtration rate (GFR) and increased urinary albumin excretion. It was originally categorised into five different stages, usually according to the estimated glomerular filtration rate (eGFR), but stage 3 CKD has now been separated into two stages, 3a and 3b (Fig. 1.1) (Johnson *et al.*, 2013). An eGFR of at least 90 mL/min/1.73m^2 with other indicators of kidney damage over three months is classified as stage 1 and represents early evidence of developing CKD, but not at a level that is dangerous to human health. However, this early development of CKD may be exacerbated by other superimposed causes of renal injury, such as high blood pressure, high blood lipids, diabetes and high blood glucose, chronic systemic

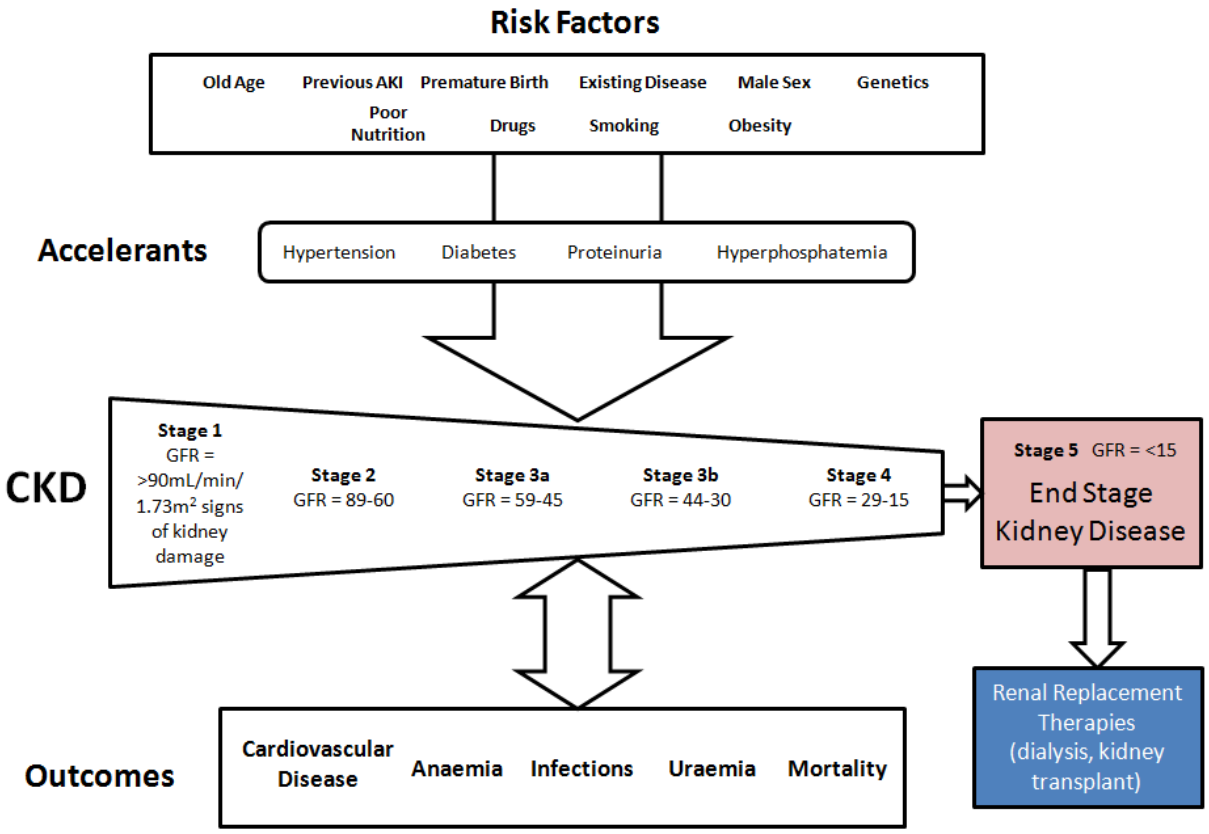

Figure 1.1: Factors that influence the development of chronic kidney disease
Chronic kidney disease (CKD) has many modifiable and non-modifiable causes. Ageing is one of the non-modifiable causes and its effects are accelerated by the presence of other age-related diseases like type 2 diabetes and hypertension. CKD is graded in stages from 1 to 5, according to an estimated glomerular filtration rate (GFR). Cardiovascular disease, infections and anaemia all exacerbate outcomes of CKD. The final stage, end stage kidney disease, causes uraemia at toxic levels and is treatable only with renal replacement therapies such as dialysis or transplantation. (AKI, acute kidney injury)

inflammation, or a build-up of environmental toxins. The functional impairment of the kidney is accompanied by pathological changes including increased tubular atrophy, interstitial fibrosis, glomerulosclerosis, renal vasculopathy and reduced regenerative capabilities of renal cells (Pannarale *et al.*, 2010).

The structural changes of CKD result in a stochastic deleterious effect on renal function. Over time, the renal damage may progress to stage 5 CKD, also known as ESKD, when renal function needs to be supplemented with dialysis, or renal transplant is necessary. Common health problems of the general population, including obesity, diabetes and cardiovascular disease (CVD), have a causative and/or synergistic relationship with CKD development. The aptly named cardio-renal syndrome is becoming increasingly defined as a disorder in itself, caused by an acute or chronic dysfunction of

the heart or kidneys leading to an acute or chronic dysfunction of the other organ (Ronco *et al.*, 2010). Although the aetiology and details of this disorder have yet to be validated, the outcomes of patients with CKD who develop co-morbid CVD are significantly poorer.

The kidneys are highly susceptible to age-related degeneration (Beeson *et al.*, 2010). They are one of the hardest working organs in the body, highly metabolising and reliant on a high energy production right throughout human life. In ageing, the kidneys show greater development of chronic pathology compared with brain, liver and heart, and this may relate to the gradual loss of renal energy through loss of mitochondrial function with ageing (Percy *et al.*, 2009). The aetiology of CKD is far reaching and includes specific diseases, such as diabetes, hypertension, or glomerulonephritis, or environmental factors such as those that influence metabolic syndrome or acute kidney injury (AKI). Each cause of CKD may have unique mechanisms that drive the progression of CKD, but often an underlying mechanism relates to mitochondrial dysfunction and oxidative stress. Oxidative stress, therefore, presents a useful target to slow the progression of CKD. However, oxidative stress is difficult to define at a cellular level, given its ubiquitous nature systemically.

The following literature review will initially describe oxidative stress, the involvement of mitochondrial dysfunction and the associated molecular pathways, the role of oxidative stress in CKD pathogenesis, how oxidative stress may be measured, and will give an update on the amelioration of CKD using antioxidant therapies.

1.2 LITERATURE REVIEW

1.2.1 Oxidative stress: role in kidney disease

Oxidative stress may be defined as a disturbance in regular cellular and molecular function caused by an imbalance between production of reactive oxygen species (ROS) and similar molecules, reactive nitrogen species (RNS), and the natural antioxidant ability of our cells (Pias and Aw, 2002; Zhuang *et al.*, 2007; Gomes *et al.*, 2009). Examples of the endogenous and exogenous sources of cellular ROS are listed in Table 1.1 and a list of the common reactive species is found in Table 1.2. Free radicals normally have a tightly regulated role as effectors of intracellular signalling pathways, by the activation of downstream targets for the maintenance of healthy tissue functionality. For example, physiological ligands act at specific targets to induce small bursts of ROS that control many physiological functions (Blanchetot *et al.*, 2002; Meng *et al.*, 2002; Rao and Clayton, 2002). Thus, the oxidative stress theories of disease development are controversial (Linnane and Eastwood,

2004, 2006; Linnane *et al.*, 2007b). Nonetheless, theories involving oxidative stress, as distinct from oxidant metabolism, explain many of the accumulated cellular deficits of disease pathogenesis.

Table 1.1: Endogenous and exogenous sources of reactive species

Endogenous factors	Exogenous factors
Mitochondrial oxidative phosphorylation	Environmental pollutants and toxins
Xanthine oxidase, NADPH oxidase	Cigarette smoke
Inflammatory cells	Hypoxia
Endosome/lysosome degradation	Hyperoxia
Angiotensin II	Radiation (sunlight, UV radiation)
Fibroblasts	Infectious microbes
Endoplasmic reticulum	High calorie diet
Peroxisomes	Glucotoxicity

Table 1.2: Common reactive species

	Free Radicals[a]	Non-Radical[b]
Reactive Oxygen Species	Superoxide ($O_2^{\bullet -}$) Hydroxyl ($OH^{\bullet}$) Peroxyl ($R\text{-}O^{-}$)	Hydrogen peroxide (H_2O_2) Organic peroxides (R-OOH) e.g. lipid peroxides Hypochlorous acid (HOCl)
Reactive Nitrogen Species	Nitric Oxide ($NO^{\bullet}$) Nitrogen dioxide (NO_2)	Peroxynitrite ($ONOO^{-}$)

[a] A free radical is defined as any molecule that has a spare electron in its outer shell.
[b] A non-radical does not contain a spare electron but is either an oxidizing agent or is easily converted to a free radical.

The kidney is highly energetic and therefore relies heavily on aerobic metabolism for the production of adenosine triphosphate (ATP) by oxidative phosphorylation (Beeson *et al.*, 2010). The reduction of molecular oxygen along the electron transport chain (ETC) within mitochondria is vital for cellular function, yet potentially devastating long-term. Highly reactive molecules that contain extra

electrons in their outer-shell are produced as by-products of oxidative phosphorylation. These ROS have the ability to damage lipids, deoxyribose nucleic acid (DNA) and proteins (Nemoto *et al.*, 2000). By-products of oxidative damage are increasingly found in various tissues with age. These by-products are believed to be a result of disturbances in the normal physiological oxidant pathways in young healthy renal cells, over time (Qiao *et al.*, 2005; Choksi *et al.*, 2007; Miyazawa *et al.*, 2009; Park *et al.*, 2011).

It is likely that, in a multifactorial process like a chronic disease, no theories for development of structural and functional deficit are mutually exclusive. The effect of age on kidney function has been well documented in a large range of mammalian models (Goyal, 1982; Clark, 2000; Esposito *et al.*, 2007; Pannarale *et al.*, 2010). Renal function is, in fact, considered a good predictor of longevity, with a close association found between a reduction in renal function and increase in all-cause mortality (Chien *et al.*, 2008; Liao *et al.*, 2009). CKD patients display increased biomarkers of oxidative stress compared to the non-CKD population (Dounousi *et al.*, 2006). Interestingly, other age-related diseases, such as neurodegenerative disease, which are also influenced by oxidative stress (Mancuso *et al.*, 2006) also have an increased incidence in the CKD population (Post *et al.*, 2010). This perhaps demonstrates oxidative stress as an important pathogenic factor in the development of multiple chronic diseases in the one patient.

1.2.2 Role of the mitochondria and reactive oxygen species

Fig. 1.2 demonstrates pathways to, and natural antioxidant neutralisation of, common ROS. The main ROS are superoxide ($O_2^{\bullet-}$), the hydroxyl radical ($OH^{\bullet}$) and hydrogen peroxide (H_2O_2). Although the mitochondria are considered the major source of ROS, other contributing sites of ROS generation include the endoplasmic reticulum, peroxisomes and lysosomes (Fig. 1.2) (Madesh and Hajnoczky, 2001; Soubannier and McBride, 2009; Vay *et al.*, 2009). Estimated levels of ROS within mitochondria are 5-10 fold higher than cystolic and nuclear compartments (Cadenas and Davies, 2000) due to the presence of the ETC within the mitochondrial inner membrane. 1-3 % of inspired molecular oxygen (O_2) is converted to the most common of the ROS, $O_2^{\bullet-}$ (Boveris and Chance, 1973; Nohl and Hegner, 1978), a powerful precursor of H_2O_2. Although cellular H_2O_2 is stable in this form, it has the potential to interact with a variety of substrates to cause damage, especially in the presence of the ferrous iron (Fe^{2+}), which leads to cleavage and formation of the most reactive and damaging of the ROS, the $OH^{\bullet}$. In healthy metabolic cells, the production of the potentially harmful H_2O_2 is countered by the catalysing actions of mitochondrial or cystolic catalase (CAT), or thiol peroxidases, into water and O_2.

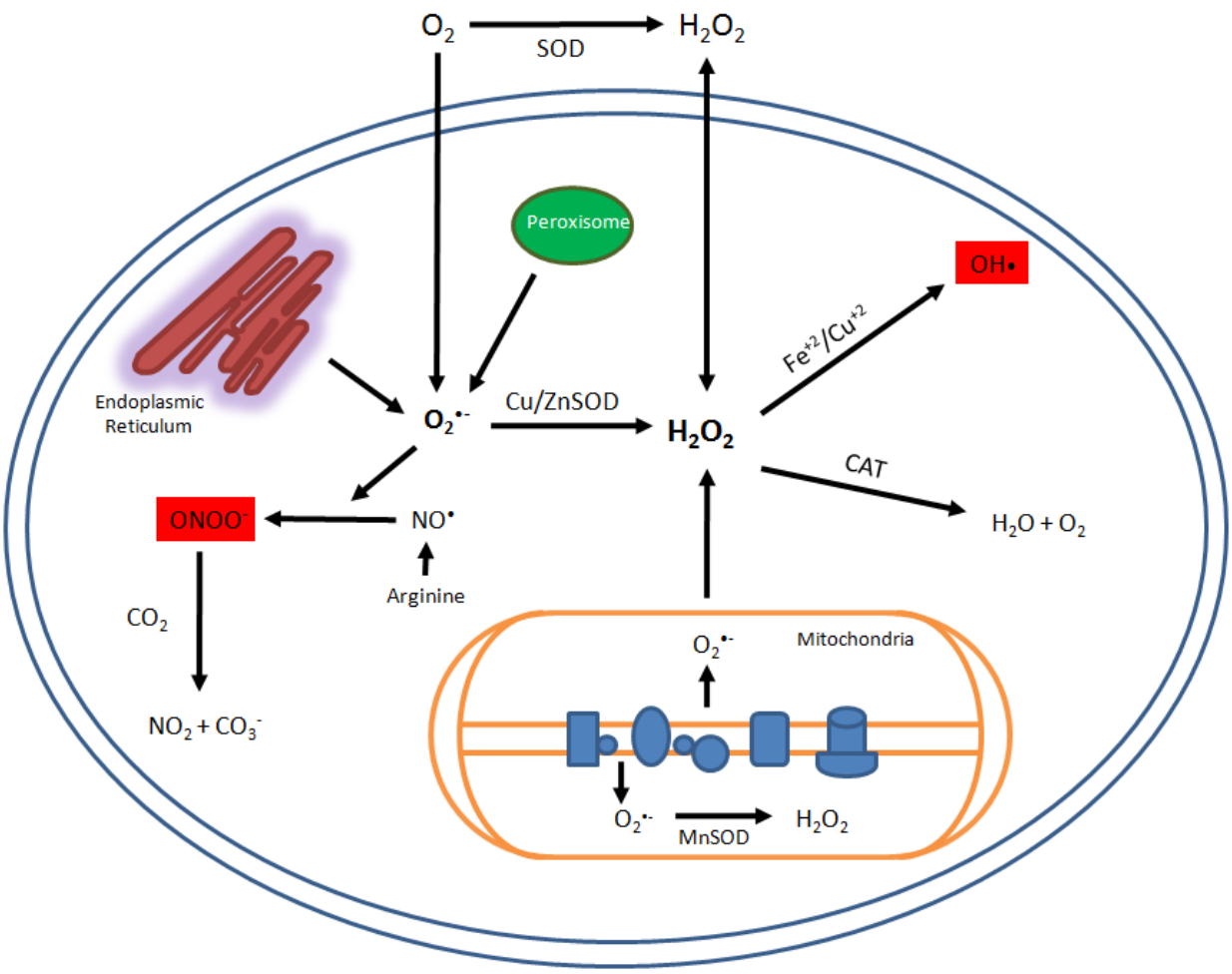

Figure 1.2: Cellular sites of free radical generation and interactions

The mitochondrion produces high levels of the superoxide anion ($O_2^{\bullet-}$) as a by-product of oxidative phosphorylation. $O_2^{\bullet-}$ is converted to stable hydrogen peroxide (H_2O_2) by manganese superoxide dismutase (MnSOD). Protein assemblage by the endoplasmic reticulum and fatty acid breakdown by peroxisomes also account for $O_2^{\bullet-}$ generation, whereby conversion to H_2O_2 occurs due to copper/zinc superoxide dismutase (Cu/ZnSOD). Catalase (CAT) is able to neutralise H_2O_2 into water (H_2O) and oxygen (O_2). In the presence of high amounts of H_2O_2, heavy metals (Fe^{+2} or Cu^{+2}) can form the highly reactive hydroxyl anion ($OH^{\bullet}$). Nitric oxide ($NO^{\bullet}$) and $O_2^{\bullet-}$ have the ability to form the highly reactive nitrogen species, peroxynitrite ($ONOO^-$), which, in the presence of carbon dioxide (CO_2) forms nitrogen dioxide (NO_2) and the reactive carbonyl species, the carboxyl anion (CO_3^-).

The ETC consists of 5 multi-enzyme complexes responsible for maintaining the mitochondrial membrane potential and ATP generation. Each of these complexes presents a site of ROS generation, however complexes I and III have been identified as primary sites of $O_2^{\bullet-}$ generation (Cadenas *et al.*, 1977; Turrens and Boveris, 1980; Turrens *et al.*, 1985; Turrens, 2003). ROS generation from mitochondrial complexes increases with age in mice (Choksi *et al.*, 2007). In humans, Granata and colleagues (2009) have reported that patients with CKD and haemodialysis patients display impaired mitochondrial respiration.

Oxidative phosphorylation is a highly orchestrated process and involves the pumping of protons into the inter-membrane space to create the mitochondrial membrane potential which is harnessed to synthesize ATP. Complex I, also known as nicotinamide adenine dinucleotide (NADH) dehydrogenase, or NADH-CoenzymeQ (NADH-CoQ) reductase, facilitates the transfer of electrons between NADH to CoQ10 (sometimes known as ubiquinone). Complex I has been identified as a major site of $O_2^{\bullet-}$ production (Liu *et al.*, 2002), increasing with age (Choksi *et al.*, 2007). Inhibition of complex I with rotenone reduces $O_2^{\bullet-}$ production significantly (Lenaz, 2001). The potential for alterations at this site with age favour the use of exogenous CoQ10 as an electron acceptor of excessive NADH derived radicals. Ubiquinol-cytochrome C oxidoreductase (Complex III) has also been identified as a major site of oxidant production. Furthermore, in an altered state, complex II can exhibit properties that would allow the reduction of O_2 to $O_2^{\bullet-}$ (Ishii *et al.*, 1998). Two mitochondrial oxidoreductase enzymes, glycerol-1-phosphate dehydrogenase and dihydroorotate dehydrogenase are also involved in the production of ROS. However, O'Toole and colleagues (2010) demonstrated recently that defects in oxidative phosphorylation may be due to the use of substrates in the respiratory chain, such as the reduced NADH and NADH oxidase, and not due to alterations in the proteins of the respiratory complexes. Thus, it is likely that both altered respiratory complexes and substrates lead to an inefficiency of electron transport and subsequent increased ROS generation, decreased ATP production and a loss of the mitochondrial membrane potential. Continual damage of this system with age produces a vicious cycle of increasing ROS generation and cell dysfunction.

Given that ROS are likely to be highly damaging molecules to cells, why have the mitochondria not evolved more efficient systems that limit mitochondrial oxidants? One possible answer is they are also involved in highly conserved basic physiological processes and are effectors of downstream pathways. Although there is evidence for this (Nemoto *et al.*, 2000; Werner and Werb, 2002), the specific mechanisms are difficult to define because of the rapidity of oxidant signalling (Cadenas and Davies, 2000). For example, protein tyrosine phosphatases are major targets for oxidant

signalling since they contain the amino acid residue cysteine that is highly susceptible to oxidative modification (Cooper *et al.*, 2002). Meng and colleagues (2002) demonstrated the oxidation of the SH2 domain of the platelet-derived growth factor (PDGF) receptor, which contains protein tyrosine phosphatases, in response to PDGF binding. This may indicate the induction of free radicals in response to receptor activation by a cognate ligand in a process that is similar to phosphorylation cascades of intracellular signalling.

Free radical damage to mitochondria with increasing age may not increase the generation of ROS, but instead inhibit mitochondrial function and ROS generation (de Grey, 2000, 2002). This theory relies on free radical damage to mitochondrial DNA (mtDNA) that causes mutations and therefore defects to complexes I and III of the ETC. This reduces mitochondrial ROS generation, and also enables mitochondria defective in mtDNA to avoid autophagy, a process traditionally believed to control intracellular removal and recycling of dysfunctional mitochondria within the cellular lysosome system. By inhibiting oxidative phosphorylation as an option for cellular energy metabolism and ATP synthesis, the cell has to utilize alternate forms of electron transport to reoxidize NADH and generate NAD+ to sustain ATP production by glycolysis. Thus, the plasma membrane redox system may facilitate the transfer of electrons from NADH inside the cell to outside the cell, and in doing so regenerate NAD+ to NADH and contribute to extracellular ROS (Close *et al.*, 2007). However, no experimental evidence exists for this theory.

Mitochondria are intimately linked to metabolism since they act, principally, as the main site for metabolism. However, there are recent and interesting investigations that highlight the importance of mitochondria during cell stress. The mitochondrial oasis hypothesis states that the NAD+ content and energetics of mitochondria determine cell survival in the fate of genotoxic stress and DNA damage, independent of the state of the cytoplasm or nucleus (Yang *et al.*, 2007a). This is achieved through an increase in mitochondrial nicotinamide phosphoribosyltransferase (Nampt), which is the biosynthetic enzyme needed to create NAD+, as well as mitochondrial NAD+-dependent deacetylases sirtuin 3 (Sirt3) and Sirt4. Furthermore, with age there is a specific loss of mitochondrial, and not nuclear, encoded oxidative phosphorylation sub-units. Thus, the decline in NAD+ that occurs with age is facilitated by a loss of nuclear-mitochondrial communication. This leads to a pseudo hypoxic state that contributes to the decline in mitochondrial function with age (Gomes *et al.*, 2013).

1.2.3 Natural defences: endogenous antioxidants

The production of ROS is usually in balance with the availability and cellular localisation of antioxidant enzymes such as superoxide dismutase (SOD), CAT and glutathione peroxidase (GPX) (Fig. 1.2). *In vivo* studies have found accumulated oxidative damage occurs from decreased levels of these enzymes rather than increased ROS production (Kokoszka *et al.*, 2001; Meng *et al.*, 2007). However, adequate levels of both are likely to be vital for normal cell function. Mitochondria possess their own pool of antioxidants to counteract their generation of ROS. Mitochondrial manganese-SOD (Mn-SOD) converts $O_2^{\bullet-}$ to H_2O_2 which is then decomposed to harmless H_2O and O_2 by CAT and Gpx (Raha *et al.*, 2000). Copper/zinc-SOD (Cu/Zn-SOD) has been implicated in stabilizing $O_2^{\bullet-}$ within other cellular compartments, especially peroxisomes, and must be considered in maintenance of the redox state of the whole cell (Angermuller *et al.*, 2009; Islinger *et al.*, 2009). Limited antioxidant actions of Cu/Zn-SOD may also occur within the inter-membrane space (Sturtz *et al.*, 2001). There is no evidence to indicate that glutathione synthesis occurs within mitochondria, however the mitochondria have their own distinct pool of glutathione required for the formation of Gpx (Soderdahl *et al.*, 2003).

Among the various endogenous defences against ROS, glutathione homeostasis is critical for a cellular redox environment and works in a critical coordinated fashion. Glutathione-linked enzymatic defences of this family include GPX, glutathione-S-transferase (GST), glutaredoxins (Grx), thioredoxins (Trx), and peroxiredoxins (Prx) (Godoy *et al.*, 2011). Many of these proteins are known to interact with each other, forming redox networks which have come under investigation for their contribution to dysfunctional oxidant pathways. Mitochondrial-specific isoforms of these proteins also exist and include Grx2, Grx5, Trx2 and Prx3 (Lillig and Holmgren, 2007; Lonn *et al.*, 2008; Hanschmann *et al.*, 2010) which may be more critical for cell survival compared to their cytosolic counterparts (Soderdahl *et al.*, 2003). Mitochondrial dysfunction, resulting in depleted ATP synthesis, has the potential to reduce the redox control of glutathione since the rate of glutathione synthesis is ATP dependent (Lash *et al.*, 2002). Intracellular synthesis of glutathione from amino acid derivatives (glycine, glutamic acid and cysteine) accounts for the majority of cellular glutathione compared with, for example, the uptake of extracellular glutathione from the bicollateral membrane in epithelial tubular cells of the renal nephron (Visarius *et al.*, 1996). This characteristic may account for different segments of the nephron being differently-susceptible to the same insult, since proximal tubular epithelial (PTE) cells lack the ability to synthesise glutathione, compared with other segments of the nephron which have that ability (Hall *et al.*, 2009). There may also be "antioxidant networks" in which there is interplay, crosstalk, and synergism to efficiently and specifically scavenge ROS. If this is the case, these antioxidant networks could be harnessed by

researchers to develop polytherapeutic antioxidant supplements to combat oxidant-related pathologies, like CKD.

1.2.4 Mitochondrial biogenesis and degradation: molecular pathways

Although oxidative stress has been recorded as a mechanistic factor in many forms of kidney disease, including CKD, the role of mitochondrial dysfunction and the molecular pathways that are involved in this process, have received little attention. Here, characteristics and molecular pathways of mitochondrial biogenesis and degradation are described. Some of these will receive attention in the research of this thesis.

Mitochondrial biogenesis and the degradation of mitochondria (mitophagy) usually occur in balance within healthy cells, including those of the kidney (Gunst *et al.*, 2013). The imbalance between mitochondrial biogenesis and mitophagy has come under investigation recently as a major contributor to oxidative stress and cellular metabolic decline (Kirkin *et al.*, 2009). It was traditionally believed that autophagy (literally, "self-eating") was a non-selective cell regulatory mechanism for the degradation of dysfunctional organelles within the cellular lysosome system (Kurz *et al.*, 2007). However, the discovery of the autophagy genes, particularly *Atg32*, as mitochondrial transmembrane receptors directing autophagosome formation, has uncovered a highly selective process of removal of damaged mitochondria (Okamoto *et al.*, 2009). A major pathway for injury-induced mitochondrial degradation is the phosphate and tensin homology-induced kinase 1 (PINK1) - Parkin 2 (Park2) pathway. Park2 is an E3 ubiquitin ligase that translocates to mitochondria and mediates mitochondrial degradation (Narendra *et al.*, 2008; Cai *et al.*, 2012). The adaptor protein p62 facilitates selective autophagy into the light chain-2 beta (LC3β)-regulated machinery for lysosomal degradation (Bjorkoy *et al.*, 2005; Geisler *et al.*, 2010). p62 is not required for Park2 translocation to damaged mitochondria, but is essential for final autophagic clearance (Geisler *et al.*, 2010). This response is enhanced by a decrease in ATP production due to dysfunctional mitochondria, and is regulated by the intracellular energy sensor, adenosine monophosphate-activated protein kinase (AMPK) (Egan *et al.*, 2011). These pathways are summarised in Figure 1.3.

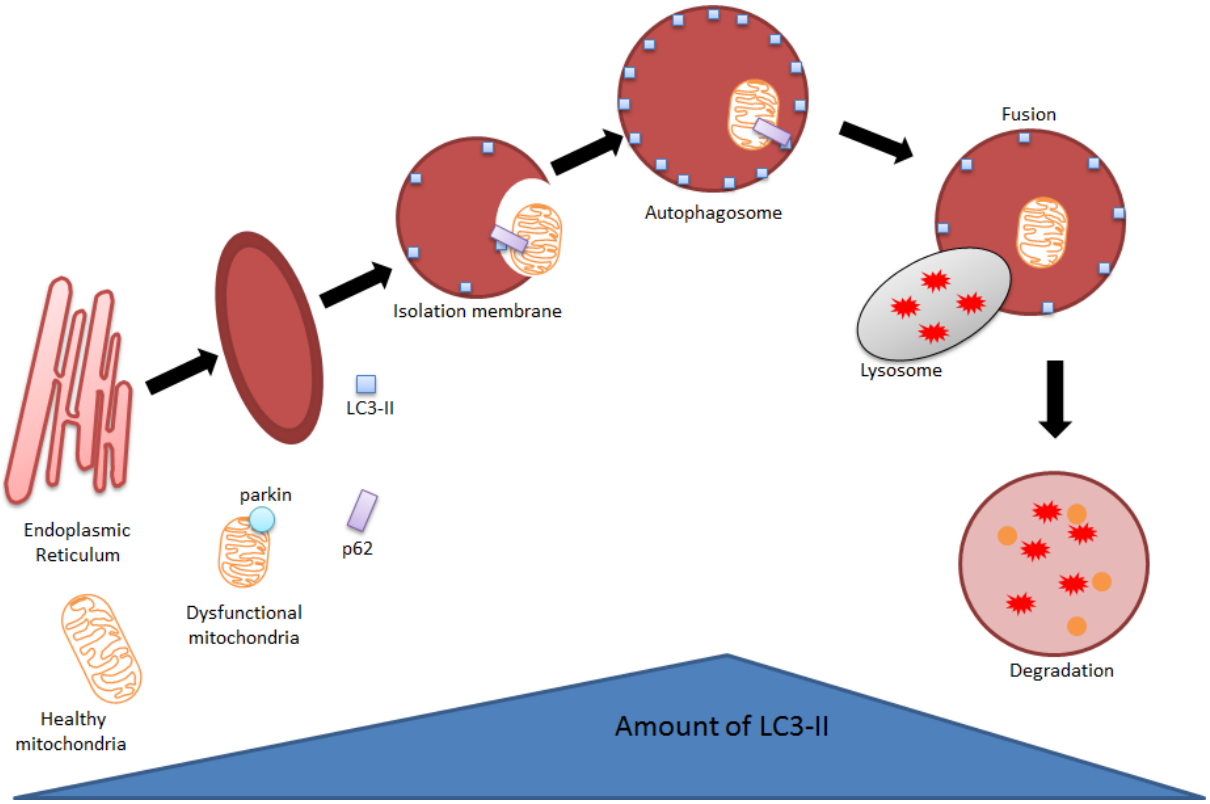

Figure 1.3: Degradation of mitochondria via autophagy (mitophagy)
Parkin is an E3 ubiquitin ligase that translocates to defective mitochondria, effectively labelling them for degradation. Autophagy is initiated by folding of the endoplasmic reticulum membrane and formation of the isolation membrane expressing light chain 3-II (LC3-II). The adapter protein p62 facilitates sequestration of parkin-labelled mitochondria into the autophagosome through LC3-II binding. Following closure of the autophagosome, lysosomes fuse to the autophagosome to form the autolysosome, and the intra-autophagosomal contents are degraded by lysosomal hydrolases.

Failure to restore mitochondrial homeostasis and function can lead to a progressive increase in ROS and ensuing oxidative stress. Peroxisome proliferator-activated receptor gamma coactivator 1-alpha (PGC-1α) is a nuclear transcription factor shown to mediate almost all aspects of mitochondrial biogenesis, and is considered a master regulator of biogenesis (Hock and Kralli, 2009). Therefore, PGC-1α activation presents a crucial target for mitochondrial preservation. Previous studies have demonstrated pharmacological peroxisome proliferator-activated receptor gamma (PPARγ) activation and induction of mitochondrial biogenesis (Hondares *et al.*, 2006; Rasbach and Schnellmann, 2007). Increasing mitochondrial biogenesis is an attractive target to reduce cellular metabolic injury and improve recovery. However, it must be realised that increasing the number of mitochondria could possibly worsen tissue hypoxia due to increased oxygen consumption.

1.2.5 Cellular apoptosis, regeneration and senescence

One of the frequently-seen structural characteristics of CKD is tubular atrophy. This involves cell deletion via apoptosis, a process first described in the kidney by Gobe and Axelsen (1987) but which has been extensively studied since. Along with the atrophic tubules, foci of regenerating tubules are often seen histologically in the kidneys of CKD patients. Although very important in maintaining renal function in the presence of significant tissue deletion, this has received less attention than apoptosis (Yang *et al.*, 2014). Finally, one of the least studied of the characteristics of tubular atrophy in CKD is the development of cell senescence (Melk et al., 2004). Apoptosis and cell senescence both have some links with mitochondrial dysfunction. The characteristics of apoptosis and the balance of regeneration, and cell senescence, will be discussed in the following section. They will also form part of the analyses in the original research chapters of this thesis.

1.2.5.1 Apoptosis

Apoptosis is a rapid, highly conserved process of gene-driven, programmed cell death required for normal physiological homeostasis (Kerr *et al.*, 1972). Apoptosis is also central to many diseases, including CKD (Yang *et al.*, 2007b; Hughson *et al.*, 2008) where the general loss of functioning renal mass of up to 25 % is attributed, at least in part, to apoptosis (Percy *et al.*, 2008). Pro-apoptotic proteases, known as caspases, play essential roles in apoptosis. ROS generation may cause suppression of phosphorylation of the anti-apoptotic B-cell lymphoma-2 (Bcl-2) protein and loss of mitochondrial membrane potential. Thus, mitochondrial dysfunction, oxidative stress and ROS are closely associated with renal apoptosis, and as a consequence, the development of CKD (Sanz *et al.*, 2008; Miyazawa *et al.*, 2009).

Figure 1.4 demonstrates some of the molecular pathways involved in apoptosis. The extrinsic pathways start, in general, with ligation of death receptors, like Fas, with ligands, like FasL and tumour necrosis factor-α (TNFα), from outside the cell. The intrinsic apoptotic pathway involves action at the mitochondria, and this might be initiated by ROS. Both pathways can impact in mitochondrial function through activation of members of the Bcl-2 family of proteins. This family has anti-apoptotic (Bcl-2, the long Bcl isoform Bcl-xl, Mcl-1) and pro-apoptotic (Bcl-2-associated x protein/Bax; Bcl-2 antagonist killer/Bak; Bid) members. Bid is crucial for the induction of death receptor-mediated apoptosis in primary tissues; but Bax is more generally recognised as a pro-apoptotic Bcl-2 protein acting at the mitochondria (Lindsay *et al.*, 2011). Once the mitochondrial membrane is injured, another set of molecules is released (cytochrome C/Cyt C) or activated (apoptotic peptidase activating factor-1/Apaf-1, caspases 9 and 3), and the structural characteristics of apoptosis become evident.

The intrinsic pathway to apoptosis is of particular importance to age-related CKD since it involves mitochondrial dysfunction and excessive ROS generation (Madesh and Hajnoczky, 2001; Ott *et al.*, 2007). Opening of the mitochondrial permeability transition pore (PTP) releases Cyt C, which had been previously bound to the inner mitochondrial membrane by an association with the anionic phospholipid, cardiolipan. Increased oxidative stress results in increased amounts of Cyt C in the cytosol, suggesting that ROS causes a dissociation of Cyt C from cardiolipan (Miyazawa *et al.*, 2009). Cytoplasmic Cyt C binds and activates caspase-9, one of the proteases known to act in the apoptotic pathways. Activated caspase-9 forms an apoptosome with Apaf-1, leading to phosphorylation and cleavage of caspase-3 and subsequent morphological changes of apoptosis (Li *et al.*, 1997; Allan and Clarke, 2009).

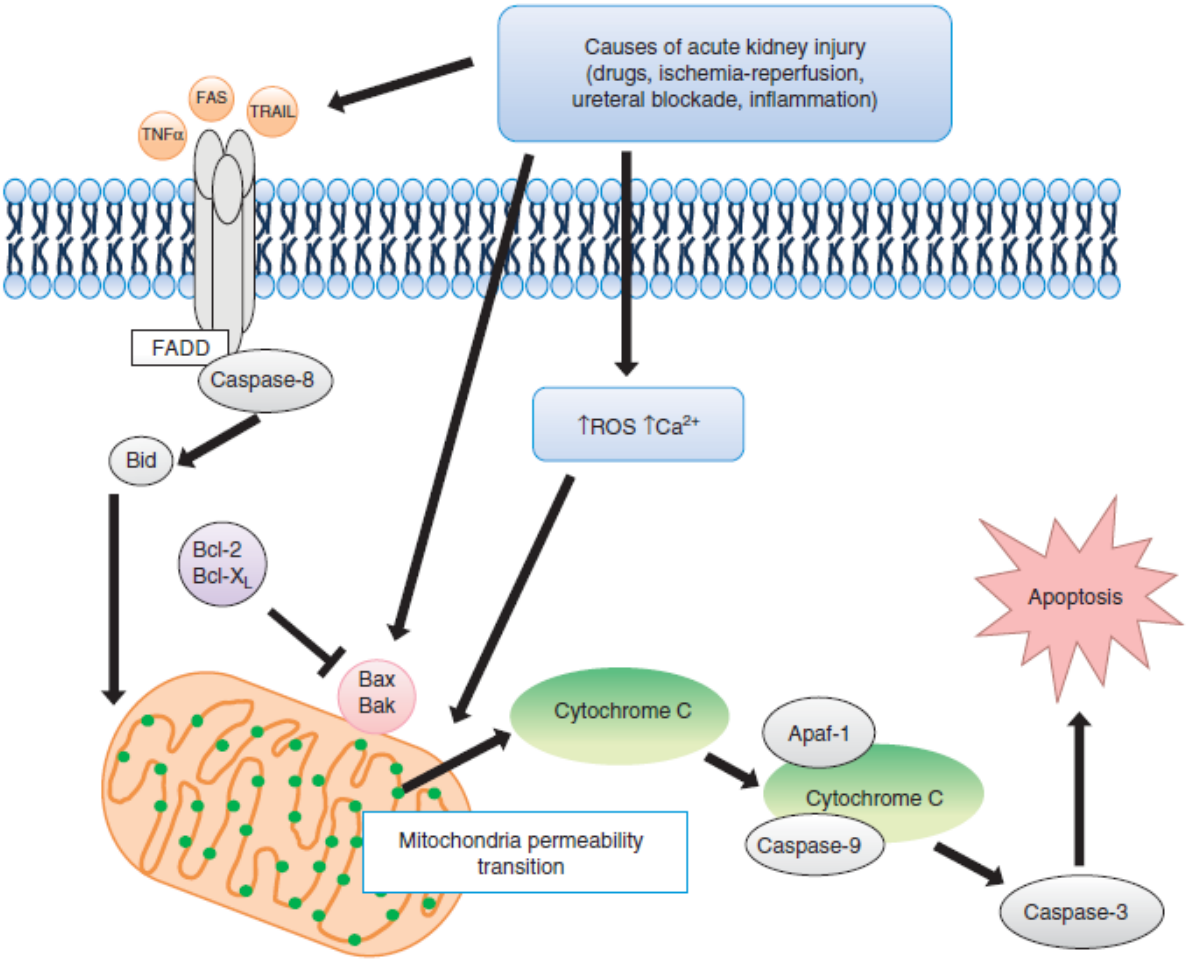

Figure 1.4: Apoptotic pathway involving cytochrome c release

During apoptosis processing using intrinsic or extrinsic pathways, cytochrome c moves from its location between the outer and inner membranes of mitochondria and is rapidly released into the cytosol. Activation and translocation of pro-apoptotic Bcl-2 family members such as Bax and Bak to the mitochondria cause the opening of the channels in the outer and inner mitochondrial membranes, thereby inducing a permeability transition. Once released, cytochrome c forms a complex with apoptotic peptidase activating factor-1 (Apaf-1) and procaspase-9, termed the apoptosome. This interaction causes cleavage and activation of caspase -9, which in turn activates the executioner caspase-3, which then induces the structural changes that are characteristic of apoptosis. (Small and Gobe, 2012)

The translocation of the Bcl-2 family proteins, especially pro-apoptotic Bax and Bak, to the mitochondria of kidney cells is the precursor to opening of the mitochondrial PTP, release of Cyt C and resultant apoptosis (Degenhardt *et al.*, 2002). Bax and Bak interact with the outer mitochondrial membrane, causing its permeabilization, however endogenous anti-apoptotic proteins (like Bcl-2 or Bcl-xl) also translocate from the cytoplasm to the mitochondrial membrane, protecting renal tubular epithelial cells against oxidative stress (Cuttle *et al.*, 2001). Apoptosis inducible factor (AIF) possesses an oxidoreductase domain which aids in the scavenging of ROS when localised within the mitochondria. However, cytosolic localisation of AIF triggers apoptosis via pro-apoptotic Bcl-2 proteins and caspase activation. This characteristic is also noted with Cyt C within and outside mitochondria which presents a possible cellular location-specific function of ROS-induced proteins as well as mitochondrial-cystolic communication by mitochondrial oxidants.

1.2.5.2 Regeneration

The regenerative ability of the kidney is limited by its own general health. It is well known that the proximal tubule has a substantial repair capacity after injury (Witzgall *et al.*, 1994), however whether a stem cell population is responsible for this proliferative response or not remains controversial. The classical model of repair after injury in epithelial cells of the proximal tubule involves a process of initial dedifferentiation and then proliferation of all surviving epithelial cells (Witzgall *et al.*, 1994; Vogetseder *et al.*, 2008). Numerous studies have also suggested a scattered intratubular progenitor cell population that is responsible for proliferation following injury (Loverre *et al.*, 2008; Lindgren *et al.*, 2011; Angelotti *et al.*, 2012). However, a recent study by Kusaba *et al.* (2014) using genetic lineage analysis, demonstrates that populations of fully differentiated PTE cells undergo dedifferentiation, to upregulate apparent stem cell markers and proliferate after injury. This provides strong evidence that epithelial dedifferentiation is responsible for regeneration rather than a resident adult stem cell population. AKI mouse models have primarily been used to define kidney regeneration, and little is known regarding this process in progressive CKD, as well a species between mouse and human.

1.2.5.3 Senescence

Most differentiated cells, as are found in the adult kidney, cannot divide indefinitely due to cellular senescence. One theory of cell senescence implicates telomeres, specialized structures that function in the protection, positioning and replication of chromosomes. Telomeres shorten after every mitotic division. The rate of telomere shortening is determined, at least in part, by the accumulation of DNA damage induced by ROS, further implicating the mitochondria in induction of senescence (Passos and Von Zglinicki, 2006). However, senescence is also associated with irreversible cell

cycle arrest, mainly in the G1 phase of the cell cycle. The senescent cells acquire a large, flat morphology, senescence-activated (acidic) β-galactosidase (β-gal) activity, and the upregulation of cyclin dependent kinase inhibitors, such as p53, $p21^{waf}$ and $p16^{ink}$ (Stein *et al.*, 1999). Oxidative stress plays a role in cell senescence: H_2O_2 downregulates casein kinase II which is required for phosphorylation of DNA-binding proteins, nuclear oncoproteins and transcription factors needed for cell proliferation and growth (Ryu *et al.*, 2006). Premature senescence also involves modification of the cellular signal transduction pathways (Goldenthal and Marin-Garcia, 2004), and a question remains as to the role of ROS and mitochondria in this modification. Lee et al (2010) recently demonstrated that increased pro-apoptotic c-Jun N-terminal kinase (JNK) was involved in the premature senescence of fibroblasts and breast carcinoma cells, accompanied by a rapid increase in mitochondrial ROS production. Basal JNK expression was also necessary for maintaining healthy levels of anti-apoptotic proteins, mitochondrial health and inhibition of cell senescence. This type of study has not been repeated in the ageing kidney, and needs investigation.

Cell senescence is a defining characteristic of CKD in ageing (Melk, 2003), yet the exact role of oxidative stress in renal cell senescence has yet to be defined. Oxidative stress induces premature senescence in fibroblast cultures (Frippiat *et al.*, 2001), and retinal epithelium during development of macular degeneration (Glotin *et al.*, 2008). The prevention of premature cell senescence with the antioxidants quercetin and vitamin E also demonstrates the essential role of oxidative stress in cell senescence (Volonte *et al.*, 2002). Given the evidence supporting increased oxidative stress with age due to increasing numbers of dysfunctional mitochondria, mitochondria may also play a novel and significant role in the premature senescence of kidney cells in CKD, but this has yet to be studied.

1.2.6 Genes driven by oxidative stress in chronic kidney disease

Knowledge of the regulatory molecular networks that determine renal health is far from complete. Understanding the transcriptional networks that maintain oxidant balance in the mature kidney will provide promising entry points for future therapeutic interventions, including for CKD. The following paragraphs summarise key aspects of transcriptional regulation in oxidative-stress induced CKD. Note that it was not possible for all regulatory molecules that are discussed here to be studied in this thesis.

1.2.6.1 Peroxisome proliferator activated receptors

Peroxisome proliferator activated receptors (PPARs) are a class of highly conserved nuclear hormone receptor superfamily of ligand-dependent transcription factors that are important regulators of metabolism (Ahmadian *et al.*, 2013). There have been three PPAR isoforms identified and characterised – PPARα, PPARγ, and PPARβ/δ. PPARα is expressed primarily in liver, heart and brown adipose tissue, where it is a major activator of fatty acid oxidation pathways (Evans *et al.*, 2004). PPARβ/δ plays a similar role to PPARα however PPARβ/δ is ubiquitously expressed, playing more of a role in skeletal muscle, liver and heart (Barish *et al.*, 2006). PPARγ exists as two isoforms – PPARγ1 and PPARγ2 – with PPARγ1 being expressed in many tissues including kidney, and PPARγ2 expression restricted to adipose tissue, however, has been shown to be induced in other tissues by a high fat diet (Medina-Gomez *et al.*, 2007; Tontonoz and Spiegelman, 2008). Ligand binding of PPARγ induces heterodimer formation with the retinoic acid receptor and complex binding to the peroxisome-proliferator response element within the promoter region of target genes involved in lipid metabolism, glucose homeostasis, cell proliferation and inflammation (Guan *et al.*, 2002). PPARγ also positively regulates mitochondrial biogenesis through the activation of PGC-1α (Portilla *et al.*, 2002; Weinberg, 2011). Therefore PPARγ may influence mitochondrial function and the maintenance of mitochondrial homeostasis to restore the intracellular redox environment (Funk *et al.*, 2010; Chiang *et al.*, 2013; Zhan *et al.*, 2013). Post-translational modifications of PPARγ have been shown to regulate its activity including phosphorylation (Hu *et al.*, 1996; Leff, 2003), acetylation (Qiang *et al.*, 2012), sumoylation (Shimizu *et al.*, 2006), and ubiquitination (Hauser *et al.*, 2000). Each modification has the potential to impart distinct features for cell or tissue specific activity of PPARγ. Specific endogenous ligands of PPARγ have not been clearly defined, however synthetic ligands such as thiazolidinediones (TZDs), are potent activators of PPARγ and are commonly used for their insulin-sensitising activities in the management of type 2 diabetes (Kung and Henry, 2012). PPAYγ expression has been shown to be increased in kidney biopsies from CKD patients of diverse aetiologies (Lepenies *et al.*, 2010) implicating a possible pathological influence in kidney disease. Nephroprotective mechanisms independent of inulin-sensitisation have been reported following PPARγ activation, including kidney structural and functional preservation in a mouse model of diabetic nephropathy despite no change in glucose, insulin or lipid levels (Calkin *et al.*, 2006); and a reduction in proteinuria in non-diabetic CKD patients (Kincaid-Smith *et al.*, 2008). However, human TZD trials in renal disease often report disparate results (Agarwal *et al.*, 2005; Pistrosch *et al.*, 2005).

1.2.6.2 The stress induced Nrf2/Keap1 axis

Nuclear factor-E2-related factor-2 (Nrf2) has received much attention over the past decade due to its ubiquitous protective regulation against cellular stress. As such, Nrf2 has formed the target of many trial therapies for common diseases (Zhao *et al.*, 2010; Joshi and Johnson, 2012; Miyata *et al.*, 2013; Yang *et al.*, 2013). Nrf2 is a transcription factor that modulates the expression of vital cytoprotective enzymes such as hemeoxygenase-1 (HO-1), PPARγ, SOD1/2, GST, and NAD(P)H:quinine oxidoreductase (NQO1) (Hybertson *et al.*, 2011). The transcriptional activation of these enzymes occurs through the binding of Nrf2 to a nucleotide motif sequence known as the antioxidant response element (ARE) (Rushmore *et al.*, 1991). During basal conditions, Nrf2 is constitutively degraded via a cullin-3-dependent pathway, following ubiquitylation labelling that appears to be promoted by the interaction with Kelch-like ECH-associated protein 1 (Keap1) (McMahon *et al.*, 2003; Zhang *et al.*, 2004). Keap1 is a strong regulator of Nrf2 activity and is vital for responding to oxidative stress to promote Nrf2 binding to ARE. Overexpression of Keap1 leads to increased levels of ubiquitin-conjugated forms of Nrf2 in cells (Nguyen *et al.*, 2005), and in *keap1*$^{-/-}$ animals, increased steady-state levels of Nrf2 (Wakabayashi *et al.*, 2003). The regulation of the Keap1-Nrf2 interaction in response to oxidative stress has yet to be fully characterised. The promotion of Nrf2 stabilisation by Keap1 disassociation and subsequent DNA binding of ARE is important (Nguyen *et al.*, 2005; Fourquet *et al.*, 2010). However, strong evidence suggests the modification of Keap1 cysteine residues by thiol-reactive chemical species, such as ROS (Dinkova-Kostova *et al.*, 2002; Zhang and Hannink, 2003; Yamamoto *et al.*, 2008; Fourquet *et al.*, 2010). Given the large numbers of cysteine residues within the primary structure of Keap1, this may prevent the interaction, or aid the disassociation, with Nrf2. Major protein kinase pathways have been implicated in Nrf2 regulation and although phosphorylation of Nrf2 has been demonstrated, it cannot be linked to its stabilisation (Kang *et al.*, 2001; Bloom and Jaiswal, 2003; Numazawa *et al.*, 2003). Furthermore, the cAMP response element-binding (CREB) protein can induce acetylation of Nrf2 and increase binding of Nrf2 to ARE, which can be decreased by sirtuin-1 (Sirt1) deacetylase (Kawai *et al.*, 2011). The hypothesis that Keap1 binding of Nrf2 occurs exclusively in the cytoplasm, and upon modification, allows Nrf2 nuclear translocation has been discarded. This outcome is in agreement with evidence that Nrf2 ARE binding occurs constitutively in healthy conditions (Nguyen *et al.*, 2005). Modulation of the Keap1-Nrf2 pathway in the kidney has been shown attenuate various pathologies that involve oxidative stress, including ischaemia-reperfusion injury, remnant kidney models, and *in vitro* models. Despite these positive benefits, the application of the potent Nrf2 activator, bardoxolone methyl, to pre-dialysis diabetic nephropathy patients resulted in increased mortality and serious adverse effects (de *et al.*, 2013). The outcome of this trial

highlights the need for more basic research into the Nrf-Keap1 pathway to harness its proven cytoprotective properties therapeutically.

1.2.6.3 Nuclear factor-kappa B

Nuclear factor-kappa B (NF-κB) comprises a family of rapid-acting nuclear transcription factors that transcriptionally-regulate a wide variety of genes involved in inflammation, immunity, apoptosis, cell proliferation and differentiation. In oxidative stress-induced kidney disease, NF-κB is activated by ROS and initiates signalling pathways involved in renal fibrosis (Greiber *et al.*, 2002; Morigi *et al.*, 2002; Sanz *et al.*, 2010) and age-related CKD (Percy *et al.*, 2009). NF-κB consists of homo- or heterodimers from five possible units of the Rel family, with the p65/p50 heterodimer being the most common form. The inhibitory protein, IκB, is associated with, and inactivates, NF-κB within the cytoplasm (Baeuerle and Henkel, 1994). Mitochondrial stress and subsequent ROS generation activates NF-κB (Morigi *et al.*, 2002). NF-κB activation in CKD is not isolated to one cell type within the kidney and has been demonstrated in podocytes, tubular cells, and mesangial cells (Massy *et al.*, 1999; Greiber *et al.*, 2002; Queisser *et al.*, 2011). It has been implicated in the transcriptional activation of the cell cycle inhibitor p21 (Pennington *et al.*, 2001; Savickiene *et al.*, 2004), linking the transcriptional regulator with renal cell senescence.

1.2.6.4 Forkhead (FoxO) proteins

The Forkhead (FoxO) proteins are a family of transcription factors believed to play a critical role in the regulation of genes in ageing (van der Horst and Burgering, 2007). They comprise FoxO1 to FoxO4, and FoxO6, however FoxO1 has most association with CKD. FoxO1 has increased levels of phosphorylation in the kidneys of elderly overweight humans with type 2 diabetes and CKD (Mussig *et al.*, 2009) and old hypertensive rats with CKD (Percy *et al.*, 2009). Increased ROS could regulate FoxO activity. Overexpression of FoxO proteins increases stress resistance including that induced by ROS (Guarente and Kenyon, 2000). Moreover, they have been linked to the upregulation of antioxidants involved in the detoxification of the harmful $O_2^{\bullet-}$ and H_2O_2 (Kops *et al.*, 2002; Nemoto and Finkel, 2002). Upregulation of FoxO also induces cell cycle arrest through the regulation of $p27^{kip1}$ and its associated cyclin dependant kinases (Kops *et al.*, 2002; van der Horst and Burgering, 2007). H_2O_2 can induce FoxO transcriptional activity and this is further confirmed by the observation that H_2O_2 treatment results in translocation of FoxOs from the cytosol to the nucleus. In addition, cell death ligands like Fas and TNFα, known to increase cellular H_2O_2 levels, also activate FoxO transcriptional activity. FoxOs induce apoptosis mainly by upregulation of pro-apoptotic genes such as those of the Bcl-2 family (Dijkers *et al.*, 2000; van der Horst and Burgering, 2007), yet they can also detoxify harmful cellular oxidants and protect cells. FoxOs can

also function in a negative feedback loop to control the cellular level of ROS and oxidative stress (Wang *et al.*, 2007).

1.2.6.5 Adapter protein p66^{shc}

The adapter protein p66^{shc} is a relatively newly-recognised mediator of mitochondrial dysfunction, first described in 1999 (Migliaccio *et al.*, 1999). Knock-out mouse models of the *p66^{shc}* gene have shown an increase in lifespan of 30 %, indicating an important role for this protein in ageing (Menini *et al.*, 2006). An isoform of the ShcA protein, p66^{shc} antagonises the actions of two other isoforms, p46^{shc} and p52^{shc}, on cell proliferation. Cellular oxidative stress induces the phosphorylation of serine 36 of p66^{shc} by protein kinase C beta (PKCβ) prior to translocation of p66^{shc} into the mitochondria. Here, it translates oxidative stress into Ca^{2+}-mediated mitochondrial damage and subsequent apoptosis (Pinton *et al.*, 2007; Arany *et al.*, 2010). As well as the general cytoplasmic location of p66^{shc}, a large proportion also exists in the mitochondria bound to heat shock protein 70. This has been shown to dissociate during stressful conditions, thereby increasing mitochondrial ROS generation and resulting in apoptosis (Orsini *et al.*, 2004). H_2O_2-induced cell injury is dependent upon a loss of mitochondrial membrane potential which can occur due to increased ROS. Ablation of the *p66^{shc}* gene decreased H_2O_2, oxidative damage and mitochondrial-mediated apoptosis (Pinton *et al.*, 2007). Activated (phosphorylated) p66^{shc} may increase mitochondrial ROS by the oxidation of Cyt C, also causing its release into the cytoplasm and induction of apoptosis (Giorgio *et al.*, 2005). Activation or opening of the PTP by ROS also induces mitochondrial dysfunction leading to apoptosis (Mather and Rottenberg, 2000). This suggests that ROS production by mitochondria is the cause and not a consequence of loss of membrane permeability transition; however, the causes and consequences of mitochondrial ROS remain elusive. Recently, histone acetylation and methylation of the p66^{shc} promoter was shown to induce both premature and replicative senescence, indicating a role of altered p66shc expression and subsequent cellular dysfunction (Zhang *et al.*, 2010). Although the role of p66^{shc} has been noted in glomerulopathies and diabetes (Menini *et al.*, 2006; Menini *et al.*, 2007) and its differential expression has been demonstrated in ageing kidneys (Percy *et al.*, 2009), the functional significance of p66^{shc} in age-related CKD has not received detailed attention.

1.2.7 Concomitant pathologies: effects on the kidneys and relationship with oxidative stress

In CKD, functional impairment correlates with tubulointerstitial fibrosis that can be characterised by inflammation, accumulation of extracellular matrix, tubular atrophy and loss of peritubular capillaries. The causes of these global CKD characteristics are, as mentioned previously,

multifactorial. In this section, the relationship between CKD and concomitant illnesses, like CVD and the interrelated epidemic of obesity in our societies, and diabetes, are briefly discussed.

An overwhelmingly large proportion of populations in Western societies is overweight or obese, and this proportion is increasing (Flegal *et al.*, 2002). Obesity is seen as a chronic disease state due to its epidemiological significance of co-morbidity and mortality, and is the most common risk factor for diabetes and CVD, both of which predispose individuals to CKD especially in ageing (Kalaitzidis and Siamopoulos, 2011). Obesity raises blood pressure by increasing renal tubular sodium reabsorption, impairing pressure natriuresis, and causing volume expansion via activation of the sympathetic nervous system and renin-angiotensin-aldosterone system and by physical compression of the kidneys, especially when there is increased visceral adiposity (Hall *et al.*, 2014). Obesity is also likely to have a direct mechanistic effect on metabolism or endocrine function, and through these, on the kidneys. Factors such as inflammation, oxidative stress, and lipotoxicity are known to contribute to obesity-mediated CKD and CVD.

Obese individuals are more likely to develop CKD and commonly show increased markers of oxidative stress, supporting redox dysregulation as a mechanism in CKD (Fox *et al.*, 2004; Noeman *et al.*, 2011). Recently, there has been interest in the novel biomarkers adiponectin and leptin in the CKD population (Kaisar *et al.*, 2008). Adipose tissue is now recognised not just as a storage system for triglycerides but as a highly active metabolic organ involved in the secretion of various adipokines. Adiponectin is a cytokine and the most common adipocyte-derived protein. This protein acts through stimulation of AMPK, inducing glucose transport (Zoccali and Mallamaci, 2011). The direct mechanistic action of adiponectin on the kidneys is yet to be defined, but serum adiponectin levels are inversely related to markers of inflammation such as C-reactive protein, TNF-α, and interleukin-6 (IL-6), in healthy individuals and those with Type-2 diabetes and CVD.

Efficient vascular and renal function relies on a healthy cellular redox balance. $NO^{\bullet}$ regulates vascular tone yet is also highly susceptible to oxidant insult. In a redox balanced state, NO synthase (NOS) converts L-arginine into $NO^{\bullet}$. However, increases in $O_2^{\bullet-}$ due to systemic oxidative stress can cause a reduction of NOS and, upon reaction with $NO^{\bullet}$, the formation of the highly reactive peroxynitrite. A systemic inflammatory response commonly observed in CKD and hypertensive patients can result in elevated leukocyte count. Leukocyte and vascular smooth muscle cells are sources of ROS which can contribute to the contraction and growth of vascular smooth muscle cells, thereby increasing systemic blood pressure (Gonzalez-Pacheco *et al.*, 2002). The role of the renin-angiotensin-aldosterone system (RAAS) is also highly relevant to CKD since angiotensin II

induces apoptosis in renal PTE cells via a process involving ROS and pro-fibrotic transforming growth factor-β (TGF-β) (Bhaskaran *et al.*, 2003).

Diabetes can cause harmful effects by mechanisms that include increasing oxidative stress, producing advanced glycation end products (AGE) and activation of PKC (Brownlee, 2001). It can cause the activation of pro-inflammatory growth factors and cytokines, such as IL-1, TNF-α, TGF-β and PDGF (Vlassara *et al.*, 1988; Doi *et al.*, 1992). Plasma oxidative stress levels are further elevated in CKD patients with diabetes and hypercholesterolemia, providing a causative or progressive role for systemic oxidative stress (Oberg *et al.*, 2004). The overproduction of ROS by the mitochondrial ETC due to increased hyperglycaemic-dependant availability of electron donors by the citric acid cycle, such as NADH and $FADH_2$, is thought to be responsible for initiating this increase in oxidative stress (Du *et al.*, 2000; Munusamy and MacMillan-Crow, 2009). Furthermore, overexpression of MnSOD attenuates the overproduction of mitochondrial $O_2^{\bullet-}$ (Du *et al.*, 2001). AGE has a major pathogenic role in diabetic nephropathy as shown by the successful use of advanced glycation inhibitors in diabetic rat and human studies (Wilkinson-Berka *et al.*, 2002; Bolton *et al.*, 2004). Damage induced by AGE occurs through mechanisms which include altering protein function (Zoellner *et al.*, 2009), modification of extracellular matrix proteins (Wang *et al.*, 2011), and the activation of AGE-receptors associated with macrophages, endothelial and mesangial cells (Yan *et al.*, 1994). Ligation of this receptor produces a ROS burst and activation of the transcription factor NF-κB, mesangial matrix expansion and glomerulosclerosis (Yan *et al.*, 1994; Reiniger *et al.*, 2010; Tang *et al.*, 2011).

1.2.8 Measuring oxidative stress

Oxidative damage may be defined as bimolecular damage caused by the direct attack of reactive species during oxidative stress (Halliwell and Whiteman, 2004). Reactive species can be measured directly, for example, by electron spin resonance (ESR) or various trapping methods, or indirectly by examining end products of their reaction with biomolecules. Assays for oxidative stress or antioxidant status, and some biomarkers, are shown in Appendix A. Oxidative stress biomarkers are progressively increased with increasing stages of CKD (Dounousi *et al.*, 2006) and decreased following renal transplantation, compared to ESKD patients (Simmons *et al.*, 2005). The positive correlation between oxidative stress levels and CKD progression is difficult to interpret given the various oxidative stress outcomes as well the influence of any overlying disorders such as diabetes and CVD. Several of the oxidative stress biomarkers that have likely pathological significance in CKD are discussed below.

1.2.8.1 The isoprostanes

Most oxidative stress biomarkers detect levels of specific end-products from free radical damage. The isoprostanes are considered the best available biomarkers of lipid peroxidation and have been investigated extensively in the study of CKD (Kim *et al.*, 2004; Simmons *et al.*, 2005; Dounousi *et al.*, 2006; Karamouzis *et al.*, 2008). Studies have focused primarily on F_2-isoprostanes, specifically 8-isoprostanes (8-*epi*-prostaglandin F2-alpha/8-*epi*-PGF2a) which are formed by non-enzymatic peroxidation of arachidonyl lipids only after exogenous antioxidants have been exhausted. F_2-isoprostanes are best detected using mass spectroscopy, and techniques have been established to detect levels in urine and plasma in humans (Calabrese *et al.*, 2007). However, F_2-isoprostanes have been criticised since they are rapidly metabolised, thereby falsely elevating the plasma isoprostane levels. Morrow and colleagues (1998) demonstrated that O_2 concentrations may also influence F_2-isoprostane levels. F_2-isoprostane levels may have low repeatability because of discrepancies in levels detected from the same person at different times of the same day (Kanabrocki *et al.*, 2002), and from day to day (Helmersson and Basu, 2001). Importantly, F_2-isoprostanes, like all end-product biomarkers, are a measure of whole body oxidative stress rather than that which occurs at a specific location, such as the kidney. Nevertheless, the use of isoprostanes has identified that levels of oxidative stress rise early in the progression of CKD (Oberg *et al.*, 2004) and relate to kidney function (Dounousi *et al.*, 2006).

1.2.8.2 Malondialdehyde

Malondialdehyde (MDA) is another end-product generated by lipid peroxidation and has been used to demonstrate increased oxidative stress during CKD (Atamer *et al.*, 2008; Terrier-Lenglet *et al.*, 2011). Unlike F_2-isoprostanes, MDA has the ability to react further and possibly cause protein and DNA adducts, thus levels of MDA should be interpreted with caution. MDA, along with other lipid peroxidation products such as 4-hydroxyalkenals, is a thiobarbituric acid reactive substance (TBARS) and earlier investigations into oxidative stress commonly used this as an assay technique (Stratta *et al.*, 1994). Most TBARS in human body fluids are unrelated to lipid peroxidation, due to their non-specific and artifactual formation (Knight *et al.*, 1988; Liu *et al.*, 1997; Halliwell and Whiteman, 2004), and simple TBARS assays from early studies should be discounted as a reliable measure of oxidative stress because of this artifactual elevation. High performance liquid chromatography (HPLC) extraction of MDA from plasma, with subsequent quantification, is now considered a reliable method for oxidative stress determination (Marsh *et al.*, 2006; Johnson *et al.*, 2007). Improved methods derivatise MDA with 2,4-dinitrophenylhydrazine, which forms specific hydrazones for MDA that can be separated by HPLC and quantified using methyl-MDA as an internal standard (Sim *et al.*, 2003). The use of *N*-methyl-2-phenylindole to determine MDA content

alone, or with 4-hydroxyalkenals, is an alternate and simple method for quantifying lipid peroxidation (Gerard-Monnier *et al.*, 1998). Urinary MDA evaluation in patients with impaired kidney function can be difficult to interpret. Renal clearance of MDA possibly provides an adaptive mechanism to prevent lipid peroxidation accumulating within kidney tubular cells, yet renal clearance of MDA would be impaired in these patients (Nath *et al.*, 1990).

1.2.8.3 Advanced oxidation protein products

Advanced oxidation protein products (AOPP) accumulate in the serum of CKD patients, especially those with uraemia and diabetes (Witko-Sarsat *et al.*, 1996; Mezzano *et al.*, 2001). This accumulation contributes to the pathogenesis of CKD (Li *et al.*, 2007). AOPP are primarily derived from serum albumin following hypochlorous acid (HOCl) free radical attack (Witko-Sarsat *et al.*, 1996; Capeillere-Blandin *et al.*, 2004; Piwowar, 2010). *In vivo* studies have demonstrated enhanced inflammation and reduced kidney function with high serum levels of AOPP (Witko-Sarsat *et al.*, 1998; Li *et al.*, 2007). AOPP as a marker of oxidative stress has yet to show a strong correlation with other more reliable markers of oxidative stress, such as F_2-isoprostanes, but it does provide a valuable indicator of oxidation-mediated protein damage. The prevalence of albuminuria/proteinuria in CKD and its impact on AOPP has not yet been investigated.

1.2.8.4 Protein carbonyls

Protein carbonyl assays quantify the carbonyl groups associated with oxidant-damaged proteins. It is important to note that protein carbonyls are not specific for oxidative stress since they also measure glycated proteins and bound aldehydes (Halliwell and Whiteman, 2004). An increase in protein carbonyls has been demonstrated in CKD patients in stages 3-5, yet no correlation was found between protein carbonyl levels and GFR (Oberg *et al.*, 2004). In addition, diabetic nephropathy patients have greater levels of protein carbonyls in plasma and lymphocytes compared to healthy control (Calabrese *et al.*, 2007).

1.2.8.5 Electron spin resonance and spin traps

Because free radicals have extremely short half-lives (Cadenas and Davies, 2000), ESR or electron paramagnetic resonance (EPR) provides a means to properly determine the contribution of free radical generation in the kidneys, and subsequent systemic oxidative stress. This method consists of using a spin trap (nitrone) to react with the initial free radical, which forms a less reactive free radical adduct (nitroxide) that can be observed and quantified using EPR spectroscopy (Swartz *et al.*, 2007). Different spin traps are used to trap specific free radicals. Commonly used spin traps include α-phenyl-N-tert-butylnitrone and 5,5-dimethyl-pyrroline N-oxide. These have been shown

to detect hydroxyl and carbon-centred radicals in the kidney after ischemia-reperfusion injury (Kadkhodaee *et al.*, 1996). More recently, 5-diisopropoxyphosphoryl-5-methyl-1-pyrroline-N-oxide was used to trap $O_2^{\bullet-}$ adducts formed in isolated mitochondria from the skeletal muscle of mice (Bhattacharya *et al.*, 2011). Spin trapping and EPR present some practical limitations, especially in humans, where they must demonstrate a safe and efficacious effect, and are costly, thereby limiting their clinical use.

1.2.8.6 γ-Glutamyl-transpeptidase

Recently, γ-glutamyl transpeptidase (GGT) was suggested as a biomarker of CKD onset through a mechanism of oxidative stress (Lee *et al.*, 2004). Extracellular GGT is required to metabolize extracellular-reduced glutathione, allowing for the intracellular synthesis of glutathione by addition of specific amino acids (Lash, 2009). Serum antioxidant levels were found to have an inverse relationship to serum GGT, indicating a redox-regulating role (Lim *et al.*, 2004). The relationship between plasma and extracellular GGT is not fully defined, but it does appear that serum GGT presents a favourable biomarker of oxidative stress. It is stable, quick and inexpensive to test, and provides an indication of whole body oxidative stress compared to specific oxidative damage to lipids, DNA or proteins.

1.2.9 Visualising metabolic changes in the kidney

With the advancement of technologies over the past decade, visualising metabolic changes in real time in the kidney has become possible. Given that metabolism, especially mitochondrial metabolism, is intimately related to ROS production, dynamic visual changes can be representative of altered cellular redox control. Intravital multiphoton microscopy (MPM) is such a technology that allows direct visualisation of metabolic changes and associated structural and functional changes, in real time, in many biological tissues including the kidney. The principles of MPM and its use in experimental nephrology have been published as part of this thesis (Small *et al.*, 2014) and will form part of the introduction to the relevant research chapter (Chapter 5). This segment gives a brief overview of MPM, specifically for kidney disease research.

The primary source of endogenous fluorescence in the majority of biological tissue is NAD(P)H/NAD+ (Zipfel *et al.*, 2003), which only fluoresces in its reduced form (NADH). NADH is a vital substrate for Complex I of the mitochondrial ETC required for oxidative phosphorylation, and its fluorescence has been used for a long time as an indicator of cellular metabolic state (Chance *et al.*, 1962; Mironov and Richter, 2001). Therefore alterations to this endogenous

fluorescence, and indirectly, NADH, indicate intracellular metabolic changes. The combination of NADH and NADPH will be referred to as NAD(P)H, since NADPH is detected by MPM on the same wavelength and therefore cannot be excluded. However, NADPH is considered to contribute minimally. Elegant experiments by Balaban and Mandel (1988) using isolated rabbit proximal tubule demonstrated that the metabolic rate and NAD(P)H redox state of epithelial cells is highly sensitive to the metabolic substrate available. In particular, NAD(P)H fluorescence and oxygen consumption increase in a linear fashion with the addition of a variety of metabolic substrates. Furthermore, anoxia results in the maximal increase in NAD(P)H fluorescence due to lack of reducing equivalents for NAD(P)H, and "backing up" of the electron transport chain causing an increase in the NAD(P)H/NAD+ ratio.

The principles of MPM allow greater compliancy for use in biological tissue, allowing intravital imaging over extended periods of time with minimal photodamage. A robust method to detect changes in NAD(P)H metabolism is to use fluorescence lifetime imaging microscopy (FLIM) in combination with MPM. The fluorescence lifetime of a fluorophore is the mean time a fluorophore remains in an excited state before emitting a photon (fluorescence) and returning to the initial ground state. The fluorescence lifetime of a fluorophore, either endogenous or synthetic, depends on the type of molecule, its conformation, and the way the molecule interacts with the surrounding microenvironment (Becker, 2012). FLIM constructs a spatial distribution map of fluorescence lifetimes of a sample imaged by confocal, multiphoton, endoscopic or wide-field microscopy (Elson *et al.*, 2004). Importantly, FLIM microscopy can be used to measure molecular environmental parameters, the metabolic state of cells and tissues via endogenous autofluorescence, drug distribution and interactions, and protein-interactions by fluorescence resonance energy transfer (FRET).

Intravital MPM can provide detailed information regarding kidney tissue oxygenation and mitochondrial redox state that often precede pathophysiological change. This information, coupled with classical oxidative stress assessments, and histopathological techniques, enables the determination of the spatial and temporal relationship of oxidative stress in the kidney.

1.2.10 Combating CKD by targeting oxidative stress

A major goal of therapy in patients with CKD is to slow, or halt, the progression to ESKD. Early detection of CKD is essential. Low-grade damage of the kidney, resulting in partial loss of functioning nephrons and/or glomeruli, activates an adaptive injury response within the remaining healthy kidney to compensate for this loss. Angiotensin II has been shown *in vivo* and *in vitro* to

induce pro-inflammatory and fibrogenic pathways (Sun *et al.*, 2000). Therefore, inhibiting the RAAS should be an effective way to slow the progression of CKD to ESKD and also slow the development of associated CVD (Masajtis-Zagajewska and Nowicki, 2009; Hoogwerf, 2010). Established CKD therapies, therefore, rely primarily on the pharmacologic blockage of the RAAS with angiotensin-converting enzyme inhibitors (ACEi) and angiotensin II receptor blockers. Despite the positive impacts of RAAS inhibition, decline of GFR continues and serum creatinine continues to be elevated (Brenner *et al.*, 2001; Lewis *et al.*, 2001). There is a great need for novel treatments and interventions. Increasing experimental evidence points to inflammation and oxidative stress as potentially rewarding targets.

Although the use of anti-oxidant therapies in the prophylactic treatment and amelioration of CKD has had limited success clinically, oxidant dysregulation occurs with age and it is therefore conceivable that a supply of antioxidants will restore the balance and the essential role of oxidants as signalling molecules. Some modifiable pathways and antioxidant treatments are summarised in Fig. 1.5, and selected antioxidants are described here.

1.2.10.1 N-acetyl cysteine

N-acetyl cysteine (NAC) acts as an essential precursor to many endogenous antioxidants involved in the decomposition of peroxides (Zafarullah *et al.*, 2003). NAC attenuates oxidative stress from various underlying causes, by replenishing intracellular glutathione stores. Glutathione is synthesized in the body by three amino acids by the catalysing intracellular enzymes gamma-glutamylcysteine synthetase and glutathione synthetase. L-glutamic acid and glycine are two precursors of glutathione that are biologically and readily available.

However, the limiting precursor to glutathione biosynthesis and the third amino acid, L-cysteine, is not readily available in a human diet. Although the primary basis for NAC supplementation is to replenish cellular cysteine levels to maintain intracellular glutathione and thus redox control, the sulfhydryl-thiol group of L-cysteine is also able to exert direct antioxidant effects by scavenging free radicals, and NAC may also exert its protective effects against 2,3,5-tris(glutathion-S-yl)-hydroquinone toxicity. This was demonstrated in isolated renal tubular epithelial cells, in part by the activation of extracellular signal regulated protein kinase (ERK) 1/2 (Zhang *et al.*, 2011). The cysteine residue of NAC also has a theoretical ability to change the intracellular redox environment by affecting intracellular signalling, promoting a reduced intracellular environment rather than an oxidised one (Diers *et al.*, 2013).

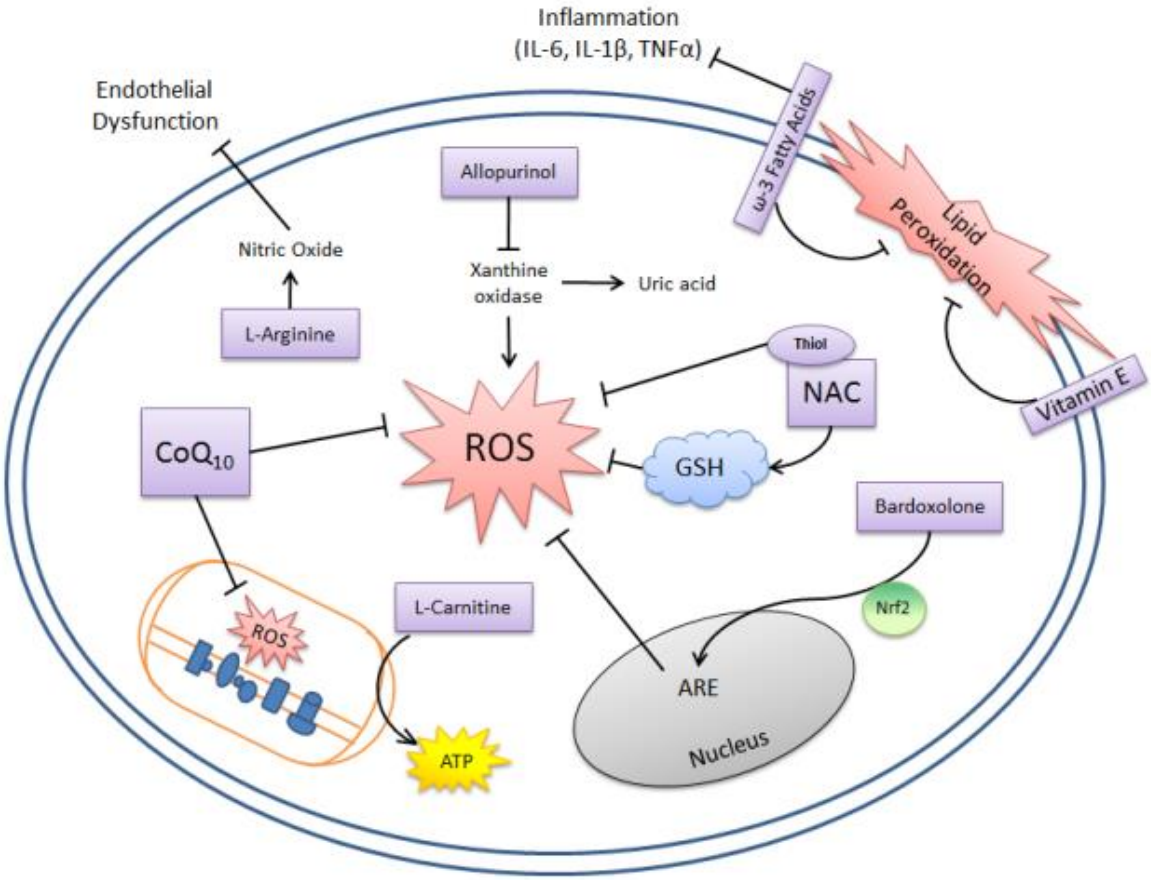

Figure 1.5: Cellular sites of reducing oxidative stress by oxidant modifying compounds
Inflammation, lipid peroxidation, and reactive oxygen species (ROS) from mitochondrial and cytoplasmic sources produce a harmful state of oxidative stress. Vitamin E incorporates into the phospholipid bilayer halting lipid peroxidation chain reactions. ω-3 fatty acids displace arachidonic acid in cell membrane and thus reduce arachidonic-derived ROS, but also significantly reduce inflammation and subsequent fibrosis. The cysteine residue of N-acetyl-cysteine (NAC) is a precursor for glutathione (GSH) synthesis, and the thiol group is able to scavenge ROS. Allopurinol inhibits xanthine oxidase derived ROS and the damaging effects of uraemia. Coenzyme Q_{10} (CoQ_{10}) enhances the efficiency of electron transport in the mitochondria thereby reducing mitochondrial derived ROS and is also able to directly scavenge ROS. Mitochondrial-targeted antioxidants accumulate in the mitochondria, reducing mitochondrial derived ROS.

The results of NAC supplementation in kidney disease have been variable and largely depend on the type and cause of kidney injury and also the timing of treatment. In cultured human PTE cells, NAC reduced lipid peroxidation and maintained the mitochondrial membrane potential, thereby preventing apoptosis following H_2O_2 administration (Ye *et al.*, 2010). Endothelial dysfunction caused by uremic toxins, such as indoxyl sulphate, induced ROS-dependent expression of the pro-inflammatory and pro-oxidant NF-κB, which was ameliorated by NAC pre-treatment (Tumur *et al.*, 2010).

Although NAC had no significant effect on markers of oxidative stress and inflammation in rats following unilateral ureteral obstruction (Pat *et al.*, 2005), it reduced kidney MDA levels in a diabetic mouse model (Ribeiro *et al.*, 2011). The treatment of CKD patients with NAC with the aim of improving renal function and preventing ESKD has been largely disappointing, with no evidence of reduction in proteinuria (Renke *et al.*, 2008; Moist *et al.*, 2010). NAC seems to exert the greatest antioxidant and anti-inflammatory properties when used against the greatest injury, such as in ESKD patients receiving either haemodialysis or peritoneal dialysis. In those cases, NAC reduced serum 8-isoprostane and the inflammatory cytokine IL-6 (Hsu *et al.*, 2010; Nascimento *et al.*, 2010). In a randomised, double-blind, placebo controlled study where 10 non-diabetic ESKD patients on maintenance haemodialysis received 1200 mg NAC daily for 7 days, fibroblast growth factor (FGF)-19 increased, which is associated with normalisation of insulin and C-peptide signalling (Li *et al.*, 2013).

1.2.10.2 Vitamin E

Vitamin E, or α-tocopherol (αTOC), is a lipid-soluble antioxidant that incorporates into the plasma membrane of cells, thereby scavenging free radicals, mainly the peroxyl radical, and thus halting lipid peroxidation chain reactions (Serbinova *et al.*, 1991). A benefit of αTOC is its ability to restore its antioxidant capacity from its oxidized form following free radical scavenging, and incorporate back into the plasma membrane. Vitamin C (ascorbic acid) is able to directly reduce αTOC (Kagan *et al.*, 1990; Kagan *et al.*, 1992; Fujisawa *et al.*, 2006), and intracellular glutathione and lipoic acid can restore αTOC indirectly by restoring vitamin C (Guo and Packer, 2000). This is a prime example of a cellular antioxidant network prone to dysregulation. Administration of αTOC to kidney PTE cells decreased cisplatin-induced ROS and increased cell viability (Schaaf *et al.*, 2002). The beneficial effects of αTOC are not limited to its antioxidant properties and, recently, attention has focused on the ability of vitamin E to promote oxygenation of the blood, and also to affect endogenous cell signalling functions that promote cell protection (Sen *et al.*, 2000).

Vitamin E foodstuffs primarily consist of α-tocotreinol, an isoform of αTOC which has higher antioxidant efficacy in biological membranes. Despite this, the uptake and distribution of α-tocotreinol is far less than αTOC. Therefore, the basis of vitamin E supplementation is to enhance αTOC levels in cell plasma membranes to prevent lipid peroxidation and resultant oxidative stress. One drawback of αTOC is that it takes several days of pre-treatment to exhibit antioxidant effects (Machlin and Gabriel, 1982). Trolox (±-6-hydroxy-2,5,7,8-tetramethylchromane-2-carboxylic acid), is an analogue of αTOC that has shown far better free radical scavenging properties owing to its water-solubility (Lucio *et al.*, 2009). Therefore, the majority of *in vivo* studies using trolox have found beneficial effects in acute cases of renal injury, such as ischemia-reperfusion, due to rapid solubility and increased potency (Eum and Lee, 2004; Wongmekiat *et al.*, 2007). A combination supplement containing both αTOC and trolox may offer greater efficacy due to the fast-acting activities of trolox combined with the sustained scavenging actions of αTOC. However, studies investigating the antioxidant effects of trolox in humans remain sparse due to its highly reactive nature.

Patients with CKD stage 4 display the largest decrease in serum αTOC levels, following a progressive decline from stage 1, indicating an increased need for αTOC in the CKD population (Karamouzis *et al.*, 2008). Interestingly, within the same cohort of patients, a positive correlation of endogenous serum αTOC levels and GFR was found (Karamouzis *et al.*, 2008). The majority of studies evaluating αTOC supplementation has largely focused on the ESKD dialysis populations compared to healthy controls. They report a reduced risk of CVD, decreased oxidative stress and increase in erythrocyte antioxidants SOD, GPX and CAT (Boaz *et al.*, 2000; Islam *et al.*, 2000; Giray *et al.*, 2003).

The use of αTOC in CKD patients is not without controversy. Recently, a placebo-controlled, double blind clinical trial in haemodialysis patients over 12-months receiving mixed tocopherols (666 IU/d) plus α-lipoic acid (600 mg/d) did not significantly alter markers of oxidative stress, inflammation, nor alter mortality and hospitalization rates (Himmelfarb *et al.*, 2014). Miller and colleagues (2005) concluded that high-dose (≥400 IU/day) vitamin E supplementation may increase all-cause mortality which may be due to αTOC displacing gamma-(γ)-tocopherol and delta-(δ)-tocopherol in the body (Huang and Appel, 2003). However, this study was highly criticized owing to bias in data analysis and numerous methodological flaws (Baggott, 2005; Blatt and Pryor, 2005; Carter, 2005; DeZee *et al.*, 2005; Hemila, 2005; Krishnan *et al.*, 2005; Lim *et al.*, 2005; Marras *et al.*, 2005; Meydani *et al.*, 2005; Possolo, 2005).

1.2.10.3 Omega-3 poly-unsaturated fatty-acids

Inflammation and fibrosis are causes, as well as consequences, of oxidative stress (Dendooven *et al.*, 2011; Irita *et al.*, 2011). Direct targeting of inflammatory and fibrotic pathways with more specific modifying compounds presents a way to indirectly decrease oxidative stress in CKD. Long chain omega(ω)-3 polyunsaturated fatty-acids, including docosahexanoic acid (DHA) and eicosapentanoic acid (EPA), have been investigated in a large range of *in vitro* and *in vivo* kidney models and found to possess anti-inflammatory properties. Recently, ω-3 fatty acid treatment of peripheral blood mononuclear cells from pre-dialysis CKD patients reduced the inflammatory markers, IL-6, IL-1β, TNF-α and C-reactive protein to levels observed in healthy subjects (Shing *et al.*, 2011). Although the beneficial effects of EPA/DHA are attributed to their anti-inflammatory properties, they are also known to enhance endogenous antioxidant defence systems, such as γ-glutamyl-cysteinyl ligase and glutathione reductase (Arab *et al.*, 2006). DHA and EPA incorporate into the phospholipid bilayer of cells where they displace arachidonic acid. Arachidonic acid can generate ROS through the cycloxygenase-2 and xanthine oxidase inflammatory pathways. DHA/EPA administration to renal epithelial cells and macrophages suppresses this pro-oxidant pathway (Kim and Chung, 2007). Furthermore, chemoattractants derived from EPA are less potent that those derived from arachidonic acid (Sperling *et al.*, 1993; Mayer *et al.*, 2003). Recently, *in vitro* studies determined that EPA and DHA attenuated TNF-α-stimulated MCP-1 gene expression by interacting with ERK and NF-κB in rat mesangial cells (Diaz Encarnacion *et al.*, 2011). Earlier evidence had shown that EPA and DHA inhibit NF-κB expression by stimulating PPARs in human kidney-2 (HK-2) cells *in vitro* (Li *et al.*, 2005). *In vivo* studies have now confirmed an improvement in kidney function and structure using EPA and DHA supplementation. There was a reduction in oxidative stress, inflammation and tubulointerstitial fibrosis through the reversal of inflammatory and oxidant pathways (An *et al.*, 2009; Peake *et al.*, 2011). Fish oil ω-3 polyunsaturated fatty acids may also provide a means to directly decrease kidney disease through improving kidney structure, as well as indirectly by decreasing inflammation and oxidative stress. Clinical studies have found fish oil treatment modulates lipid levels (Harris, 1997; Bouzidi *et al.*, 2010), and has antithrombotic (Woodman *et al.*, 2002; Cohen *et al.*, 2011) and antihypertensive effects due to vascular and endothelial actions (Matsumoto *et al.*, 2009).

1.2.10.4 Allopurinol

Uric acid is the hepatic end-product of purine metabolism in humans, synthesised by the enzyme xanthine oxidase which catalyses the oxidation of hypoxanthine to xanthine and finally to uric acid. Uric acid is a nitrogenous waste product which may also possess antioxidant activity (Miller and RiceEvans, 1996). However, uric acid at toxic levels has been implicated in the progression of

CKD. Increased serum uric acid levels (hyperuricaemia) may arise from increased purine metabolism, increasing age and decreased renal excretion, and have harmful systemic effects. Hyperuricaemia is associated with an increased risk for developing CKD and enhances its progression. A 20.6 % prevalence of hyperuricaemia was found in a cross-sectional study of 18,020 CKD patients (Shan *et al.*, 2010), and a positive correlation was found between serum uric acid and serum creatinine with impaired renal function (Chen *et al.*, 2009). Retention of uremic toxins promotes inflammation, and oxidative stress, by priming polymorphonuclear lymphocytes, activating IL-1β and IL-8 (Martinon *et al.*, 2006) and stimulating the innate immune response through CD8+ cells (Sakamaki *et al.*, 2008). Additionally, uric acid synthesis can promote oxidative stress directly through the activities of xanthine oxidase, which produce $NO^{\bullet}$, and ROS such as NADPH (Sanchez-Lozada *et al.*, 2008). Allopurinol treatment aims is to inhibit xanthine oxidase to decrease serum uric acid and its associated toxic effects.

Allopurinol and its metabolite, oxypurinol, act as competitive substrates for xanthine oxidase. They enhance urinary urate excretion and block uric acid reabsorption by urate transporters in the proximal tubule, thereby facilitating enhanced uric acid excretion (Sanders *et al.*, 1997; El-Sheikh *et al.*, 2008; Riegersperger *et al.*, 2011). Allopurinol treatment of diabetic mice attenuated hyperuricaemia, albuminuria, and tubulointerstitial injury (Kosugi *et al.*, 2009). Allopurinol may also have antioxidant activities in addition to its enzyme inhibitory activities, by scavenging $OH^{\bullet}$ as well as chlorine dioxide and HOCl (Das *et al.*, 1987; Moorhouse *et al.*, 1987). Although later *in vivo* studies revealed that rat serum, obtained after oral administration of allopurinol, did not contain allopurinol levels sufficient to scavenge free radicals (Klein *et al.*, 1996), inhibition of xanthine oxidase-dependent production of $NO^{\bullet}$ and ROS provides allopurinol an indirect mechanism for decreasing oxidative stress in hyperuricaemic CKD patients. Interventional studies of use of allopurinol in renal disease have shown improved uric acid levels, GFR, cardiovascular outcomes and delayed renal disease progression. A prospective randomised trial of 113 patients with GFR <60 ml/min/1.73m^3 given allopurinol 100 mg/d for 2 years found an increase in GFR of 1.31 ml/min/1.73m^3 compared to the controls which decreased, and a 71 % decreased risk of CVD (Goicoechea *et al.*, 2010). Kanbay and colleagues (2007) found that allopurinol at 300 mg/d over 3 months improved GFR, uric acid and C-reactive protein levels but had no change on proteinuria. Allopurinol given to ESKD patients on haemodialysis reduced the risk of CVD by decreasing serum low density lipoproteins, triglycerides and uric acid (Shelmadine *et al.*, 2009). Large, long-term interventional studies investigating kidney function in the CKD population are needed to fully determine if allopurinol is nephroprotective via anti-oxidant mechanisms.

1.2.10.5 Coenzyme Q_{10}

The kidneys contain the highest endogenous levels of CoQ_9 and CoQ_{10} compared to all other organs (Lass *et al.*, 1999; Lass and Sohal, 2000). This is likely due to the reliance of the kidney on aerobic metabolism, and the high density of mitochondria in the epithelial cells of the nephron. Endogenous CoQ_{10} levels must be maintained to ensure mitochondrial health, and this forms the rationale for CoQ_{10} therapy. CoQ_{10} is a fundamental lipid-soluble component of all cell membranes including those enclosing subcellular compartments. The physiological roles of CoQ_{10} act mostly within the mitochondria where it has three well-characterised functions: (1) the transfer of electrons from Complexes I and II to Complex III along the ETC of the inner mitochondrial membrane and subsequent membrane polarisation and ATP generation (Merker *et al.*, 2007; Ohnishi *et al.*, 2008); (2) the pro-oxidant generation of $O_2^{\bullet-}$ and H_2O_2 (James *et al.*, 2004; Linnane *et al.*, 2007a); and (3) the anti-oxidant quenching of free radicals (Nohl *et al.*, 1999). The continual oxidation-reduction cycle, and existence of CoQ_{10} in three different redox states, explains its actions as an important cellular redox modulator through its pro-oxidant and antioxidant actions. The fully oxidised form of CoQ_{10}, or ubiquinone, is able to accept electrons, primarily from NADH, to become fully reduced (ubiquinol - CoQ_{10}-H_2). The reduced form of CoQ_{10} is able to give up electrons, thereby scavenging free radicals. The intermediate of ubiquinone and ubiquinol is the univalently-reduced ubisemiquinone (CoQ_{10}-H^+) which acts as a pro-oxidant to form $O_2^{\bullet-}$ and, subsequently, H_2O_2.

The major antioxidant role of CoQ_{10} is in preventing lipid peroxidation directly, and by interactions with αTOC (Frei *et al.*, 1990). Ubiquinol is able to donate a hydrogen atom and thus quench peroxyl radicals, preventing lipid peroxidation chain reactions. CoQ_{10} and αTOC co-operate as antioxidants through the actions of CoQ_{10}-H_2 restoring α-tocopheroxyl back to αTOC (Kagan *et al.*, 1990; Stoyanovsky *et al.*, 1995). However, the reactivity of αTOCs with peroxyl radicals far exceeds that of ubiquinols with peroxyl radicals, suggesting that, *in vivo*, ubiquinols do not act as antioxidants but regenerate the antioxidant properties of αTOCs (Lass and Sohal, 1998). This is in accordance with *in vivo* studies investigating the effects of CoQ_{10} supplementation which have primarily found a limited antioxidant capacity. The role of CoQ_{10} as a pro-oxidant in all biological membranes including the Golgi, endosome/lysosome systems, as well as mitochondria has led to much criticism regarding the claimed antioxidant power of CoQ_{10} supplementation in humans (Linnane *et al.*, 2007a). Nonetheless, many *in vitro* studies demonstrate antioxidant properties of CoQ_{10} in single cells. The benefits of CoQ_{10} supplementation in humans is attributed to its ability to maintain efficient mitochondrial energy metabolism and thus prevent mitochondrial dysfunction, rather than act as a direct cellular antioxidant. CoQ_{10} supplementation *in vivo* reduced protein oxidation in skeletal muscle of rats but had no effect on mitochondrial H_2O_2 production in the

kidney (Kwong *et al.*, 2002). However, Ishikawa and colleagues (2011) demonstrated a decrease in kidney $O_2^{\bullet-}$ levels in hemi-nephrectomised rats on a CoQ_{10} supplemented diet, and increased renal function, compared to rats on a control diet. There is a general lack of human studies investigating CoQ_{10} therapy for the treatment and/or prevention of CKD. CoQ_{10} levels decrease with age, but there are no studies measuring endogenous CoQ_{10} levels in CKD patients and this could prove vital in the identification of any population where CoQ_{10} therapy may have beneficial outcomes.

1.2.10.6 Mitochondrial-targeted antioxidants

Mitochondrial-targeted compounds have created much interest for their application in reducing oxidative stress, due to the well-defined role of the mitochondria as the major cellular source of ROS. One of the most tested is the mitochondrial-targeted derivative of endogenous CoQ_{10}, termed MitoQ (mitoquinone mesylate). The approach of this compound and those alike, such as mitochondrial-targeted vitamin E (MitoVit E), consists of covalently attaching a lipophilic cation to an alkyltriphenylphosphonium allowing rapid accumulation into the mitochondria driven by the large negative value of the mitochondrial membrane potential. Most evidence supporting the use of MitoQ as a nephroprotective agent lies in *in vivo* experimental models. MitoQ has been shown to accumulate in the kidneys, comparable to levels that protect cells in culture, and has been safely administered long-term to mice (Graham *et al.*, 2009; Rodriguez-Cuenca *et al.*, 2010). Administration of MitoQ in a rat model of diabetic nephropathy decreased mesangial expansion and tubulointerstitial fibrosis, thereby improving renal function (Chacko *et al.*, 2010). Human trials have shown that MitoQ can decrease biomarkers of liver inflammation in hepatitis C patients (Gane *et al.*, 2010). However, a larger scale double-blind, placebo-controlled study found that MitoQ did not slow the progression of untreated Parkinson's disease, a disease associated with mitochondrial oxidative stress (Snow *et al.*, 2010). The effect may be tissue specific, and early intervention with MitoQ in CKD patients could prove fruitful given that oxidative stress is evident early in CKD progression (stages 1-3).

1.2.10.7 Targeting the Nrf2 pathway

Bardoxolone methyl (2-cyano-3,12-dioxooleana-1,9(11)-dien-28-oic acid/CDDO-Me) demonstrated a high level of promise to the nephrology community for halting the early progressive decline of GFR in type 2 diabetic patients (Pergola *et al.*, 2011a; Pergola *et al.*, 2011b). Bardoxolone methyl is a triterpenoid derived from natural plant products and is a potent activator of the Nrf2 pathway (Eskiocak *et al.*, 2010; Nagaraj *et al.*, 2010; Honda *et al.*, 2011). However, initial hopes were doused following the termination of a subsequent large-scale, randomised, placebo controlled trial in type 2 diabetes-stage 4 CKD patients, due to a higher rate of cardiovascular events and failure to

reduce the risk of ESKD or death from cardiovascular causes (de *et al.*, 2013). The apparent failure of bardoxolone methyl was criticised largely due to a lack of scientific rigor in pre-clinical models, and rush to proceed with the large phase III trial despite strong evidence of serious adverse events in earlier phase II trials (Tayek and Kalantar-Zadeh, 2013). Prior to publication of the results of the phase IIa trial (BEAM) in stage 3b-4 CKD patients with type 2 diabetes, no publications existed using *in vivo* animal models examining renal or cardiovascular parameters following bardoxolone administration. All published data, prior to the BEAM results, principally examined the anti-tumorigenic characteristics of bardoxolone methyl in mouse studies (Liby *et al.*, 2007; Ling *et al.*, 2007; Gao *et al.*, 2008; Liby *et al.*, 2008; Liby *et al.*, 2009; Auletta *et al.*, 2010; Li *et al.*, 2010; Liby *et al.*, 2010; Nagaraj *et al.*, 2010; Saha *et al.*, 2010). Wu et al (2011) demonstrated, at approximately the same time as the BEAM trial results were published, that bardoxolone administration attenuated ischaemia-reperfusion induced AKI in a mouse model, that was associated with increased Nrf2, PPARγ, and HO-1 mRNA levels. A subsequent *in vivo* model demonstrated deleterious effects of bardoxolone methyl and its analogs in diabetic nephropathy (Zoja *et al.*, 2013). Despite this, rodent models examining kidney parameters continually showed efficacy of bardoxolone methyl and triterpenoid analogs (Reisman *et al.*, 2012; Chin *et al.*, 2013; Ding *et al.*, 2013), giving reason to continue research into targeting the Nrf2 pathway. As previously mentioned, the Keap1-Nrf2 pathway is a highly conserved, ubiquitous response not only to stress, but also responsible for constitutive expression of genes regulated by ARE during basal conditions. Considering the superior potency of bardoxolone methyl to upregulate Nrf2-ARE-dependent genes (Walsh *et al.*, 2014), it comes as little surprise that deleterious outcomes result from its constant activation. Therefore, modulating Nrf2 activation requires a greater understanding of basal Nrf2 regulation, the exact role of the Keap1-Nrf2 interaction, and how Nrf2 regulation is altered in metabolically unstable disease populations such as CKD.

1.2.11 Exercise and lifestyle modification in CKD

The “magic bullet” approach to reduce oxidative stress is increasingly being recognised as unlikely given the vast complexity and interactions that incorporate oxidative stress. Exercise and lifestyle modification improve general health and the burden of disease (Sattelmair *et al.*, 2011; Belardinelli *et al.*, 2012; Ezzati and Riboli, 2013; Wang *et al.*, 2013). Regular physical activity alone reduces biomarkers of oxidative stress and increases endogenous antioxidants via a stress induced hormetic response. Nevertheless, convincing, practical and realistic implementation of exercise and lifestyle interventions to large populations of people, let alone chronic disease populations, is an enormous challenge. A greater understanding of the natural ability of the body to invoke a systemic protective

response is needed to determine whether these processes can be harnessed for the benefit of the chronic disease population such as CKD.

There is a variety of biochemical, cellular, and systemic adaptations that occur in response to exercise that are intimately linked to redox control (Baar, 2014; Marton *et al.*, 2014). ROS increase during and following exercise (Davies *et al.*, 1982; Alessio and Goldfarb, 1988; Radak *et al.*, 2001). This is a paradox given that exercise decreases the incidence of oxidative stress-related diseases, and is a further example of beneficial ROS signalling that is the result of exercise-induced adaptation. The site of increased ROS production is difficult to identify and is assumed to be from mitochondria, given that exercise causes an increase in oxygen consumption. However, as Gomez-Cabrera *et al* (2008) describe, actively-respiring mitochondria that produce ATP from ADP, with a high electron flow from O_2, produce one tenth of the ROS that are produced from resting state mitochondria (2 %) (Chance *et al.*, 1979). Therefore, mitochondria as a source of increased ROS production in exercise should be reconsidered. Potential extracellular sources of exercise-induced ROS may occur given that the response to exercise is systemic and has been suggested to arise from xanthine oxidase activity (Hellsten *et al.*, 1988; Pattwell *et al.*, 2004). This is further supported from studies using allopurinol to prevent oxidation of glutathione and lipid peroxidation following exhaustive exercise (Vina *et al.*, 2000). NADPH oxidases and phospholipase-A2-dependent processes have also been shown to contribute (Nethery *et al.*, 1999; Frasier *et al.*, 2013; Sakellariou *et al.*, 2014). The importance of exercise-induced ROS signalling was highlighted in a recent study investigating the effects of a combination of vitamin C (1000 mg/day) and vitamin E (400 IU/day) on insulin sensitivity and ROS-sensitive transcriptional regulators (Ristow *et al.*, 2009). The antioxidant combination prevented increased insulin sensitivity and upregulation of PPARγ, PGC-1α and PGC-1β following physical exercise (Ristow *et al.*, 2009). Similar findings were found in a rat model demonstrating a failure of training-induced mitochondrial biogenesis following oral administration of vitamin C (Gomez-Cabrera *et al.*, 2008). However, a recent study demonstrated no differences in the exercise-induced adaptations of GLUT4, SOD 1/2, PGC-1α and mitochondrial biogenesis of vitamin C and E supplementation in a rat model (Higashida *et al.*, 2011).

There is strong evidence showing that skeletal muscle contraction induces antioxidant adaptation to chronic exercise training. Of the known antioxidant responses, SOD activity (primarily MnSOD) and GPX, have been demonstrated as the most consistent, by increasing in an exercise-dependent manner (Alessio and Goldfarb, 1988; Lawler *et al.*, 1993; Leeuwenburgh *et al.*, 1994; Powers *et al.*, 1994; Budiono *et al.*, 2012). The skeletal muscle adaptation to exercise is clearly the most pronounced and most well-studied. However, this raises a question: is the systemic response to

exercise a consequence of all cells responding to exercise the same way as skeletal muscle? This is interesting considering that changes to antioxidant/oxidative stress biomarkers have been demonstrated in various other organs such as brain, kidney, heart and liver, and all appear to have a similar protective response despite reacting differently to changes in oxygen supply during exercise (Radak *et al.*, 1996; Navarro *et al.*, 2004; Radak *et al.*, 2004; Iemitsu *et al.*, 2006; Radak *et al.*, 2008). This suggests that an extracellular source of cytoprotective signalling may account for such a systemic response to exercise.

Mitochondrial biogenesis is a consistent adaptation to exercise, and seems to contribute to the majority of gained benefits to systemic redox control (Baar *et al.*, 2002; Koltai *et al.*, 2012; Marton *et al.*, 2014). Mitochondrial biogenesis is presumed to occur due to increased reliance on aerobic metabolism, and is initiated by increased ROS signalling (Kang *et al.*, 2009). Metabolic regulation of PGC-1α is central not only to exercise-dependent mitochondrial biogenesis, but also upregulation of antioxidant enzymes and cytoprotective responses via coactivation of Nrf2 and upregulation of SOD1/2, GPX, CAT and HO-1 (Kim and Vaziri, 2010; Wu *et al.*, 2011). The activity of PGC-1α is highly susceptible to changes in metabolism and is therefore regulated in many ways in response to exercise. PGC-1α phosphorylation is known to increase translocation to the nucleus and its ability to bind transcription factors for mitochondrial biogenesis (Puigserver *et al.*, 2001). Furthermore, deacetylation by specific deacetylases increases nuclear translocation and cofactor recruitment (Rodgers *et al.*, 2005). Sirt1 is a NAD+-dependent deacetylase and has been shown to deacetylate PGC-1α. Metabolic alterations, such as exercise, increase Sirt1 activity since lactate levels rise in skeletal muscle and change the redox state by increasing NAD+ and the ratio of NAD+/NADH (Li *et al.*, 2009). A Sirt1 knock-out mouse exercise model surprisingly demonstrated unaltered PGC-1α acetylation and mitochondrial biogenesis compared to wild type animals (Philp *et al.*, 2011), yet demonstrated a reduction in an acetyltransferase of PGC-1α (general control of amino-acid synthesis 5 – GCN5), demonstrating a Sirt1-independent mitochondrial biogenesis pathway.

Increasing numbers of mitochondria allow lower levels of respiratory activity for the same degree of ATP production. The previously mentioned elusive site of exercise-dependent increased in ROS signalling could be explained by resting state respiring mitochondria in increased number due to the exercise-induced adaptation of mitochondrial biogenesis. However, this explanation would only account for the sustained increase in antioxidant/cytoprotective proteins and enzymes following mitochondrial biogenesis, occurring following repeated sustained exercise, and not responsible for the initiation of exercise-induced ROS signalling.

The benefits gained from physical activity depend on intensity, duration, and initial health of the individual. Continued research into the optimal intensity and duration for an individual to induce the greatest health benefits must be continued and harnessed. However, as a substantial body of evidence demonstrates (Sattelmair *et al.*, 2011; Belardinelli *et al.*, 2012; Ezzati and Riboli, 2013; Wang *et al.*, 2013), as does common sense, any exercise is better than none (Bharakhada *et al.*, 2012). There is still a lack of evidence regarding the association between exercise, oxidative stress, and CKD.

1.3 HYPOTHESIS AND AIMS

CKD is a common and serious problem that adversely affects human health, limits longevity, and increases costs to healthcare systems worldwide. Its increasing incidence cannot be fully explained by traditional risk factors. Oxidative stress is prevalent in CKD patients and is considered to be an important pathogenic mechanism. Oxidative stress develops from an imbalance between free radical production often increased through dysfunctional mitochondria and reduced anti-oxidant defences. Perturbations in cellular oxidant handling influence downstream cellular signalling and, in the kidney, promote renal cell apoptosis and senescence, decreased regenerative ability of cells, and fibrosis.

The overall hypotheses tested in this thesis were that: (1) oxidative stress impacts adversely on cellular bioenergetics in the kidney and leads to loss of functioning kidney tissue in chronic kidney pathologies; and (2) modulation of oxidative stress will minimise the development and progression of injury to kidney cells.

The aims of this thesis were to:

1. Use an *in vitro* model of kidney injury from oxidative stress to determine how the failure of balance between oxidative stress and oxidant control in PTE cells causes kidney cell injury, and then to determine whether exogenous antioxidants can prevent and restore renal cell bioenergetics and reduce cell injury (Chapters 3 and 4);
2. Use an *in vivo* model of oxidative stress-induced kidney injury, with molecular and metabolic imaging, to measure potential oxidative stress biomarkers in association with changes in kidney structure and function, and to determine whether treatment with an antioxidant modulates kidney disease pathology (Chapters 5 and 6);

3. Explore the links between increasing oxidative stress and development of CKD in patients who are undergoing significant lifestyle change in conjunction with standard nephrology care, and to determine if biomarkers of oxidative stress correlate with clinical markers of renal function in CKD patients (Chapter 7).

CHAPTER 2

Materials and Methods

This Chapter presents the general materials and methods for this thesis. More specific details are given in the original research Chapters (Chapters 3-7) for methods specific to those Chapters.

2.1 MATERIALS

All chemicals were of high purity and, unless otherwise indicated, were obtained from Sigma-Aldrich (St. Louis, MO, USA). HK-2 cells were obtained from the American Type Culture Collection (ATCC) (Rockville, MA, USA), unless otherwise indicated. All plasticware for tissue culture was either Nunc brand (In Vitro Technologies, Noble Park North, Australia) or Corning Plastic (Sigma-Aldrich; St. Louis, MO, USA). Fetal bovine serum (FBS) was from Gibco (Invitrogen/Life Technologies Pty Ltd, Mt. Waverley, Australia). Antibiotics for tissue culture were obtained from BioWhittaker (Edward Keller Australia, Silverwater, Australia). Growth media were obtained from Invitrogen Pty Ltd (Life Technologies Pty Ltd, Mt. Waverley, Australia). The protein assay kit was from Pierce Pty Ltd (Quantum Scientific, Murarrie, Australia). The ApopTag® Peroxidase *In Situ* Apoptosis Detection Kit was supplied by Serologicals Corporation (Millipore Pty Ltd, North Ryde, Australia). Primary antibodies, their dilutions and suppliers are listed in sections on Western Immunoblots and immunohistochemistry (IHC). All secondary antibodies were from Zymed Laboratories (Invitrogen/Life Technologies, Mt. Waverley, Australia) and dilutions are listed in relevant chapter sections. The polyvinylidene difluoride (PVDF) membrane for Western immunoblots was from PerkinElmer (Thermo Fisher Scientific, Scoresby, Australia). Mice were purchased from the Translational Research Institute (TRI) Biological Research Facility breeding house (Woolloongabba, Australia). Powdered food for the mouse diet was from Specialty Feeds (Glen Forrest, Australia) and was donated from the laboratories of Professor Lindsay Brown (School of Health, Nursing and Midwifery, University of Southern Queensland, Toowoomba, Australia).

2.2 CELL CULTURE

HK-2 cells are adult human kidney PTE cells that have been transfected with human papilloma virus (HPV 16) E6/E7 genes, and are therefore immortalised. They were selected because they are highly representative of freshly isolated PTE cells based on histochemical, immune, cytochemical, and functional characteristics (Ryan *et al.*, 1994). Freshly isolated human tubular epithelial cells have disadvantages owing to a limited availability of human sources and inherent patient variability of culture isolates, time-consuming and difficult isolation techniques, and limited ability of the cells for multiple passaging without inherent senescence (Vesey *et al.*, 2009).

2.2.1 Cell culture

HK-2 cells were maintained routinely in 25 cm^2 or 75 cm^2 cell culture flasks containing Dulbecco's modified Eagle's medium (DMEM)/Ham's F12 containing 10% FBS with penicillin (1000 U/mL) and streptomycin (1000 U/mL). This will be termed "normal growth medium" in this thesis. Cells were grown in a humidified atmosphere of 95% air and 5% carbon dioxide (CO_2) at 37˚C in a tissue culture incubator. Frozen stocks of cultures were stored in liquid nitrogen at -196 ˚C. Stocks were checked routinely for mycoplasma contamination and were always found to be uncontaminated.

2.2.2 Sub-culturing techniques

Cultures were passaged every 3-5 days when flasks were 90-100% confluent. HK-2 cells are adherent and were trypsinised using either 2.5% trypsin/versene solution or 2.5% trypsin/ethylenediaminetetraacetic acid (EDTA) at 37 ˚C until cells detached from the tissue culture flasks. Cell suspensions were transferred to a sterile 5 or 10 mL tube and centrifuged at 1000-1200 revolutions per minute (rpm) for 5 min to pellet the cells. Cell pellets were resuspended in 5-10 mL of normal growth medium and transferred to sterile 25 cm^2 or 75 cm^2 tissue culture flasks containing 5-10 mL of growth medium. Aseptic technique was used, and normal growth medium was often filtered using a 0.2 µm syringe-adaptable filter. Following centrifugation and re-suspension, cells were also either plated directly into 24-well multi-well culture plates containing sterile glass coverslips (12 mm diameter; Lomb Scientific, Taren Point, NSW, Australia) for microscopy, or plated into 6-well multi-well tissue culture plates or 100 mm tissue culture dishes for protein extraction, or 96-well plates for the MTT assay (section 2.2.5) or the fluorimetry assay (Section 2.2.6). Petri dishes routinely contained a coverslip that was fixed and stained for histology. Cells were grown for 24-48 h prior to treatment or until 80-90 % confluent. Phosphate buffered saline (PBS) was routinely used to wash cells.

2.2.3 Frozen stocks of cell lines

Frozen stocks of the cell lines were prepared periodically. Trypsinised cells were centrifuged, the supernatant discarded, and the cells were re-suspended in 1 mL of normal growth medium with 10 % dimethyl sulphoxide (DMSO). Resuspended cells were transferred to labelled cryogenic tubes and frozen at -80 ºC in an insulated isopropanol-filled freezing container (Nalgene, Thermo Fisher Scientific, Scoresby, Australia; Cat. no. 5100-0001) which regulated the freezing rate. Frozen cells were then relocated to liquid nitrogen for long-term storage.

2.2.4 Cell treatments

Specific cell treatments are described in relevant chapters. H_2O_2 cell treatment was common throughout *in vitro* studies and is therefore described here. A 5% H_2O_2 solution was prepared from a 30 % H_2O_2 stock solution by diluting 1:6. A 1 mM solution was prepared by adding 10.2 µL of the dilution to 15 mL normal growth medium. A serial dilution was prepared according to Table 2.1.

Table 2.1: H_2O_2 serial dilution

H_2O_2 Concentration	Volume of 1mM H_2O_2	Volume of Media
1 mM	5 mL	0 mL
0.8 mM	4 mL	1 mL
0.6 mM	3 mL	2 mL
0.4 mM	2 mL	3 mL
0.2 mM	1 mL	4 mL
0 mM (Control)	0 mL	5 mL

In preparation for treatment, cells were grown to 80-90 % confluence in appropriate culture vessels, as described in Section 2.2.2. Cells were washed X 1 with sterile PBS or culture media before the addition of treatments. Volumes added and incubation times are stated within specific treatment methods in relevant Chapters, and varied depending on the culture vessel and treatment used. For experiments involving co-treatments, chemicals were prepared at double the concentration and then combined at a 1:1 ratio to obtain the required concentration within the cell culture medium. All cell culture treatment studies included appropriate controls including an untreated culture. Vehicle controls were included where necessary. Concentration of vehicle controls was always less than 1 % in the treatments and, in general, caused no change from normal growth media.

2.2.5 Cell viability assay

Cell viability was measured using the assay based on the reduction 3-[4,5-dimethylthiazol-2-yl]-2,5-diphenyltetrazolium bromide (MTT) (Sigma, Missouri, USA). Following cell treatments in 96-well plates, 100 µL of MTT solution prepared in serum-free growth medium (0.5 mg/mL) were added to wells and incubated for 90 min at 37 ˚C. Culture medium was removed and formazan crystals were dissolved in 200 µL DMSO. Absorbance was measured in a microplate reader at 570 nm with background collection at 690 nm.

2.2.6 Cell fluorimetry assays

Dihydroethidium (DHE) was used as a marker of ROS production in HK-2 cells since the oxidation of hydroethidine to ethidium is mediated by superoxide production. JC-1 was used to assess changes to the mitochondrial membrane potential since JC-1 fluoresces red when internalised into healthy polarised mitochondria, and green when it is in the cytoplasm unable to be taken into mitochondria with a depolarised membrane potential. HK-2 cells were seeded into black, clear-bottom 96-well plates, incubated overnight, and subjected to treatments. Conditioned media were removed, cells were washed, and either 5 µM DHE or 3 µM JC-1 in serum-free DMEM Ham's F12 medium were added and incubated for 30 min. Cells were washed X2 in Hank's Buffered Solution (HBS) before fluorimetry was read. Fluorescence was read on a Synergy Mx multi-mode microplate reader (BioTek, Winooski, VT) with DHE excited at 535 nm, JC-1 (red) at 525 nm, JC-1 (green) at 490 nm, and emission detected at 610 nm (DHE), 590 nm (JC-1-red), and 530 nm (JC-1-green). Emitted fluorescence values were normalised to protein concentration determined by the Pierce bicinchoninic acid (BCA) protein assay (Pierce Chemical Co., Rockford, Illinois, USA) (Section 2.5.2), which was performed using protein extracted from the black 96-well plate and transferred to a clear 96-well plate.

2.2.7 ATP luminescence assay

ATP production was measured using a luciferase-based luminescence assay (Promega, Sydney, Australia). Cells were seeded into white opaque 96-well plates and treated as previously described. Chemiluminescent reagent was added and cell lysis induced prior to measuring luminescence at an integration time of 0.5 sec using a Titertek-Berthold Luminometer (Titertek-Berthold Detection Systems, Pforzheim, Germany).

2.2.8 Malondialdehyde assay for lipid peroxidation

A colorimetric assay (Bioxytech LPO-586 Assay, OxisResearch Products, Percipio Biosciences Inc., USA) for lipid peroxidation was conducted as a measure of oxidative stress in treated HK-2 cells. The assay measures malondialdehyde (MDA) content. MDA is generated from polyunsaturated fatty acid peroxides following lipid peroxidation. The shift in absorbance is based on the reaction of N-methyl-2-phenylindole with MDA which produces a stable chromophore. Absorbance is then read in triplicate at 620 nm using an ELISA plate reader. Protein extraction was performed in a similar method to that used for Western immunoblotting, with addition of 0.5 M butylated hydroxytoluene (BHT) to prevent any further oxidation of cells during protein extraction and sample preparation, in accordance with the manufacturer's guidelines. Cells treated with 1 mM H_2O_2 were used in addition to treatments, as a positive control representing high oxidative stress.

Protein was analysed according to the supplier's instructions (www.oxisresearch.com/pub/PDF/inserts/75820605.pdf). Protein concentration was determined by a BCA protein assay (Section 2.5.2) and spectroscopy was carried out at 540 nm. MDA absorbance values were then normalised according to the protein concentration of each cell homogenate.

2.2.9 Total antioxidant capacity assay

The OxiSelect^{TM} TAC Assay Kit (Cell Biolabs, Inc., Jomar Bioscience Pty Ltd., Welland, Australia) was used to determine the total antioxidant capacity (TAC) by measuring the reduction of the copper ion coupled to a chromogenic reagent, measured at 490 nm. Uric acid was used as a standard. The kit was used according to the manufacturer's protocol. Treated and control cultures were washed X3 in PBS for 5 min before being lysed in PBS by sonification. Cell debris was removed by centrifugation at 10000 g for 10 min at 4 ºC. Protein concentration was determined by the BCA assay (Section 2.5.2) and spectroscopy performed at 540 nm so that 100 µg of protein was analysed for each treatment.

2.3 CELL CULTURE MICROSCOPY

2.3.1 Fixation

Cell culture growth medium was discarded from control and treated cells on coverslips, followed by washing X 1 with PBS, pH 7.4. Cells were then fixed in 4% paraformaldehyde (PF) (Appendix B) for 30 min at room temperature (RT) or overnight at 4 °C. Cells were washed twice in PBS then either stained immediately or stored in PBS at 4 °C. For immunocytochemistry microscopy, cells on coverslips were fixed in 100 % methanol at -20 °C for 5 min prior to PBS washes.

2.3.2 Haematoxylin and eosin (H&E) staining of cell culture

Following fixation, PBS was discarded and cells were permeabilized with 0.2 % Triton X-100 in PBS for 10 min. Mayer's haematoxylin stain was filtered (0.22 µm) onto coverslips for approximately 10 min. The haematoxylin was removed and cells "blued" in normal tap water for 2 X 2 min, then with a "blueing" agent of 0.2 % (w/v) aqueous sodium carbonate for a further 5 min to intensify the stain. Cells were dehydrated in a series of ethanol solutions (70 %, 95 %, 100 %) for 5 min each. The final 100 % ethanol solution was removed prior to adding eosin solution for 5 min. This was followed by 2 X 2 min washes in 100 % ethanol. Cells were transferred into a glass dish by small tweezers where they were cleared in xylene for 5 min. Coverslips were mounted onto slides using Depex mounting medium. Adequate time was allowed for the mounting medium to dry prior to light microscopy, or digital scanning.

2.3.3 Cytological assessment of apoptosis

H&E stained coverslip-cultures were viewed using light microscopy or Aperio Image Scope digital histology software. The morphological features of apoptosis (Kerr *et al.*, 1995; Gobe, 2009) that were used were: (i) shrunken eosinophilic cells with condensed, marginated nuclear chromatin and intact cell membrane; (ii) discrete apoptotic bodies compromising large, dense, pyknotic nuclear fragments usually surrounded by a narrow eosinophilic cytoplasmic rim; and (iii) clusters of small apoptotic bodies (assessed as a single apoptotic occurrence) (Fig 2.1). Cells with nuclear features of apoptosis not showing the characteristics of secondary necrosis (swollen cytoplasm), known to occur in cell culture were also counted as apoptosis. Apoptosis was counted in at least 10 microscopic fields at x200 per coverslip culture and a minimum of 1000 cells was counted. Counts of apoptosis were calculated as a percentage of total cells (normal plus apoptotic) per field.

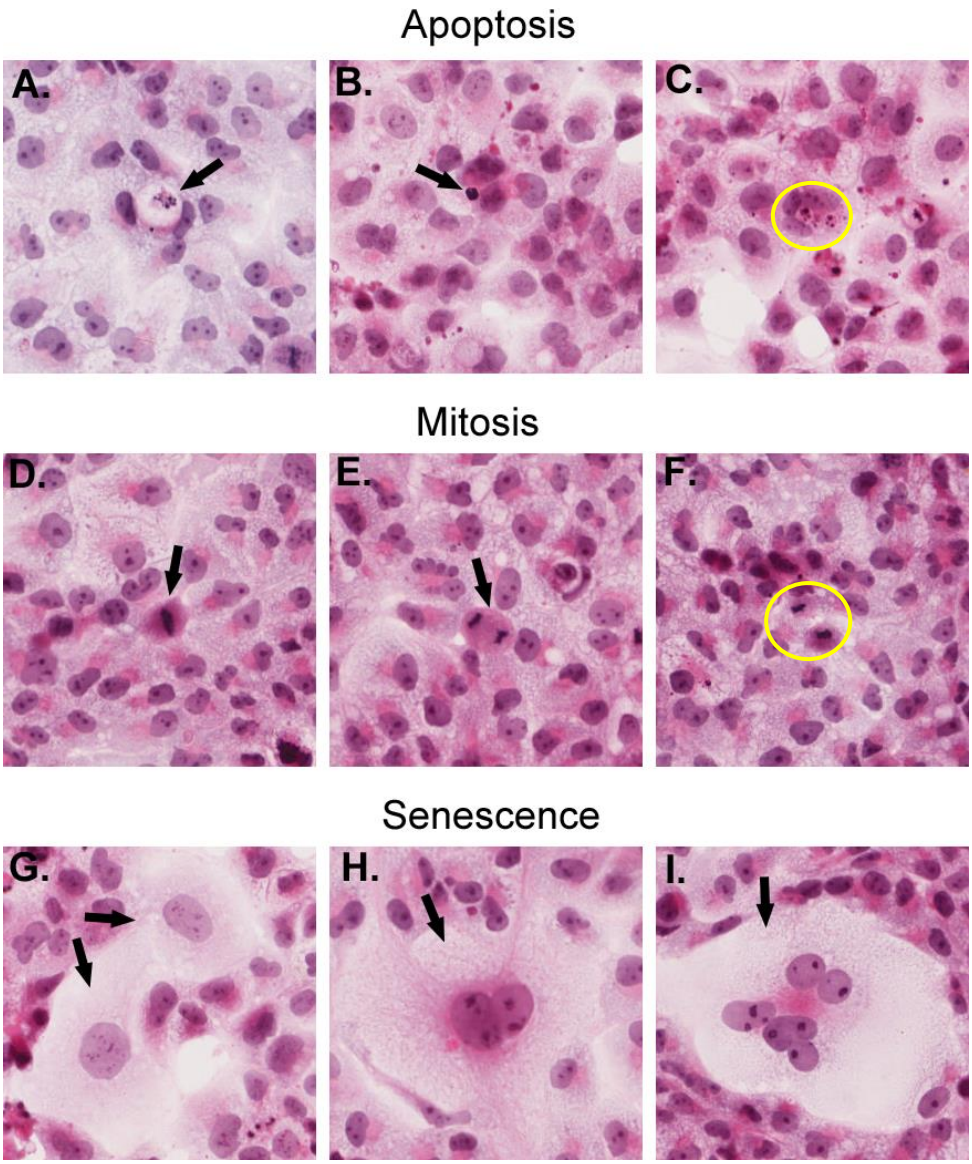

Figure 2.1: H&E-stained HK-2 cells undergoing apoptosis, mitosis and senescence
Apoptosis was identified by shrunken eosinophilic cells with condensed, marginated nuclear chromatin and intact cell membrane (A.), discrete apoptotic bodies compromising large, dense, pyknotic nuclear fragments usually surrounded by a narrow eosinophilic cytoplasmic rim (B.), and clusters of small apoptotic bodies assessed as a single apoptotic occurrence (C.). Mitosis was identified by the formation of mitotic spindles occurring during metaphase and remaining visible in anaphase (D.), and cells in the later stages of mitosis, telophase (E.) or undergoing cytokinesis (F.). Morphological senescence was identified as large cells, at least 3-4 times the diameter of non-senescing cells (G.), often appearing with multiple and bi-lobed nuclei per senescent cell (H. and I.).

2.3.4 Cytological assessment of mitosis or cell senescence

The morphological characteristics used to distinguish mitosis were: (i) formation of mitotic spindles occurring during metaphase and remaining visible in anaphase; or (ii) cells in the later stages of mitosis, telophase or undergoing cytokinesis. Cell senescence was assessed initially by the presence of large cells, at least 3-4 times the diameter of non-senescing cells (Figure 2.1).

2.3.5 Cell culture immunohistochemistry (IHC)

After fixation of coverslip cultures and washing in PBS, cells were permeabilized with 0.2 % Triton-X100 in PBS for 10 min, then non-specific binding of peroxidase or antibody was blocked with 0.1 % sodium azide in 0.3 % H_2O_2 in Tris-buffered saline (TBS) for 10 min, followed by 4 % blotto in TBS for 20 min. The primary antibody was diluted in 1 % bovine serum albumin (BSA) prepared in TBS was applied at 4 ^{o}C overnight. Negative controls were prepared without primary antibody, or with non-specific serum. The LSAB+ peroxidase kit (DAKO Australia Pty Ltd, Campbellfield, Australia) was used for application of the secondary antibody and for the Horseradish Peroxidase (HRP) reaction and diaminobenzidine 2-hydrochloride (DAB) chromogen reaction. Cells were lightly counterstained with haematoxylin, dehydrated in a series of ethanols, cleared in xylene then mounted in Depex.

2.3.6 Cell culture immunofluorescence (IF)

After fixation of coverslips cultures and washing in PBS, cells were permeabilised with 0.2 % Triton-X100 in PBS for 10 min, then non-specific antibody binding was blocked with 10 % bovine calf serum (BCS) in PBS solution for 30 min. A primary antibody solution (Table 2.2) diluted in the blocking solution was added for 2 h and room temperature. Coverslips were washed in PBS for a total time of 20 min at least 6 X. The appropriate diluted secondary antibody solution was applied and incubated for 30 min at room temperature before washing coverslips in PBS for a total time of 20 min with at least 6 washes. Mount coverslips onto glass slides using aqueous mounting medium.

2.3.7 MitoTracker Red CMXRos confocal microscopy

MitoTracker Red CMXRos (Invitrogen Australia Pty Ltd, Mt Waverley, Australia) is a fluorescent dye that localises to mitochondria with a healthy mitochondrial membrane potential. The dye fades as mitochondria lose mitochondrial membrane potential. Cells were first washed in PBS then incubated, shielded from light, in 100 nM MitoTracker Red for 30 min. Cells were then washed X 2 in PBS, fixed in 4 % PF for 30 min at 4 ºC, then washed X 3 in PBS before being mounted onto glass slides using Vectashield anti-fade aqueous mounting medium (Vecta Laboratories, Abacus ALS, East Brisbane, Australia) with 4',6-diamidino-2-phenylindole (DAPI) blue nuclear fluorescent

dye. Cells were observed at 579 nm using a Zeiss 510 Meta confocal fluorescence microscope with Zen 2008 software, with x63 oil objective to obtain photographs. To analyse the mean intensity of MitoTracker Red CMXRos fluorescence for each treatment, cells were visualised using a Nikon FN-S2N fluorescence microscope (x63 objective) with a Nikon DS-U2/L2 USB camera and NIS-Elements microscopy software. This allowed the florescence intensity of a single cell to be determined and expressed as arbitrary units (AU). 5 representative fields for each treatment were captured, the fluorescence of each cell within that field was measured, and an overall mean intensity calculated.

2.3.8 JC-1 confocal microscopy

JC-1 is a cationic fluorophore that possesses a mitochondrial membrane potential-dependent accumulation in mitochondria. A decrease in red fluorescence and increase in green fluorescence indicates mitochondrial membrane depolarisation. Cells on coverslips were washed in PBS then incubated in 3 µM JC-1 in serum-free medium for 30 min. Cells were then exposed to 0.4 mM H_2O_2 (moderate oxidative stress) and 1 mM H_2O_2 (high oxidative stress) in serum-free media for 1 h. Coverslips were washed in PBS then fixed in 4 % PF for 30 min at 4 ºC, washed X 3 in PBS then mounted onto glass slides using Vectashield mounting medium with DAPI. Cells were then visualised at 590 nm (red), 529 nm (green) and 460 nm (blue) using the laser scanning confocal florescence microscopy stated in Section 2.3.6 (x63 oil objective). For live cell imaging, 1 X 10^4 cells/mL were seeded onto glass bottom dishes (MatTec Corporation, Loveland, USA) and allowed 24 h to adhere. Cells were incubated in 3 µM JC-1 for 30 min. A representative field of cells was then visualised using a Zeiss 510 Meta confocal fluorescence microscope with Zen 2008 software, x63 objective, and a live-cell imaging chamber at 37^{o}C and 5% CO_2 in air, to assess fluorescence leaching or alteration of mitochondrial membrane potential because of exposure to the laser. H_2O_2 treatment was added to the cells and the same field viewed over a total of 25 min. A timed series of photos was taken in consecutive 5 min intervals to investigate the shift from red (590 nm) to green (460 nm) fluorescence under oxidative stress.

2.3.9 Transmission electron microscopy

The transmission electron microscopy (TEM) preparation work and imaging was performed under the supervision and assistance of Drs Richard Webb, Robin Webb, and Kathryn Green at the Centre for Microscopy and Microanalysis, University of Queensland, St Lucia, Australia.

For immuno-labelling of Bax, cell samples were taken from trypsinised suspensions following treatment, re-suspended in PBS, then re-suspended in 2 mL 3 % glutaraldehyde in Sorensen's

buffer, pH 7.4, for 30 min. The fixed samples were spun down, resuspended in Sorensen's buffer, and stored at 4 º C. Cells were post-fixed in osmium tetroxide in PBS then embedded in Epon resin. Semi-thin sections were cut, stained with toluidine blue and viewed under a light microscope to select areas for preparation of ultra-thin sections. Selected areas were cut onto copper grids using an ultramicrotome. Prior to labelling and at room temperature, grids were washed 3 X in PBS and blocked to prevent non-specific binding, for 15 min in 0.2 % BSA 0.2 % fish skin gelatin, 20 mM glycine in PBS. Bax primary antibody (Table 2.2) dilated 1:70 in blocking buffer was applied to grids for 30 min, then was washed 4 X in blocking buffer, before adding anti-rabbit-10nm-gold secondary antibody diluted 1:70 in blocking buffer for 30 min. Grids were washed 4 X in PBS, then 4 X in water, before being counterstained with 4 % uranyl acetate in 2 % methylcellulose solution. Images were acquired using a Jeol 1010 TEM. For mitochondrial ultrastructure, cells were grown on sapphire disks in control and H_2O_2 treatment culture conditions. High-pressure freezing fixation was used for optimal preservation of structure prior to 4 % uranyl acetate and Reynolds lead citrate staining.

2.4 HISTOLOGY AND IMMUNOHISTOCHEMISTRY

IHC was performed on coverslip cell cultures or paraffin-embedded sections of mouse kidney. In general, antibodies used in the Western blotting process were used at a higher concentration for IHC. Antibody dilutions for IHC are listed in Table 2.2. This work was carried out at the Histology Facility, Queensland Institute for Medical Research by Mr Clay Winterford.

2.4.1 Haematoxylin and eosin staining of mouse kidney

H&E staining was routinely performed for all blocked tissue, prior to any staining for IHC, ApopTag or Masson's Trichrome. 3-4 µm sections were cut from paraffin embedded mouse kidney, dewaxed in xylene and rehydrated in descending grades of alcohol. Sections were briefly washed in water before staining in Mayer's haematoxylin for 5-10 min. Sections were washed in water for 2 min before the nuclear stain was blued in Scott's solution (potassium bicarbonate 2 g/mL, magnesium sulphate 20 g/mL in distilled water [dH_2O]), and washed in water for 2 min. Sections were washed in 70 % alcohol before alcoholic eosin was added as a counter stain for 1-3 min. Absolute alcohol was used to dehydrate the sections before being cleared in xylene and mounted using Depex.

2.4.2 Masson's Trichrome stain for collagen

This method applies the principle that larger molecular-sized dyes can replace (differentiate) smaller sized dyes that are first applied. This applies only for structures it can penetrate, such as collagen, but not in those it cannot penetrate, such as muscle or fibrin. Phosphotungstic acid can be replaced by the larger molecular sized dye Aniline Blue, which results in collagen being stained. 3-4 µm mouse kidney sections were dewaxed and rehydrated to PBS using standard protocol. Sections were treated in Bouin's fluid for 1 h at 56 ºC to add intensity to the colour, then washed in running water for 5 min or until colourless. Celestine Blue Stain R was added for 5 min, then washed in running water, followed by Mayer's haematoxylin for 5 min. Sections were again washed in running water before 0.5 % acetic alcohol was added for 30 sec to differentiate nuclei, and washed off with water. Sections were then covered with Biebrich Scarlet-Acid Fuchsin. Following 15 min, 1-2 drops of dH_2O were added and sections were covered with 5 % tungstophosphoric acid solution for 20 min. The solution was drained and aniline blue solution was added for 20 min before being washed in 1 % acetic acid for 3 min. Sections were dehydrated to absolute alcohol, cleared in xylene and mounted using Depex.

2.4.3 ApopTag® peroxidase *in situ* apoptosis detection in mouse kidney

This method labels apoptotic cells by modifying DNA fragments, utilizing terminal deoxynucleotidyl transferase (TdT) for detection of apoptotic cells by specific staining. TdT catalyses a template-independent addition of nucleotide triphosphates to the 3'-OH ends of double-stranded or single-stranded DNA. DNA fragments which have been labeled with a digoxigenin-nucleotide bind an anti-digoxigenin antibody that is conjugated to peroxidase. The bound peroxidase antibody, conjugated enzymatically, generates a permanent, intense, localized chromogenic stain, providing sensitive detection. Methods were followed according to the manufacturer's protocol (Millipore, S7100, CA, USA). Briefly, 3-4 µm paraffin sections were dewaxed and rehydrated with PBS using standard protocol. Freshly diluted proteinase K (20 µg/mL in 0.05 M Tris-HCl, 0.01 M $CaCl_2$ pH 8.0) was added to the section for 10 min at room temperature before being washed 2 X in PBS. The sections were decanted of excess buffer and the equilibration buffer was added directly onto the section for 10 min. The equilibration buffer was removed and the working strength TdT enzyme was applied for 1 h at 37 ºC. TdT enzyme was removed prior and the stop wash buffer was added before incubating for 10 min and washing X 3 in PBS. Anti-digoxygenin conjugate was added underlying a plastic coverslip for 30 min at room temperature before being washed X 4 in PBS. Colour was developed in DAB with H_2O_2 as a substrate for 5 min. Sections were washing in running water for 5 min and then counterstained with Mayer's haematoxylin for 2 min.

2.4.4 Mouse kidney IHC for proliferating cell nuclear antigen

Table 2.2 gives primary and secondary antibody dilutions for all IHC and IF. Proliferating cell nuclear antigen (PCNA) was used to verify morphological identification of mitosis. PCNA identifies cycling cells but is an accepted measure of cell proliferation. Paraffin blocks of fixed mouse kidney (commonly four kidneys per slide in a tissue array) were sectioned onto Superfrost ® Plus slides (Menzel-Glasser, Braunschweig, Germany) at 3-4 µm thickness and air dried overnight at 37 ºC. Sections were dewaxed and rehydrated through descending graded alcohols to TBS, pH 7.4 prior to the blocking of endogenous peroxidase activity by incubating the sections in 2.0 % H_2O_2 in TBS for 10 min. Sections were washed X 3 in TBS, pre-treated with 0.2 M hydrochloric acid (HCl) for 20 min at RT, and washed a further 3 X in TBS. Endogenous immunoglobulin was blocked by incubating the sections in Biocare Medical Mouse Block M (Metagene.com.au; cat. no. RBM961) + Jackson ImmunoResearch (East Brisbane, Australia) anti-mouse $F(ab')_2$ fragments diluted 1:50 for 60 min, then washing X 3 in TBS. Normal goat serum (10%) was added for 30 min to stop non-specific binding. Excess normal serum was decanted from the sections and the diluted primary antibody for PCNA (Table 2.2) was incubated 90 min at room temperature. Sections were washed X 3 in TBS prior to the addition of Biocare Medical Mach2 anti-mouse for 30 min at room temperature. Following another 3 washes in TBS, colour was developed in DAB with H_2O_2 as the substrate for 5 min. Sections were washed in gently running tap water for 5-10 min to remove excess chromogen. Mayer's haematoxylin was added as a light counterstain before the sections were dehydrated through ascending graded alcohols, cleared in xylene, and mounted using Depex.

Table 2.2: Primary and secondary antibodies used for immunohistochemistry and immunofluorescence

Primary Antibody	Supplier Ab name	Source	Supplier	Catalogue number	Dilution
8-OHdG	8-OhdG (K-20)	Goat (polyclonal)	Santa Cruz	sc-130085	1:100 (IHC)
β-Gal	B-Gal (14B7)	Mouse (monoclonal)	Cell Signaling	2372	1:500 (IF)
p62	SQSTM1 (D-3)	Mouse (monoclonal)	Santa Cruz	sc-28359	1:500 (IF)
PCNA	PCNA	Mouse (monoclonal)	Vector Laboratories	VP-P980	1:75 (IHC)
p-PPARγ	p-PPARγ (Ser 112)-R	Rabbit (polyclonal)	Santa Cruz	sc-28001-R	1:100 (IHC)
PPARγ	PPARγ (H-100)	Rabbit (polyclonal)	Santa Cruz	sc-7196	1:100 (IHC)

Secondary Antibody	Supplier	Catalogue number	Dilution
Goat Probe and Goat-on-Rodent HRP-Polymer	Biocare Medical	GHP516 G, H, L	1:300
Goat Anti-Mouse-HRP (MACH 2 Mouse HRP-Polymer)	Biocare Medical	MHRP520 G, H, L, MM	1:300
Goat Anti-Rabbit-HRP (MACH 2 Rabbit HRP-Polymer)	Biocare Medical	RHRP520 G, H, L, MM	1:300
Anti-Mouse Alexa-Fluor Green	Molecular Probes	A-11001	1:50

Ab = antibody; Appropriate dilutions for both primary and secondary antibodies and names of suppliers are included for all proteins.

2.4.5 Mouse kidney IHC for 8-hydroxy-2'-deoxyguanosine

8-hydroxy-2'-deoxyguanosine (8-OHdG) is an indicator of oxidative stress in cells. Paraffin blocks of mouse kidney in tissue arrays were sectioned onto Superfrost ® Plus slides (Menzel-Glasser, Braunschweig, Germany) at 3-4 µm thickness and air dried overnight at 37 ºC. Sections were dewaxed and rehydrated through descending graded alcohols to PBS, pH 7.4, prior to the blocking of endogenous peroxidase activity by incubating the sections in 1.0 % H_2O_2, 0.1 % sodium azide in PBS for 10 min. Sections were washed X 3 in PBS prior to adding freshly-diluted proteinase K (20 µg/mL in 0.05 M Tris-HCl, 0.01 M $CaCl_2$, pH 8.0) to the section for 10 min at room temperature. Sections were washed 3 X in PBS with the first wash containing 0.5 % Triton X-100. Normal donkey serum (10 %) was applied for 30 min. Excess normal serum was decanted from the sections and the diluted primary antibody for 8-OHdG (Table 2.2) was added for 1 h at RT. Sections were washed 3 X in PBS, with the first wash containing 0.5 % Triton X-100, before adding Biocare Medical Goat Probe for 15 min. Sections were washed 3 X in PBS prior Biocare Medical Goat Polymer HRP was added for 15 min, then washed 3 X in PBS. Colour was developed in DAB with H_2O_2 as the substrate for 5 min and the sections were washed in gently running tap water for 5-10 min to remove excess chromogen. Sections were counterstained in Mayer's haematoxylin, then dehydrated through ascending graded alcohols, cleared in xylene, and mounted using depex.

2.5 WESTERN IMMUNOBLOT

All primary and secondary antibody dilutions for Western immunoblotting are in tables 2.3 and 2.4.

2.5.1 Protein extraction

Cell cultures for protein extraction were grown in 6-well tissue culture plates or 100 mm petri dishes. Each vessel routinely contained a coverslip that was fixed and stained with H&E to compare morphological changes with any changes in protein expression. Remaining cells were washed twice in ice-cold PBS then incubated on ice with radioimmuno precipitation assay (RIPA) cell lysis buffer (Appendix B) containing protease and phosphatase inhibitors (10 µg/mL leupeptin, 10 µg/mL aprotinin, 100 µg/mL phenylmethanesulphonyl fluoride, 1 mM sodium vanadate) for 5 min. Cells were scrapped to one side and transferred to a sterile 1.5 mL Eppendorf tube. To ensure complete lysis and disruption of cell membranes, cells underwent probed sonication twice for 5 sec each. Cell debris was removed by centrifugation at 13,000 rpm for 20 min at 4 ºC. Mouse kidney tissue for protein extraction was snap frozen in liquid nitrogen at time of harvest and stored at -80 ºC. Kidney tissue (approximately 0.1 g) was transferred to a 5 mL flat bottom specimen container and suspended in 1 mL RIPA lysis buffer and with the additives mentioned above. Tissue was homogenised with an electric motorised tissue homogeniser for 10 sec X 2. To ensure complete disruption of cell membranes, homogenates were probe-sonicated twice for 5 sec. Cell debris was removed by centrifugation at 13,000 rpm for 20 min at 4 ºC. Centrifugation was repeated for tissue homogenates owing to the large amount of cell debris. Protein concentration was determined by the BCA protein assay and spectroscopy.

2.5.2 BCA protein assay

The Pierce BCA Protein Assay Kit (Pierce Chemical Co cat. no. 23227) was used. The BCA Working Reagent (WR) was prepared by mixing 50 units of BCA Reagent A with 1 unit of BCA Reagent B. The total volume of WR required was calculated by (number of standards + number of unknowns) x (number of replicated) x (200 µL of WR per sample). The following microplate procedure was used: 20 µL of each standard replicate was pipetted into a microplate well. The working range of the standards was 20-2,000 µg/mL and the amount per well was 50, 37.5, 25, 18.75, 12.5, 6.25, 3.125, 0.625, and 1 µg. Sample volumes of 2-5 µL were used depending upon the available lysate volume. 200 µL of the WR were added to each well. The plate was incubated at 37 ºC for 30 min then removed from the incubator and allowed to cool to RT. Absorbance was read at 562 nm using a Labsystems iEMS Reader MF (Thermo, Helsinki, Finland). GraphPad Prism 5 or 6

was used to generate a BCA standard curve and polynomial fourth order function to calculate each sample protein concentration.

Table 2.3: Primary antibodies used in Western immunoblotting

Primary Antibody	Supplier Ab name	Ab Source	Supplier	Catalogue Number	Western dilution
Bax	Bax (P-19)	Rabbit (polyclonal)	Santa Cruz	sc-526	1:1000
Bcl-X_L	Bcl-X_L	Rabbit (polyclonal)	Santa Cruz	sc-7195	1:1000
GAPDH	GAPDH	Rabbit (polyclonal)	Sigma	G9545	1:10000
HO-1	HO-1	Rabbit (polyclonal)	Abcam	ab13243	1:1000
Keap1	KEAP1	Rabbit (polyclonal)	Aviva Systems Biology	ARP38981_P050	1:1000
LC3β	MAP LC3β (N-20)	Goat (polyclonal)	Santa Cruz	sc-16755	1:1000
Nrf2-α	GABPA	Rabbit (polyclonal)	Aviva Systems Biology	P100832_T100	1:1000
Nrf2-β	GABPB2	Rabbit (polyclonal)	Aviva Systems Biology	P100925_P050	1:1000
p16	p16	Mouse (monoclonal)	Santa Cruz	sc-9968	1:1000
p62	SQSTM1 (D-3)	Mouse (monoclonal)	Santa Cruz	sc-28359	1:1000
$p66^{shc}$	p66Shc	Rabbit (polyclonal)	Upstate Biotechnologies	07-150	1:1000
Park2	Park2	Rabbit (polyclonal)	Aviva Systems Biology	ARP43038_P050	1:1000
PGC-1α	PGC-1 alpha	Rabbit (polyclonal)	Novas Biologicals	NBP1-04676SS	1:1000
PPARα	PPARα (H-98)	Rabbit (polyclonal)	Santa Cruz	sc-9000	1:500
p-PPARγ	p-PPARγ (Ser 112)-R	Rabbit (polyclonal)	Santa Cruz	sc-28001-R	1:100
PPARγ	PPARγ (H-100)	Rabbit (polyclonal)	Santa Cruz	sc-7196	1:1000
SOD-2	SOD2	Rabbit (polyclonal)	Aviva Systems Biology	ARP58529_P050	1:5000
TGF-β1	TFG β1 (V)	Rabbit (polyclonal)	Santa Cruz	sc-146	1:1000

Table 2.4: Secondary antibodies used in Western immunoblotting

Secondary Antibody	Supplier	Catalogue Number	Western Dilution
Goat Anti-Rabbit IgG (H+L) HRP conjugate	Invitrogen	G21234	1:2000
Rabbit Anti-Mouse IgG (H+L) HRP	Invitrogen	61-6420	1:2000
Rabbit Anti-Goat IgG (H+L) HRP	Invitrogen	81-1620	1:2000

Ab = antibody; appropriate dilutions for both primary and secondary antibodies and suppliers are included for all proteins. Primary antibody refers to the protein of interest referred to within text, and the supplier antibody name refers to the technical name of the antibody specified within a datasheet, which is commonly a synonym.

2.5.3 SDS-PAGE, Western immuno-transfer and protein visualisation

Lysates were resolved using 10 % sodium dodecyl sulphate polyacrylamide gel electrophoresis (SDS-PAGE) with either 10 or 15 lanes per gel. Using protein extracts from cells and kidney homogenates, 20-50 µg of total protein were loaded onto each gel lane. Electrophoresis was at 30 mA/gel until the band of protein was observed to reach the bottom of the gel. Protein was then transferred to a PVDF membrane using a Bio-Rad Mini Protean 3 unit (Bio-Rad Laboratories Pty Ltd, Gladesville, Australia). At this stage, PVDF membranes were stained using Ponceau Solution to visualise and confirm the protein transfer as well as check for even distribution of protein between lanes. If an error was visualised, the protocol was halted at this step. Non-specific binding of antibodies to the membrane was inhibited by incubation in 5 % skim milk powder in Tis buffered saline-Tween 20 (TBST) buffer (blotto) (Appendix B) for 1 h with continuous rocking. Primary antibodies were prepared in 1 % blotto solution and incubated overnight at 4 ºC on a continual rotator. Information on antibodies and their dilutions are presented in Table 2.2. Probed membranes were washed 3 X 5 min in TBST then incubated with the appropriate secondary antibody diluted in 1 % blotto for 1 h at RT with continuous motion. Membranes were washed 3 X 5 min in TBST before having Supersignal West Pico chemiluminescent substrate (Pierce Chemical Co., Rockford, Illinois, USA; cat. no. 1859674 and 1859675) added after being placed in a developing cassette. Protein bands were detected using enhanced chemiluminescence (ECL) imaging onto X-ray film (Kodak X-Omat AR-5 or Fuji Rx XR Film) and scanned using a Canon Canoscan 8400F at 300 dpi. Scion Image software version Alpha 4.0.3.2 or ImageJ (1.46r, National Institutes of Health, USA) was used to quantify the density of the bands in arbitrary densitometry units (ADU). Even loading of lanes (protein loading control) was assessed using glyceraldehyde 3-phosphate dehydrogenase (GAPDH) immunoblots. These were also used to normalise densitometry from the same membrane following stripping of the probed antibody. Membrane stripping involved adding the probed membrane to stripping buffer (1 M Tris, 20% SDS, 14.3 M β-mercaptoethanol) at 50 ºC for 30 min.

2.6 *IN VIVO* STUDIES

2.6.1 Animals

Male C57Bl6 mice weighing 20-30 g were purchased from The University of Queensland Biological Resource Facility. Mice were housed at the University of Queensland Biological Resource Facility at the Translational Research Institute and Princess Alexandra Hospital campuses. Animals were housed with 12 h light - 12 h dark and unlimited access to food and water during normal conditions. Diet was regulated during NAC antioxidant therapy studies.

2.6.2 Surgical procedure and ischaemia-reperfusion model

For the ischaemia-reperfusion (IR) experiments, 20-30 g mice (4-6 weeks old) were anaesthetised using a ketamine/xylazine combination (10 mg/mL and 1 mg/mL, respectively) administered via intra-peritoneal injection at a dose of 10 μL/g body weight. Mice were shaved on the left and right flanks, placed on a heated pad (38 °C), moistened eye lubricant and gauze were placed over the eyes, and the kidney on the left side was exposed using a flank incision through the skin and the muscle layers. The renal artery was cleared of fat and a non-traumatic vascular microclamp was placed over the vessels for 20 min. Vessel occlusion was confirmed by darkening of the kidney. The kidney was placed within the body cavity and moistened gauze was placed over this skin incision. The mouse was turned to its right side, and the procedure repeated. The second skin incision was covered with moistened gauze. Following 20 min of left renal vessel occlusion, the microclamp was removed from the left side, and the animal turned to remove the microclamp from the right side (approximately 20 min occlusion). In each case, reflow to the kidney was confirmed by a return to normal colour of the kidney. For chronic injury in the kidney, the muscle and skin incisions were sutured with 4-0 silk, and mice were allowed to recover for 21 days. 21 days was selected for chronic injury from our previous research into IR-induced injury in rodents which show progression to chronic injury at 14 and 28 days (Gobe *et al.*, 1990; Gobe *et al.*, 2014). In addition, we calculated that 21 days in a mouse was equivalent in a human to 2 years.

2.6.3 Intravital multiphoton microscopy of kidney ischaemia-reperfusion

After anaesthesia was obtained, the animal was shaved on the left and right flank. Surgical procedure was carried out on a heating platform set to 38 °C. The left kidney was externalised by making a small incision on the left flank through the retroperitoneum. For intravital imaging during ischaemia (when the microclamp is on) and during initial reperfusion (when the microclamp is just released) only the left kidney was externalised to prevent major trauma to the mouse and excess

body temperature loss. Renal vessels were occluded (as described in Section 2.4.1) and the mouse was moved to the multiphoton microscope (MPM) stage making sure to place the kidney over the objective bathed in dH_2O. A heated jacket was placed over the mouse to maintain the normal body temperature (heated jacket at 38 °C) and images of the ischaemic kidney were acquired over 20 min from when the microclamp was attached. Intravital imaging during initial reperfusion was performed by releasing the microclamp following the 20 min renal ischaemia period, then quickly replacing the mouse to the microscope stage with the reperfused kidney over the objective bathed in warm dH_2O and covering with the heated jacket. Images were acquired over 40 min from when the clamp was removed. Both left and right kidneys from healthy control mice and 21-day IR mice were imaged by the same procedure, with clamping omitted at the time of MPM.

2.6.4 Intravital mitochondrial function assessment

Tetramethylrhodamine methyl ester (TMRM) was infused intravenously (iv) and visualised via MPM to determine mitochondrial health following 21-days post IR injury. TMRM is a cell-permeant, cationic fluorophore that is readily sequestered by active mitochondria with a polarised membrane potential. TMRM is ideal for MPM since the excitation wavelength does not overlap with NADH endogenous fluorescence excitation that commonly occurs with other mitochondrial membrane potential-dependant fluorescent probes (Hall *et al.*, 2013). Prior to infusion, mice were prepared as previously described (Section 2.4.2) and images were captured at 740 nm (NADH) (Figure 2.2) and 800 nm (TMRM) excitation to gain a matched background signal. 20 µL of a 5 µg/mL TMRM solution prepared in 0.9% saline or PBS, was infused into the tail vein. This volume and concentration would result in 0.1 µg/mL plasma concentration of TMRM. The kidneys were then immediately imaged with MPM. Z-stack images were acquired shortly after infusion at both 740 nm and 800 nm excitation in at least three separate fields per kidney.

2.6.5 Intravital MPM image acquisition and analysis

Images were captured using a X20 objective on a Nikon Ti Eclipse - LaVision MPM (LaVision BioTec GmbH, Bielefeld, Germany) equipped with an ultrashort (85 fs pulse width) pulsed mode-locked 80 MHz Titanium:Sapphire MaiTai laser (Spectra Physics, Mountain View, USA) and ImSpector Pro software. The excitation wavelength was set to 740 nm for NADH fluorescence, 900 nm for collagen (Figure 2.3) via second harmonic generation (SHG), and 800 nm for TMRM. For TMRM experiments, using only control and 21-day post IR injury mice, background readings were obtained at 740 nm and 800 nm excitation prior to TMRM infusion. Emitted light was collected using three photomultiplier tube filters: 447 nm – 460 nm (blue), 485 nm – 550 nm (green), 575 nm – 630 nm (red). The objective was placed in a field of view that visualised detailed tubular

structures and serial (30-50) penetrating slice images were acquired from the renal cortex to a depth of 50-70 μm. A minimum of three fields of view per kidney was obtained. The image analysis software Imaris x64 7.6.0 (Bitplane Scientific Software, Zurich, Switzerland) was used to adjust the minimum and maximum exposure settings consistently throughout all acquired images for standardised quantification of fluorescence intensity. ImageJ (1.46r, National Institutes of Health, USA) was used to obtain mean fluorescent intensity values for NADH and TMRM detected fluorescence. For each of the three fields captured per kidney, the epithelial layer of definitive continuous tubules were selected and measured for mean intensity. Eight tubules per z-slice image were measured from five selected z-slice images per z-stack.

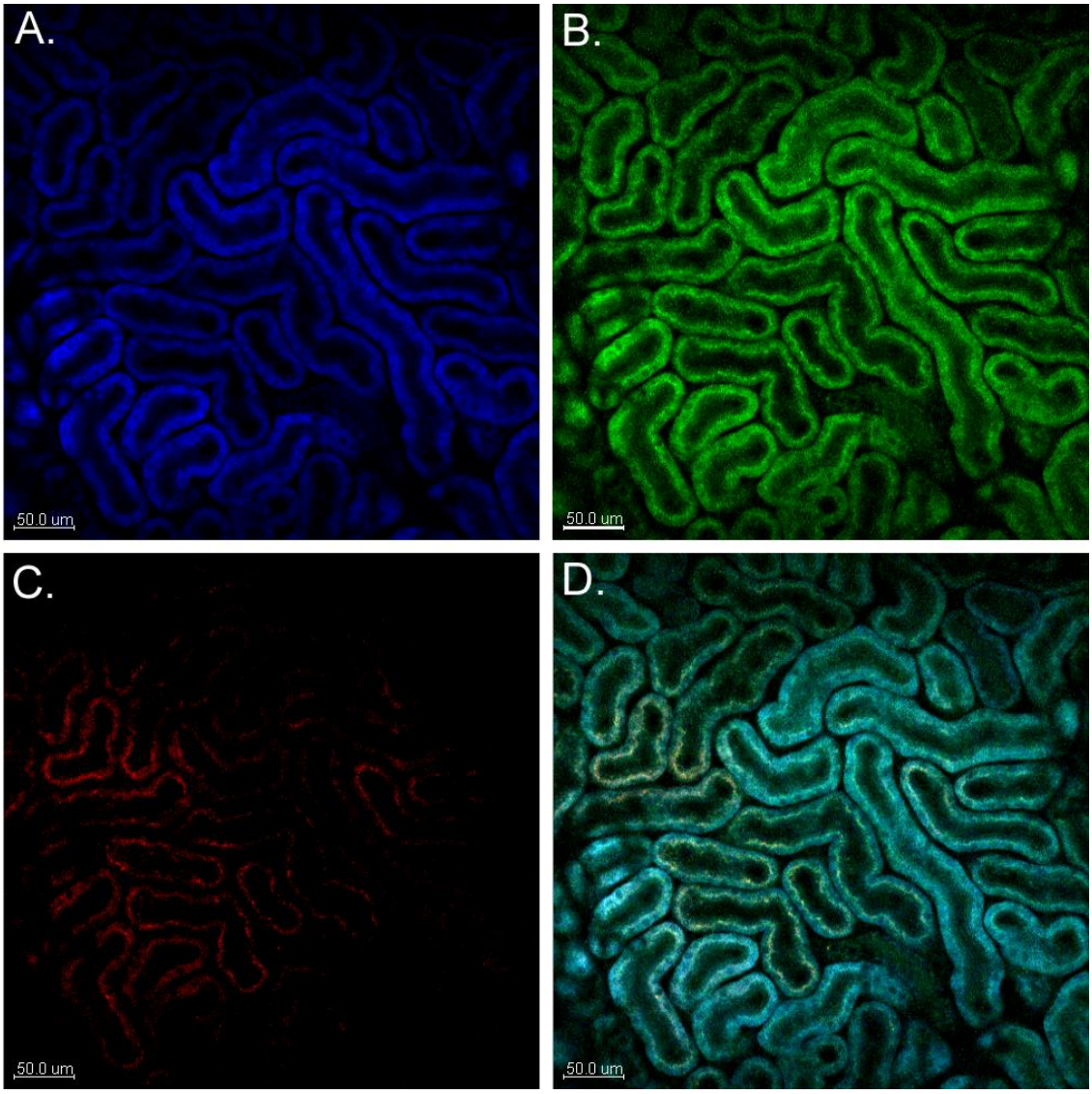

Figure 2.2: 740 nm excitation MPM of intravital mouse kidney cortex
Representative healthy control kidney from mouse exciting fluorescence at 740 nm and detecting emission in three channels: Blue (A.); 447 nm – 460 nm. Green (B.); 485 nm – 550 nm. Red (C.); 575 nm – 630 nm (red). (D.) depicts a combined image from all three channels. Image was captured 29 µm below renal capsule.

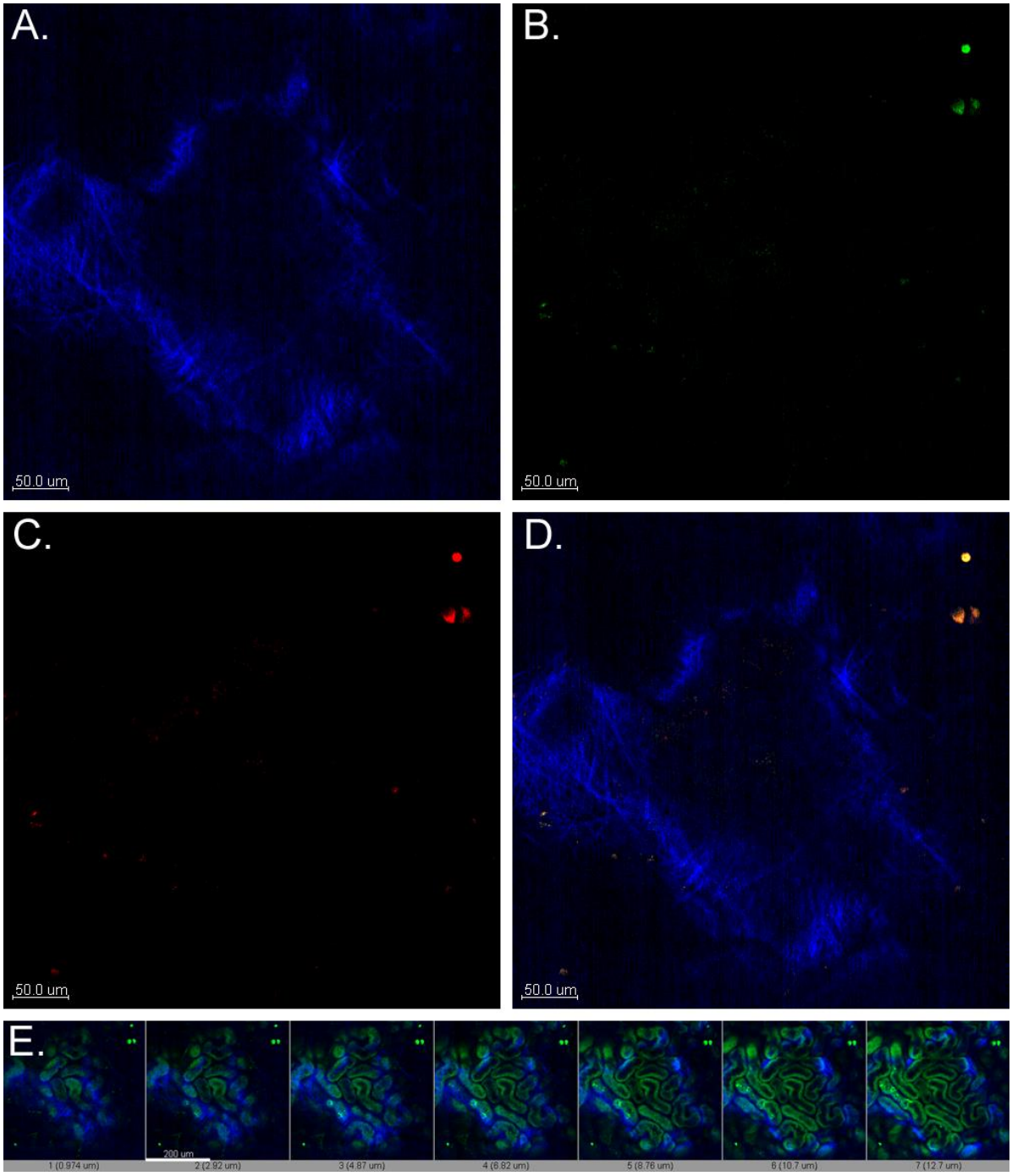

Figure 2.3: 900 nm excitation MPM of intravital mouse kidney capsule and cortex
Representative healthy control kidney from mouse exciting fluorescence at 900 nm and detecting emission in three channels: Blue (A.); 447 nm – 460 nm. Green (B.); 485 nm – 550 nm. Red (C.); 575 nm – 630 nm (red). (D.) depicts a combined image from all three channels. A-D images were captured 6.82 µm below outermost capsule which can be visualised in sequential slice images (E.).

2.6.6 Multiphoton fluorescence lifetime imaging microscopy

Dr Washington Y Sanchez performed and provided expert assistance with kidney FLIM experiments. FLIM was performed on mouse kidney post-sacrifice. Kidneys were harvested after euthanasia of the mice, and placed on ice. A custom-made kidney section apparatus was used to slice 1 mm thick sections through the middle of a coronal section from the kidney. The section was placed on a glass microscopy slide with an overlying glass coverslip taped down for stabilisation (Fig 2.4). Three areas each from both cortex and medulla were captured for FLIM data per kidney. Time from death to first image capture was no more than 30 min. Images were captured using a DermaInspect system (JenLab GmbH, Jena, Germany) equipped with an ultrashort (85 fs pulse width) pulsed mode-locked 80 MHz Titanium:Sapphire MaiTai laser (Spectra Physics, 25 Mountain View, USA). The excitation wavelength was set to 740 nm for kidney autofluorescence with an emission signal range of 350 to 650 nm established through the use of a BG39 bandpass filter. Images were recorded with a 40 x objective. The laser power was set to 15 mW and the acquisition time for obtaining images was 13.4 s per frame. FLIM data were collected with a time-correlated single-photon counting (TCSPC) SPC-830 detector (Becker & Hickl GmbH, Berlin, Germany) integrated into the DermaInspect MPM system. The TCSPC module assembles a photon distribution of the scan area across the χ and Υ coordinates taken from four photon counters, with only three used for this project. The model determines the time of arrival for each photon detected within the fluorescence decay. Fluorescence emission was spectrally resolved between three linearly-arranged photon counters through the use of three dichroic filters in the beam path, spectrally dividing the emission light into three channels for each photon counter: 350 to 450 nm (reduced nicotinamide adenine dinucleotide phosphate – NAD(P)H), 450 to 515 nm (NAD(P)H, flavin adenine dinucleotide phosphate – FAD), and 515 to 610 nm (FAD). Each FLIM image was collected at an exposure of 13.4 s and acquisition image size of 214 x 214 μm.

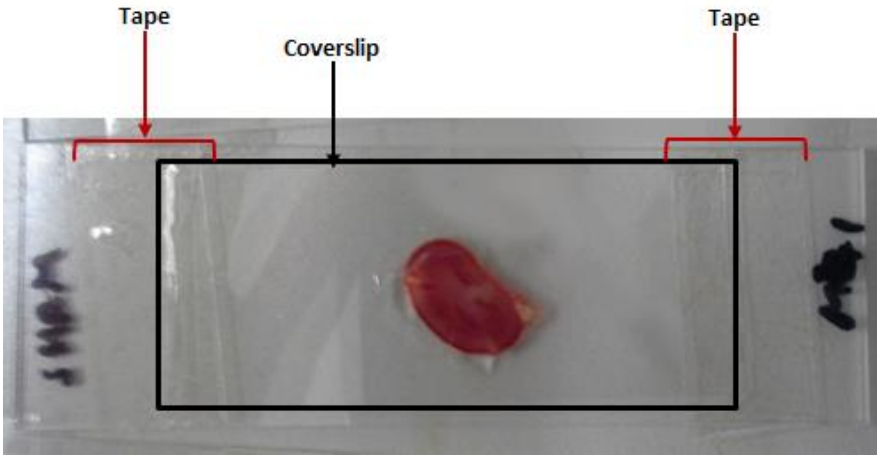

Figure 2.4: Mouse kidney section preparation for MPM FLIM microscopy
A 1 mm thick coronal section of a freshly harvested mouse kidney was placed onto a glass microscopy slide. A glass coverslip was overlaid on the kidney slice and adhered to the slide by adhesive tape.

2.6.7 FLIM data analysis

FLIM data analysis was performed using SPCImage 4.8 (Becker and Hickl GmbH). FLIM data are composed of an array of pixels containing several time channels distributed across the fluorescence decay curve. The decay curve represents a sum of multiple exponentials, or components, as each pixel contains an overlay of fluorescence from several endogenous fluorophores at various conformations. A double-exponential decay model function was used. The fitted decay curve establishes two lifetimes: the short (τ_1) and long (τ_2) fluorescence decay lifetimes (ps) and with corresponding relative amplitude coefficients α_1 and α_2 (%), respectively. The lifetime of NAD(P)H is resolved as a two-component system with the short (~0.3-4 ns) and long (~2.3 ns) lifetime represented as the free and protein-bound conformations, respectively (Lakowicz *et al.*, 1992; Niesner *et al.*, 2004; Berezin and Achilefu, 2010). The free-to-bound ratio of NAD(P)H, represented by the ratio of the amplitude coefficients for the short and long lifetimes (i.e. α_1/α_2), is related to the NADH/NAD+ ratio and was used as an indicator for redox changes within the cell (Bird *et al.*, 2005).

2.7 CLINICAL STUDIES

2.7.1 Study design

This study was a substudy of an ongoing open-label randomised controlled trial, known as the LANDMARK-III trial (Longitudinal Assessment of Numerous Discrete Modifications of Atherosclerotic Risk Factors in Kidney Disease). LANDMARK-III is a 3-year study comparing the effect of a nurse practitioner-led model of care with standard nephrology care on cardiovascular risk

factors. Patients were screened at the Princess Alexandra Hospital Nephrology Department, Brisbane, Australia.

2.7.2 Participants

Patients were eligible for inclusion if they were aged 18-75 years, had moderate CKD (eGFR 25-60 ml/min/1.73 m^2), and had one or more uncontrolled yet modifiable cardiovascular risk factors that were: blood pressure (BP) exceeding target (>130/80 mmHg, or >120/75 mmHg for those with diabetes or proteinuria > 1 g/ 24 h), overweight (body mass index [BMI] >25 kg/m^2), poor diabetic control (haemoglobin A1c [HbA1c] >7%), or hyperlipidaemia (low-density lipoprotein [LDL-C] <2.5 or <2.0 mmol/L in those with diabetes or existing coronary heart disease). Exclusion criteria were: intervention for, or symptomatic, coronary artery disease (within 3 months), current heart failure (according to New York Heart Association class III and IV) or significant valvular heart disease, pregnant or planning to become pregnant, previous kidney transplant, and life expectancy or anticipated time to dialysis or transplant <6 months. Participants provided written informed consent and the study complied with the Declaration of Helsinki.

2.7.3 Patients groups

2.7.3.1 Control group

The control group received standard nephrology care, which included review by a nephrologist, recommended lifestyle modification but no specific information or education, and referral to an allied health professional on an *ad hoc* basis.

2.7.3.2 Exercise and Lifestyle intervention group

In addition to standard nephrology care, cardiovascular risk factor management was provided by a multidisciplinary clinic including a CKD nurse practitioner, dietician, exercise physiologist, diabetic educator, psychologist, and social worker to target risk factors to national guidelines (Johnson, 2007; NHF, 2010). The exercise-training component involved 150 min of moderate intensity exercise per week, with 8 weeks of training supervised by an accredited clinical exercise physiologist. Patients attended gym sessions two to three times per week. The sessions included a warm-up, 20-30 min of aerobic activity using a treadmill, stationary bike, or rowing ergometer, and whole body resistance training with machines and free weights. On completion of the gym-based training, patients began a home-based program and were provided a booklet depicting resistance exercise using Thera-Bands and a Swiss ball. Regular contact was maintained *via* telephone and Email. Participants were questioned on their ability to maintain the prescribed exercise and if they identified difficulty, they were encouraged to attend gym-based refresher visits. Patients performed

exercise at a moderate intensity, with perceived exertion of 11-13 on a 20-point Borg scale (include reference), and was tailored individually. Patients also underwent 4 weeks of group behaviour and lifestyle modification facilitated by a dietician and psychologist. The program focused on sustainable diet and behaviour change to assist with weight loss. The dietician therapy complied with the Evidence-Based Practice Guidelines for Nutritional Management of CKD for patients with eGFR between 25 and 60 mL/min/1.73 m^2 (Ash *et al.*, 2006).

2.7.4 Sample collection and handling

Venous blood (10 mL) samples were collected following an overnight fast using ethylenediaminetetraacetic acid (EDTA) vacucontainers (BD Diagnostics, NJ, USA). For oxidative stress analysis (isoprostanes, GPX, and TAC), samples were stored on ice before being centrifuged at 2000g at 4 ºC for 10 min. Plasma was separated and stored at -80 ˚C with BHT (10 µL of 100 mM to each 1.5 mL Eppendorf tube) to prevent artifactual oxidation. Routine blood biochemistry and additional blood measures of lipids, haemoglobin, phosphate, creatinine, C-reactive protein (CRP), albumin, glucose and insulin were conducted using standard laboratory techniques by Queensland Health Pathology Service at the Princess Alexandra Hospital (Woolloongabba, Brisbane, Australia). The Modification of Diet in Renal Disease-175 formula (Levey *et al.*, 2006) was used to estimate eGFR and insulin resistance was computed using the homeostatic model assessment of insulin resistance method (Matthews *et al.*, 1985).

2.7.5 F_2-isoprostanes assay

Dr David Briskey, in the laboratory of Prof Jeff Coombes (School of Human Movement Studies, University of Queensland), was responsible for performing all measurements for isoprostanes. Detailed methods outlining the development and troubleshooting of the method used to measure plasma F_2-isoporostanes have been published (Briskey *et al.*, 2014). Briefly, a liquid-liquid extraction method prior to determination of total isoprostanes using negative chemical ionization gas chromatography-tandem mass spectroscopy in plasma was used. F_2-isoprostane extraction involved vortexing the plasma sample with the internal standard (8-iso-$PGF_{2\alpha}$-d_4), methanolic sodium hydroxide (NaOH) for saponification and dH_2O for 5 sec, then incubating in a water bath at 42 ºC for 60 min before placing on ice for 10 min. Proteins were precipitated out of the solution by adjusting to pH 3 using 3 M HCl and vortexing for 5 sec. Neutral lipids were then removed by adding hexane, gently mixing on a circular mixer at 20-30 rpm for 10 min, centrifuging (3000 x g) for 10 min at RT, then removing the supernatant using a glass Pasteur pipette into a clean glass tube. Extracts were dried under nitrogen stream at 40 ºC until completely dry. Dry extracts were

then reconstituted in acetonitrile and vortexed for 5 sec before being transferred into silonized glass inserts where they were again dried under a nitrogen stream at 40 ºC prior to derivatization. Derivatization involved adding pentafluorobenzylbromide (10% in acetonitrile) and di-isopropylethylamine (10% in acetonitrile) to the extract, vortexing for 5 sec, and incubating at RT for 30 min to allow the reaction to proceed. Extracts were then dried for 30 min under nitrogen gas before being mixed with anhydrous pyridine and bis-(trimethylsily)trifluoroacetamide and trimethylchlorosilane (99:1), vortexed for 5 sec and incubated for 20 min at 45 ºC. Anhydrous hexane was added to the extract prior to loading into an autosampler carrier vial. Gas chromatography-tandem mass spectroscopy (GC-MS) was used to analyse samples for total isoprostane concentration using a Varian 320 MS/MS, with Varian 450 gas chromatograph equipped with a CP8400 auto sampler. The Varian MS Workstation System control software version 6.9.2 (Varian, Agilent.com) was used to analyse the data. 1 µL of sample was introduced in splitless mode (entire sample) using a 10 µL Hamilton syringe. After 1 min the injector port was switched to a 1:20 split. A Varian FactorFour Capillary Column (VF5 MS 30 m x 0.25 mm ID, DF-0.25) using helium as the carrier gas at a flow rate of 1.0 mL/min with the injector operated at 250 ºC was used. The column oven was started at 160 ºC for 1 min before being increased by 20 ºC at 1 min intervals to reach 300 ºC where it was held for 10 min. The total column oven run time is 18 min with the isoprostane peak eluted at approximately 9-10 min. The mode was set to run in negative chemical ionization mode at 70 eV. The chemical ionisation gas and collision gas was argon run at an ion source pressure of 4.20 Torr and 2.00 mTorr, respectively. The mass spectrometer was operating at a transfer line temperature of 250 ºC, ion volume temperature of 200 ºC, and collision energy of 17 V. The detector operated at 1700 V. The peak identification of isoprostanes within a sample was established by comparing the retention time and the fragmentation pattern of a standard and deuterated standard. The mass size and transition of isoprostanes and the respective deuterated standard were established at *m/z* 569.3/299.3 and 573.3/303.3 respectively.

Final total isoprostane concentrations were calculated by producing a standard curve by injecting known amounts of F_2-isoprostane (200, 400 and 800 pg/ml) and F_2-isoprostanes-d_4 (internal standard). Comparing the ratio of internal standard to isoprostanes in both the aqueous standards and biological samples allows for quantification of the total isoprostanes. Percentage recovery of the internal standard added to biological samples compared to the aqueous standards determined the efficiency of the of the extraction process. Internal standard addition to each biological sample allows for the variability in recovery of every sample to be accounted for. This assay was validated by determining the average coefficient of variance of over 1000 different samples analysed in duplicate over 12 months. Pooled samples from “sick” individuals (chronic disease patients who

have plasma samples that would otherwise be discarded, and typically have high isoprostanes levels) and young healthy individuals (typically have low isoprostanes), acted as high and low quality control (QC) samples, respectively. QC samples were extracted in conjunction with study samples at the time of assay. Accuracy was assessed by comparing plasma samples spiked with known amounts of isoprostanes, and analysed in duplicate on multiple occasions. F_2-isoprostane concentrations were separately quantified in these samples, unspiked samples and aqueous standards (Briskey *et al.*, 2014).

2.7.6 Glutathione peroxidase assay

GPX was measured from plasma using slightly modified published methods (Wheeler *et al.*, 1990; Andersen *et al.*, 1997). This assay is based on the oxidation of NADPH following the reduction of t-butyl hydroperoxide. The oxidation of NADPH to NADP+ is accompanied by a decrease in absorbance at 340 nm and the rate of this decrease is proportional to the GPX activity in the sample. An automated assay was performed using the COBAS MIRA system (Roche Diagnostics, Australia) following sample and reagent preparation. Briefly, each sample was incubated for 50 sec with the sample reagent consisting of 0.25 mM NADPH, 0.205 units/mg glutathione reductase, 1.01 mM glutathione in Tris-HCl buffer (0.1 M Tris, 0.5 mM EDTA sodium salt, pH 7.55). The reaction was started by the addition of 0.13% aqueous t-butyl hydroperoxide and absorbance at 340 nm was recorded for 450 sec. High and low QC samples were run simultaneously with patient samples and acted as internal controls for accuracy and validity. The linear portions of the absorbance curves were identified between two time points and were kept consistent for all calculations to determine the difference in absorbance over time. Sample absorbance per minute was converted to GPX units (U) to incorporate total volume in the cuvette (225 µL) and the molar extinction coefficient of NADPH (6.22×10^3 $L.mol^{-1}.cm^{-1}$).

2.7.7 Total antioxidant capacity assay

TAC of patient plasma was measured using a similar method to that described previously (Rice-Evans and Miller, 1994). The principle of this assay is based on the inhibition of the absorbance of the radical cation, 2,2'-azinobis(3-ethylbenzothiazoline 6-sulfonate) ($ABTS^+$) from any substance within plasma that possesses antioxidant properties. The $ABTS^+$ cation is formed by the interaction of ABTS with the ferrylmyoglobin radical species that is generated by the activation of metmyoglobin with H_2O_2. Antioxidant compounds suppress the absorbance of $ABTS^+$ to an extent that is dependent on time and the antioxidant capacity within the serum. The assay was performed in conjunction with Trolox standards prepared in PBS (0 mM – 2.5 mM at 0.5 mM intervals). Briefly, samples and Trolox standards were added to a 150 µM ABTS and 2.5 µM metmyoglobin

solution in PBS prior to starting the reaction with the addition of 75 µM H_2O_2. Absorbance was measured at 734 nm prior to H_2O_2 addition and 6 min after. Trolox standards were plotted as concentration versus change in absorbance at 734 nm over 6 min. Sample absorbance change values were interpolated from the Trolox standard curve and expressed as the mM concentration of a Trolox solution having the antioxidant capacity equivalent to a 1 mM solution under investigation (mmol/L).

2.8 STATISTICS

Specific statistical analysis is outlined in the relevant research chapters. Briefly, for *in vitro* and mouse experiments, the measured parameters were expressed as mean ± SEM, and an independent samples t-test was utilised for comparison between two groups. A one way analysis of variance (ANOVA) was used for comparisons between more than two groups, and where relevant, a Tukey's post-hoc comparison. A two-way ANOVA was utilised to test the interaction between two independent variables, and where relevant, a Bonferroni's post-hoc comparison.

Dr Anne Bernard from QFAB Biostatistics, Translational Research Institute, Brisbane, Australia advised on statistical analysis regarding human clinical measures. Full statistical methods are outline in Chapter 7. Briefly, data were tested for normality using Shapiro-Wilk tests, and appropriate tests were performed on data following log transformation (expressed as natural logarithm, Log_e). Data were expressed as mean ± SD for normally distributed data, or median ± interquartile range for non-normally distributed data.

Statistical significance was determined at $p \leq 0.05$.

CHAPTER 3

In Vitro Model of Kidney Damage and the Role of Oxidative Stress

This chapter examines the separate, and cumulative, effects of cellular processes common to kidney diseases, namely, oxidative stress, mitochondrial dysfunction and cell senescence. The contents of this chapter have been published (Small *et al*., 2012, Appendix A). Below is a modification of that publication consistent with the format of this thesis.

3.1 INTRODUCTION

CKD affects approximately 10-15 % of the adult population in industrialized countries and the incidence of CKD, and its associated end stage disease, is increasing. Although diabetes and hypertension are known causes of CKD, ageing alone causes gradual loss of kidney function independent of any other pathology (Inagami, 2011). Oxidative stress increases with ageing (Finkel and Holbrook, 2000), and has been described in the pathogenesis of diabetes (Singh *et al.*, 2011) and hypertension (Carnicer *et al.*, 2012). Oxidative stress, as a significant cause of CKD and the associated loss of functioning renal mass, is still debated. Mitochondria are increasingly recognised as key participants in renal cellular metabolism (Cuttle *et al.*, 2001), including generation of energy in the form of ATP, regulation of calcium homeostasis (Vay *et al.*, 2009), tissue O_2 gradients, apoptosis (Madesh and Hajnoczky, 2001), and cell signalling (Soubannier and McBride, 2009). However, their contribution to CKD is largely unknown.

The kidney is a highly metabolic organ that relies heavily on oxidative phosphorylation, accounting for approximately 10 % of whole body O_2 consumption. Mitochondrial energy generates 95 % of required ATP for the kidney (Rieg and Vallon, 2009). The PTE cells, often most atrophic in CKD, contain many large active mitochondria (Hall *et al.*, 2009). A decrease in mitochondrial efficiency and subsequent cell function could have a significant impact on CKD development and renal failure. Mitochondria are also a major cellular producer of ROS and are themselves targets of ROS-mediated damage (St-Pierre *et al.*, 2002). Along the respiratory chain complexes of the inner mitochondrial membrane, reduction in molecular O_2 yields ROS mainly in the forms of $O_2^{\bullet}$- and H_2O_2. Defining mitochondrial dysfunction in the highly-metabolic PTE cells may hold a key to explaining how oxidative stress contributes to the pathogenesis of kidney diseases like CKD.

Cell senescence is commonly observed in CKD with increased levels of senescence-associated β-gal and lipofuscin granules predominately in tubular cells (Melk, 2003), and to a lesser extent in glomerular mesangial cells (Jiao *et al.*, 2012). Senescent kidney cells can die or persist in a damaged form, showing little function and an inability to proliferate (Stenvinkel and Larsson, 2013). Persisting senescent cells can compromise the healthy functioning of the kidney and reduce

the ability of the ageing nephron to cope with disease stresses, since it is the tissue in its whole form that accounts for function rather than individual cells. Senescent cells have been shown to secrete multiple pro-inflammatory growth factors, cytokines and chemokines (Campisi and d'Adda, 2007) therefore promoting inflammation, but also presenting promising targets to inhibit the many co-morbid conditions associated with inflammation in CKD. Oxidative stress itself can induce premature senescence in non-renal cells: in fibroblast cultures (Frippiat *et al.*, 2001); and in retinal epithelium during macular degeneration (Glotin *et al.*, 2008). Senescing cells undergo irreversible cell cycle arrest, mainly in G1 phase, have increased β-gal activity, and up-regulation of cyclin-dependent kinase inhibitors, like $p16^{ink4a}$ (Stein *et al.*, 1999). Oxidative stress may cause premature senescence of kidney cells in CKD. However, the mechanisms underlying mitochondrial dysfunction and subsequent oxidative stress-induced premature senescence in the kidney remain largely undefined. We had previously demonstrated that protecting the mitochondria in renal PTE protects these cells from increasing apoptosis (Cuttle *et al.*, 2001). The aim of the current study was, therefore, to use an *in vitro* model to investigate the separate and cumulative effects of oxidative stress, mitochondrial dysfunction and cell senescence in promoting loss of renal tubular epithelium.

3.2 MATERIAL AND METHODS

Complete methods are outlined in Chapter 2. Below is a brief summary of the experimental materials and methods used specifically for this chapter.

3.2.1 Experimental design

HK-2 cells were grown in normal culture conditions outlined in Chapter 2. Following H_2O_2, apigenin (API) and NAC dose response studies, they were grown to 80-90 % confluence then treated for 18 h with 0.4 mM H_2O_2 for oxidative stress, and 100 µM API to induce renal cell senescence (Ryu *et al.*, 2006). DMSO as a vehicle control was <1 % in growth medium. NAC was used as an antioxidant as a pre- and co-treatment at 10 mM (N=3 replicates).

3.2.2 Determination of ATP, oxidative stress and cytotoxicity

ATP levels (luciferase-based bioluminescence assay, Promega, Sydney, Australia); lipid peroxidation with MDA (Bioxytech LPO-586 Assay, OxisResearch Products, Percipio Biosciences Inc., CA); and TAC (OxiSelect™ TAC Assay Kit, Cell Biolabs, San Diego, CA) were measured according to the manufacturers' protocols and with appropriate controls. As a measure of cytotoxicity, lactate dehydrogenase (LDH) was measured as a % of maximal LDH release from

cells treated with 5 mM H_2O_2 (Cytotoxicity Detection Kit^{PLUS}, Roche Diagnostics, Castle Hill, Australia).

3.2.3 Mitochondrial function

MitoTracker Red CMXRos (Invitrogen Australia) localises to mitochondria with healthy membrane potential, and fades as mitochondria lose membrane potential. HK-2 cells were incubated 30 min with 100 nM MitoTracker Red before being fixed in 4 % PF and mounted for microscopy (Vectashield anti-fade, Vecta Laboratories, East Brisbane, Australia). DAPI was used to label nuclei. A Zeiss 510 Meta confocal fluorescence microscope with Zen 2008 software (X63 oil lens; 579 nm) was used. Mean fluorescence intensity was analysed (Nikon FN-S2N fluorescence microscope, NIS Image software, X63 objective).

JC-1 is a fluorophore that has mitochondrial membrane potential-dependent accumulation in mitochondria. Decrease in red and increase in green fluorescence indicates mitochondrial membrane depolarisation. JC-1 (3 µM) was applied 30 min preceding H_2O_2 exposure and then for 1 h of 0.4 mM H_2O_2 or 1 mM H_2O_2 (as high oxidative stress control). Cells on coverslips were fixed (4 % PF) before being mounted on glass slides (Vectashield mounting medium with DAPI) and visualised at 590 nm (red), 529 nm (green) and 460 nm (blue) using confocal florescence microscopy (X 63 oil lens). For live cell imaging, HK-2 cells were seeded onto MatTek Corp (Ashland, MA) glass bottom dishes before JC-1 incubation. Cultures were placed in a live-cell imaging chamber (Zeiss Axiovert 200M Live Cell Imager) at 37 ^{o}C and 5 % CO_2 in air. A representative field was then visualised using confocal microscopy to assess background laser-induced fluorescence leaching. H_2O_2 treatment was then added to the cells and the same field photographed over 25 min at consecutive 5 min intervals.

3.2.4 Light and fluorescence microscopy

Cells were fixed in 4 % PF or 100 % ice-cold methanol for 30 min at 4 ^{o}C for H&E staining or fluorescence microscopy, respectively. H&E stained cells were assessed using the Aperio ScanScope XT system (Aperio Technologies, Vista, CA) for % apoptosis, mitosis and cell senescence by counting cells with noted morphological characteristics (Chapter 2, Section 2.3.3 – 2.3.4) in ten frames of cells (X 200 magnification; an approximate total of 800-1000 cells) for each treatment (Hughes and Gobe, 2007). The ApopTag® Peroxidase *In Situ* Apoptosis Detection Kit (Merck-Millipore Pty Ltd, Kilsyth, Victoria, Australia) was used for identifying and verifying apoptosis according to our published methods (Hughes and Gobe, 2007). Ki67 (Santa Cruz Biotechnology Inc, Santa Cruz, CA; 1:100) immunocytochemistry was used to assess proliferative

activity. Senescent cell morphology and SA-β-gal immunofluorescence (Cell Signalling Technologies, Danvers, USA; 1:500) for cell senescence were used in parallel. Senescent cells had reduced staining saturation (Chen and Ames, 1994) and were 3-4 times the diameter of control cells.

3.2.5 Western immunoblotting for Bax, Bcl-X_L and $p16^{Ink4a}$

Protein was extracted by lysing HK-2 cells in RIPA buffer and following an established protocol (Chapter 2, Section 2.5). Protein concentration was determined (Pierce BCA assay) and 40 µg of each protein separated (10 % SDS-polyacrylamide gel electrophoresis). Immunoblotting was performed against Bax (1:1000, Santa Cruz Biotechnology); Bcl-X_L (1:1000, Zymed); GAPDH (1:1000; Sigma); and $p16^{Ink4a}$ (1:100; gift from A/Prof. Brian Gabrielli) (Wang *et al.*, 1996). HRP-conjugated secondary antibodies were used. Protein bands were visualised using ECL. Scion Image software Alpha 4.0.3.2 was used for densitometry. GAPDH immunoblots were used to normalise densitometry.

3.2.6 Immuno-transmission electron microscopy (Bax)

TEM and immuno-gold labelling were used to assess subcellular localisation of Bax following H_2O_2 treatment. The protocol is outlined in Chapter 2, Section 2.3.8.

3.2.7 Statistical analysis

Values reported are means ± SEM. Data were analysed using ANOVA and Tukey's post hoc analysis, two-way ANOVA and Bonferroni's post hoc test, or student's *t*-test where appropriate, with statistical significance at $p<0.05$.

3.3 RESULTS

3.3.1 ATP, lipid peroxidation and total antioxidant capacity assays indicate oxidative stress with all treatments

API and H_2O_2, alone or in combination, significantly increased MDA ($p<0.05$; Fig. 3.1A) indicating oxidative stress. API, alone or in combination with H_2O_2, significantly reduced TAC ($p<0.05$; Fig. 3.1B), whereas H_2O_2 alone significantly increased TAC ($p<0.05$; Fig. 3.1B). Both API and H_2O_2 resulted in loss of ATP; however both treatments were necessary for a significant ATP loss compared to untreated controls (Fig. 3.1C).

3.3.2. Confocal fluorescence microscopy and live cell imaging indicate loss of mitochondrial function with all treatments

MitoTracker Red fluorescence was significantly reduced following API and/or H_2O_2 exposure (Figs 3.2A-E) ($p<0.05$). There was no additive effect when H_2O_2 was delivered with API. Live cell imaging captured the loss of mitochondrial membrane permeability in the kidney cells with oxidative stress (H_2O_2). Results of time lapse photography (Figs 3.2F-K) using JC-1 demonstrated healthy polarised mitochondrial membrane (red fluorescence) transitioning to green fluorescence and dysfunctional mitochondria. Fixed cells (JC1, Figs 3.2L-M) also showed mitochondrial depolarisation in response to oxidative stress. Concomitant apoptosis is indicated (arrow, Fig. 3.2M).

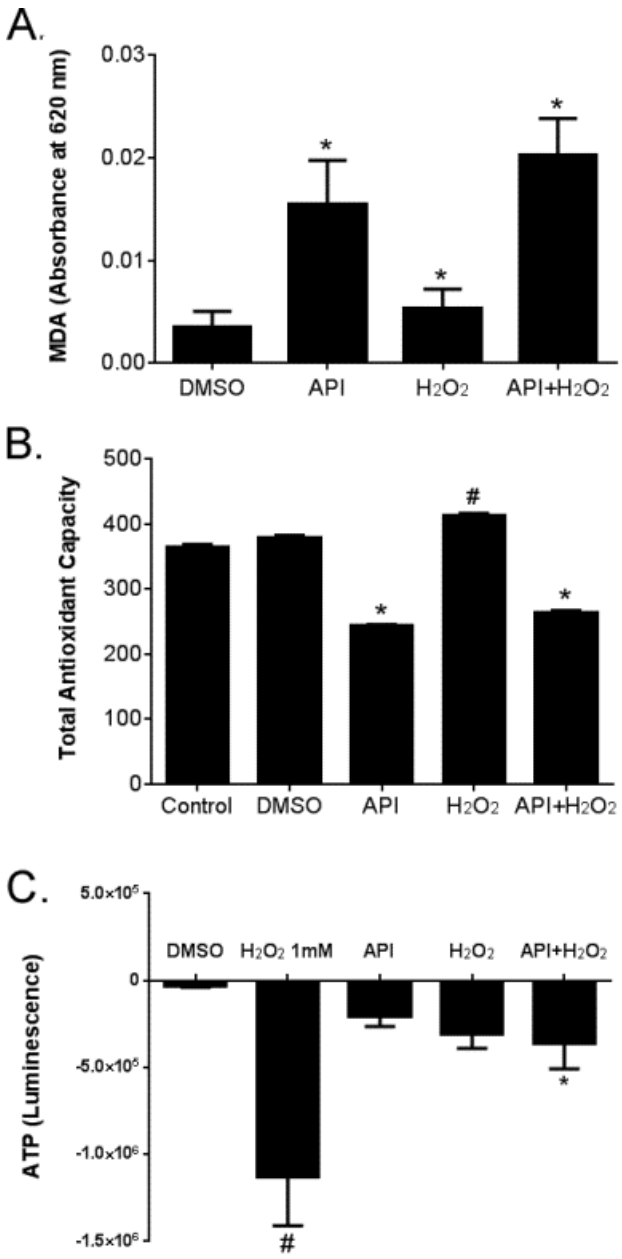

Figure 3.1: Lipid peroxidation, total antioxidant capacity and ATP generation following oxidative stress and cell senescence

In A, lipid peroxidation was measured by malondialdehyde (MDA) assay. Cells exposed to API, H_2O_2, or API+H_2O_2 had a significant increase in MDA compared to DMSO vehicle controls (*, $p<0.05$ compared to DMSO). In B, total antioxidant capacity was measured by colorimetric assay. Cells exposed to API or API+H_2O_2 had a significant reduction in total antioxidant capacity compared to DMSO controls. H_2O_2 induced a small but significant increase in total antioxidant capacity (*, $p<0.05$ compared to DMSO; #, $p<0.05$ compared to untreated controls). In C, ATP generation was measured by luminescence assay. 1 mM H_2O_2 was used to demonstrate maximal ATP loss. Compared with untreated controls, H_2O_2 caused the greatest ATP loss (*, $p<0.05$ compared to DMSO; #, $p<0.05$ compared to all).

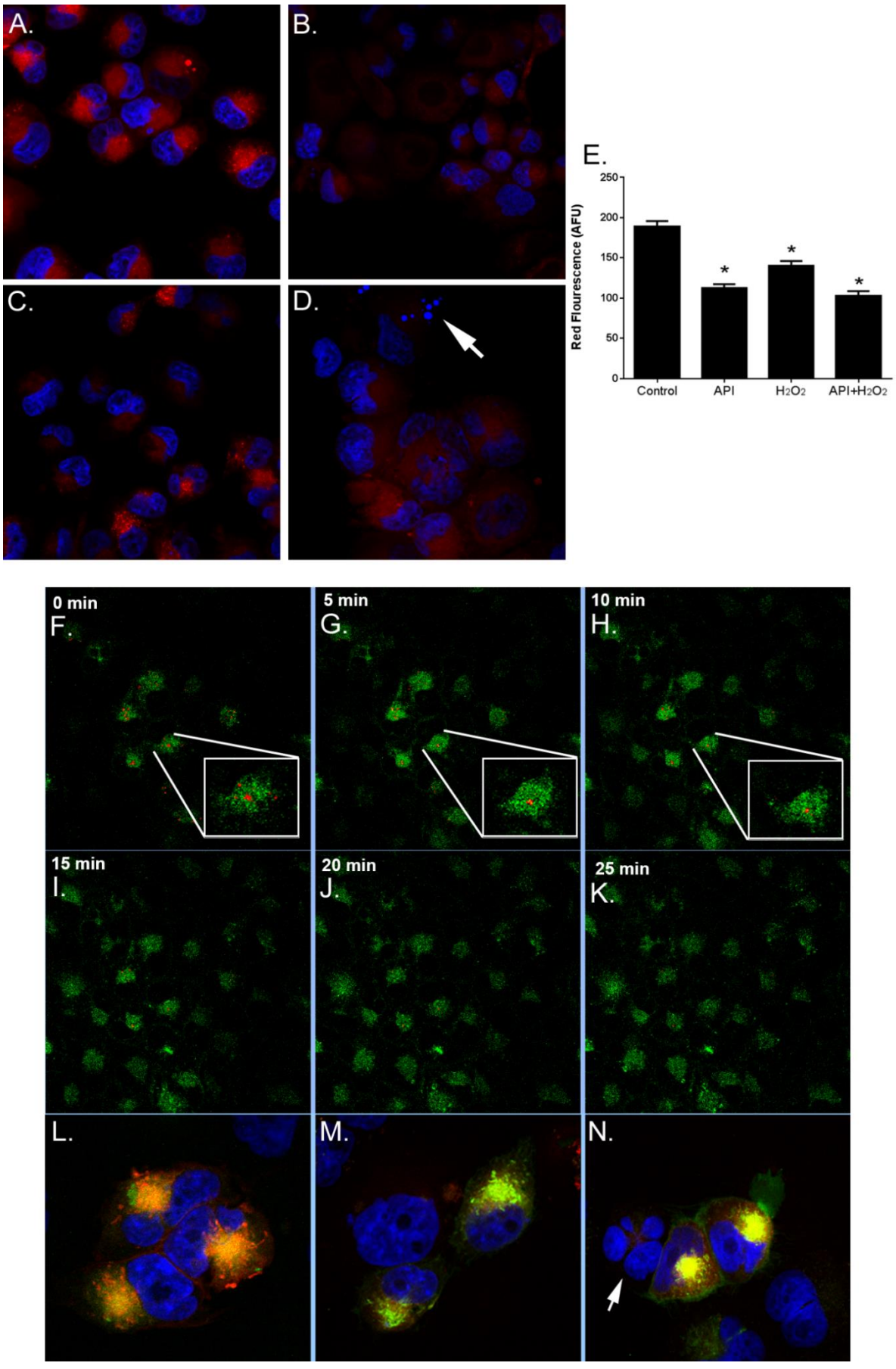

Figure 3.2: Live and fixed cell imaging verified mitochondrial dysfunction with oxidative stress and cell senescence

(Legend for Fig 3.2)
MitoTracker Red CMXRos confocal fluorescence microscopy is demonstrated in A-D and fluorimetry is presented graphically in E as arbitrary fluorescence units (AFU). Compared with control cultures (A), all treatments (B = API; C = H_2O_2, and D = API+H_2O_2) had decreased MitoTracker Red. In E, AFU were significantly decreased in all treatments (*, $p<0.05$ compared to untreated controls). Confocal fluorescence microscopy using live cell imaging and JC-1 labelling is indicated in F-H. F demonstrates the control cells, and G and H demonstrate mitochondrial membrane depolarisation over 20 min exposure to H_2O_2. There was a gradual decrease in red fluorescence (polarised mitochondria, ~590 nm) to predominantly green fluorescence (depolarised mitochondria, ~525 nm). Mitochondrial depolarisation was also demonstrated by JC-1 pre-treatment, oxidative stress, then fixing the cells before confocal microscopy (I-K). Control cells (I) have red fluorescing mitochondria. J and K demonstrate the predominance of green fluorescence after exposure to H_2O_2, again demonstrating mitochondrial membrane depolarisation. Apoptosis is also seen in K (DAPI-stained nuclear condensation and fragmentation, arrow).

3.3.3 Oxidative stress as a mechanism unifies outcomes of increased renal cell apoptosis, decreased mitosis and cell senescence

Apoptosis was increased, and mitosis decreased, by all treatments. API in association with H_2O_2 produced greatest effect (Fig. 3.3A; $p<0.05$). These results were supported by the cytotoxicity assay (Fig. 3.3B). Representative photomicrographs of morphological characteristics of apoptosis, mitosis and senescence are demonstrated in Fig. 3.3C-G. ApopTag labelling is demonstrated in Figs 3.3H-L. Ki67 immunocytochemistry is demonstrated in Figs 3.3M-Q. Representative Western immunoblots of Bax and Bcl-X_L (Fig. 3.4A) and densitometry (Fig. 3.4B) demonstrated increased Bax and decreased Bcl-X_L, with a pro-apoptotic ratio of Bax:Bcl-X_L increased, with all treatments. Using immuno-electron microscopy, oxidative stress alone resulted in enhanced translocation of Bax to mitochondria demonstrated in Figs 3.5 and 3.6. The greatest increase was observed with API+H_2O_2 (all $p<0.05$).

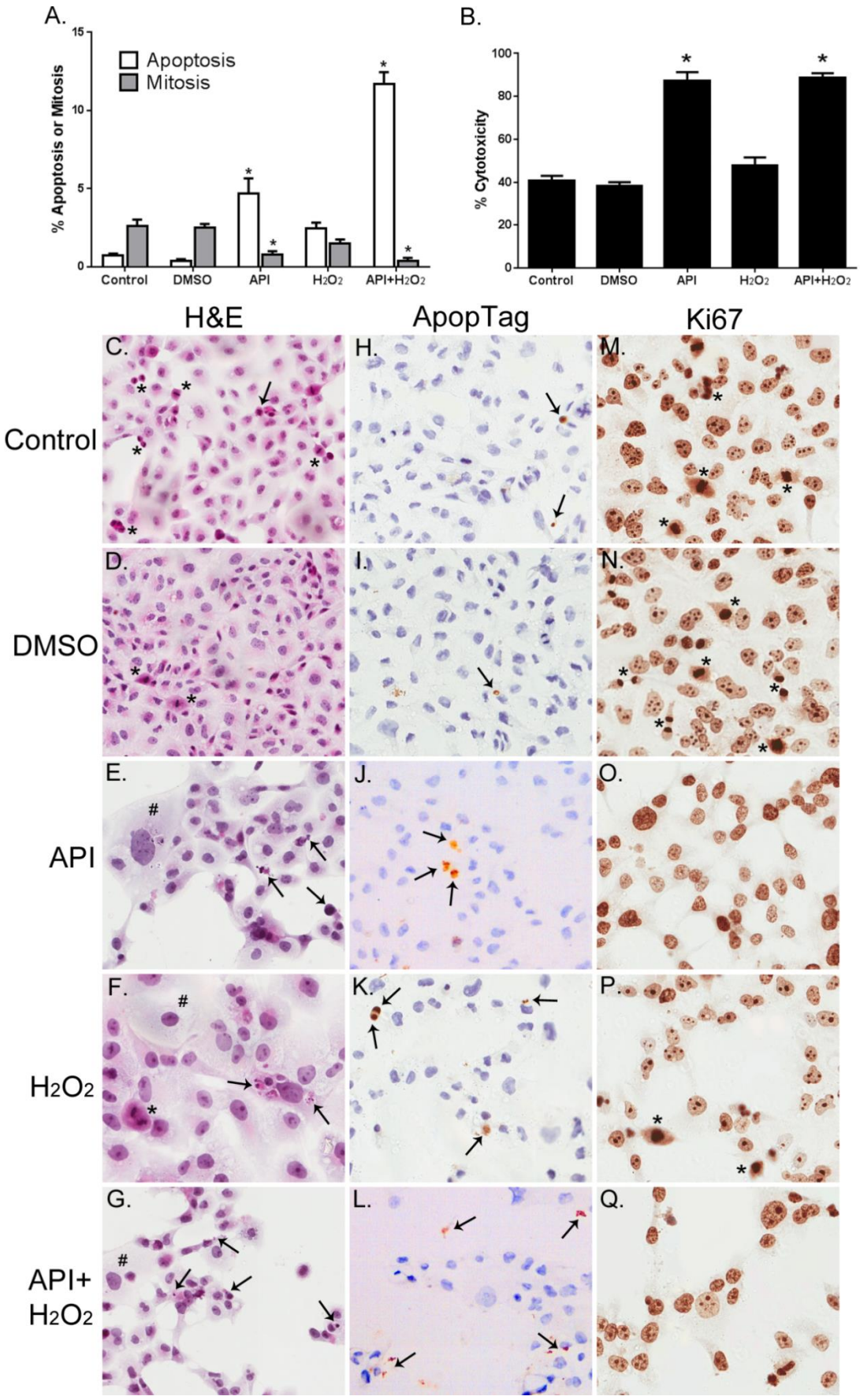

Figure 3.3: Increased apoptosis and decreased mitosis occur with oxidative stress and senescence

(Legend for Fig 3.3)
Graph A demonstrates the mean ± SEM of % apoptosis and mitosis. Apoptosis increased significantly with all treatments compared with control or DMSO but was greater than the addition of counts for API and H_2O_2 in the API+H_2O_2 treatment, indicating a synergistic effect of the treatments (*, $p<0.05$ compared to control). Mitosis decreased in all treatments compared to control and DMSO (#, $p<0.05$ compared to control). Graph B represents the mean ± SEM of lactate dehydrogenase (as % maximal cytotoxicity of HK-2 cells exposed to 5 mM H_2O_2). API and API+H_2O_2 produced the greatest % cytotoxicity compared with untreated cells and DMSO controls (*, $p<0.05$ compared to untreated control). Representative histology is demonstrated in C-Q. (C, H, M = control; D, I, N = DMSO; E, J, O = API; F, K, P = H_2O_2; G, L Q = API+H_2O_2).The morphological characteristics of apoptosis (arrows), and mitosis (*) and senescence (#) are shown in H&E stained cells (C-G) Verification of apoptosis with ApopTag (brown nuclei, arrows) is demonstrated in H-L. In M-Q, proliferative activity was identified using Ki67 immunocytochemistry (positive nuclei as intense brown, *).

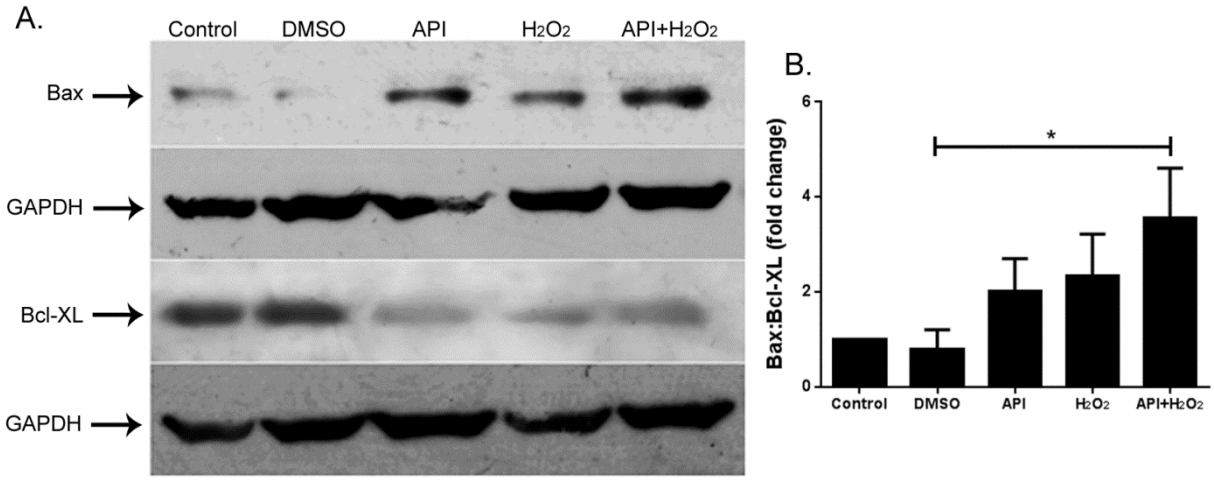

Figure 3.4: Western immunoblot and densitometry for Bax and Bcl-X_L expression
Representative examples of Western immunoblots for pro-apoptotic Bax and anti-apoptotic Bcl-X_L plus the GAPDH loading controls for those blots are demonstrated in A, and the relative densitometry is demonstrated in B. Blots and densitometry are labelled with control, DMSO vehicle, API, H_2O_2, or API+H_2O_2. All treatments resulted in increased Bax and decreased Bcl-X_L. Densitometry (B) was normalised to GAPDH, calculated as a fold change of controls, and presented graphically as a ratio of Bax:Bcl-X_L. The pro-apoptotic ratio of Bax:Bcl-X_L increased with all treatments compared with DMSO with the greatest increase observed in the API+H_2O_2 treatment (*, $p<0.05$).

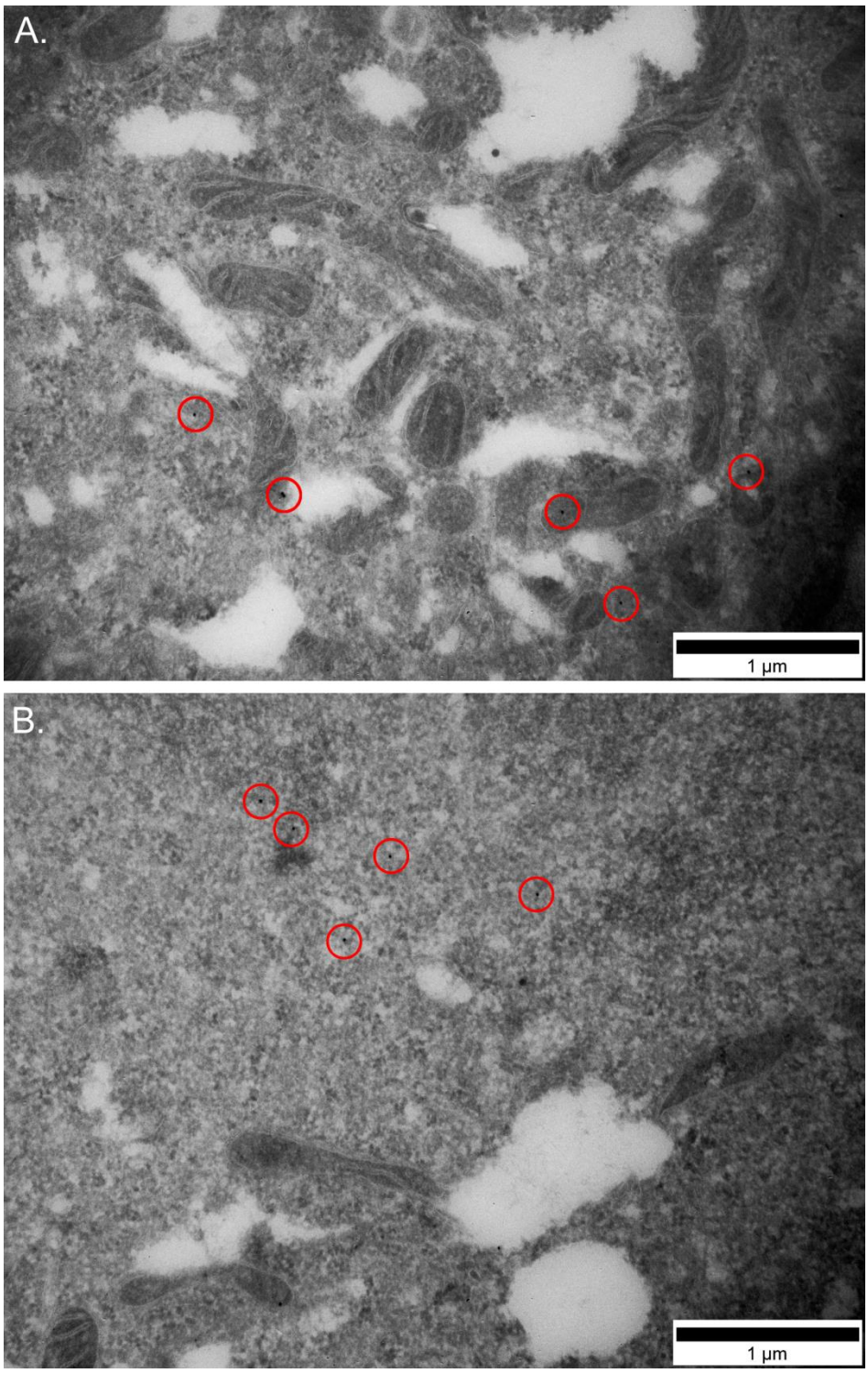

Figure 3.5: Pro-apoptotic Bax protein does not associate with mitochondria in healthy cells
Untreated HK-2 cells were imaged using transmission electron microscopy following immuno-gold (10 nm – red circle) labelling of Bax. Both A. and B. reveal predominately cytoplasmic localisation of Bax surrounding structurally healthy mitochondria.

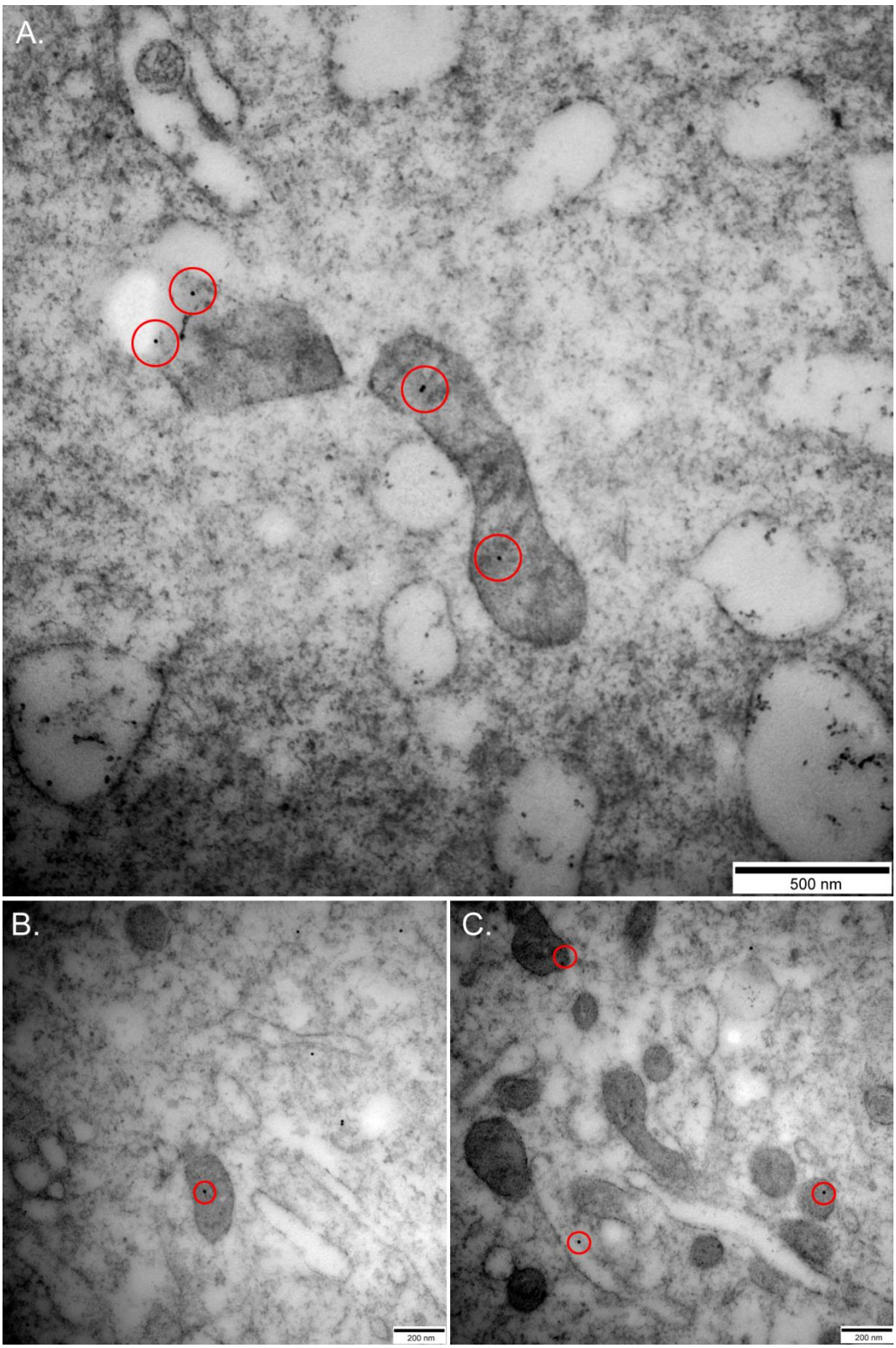

Figure 3.6: Pro-apoptotic Bax protein associates with mitochondria during conditions of oxidative stress

H_2O_2 treated HK-2 cells were imaged using transmission electron microscopy following immuno-gold (10 nm – red circle) labelling of Bax. A-C reveals mitochondrial localisation of Bax and the presence of swollen mitochondria with distorted cristae.

Percentage senescent cells and β-gal immunofluorescence are presented in Figs 3.7A and 3.7B, respectively. API and API+H_2O_2 produced significant morphological changes of senescence ($p<0.001$ compared to DMSO), but all treatments caused increased β-gal immunofluorescence ($p<0.05$ compared to DMSO). Examples of immunofluorescence demonstrated little β-gal in controls (Fig. 3.7C), versus extensive punctuate green cytoplasmic fluorescence in Fig. 3.7D (API treatment).

Expression of the cell cycle regulator $p16^{Ink4a}$ (Figs 3.8A-C) did not change with API or H_2O_2 treatments at 2 h exposure. However, a significant increase was demonstrated following H_2O_2 at 18 h.

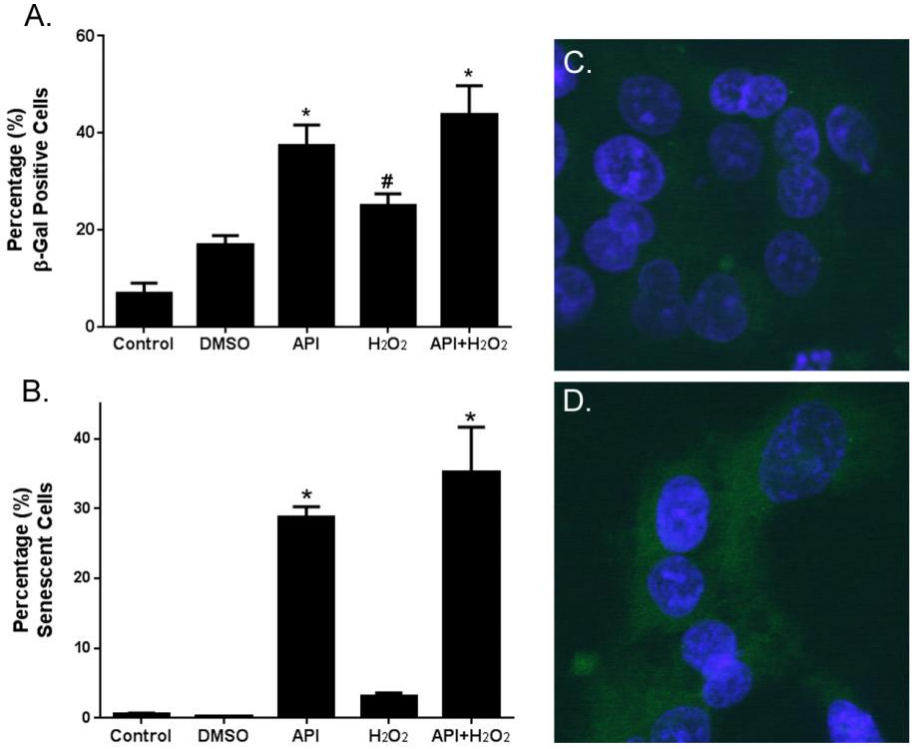

Figure 3.7: Induction of senescence in HK-2 cells
Senescence was identified and quantified using morphology (enlarged cells with reduced staining saturation) in A, and using immunofluorescence of senescence-activated β-galactosidase (SA-β-gal) (B-D). API and API+H_2O_2 produced significant changes in senescence morphology (B; *, $p<0.05$ compared with controls), however SA-β-gal (A) was significantly increased by all treatments (*, $p<0.05$ compared to DMSO; #, $p<0.05$ compared to untreated controls). In the examples in C and D, immunofluorescence for controls (C) had little labelling versus extensive punctuate green fluorescence in the cytoplasm of API-treated cells. DAPI-stained nuclei are blue.

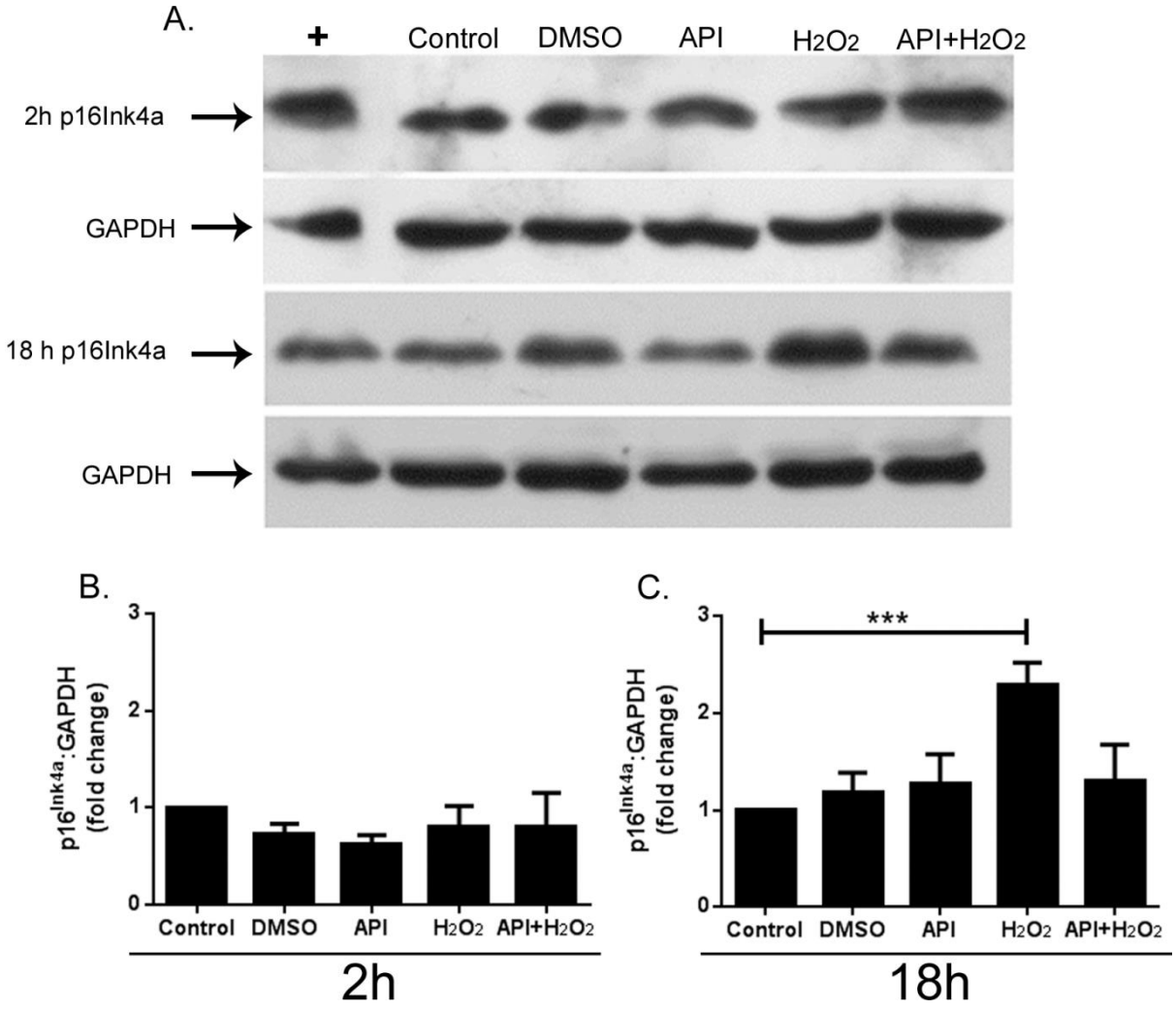

Figure 3.8: Western immunoblot and densitometry for $p16^{Ink4a}$

Examples are demonstrated of Western immunoblots for the cell cycle regulator $p16^{Ink4a}$ at 2 h and 18 h treatment, plus the GAPDH loading controls. Suberohydroxamic acid (SBHA) (indicated by + in blots) was used as a positive control for induction of $p16^{Ink4a}$ expression. Blots and densitometry are labelled with control, DMSO vehicle, API, H2O2, or API+H2O2. $p16^{Ink4a}$ expression did not change significantly at 2 h following all treatments, however at 18 h exposure to H_2O_2 there was significantly increased $p16^{Ink4a}$ expression (***, $p<0.05$ compared to C).

3.3.4 The antioxidant NAC protects renal cells from oxidative stress and senescence

NAC significantly modulated apoptosis for all treatments, restored the mitotic potential of H_2O_2 treated cells, and decreased senescence morphology induced by API and H_2O_2 ($p<0.05$; Figs 3.9A-C).

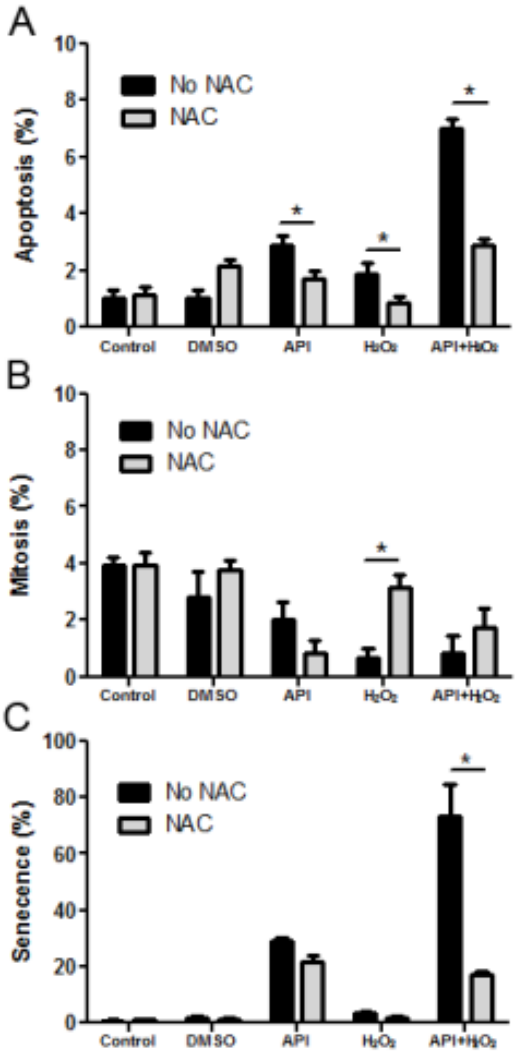

Figure 3.9: The antioxidant NAC ameliorates effects of oxidative stress and senescence
Percentage apoptosis (A), mitosis (B) and senescence (C) are shown. Cells were pre-treated with the antioxidant N-acetyl cysteine (NAC) (10 mM), or with vehicle control, for 2 h prior to the treatments. Significant changes are indicated by * ($p<0.05$). NAC significantly modulated apoptosis for all treatments, restored the mitotic potential of H_2O_2 treated cells, and decreased senescence induced by API+H_2O_2.

3.4 DISCUSSION

Although oxidative stress and cell senescence may contribute to renal cell dysfunction and attrition in CKD, the involvement of the mitochondria and their health or dysfunction in the pathogenesis of CKD had not been well defined. This study used an *in vitro* kidney disease model with oxidative stress and cell senescence to investigate their involvement in kidney epithelial cell dysfunction, as a cell culture model of oxidative stress in CKD. The results have provided evidence that oxidative stress and cell senescence combine to cause most renal cell loss, as well as decrease the renal cell proliferative activity, and both involve mitochondrial destabilization.

One of the unusual outcomes was that the flavonoid API, used successfully here and elsewhere (Ryu *et al.*, 2006) to induce renal cell senescence, also caused increased lipid peroxidation (increased MDA), decreased TAC, and caused greatest mitochondrial dysfunction with or without concurrent H_2O_2. Lagao *et al* have recently reported, using mitochondria isolated from rat brain and heart, that API (10 μM) inhibited the activity of Complex I of the electron transport chain by affecting the binding of the coenzyme substrate (Lagoa *et al.*, 2011). Increased reliance on Complex I to III electron transfer reduces the efficiency of oxidative phosphorylation, perhaps leading to mitochondrial dysfunction. These results and our own suggest that the oxidative stress produced by API may exhaust antioxidant stores. In our study, API did not alter the expression of the cell cycle regulator $p16^{ink4a}$ after 2 h or 18 h indicating that API-induced kidney cell senescence may occur via $p16^{Ink4a}$ independent mechanisms. The apparent lack of $p16^{ink4a}$ activity may indicate a protective mechanism, thereby ceasing their progression to transcription. Transcriptional regulation by API may need to be investigated, such as was published by Liu and colleagues (Liu *et al.*, 2005) for the inhibitory action of API on vascular endothelial growth factor and angiogenesis.

Apoptosis and mitosis contribute in renal homeostasis by ensuring adequate cell numbers for healthy renal function. Loss of functioning renal cells (increased apoptosis), decreased mitosis and increased cell senescence reflect a decreased ability for the kidney to metabolise and repair in CKD (Vogetseder *et al.*, 2008; Percy *et al.*, 2009). All of these characteristics featured in the current experiments. API and H_2O_2 were pro-apoptotic, notably with a synergistic effect seen on renal cell apoptosis when the treatments were combined. The pro-apoptotic effect of API has been recorded previously, but mostly in investigations of cancer treatments, where it caused apoptosis in cervical and prostate cancer cell lines when trialled as a therapy against cancer growth (Zheng *et al.*, 2005; Shukla and Gupta, 2006).

Apoptosis, as a result of oxidative damage, is well-recognised. In CKD, apoptosis may initially act as a cellular adaptive response to oxidative stress to eliminate dysfunctional cells. The outcome for the whole kidney, however, is likely to be renal atrophy with loss of renal function. The Bcl-2 family proteins, including pro-apoptotic Bax and anti-apoptotic Bcl-X_L, regulate the intrinsic, mitochondrial-dependent, pathway of apoptosis (Madesh and Hajnoczky, 2001; Chipuk *et al.*, 2010). Changes in the ratio of pro-apoptotic Bax to anti-apoptotic Bcl-X_L following oxidative insult have been seen previously in renal epithelium (Cuttle *et al.*, 2001; Ye *et al.*, 2010). In the current experiments, there was a similar pro-apoptotic change with all treatments.

NAC is a free radical scavenger that has been used successfully to reduce injury in a variety of nephrotoxic and ischemic experimental and clinical renal models, and has had some success in CKD patients (Alonso *et al.*, 2004). When it was used concurrently with API and/or H_2O_2, it significantly reduced apoptosis and senescence and also restored the regenerative capacity of the kidney. However, antioxidant therapy is sometimes disappointing in models of CKD (Quiroz *et al.*, 2009) and it will be important to repeat these studies in the whole animal (Chapter 6).

In conclusion, the cellular and biomolecular alterations in the kidney during CKD are undoubtedly very complex, but the present investigation provides evidence that oxidative stress and cell senescence together produce greatest renal cell loss and mitochondrial destabilisation. The antioxidant NAC attenuated many of the characteristics that likely contribute to CKD. A more targeted approach to antioxidant therapy in CKD may limit mitochondrial dysfunction, with improved outcome for CKD patients. The model may serve as a baseline to test the role of mitochondria after various putative causes of CKD, and to further analyse the benefits of antioxidants in ameliorating mitochondrial dysfunction in CKD.

CHAPTER 4

The Role of PPARγ in Oxidative Stress-Induced Kidney Damage

Oxidative stress encompasses more than an imbalance between ROS and endogenous antioxidants. Oxidative stress also affects intracellular signalling pathways that are vital for normal cell function. Mitochondrial dysfunction was identified in Chapter 3 as a major contributor to oxidative stress-induced injury to epithelial cells of the kidney. This chapter defines the role of a specific oxidant signalling regulatory mechanism, one regulated by PPARγ. The study sought to (1) investigate the role of PPARγ in oxidative stress and mitochondrial destabilisation causing damage and loss of kidney PTE cells; and (2) to determine whether PPARγ modulation could protect kidney PTE cells from oxidative stress-induced damage by preserving mitochondrial function. The contents of this Chapter have been published (Small *et al.*, 2014, Appendix A). The report in this chapter is a modification consistent with the format of this thesis.

4.1 INTRODUCTION

Alterations in the bioenergetic controls of kidney cells can lead to a failure in oxidant handling, leading to a state of oxidative stress in kidney disease. The causes are multiple, from high glucose of diabetes, to ischaemia-reperfusion, toxins and AKI, to the long-term effects of ageing and development of CKD. Kidney atrophy, often due to apoptosis of the PTE cells, is a common characteristic of these diseases and therefore presents a crucial target to preserve kidney health (Nath, 1992; Niizuma *et al.*, 2011). Oxidative stress is a mediating factor in mitochondrial dysfunction and subsequent cell dysregulation and death during kidney disease (Granata *et al.*, 2009; Small *et al.*, 2012; Xu *et al.*, 2013). The importance of mitochondrial dysregulation comes from the large number of mitochondria in the PTE cells and their heavy reliance on oxidative phosphorylation for ATP-dependent active solute transport in the nephron (Hall *et al.*, 2011). Identifying oxidant-handling pathways that are perturbed in the kidney during oxidative stress is necessary for development of reliable targeted therapies.

PPARγ is a member of the highly conserved nuclear hormone receptor superfamily of ligand-dependent transcription factors that play central roles in lipid metabolism, glucose homeostasis, cell proliferation and inflammation (Ahmadian *et al.*, 2013). Ligand binding induces heterodimer formation with the retinoic acid receptor and complex binding to the peroxisome-proliferator response element within the promoter region of target genes (Guan *et al.*, 2002). Phosphorylation may modulate the activity of PPARγ through activating multiple kinase signalling pathways, including ERK and AMPK. However, PPARγ phosphorylation does not always indicate activation of PPARγ (Hu *et al.*, 1996; Zhang *et al.*, 1996; Camp and Tafuri, 1997). Its altered expression may

also be important for overall outcome that largely depends on tissue type and mode of PPARγ modulation.

The family of TZDs consists of potent pharmacological agonists of PPARγ, commonly used in the treatment of type 2 diabetes where it modulates insulin levels. The targeting of PPARγ, however, is not limited to diabetes. First, PPARγ mRNA expression is increased in kidney biopsies of CKD patients of diverse aetiologies (Lepenies *et al.*, 2010) raising the possibility of mechanisms not dependent on insulin. Second, the TZD rosiglitazone attenuated kidney structural and functional damage in a mouse model of diabetes, yet no change was observed in glucose, insulin or lipid levels (Calkin *et al.*, 2006). Finally, a reduction in proteinuria was achieved in patients with non-diabetic kidney disease of various aetiologies following 4 months of rosiglitazone treatment (Kincaid-Smith *et al.*, 2008). A possible explanation for the diverse outcomes from PPARγ agonist success is that PPARγ also positively regulates mitochondrial biogenesis through the activation of the PGC-1α. Thus, PPARγ may influence mitochondrial function (Funk *et al.*, 2010; Chiang *et al.*, 2013). This is important given the vital role mitochondria play in regulating the intracellular redox environment (Zhan *et al.*, 2013). Healthy mitochondrial function relies on the degradation of defective mitochondria via activation of selective autophagy pathways (mitophagy) and up-regulation of mitochondrial biogenesis pathways to restore a healthy pool of functioning mitochondria (Weinberg, 2011). PPARα, an alternate isoform of PPAR, also plays a role in mitochondrial biogenesis, but is more widely expressed in skeletal muscle and liver than the kidney (Guan and Breyer, 2001).

Several molecular pathways may be involved for any influence of PPARγ on mitochondrial function. A major pathway for injury-induced mitochondrial degradation is the PINK1-Park2 pathway. Park2 is an E3 ubiquitin ligase that translocates to mitochondria and mediates mitochondrial degradation (Narendra *et al.*, 2008; Cai *et al.*, 2012). The adaptor protein p62 facilitates selective autophagy into the LC3β regulated machinery for lysosomal degradation (Bjorkoy *et al.*, 2005; Geisler *et al.*, 2010). p62 is not required for Park2 translocation to damaged mitochondria, but is essential for final autophagic clearance (Geisler *et al.*, 2010). PGC-1α is a nuclear transcription factor shown to mediate almost all aspects of mitochondrial biogenesis and is therefore considered a master regulator of biogenesis (Hock and Kralli, 2009). Failure to restore mitochondrial homeostasis and function can lead to a progressive increase in ROS and ensuing oxidative stress. Therefore, PGC-1α activation presents a crucial target for mitochondrial preservation. Previous studies have demonstrated TZD induction of mitochondrial biogenesis (Hondares *et al.*, 2006; Rasbach and Schnellmann, 2007).

This study sought to (1) investigate the role of PPARγ in oxidative stress and mitochondrial destabilisation in damage and loss of human kidney proximal tubular cells; and (2) determine whether PPARγ modulation can protect human kidney PTE cells from oxidative stress-induced damage by preserving mitochondrial function.

4.2 METHODS AND MATERIALS

Complete methods are outlined in Chapter 2. Below is a brief summary of the experimental materials and methods that are specific for this chapter.

4.2.1 Experimental design

HK-2 cells were grown in normal culture conditions outlined in Chapter 2. Cells were treated with H_2O_2 0.2 mM – 1.0 mM for 2 h and 18 h to induce oxidative stress. In some treatments, the PPARγ agonists troglitazone, rosiglitazone and pioglitazone were used as treatments for 2 h prior to and during H_2O_2 exposure. Troglitazone (#T2573) and pioglitazone (#E6910) were purchased from Sigma-Aldrich (Castle Hill, Australia); rosiglitazone (#71740) was purchased from Cayman Chemicals (Ann Arbor, USA). All were dissolved as stock solutions in DMSO and stored frozen as small aliquots. A DMSO vehicle control was always used for these experiments.

4.2.2 Western immunoblot

Western blots were performed from whole cell lysates dissociated in lysis buffer. Protein was separated by SDS-PAGE on 10 % acrylamide gel and electrophoretically transferred onto PVDF membrane. Membranes were blotted using antibodies against PPARγ, phosphorylated PPARγ (p-PPARγ; phosphorylation site *Ser112*), PPARα, PGC-1α, Park2, p62, LC3β, and GAPDH for loading control (see Table 2.3 for dilutions and suppliers). Appropriate secondary antibodies (see Table 2.4 for dilutions and suppliers) were used and visualised with ECL and X-ray film. Scion software (Release Alpha 4.0.3.2) was used to quantify bands for densitometry that was normalised to GAPDH.

4.2.3 Light and fluorescence microscopy

Cells were grown on glass coverslips for treatments and fixed in 4 % PF. Immunofluorescence and cytochemistry were used to assess p62 cellular localisation. Apoptosis and mitosis were assessed using morphology (Gobe, 2009) following H&E staining and digital scanning using Aperio

ImageScope histology software. Results are expressed as a % apoptotic or mitotic cells per field of view.

4.2.4 Oxidative stress and mitochondrial function

Oxidative stress was determined and quantified using microfluorimetry detection of the oxidation of dihydroethidium (DHE) to ethidium. $O_2^{\bullet-}$ selectively oxidises this reaction, and is an essential precursor to harmful cellular oxidants, such as $OH^{\bullet}$ and $ONOO^-$. Cells were cultured in black 96-well plates and treated as previously described. The growth medium was then replaced with DHE-supplemented normal growth media and incubated for 30 min. Fluorescence intensity was measured at 536 nm excitation and 610 nm emission (Synergy Mx Multi-Mode Microplate reader, BioTek, Winooski, VT). Fluorescence values were normalised to protein content for corresponding wells and expressed as DHE fluorescence per µg protein. JC-1 was used to assess the mitochondrial membrane potential and was quantified using the same technique. A decrease in red fluorescence (JC-1 aggregate uptake into healthy mitochondria) and increase in green fluorescence (JC-1 in cytoplasm) indicates mitochondrial membrane depolarisation. ATP production was measured using a luciferase-based luminescence assay (Promega, Sydney, Australia). Cells were seeded into white opaque 96-well plates and treated as previously described. Chemiluminescent reagent was added and cell lysis induced prior to measuring luminescence at an integration time of 0.5 sec using a Titertek-Berthold Luminometer (Titertek-Berthold Detection Systems, Pforzheim, Germany).

4.2.5 Mitochondrial health

MitoTracker Red CMXRos (Invitrogen^{TM}, Mulgrave, Australia) and confocal fluorescence microscopy were used to determine mitochondrial density. MitoTracker localises to mitochondria with a healthy mitochondrial membrane potential. Cells were grown on glass coverslips and exposed MitoTracker Red CMXRos for 30 min following treatments as previously described. Coverslips were mounted following fixation in 4 % PF and DAPI staining. Cells were observed at x63 with a Zeiss 510 Meta confocal fluorescence microscope using Zen 2008 software. Transmission electron microscopy was used to visualise the ultrastructure of mitochondria, according to an established protocol outlined in Chapter 2, Section 2.3.8.

4.2.6 Cell viability

Cell viability was measured using the MTT assay. Absorbance was measured in a microplate reader at 570 nm with background collection at 690 nm.

4.2.7 Transmission electron microscopy

TEM was used to assess mitochondrial ultrastructure. The protocol is outlined in Chapter 2, Section 2.3.8.

4.2.8 Statistical analysis

Values reported are mean ± SEM. Data were analyzed using ANOVA and Tukey's post hoc analysis, two-way ANOVA and Bonferroni's post hoc test, or student's t-test where appropriate. Significance was established at $p < 0.05$.

4.3 RESULTS

4.3.1 Oxidative stress decreased PPARγ expression and increased PPARγ serine 112 (*Ser112*) phosphorylation

HK-2 cells displayed a dose-dependent significant increase in apoptosis and dose-dependent decrease in mitosis following oxidative stress at both 2 h and 18 h (Fig 4.1A and B). This was associated with a decrease in PPARγ protein levels (Fig 4.2A; $p<0.001$ starting at 0.4 mM H_2O_2) and a dose-dependent increase in p-PPARγ levels (Fig 4.2A; $p<0.001$ starting at 0.4 mM H_2O_2) following 2 h exposure to H_2O_2. Following 18 h H_2O_2 exposure (Fig 2B), PPARγ and p-PPARγ returned to basal levels indicating that oxidative stress promotes phosphorylation of PPARγ as an early response. Conversely, PPARα expression decreased in a dose-dependent manner following 2 h exposure to H_2O_2 (Fig 4.2A; $p<0.05$ starting at 0.4 mM H_2O_2) and returned to control levels following 18 h H_2O_2 exposure (Fig 4.2B).

4.3.2 Oxidative stress induced mitochondrial dysfunction

Mitochondrial function was significantly reduced following exposure to H_2O_2 for both 2 h and 18 h (Fig 4.3). 0.6 mM H_2O_2 significantly increased DHE fluorescence indicating enhanced levels of $O_2^{\bullet-}$ production and confirming an intracellular state of oxidative stress (Fig 4.3A; $p<0.05$). The mitochondrial membrane potential significantly decreased, indicated by a decrease in JC-1 red fluorescence intensity (Fig 4.3B; $p<0.01$ starting at 0.4 mM H_2O_2) and increase in JC-1 green fluorescence intensity (Fig 4.3C: $p<0.01$ starting at 0.4 mM H_2O_2). Confocal microscopy revealed that, compared with untreated HK-2 cells (Fig 4.3H), uptake of MitoTracker Red CMXRos fluorescence was impaired following H_2O_2 exposure at both 2 h (Fig 4.3I) and 18 h (Fig 4.3J). Mitochondrial ultrastructure (Figs 4.3D-G) revealed abundant elongated mitochondria with clear cristae in untreated HK-2 cells (Figs 4.3D and E), compared with Fig 3F (segmented and swollen mitochondria) and Fig 4.3G (cristae absent) following H_2O_2 exposure. These changes relate to a

significant dose-dependent decrease in ATP production by mitochondria following H_2O_2 exposure at both 2 h (Fig 4.4A; $p<0.001$ at 0.4 mM H_2O_2) and 18 h (Fig 4.4B; $p<0.001$ at 0.4 mM H_2O_2), indicating impaired oxidative phosphorylation.

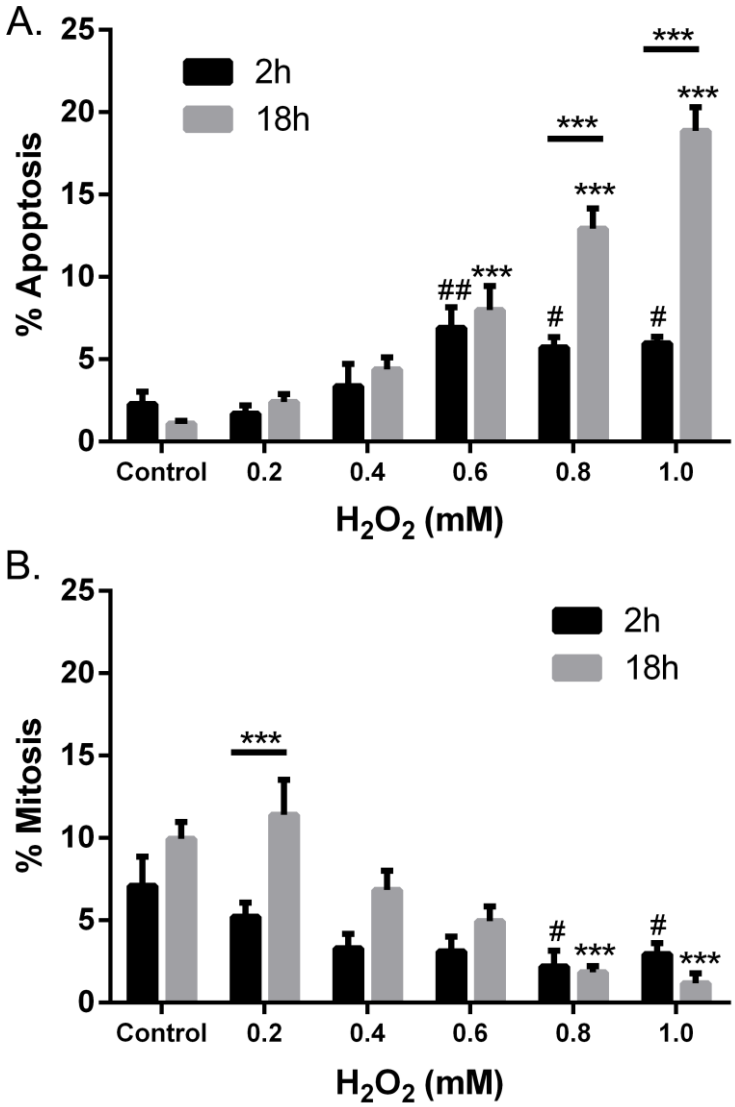

Figure 4.1: Oxidative stress promotes apoptosis and impairs mitosis in HK-2 cells
HK-2 cells were exposed to H_2O_2 at concentrations ranging from 0.2 mM to 1.0 mM. % apoptosis significantly increased in a dose-dependent manner following H_2O_2 exposure at both 2 h and 18 h (A.). % mitosis significantly decreased in a dose-dependent manner following H_2O_2 exposure at both 2 h and 18 h (B.). Results are expressed as mean ± SEM (*** $p<0.001$, compared to 18 h Control; # $p<0.05$; ## $p<0.01$, compared to 2 h Control; bar, compared as indicated).

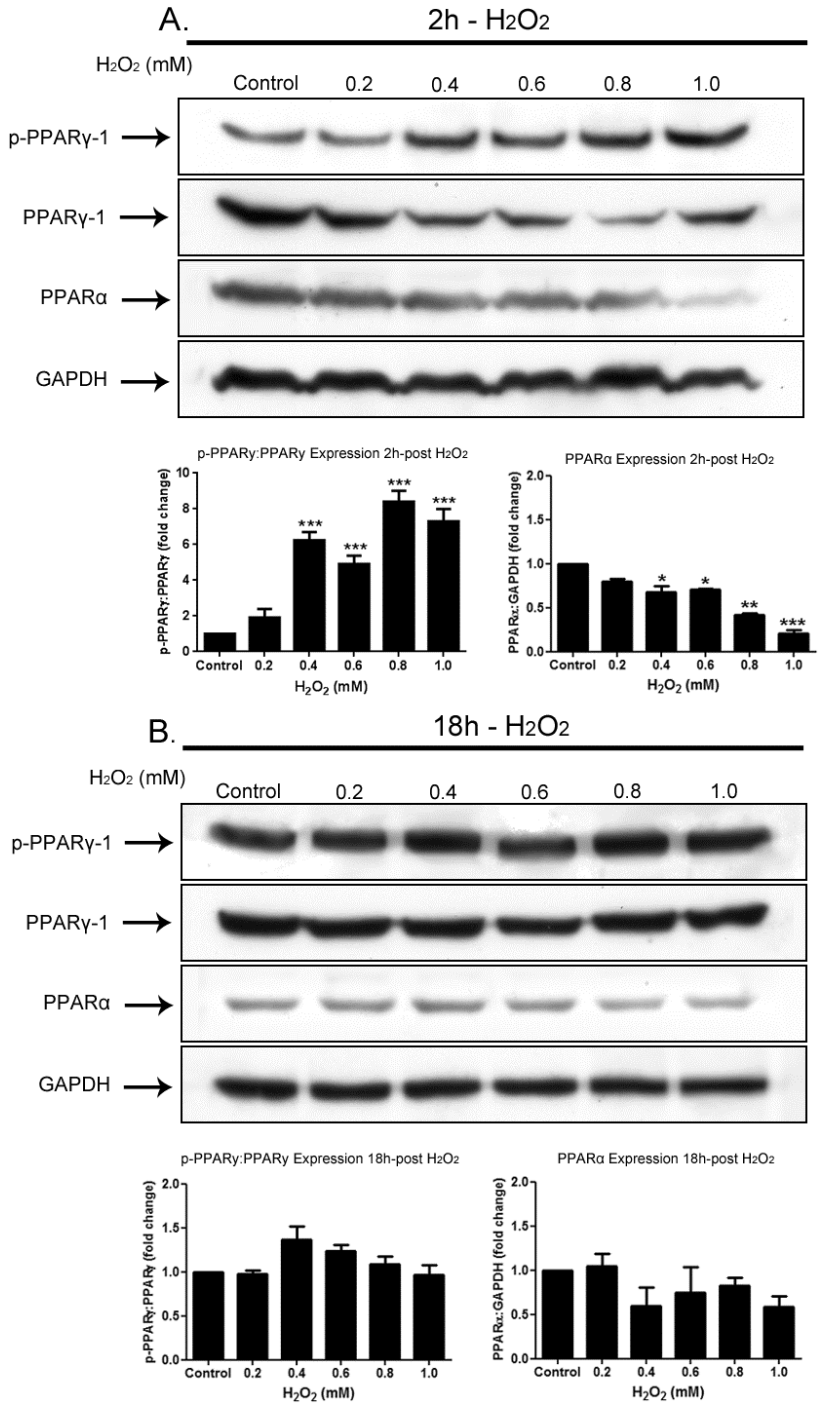

Figure 4.2: PPARγ and PPARα expression at 2 h and 18 h

HK-2 cells were exposed to a range of H_2O_2 concentrations (0.2 mM – 1.0 mM) for 2 h and 18 h. Representative Western blots are supplied. There was a dose-dependent significant increase in PPARγ phosphorylation (p-PPARγ) following 2 h H_2O_2 exposure (A.) that corresponded to a decrease in PPARγ expression. PPARα significantly increased in a dose-dependent manner following 2 h H_2O_2. 18 h H_2O_2 (B.) did not significantly alter PPARγ phosphorylation or PPARα expression. p-PPARγ and PPARγ were expressed as a ratio, and PPARα protein expression was normalised to GAPDH expression. Results are expressed as mean ± SEM (* $p<0.05$; ** $p<0.01$; ***$p<0.001$, compared to Control).

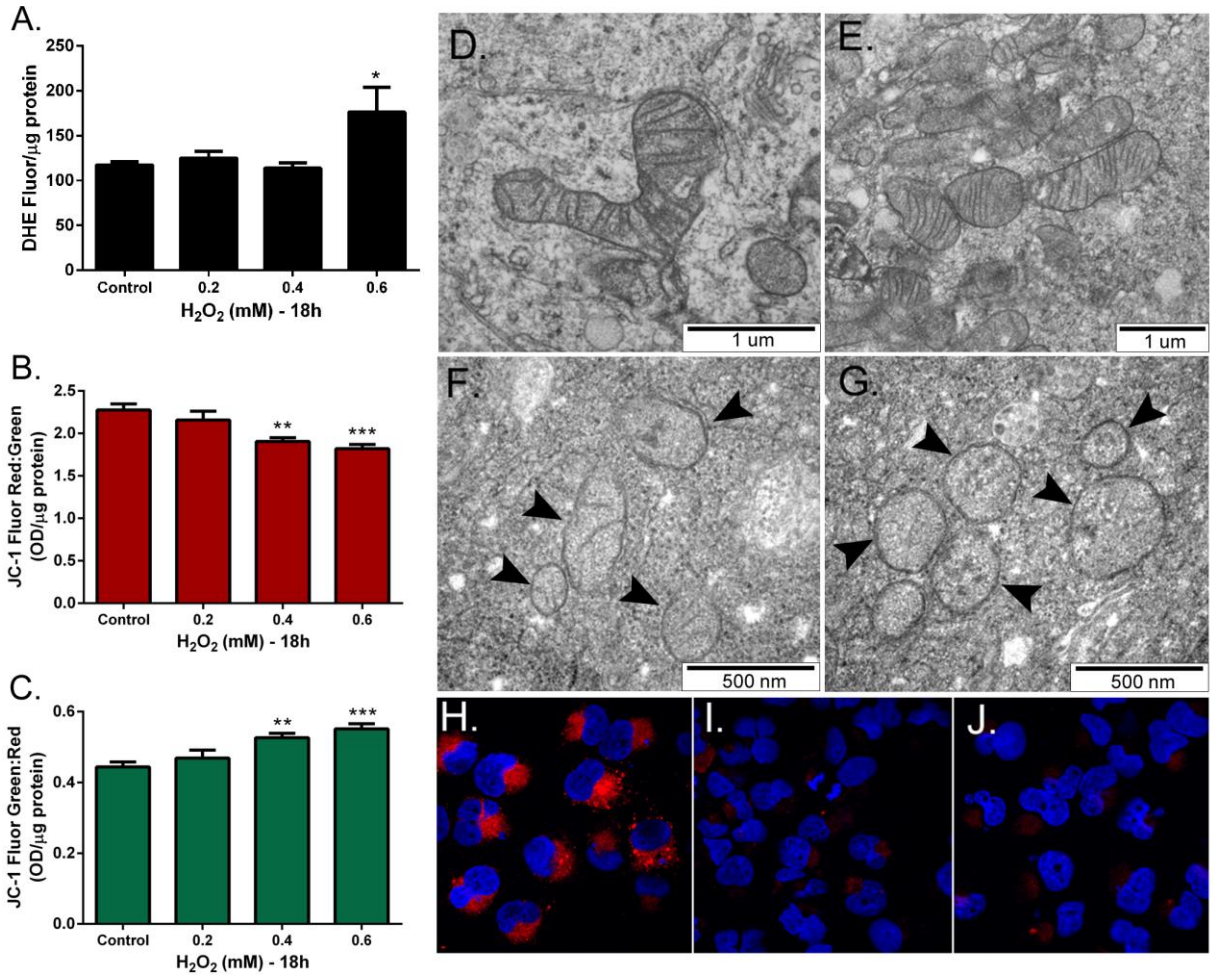

Figure 4.3: Oxidative stress induces mitochondrial dysfunction

HK-2 cells were exposed to a range of H_2O_2 concentrations (0.2 mM – 0.6 mM) for 2 h and 18 h. DHE and JC-1 fluorescence was quantified by fluorimetry at 18 h. DHE fluorescence significantly increased following 0.6 mM H_2O_2 exposure demonstrating ROS generation at 18 h (A.). JC-1 red fluorescence significantly decreased in a dose-dependent manner (B.) while increasing in green fluorescence (C.) indicating mitochondrial membrane depolarisation at 18 h. Transmission electron microscopy revealed elongated morphologically healthy mitochondria with cristae in untreated HK-2 cells (D. and E.) and segmented, swollen mitochondria (F.) often with absent cristae (G.) in 0.6 mM H_2O_2 treated HK-2 cells at 18 h (arrow heads). MitoTracker Red CMXRos uptake was visualised with confocal microscopy and shown to decline following both 2 h (I.) and 18 h (J.) of 0.6 mM H_2O_2 exposure compared to untreated HK-2 cells (H.). Results are expressed as mean ± SEM (* $p<0.05$; ** $p<0.01$; ***$p<0.001$, compared to Control).

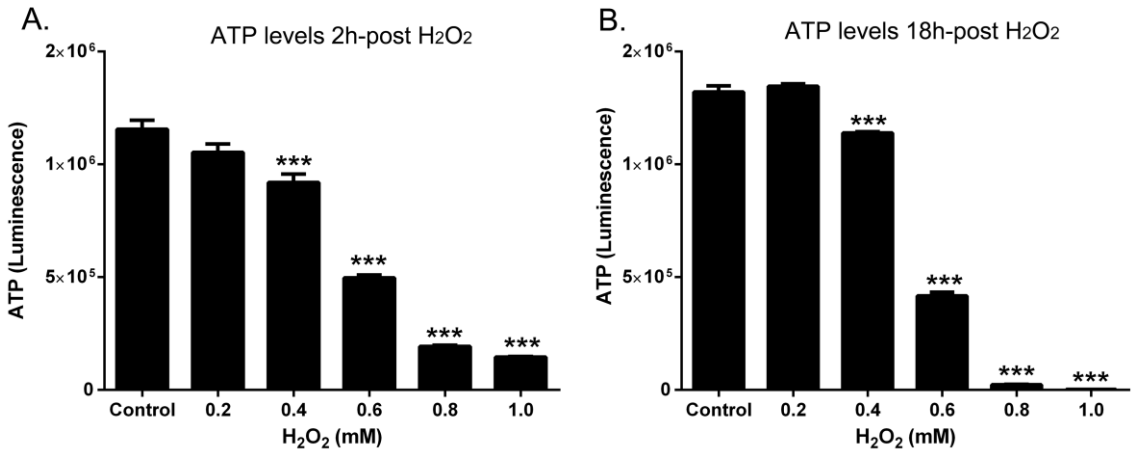

Figure 4.4: Oxidative stress impairs cellular ATP production
HK-2 cells were exposed to a range of H_2O_2 concentrations (0.2 mM – 1.0 mM) for 2 h and 18 h. ATP assay was performed based on luminescence. ATP levels significantly decreased in a dose-dependent manner following H_2O_2 exposure for both 2 h (A.) and 18 h (B.). Results are expressed as mean ± SEM (***$p<0.001$, compared to Control).

4.3.3 Oxidative stress-induced PPARγ dysregulation impaired mitochondrial autophagy (mitophagy) and biogenesis

Following oxidative stress and the initial insult affecting mitochondrial function (Figs 4.3 and 4.4), the cellular autophagy machinery needed for selective mitochondrial clearance was upregulated. These results are presented in Fig. 4.5. 2 h H_2O_2 exposure significantly increased Park2 expression (Fig 4.5A; $p<0.01$ at 0.4 mM H_2O_2) indicating effective tagging of defective/damaged mitochondria for autophagic clearance. Simultaneously, expression of the adapter protein p62 was significantly down-regulated (Fig 4.5B; $p<0.05$ at 0.4 mM H_2O_2), and a significant increase was seen in LC3β protein levels (Fig 4.5C; $p<0.01$ at 0.6 mM H_2O_2), demonstrating early selective autophagy of mitochondria (mitophagy). Park2 expression did not alter significantly following extended (18 h) H_2O_2 exposure (Fig 4.5D), yet there was a significant increase in p62 and LC3β protein levels, indicating impaired p62 degradation with intracellular accumulation. Altered p62 expression seen by Western immunoblot, and assumed intracellular accumulation, was verified using confocal microscopy (Figs 4.5G-I). There was a decrease in the PPARγ co-activator and mitochondrial biogenesis marker PGC-1α following 2 h H_2O_2 exposure (Fig 4.6A; $p<0.05$ at 0.4 mM H_2O_2) that corresponded with the changes in Park2, p62 and LC3β. The cumulative results demonstrate impaired PPARγ-dependent mitochondrial biogenesis.

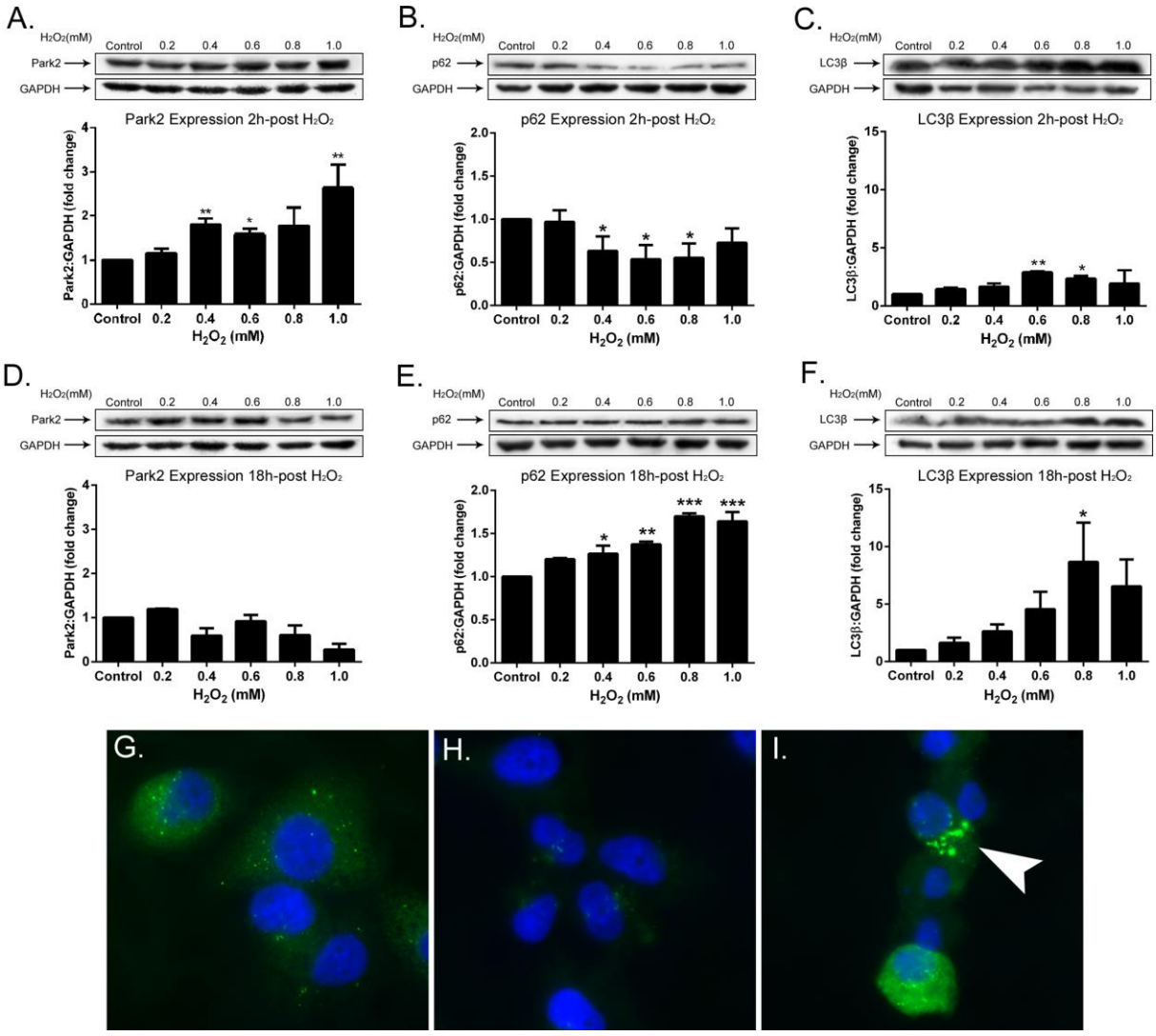

Figure 4.5: Oxidative stress promotes selective mitochondrial autophagy (mitophagy)
HK-2 cells were exposed to a range of H_2O_2 concentrations (0.2 mM – 1.0 mM) for 2 h and 18 h. Cells were lysed and Western blot analysis performed. Immunofluorescence of p62 was performed (anti-p62 is green fluorescence and nuclear DAPI is blue). Protein levels of Park2 (A.) and p62 (B.) significantly increased and decreased, respectively, in a dose-dependent manner, while LC3β (C.) significantly increased following 2 h H_2O_2 exposure. Park2 protein levels returned to control levels following 18 h H_2O_2 (D.), while p62 (E.) and LC3β (F.) expression significantly increased in a dose-dependent manner. Immunofluorescence revealed decreased cytoplasmic localisation of p62 following 2 h H_2O_2 (H.) compared to untreated HK-2 cells (G.), which increased following 18 h H_2O_2 (I.) to show a punctate perinuclear cytoplasmic pattern (white arrowhead). Protein expression was normalised to GAPDH expression. Results are expressed as mean ± SEM (* $p<0.05$; ** $p<0.01$; ***$p<0.001$, compared to Control).

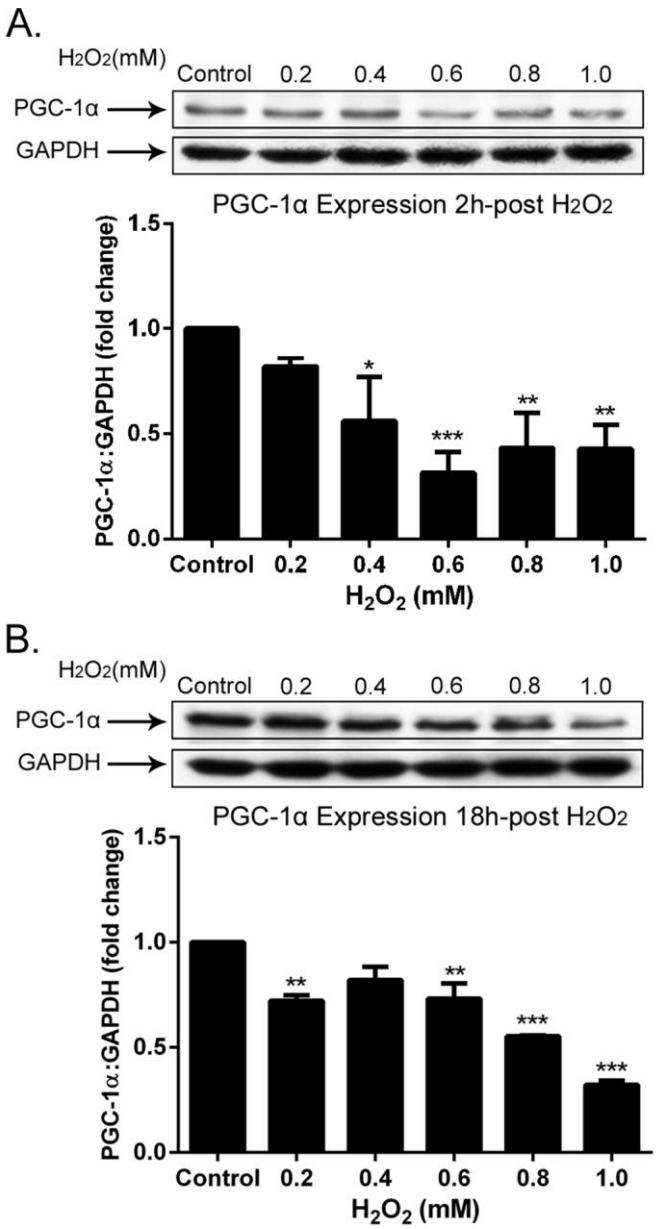

Figure 4.6: Oxidative stress impairs PGC-1α-dependent mitochondrial biogenesis that persists long-term

HK-2 cells were exposed to a range of H_2O_2 concentrations (0.2 mM – 1.0 mM) for 2 h and 18 h. Cells were lysed and Western blot analysis performed. Protein levels of PGC-1α significantly decreased in a dose-dependent manner following both 2h (A.) and 18 h (B.) of H_2O_2 exposure. Protein expression was normalised to GAPDH expression. Results are expressed as mean ± SEM (* $p<0.05$; ** $p<0.01$; ***$p<0.001$, compared to Control).

4.3.4 PPARγ activation does not protect kidney proximal tubular cells from oxidative stress induced damage

PPARγ expression and phosphorylation changes with selective PPARγ TZD agonists were tested to determine whether this protected cells from oxidative stress. The TZD agonists were delivered 2 h prior to H_2O_2 (0.6 mM) exposure and during the 2 h and 18 h H_2O_2 treatment periods. Concentrations of the TZD agonists (rosiglitazone and troglitazone at 10 µM; pioglitazone at 1 µM) were chosen from preliminary data (Appendix C) and were consistent with concentrations used in similar previous studies (Hondares *et al.*, 2006; Fujisawa *et al.*, 2009; Martin *et al.*, 2012; Miglio *et al.*, 2012; Chiang *et al.*, 2013). Expression of p-PPARγ was calculated as a ratio of PPAR and then a fold change on control cells compared for each of the TZDs at 2 h (Figs 4.7A-C) and 18 h (Figs 4.7G-I). H_2O_2 exposure alone caused a significant increase in *Ser112* phosphorylation of PPARγ at both 2 h and 18 h (Figs 4.7A-C; $p<0.05$ and Figs 4.7G-I; $p<0.001$, respectively). This occurred in conjunction with a significant decrease in cell viability compared with control cells at 2 h and 18 h (Figs 4.7D-F; $p<0.001$ and Figs 4.7J-L; $p<0.001$, respectively). The cell viability was not improved above H_2O_2 levels when each of the PPARγ agonists was used in combination with H_2O_2 for 2 h (Figs 4.7D-F). Thus, these results demonstrate a lack of protection by TZDs against oxidative stress-induced loss of viability at a time when p-PPARγ:PPAR was significantly increased. Following extended exposure to PPARγ agonists and H_2O_2 (18 h), cell viability levels remained significantly low (Figs 4.7J-L; $p<0.001$), with the cell viability of the dual TZD and H_2O_2 treatment showing a further significant reduction with rosiglitazone and troglitazone (Figs 4.7J and K; $p<0.05$). Expression of p-PPARγ:PPARγ remained significantly increased at 18 h for rosiglitazone combined with H_2O_2 (Fig 4.7G; $p<0.001$), while the ratio returned to that observed in untreated controls following troglitazone co-treatment (Fig 4.7H) and lower than untreated controls with pioglitazone co-treatment (Fig 4.7I; $p<0.01$). Extended exposure of TZD agonists for 18 h prior to H_2O_2 exposure also demonstrated no protection to cell viability and significantly decreased cell viability when either TZD was used alone (Fig 4.7M-O; $p<0.01$). A representative TZD (troglitazone), used in combination with H_2O_2, was assessed for apoptosis and mitosis (Fig 4.8A-B). Pre-exposure to troglitazone did not prevent the significant increase in apoptosis caused by H_2O_2 alone (Fig 4.8A; $p<0.05$). Using a high concentration of troglitazone (100 µM) significantly increased apoptosis alone or with H_2O_2 (Fig 4.8A; $p<0.05$). Similarly, troglitazone did not prevent reduced mitosis caused by H_2O_2 alone (Fig 4.8B; $p<0.001$). Using a high concentration of troglitazone (100 µM) significantly reduced mitosis alone or in combination with H_2O_2 (Fig 4.8B; $p<0.001$).

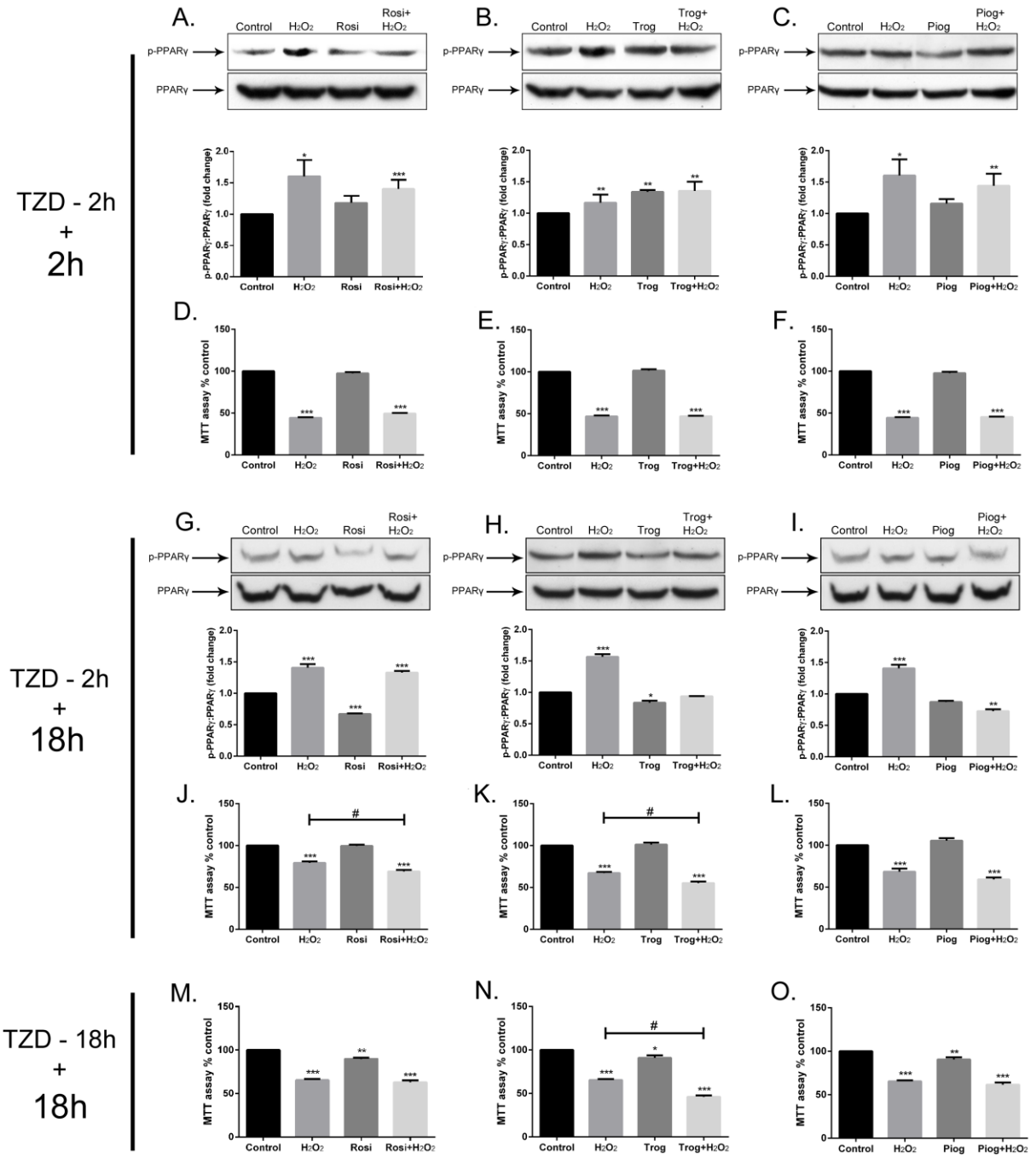

Figure 4.7: PPARγ activation does not protect HK-2 cells against oxidative stress induced injury

HK-2 cells were exposed for 2 h (A. – L.) or 18 h (M. – N.) with either rosiglitazone (Rosi – 10 µM), troglitazone (Trog – 10 µM) or pioglitazone (Piog – 1 µM) followed by 2 h and 18 h exposure to H_2O_2 (0.6 mM) in combination with Rosi, Trog or Piog. Western blot analysis and MTT assay were performed. At 2 h, H_2O_2 alone and in combination with Rosi significantly increased the fold difference in the p-PPARγ:PPARγ ratio compared with controls (A.). H_2O_2 and Trog treatment alone or in combination, significantly increased p-PPARγ:PPARγ (B.). H_2O_2 treatment alone or in combination with Piog significantly increased p-PPARγ:PPARγ (C.). Cell viability significantly decreased following H_2O_2 treatment alone and in combination with Rosi (D.), Trog (E.) or Piog (F.). At 18 h, H_2O_2 exposure alone and in combination with Rosi significantly increased p-PPARγ:PPARγ, while Rosi treatment alone significantly decreased p-PPARγ:PPARγ (G.). H_2O_2

exposure alone significantly increased, while Trog treatment alone significantly decreased, p-PPARγ:PPARγ (H.). H_2O_2 treatment alone significantly increased p-PPARγ:PPARγ, which was significantly decreased when H_2O_2 was used in combination with Piog (I.). Cell viability was significantly decreased following H_2O_2 exposure alone, and this was significantly enhanced when combined with Rosi (J.) or Trog (K.). Pioglitazone treatment in combination with H_2O_2 significantly decreased cell viability compared to Control (L.). Treatment with TZD for an extended period (18 h) prior to H_2O_2 co-treatment for 18 h significantly decreased cell viability alone or in combination with Rosi (M.), Trog (N.) or Piog (O.). Results expressed as mean ± SEM (* $p<0.05$; ** $p<0.01$; ***$p<0.001$, compared to Control; # $p<0.05$, compared as indicated).

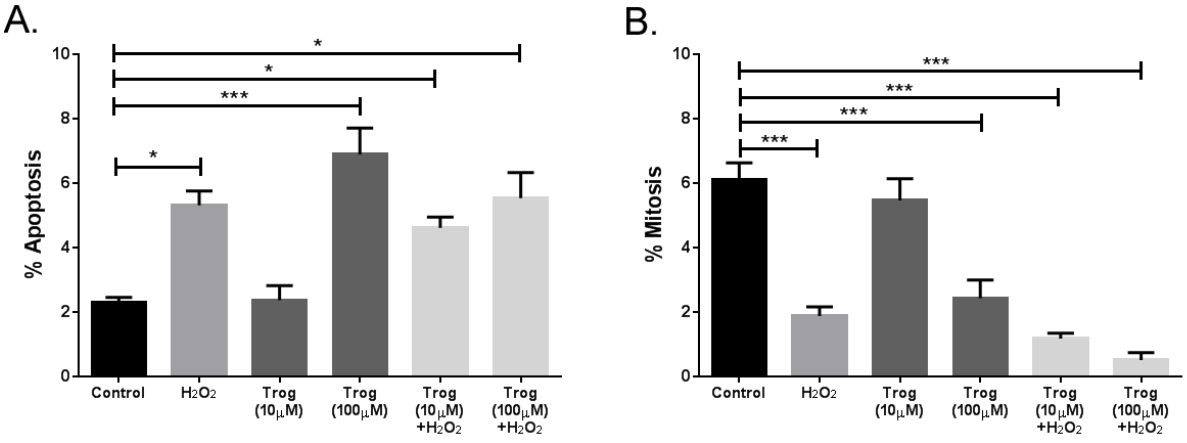

Figure 4.8: The PPARγ agonist troglitazone does not protect against oxidative stress induced apoptosis or reduced mitosis

HK-2 cells were exposed for 2 h with troglitazone (Trog – 10 µM or 100 µM) followed 18 h exposure to H_2O_2 (0.6 mM) in combination with Trog. Apoptosis and mitosis were quantified using morphology and H&E staining. H_2O_2 alone or in combination with Trog (both 10 µM and 100 µM) resulted in a significant increase in apoptosis. Trog (100 µM) was sufficient to significantly increase apoptosis alone. H_2O_2 alone or in combination with Trog (both 10 µM and 100 µM) resulted in a significant decrease in mitosis. Trog (100 µM) was sufficient to significantly decrease mitosis. Results expressed as mean ± SEM (* $p<0.05$; ***$p<0.001$, compared to Control).

4.4 DISCUSSION

Oxidative stress and mitochondrial dysfunction have been implicated in the pathogenesis of kidney disease of diverse causes, including diabetes and CKD, two diseases of increasing incidence (Dounousi *et al.*, 2006; Gomes *et al.*, 2009; Granata *et al.*, 2009). However, the molecular mechanisms are still unclear. Here, oxidative stress-induced PPARγ alterations were associated with mitochondrial destabilisation and a failure to restore mitochondrial health due to defective activation of PPARγ-dependent biogenesis pathways. Furthermore, selective PPARγ activation

enhanced oxidative stress-mediated tubular cell damage that was associated with PPARγ *Ser112* phosphorylation. The results suggest that, despite positive benefits in other tissues, PPARγ activation may be detrimental to kidney PTE cells in the scenario of oxidative stress-induced injury.

Our results demonstrate that PPARγ is present in kidney PTE cells and is responsive early in oxidative stress-induced injury. The associated increase in *Ser112*-phosphorylation of PPARγ (p-PPARγ) was not beneficial to cellular outcome in these cells. The increase in the p-PPARγ:PPARγ ratio may be injurious to cells via development of mitochondrial dysfunction. However, at 18h exposure to oxidative stress, the p-PPARγ:PPARγ ratio was not elevated, perhaps demonstrating that early stress-induced PPARγ dysregulation stimulates a series of persistent negative cellular events, primarily targeting mitochondrial homeostasis.

Oxidative stress-induced post-translational modifications to PPARγ, including phosphorylation, have had little study in kidney PTE cells. In adipocytes, mitogen-activated protein kinase-induced phosphorylation of PPARγ at *Ser112* was linked to decreased transcriptional activity of PPARγ by inhibition of ligand binding and co-factor recruitment (Hu *et al.*, 1996; Zhang *et al.*, 1996; Camp and Tafuri, 1997). In addition, PPARγ phosphorylation at *Ser87* by AMP kinase in Baby Hamster Kidney (BHK) cells repressed the transactivating function of the receptor (Leff, 2003). Our data, demonstrating a decrease in PPARγ transcriptional activity, along with a failure to upregulate PGC-1α and mitochondrial biogenesis, at a time of increased *Ser112* PPARγ phosphorylation in the human kidney PTE cells, agree with those reports. The decrease in total functional PPARγ is likely due to phosphorylation. Similar results have been shown in kidney mesangial cells exposed to a high glucose environment (Whiteside *et al.*, 2009), a mechanism of kidney injury involving increased oxidative stress (Stanton, 2011; Shao *et al.*, 2013).

PTE cells of the kidney have a high density of mitochondria (Hall *et al.*, 2009). It is likely, therefore, that the relationship between PPARγ and mitochondrial function will be especially important. Yang and colleagues have previously shown, in an *in vivo* rat model of ageing, that PPARγ activation attenuates age-related mitochondrial injury in the kidney by maintaining the integrity of the mitochondrial membrane potential (Yang *et al.*, 2009). However, these results represent outcome from the heterogeneous renal cell population, and not specifically mitochondria from PTE cells. The majority of *in vitro* studies, that demonstrate protective actions of PPARγ, do so in glomerular cell types, namely podocytes and mesangial cells (Yang *et al.*, 2006; Kanjanabuch *et al.*, 2007; Miglio *et al.*, 2012). Our results demonstrate oxidative stress-induced PTE cell mitochondrial dysfunction that is associated with a decreased p-PPARγ:PPARγ ratio. This alteration

is persistent, indicating that PPARγ induces negative downstream effects. We hypothesised that PPARγ phosphorylation induced disruptions to the mitochondrial homeostatic machinery, and was responsible for this persistent cumulative dysfunction.

Autophagy is a highly conserved protective response to eliminate damaged cellular components. Mitochondrial homeostasis relies on the degradation of defective mitochondria and upregulation of mitochondrial biogenesis to restore a healthy pool of functioning mitochondria (Egan *et al.*, 2011). Our results demonstrate significant perturbation to these pathways during oxidative stress. The induction of selective mitophagy mediated by the Park2-p62-LC3β pathway is evident following the initial (2 h) response to oxidative stress. However, long-term (18 h) oxidative stress facilitates significant impairments to this system, indicated by p62 aggregation. Park2 upregulation following 2h oxidative stress demonstrates labelling and translocation of the E3-ligase, Parkin, to depolarised mitochondria and initiate poly-ubiquination to signal p62 binding (Geisler *et al.*, 2010). p62 degradation has been shown to be a consistent marker of selective autophagy due to its clearance within the autophagosome (Komatsu *et al.*, 2010; Komatsu *et al.*, 2012; Jiang *et al.*, 2013; Wang *et al.*, 2013), and our results further confirm this with enhanced LC3β expression. Mitophagy has received little study in the kidney, with Parkin-mediated mitophagy previously shown to be dependent upon p62 in HeLa and neuroblastoma cell lines (Geisler *et al.*, 2010). Recently, Ishikawa and colleagues used rat AKI models to demonstrate that increased mitophagy in the kidney was highly influenced by ROS (Ishihara *et al.*, 2013). The results of the present investigation show an increase in p62 following 18h oxidative stress, demonstrating impaired selective turnover and accumulation of p62. Previous studies have demonstrated liver injury is accompanied by the formation of p62-positive inclusions, and that the removal of p62 attenuated this injury (Komatsu *et al.*, 2007). Impaired selective mitochondrial autophagy caused by persistent ROS production and ensuing oxidative damage results in p62 accumulation, which further contributes to cellular dysfunction. This result was compounded by the failure of PPARγ to activate PGC-1α to stimulate mitochondrial biogenesis and restore the cellular redox environment. This change would have provided a continuation of negatively-regulating intracellular signalling, with persistent oxidative stress and reduced mitochondrial-dependent ATP production. This_demonstrates early, persistent, and indirect mitochondrial dysfunction resulting from a failure of PGC-1α activity following oxidative stress.

PPARγ agonist treatment has previously been shown to protect against mitochondrial dysfunction in other cell types, including neuronal (Fuenzalida *et al.*, 2007; Wu *et al.*, 2009) and endothelial cells (Fujisawa *et al.*, 2009). In the kidney, disparate results have been described previously and largely

depend on the cell type and cause of injury (Kanjanabuch *et al.*, 2007; Whiteside *et al.*, 2009; Wu *et al.*, 2009). Important to note is that PPARγ *Ser112* phosphorylation has been shown to modify PPARγ activity, rather than act as a marker of PPARγ activation. PPARγ agonists can inhibit obesity-linked *Ser273* phosphorylation of PPARγ by cyclin-dependent kinase 5 in adipose tissue (Choi *et al.*, 2010). Our results show an inability of rosiglitazone to inhibit PPARγ *Ser112* phosphorylation during oxidative stress, therefore preventing classical downstream actions of PPARγ, primarily the upregulation of PGC-1α and maintenance of mitochondrial homeostasis (Rasbach and Schnellmann, 2007; Hock and Kralli, 2009). This finding appears to be unique to kidney tubular cells. Of note is that PPARα is an alternate inducer of PGC-1α-dependent mitochondrial biogenesis (Portilla *et al.*, 2002; Weinberg, 2011), and its downregulation in response to oxidative stress further impairs the restoration of mitochondrial homeostasis. The ability of rosiglitazone and troglitazone to decrease PTE cell viability following extended oxidative stress is a novel finding and may result from the inability to prevent PPARγ phosphorylation, not only at *Ser112*, but other sites of phosphorylation including *Ser273* and *Ser82* that were not studied here.

In summary, our findings describe oxidative stress-induced PPARγ alterations and resulting mitochondrial destabilisation, and a failure to restore mitochondrial health due to defective activation of PPARγ-dependent biogenesis pathways. These changes may contribute to the pathogenesis of diverse kidney disease, including CKD. A novel finding is that activation of PPARγ by TZD enhances oxidative stress-mediated tubular cell damage that is associated with PPARγ *Ser112* phosphorylation. This may account for tubular damage, and a lack of therapeutic benefit of TZD, seen in some human trials.

CHAPTER 5

In Vivo Model of Oxidative Stress-Induced Kidney Injury

Chapters 3 and 4 investigated specific pathways that are perturbed and could contribute to oxidative stress in one important cell type in the kidney, the PTE cell. However, the renal microenvironment is a complex three-dimensional network of heterogeneous cell populations comprising glomeruli, tubules, interstitial space and vasculature. Alterations that occur in one cell are likely to have a stochastic effect not only on neighbouring structures, but on whole organ physiology. Therefore, an *in vivo* model of oxidative stress-induced kidney injury was used to investigate alterations identified in Chapters 3 and 4, as well as identify temporospatial changes in the kidney resulting from oxidative stress.

5.1 INTRODUCTION

The pathophysiology of CKD, of multiple causes, involves persistent, insidious, cycles of common disease processes including cell death, fibrosis, senescence and inflammation. However, an important concept in understanding the pathogenesis of CKD and its progression to ESKD is that this likely involves common processes that are independent of the original cause of CKD. Important characteristics of CKD progression, that are independent of its cause, include reductions in renal mass and nephron number, vascular insufficiency, cell cycle disruption and maladaptive repair mechanisms. Clinical AKI, and experimental studies using AKI models, also highlight these characteristics of injury, leading to the suggestion of common integrated clinical syndromes (Fig 5.1) (Chawla and Kimmel, 2012). The early teaching that patients who survive an episode of AKI achieve full or nearly full recovery (Clarkson *et al.*, 2008), has been surpassed by current evidence, from a diverse range of large population studies, demonstrating a significant risk for the progression to advanced stage CKD in patients that survive a single episode of AKI (Ishani *et al.*, 2009; Chawla *et al.*, 2011; Coca *et al.*, 2012).

As demonstrated in Chapters 3 and 4, mitochondrial alterations influence PTE cell outcome during oxidative stress. Oxidative stress, mitochondrial dynamics and metabolism have all been shown to play an intimate role in AKI, however the role of mitochondrial function during progressive renal pathologies, such as CKD and ESKD, has not yet received detailed investigation.

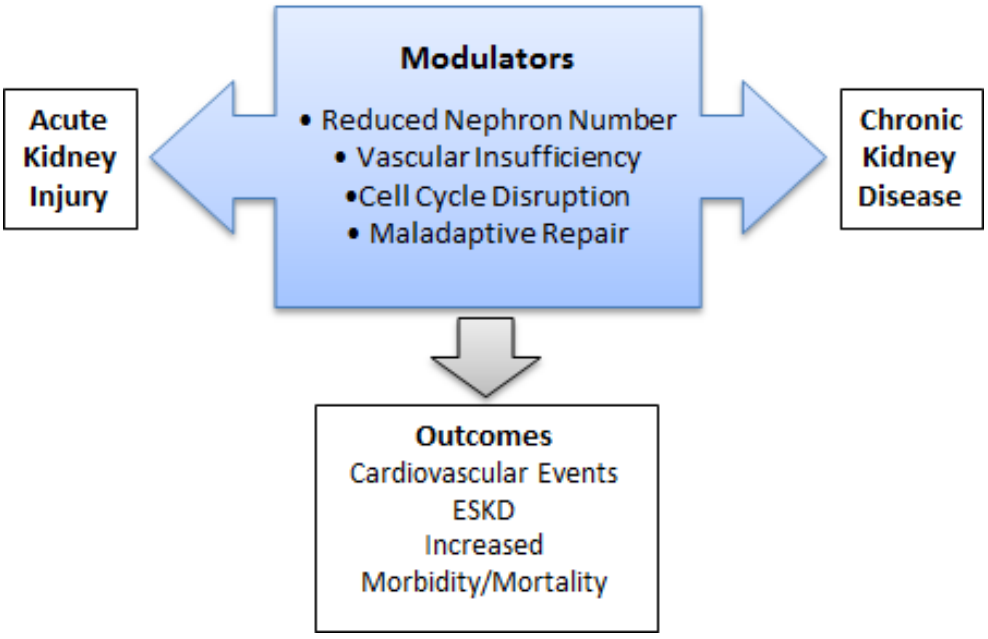

Figure 5.1: Acute kidney injury and chronic kidney disease as an integrated syndrome
Acute kidney injury and chronic kidney disease has a bi-directional relationship that is modulated by some common pathological mechanisms such as reduced nephron number, vascular insufficiency, cell cycle disruption, and maladaptive repair. These mechanisms primarily contribute to common outcomes of this progression such as increased cardiovascular events, end stage kidney disease (ESKD), and increased morbidity and mortality.

IR injury is a common cause of AKI. The kidney has minimal glycolytic capacity owing to an abundance of PTE cells, high activity, and reliance on oxidative phosphorylation for ATP synthesis, increasing the susceptibility to hypoxia (Basile *et al.*, 2001). The dynamics of mitochondria during ischaemia and following reperfusion have been extensively studied and are shown to involve oxidative stress and overproduction of ROS (Hall *et al.*, 2013). The current understanding of mitochondrial dynamics during ischaemic starvation is characterised by depletion in ATP, depolarisation of the mitochondrial membrane potential (MMP), disruption of the inner mitochondrial membrane (IMM) cristae that house the ETC, due to a loss of ATP-dependent actin polymerisation, and mitochondrial swelling due to a loss of osmotic regulation. Re-energising mitochondria is necessary for ATP recovery and cell survival following ischaemia. However, alterations to the ETC components of the IMM cristae lead to a defect in the functional capacity of mitochondria to produce ATP through oxidative phosphorylation. At the point of reperfusion, and the re-presentation of O_2 to damaged components of the ETC, increased mitochondrial ROS production is thought to contribute significantly to the pathogenesis of kidney IR injury. Within the literature, there has been a broad classification of mitochondrial dysfunction following IR injury. The fate of the cell during reperfusion, either via cell death, senescence, impaired function or

complete restoration (reversible injury), appears to be determined by the ability of mitochondria to restore cell metabolism and redox control. Mitochondrial dysfunction should not exclude the homeostasis of mitochondrial degradation and regeneration via biogenesis, as these also contribute significantly to the subsequent cell fate and function. Furthermore, the basis of our current understanding of mitochondrial biology *in vivo* during normal and diseased conditions is primarily based on the extrapolation of *in vitro* experimental evidence from isolated cells or organelles. There has been little investigation of the contribution of mitochondrial ROS *in vivo*, and their contribution to IR-induced AKI.

The kidneys constitute less than 0.5 % of body mass but receive greater than 20 % of the total cardiac output which is filtered within the kidneys. Thus, the metabolism of the kidneys is vitally important for overall health. The supply and utilisation of metabolic substrates for oxidative phosphorylation, such as NADH and FAD, is necessary for mitochondrial and cellular function. NADH is a metabolic substrate for complex 1 of the mitochondrial ETC and exists primarily in two forms - oxidised NAD+ and reduced NADH. These two molecules are continually being cycled through a redox reaction and are, therefore, vital to maintaining a healthy intracellular redox environment. NADH is produced from the conversion of oxidised NAD+ in the citric acid cycle (Figure 5.2). The biosynthesis of NAD+ can occur either through *de novo* production from tryptophan or aspartic acid, or from the salvage of preformed compounds containing nicotinamide (nicotinic acid and nicotinamide) commonly obtained through the diet. An amount of NAD+ is phosphorylated by NAD+ kinase to form NADP+ that can go on to be reduced to form NADPH. NADP+ is similar to NAD+, however it plays a different role in metabolism. The reduced forms of the NADP+/NADPH and NAD+/NADH ratios (NADPH and NADH, respectively) are the major components. NADPH is primarily required as a reducing agent for cellular anabolic reactions such as lipid and nucleic acid synthesis and is considered to play little part in renal metabolism given its high energy requirements. FAD is another important metabolic substrate linked to mitochondrial regulation. FAD is a redox cofactor and can exist in two different forms depending on its state within a redox reaction – oxidised FAD and reduced $FADH_2$. $FADH_2$ is generated by the citric acid cycle and binds with complex II of the mitochondrial ETC that oxidises succinate to fumarate. Two hydrogen ions are left within the inner-mitochondrial membrane to contribute to the polarisation of the MMP.

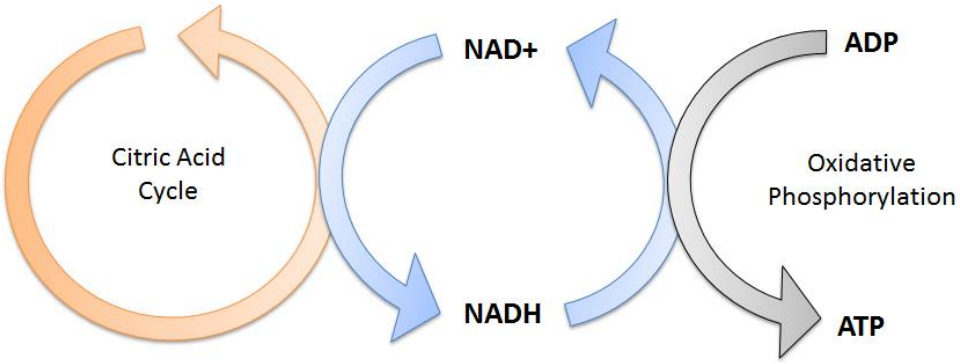

Figure 5.2: Simplified schematic of integrated metabolism that occurs within mitochondria to produce ATP

NADH is produced from the conversion of oxidised NAD+ in the citric acid cycle which then acts as a substrate for complex I of the mitochondrial electron transport chain for oxidative phosphorylation that drives the conversion of ADP to ATP. Perturbation to any point of this cycle can result in cell dysregulation due to a reduction in ATP production.

As mentioned in Chapter 1, Section 1.2.9, the spectral properties of NAD+, NADH, FAD and $FADH_2$ can indicate dynamic metabolic processes (the combination of NADH and NADPH will be refered to as NAD(P)H, since NADPH is detected by MPM on the same wavelength and therefore cannot be excluded. However, NADPH is considered to contribute minimally). Direct *in vivo* visualisation of metabolic substrates can be achieved through MPM and FLIM techniques. The basic principles of fluorescence apply to MPM imaging. Fluorescence occurs by the absorption of a photon by a fluorophore that brings an electron from the fluorophore to an excited state. The electron returning to its ground state causes the release of a photon (fluorescence emission photon), which is then efficiently detected (Coling and Kachar, 2001; Ghiran, 2011). The initial excitation photon is typically of a high energy. This is known as single-photon fluorescence. MPM fluorescence is based on the simultaneous absorption of two low-energy, near-infrared wavelength, photons by a fluorophore; hence the alternative name "two-photon fluorescence" (Figure 5.3). Three-photon excitation and second harmonic generation work on similar principles and can also be used to visualise fluorescent optical sections (Zipfel *et al.*, 2003). Although the energy of either of these photons is too low to raise an electron to an excited state, it is the combination of the two energies that is sufficient to excite and thus release a fluorescence emission photon. This approach is far more compliant to biological tissue due to significantly reduced phototoxicity. A further advantage of using near-infrared wavelengths, instead of ultraviolet light, for fluorescence excitation is the reduction of scattering and increase in imaging penetration depth in the sample from approximately 20 µm to 500-600 µm. However, in the kidney, the maximal penetration depth is approximately 150 µm owing to substantial scattering of emission photons from the high refractory index and heterogeneity of kidney tissue (Young *et al.*, 2011a; Young *et al.*, 2011b).

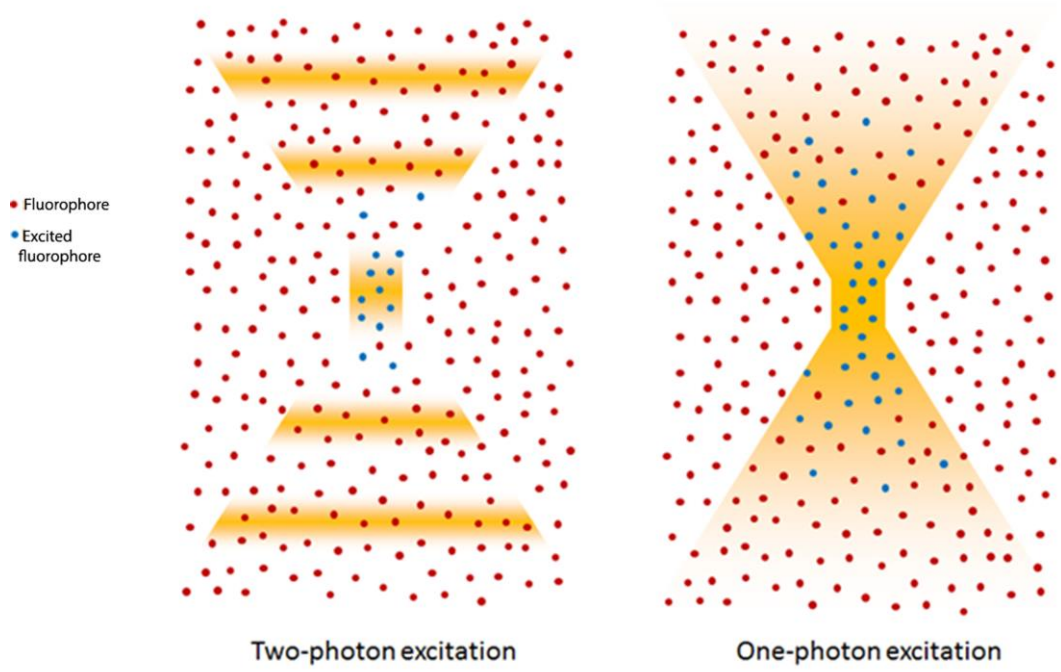

Figure 5.3: Pictorial representation of one-photon and two-photon fluorescence
Two-photon excitation occurs via simultaneous absorption of infrared laser pulses at a single point, compared to one-photon excitation which uses visible or ultraviolet light lasers that excite photons throughout the biological material, and thereby may casue phototoxicity.

A useful application of FLIM in conjunction with MPM in the kidney is measuring the fluorescence lifetime of NAD(P)H. NAD(P)H lifetime measurements are widely used for metabolic and redox imaging *in vitro* and *in vivo* (Bird *et al.*, 2005; Skala *et al.*, 2007a; Skala *et al.*, 2007b; Sanchez *et al.*, 2010; Leite-Silva *et al.*, 2013; Thorling *et al.*, 2013). The lifetime of NAD(P)H is resolved as a two-component system with the short (α_1) (~0.3-4 ns) and long (α_2) (~2.3 ns) lifetime represented as the free and protein-bound conformations, respectively (Lakowicz *et al.*, 1992; Niesner *et al.*, 2004; Berezin and Achilefu, 2010). As previously mentioned, the oxidised form of NADH, NAD+, is not fluorescent and the ratio of NADH:NAD+ has been used previously as a measure of the redox state of the cell. Bird and colleagues demonstrated that the free-to-bound ratio of NAD(P)H, represented by the ratio of the amplitude coefficients for the short and long lifetimes (i.e. α_1/α_2), is related to the NADH/NAD+ ratio and can be used as an indicator for redox changes within the cell (Bird *et al.*, 2005). FAD is also examined routinely by FLIM for intracellular metabolic and redox states. While FAD can be found in a free and protein-bound conformation, the former has a significantly higher quantum yield with a lifetime of 2.91 ns (Berezin and Achilefu, 2010). In contrast to NAD(P)H, only the oxidised form of FAD is fluorescent and is used to measure changes in the redox state of the cell in combination with NADH (Chance *et al.*, 1979). The fluorescence lifetimes of NAD(P)H and FAD are useful indicators of IR injury within the liver and kidney *in vivo* (Abulrob *et al.*, 2007;

Thorling *et al.*, 2011; Thorling *et al.*, 2013). The fluorescence lifetime changes associated with necrosis and apoptosis have also been described and can be used to measure tissue responses to drug treatments and disease states within the kidney (Wang *et al.*, 2008; Sanchez *et al.*, 2010; Yu *et al.*, 2011)

There are many pathological mechanisms responsible for driving the progression of CKD. Structural defects give rise to reduced renal function and result in a viscious cycle of increased systemically-circulating toxins and a failure of compensatory and protective mechanisms. However, changes in cellular metabolism often underlie subsequent structural changes and perturbed cell signalling common to all pathogenic mechanisms. The aim of this chapter was to use *in vivo* MPM to visualise IR-induced tubular redox changes and tubulointerstitial damage in real-time and correlate these with histology and markers of oxidative stress.

5.2 MATERIALS AND METHODS

5.2.1 Animals and kidney ischaemia-reperfusion injury model

Male 4-6 week old C57Bl6 mice were anaesthetised using a ketamine/xylazine combination (10 mg/mL and 1 mg/mL, respectively) administered via intra-peritoneal injection at a dose of 10 μL/g body weight. Bilateral kidney IR injury was induced according to the protocol outlined in Chapter 2, Section 2.6.2. Briefly, the left kidney was exposed via a flank incision and the renal artery was cleared of fat before a non-traumatic vascular microclamp was placed over the vessels. The left kidney was placed within the body cavity, the mouse turned to its right side, and the procedure repeated. The microclamps were removed following 20 min occlusion of left or right renal vessels. For chronic injury to the kidney, the muscle and skin incisions were sutured, and mice were allowed to recover for 21 days. From previous experiments (Gobe *et al.*, 1990; Gobe *et al.*, 2014), significant progression to CKD had been observed to occur by 21 days. For intravital MPM during IR injury, a modified protocol was performed (Section 5.2.2). All experiments were approved by the University of Queensland Animal Ethics Committee 2013 – AEC No: MED/053/12/CKDR.

5.2.2 Intravital MPM of kidney ischaemia-reperfusion injury

A detailed protocol is outlined in Chapter 2, Section 2.6.3. Briefly, mice were anaesthetised and the left kidney externalised by making a left flank incision. Renal vessels were occluded and the mouse was moved to the MPM stage. A heated jacket (38 ºC) was placed over the mouse to maintain normal body temperature and images of the ischaemic kidney were acquired over the 20 min period from when the clamp was attached. Intravital imaging during initial reperfusion was performed by

releasing the microclamp, then quickly replacing the mouse to the MPM stage. Images were acquired over a 40 min period from when the microclamp was removed. Both left and right kidneys from healthy control mice and 21-day IR mice were imaged by the same procedure, with clamping omitted at the time of MPM. Images were captured using a Nikon Ti Eclipse – LaVision MPM equipped with an ultrashort pulse mode locked 80 MHz Titanium:Sapphire MaiTai laser and ImSpector Pro software. The excitation wavelength was set to 740 nm for NAD(P)H fluorescence and 900 nm for collagen. Emitted light was collected using three photomultiplier tube filters: 447 nm – 460 nm (blue), 485 nm – 550 nm (green), 575 nm – 630 nm (red). The objective was placed in a field of view that visualised detailed tubular structures and serial (30-50) penetrating slice images were acquired from the renal cortex to a depth of 50-70 μm. A minimum of three fields of view per kidney was obtained. Imaris x64 7.6.0 software was used to adjust the minimum and maximum exposure settings consistently throughout all acquired images for standardised quantification of fluorescence intensity. ImageJ was used to obtain mean fluorescence intensity values for NAD(P)H (green channel). For each of the three fields captured per kidney, the epithelial layer of definitive continuous tubules was selected and measured for mean intensity. Eight tubules per z-slice image were measured from five selected z-slice images per field.

5.2.3 Fluorescence lifetime imaging microscopy

FLIM was performed on mouse kidney slices immediately post-sacrifice in healthy control and 21-day IR mice (2 kidneys for controls or 21-day IR, 3 fields of view per kidney). A detailed protocol is outlined in Chapter 2, Section 2.6.7. Briefly, kidneys were harvested after euthanasia of mice and placed on ice. A coronal kidney section was placed on a glass slide and overlayed with a glass coverslip. Time from death to first image capture was no more than 30 min. Images were captured using a DermaInspect system equipped with an ultrashort pulsed mode-locked 80 MHz Titanium:Sapphire MaiTai laser. The excitation wavelength was set to 740 nm for kidney endogenous fluorescence with emission signal range of 350 to 650 nm. FLIM data were collected with a time-correlated single-photon counting (TCSPC) SPC-830 detector integrated into the DermaInspect MPM system. Fluorescence emission was spectrally resolved between three linearly arranged photon counters through the use of three dichroic filters that divide the emission light into three channels for each photon counter: 350 to 450 nm (NAD(P)H), 450 to 515 nm (NAD(P)H and FAD), and 515 to 610 nm (FAD). FLIM data analysis was performed using SPCImage 4.8.

5.2.4 Histology

Following intravital MPM, kidneys were cut transverse to the length of the kidney at the equatorial plane, and half was fixed in 4 % formalin overnight, embedded in paraffin, and stained with H&E

according to the protocol outlined in Chapter 2, Section 2.4.1. Stained slides were scanned using Aperio ScanScope software software and visualised using ImageScope software.

5.2.5 Western immunoblotting

Following intravital MPM and euthanasia, the second half of the kidneys (after tissue collection for histology, see Section 5.2.4) was snap frozen in liquid nitrogen and stored at -80 ºC. Kidney tissue proteins were extracted and Western immunoblotting was performed for TGF-β1, SOD2, Keap1 and Nrf2, as outlined in Chapter 2, Section 2.5.

5.3 RESULTS

5.3.1 Histopathology of renal ischaemia-reperfusion injury

Figure 5.4 gives an overview of the kidney structure from controls (A), IR mice 20-40 min (early) after reperfusion (B), and IR mice 21 days after reperfusion (C). Kidneys from control mice had no abnormal structures. Kidneys from early IR mice showed evidence of cell swelling and eosinophilia especially in the outer stripe of the outer medulla (straight segment of the proximal tubule [S3] and thick ascending limb of the Loop of Henle), and cast formation along the nephron. The IR kidneys at 21 days showed diffuse areas of atrophy (intensely stained purple because of atrophic epithelial structures staining with haematoxylin in C) within the outer medulla but also radiating up into the cortex.

Figure 5.5 demonstrates high power microscopy of the control and early IR kidneys. In A and B, normal kidney structure of the cortex (A) and medulla (B) is demonstrated. IR kidneys that had had 20 min bilateral renal ischaemia and then were collected after the early reperfusion time, during which they had been viewed with MPM (20-40 min), are demonstrated in C and D. C shows minimal disruption of the cortex but some epithelial cell swelling and cast formation, in contrast with D, where there is clear evidence of epithelial cell swelling and eosinophilia in the proximal tubule straight segment and the thick ascending limb of the Loop of Henle.

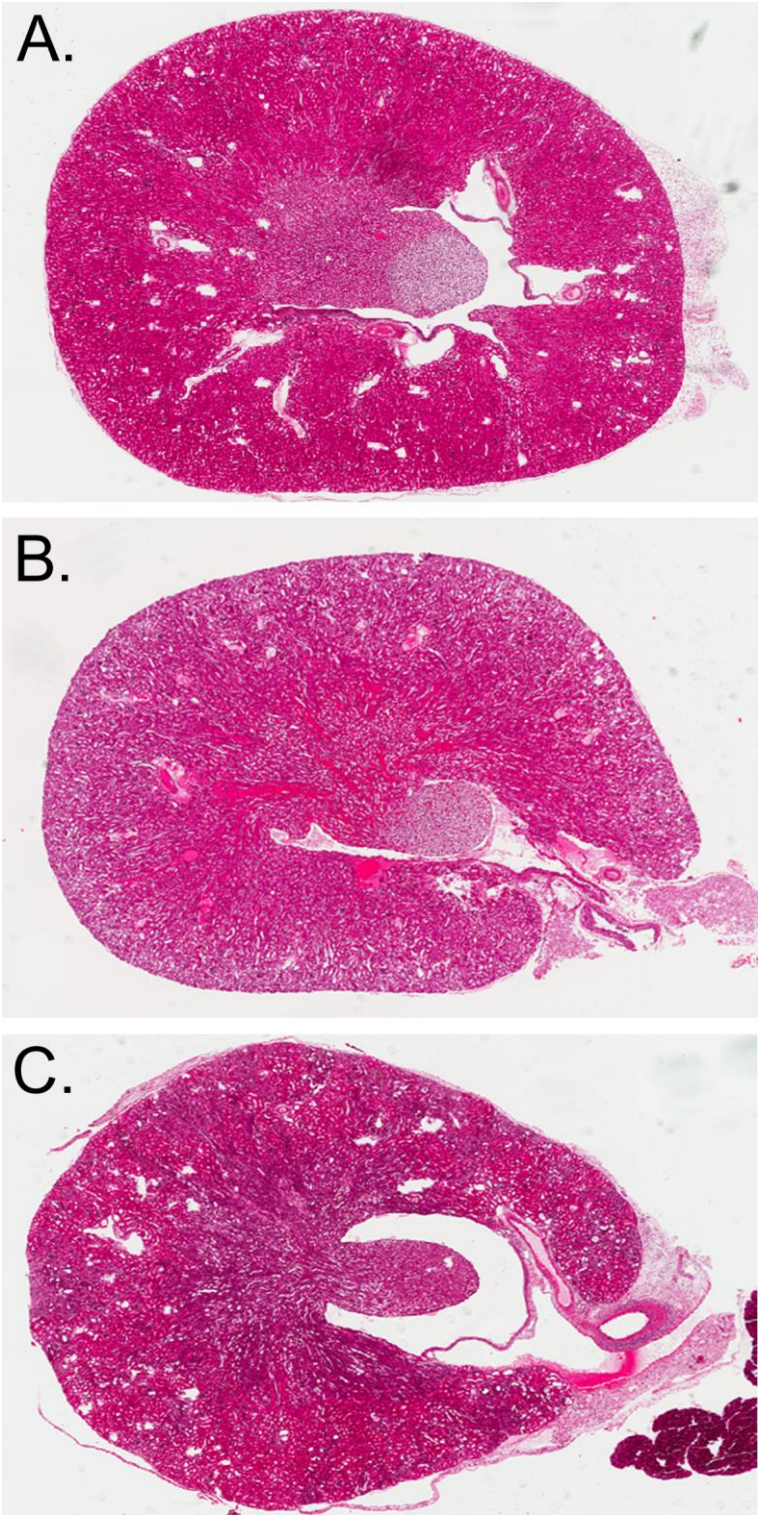

Figure 5.4: Overview of the kidney structure for IR experiments
Kidneys from controls (A), IR mice 20-40 min (early) after reperfusion (B), and IR mice 21 days after reperfusion (C) are demonstrated. The changes in B are subtle at this magnification but show general swelling around the outer stripe of the outer medulla, and debris in the lumens of the nephrons. In C areas of atrophy (intense stain) are clearly visible in the medulla, and radiating up into the renal cortex**.**

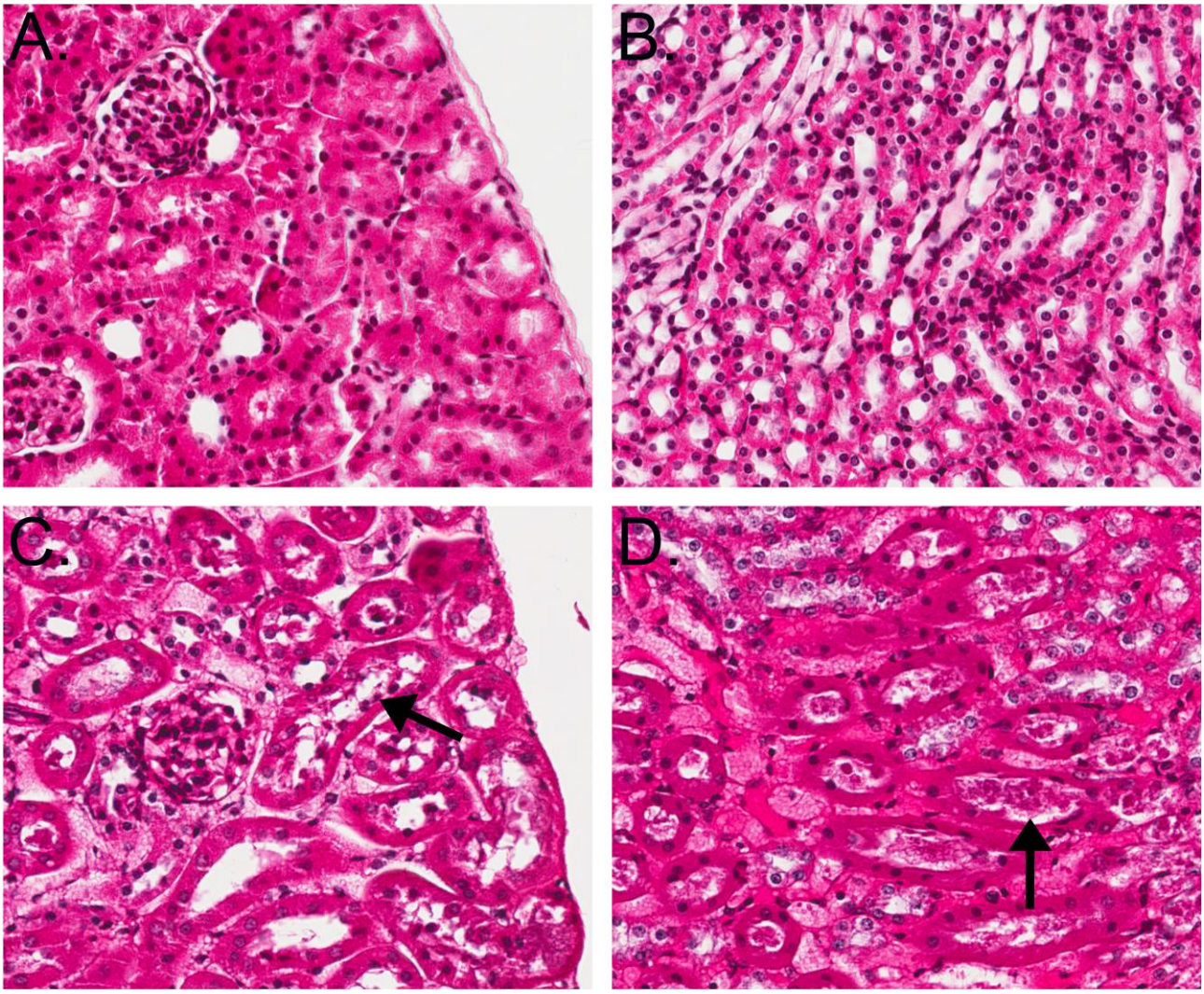

Figure 5.5: Early IR changes to kidney structure
Control kidney cortex is demonstrated in (A.) and control kidney medulla is demonstrated in (B.). (C.) demonstrates early changes to the cortex at reperfusion. Cast material can be found in the lumen of tubules (arrow), disappearance of the brush border, and peritubular vascular expansion. (D.) demonstrates early changes to the medulla at reperfusion. Red blood cell accumulation is observed within thick straight tubules (arrow) and peritubular vascular expansion.

Figure 5.6 demonstrates higher power microscopy of the control and 21 day IR kidneys. In A, normal kidney structure of the cortex is demonstrated. Cortex was selected because this is the zone of the kidney that can be visualised by MPM. IR kidneys that had had 20 min bilateral renal ischaemia and then were collected after 21 days are demonstrated in B and C (cortex) and D (medulla). All show evidence of atrophy. Although the vicinity of the glomeruli to the renal casule should have allowed their visualisation using MPM, in only one instance was a glomerulus seen as a round, non-fluorescent area. Figure 5.7 demonstrates specific microscopic features of the cortex of 21 day IR kidneys. Control kidney cortical structure is demonstrated in A. In B, a distinct subcapsular intensely-stained atrophic region is seen with relatively healthy tubules deeper in the cortex. C and D demonstrate some of the pathological characteristics of the atrophic cortical regions, with apoptosis (arrows) and a golden, probably lipofuscin, pigment indicated by asterisks. Lipofuscin pigment is an indicator of autophagy.

5.3.2 Renal ischaemia-reperfusion injury promotes structural and metabolic changes that can be visualised by intravital multiphoton microscopy

Intravital MPM (Excitation: 740 nm) allows clear visualisation of the renal cortical network in healthy control kidney from endogenous NAD(P)H fluorescence (Fig 5.8A-C). Cellular boundaries and tubular architecture was identifiable showing tubular lumen and interstitial space. During 20 min ischaemia, tubular diameter increased causing a reduction in the interstitial space, luminal material was present (Fig 5.8D-F), and NAD(P)H fluorescence significantly increased (Fig 5.8J; $p<0.01$ compared to control). The greatest amount of tubular and cellular damage occurred at the early stages of reperfusion (5 to 40 min following the release of the microclamp). Tubular epithelial cell effacement and the formation of cast material, were well as the appearance of epithelial cell striations, are apparent at this time (Figure 5.8G-I).

Chronic renal pathology was evident 21 days following IR when visualised with intravital MPM (Fig 5.9) with widespread areas of tubular atrophy containing highly fluorescent punctate regions most likely demonstrating enlarged lysosomes (Fig 5.9D-E). Within areas of observable atrophic pathology, were structurally-normal cortical tubules which contained a significantly higher NAD(P)H fluorescence compared to control kidneys (Fig 5.9G). Areas of observable pathology were highly variable as is demonstrated in Fig 5.9E. The endogenous fluorescence of the kidney cortex (collagen) was visualised at an excitation of 900 nm via second harmonic generation. This is clearly depicted by a 3D-reconstruction from Z-stack images co-detecting endogenous NAD(P)H fluorescence of tubules and collagen of the renal capsule (Fig 5.10A). The capsule appeared to thicken by 21 days after IR compared to control kidneys. This was consistent with histological

observations (Fig 5.6 and 5.7B). Collagen was not detected within the tubulointerstitial space via MPM (900 nm).

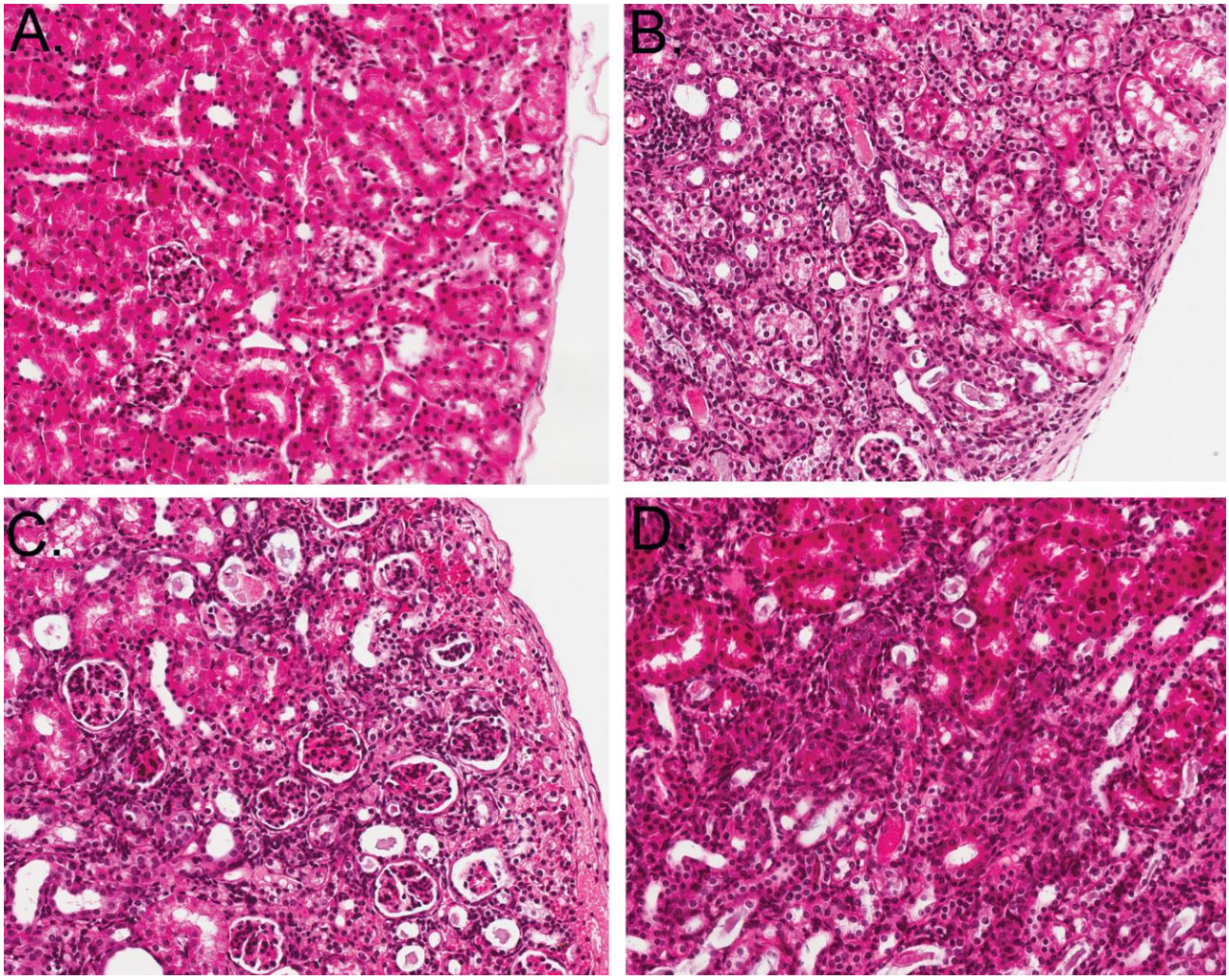

Figure 5.6: 21 day IR pathology
Control kidney cortex is demonstrated in A. B and C demonstrate areas of atrophy in the cortex of 21 day IR kidneys. In both, there is thickening of the capsular membrane. In B, atrophic tubules intermix with relatively healthy tubules in the subcapsular region. In C, there is general subcapsular atrophy, and here the glomeruli are close enough to the renal capsule to allow visualisation with MPM. In D, the medulla of the IR kidneys showed evidence of previous acute injury that had healed and had developing fibrosis. These regions were too deep in the kidney to be seen by MPM.

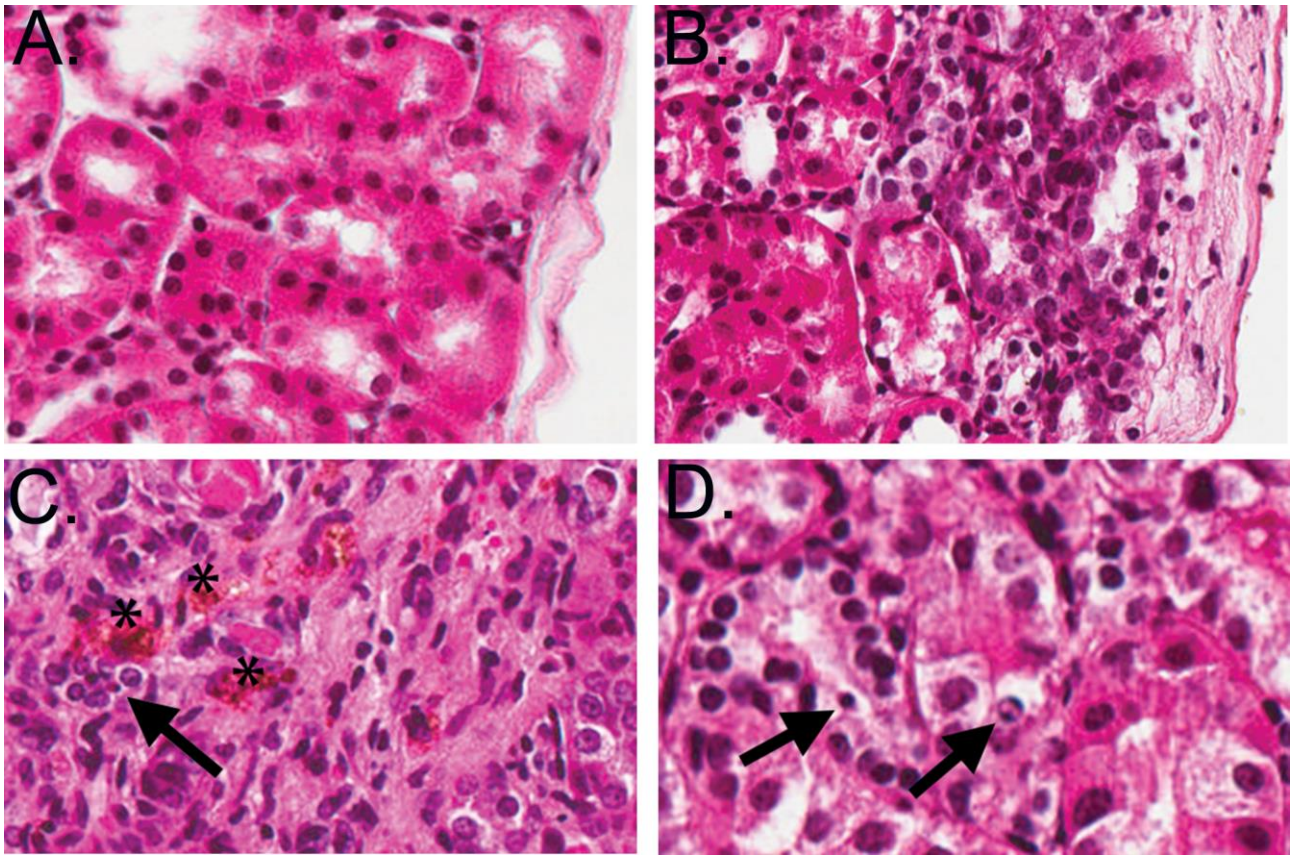

Figure 5.7: High power microscopy 21 days post IR injury
Control kidney cortical structure is demonstrated in A. In B, a distinct subcapsular intensely stained atrophic region is seen with relatively healthy tubules deeper in the cortex. C and D demonstrate some of the pathological characteristics of the atrophic cortical regions, with apoptosis (arrows) and a golden, probably lipofuscin, pigment indicated by asterisks.

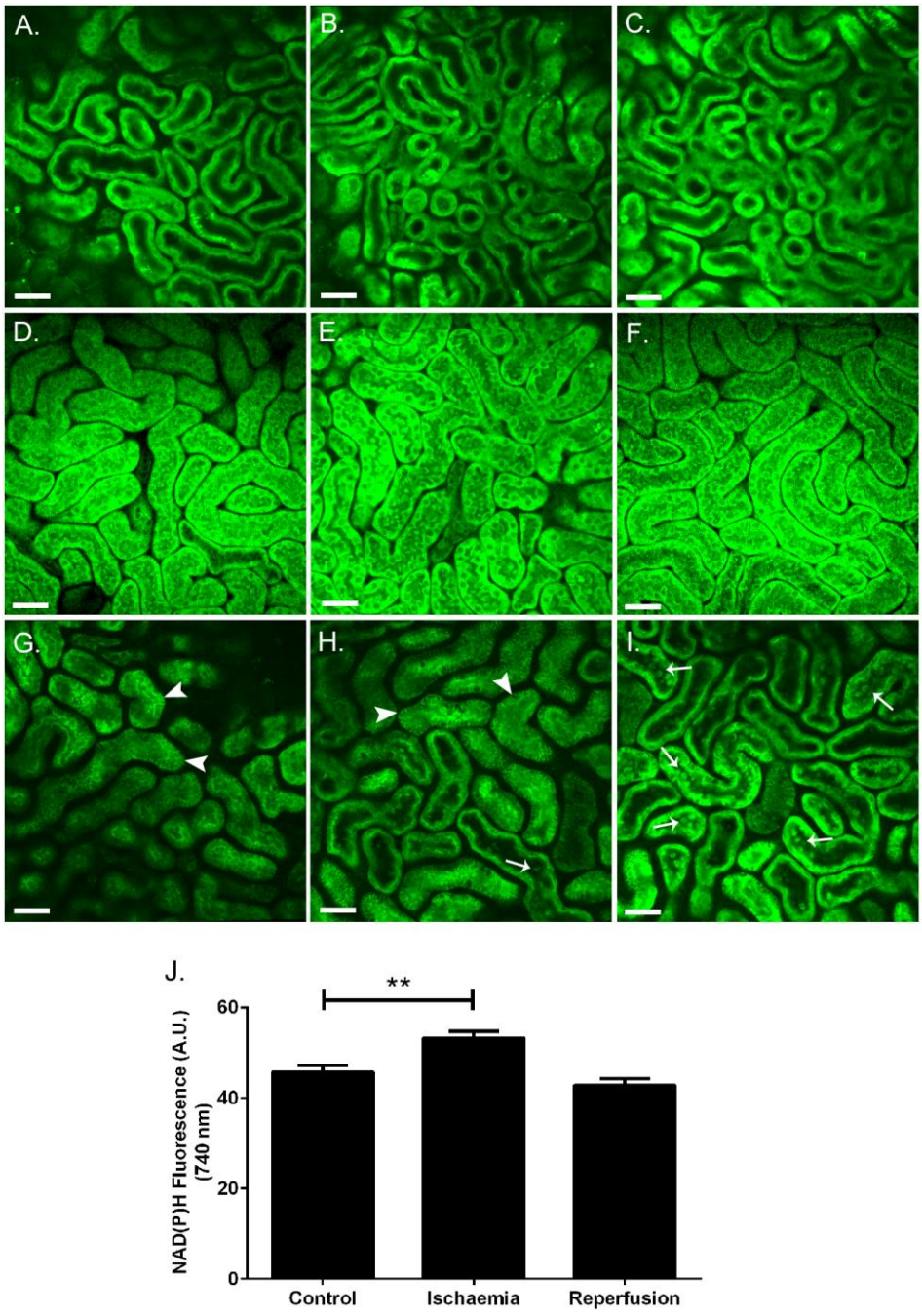

Figure 5.8: Intravital MPM demonstrates metabolic and structural alterations during kidney IR injury

Endogenous fluorescence of NAD(P)H excited at 740 nm in the healthy control kidney cortex clearly demonstrates the cortical tubular network with distal tubules, proximal tubules with associated brush border, and interstitial space (A.-C.). During 20 min ischaemia, tubular swelling and a reduction in interstitial space is evident (D.-F.) and is associated with a significant increase in tubular cell NAD(P)H endogenous fluorescence (J.). Tubular pathology is apparent during immediate reperfusion (G.-I.), demonstrated by epithelial cell striations (arrow head), tubular cell effacement and the formation of cast material (arrow) all of which indicating a loss of cell integrity, in some cases early cell death, but also perhaps repairable damage. Results expressed as mean ± SEM tubular epithelial cell fluorescence a 740 nm (** $p<0.01$ compared as indicated). Scale bar represents 50 µm.

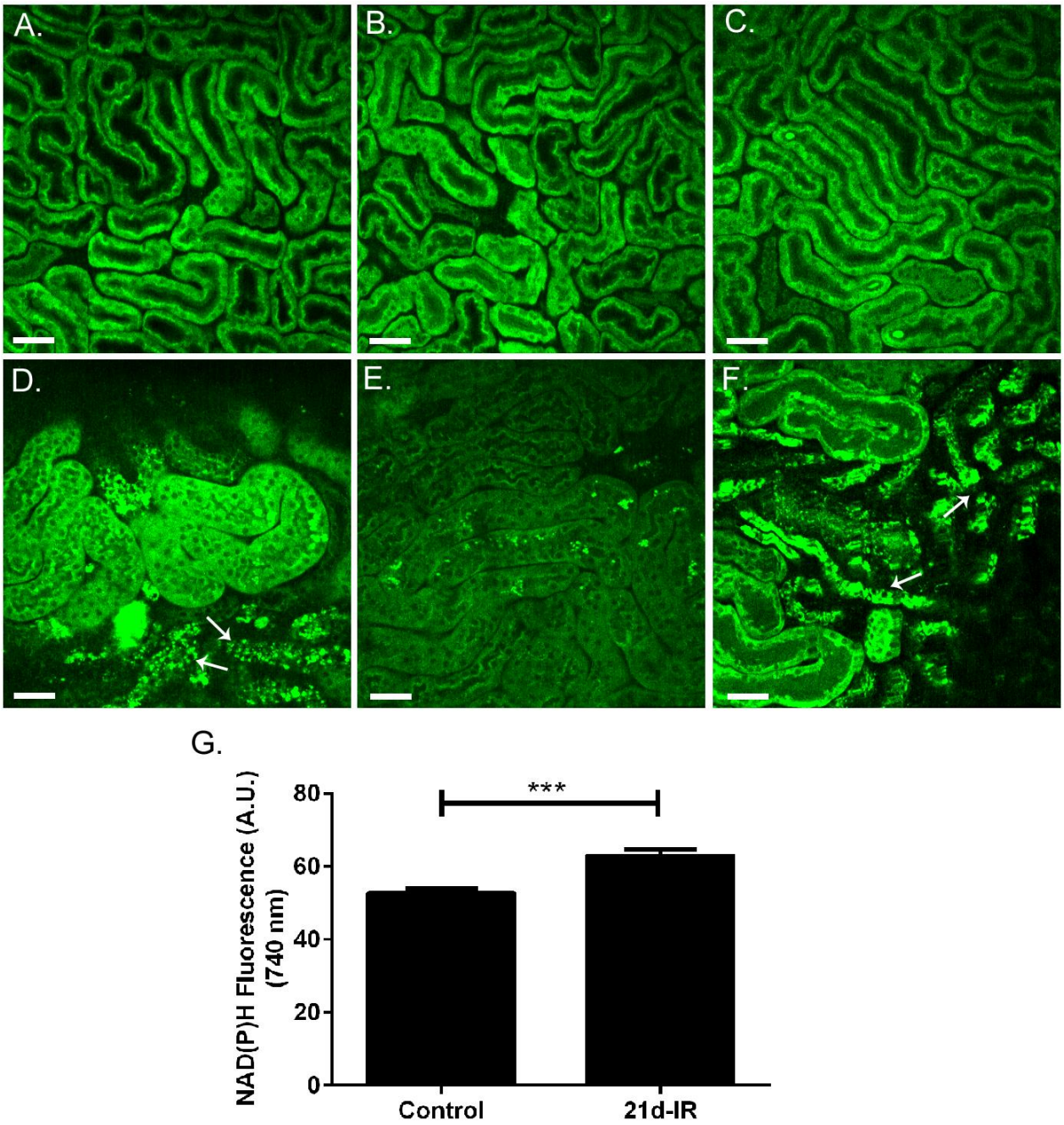

Figure 5.9: Intravital MPM demonstrates metabolic and structural alterations in the chronically damaged kidney following IR injury

Endogenous fluorescence of NAD(P)H excited at 740 nm in the healthy control kidney cortex clearly demonstrates the cortical tubular network with distal tubules, proximal tubules with associated brush border, and interstitial space (A.-C.). 21-days following IR injury (21d-IR) (D.-F.), there was widespread areas of tubular atrophy with highly fluorescent punctate regions most likely demonstrating enlarged lysosomes (arrow). Tubular structure was highly variable with structurally normal tubules appearing directly within areas of atrophy, which demonstrated a significantly greater NAD(P)H fluorescence signal (G.). Results expressed as mean ± SEM tubular epithelial cell fluorescence a 740 nm (*** $p<0.001$ compared as indicated). Scale bar represents 50 µm.

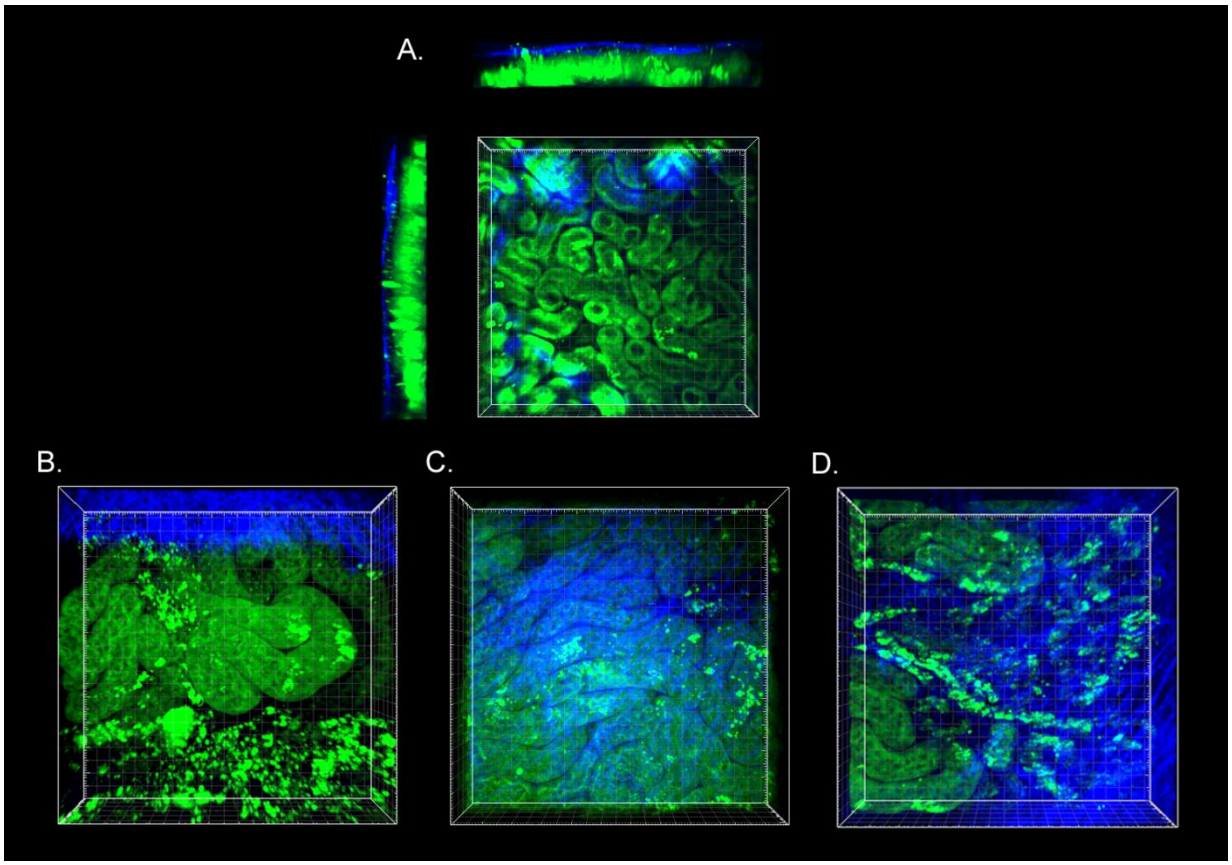

Figure 5.10: Three-dimensional reconstruction of kidney cortex using endogenous NAD(P)H and collagen fluorescence with MPM

(A.) Healthy control kidney demonstrates a normal cortical tubular architecture underlying the renal capsule. Green – Ex: 740 nm; Blue – Ex: 900 nm. (B.-C.) 21-days post IR, tubular pathology is present demonstrated by areas of tubular atrophy. The kidney capsule can be visualised and was shown to be thicker. However no collagen was detected using MPM within areas of atrophic damage within the parenchyma of the cortex.

5.3.3 Ischaemia-reperfusion injury promotes long-term alterations to tubular cell metabolism in the kidney cortex

Representative FLIM images of the τ_m (pseudocoloured according to the average weighted lifetime τ_m) are shown in Figure 5.11 across three spectral channels depicting NAD(P)H, NAD(P)H/FAD and FAD from control and 21d-IR kidney cortex. The results demonstrate that, in the first channel (E_m 350-450 nm; NAD(P)H), there is a change in the τ_m demonstrated by a shift from blue to green pseudocolour of NAD(P)H in 21d-IR kidneys compared to control (Fig 5.11A and B). This indicates an increase in the τ_m of NAD(P)H (Fig 5.11D). This observation is also demonstrated in the histogram data by a right shift of the 21d-IR kidneys compared to control (Fig 5.11C). Channel 2, which detects both NAD(P)H and FAD, demonstrated a significant increase in the τ_m of NAD(P)H/FAD following 21d-IR compared to the control kidney (Fig 5.11E, F and H). This was further demonstrated with a right shift of the 21d-IR NAD(P)H/FAD lifetime compared to control (Fig 5.11G). Isolating the spectral properties of FAD in channel 3 demonstrated no significant differences between control and 21d-IR kidneys (Fig 5.11I-L), suggesting that major differences in channel 2 are primarily due to τ_m changes to NAD(P)H.

5.3.4 Ischaemia-reperfusion injury promotes chronic impairments to redox signalling in the kidney

Oxidative stress-responsive proteins were shown to be significantly altered following early acute injury to the kidney and at 21 days post IR (Fig 5.12). Nrf2 is a transcription factor responsible for the expression of vital cytoprotective genes, and was shown to be significantly upregulated early after initial reperfusion and significantly decreased following long-term injury compared to control (Fig 5.12A-B; *** $p<0.001$). The intracellular inhibitor of Nrf2, Keap1, and the mitochondrial antioxidant protein, SOD2, decreased significantly following 21d-IR (Fig 5.12C; *** $p<0.001$ and Fig 5.12D; * $p<0.05$). The pro-fibrotic cytokine TGF-β1 significantly decreased following early reperfusion but was significantly increased following 21d-IR compared to control kidneys (Fig 5.12E; $p<0.01$).

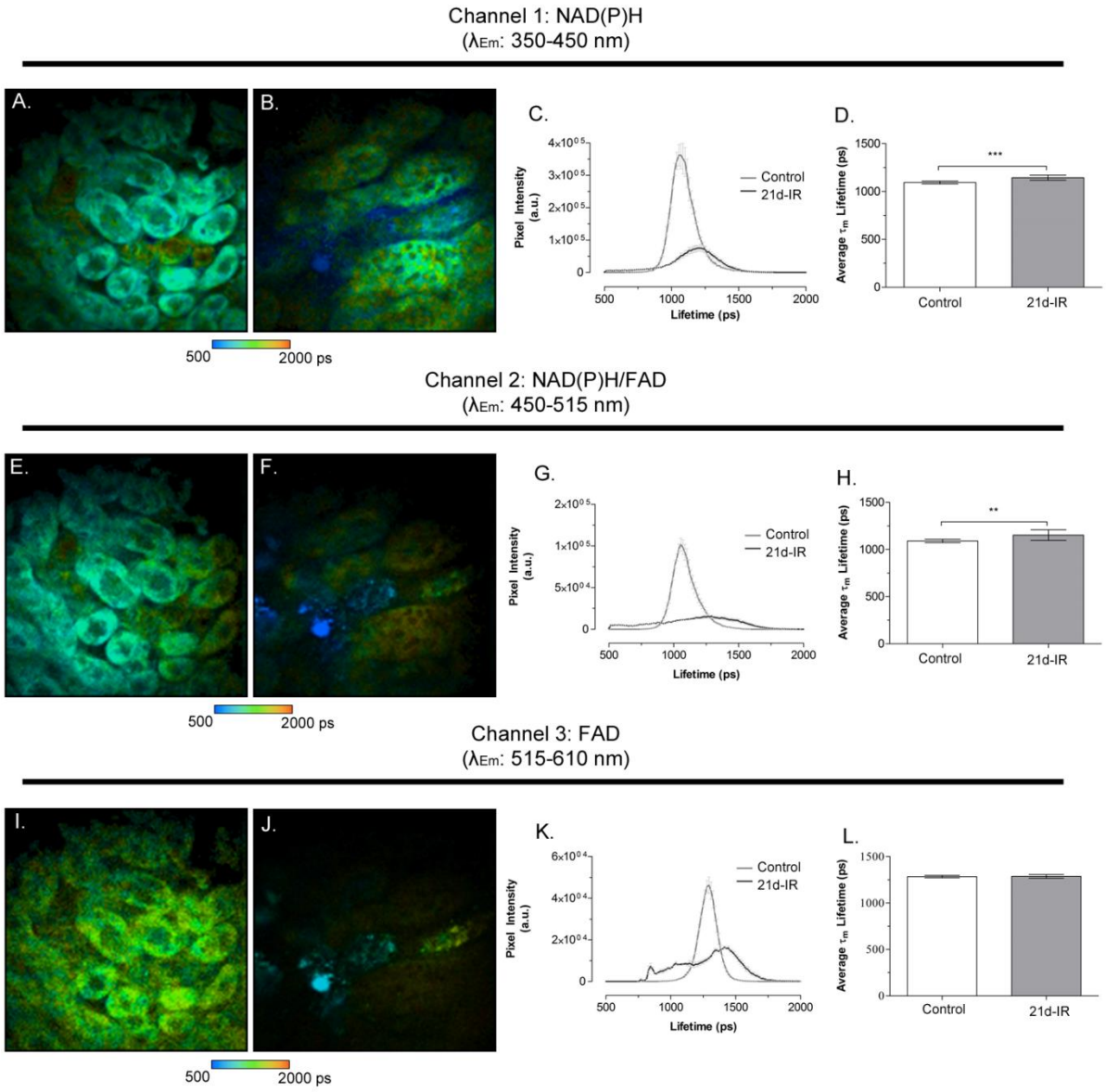

Figure 5.11: Fluorescence lifetime imaging microscopy

FLIM suggests alterations in the average weighted fluorescence lifetime (τ_m) in the kidney cortex following 21-days post IR. Kidneys were imaged immediately post-sacrifice to allow medulla and cortex to be seen. FLIM data were measured within three spectral ranges using excitation at 740 nm (pseudo colour range is indicated in the parenthesis below images): 350-450 nm, 450-515 nm, and 515-620 nm to capture NAD(P)H, NAD(P)H/FAD, and FAD respectively. Representative images are shown in (A, B, E, F, I and J). Histograms (C, G and K) represent the average pixel intensity for each τ_m lifetime and the corresponding average τ_m lifetimes from the three spectral channels are graphed (D, H and L). The τ_m of NAD(P)H and NAD(P)H/FAD significantly increased 21d-IR compared to control and no change in τ_m was observed in FAD alone. Results represent mean ± SEM (N = 2 kidneys and three fields per view per kidney. ** $p<0.01$ as indicated).

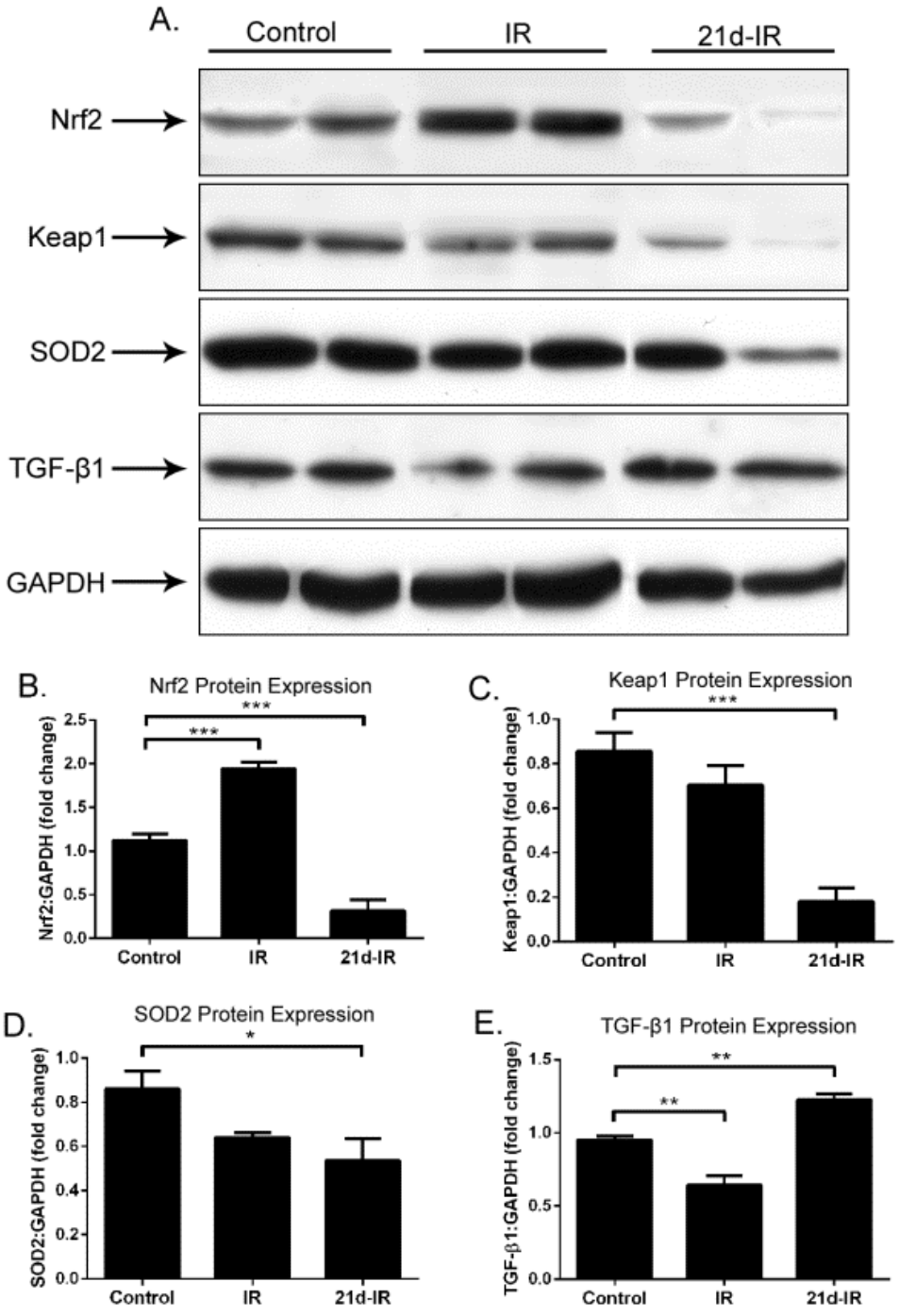

Figure 5.12: IR-injury promotes chronic impairments to redox signalling in the kidney
Protein was extracted from whole kidneys after intravital MPM at early reperfusion (IR) and 21-days post IR (21d-IR) and probed via Western blotting. Representative Western immunoblots for Nrf2, Keap1, SOD2 and TGF-β1 are shown in (A.). Following early reperfusion there was a significant increase in Nrf2 protein expression that was significantly decreased compared to healthy kidneys at 21d-IR (B.). Keap1 (C.) and SOD2 (D.) significantly decreased at 21d-IR and while TGF-β1 increased. Protein expression was normalised to GAPDH protein expression. Results are expressed as mean ± SEM (* $p<0.05$; ** $p<0.01$; *** $p<0.001$ compared as indicated).

5.4 DISCUSSION

The progression to advanced stage CKD following AKI may be modulated by common pathological mechanisms, such as reduced nephron number, vascular insufficiency, cell cycle disruption and maladaptive repair (Chawla and Kimmel, 2012; Coca *et al.*, 2012). The underlying mechanisms behind these common modulators of injury remain to be defined. Here, oxidative stress and metabolic alterations within PTE cells of the kidney (renal cortex) are presented as common contributors to the initiation and progression of chronic alterations in the kidney following IR-induced AKI. Furthermore, to our knowledge, we are the first to apply intravital MPM to visualise chronic alterations in the kidney following IR-induced AKI.

Our results demonstrate significant structural and metabolic changes during renal ischaemia and during early reperfusion in the tubulointerstitial region of the kidney cortex. Tubular epithelial cell swelling causing a reduction in interstitial space was observed during ischaemia. Cell swelling is a common observation during hypoxic conditions within many cell types (Heiss, 2012), and in tubular epithelial cells of the renal cortex is due to osmotic dysregulation by disturbed sodium potassium (Na^+/K^+) ATPase function (Molitoris *et al.*, 1992; Coux *et al.*, 2009). Decreased ATP-dependent cellular functions are further demonstrated by our observed increase in endogenous NAD(P)H fluorescence since NADH is a substrate for complex I of the ETC. Decreased O_2 supply coupled with the minimal glycolytic capacity of tubular epithelial cells cause underutilisation of NADH to be oxidised into NAD+ (non-fluorescent by MPM) by complex I of the ETC. This "backing up" of NADH results in increased endogenous fluorescence. The results are consistent with intravital MPM results from rats with AKI after IR injury (Hall *et al.*, 2013), and similar findings have been demonstrated in brain with microregional hypoxia (Polesskaya *et al.*, 2012) and in assays of NADH in isolated renal tubule preparations after various short-chain fatty acid, carboxylic acid, and amino acid treatments (Balaban and Mandel, 1988). Interestingly, early studies investigating renal IR-induced injury have demonstrated that the occlusion of small vessels caused by tubular swelling can contribute to the pathology of ensuing reperfusion injury (Obermuller *et al.*, 1997). Furthermore, loss of osmotic regulation due to ATP depletion has similar effects on mitochondria, inducing swelling and disappearance of the IMM (Kaasik *et al.*, 2007). ROS generation and the peroxidation of cardiolipan during ischaemia have been suggested to result in IMM disruption (Lesnefsky *et al.*, 2009; Wiswedel *et al.*, 2010).

An important component of the IMM is the ETC for effective ATP production via oxidative phosphorylation. It has been well documented that the majority of IR-induced injury occurs at the

point of reperfusion (Plotnikov *et al.*, 2007; Lejay *et al.*, 2014). Intravital MPM at early reperfusion enabled the visualisation of dynamic tubular pathological changes, including epithelial cell effacement, cast formation, and cellular striations, all of which indicate loss of cell integrity, in some cases early cell death, but also perhaps repairable damage. Increased mitochondrial ROS production is thought to be the major pathological process when O_2 is re-presented to damaged components of the ETC of the IMM, as seen in reperfusion. Depleted ATP also causes significant impairment to ATP-dependent actin polymerisation (Atkinson *et al.*, 2004) causing cytoskeletal changes in tubular epithelial cells and resulting in the breakdown of the brush border, cell-cell contact, disruption of barrier function and cell detachment (Sharfuddin and Molitoris, 2011). Mitochondrial permeability transition due to cristae disruption can also result in the release of Cyt C from the IMM and the initiation of apoptosis (Madesh and Hajnoczky, 2001; Halestrap, 2010). Our results demonstrate histological tubular epithelial cell apoptosis in kidney sections collected following early reperfusion. Apoptosis and acute tubular necrosis are common pathological mechanisms after kidney IR injury resulting in reduced kidney function (Heyman *et al.*, 2011).

Increased ROS generation has previously been shown to upregulate important genes responsible for cytoprotection (Kensler *et al.*, 2007; Fourquet *et al.*, 2010; Shelton *et al.*, 2013). Our results demonstrate that the kidney responds well to the initial acute injury, at the time of early reperfusion, indicated by the upregulation of Nrf2 following IR-induced ROS generation. Downstream targets of Nrf2 include HO-1, PPARγ, and GPX responsible for neutralisation of increased ROS and maintenance to the intracellular redox environment (Wu *et al.*, 2011; Sadi *et al.*, 2014). Interestingly, the intracellular inhibitor of Nrf2, Keap1, did not change significantly at the corresponding time point, indicating that the dissociation of Keap1 from Nrf2, as the mechanism of inhibiting Nrf2, rather than decreased Keap1 protein levels, which is consistent with other findings (Kim *et al.*, 2014).

The early acute phase response to IR-injury was followed by dampened regulation of cytoprotective defences promoting an oxidative stress environment. Decreased levels of Nrf2 were observed following 21-days post IR-injury indicating a failure of antioxidant responses and promotion of ROS. Impaired Nrf2-Keap1 signalling has been previously demonstrated in CKD rodent models in association with decreased renal function and increased tubulointerstitial damage (Kim and Vaziri, 2010; Aminzadeh *et al.*, 2013). Similar results were seen with neurodegenerative disease (Jin *et al.*, 2013) and age-related macular degeneration (Sachdeva *et al.*, 2014). Furthermore, the mitochondrial endogenous antioxidant SOD2, decreased during chronic injury implicating mitochondrial dysfunction and the promotion of mitochondrial-derived ROS production. ROS have

been previously shown to promote TGF-β1 activation of tubulointerstitial myofibroblasts, aiding in their proliferation and the deposition of collagen (Bondi *et al.*, 2010). However, detection of collagen using MPM (second harmonic generation/SHG) detected fluorescence of the kidney capsule but did not detect collagen within the tubulointerstitial region of the cortex. Pena and colleagues (2005) have demonstrated high optical activity by SHG from type I collagen, which is the predominate collagen type throughout the body including the kidney capsule (Di *et al.*, 2002), compared to type IV collagen that has little or no SHG optical activity and mainly constitutes basil lamina (Yurchenco and Schittny, 1990). This is primarily due to the fibrillar and nonfibrillar nature of collagen type I and type IV respectively, and highlights that SHG microscopy is sensitive to the organisation of collagen molecules in the tissue rather than the collagen type (Pena *et al.*, 2005). The results in the present study suggested a thickening of the kidney capsule 21d-IR compared to the healthy kidney capsule which was confirmed following standard histological morphology. The dysregulation of Nrf2, Keap1, SOD2 and TGF-β1 implicate redox alterations within the chronically damaged kidney. These findings are also consistent with, and likely result from, observable alterations to tubular epithelial metabolism in the chronically damaged kidney.

Significant impairment to cortical tubular epithelial cell structure and metabolism was observed 21-days following IR-induced injury. Widespread yet focal areas of tubulointerstitial atrophy and the presence of structurally-normal tubules adjacent to atrophic tubules were observed, suggesting cross-talk was possible between sites of persistent and chronic damage, and the normal-looking tubules. Increased endogenous NAD(P)H fluorescence within structurally-normal tubules located within areas of atrophy suggest impaired NADH metabolism and mitochondrial function due to reduced O_2 delivery. Traditionally, it is the outer stripe of the outer medulla that is damaged acutely in IR-induced AKI. MPM did not allow its visualisation, due to a restriction of depth of excitation approximately 70 μm beneath the kidney capsule (Small *et al.*, 2014). It is well documented that the outer stripe of the outer medulla is highly susceptible not only to ischaemic insult, but also toxic insult (Yamamoto *et al.*, 1984a, b). This region of the kidney has the greatest oxygen concentration, mainly due to constitutive S3 segments of the proximal tubule that contain a high density of mitochondria (Venkatachalam *et al.*, 1978). Nevertheless, the renal cortex accounts for 80 % of oxygen in the kidney, which is mainly accounted for by the remainder of the proximal tubule, making it an important site to consider. Depth restriction remains a challenge to intravital MPM preventing an accurate comparison between medullary and cortical dynamics in response to AKI and ensuing chronic pathology. Different approached to this limitation are explored in Chapter 6. However, MPM provided novel data on the participation of cortical regions to IR injury of the kidney.

Tubular atrophy and subsequent whole organ atrophy are primarily due to increased levels of apoptosis respective to levels of mitosis (Gobe and Axelsen, 1987; Gobe *et al.*, 1990). Continuing apoptosis in preserved tubules would occur due to the inflammatory infiltrate and a developing hypoxic environment due to vascular insufficiency. *In vivo* MPM investigations of brain have demonstrated increased endogenous NAD(P)H fluorescence when tissue oxygen levels are less than 10 mmHg (Polesskaya *et al.*, 2012). Low O_2 levels reduce the activity of the mitochondrial complex I and the conversion of NADH to NAD+, resulting in increased fluorescence detection. Reduced nephron number due to tubular atrophy likely induces a compensatory function in remaining tubules and subsequent increase in ATP demand. Hypoxia causes mitochondrial dysfunction within these functional remaining tubules which reduces ATP synthesis, further enhancing ATP demand, and producing a vicious cycle of metabolic insufficiency. Cell death via apoptosis or autophagy resulting in perturbed tubular function is the ultimate result. An alternate theory may argue that the compensatory nature of these functional remaining tubules results in a greater density of mitochondria. This would produce higher basal levels of NADH. However, greater levels of O_2 supply would be needed to maintain NADH turnover and oxidative phosphorylation, which is highly unlikely given that vascular insufficiency is a hallmark of all chronic kidney pathologies and was observed histologically in the present study.

Our preliminary observations investigating the fluorescence lifetime changes of NAD(P)H and FAD suggest impaired NAD(P)H dynamics in the chronically-damaged kidney following AKI. We identified an increase in the τ_m observed in both the 350-450 and 450-515 nm spectral channels, both of which encompass NAD(P)H endogenous fluorescence (Yu *et al.*, 2012). A lack of any change in the 515-620 spectral channel, which predominately isolates FAD endogenous fluorescence, supports the conclusion that NAD(P)H is responsible for the τ_m changes detected in the 450-515 nm spectral channel. Interestingly, previous studies have demonstrated that increased τ_m of NAD(P)H is associated with ischaemic necrosis and apoptosis in skin and cancer cell lines (Wang *et al.*, 2008; Sanchez *et al.*, 2010). Both of these processes are associated with oxidative damage which may alter the protein recruitment of NAD(P)H and result in an increased lifetime fluorescence that we observe. However, further investigations are required to identify the changes associated with protein binding in NAD(P)H in chronically-damaged kidneys following IR-injury, such as the redox ratio which provides an expression of free and bound NAD(P)H (Skala *et al.*, 2007a). FLIM was performed on kidney slice preparations immediately after kidney collection, compared to MPM which was performed intravitally. Nonetheless, the validity of lifetime changes is supported by the obvious preservation of the tissue within the time until first image. In addition,

the comparative nature between two different samples (control and 21d-IR), rather than dynamic changes due to experimental intervention to the same tissue, also supports data validity. It has been described previously that *ex-vivo* skin maintains NAD(P)H autofluorescence when kept at 4 ºC for 7 days despite the possibility of post-death changes, such as autolysis. The kidney is likely to have a shorter half-life of endogenous fluorescence given the high reliance on aerobic metabolism, although there are no previous studies that have investigated this.

In summary, this study strongly suggests that NAD(P)H alterations influence oxidative stress in IR-induced AKI and future development of progressive CKD. The early stages of IR damage in the kidney were characterised by significantly increased NAD(P)H endogenous fluorescence. At reperfusion, structural damage in the tubulointerstitial regions of the cortex occurred rapidly. By 21d-IR, there was focal tubular atrophy and significantly increased NAD(P)H fluorescence in functional remaining tubules. Compared with control kidneys, molecular analysis demonstrated increased Nrf2 expression at reperfusion but decreased at 21d-IR. Mitochondrial SOD2 decreased. In conclusion, mitochondrial dysfunction is persistent in functional remaining tubules of the chronically-damaged kidney following AKI. The results present oxidative stress and mitochondrial preservation as crucial *in vivo* targets following AKI to prevent progression to CKD.

CHAPTER 6

Targeting Oxidative Stress in Kidney Disease

Chapters 3 to 5 have demonstrated that intracellular oxidative stress and impairments to cellular metabolism are major contributing factors to kidney dysfunction and the progression to chronic damage. The known contribution of oxidative stress due to mitochondrial dysfunction suggests that targeting excess ROS production will attenuate progressive kidney injury. In Chapter 3, *in vitro* evidence suggested that use of an exogenous antioxidant could benefit oxidative stress-induced kidney injury, including by reducing apoptosis. Targeting anti-oxidant defence mechanisms against oxidative stress is a broad area of research that has attracted many different approaches. The aims of Chapter 6 were (1) to use an *in vitro* model of oxidative stress-induced kidney injury to determine which antioxidant/s best prevented cell damage, and (2) to then translate these benefits into an *in vivo* model of chronic kidney injury following AKI after IR-induced injury.

6.1 INTRODUCTION

Progression of chronic diseases, including chronic kidney diseases, is driven by numerous deleterious and converging physiological processes, regardless of the cause. Targeting the progressive nature of disease is increasingly difficult and further exaggerated by advanced stage disease. Oxidative stress is a cellular process that contributes to the myriad of pathological events attributed to progressive kidney disease including fibrosis, apoptosis, senescence, vascular insufficiency and maladaptive repair. As suggested from findings in Chapter 5, metabolic alterations within the kidney are intimately linked to oxidative stress, mitochondrial dysfunction, and the promotion of ROS generation. This presents oxidative stress and ROS as underlying common contributors, and targets to reduce the pathological consequences and progression of CKD.

That antioxidant therapy is successful in reducing AKI has been demonstrated best in contrast-induced nephropathy (Hsu *et al.*, 2012; Kongkham *et al.*, 2013), renal IR-injury (Seguro *et al.*, 2012; Peerapanyasut *et al.*, 2014), and acute toxin nephropathies (Parra *et al.*, 2003; Kadkhodaee *et al.*, 2007). Targeting oxidative stress in progressive kidney diseases, such as CKD, with the use of exogenous antioxidant compounds has produced ambivalent findings primarily due to the use of small patient populations and suboptimal study quality. The outcomes have been of insufficient power to confirm any benefit. A recent meta-analysis of 10 studies assessing antioxidant therapy in haemodialysis, transplant recipients and non-dialysis CKD patients found that antioxidant therapy significantly reduced the development of ESKD, but showed no clear benefit on cardiovascular and all-cause death or major cardiovascular events in CKD patients (Jun *et al.*, 2012). Pre-clinical *in vivo* models commonly demonstrate beneficial results of antioxidant interventions, primarily in AKI models. Considering that AKI is commonly followed by insidious maladaptive and progressive

kidney pathology with asymptomatic kidney functional decline (Kang *et al.*, 2002; Lafrance and Miller, 2010), the apparent benefit of antioxidant therapy to reduce the onset of CKD is less clear. Recently, Himmelfarb *et al.* (2014) conducted a well-powered trial investigating whether mixed tocopherols and α-lipoic acid would alter oxidative stress and inflammation biomarkers in maintenance haemodialysis patients, and found no detectable change compared to placebo controls. These data highlight the need for more basic research into oxidative stress to design appropriate targets.

Chapter 1 Section 1.2.9 provided detailed information about the mechanism of action of selected antioxidants and reviewed their current use for CKD (Small *et al.*, 2012). Briefly, NAC acts as an essential precursor to many endogenous antioxidants involved in the decomposition of peroxides (Zafarullah *et al.*, 2003; Zhang *et al.*, 2011), as well as replenishing intracellular glutathione stores. In addition, the sulfhydryl-thiol group of L-cysteine is able to exert direct antioxidant effects by scavenging free radicals. NAC seems to exert the greatest antioxidant and anti-inflammatory properties when used against the greatest injury, such as in ESKD patients receiving either haemodialysis or peritoneal dialysis. In those cases, NAC reduced serum F_2-isoprostanes and the inflammatory cytokine IL-6 (Hsu *et al.*, 2010; Nascimento *et al.*, 2010). In a randomised, double-blind, placebo-controlled study where 10 non-diabetic ESKD patients on maintenance haemodialysis received 1200 mg NAC daily for 7 days, pro-fibrotic FGF-19 was decreased (Li *et al.*, 2013). αTOC is a lipid-soluble antioxidant that incorporates into the plasma membrane of cells scavenging free radicals and preventing lipid peroxidation (Serbinova *et al.*, 1991). Despite this, αTOC as a therapeutic agent remains controversial owing to trials demonstrating increased risk of prostate cancer and all cause-mortality with its use. CoQ_{10} is another fundamental component of the lipid membrane that acts primarily within mitochondria for electron transfer, membrane polarisation and ATP generation, and is a popular compound as an antioxidant therapy. There is a general lack of human studies investigating CoQ_{10} therapy for the treatment and/or prevention of CKD despite positive pre-clinical models. CoQ_{10} levels decrease with age, but there are no studies measuring endogenous CoQ_{10} levels in CKD patients and this could prove vital in the identification of populations where CoQ_{10} therapy may have beneficial outcomes.

Oxidative stress incorporates the disruption of vital intracellular signalling networks that are redox sensitive. Nrf2-Keap1 dynamics during an oxidative stress environment and developing renal pathologies have gained increased attention as a result of the thwarted BEACON trial (de *et al.*, 2013). The results, where Nrf2 was targeted with bardoxolone methyl, suggest that altering such up-stream, highly conserved targets can have negative systemic consequences (Tayek and Kalantar-

Zadeh, 2013). Furthermore, as demonstrated in Chapter 4 (Small *et al.*, 2014), oxidative stress-induced alterations to PPARγ can disrupt important PPARγ-dependent processes such as mitochondrial homeostasis and mitophagy in PTE cells. It is not known whether these effects occur during AKI and CKD.

This chapter aimed to determine whether targeting oxidative stress could improve mitochondrial dysfunction and metabolic alterations following AKI and during any subsequent progression to CKD.

6.2 MATERIALS AND METHODS

6.2.1 Materials

Powdered mouse food (normal feed) from Specialty Feeds (Glenn Forrest, WA) was a gift from Prof. Lindsay Brown (Southern Cross University, Lismore, Australia). NAC (catalogue number A7250), αTOC (catalogue number T3251) and Trolox (Tlx – catalogue number 238813) were purchased from Sigma-Aldrich (St. Louis, MO, USA). Coenzyme-Q_{10} was a gift from A/Prof. Luis Vitetta and Medlab (Alexandria, NSW).

6.2.2 Cell culture model

Dose-response experiments were performed on HK-2 cells for each chosen antioxidant to obtain the highest concentration that did not significantly damage the cultures. This was assessed by measuring cell death (mainly, morphological features of apoptosis) or mitosis (morphological assessment described in Chapter 2 Sections 2.3.2 – 4). Concentrations were as follows; NAC – 0.01, 0.1, 1.0, 10, 20 mM; αTOC – 0.1, 0.5, 1.0 mg/ml; Tlx – 1.0, 1.5, 2.0 mM; CoQ_{10} – 0.01, 0.1, 1.0, 10 μM;. Stock concentrations were prepared using DMSO for Tlx and NAC and ethanol (EtOH) for αTOC and CoQ_{10}. The final working concentration of the vehicle never exceeded 1 % in culture and an appropriate vehicle-control was used throughout all experiments. Oxidative stress was induced using 0.6 mM H_2O_2 exposed to HK-2 cells over 18 h. This induced a significant increase in apoptosis and decrease in mitosis and, after dose-response studies, was therefore chosen as the treatment concentration for co-treatment studies with antioxidants. For co-treatment studies, HK-2 cells were exposed to the selected antioxidant alone for 2 h prior to co-administration of 0.6 mM H_2O_2 and the antioxidant for 18 h. Appropriate controls were always used.

6.2.3 *In vivo* mouse model

4-6 week old male C57Bl6 were housed in temperature controlled boxes with a 12 h light – 12 h dark cycle. Mice were fed a normal powdered food diet or a normal powdered food diet with the addition of 5 % NAC since this oral dosage has previously been shown to be beneficial (Malins *et al.*, 2002). The average 30 g male C57Bl6 mouse consumes 4.5 g of dry food daily (Bachmanov *et al.*, 2002). Mice were an average weight of 25 g with no mouse weighing greater than 30 g. Therefore each mouse (individually housed) was allotted 4.5g of food each day. Mice consumed either the normal powdered food or powdered food with 5% NAC (NAC diet). They did not consume the full amount provided within a 24 h period, by observation. However, there was no difference in the residue food amounts for control or NAC-fed mice, indicating they consumed equivalent food amounts. Mice were fed the diets one week prior to kidney IR surgery, and for 21-days following kidney IR. Intravital MPM and kidney collection occurred following initial kidney IR injury and at 21-days post IR. (N = 4 – 6 animals per group). All experiments were approved by the University of Queensland Animal Ethics Committee 2013 – AEC No: MED/053/12/CKDR.

6.2.4 Western immunoblotting

Protein expression levels were determined for p-PPARγ, PPARγ, Keap1, Nrf2, SOD2, HO-1 and TGF-β1 from whole kidney protein extracts, using methods described in Chapter 2 Section 2.5. GAPDH was used as a loading control and densitometry was used to semi-quantitate protein expression.

6.2.5 Mouse kidney histology and immunohistochemistry

Kidneys were collected from control mice, those at early reperfusion, and at 21-days following IR surgery. H&E, Masson's Trichrome stain, *in situ* enzymatic ApopTag, and IHC for PCNA, 8-OHdG, p-PPARγ, PPARγ were performed according to protocols detailed in Chapter 2 Section 2.4. Morphometry was performed using ImageScope following digital scanning of slides using the Aperio ScanScope XT slide scanning system (Aperio Technologies Inc., Vista, California, USA) at x20 magnification. Entire kidney sections were analysed and separated into cortex and medulla. Algorithms selected for quantification were as follows: IHC Nuclear v1, Version 1 for ApopTag and PCNA staining, with strong positive (+3) and positive (+2) included into mean values; Positive Pixel Count v9, Version 9.1 for 8-OHdG staining, with strong positive (+3) only included into mean values; and Masson's Trichrome stain using the Positive Pixel Count v9, Version 9.1 algorithm, with Total Negative Pixels included into mean values since blue is detected as negative staining.

6.2.6 Intravital MPM of kidney IR injury

The same protocol was used as described in Chapter 5 and is detailed in Chapter 2, Section 2.6. The mitochondrial membrane potential dependent dye TMRM was infused intravenously and imaged with intravital MPM to assess mitochondrial dynamics in the chronically-damaged kidney. These methods are outlined in Chapter 2, Section 2.6.4.

6.2.7 Fluorescence lifetime imaging microscopy

The same protocol was used as described in Chapter 5 and is detailed in Chapter 2, Sections 2.6.7 and 2.6.8. As an extension to FLIM data described in Chapter 5, more replicates were performed (N = two animals per group, both kidneys were analysed, N = 4), as well as differentiating the medulla from the cortex. Areas of focal fibrotic change were analysed.

6.3 RESULTS

6.3.1 *In vitro* models support NAC as a superior antioxidant to prevent oxidative stress-induced kidney injury

Apart from 1 mg/ml, αTOC significantly increased apoptosis in a dose-dependent manner compared to untreated and vehicle control HK-2 cells (Fig 6.1A); $p<0.001$). 1.0 mg/ml also had no detrimental effect on mitosis in controls (Fig 6.1B). 1.0 mg/ml αTOC was then applied as an antioxidant in combination with H_2O_2. 2 h pre-treatment with 1.0 mg/ml αTOC prior to and during 18 h H_2O_2 did not attenuate H_2O_2-induced apoptosis (Fig 6.1C) or reduced mitosis (Fig 6.1D). A non-significant trend of increased apoptosis when αTOC was used in conjunction with H_2O_2, compared to H_2O_2 treatment alone, suggests αTOC could promote apoptosis (Fig 6.1C). Tlx (water soluble αTOC) significantly increased apoptosis when used at 2 mM (Fig 6.2A; $p<0.001$), but none of the lesser concentrations had detrimental effects. No treatment concentrations had any significant effect on mitosis (Fig 6.2B). 1 mM Tlx was selected as the treatment concentration and was therefore applied in combination with H_2O_2. 1 mM Tlx pre-treatment for 2 h, and during 18 h H_2O_2 exposure, did not attenuate H_2O_2-induced apoptosis (Fig 6.2C) or decreased mitosis (Fig 6.2D). CoQ_{10} did not alter levels of apoptosis (Fig 6.3A) or mitosis (Fig 6.3B) at concentrations ranging from 0.001 to 10 µM. The highest soluble CoQ_{10} concentration (10 µM) was chosen to be used in combination with H_2O_2. 2 h exposure of 10 µM CoQ_{10} prior to and during 18 h H_2O_2 exposure did not attenuate H_2O_2-induced apoptosis (Fig 6.3C) or reduced mitosis (Fig 6.4D). In the NAC dose response tests, only 20 mM significantly increased apoptosis in HK-2 cells compared to untreated and vehicle control cultures (Fig 6.4A; $p<0.001$). There was no significant alteration in mitosis (Fig 6.4B). 10 mM NAC did not significantly alter apoptosis or mitosis and was therefore chosen to use in combination

with H_2O_2. 2h exposure to NAC prior to and during 18h H_2O_2 exposure significantly reduced H_2O_2-induced apoptosis (Fig 6.4C; $p<0.001$) but did not improve the H_2O_2-induced reduction in mitosis (Fig 6.4D). The DMSO vehicle significantly reduced H_2O_2-induced apoptosis (Fig 6.4C; $p<0.05$).

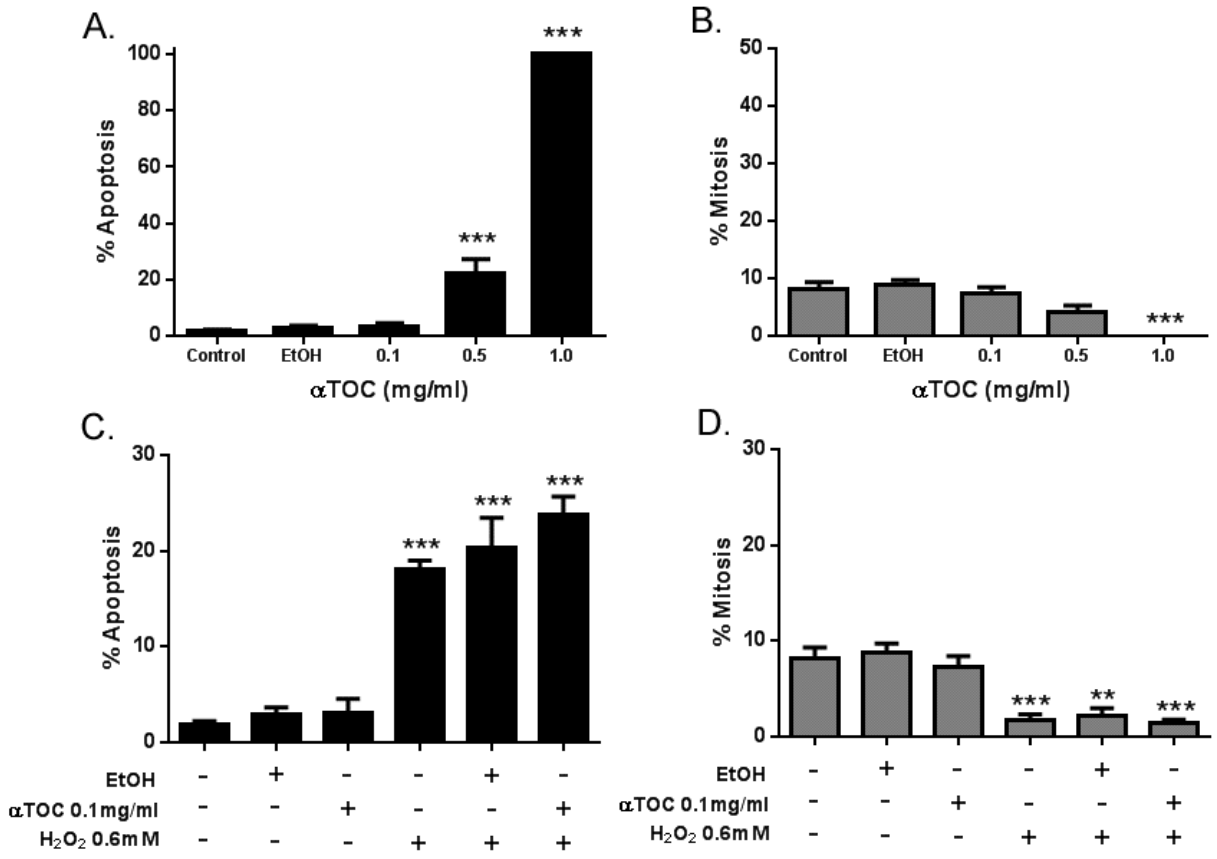

Figure 6.1: The antioxidant αTOC promotes oxidative stress induced apoptosis
After dose-response studies as described in text, HK-2 cells were exposed to 0.1 mg/ml αTOC 2 h prior to and during 18 h H_2O_2 treatment. The combination of αTOC and H_2O_2 induced a significant increase in apoptosis similar to that observed in cells treated with H_2O_2 alone (C.). The combination of αTOC and H_2O_2 induced a significant decrease in mitosis similar to that observed in cells treated with H_2O_2 alone (D.). Within the graphs the ethanol vehicle is indicated by EtOH. Results are expressed as means ± SE (** $p<0.01$; *** $p<0.001$ compared to untreated control).

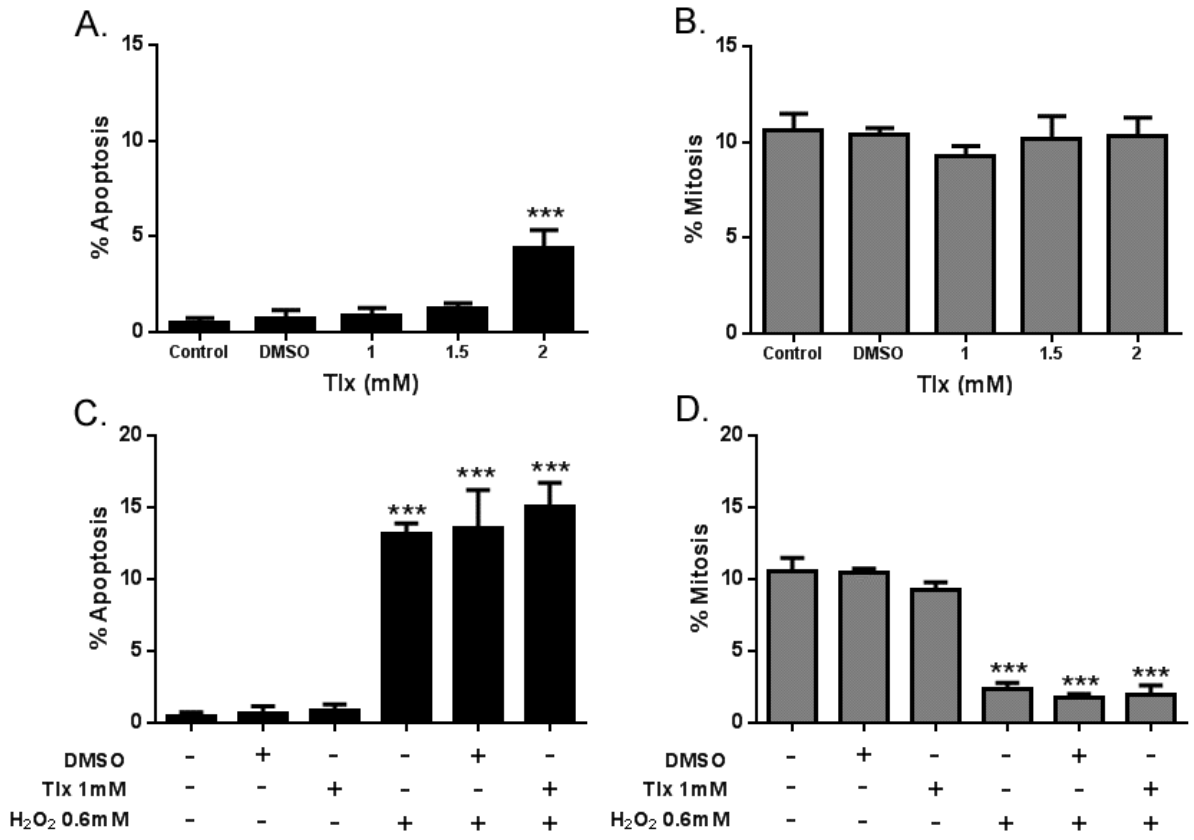

Figure 6.2: The antioxidant Tlx does not protect against oxidative stress induced apoptosis or reducted mitosis

In the dose response tests, Trolox (Tlx) significantly increased apoptosis at a concentration of 2 mM (A.) Tlx did not affect levels of mitosis (B.). HK-2 cells were exposed to 1 mM Tlx 2 h prior to and during 18 h H_2O_2 treatment. In a scenario of oxidative stress (0.6 mM H_2O_2), Tlx did not decrease the significant increase in % apoptosis induced by H_2O_2 alone. (C.). Tlx also did not improve the low levels of mitosis induced by H_2O_2 alone (D.). Within the graphs the dimethyl sulfoxide vehicle is indicated by DMSO. Results are expressed as mean ± SE (*** $p<0.001$ compared to untreated control).

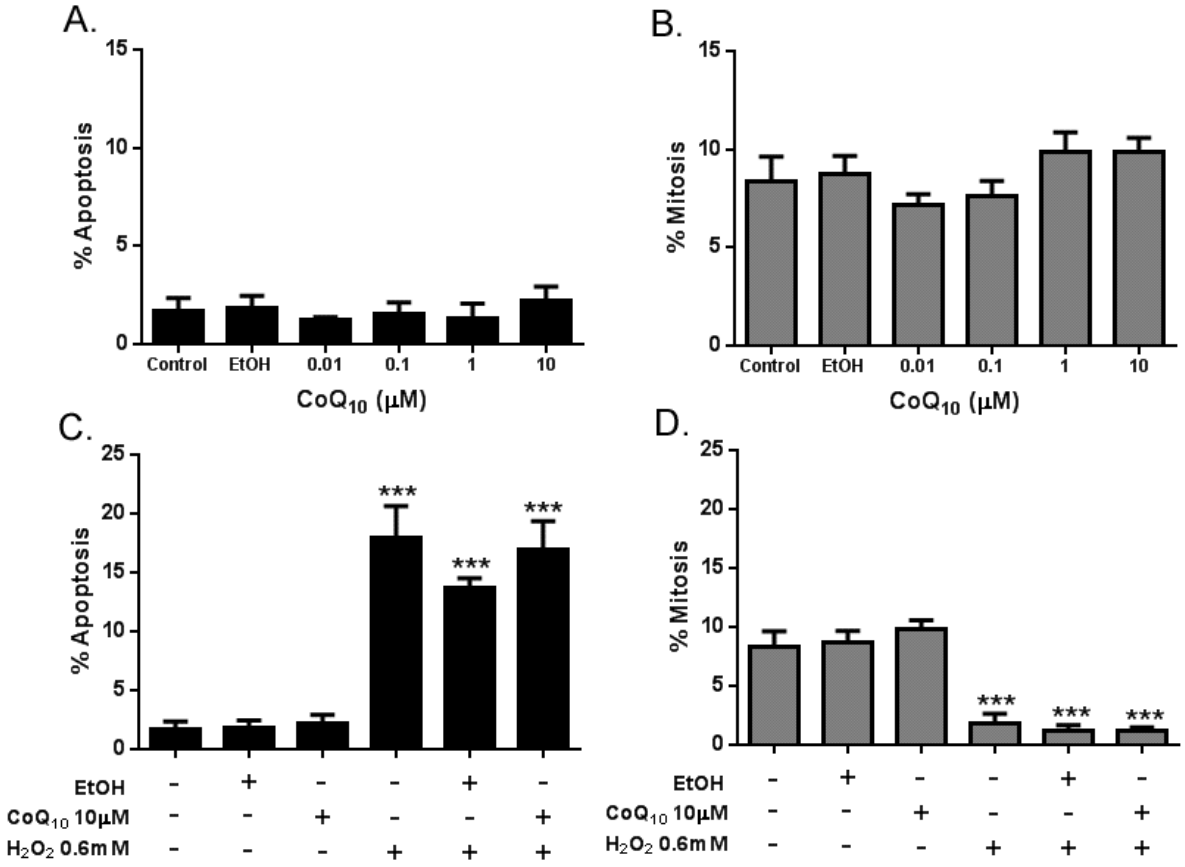

Figure 6.3: The antioxidant CoQ_{10} does not protect against oxidative stress induced apoptosis or reduction in mitosis

CoQ_{10} at concentrations of 0.01 – 10 μM did not alter levels of apoptosis (A.) or mitosis (B.). HK-2 cells were exposed to 10 μM CoQ_{10} 2 h prior to and during 18 h H_2O_2 treatment. CoQ_{10} had no significant effect on levels of apoptosis induced by H_2O_2 alone (C.). Similarly, CoQ_{10} did not improve the reduced levels of apoptosis induced by H_2O_2 alone (D.). Within the graphs the ethanol vehicle is indicated by EtOH. Results are expressed as mean ± SE (*** $p<0.001$ compared to untreated controls).

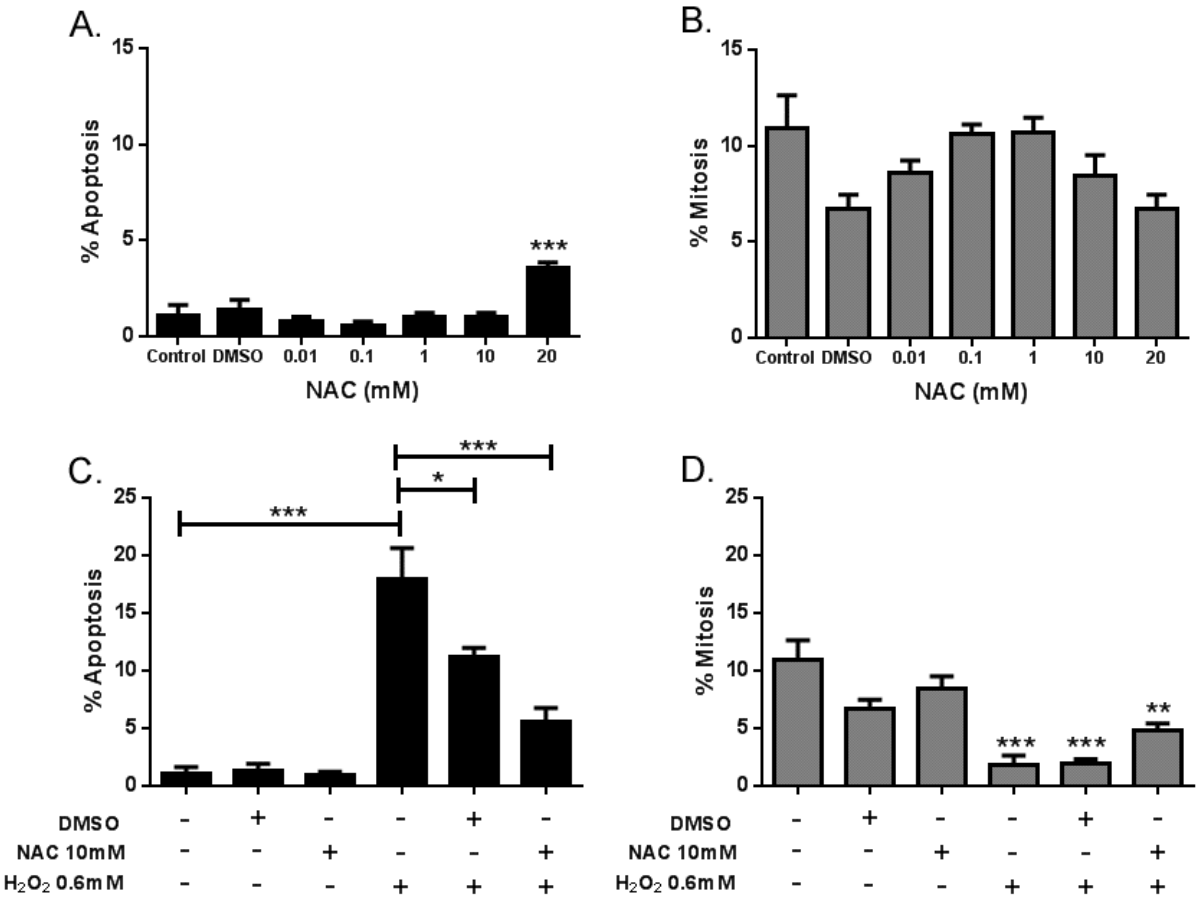

Figure 6.4: The antioxidant NAC attenuates oxidative stress induced apoptosis and a reduction in mitosis

In the dose response tests, NAC significantly increased apoptosis only at a concentration of 20 mM (A.). There was no significant effect at 0.01 – 10 mM compared to untreated controls (A.). NAC did not significantly alter levels of mitosis (B.). HK-2 cells were exposed to 10 mM NAC 2 h prior to and during 18 h H_2O_2 treatment. Oxidative stress significantly increased apoptosis. NAC significantly decreased oxidative stress-induced apoptosis (C.). Note that DMSO also significantly improved outcome in H_2O_2-induced apoptosis. The addition of NAC significantly improved outcome in the H_2O_2-induced reduction in mitosis (D.). Within the graphs the dimethyl sulfoxide vehicle is indicated by DMSO. Results are expressed as mean ± SEM (* $p<0.05$; ** $p<0.01$; *** $p<0.001$ compared to untreated control, and as indicated).

6.3.2 Progression of chronic kidney pathology following acute kidney injury is enhanced by the antioxidant NAC

The progression of fibrosis was evident at 21d-IR by significantly increased interstitial collagen deposition, detected by Masson's Trichrome staining, within the interstitial spaces at 21d-IR compared to control kidneys from mice fed a normal diet (Fig 6.5A, C and G; $p<0.05$) and mice fed a normal diet + 5% NAC (NAC diet; Fig 6.5D, F and G; $p<0.001$). Tubular damage at early reperfusion (IR), regardless of diet, is evident by the presence of cell debris within tubules (Fig 6.5B and E). PCNA IHC demonstrates significantly increased proliferation of cells within the interstitium, likely to be myofibroblasts, at 21d-IR compared to control kidneys from mice fed a normal diet (Fig 6.5H, J and K; $p<0.01$) and mice fed the NAC diet (Fig 6.5 L, N and K; $p<0.001$). The interstitial cell PCNA labelling was further enhanced in the kidneys of mice fed the NAC diet (Fig 6.5K; $p<0.001$). TGF-β1 protein expression from whole kidney extracts was significantly increased in mice fed the NAC diet compared to mice fed a normal diet (Fig 6.5O and P; $p<0.05$) and remained significantly increased at 21d-IR regardless of diet compared to control mice on a normal diet (Fig 6.5O and P; $p<0.01$). Apoptosis was significantly increased within tubular epithelial cells at IR in mice fed a normal diet (Fig 6.7A, B and G; $p<0.05$). Apoptosis was attenuated in mice fed the NAC diet (Fig 6.7D, E and G; $p<0.05$) at this acute time. Apoptosis remained significantly increased at 21d-IR regardless of diet compared to control kidneys (Fig 6.7A, C and G; $p<0.05$. Fig 6.7D, F and G; $p<0.001$) and was significantly enhanced in mice fed the NAC diet (Fig 6.7C, F and G; $p<0.001$ compared to 21d-IR normal diet). Representative images demonstrating kidney capsule thickening at 21d-IR compared to control, acquired by intravital MPM and second harmonic generation of fibrillar collagen, are shown in Fig 6.6A and B. Fibrillar collagen appears to penetrate the cortex overlying sites of tubular atrophy.

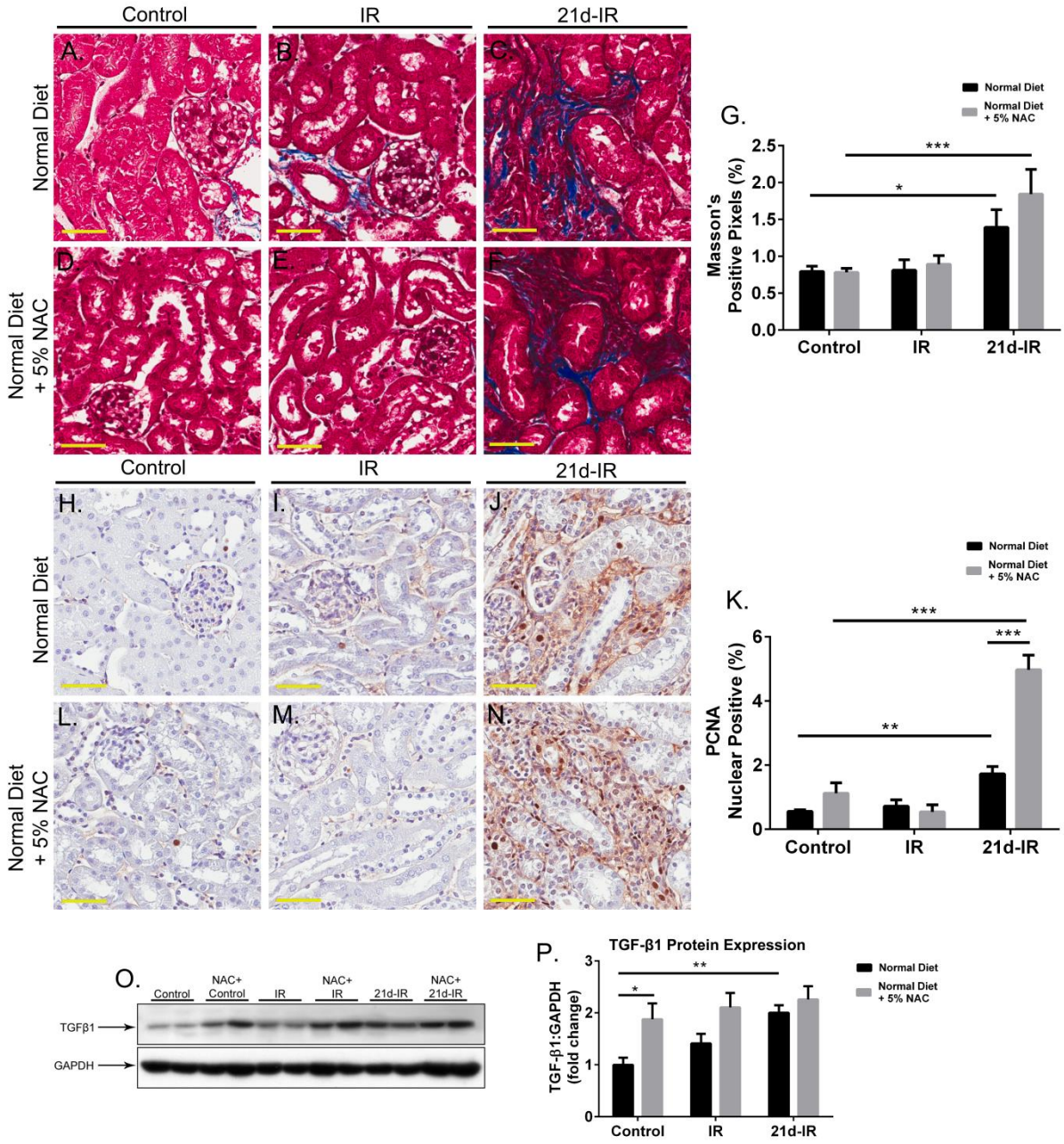

Figure 6.5: Progression to fibrosis following AKI is enhanced by the antioxidant NAC

Masson's Trichrome staining and morphometry (A.-G.) demonstrate increased interstitial collagen deposition 21-days following IR injury (21d-IR) compared to healthy controls and early reperfusion (IR) for both normal diet (A.-C.) and normal diet + 5% NAC (NAC diet; D.-F.). Proliferation detected by proliferating cell nuclear antibody (PCNA) and quantified by morphometry (H.-N.) increased within the interstitium of the cortex 21d-IR for both normal diet (H.-J. and K.) and the NAC diet (K.-N.). The NAC diet enhanced interstitial cell proliferation for 21d-IR compared to mice on a normal diet (K.). Transforming growth factor-beta-1 (TGF-β1) from whole kidney protein extracts, detected by western immunoblotting (O.) and quantified by densitometry (P.), increased in mice on a normal diet for 21d-IR compared to control. The NAC diet increased TGF-β1 expression compared to mice on a normal diet in control kidneys (P.). Results expressed as mean ± SE (* $p<0.05$; ** $p<0.01$: *** $p<0.001$ compared as indicated). Scale bar represents 50 µm.

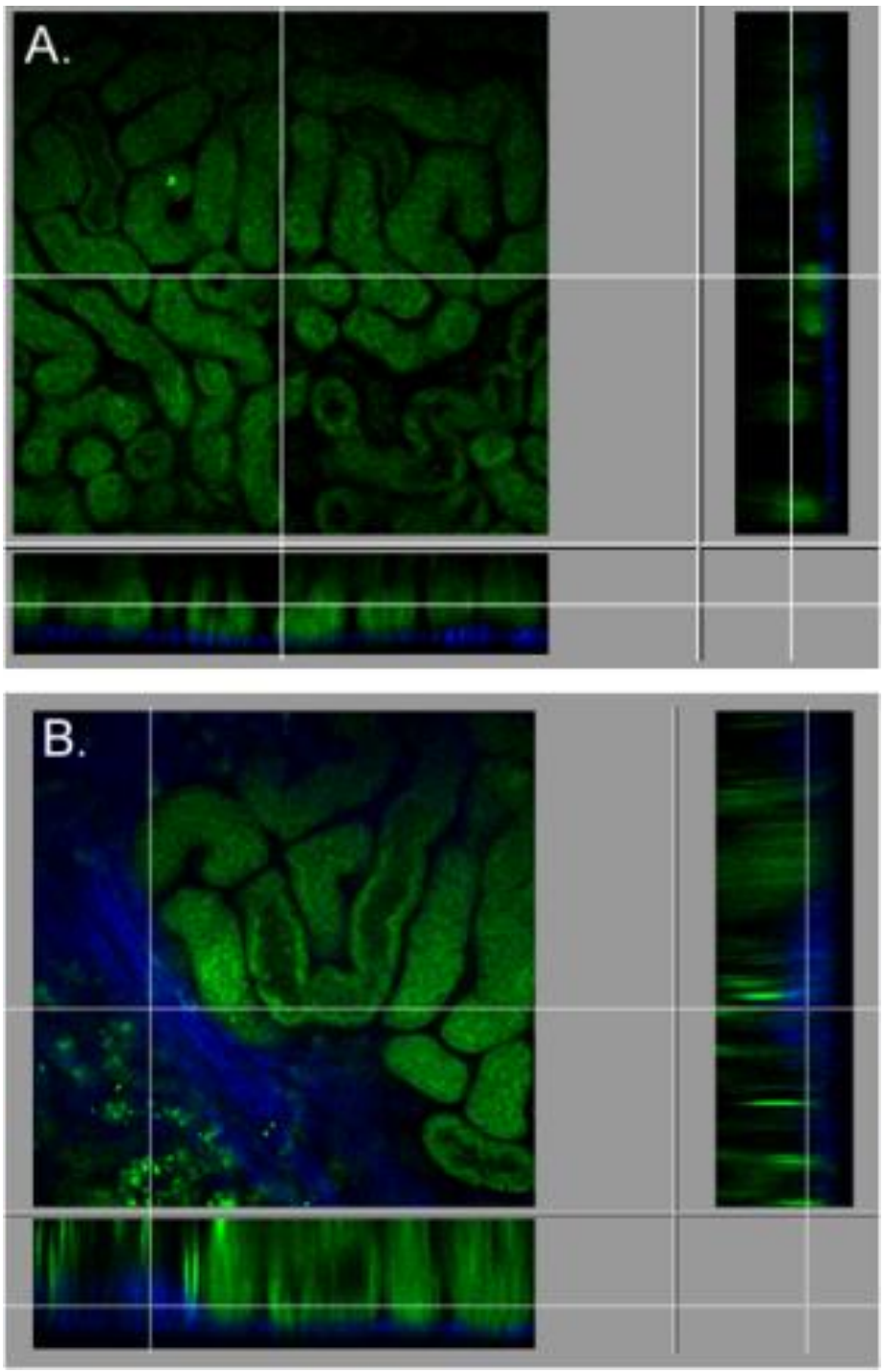

Figure 6.6: Kidney capsule thickening in the chronically damaged kidney detected by MPM Z-stack reconstruction and section view of the mouse kidney acquired with intravital MPM is demonstrated. Green shows NAD(P)H endogenous fluorescence excited at 740 nm depicting the renal cortical tubular network. Blue shows fibrillar collagen endogenous fluorescence excited at 900 nm depicting type 1 collagen of the renal capsule. A thin and uniform renal capsule composed of collagen can be visualised in the healthy control kidney with 900 nm excitation (A.). At 21-days following IR injury (21d-IR; normal diet), the renal capsule was noticeably thicker in regions overlying areas of cortical tubular atrophy (B.).

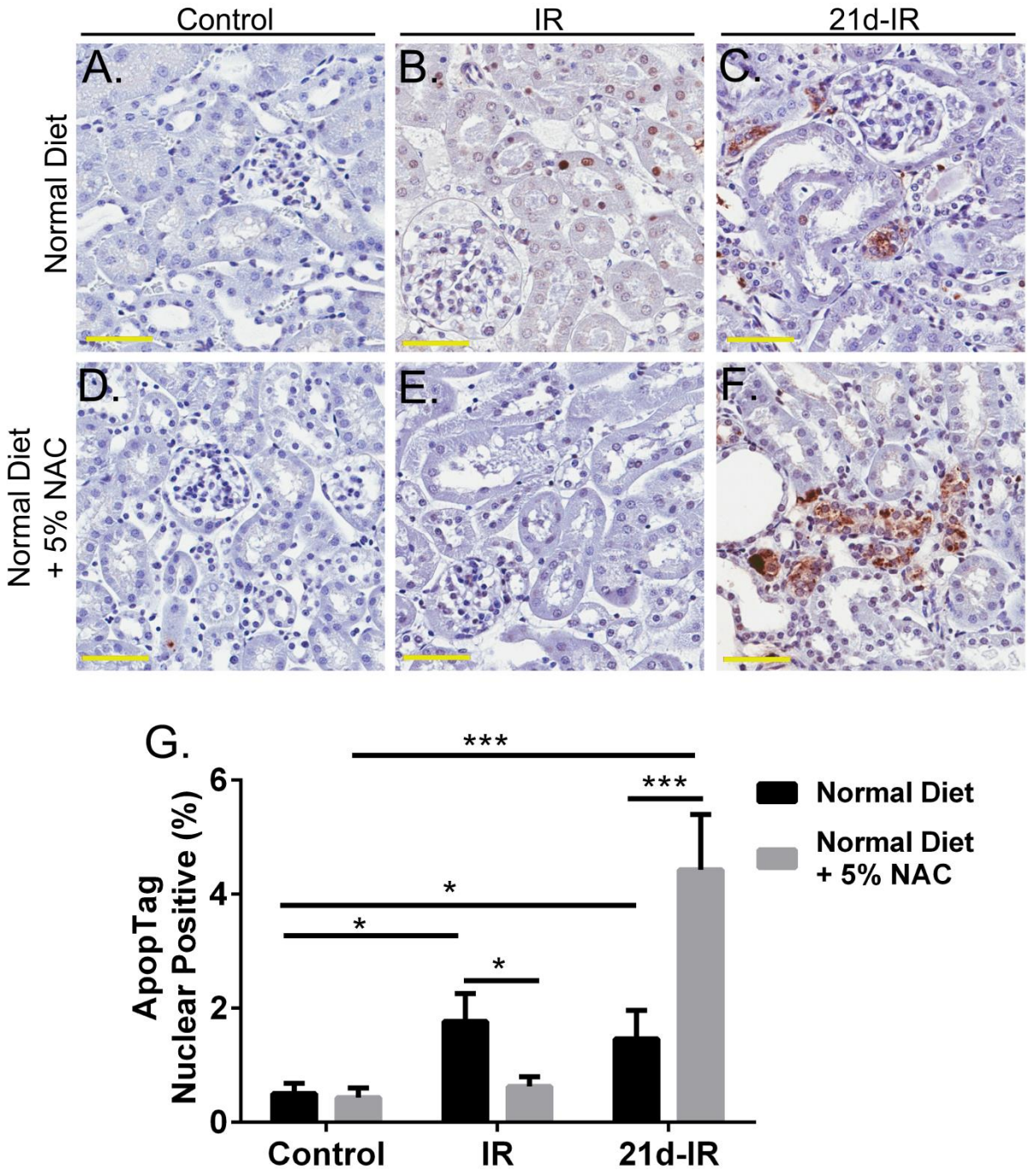

Figure 6.7: NAC prevents apoptosis following AKI and enhances apoptosis during chronic kidney pathology

The enzymatic *in situ* stain ApopTag labels apoptotic cells and bodies (A.-E.). Labelling was quantified with morphometry (G.). Apoptosis significantly increased in tubular epithelial cells at early reperfusion (IR) (B.) and 21-days following kidney IR-injury (21d-IR) (C.) in mice on a normal diet. The 5% NAC dietprevented tubular cell apoptosis at IR (E.) but significantly enhanced apoptosis at 21d-IR (F.) compared to mice on a normal diet. Results expressed as mean ± SE (* $p<0.05$; ** $p<0.01$: *** $p<0.001$ compared as indicated). Scale bar represents 50 µm.

6.3.3 NAC enhances chronic oxidative damage in progressive kidney pathology by altering endogenous antioxidant responses

The oxidative damage marker 8-OHdG was weakly positive in the tubular epithelium of control kidneys regardless of the type of diet (Fig 6.8A and D). Distal tubular epithelium possessed stronger 8-OHdG positivity than proximal tubular epithelium (Fig 6.8A and D). There was no significant increase in 8-OHdG immediately after reperfusion (IR) regardless of the diet (Fig 6.8B and E). However, at 21d-IR, there was a significant increase in 8-OHdG that was further enhanced by the NAC diet (Fig 6.8C, F and G; $p<0.001$).

Nrf2 protein expression from whole kidneys significantly increased at IR in mice on a normal diet demonstrating a cytoprotective response (Fig 6.8H; $p<0.05$). This did not occur in mice on the NAC diet. An non-significant increase was observed in Nrf2 expression in 21d-IR mice on the NAC diet compared to control (Fig 6.8H; $p<0.0587$). Keap1 protein expression did not alter significantly (Fig 6.8I).

Western immunoblotting detected HO-1 protein expression at approximately 32-34 kDa plus a lighter HO-1 protein ($HO\text{-}1_{Truncated}$) consistent with C-terminal truncation (Lin *et al.*, 2007b) (Fig 6.8J representative western blot). HO-1 protein expression significantly increased at 21d-IR compared to control kidneys regardless of diet (Fig 6.8J; $p<0.01$ and $p<0.001$ compared to respective control kidneys). Mice on the NAC diet had significantly higher HO-1 expression at IR compared to mice on a normal diet (Fig 6.8J; $p<0.05$).

SOD2 protein expression significantly decreased at 21d-IR compared to control kidneys regardless of diet (Fig 6.8K; $p<0.05$ and $p<0.05$ compared to respective controls). NAC diet significantly reduced SOD2 compared with normal diet at 21d-IR (Fig 6.8K; $p<0.05$).

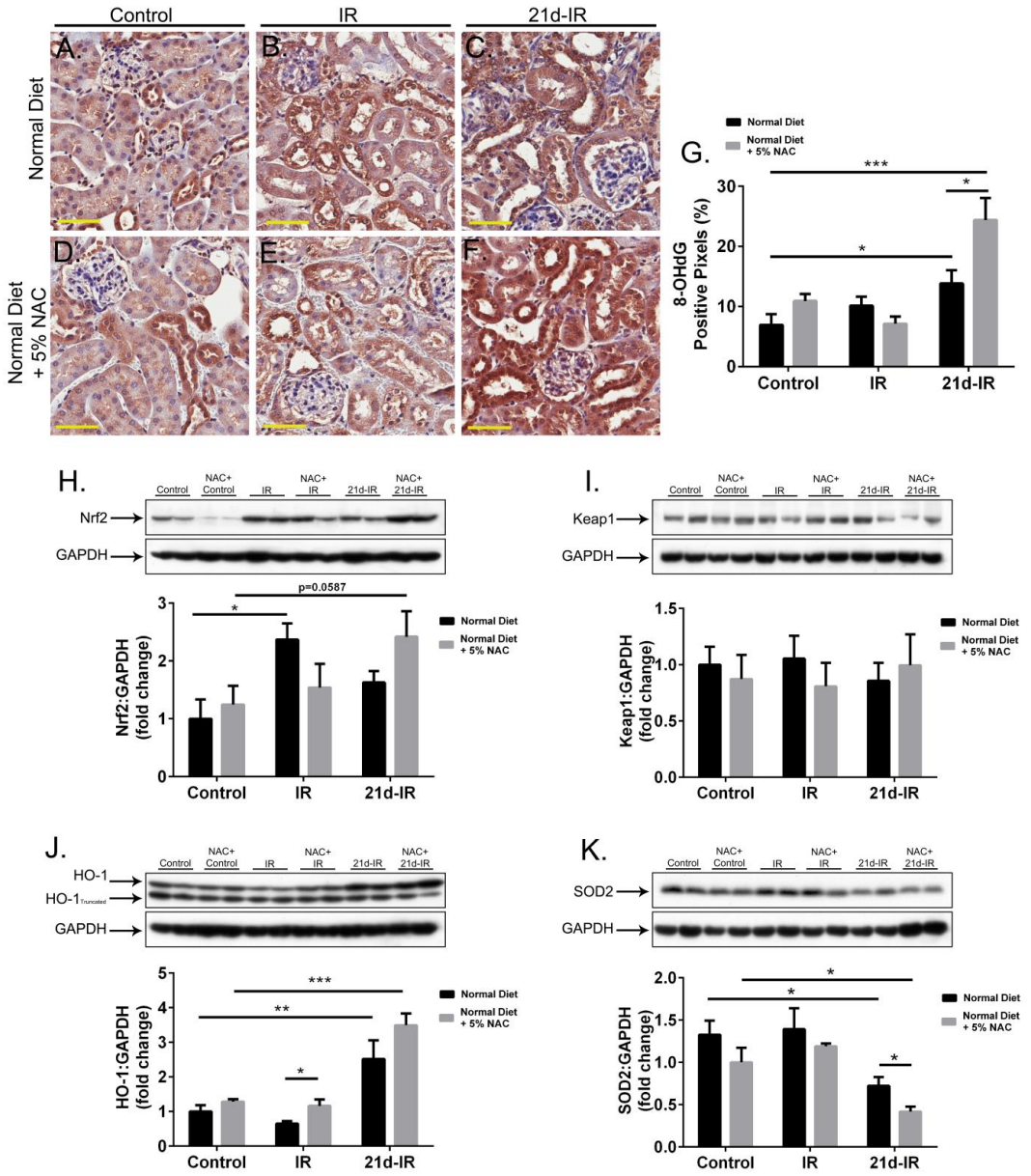

Figure 6.8: NAC enhances oxidative damage in the chronically damaged kidney following AKI

8-OHdG IHC (A.-F.) and morphometry (G.) demonstrate increased oxidative damage 21-days following IR injury (21d-IR) for mice on a normal diet and mice with the addition of 5 % NAC (NAC diet), compared to control kidneys (G.). NAC diet significantly enhanced 8-OHdG positivity at 21d-IR compared to mice on a normal diet (C., F., and G.). Nuclear factor like-2 (Nrf2) protein expression increased in mice on a normal diet at early reperfusion (IR), and an increase trend was observed at 21d-IR in mice on the NAC diet (H.). No changes were observed in Kelch-like ECH-associated protein 1 (Keap1) protein expression (I.). Heme-oxygenase-1 (HO-1) protein expression increased at 21d-IR in mice on a normal diet and on the NAC diet compared to control kidneys (J.). Apart from the normal 32-34kDa band, a band for truncated HO-1 was detected (J. – representative Western blot). Superoxide dismutase-2 (SOD2) decreased at 21d-IR in mice on a normal diet compared to controls. SOD2 was further decreased in mice on the NAC diet (K.). Results expressed as mean ± SE (* $p<0.05$; ** $p<0.01$: *** $p<0.001$ compared as indicated). Scale bar represents 50 µm.

6.3.4 Serine 112 phosphorylation of PPARγ-1 is associated with chronic kidney pathology following acute kidney injury *in vivo*

Localisation of PPARγ and p-PPARγ protein was investigated using IHC in kidney sections from the MPM animals, comparing mice on a normal diet (Fig 6.9A-F) and the NAC diet (Fig 6.9G-L). PPARγ expression was low and localised to the brush border of proximal tubular epithelial cells in the cortex of control kidneys regardless of diet (Fig 6.9A and G). p-PPARγ expression was localised to nuclei of tubular epithelial cells in the cortex regardless of diet (Fig 6.9D and J). At IR, PPARγ expression was lost from the brush border and appeared within punctate regions of tubular epithelial cells and glomerular cells (Fig 6.9B and H) whilst p-PPARγ nuclear expression was maintained in tubular epithelial cells (Fig 6.9E and K) regardless of diet. Brush border localisation of PPARγ was low in atrophic tubules at 21d-IR regardless of diet (Fig 6.9C and I), but localised to interstitial cells in mice fed the NAC diet (Fig 6.9I). Nuclear labelling of p-PPARγ within tubular epithelial cells appeared greater in atrophic areas at 21d-IR regardless of diet (Fig6.9F and L). Western immunoblotting identified protein expression of both PPARγ-1 and PPARγ-2 isoforms. Only phosphorylation (*ser112*) of PPARγ-1 (p-PPARγ-1) was seen (Fig 6.9M). PPARγ-2 protein expression significantly increased at IR compared to respective control kidneys regardless of diet (Fig 6.9N; $p<0.05$ and $p<0.01$ compared to control normal diet and the NAC diet, respectively), whereas PPARγ-1 expression did not alter (Fig 6.9O). Mice on a normal diet had significantly lower PPARγ-1 protein expression at 21d-IR compared to mice on the NAC diet (Fig 6.9O; $p<0.05$). The p-PPARγ-1 to PPARγ-1 ratio significantly increased at 21d-IR in kidneys of mice on both types of diet compared to control mice (Fig 6.9P; $p<0.01$ and $p<0.05$ for mice on a normal diet and the NAC diet, respectively).

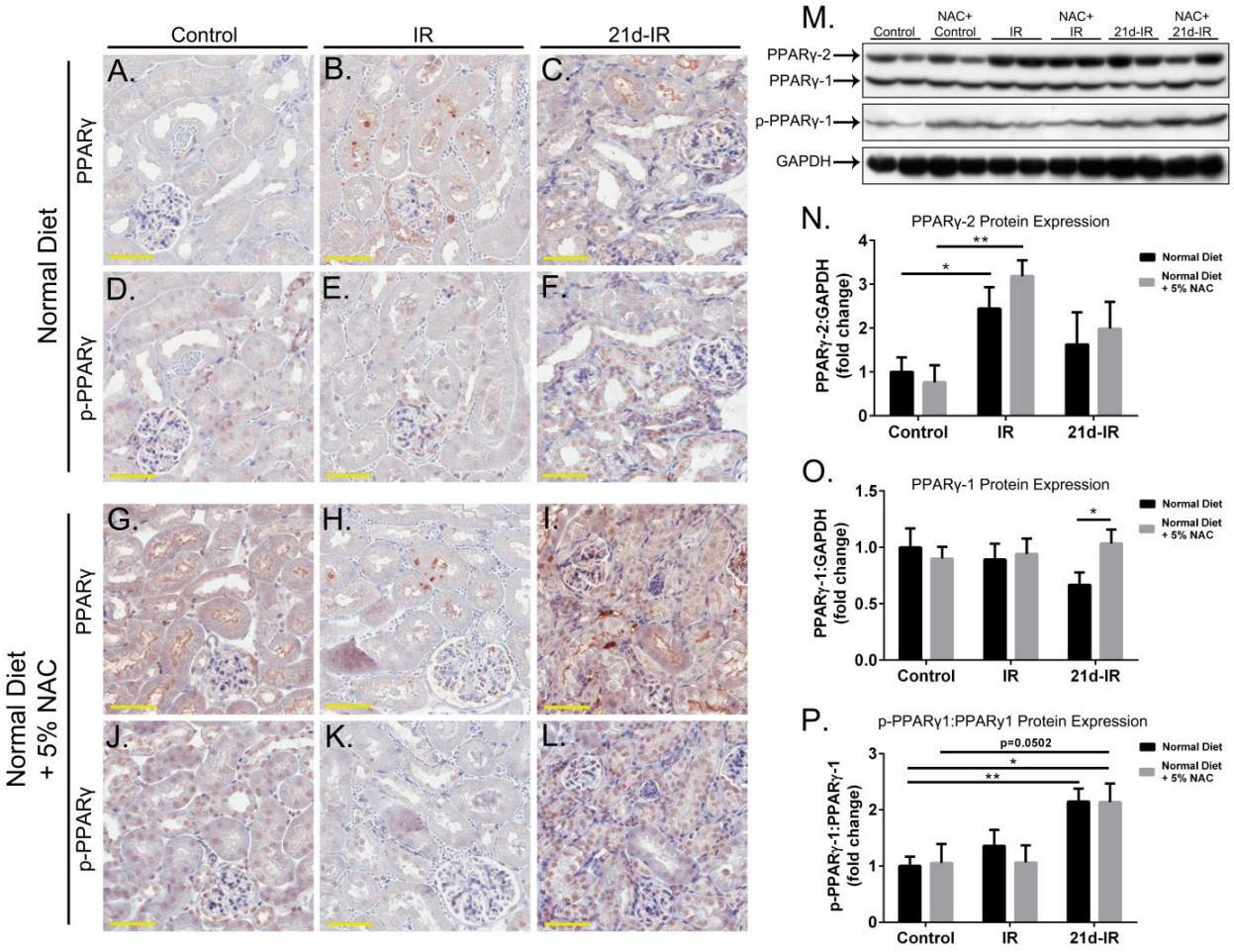

Figure 6.9: *Ser112* phosphorylation of PPARγ is associated with chronic kidney pathology following AKI

PPARγ and p-PPARγ protein localisation was examined by IHC, comparing mice on a normal diet (A.-F.) and normal diet + 5% NAC (NAC diet; G.-L.) in control kidneys, early reperfusion (IR) and 21-days following IR-injury (21d-IR). Control kidneys regardless of the type of diet demonstrated cytoplasmic and brush-border localisation of PPARγ within proximal tubular cells (A. and G.) and nuclear localisation of p-PPARγ (D. and J.). Punctate regions within tubular cells positive for PPARγ were apparent at IR regardless of the type of diet (B. and H.) and no change was observed in p-PPARγ localisation (E. and K.). 21d-IR PPARγ expression was localised primarily to the interstitium (C. and I) which matched nuclear localisation of p-PPARγ (F. and L.). Western blotting of whole kidney extracts for PPARγ protein expression detected PPARγ-1 and PPARγ-2 isoforms. Only phosphorylation of PPARγ-1 was detected (p-PPARγ-1) (M.). Densitometry demonstrated increased PPARγ-2 expression at IR in mice regardless of diet (N.) and decreased PPARγ-1 expression at 21d-IR in mice on a normal diet compared to mice on the NAC diet (O.). The p-PPARγ-1:PPARγ-1 ratio was significantly increased at 21d-IR in the kidneys on mice on a normal diet compared to control kidneys (P.). Results are expressed as mean ± SE (* $p<0.05$; ** $p<0.01$: *** $p<0.001$ compared as indicated). Scale bar represents 50 µm.

6.3.5 Metabolic alterations in the kidney cortex underlie the progression of chronic kidney pathology following AKI that is not prevented by the antioxidant NAC

Intravital MPM at 740 nm excitation demonstrated no observable differences in the renal cortical tubular network structure or mean NAD(P)H fluorescence between mice on a normal diet and on the NAC diet (Fig 6.10A, E and I). During 20 min of kidney ischaemia, tubular epithelial cell swelling was associated with a significant increase in mean NAD(P)H fluorescence, regardless of diet (Fig 6.10B, F and I; $p<0.001$ compared to respective controls), and a reduction in interstitial space that occurred with both diet regimens. Tubular and cellular damage was observed at the early stages of reperfusion (IR; 5 to 40 min follow end of ischaemia), and this was indicated by epithelial cell striations, cell effacement and the formation of cast material in kidneys of mice on either diet. NAD(P)H fluorescence returned to control levels (Fig 6.10C, G and I). The mean NAD(P)H fluorescence within tubular epithelial cells was significantly lower in mice on normal diet compared to the NAC diet (Fig 6.10I; $p<0.05$). Chronic kidney pathology (tubular atrophy, interstitial expansion) was apparent at 21d-IR. The areas of tubular atrophy contained highly fluorescent punctate regions, perhaps indicating enlarged lysosomes (Fig 6.10D and H). Remnant tubules possessed significantly higher NAD(P)H endogenous fluorescence compared to controls. This was enhanced in mice on the NAC diet (Fig 6.10D, H and I; $p<0.001$ compared to respective controls. $P<0.05$ compared to 21d-IR normal diet).

Intravital MPM has restricted depth in the kidney, hindering analysis, and so kidney slice preparations were imaged immediately after animal euthanasia, by MPM coupled with FLIM. This allowed visualisation of the cortex and medulla (Fig 6.11 and 6.12), and each zone of the kidney was then compared. Figure 6.11A demonstrates FLIM images (pseudocoloured according to averaged weighted lifetime τ_m) across three spectral channels that detect NAD(P)H, NAD(P)H/FAD, and FAD, from kidneys cortex from control or 21d-IR mice, whether on an NAC diet or not. The data demonstrate that, in all spectral channels, there was a decrease in τ_m between control kidney cortex and 21d-IR regardless of diet, indicated by a change from green to blue within representative images. This observation was also seen in τ_m lifetime histograms by a left-shift in 21d-IR τ_m peaks compared to control τ_m peaks, regardless of diet (Fig 6.11B-D). The average τ_m significantly decreased at 21d-IR in mice on a normal diet for NAD(P)H (Fig 6.11E; $p<0.01$), NAD(P)H/FAD (Fig 6.11F; $p<0.001$), and FAD (6.11G; $p<0.001$), and in mice on the NAC diet for NAD(P)H (Fig 6.11E; $p<0.01$ compared to control normal diet), NAD(P)H/FAD (Fig 6.11F; $p<0.01$), and FAD (6.11G; $p<0.001$). 21d-IR mice on a normal diet had a significantly lower FAD average τ_m compared to mice on a NAC diet at 21d-IR (Fig 6.11G; $p<0.001$).

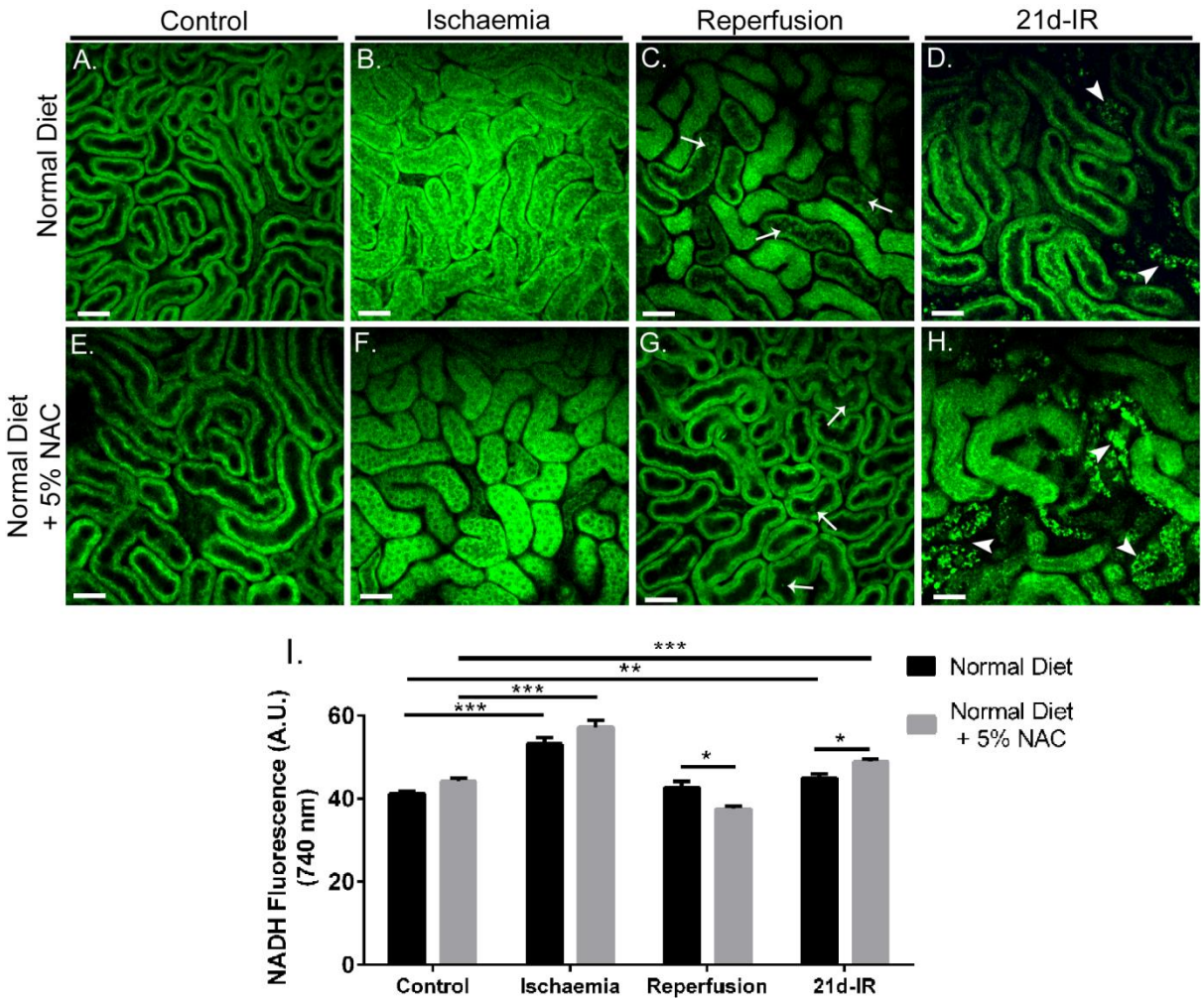

Figure 6.10: Intravital MPM demonstrates metabolic and structural alterations in chronic kidney pathology following kidney IR-injury that it not attenuated by NAC

Endogenous fluorescence of NAD(P)H, excited at 740 nm, in healthy control kidney cortex demonstrates the cortical tubular network with distal tubules, proximal tubules with associated brush border, and interstitial space that was unaltered in mice fed 5% NAC (NAC diet; A. and E.). During 20 min ischaemia, tubular swelling and a reduction in interstitial space was evident in both normal diet (B.) and the NAC diet (F.) and was associated with a significant increase in tubular cell NAD(P)H endogenous fluorescence (I.). Epithelial cell detachment and cast material formation (arrow) was evident at early reperfusion in both normal diet (C.) and the NAC diet (G.). 21-days following IR injury (21d-IR) there was widespread tubular atrophy with highly fluorescent punctate regions perhaps demonstrating enlarged lysosomes (arrowhead). Tubular structure was highly variable with structurally normal tubules appearing within areas of atrophy, perhaps allowing crosstalk between these tubules. There was a significantly greater NAD(P)H fluorescence signal in the normal-looking tubules for both normal diet (D. and I.) and the NAC diet (H. and I.). Results are expressed as mean ± SE tubular epithelial cell fluorescence a 740 nm (* $p<0.05$; ** $p<0.01$: *** $p<0.001$ compared as indicated). Scale bar represents 50 µm.

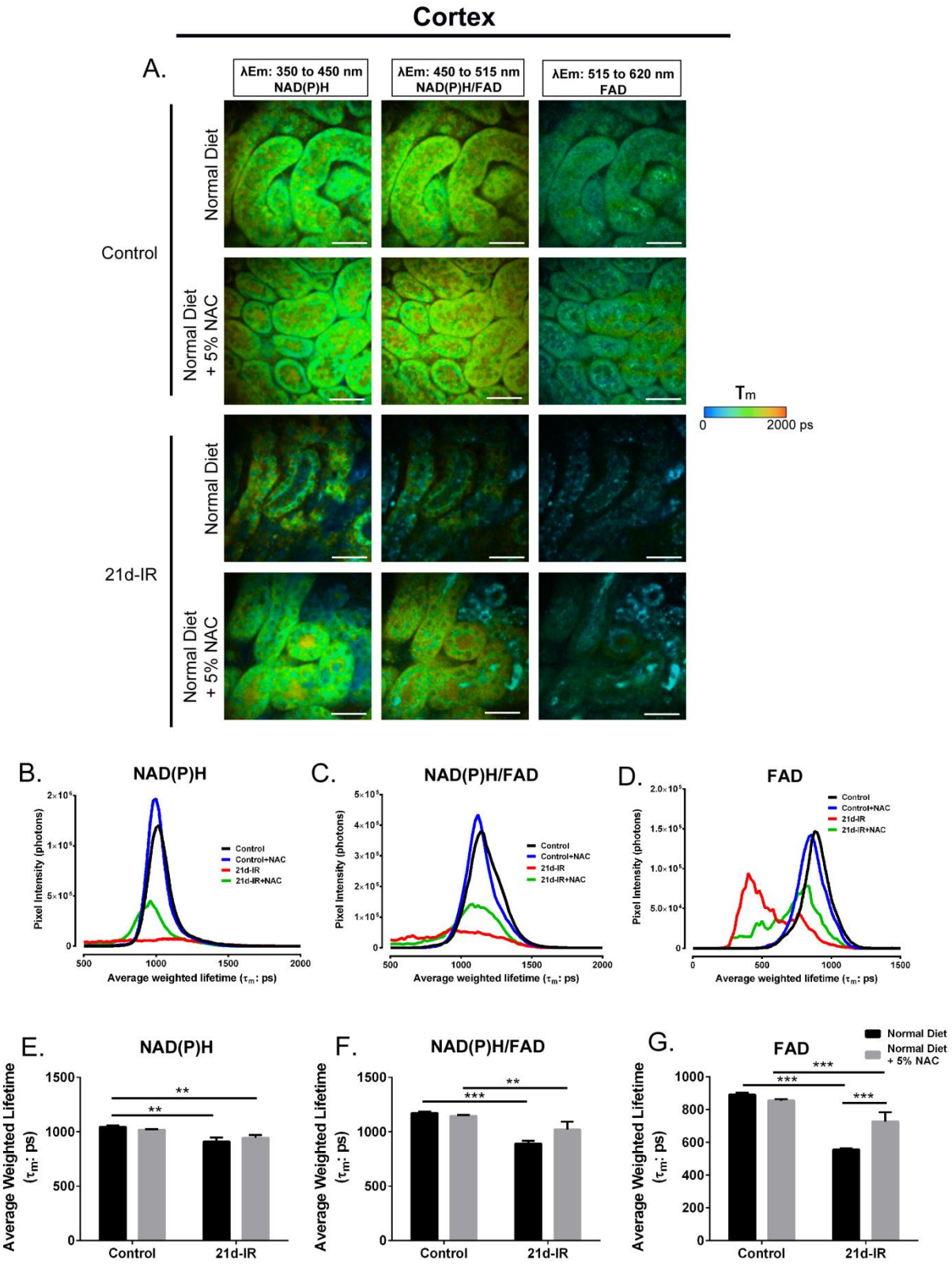

Figure 6.11: Fluorescence lifetime imaging microscopy in the cortex of the chronically damaged mouse kidney following NAC therapy

(Legend for Fig 6.11)
Representative average weighted fluorescence lifetime (τ_m) images of control and 21-day following IR-injury (21d-IR) in the cortex of the kidney from mice on a normal diet, or a normal diet + 5% NAC (NAC diet) are shown in (A.). Fluorescence lifetime data were measured within three spectral ranges (pseudocolour range from blue-red indicated in colour bar): 350 to 450 (750 to 1500 ps) to capture NAD(P)H, 450 to 515 (1000 to 1750 ps) to capture NAD(P)H/FAD, and 515 to 620 nm (500 to 1750 ps) to capture FAD. τ_m lifetime histograms, representing the average pixel intensity for each τ_m lifetime, are shown (B.-D.). The corresponding average τ_m lifetimes from the three spectral channels are charted for control and 21d-IR kidney cortex from mice with or without NAC (E.-G.). τ_m lifetime histograms demonstrate a decreased pixel intensity for 21d-IR kidneys in the cortex regardless of diet and within all three spectral channels (B.-D.). An observable left-shift is apparent in 21d-IR kidney cortex compared to control kidneys, which is more pronounced in mice on a normal diet (B.-D.). The τ_m detected in all three spectral channels was significantly decreased in the cortex of 21d-IR kidneys compared to respective control kidneys, regardless of diet (E.-G.), and this was enhanced for FAD in mice on a normal diet (G.). Results are expressed as mean ± SE (* $p<0.05$; ** $p<0.01$: *** $p<0.001$ compared as indicated). Scale bar represents 30 µm.

Figure 6.12A demonstrates FLIM images of the kidney medulla in control and 21d-IR mice on the NAC diet or not, across the same three spectral channels as 6.11A. The data demonstrate alterations to the τ_m within all spectral channels in the medulla at 21d-IR compared to controls, especially in mice on the NAC diet (Fig 6.12A). These changes are not apparent in τ_m histogram data (Fig 6.12B-D), yet are confirmed when τ_m is averaged (Fig 6.12E-G). The average τ_m significantly decreased at 21d-IR in mice on the NAC diet for NAD(P)H (Fig 6.12E; $p<0.01$), NAD(P)H/FAD (Fig 6.12F: $p<0.01$), and FAD (Fig 6.12; $p<0.01$) compared to mice on an NAC diet that did not undergo 21d-IR. Mice on a normal diet at 21d-IR had a significantly decreased average τ_m within the NAD(P)H/FAD spectral range compared to control mice (Fig 6.12F; $p<0.05$).

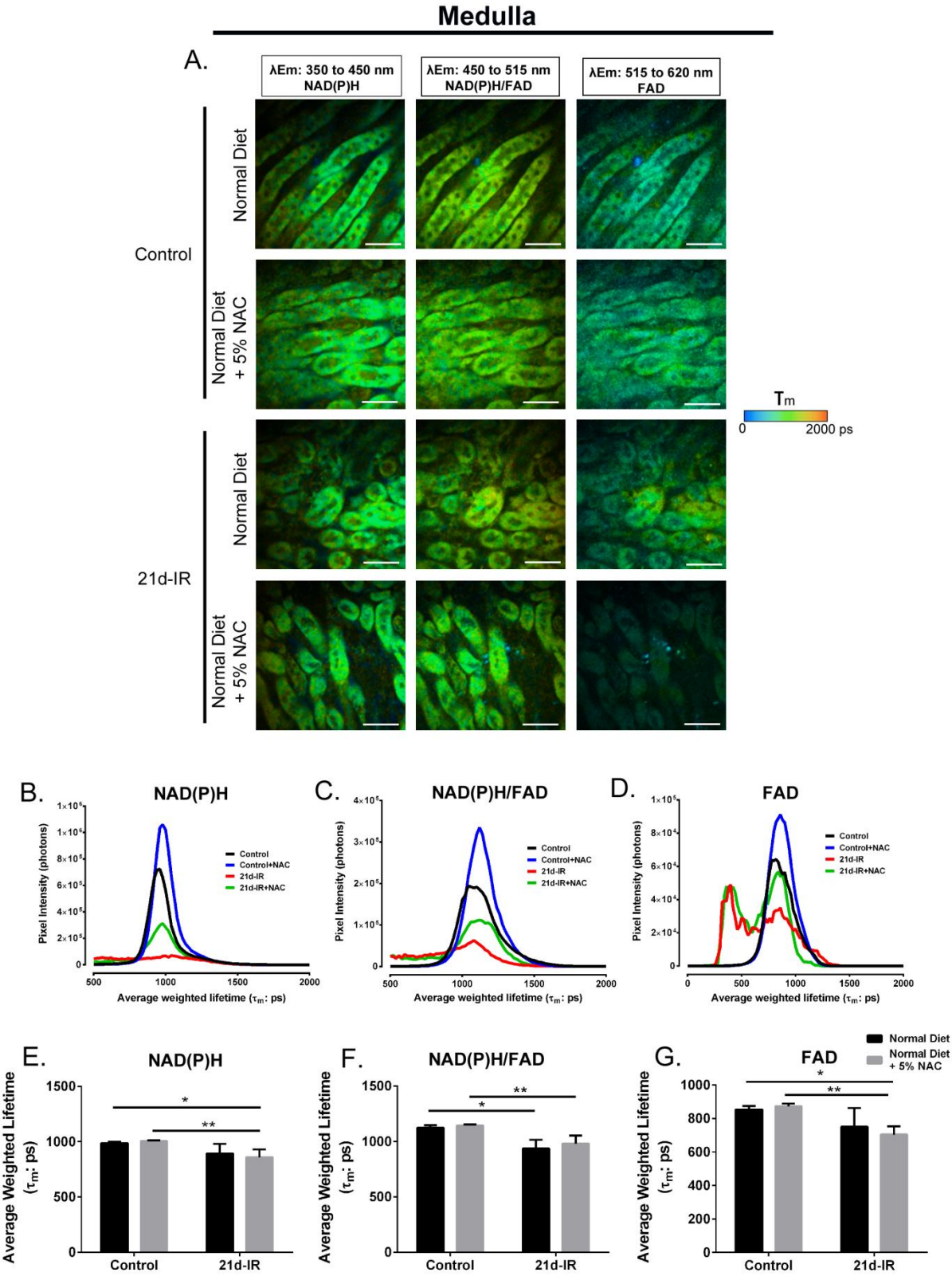

Figure 6.12: Fluorescence lifetime imaging microscopy in the medulla of the chronically damaged mouse kidney following NAC therapy

(Legend for Fig 6.12)
Representative average weighted fluorescence lifetime (τ_m) images of control and 21-day following IR-injury (21d-IR) in the medulla of the kidney from mice on a normal diet, or a normal diet + 5% NAC (NAC diet) are shown in (A.). Fluorescence lifetime data were measured within three spectral ranges (pseudocolour range from blue-red indicated in colour bar): 350 to 450 (750 to 1500 ps) to capture NAD(P)H, 450 to 515 (1000 to 1750 ps) to capture NAD(P)H/FAD, and 515 to 620 nm (500 to 1750 ps) to capture FAD. τ_m lifetime histograms, representing the average pixel intensity for each τ_m lifetime, are shown in (B.-D.). The corresponding average τ_m lifetimes from the three spectral channels are charted for control and 21d-IR kidney medulla from mice with or without NAC (E.-G.). τ_m lifetime histograms demonstrate high pixel intensity for control kidney medulla in mice on an NAC diet, and low pixel intensity for 21d-IR kidney medulla regardless of diet, within all three spectral channels (B.-D.). The τ_m detected in the NAD(P)H and FAD channels (E. and G., respectively) was significantly decreased in the medulla of 21d-IR kidneys compared to control kidneys in mice on the NAC diet. The NAD(P)H/FAD channel detected a decreased τ_m in the medulla of the 21d-IR kidney regardless of diet (F.). Results are expressed as mean ± SE (* $p<0.05$; ** $p<0.01$ compared as indicated). Scale bar represents 30 μm.

6.3.6 Mitochondrial dysfunction within remnant cortical tubules indicates a site of persistent oxidative stress

τ_m changes in NAD(P)H of the chronically damaged kidney were further investigated since NADH is a vital metabolic substrate for complex 1 of the ETC within mitochondria. Figure 6.13 A and D show representative redox FLIM images of the kidney cortex and medulla, respectively, that are pseudocoloured according to the ratio of free (α_1) to bound (α_2) NAD(P)H (redox ratio). The redox ratio appears higher in the cortex of 21d-IR kidneys regardless of diet (red) compared to control kidneys regardless of diet (green) (Fig 6.13A). The relationship is also observed in the medulla (Fig 6.13D). This observation is also seen in the α_1/α_2 histograms which show a right-shift at 21d-IR, regardless of diet, primarily within a secondary peak in both the cortex (Fig 6.13B) and medulla (Fig 6.13E). The average redox ratio significantly increased in the cortex at 21d-IR regardless of diet (Fig 6.13C; $p<0.001$ compared to respective controls). Mice on the NAC diet had a significantly increased redox ratio in the medulla, that did not occur in mice on a normal diet (Fig 6.13F; $p<0.001$). This indicates an increase in free NAD(P)H or decrease in bound NAD(P)H in the cortex of the chronically-damaged kidneys. This change was also present in the renal medulla of mice on the NAC diet.

To further investigate apparent mitochondrial dysfunction in the cortex of the chronically-damaged kidney *in vivo*, the mitochondrial membrane potential-dependent dye TMRM, was infused into mice and imaged with intravital MPM (Fig 6.14). Three representative images demonstrate uptake of TMRM into tubules of the cortex in healthy kidney (Fig 6.14A-C), which is impaired in tubules of

21d-IR kidneys (Fig 6.14D-F) demonstrating mitochondrial dysfunction. TMRM quantification per tubular epithelium was shown to be significantly decreased at 21d-IR compared to control (Fig 6.14G; $p<0.001$). TMRM and NAD(P)H co-localisation to the basolateral region of tubular epithelium in control mice confirmed mitochondrial accumulation (Fig 6.14H-J), which was disrupted at 21d-IR (Fig 6.14K-M).

Z-stack 3D reconstructions of healthy control regions of the cortex following TMRM infusion demonstrated NAD(P)H and TMRM fluorescence and accumulation within normal tubular epithelial cells (Fig 6.15A-C). Three representative areas of atrophic regions within the cortex at 21d-IR demonstrated remnant, structurally-normal tubules that retained NAD(P)H endogenous fluorescence yet displayed impaired TMRM uptake and ensuing mitochondrial dysfunction (Fig 6.15D-F).

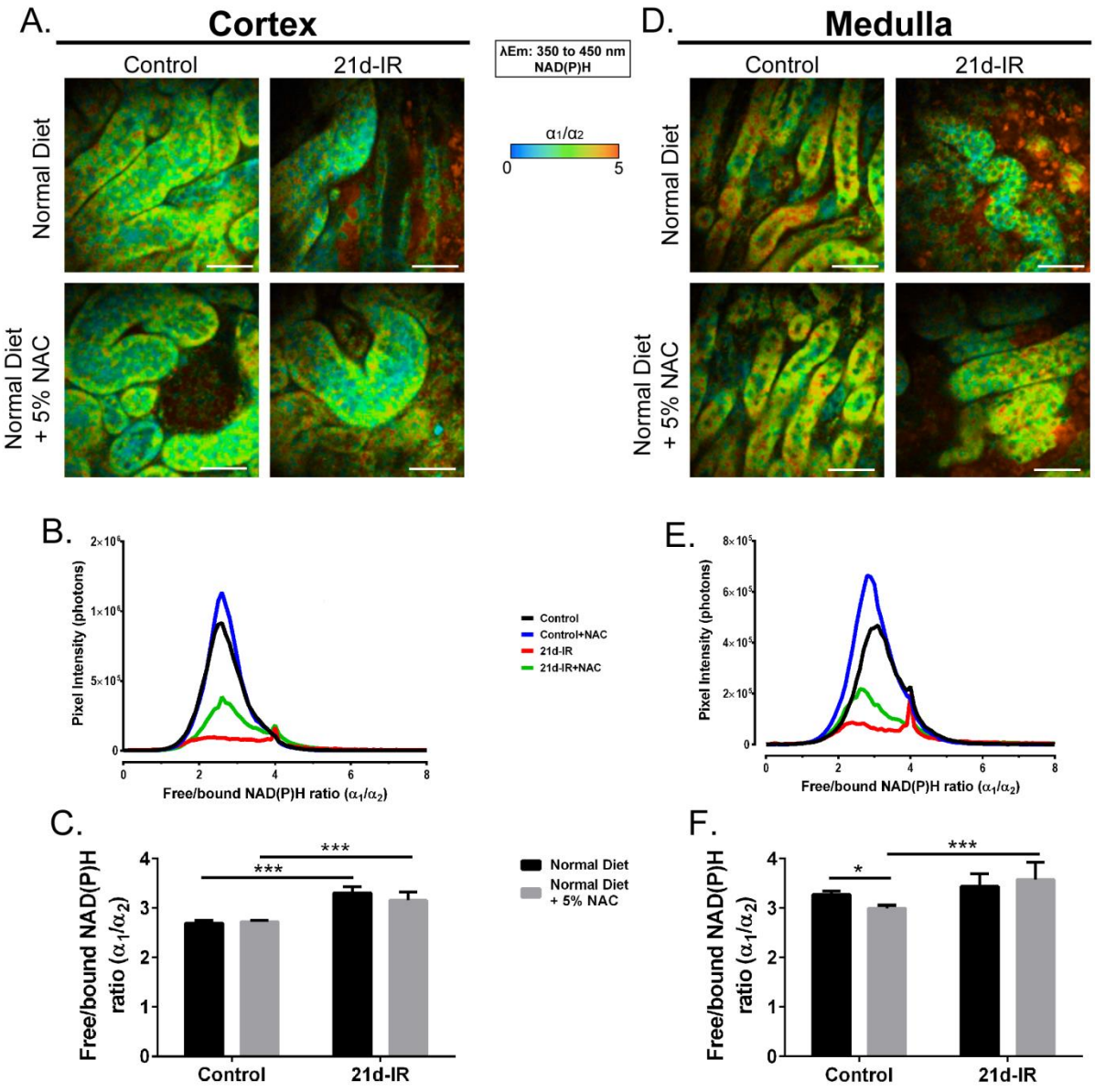

Figure 6.13: Changes in the redox ratio (α_1/α_2) in the chronically damaged mouse kidney following NAC therapy

Representative redox images of control and 21-days following IR-injury (21d-IR) kidney cortex (A.) and medulla (D.) from mice on a normal diet, or on a normal diet + 5% NAC (NAC diet), depict changes in the free (α_1) to bound (α_2) NAD(P)H ratio. Fluorescence lifetime data were measured in the 350 to 340 nm spectral channel to capture NAD(P)H and pseudocoloured according to the α_1/α_2 range 0 to 5 (blue to red). Redox ratio histograms, representing the average pixel intensity for each redox ratio value, are shown in (B.) and (E.) for the cortex and medulla, respectively. The corresponding average redox ratios are charted for the control and 21d-IR kidneys for cortex (C.) and medulla (F.). The pixel intensity for the average redox ratio was noticeably decreased in 21d-Ir kidneys regardless of diet in both the cortex (B.) and medulla (E.). The redox ratio was increased in the cortex of 21d-IR kidneys compared to controls regardless of diet (C.). Mice on the NAC diet had increased redox ratio in the medulla of the kidney at 21d-IR compared to control mice (F.). The NAC diet decreased the redox ratio in the healthy control kidney (F.). Results are expressed as mean ± SE (* $p<0.05$; *** $p<0.001$ compared as indicated). Scale bar represents 30 µm.

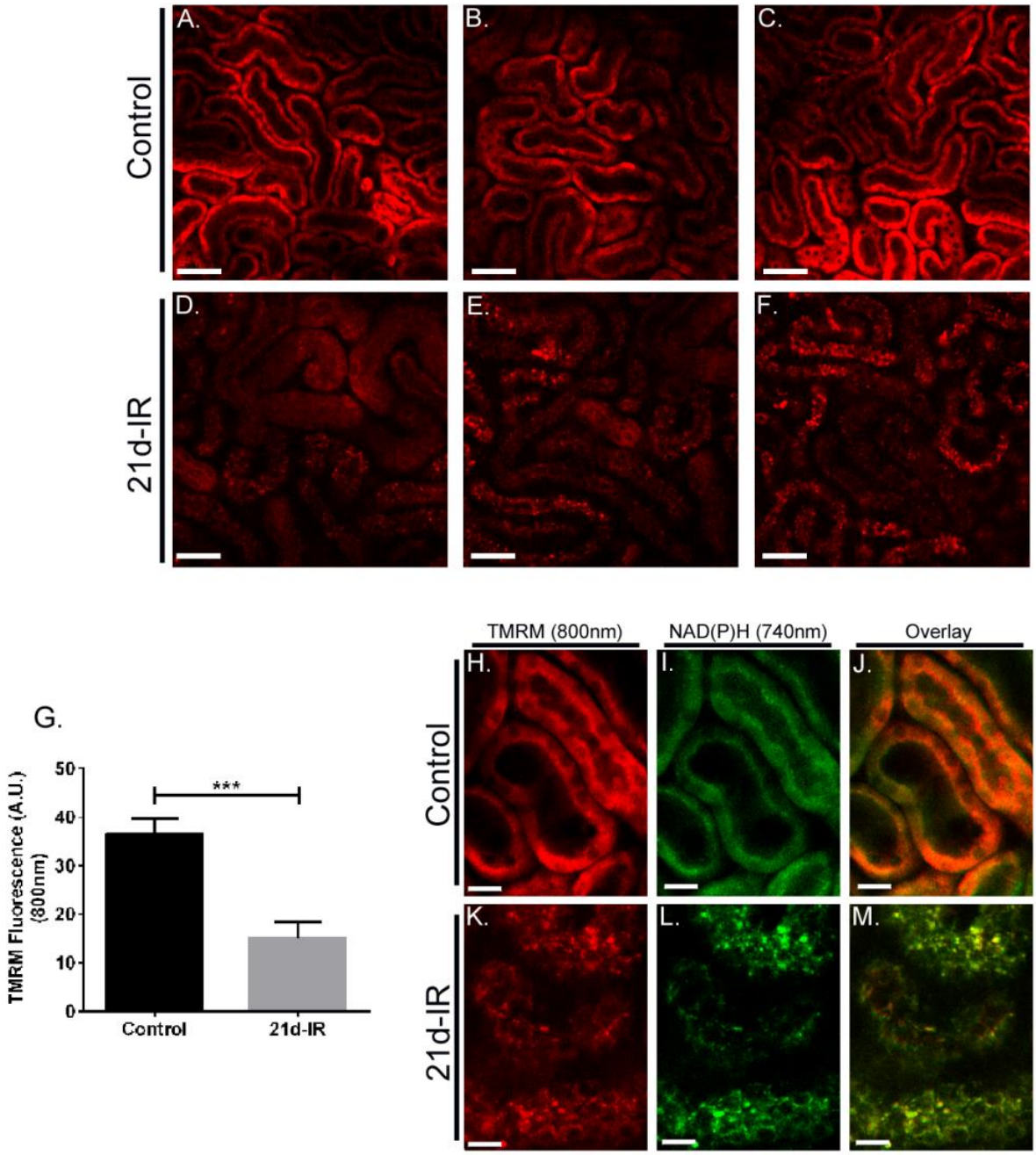

Figure 6.14: *In vivo* imaging reveals impaired mitochondrial function within tubular epithelial cells of the kidney cortex 21-days following ischaemia-reperfusion injury

The mitochondrial membrane potential-dependent fluorophore tetramethylrhodamine methyl ester (TMRM) was infused into mice and imaged with intravital MPM at excitation 800 nm (pseudocoloured red). Three representative images of the healthy control kidney revealed accumulation of TMRM into tubular epithelial cells (A.-C.). Accumulation of TMRM into tubular epithelial cells of the cortex 21-days following IR-injury (21d-IR) was noticeably reduced in three representative images (D.-F.). TMRM fluorescence quantification per tubule demonstrated a significant decrease in TMRM accumulation compared to control (G.). The co-localisation of TMRM (H.) and NAD(P)H (excitation at 740 nm) (I.) to the basolateral region of tubular epithelial cells (J.) confirmed mitochondrial accumulation. Basolateral localisation of TMRM and NAD(P)H fluorescence was disrupted at 21d-IR with the formation of punctate vesicles, perhaps enlarged lysosomes, strongly detected at both excitations (K.-M.). Results are expressed as mean ± SE (*** $p<0.001$ compared to control). Scale bar represents 50 µm (A.-F.) and 15 µm (H.-M.).

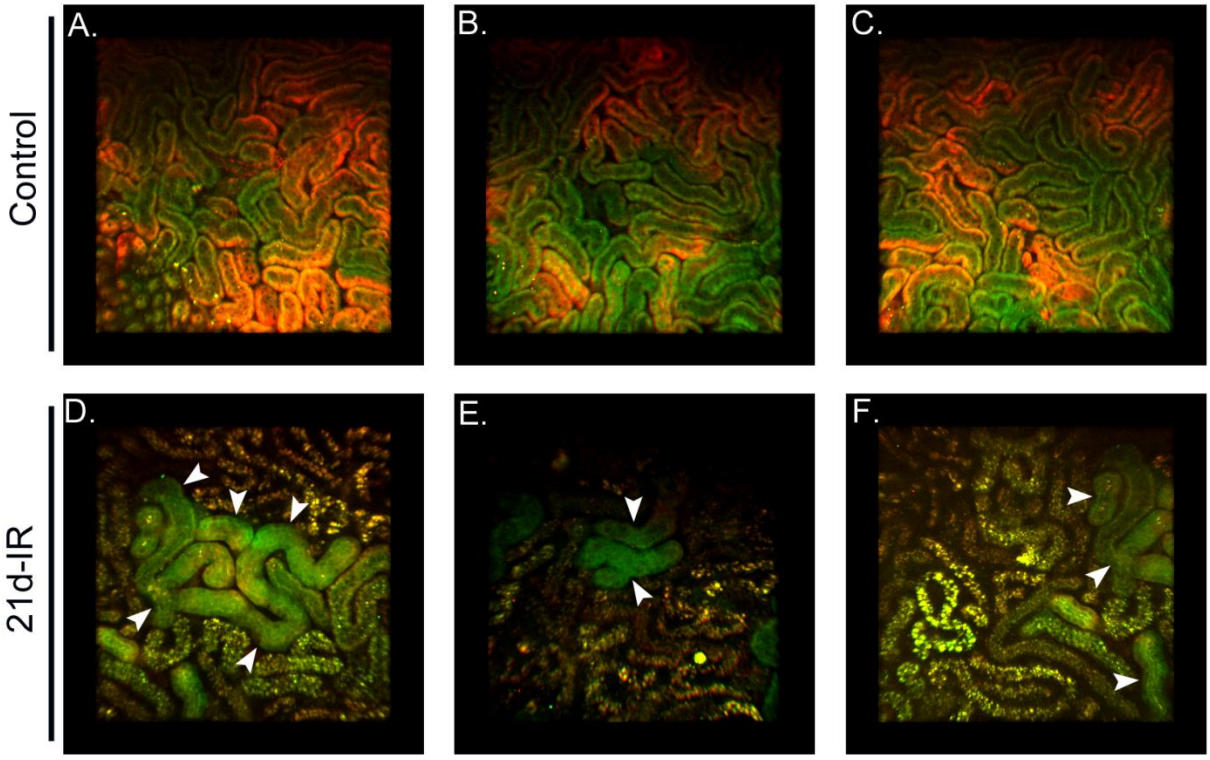

Figure 6.15: Remnant tubules in the kidney cortex 21-days post ischaemia-reperfusion injury are a site of persistent mitochondrial dysfunction

Three representative fields (z-stack 3-dimensional reconstructions) of the healthy control kidney (A.-C.) depict green NAD(P)H autofluorescence (excitation 740 nm) and red TMRM fluorescence (excitation 800 nm) accumulation within normal tubular epithelial cells. Three representative z-stack 3D reconstructions 21-days following IR-injury (21d-IR) (D.-F.), demonstrate the appearance of remnant, structurally-normal tubules within areas of tubular atrophy, that have low TMRM accumulation yet retain NAD(P)H fluorescence (arrow heads).

6.4 DISCUSSION

Despite numerous reported positive benefits of antioxidant therapy against AKI, targeting oxidative stress in chronic progressive kidney disease has yielded limited and often disappointing results in patient cohorts (Jun *et al.*, 2012; Himmelfarb *et al.*, 2014). The results of the present study further support the use of a known general antioxidant (NAC) to target systemic oxidative stress to reduce early IR-induced AKI. However, we provide new evidence that the ensuing progression to chronic kidney pathology can be enhanced by antioxidant therapy by eliminating redox-sensitive endogenous cytoprotective signalling. Furthermore, we provide a description of metabolic alterations in the chronically-injured kidney that are specific to mitochondrial dysfunction and have only previously been described in models of acute injury.

In vitro experiments demonstrated a superior benefit of the antioxidant NAC to reduce oxidative stress-induced apoptosis of kidney PTE cells, compared to other commonly-used antioxidant therapies vitamin E (αTOC and Tlx) and CoQ_{10}. NAC is consistently a successful antioxidant therapy in cell culture models of oxidant-induced injury (Zhong *et al.*, 2009; Ye *et al.*, 2010; Zhang *et al.*, 2011). This may be due to the potency of the sulfhydryl-thiol group of L-cysteine directly scavenging ROS, in such a confined system as cell culture. The results showing a lack of benefit conferred by vitamin-E derivatives, αTOC and Tlx, contribute to a growing body of evidence that implicates vitamin-E with negative outcomes (Miller *et al.*, 2005; Klein *et al.*, 2011), including a study demonstrating its pro-apoptotic actions (Jia *et al.*, 2010). CoQ_{10} also did not alter oxidative stress-induced apoptosis. The major contributing factor in cell culture is the low solubility of CoQ_{10}, owing to a long isoprenyl side chain, which would limit its ability to enter the cell and the mitochondria, where the majority of beneficial actions would be exerted (Sohal *et al.*, 2006). The bioavailability of CoQ_{10} *in vivo* also remains a challenge (Bhagavan and Chopra, 2006). Tubular cell apoptosis remains a common contributing factor to AKI and CKD pathogenesis (Gobe *et al.*, 2014). Therefore the ability of NAC to attenuate oxidative stress-induced pathological processes *in vitro* was investigated *in vivo*.

A diet of 5% NAC for one week attenuated tubular epithelial cell apoptosis in the kidney cortex at the time of early IR-induced injury, demonstrating acute protection. These findings are consistent with human clinical trials investigating NAC pre-treatment against AKI, including contrast-induced nephropathy (Kay *et al.*, 2003), and cardiovascular bypass surgeries (Santana-Santos *et al.*, 2014). IR injury of the kidney primarily occurs at the time of reperfusion. At this time, re-presentation of oxygen to components of the mitochondrial ETC membrane complexes, previously damaged from a

failure of ATP-dependent actin polymerisation during ischaemia, subsequently causes ROS production (Atkinson *et al.*, 2004; Plotnikov *et al.*, 2007). This mechanism is supported by visualising NAD(P)H dynamics during IR-induced injury with intravital MPM. Increased NAD(P)H fluorescence demonstrates a failure of ETC complex 1 to convert NAD+, in both normal and NAC-treated mice. The apparent decrease in NAD(P)H fluorescence in NAC-treated mice, compared to normal diet, may represent efficient ETC complex 1 activity at reperfusion due to NAC detoxification of ROS and subsequent improvement in mitochondrial membrane damage (Brunet *et al.*, 1995).

Nrf2-Keap1 dynamics during an oxidative stress environment promote the upregulation of cytoprotective enzymes and proteins to protect against cell damage (Kensler *et al.*, 2007). Interestingly, Nrf2 upregulation at the time of early reperfusion was prevented in mice on an NAC diet. Nrf2 nuclear translocation and binding to the ARB sequence is regulated through increased intracellular ROS signalling forming a highly conserved cytoprotective response (Zhang and Hannink, 2003; Sekhar *et al.*, 2010). Recent studies demonstrate that Nrf2 dissociation from Keap1, a substrate adapter for the ubiquitin E3 ligase complex, occurs by ROS modification of the Keap1 cysteine 288 residue (Kim *et al.*, 2014). NAC, as a general cellular antioxidant, has the ability to eliminate intracellular ROS, and thereby eliminate ROS signalling that is dependent on cysteine modification, such as cysteine 288 of Keap1. This would result in maintained binding of Keap1 to Nrf2, subsequent degradation, and failure to upregulate cytoprotective responses through ARB binding. Furthermore, the cysteine residue of NAC forms a competitive antagonist type mechanism for ROS-dependent Nrf2 activation. The anti-apoptotic effect of NAC early after reperfusion can be attributed to immediate ROS detoxification and protection of the intrinsic mitochondrial apoptotic pathway (Higuchi *et al.*, 1998). This is supported by the *in vitro* experiments in the present study, which represent a more acute model of ROS-induced kidney cell apoptosis. However, an underlying disruption to kidney cell redox control is apparent during the ensuing progression of disease following AKI. The ability of NAC to prevent a highly conserved cytoprotective response to IR, in kidney cells with disrupted redox control, becomes apparent during the progression of disease following AKI.

Maladaptive repair is a defining characteristic of the progression to CKD from AKI (Bonventre and Yang, 2011; Yang *et al.*, 2011). The underlying mechanisms driving maladaptive repair following AKI are poorly understood, yet are associated with cell cycle arrest (Yang *et al.*, 2010), interstitial proliferation and fibrosis (Chen *et al.*, 2011), and enhanced cell death (Gobe *et al.*, 2014). Our findings demonstrate that a perturbed redox environment due to prolonged NAC therapy can

promote fibrosis and the secretion of pro-fibrotic TGF-β1, and these changes may enhance other characteristics of maladaptive repair, such as increased apoptosis of tubular epithelial cells in the cortex. In the current study, increased PCNA labelling was found in cells within the interstitial areas at 21d-IR, consistent with increased myofibroblast or macrophage/monocyte proliferation (Forbes *et al.*, 2000). Myofibroblasts and macrophages are known to secrete fibrogenic factors like TGF-β1 (Okada *et al.*, 2005). This process, combined with increased apoptosis of tubular epithelial cells, demonstrates disrupted repair mechanisms that result in chronic kidney pathology. It is important to note that some PCNA-positive cells were found within the tubular epithelium, indicating an attempt to repair via epithelial cell repopulation to preserve a functional tubule. This repair mechanism has gained recent attention and indicates the importance of remnant tubules within areas of focal fibrotic change (Kusaba *et al.*, 2014), as observed in the present study.

Kidney function was not measured in the current investigation and this may be seen as a criticism. However, we would expect the greatest degree of functional impairment to occur at 1-4 days post reperfusion (Vesey *et al.*, 2004; Johnson *et al.*, 2006), and to then return to normal levels at 3 weeks post-IR. This is also representative of functional decline and re-establishment in human AKI. Reduced kidney function at 21d-IR in the present study was not expected since substantial areas of functional kidney parenchyma were observed histologically thereby allowing compensation to occur. In addition, the aim of this study was to understand the underlying alterations to kidney cell metabolism and redox control, using the novel methods of MPM and FLIM.

Our description of the ability of NAC to enhance fibrosis is novel, and is in contrast to previous studies reporting the antifibrotic actions of NAC within isolated pro-fibrotic hepatic stellate cells (Meurer *et al.*, 2005), and fibroblasts (Kopp *et al.*, 2006). However, these studies were carried out *in vitro* and highlight the superior antioxidant mechanisms of NAC in the cell culture environment, as was noted here earlier. Borkham-Kamphorst *et al.* (2005) demonstrated that phosphorylation of PDGF, ERK or protein kinase B could not be inhibited despite high NAC administration to hepatic stellate cells *in vitro*. Therefore PDGF-dependent activation of ERK in renal myofibroblasts, and their subsequent proliferation and collagen synthesis, may play an important role i*n vivo* in response to NAC following AKI-induced progressive fibrosis. In support of NAC-induced TGF-β1 expression *in vivo*, an hepatic bile-duct ligation mouse model of liver fibrosis analysed TGF-β1 expression in livers of mice given NAC orally. Sham surgery mice with NAC had increased TGF-β1 expression, compared to sham mice on a normal diet, however, the increase was, unfortunately, not analysed for significance (Galicia-Moreno *et al.*, 2012). Recent evidence suggests that TGF-β1 can suppress Nrf2 activation (Ryoo *et al.*, 2014). This is interesting given that, in our study, TGF-β1

levels were high in NAC-treated control kidneys and may suggest that NAC-induced TGF-β1 expression inhibits Nrf2 activation at a time of early reperfusion, rather than NAC saturation of ROS and the prevention of Keap1 cysteine 288 modification, as previously suggested. Nevertheless, the work by Ryoo et al (2014) supports our findings that NAC dampens the Nrf2-dependent cytoprotective response following kidney IR injury. The mechanism by which NAC induces TGF-β1 in the kidney requires further investigation, yet is likely to involve alterations to the redox environment, that include a pro-oxidant role. There have been studies that suggest harmful effects of NAC in various clinical settings (Peake *et al.*, 1996; Childs *et al.*, 2001; Spapen *et al.*, 2005; Laisalmi-Kokki *et al.*, 2009), including a randomised placebo-controlled study showing a trend for increased mortality in multisystem organ failure (Molnar *et al.*, 1999). This highlights the importance of basic research into the mechanisms of NAC within the kidney, especially in progressive kidney disease.

Oxidative stress incorporates alterations in normal cell redox networks, which are vital for physiological cell function. Long-term alterations following IR-induced injury lead to increased HO-1 expression. HO-1 is the inducible HO isoform responsible for the degradation of heme in tissues, and the induction of HO-1 is recognized as a protective response against virtually any insult, including AKI (Chen *et al.*, 2005; Bolisetty *et al.*, 2010; Stec *et al.*, 2012). We report unchanging HO-1 expression at immediate (30-40 min) reperfusion. Zager *et al.* (2012) demonstrated that peak HO-1 expression in the kidney occured at 4 h following reperfusion, thus observable increases in HO-1 at 30-40 min may not occur. Despite genetic knock in/out mouse models confirming a protective relationship, physiological HO-1 induction in response to IR injury does not prevent overall damage (Mayer *et al.*, 2003; Bolisetty *et al.*, 2010; Kezic *et al.*, 2013). Thus, many researchers use HO-1 expression as a marker of oxidative stress, rather than an indicator of a full cytoprotective response. We demonstrate an increase in HO-1 expression at 21d-IR that is associated with maladaptive repair and fibrosis. Within the tissue milieu, HO-1 induction is likely responding to an oxidative stress environment indicated by enhanced 8-OHdG detection, and so is likely to be an attempt to promote antioxidant and cytoprotective benefit. The detection of an HO-1 isoform of lower kDa size to the normal HO-1 indicates protease-mediated truncation of HO-1 at the C-terminal domain (Yoshida *et al.*, 1991). The functional relevance of this truncation has been explored by Lin and colleagues and shown to aid nuclear-cytoplasmic HO-1 shuttling and altered binding of transcription factors involved in oxidative stress, thereby affording protection against H_2O_2 (Lin *et al.*, 2007a). We noted an observable decrease in $HO\text{-}1_{Truncated}$ at 21d-IR compared to healthy controls, regardless of diet, suggesting that truncated HO-1 may be more functionally-relevant in a chronic oxidative stress environment in the kidney. Alternatively, the

truncation of HO-1 by oxidative stress may prevent its translocation to the nucleus. This functionality appears relevant in the murine kidney, however only the un-truncated isoform was detected in human PTE cells with and without oxidative challenge (our data, not shown).

We have previously demonstrated (Chapter 4) that oxidative stress induces PPARγ alterations and mitochondrial destabilisation within isolated PTE cells (Small *et al.*, 2014). The results presented in the current Chapter support the association between increased PPARγ *ser112* phosphorylation and a failure to induce cytoprotective responses during an oxidative stress environment in the kidney. However, the cell types involved, and responsive PPARγ isoforms, are more diverse following kidney IR-induced injury. The heavier PPARγ-2 isoform was detected from whole kidney protein extracts and was found to be especially responsive during early IR compared to PPARγ-1. This indicates that the punctate regions within PTE cells seen via IHC are more likely to be attributable to PPARγ-2. This is in contrast to our *in vitro* studies detecting only PPARγ-1 from isolated PTE cells, and may indicate species differences, or PPARγ-2-mediated responses within glomerular cell types that were detected by IHC (Zhu *et al.*, 2011; Miglio *et al.*, 2012). PPARγ-1 and PPARγ-2 regulate similar genes, yet PPARγ-2 is the dominant isoform expressed in adipose tissue of rodents (Chawla *et al.*, 1994; Tontonoz *et al.*, 1994).

PPARγ is an important regulator of PGC-1α and subsequent mitochondrial biogenesis (Rasbach and Schnellmann, 2007; Hock and Kralli, 2009). Furthermore, at 21d-IR total PPARγ-1 and PPARγ-2 remained relatively unaltered compared to control, yet *ser112* phosphorylation of PPARγ-1 increased and was primarily localised to nuclei of atrophic tubules within regions of fibrotic change. These findings are consistent with decreased cell and mitochondrial function due to PPARγ-1 phosphorylation within PTE cells when oxidative stress is involved in the damage, and further contributes to a cycle of oxidative stress and tissue damage, progressing fibrotic change. These differential expression profiles of PPARγ-1 and PPARγ-2 may suggest different and unique mechanisms of the two isoforms in response to injury in the kidney, whereby PPARγ-2 plays an early adaptive and protective role against injury, whereas PPARγ-1 is primarily influenced by post-translational phosphorylation long-term. Targeting PPARγ with TZD agonists has proved beneficial in rodent models of kidney IR-induced injury (Yang *et al.*, 2009; Miglio *et al.*, 2012). Interactions resulting from therapeutic PPARγ activation on tubular epithelial cells preventing the ensuing phosphorylation may prove beneficial in preserving renal function. Important to note is a relative lack of effect of an NAC diet on PPARγ responses following kidney injury, besides maintaining total PPARγ-1 expression at 21d-IR. PPARγ plays a vital role in fatty acid oxidation and metabolism, which suggests that the influence of NAC cannot alter these processes.

The metabolic coenzymes NAD(P)H and FAD are the primary electron donor and acceptor, respectively, in oxidative phosphorylation. The results in this Chapter present the first demonstration of differences in the redox and metabolic state of kidney tubular epithelial cells between healthy and IR-induced chronic damage. Using FLIM, the main metabolic changes were observed in the cortex, rather than medulla, of the chronically-damaged kidney. This is consistent with a high O_2 tension in the cortex (Epstein *et al.*, 1994), and an unexpected result because the medulla, particularly the outer stripe of the outer medulla, is thought to be the main site of injury in the IR-injured kidney (Bonventre and Yang, 2011). Using MPM for observations of changes in metabolism presented technical limitations on measuring changes in the outer stripe of the outer medulla, where the severity of ischaemic AKI is most pronounced. However, within the cortex, a decrease in τ_m was observed in all spectral channels that encompass NAD(P)H and FAD endogenous fluorescence. This result indicates that the cortex is also a critical site of metabolic dysfunction in IR-induced kidney injury. Decreased NAD(P)H τ_m has been observed previously in photo-damaged skin compared to solar-protected skin (Sanchez *et al.*, 2013), and in hepatocytes following IR injury at 4 h (Thorling *et al.*, 2013), and is attributed to metabolic damage, namely oxidative damage due to ROS generation. NAD(P)H may be recruited by proteins related to oxidative repair, causing the lifetime changes we observe. Contrasting differences have been observed in NAD(P)H τ_m changes due to IR-induced necrosis and apoptosis, that are associated with increases in NAD(P)H τ_m (Skala *et al.*, 2007; Wang *et al.*, 2008; Sanchez *et al.*, 2010). Despite these processes also involving oxidative stress, they represent a more acute response to injury that may result in alternative NAD(P)H protein recruitment compared to that observed in chronic injury, which contributes to a persistent and underlying metabolic dysfunction.

Using FLIM, the protein-binding interactions of NAD(P)H were investigated further, with the ratio of free to bound NAD(P)H (α_1/α_2) found to increase. Considering that all values are greater than 1, an increased ratio demonstrates either an increase in free NAD(P)H or decrease in protein-bound NAD(P)H. NAD(P)H binding primarily occurs on the mitochondrial membrane (complex I). Therefore, a decreased redox ratio indicates impaired mitochondrial function, and is consistent with intravital MPM data, describing complex I-deficient backing up of NAD+ at 21d-IR. Similar NAD(P)H binding dynamics were not observed in the medulla, except under NAC conditions, indicating that long-term NAC therapy contributes to metabolic dysfunction, that is usually preserved in the medulla following IR-induced injury. Conesa *et al.* (2001) have previously demonstrated that NAC can enhance renal medullary perfusion, suggesting that increased O_2 presentation to deficient mitochondria can potentiate metabolic impairments long-term. Further studies are required to identify the specific protein binding associations of NAD(P)H in the cortex

of the chronically-damaged kidney. Decreased FAD τ_m likely demonstrates decreased protein-bound FAD to the succinate dehydrogenase enzyme complex of complex II of the ETC and, in addition, decreased free FAD due to decreased complex II utilisation and re-presentation of FAD to the citric acid cycle. Both explanations underlie impaired metabolism and/or mitochondrial dysfunction within tubular epithelial cells of the cortex. The results, showing that NAC diet significantly enhanced the observed decrease in FAD at 21d-IR, further contribute to the evidence within this chapter, that altering the cellular redox environment in the kidney through exogenous means, can worsen outcome after injury, perhaps by functional metabolic impairments.

The intimate relationship between mitochondria and metabolism in the kidney has been previously recognised. In the present study, growing evidence of mitochondrial dysfunction and subsequent metabolic impairment in the chronically-damaged kidney has been presented, including reduced SOD2 expression and an increased redox ratio. Furthermore, 8-OHdG, which was used to assess oxidative damage, revealed predominant cytoplasmic localisation that is consistent with mitochondrial DNA damage (Tan *et al.*, 2013). Mitochondrial DNA is more susceptible than nuclear DNA to increased oxidative damage and mutations because of a lack of histone protection and limited capacity of DNA repair systems (Lum and Roebuck, 2001; Stadtman and Levine, 2003). This indicates oxidative stress-induced mutations to mitochondrial DNA could contribute to mitochondrial destabilisation in IR-induced chronic kidney damage, and thus increase impaired tubular metabolism. Of particular importance is the presence of remnant tubules within areas of focal fibrotic change in the kidney cortex, that display reduced mitochondrial function indicated by impaired TMRM uptake. This has important implications for mitochondrial-targeted therapies that rely on mitochondrial membrane potential differences to accumulate within mitochondria to exert beneficial effects. The current lipophilic triphenylphosphonium cation, MitoQ, is reliant on this process and this may explain the lack of effect in clinical trials of MitoQ as a disease modifying therapy for Parkinson's disease (Snow *et al.*, 2010). More so, the apparent structural normality of these tubules that remain in such damaged areas is at odds with their measured dysfunction in metabolism. Crosstalk between the atrophic tubules and these structurally-normal tubules may explain subsequent disease progression and this is worthy of future investigation. Mitochondrial dysfunction is a common driver of ROS generation (Che *et al.*, 2014), as well as causing a reduction in ATP-dependent processes. The stimulus for sustained mitochondrial dysfunction during chronic progression is most likely explained by chronic tubular hypoxia caused by peritubular capillary loss (Basile *et al.*, 2001). Persistent ROS generation, and cell cycle arrest and secretion of fibrogenic factors which has been recently demonstrated (Yang *et al.*, 2010; Canaud and Bonventre, 2014), may contribute to stimulating focal progressive and chronic change to decrease kidney function. An

alternative explanation may be that terminally-differentiated PTE can re-express apparent stem-cell markers during injury-induced de-differentiation and repair, to repopulate epithelial cells following AKI (Kusaba *et al.*, 2014). Remnant tubules may represent these sub-populations of cells.

In summary, our study presents data that suggest metabolic dysfunction of tubular epithelial cells, resulting from AKI, at least in part underlies the progression of CKD. The antioxidant NAC did not reduce oxidative damage and significantly altered the cellular redox environment to promote metabolic and mitochondrial dysfunction. The results of this study do not support the use on long-term general antioxidant therapy, such as with NAC, in chronic kidney pathologies. We believe that NAC saturates vital ROS-dependent intracellular signalling networks, thereby preventing conserved cytoprotective responses. The results do, however, present mitochondrial preservation, and a reduction of excess mitochondrial-derived ROS, as therapeutic targets. The contribution of oxidative stress to AKI and future CKD is an important process within the cellular milieu of the kidney, which requires specific and target therapies rather than a general approach.

CHAPTER 7

Oxidative Stress Biomarkers in Chronic Kidney Disease

Chapters 3-6 have investigated the role of oxidative stress in cell culture and animal models. However, oxidative stress is also being given consideration as a cause of disease progression in CKD patients. Chapter 7 examines biomarkers of oxidative stress in stage 3-4 CKD patients to understand the relationship of these factors on the progression of the disease.

7.1 INTRODUCTION

Systemic biomarkers of oxidative stress have been associated with the progression of CKD (Witko-Sarsat *et al.*, 1996; Dounousi *et al.*, 2006; Karamouzis *et al.*, 2008; Kuchta *et al.*, 2011). Furthermore, biomarkers of oxidative stress have been shown to decrease following renal intervention therapies, such as kidney transplantation (Simmons *et al.*, 2005; Vostalova *et al.*, 2012). However, as is demonstrated in numerous chronic disease patient clinical trials, not necessarily in CKD, reducing oxidative stress through dietary antioxidant compounds has yielded little benefit to disease progression (Bjelakovic *et al.*, 2012; Jun *et al.*, 2012). The complexity and heterogeneity of a typical CKD patient population, with associated co-morbidities and poor lifestyle habits, highlights the importance of identifying and characterising alterations to the systemic redox environment during CKD, to employ appropriate therapies to target oxidative stress in this population.

CVD is the leading cause of morbidity and mortality in the CKD population, with patients more likely to die from CVD than progress to ESKD (Go *et al.*, 2004). Oxidative stress has been implicated as common modulator linking CKD and CVD (Cachofeiro *et al.*, 2008; Rubattu *et al.*, 2013). This association and increased risk is compounded by common co-morbidities of CKD and lifestyle diseases, including obesity, Type 2 diabetes and hypertension (Jha *et al.*, 2013). Conventional pharmacological strategies targeting CVD and co-morbidities are only partially effective in reducing the progression of CKD (Brenner *et al.*, 2001; Lewis *et al.*, 2001). The variety of contributing factors to CVD risk within CKD suggests a comprehensive strategy to modify disease progression. This was demonstrated in a recent comprehensive trial targeting modifiable CVD and lifestyle risk factors in moderate (stage 3 and 4) CKD patients through exercise training and lifestyle intervention, which resulted in significant improvements in cardiorespiratory fitness, body composition and diastolic function (Howden *et al.*, 2013). Improvements in cardiovascular function are attributed to systemic adaptation of physical exercise. However, the influence of physical exercise on metabolism and systemic redox homeostasis has been suggested to underlie the proven benefits on health and the burden of disease (Radak *et al.*, 2008; Radak *et al.*, 2013).

Systemic adaptations to regular physical exercise include decreased ROS production (Radak *et al.*, 2004) and increased activity of antioxidant enzymes (Alessio and Goldfarb, 1988; Radak *et al.*, 2001), which favour a reduction in oxidative stress. Mitochondrial biogenesis is a consistent adaptation to regular physical exercise that plays a central role in correcting redox homeostasis (Marton *et al.*, 2014). Initial increases in ROS as a result of physical exercise have been demonstrated to promote cellular adaptations to exercise via vital ROS-dependent intracellular signalling promoting cytoprotection (Gounder *et al.*, 2012; Muthusamy *et al.*, 2012). This ability of the body to adapt to challenges of physical stress demonstrates a highly conserved physiological adaptation to promote health over time. Harnessing these adaptations in the CKD population is a promising mechanism to what already is a disrupted metabolic environment.

Measuring a dynamic process such as oxidative stress is difficult, and primarily relies on the quantification of specific end-products from free radical damage. F_2-isoporstanes (IsoP) are considered stable and one of the better available measures (Tucker *et al.*, 2013). IsoPs are end-products of non-enzymatic peroxidation of arachidonyl lipids and have been studied extensively in the relationship between oxidative stress and CKD (Roberts and Morrow, 2002; Dounousi *et al.*, 2006; Karamouzis *et al.*, 2008). A change in endogenous antioxidant levels can influence the overall development of oxidative damage and should, therefore, be considered in assessments of systemic oxidative stress (Calderon-Salinas *et al.*, 2011; Sedighi *et al.*, 2014). Identifying site specific changes in ROS generation *in vivo* is difficult to assess, however, considering that oxidative stress likely influences overall disease progress, systemic markers need to be considered.

The primary aim of this study was to investigate the effect of exercise training and lifestyle intervention on systemic biomarkers of oxidative stress in stage 3-4 CKD patients, over a 12-month period. The secondary aim was to determine any association between oxidative stress biomarkers and changes in clinical parameters.

7.2 MATERIALS AND METHODS

Many people were involved in many aspects of this study. These include Dr Erin Howden and Kassia Weston from the Centre for Research Excellence, Physical Activity and Health, The University of Queensland; and the renal research and data management team at the Nephrology Department, Princess Alexandra Hospital, Brisbane Australia. Dr Anne Bernard from QFAB provided statistical support. A/Prof Nicole Isbel is the LANDMARK III-trial leader.

7.2.1 Study design

This study was a sub-study of an ongoing open-label randomised controlled trial, known as the LANDMARK-III trial (Longitudinal Assessment of Numerous Discrete Modifications of the Atherosclerotic Risk Factors in Kidney Disease). LANDMARK-III is a 3-year study comparing the effect of a nurse practitioner-led model of care with standard nephrologic care on cardiovascular risk factors. Patients were screened at the Princess Alexandra Hospital Nephrology Department.

7.2.2 Participants

The study received approval from the Princess Alexandra Human Research Ethics Committee (HREC 2007/190) and University of Queensland Medical Research Ethics Committee (MREC 2008000184), and was registered at www.anzctr.org.au (Registration Number ANZCTR 12608000337370). Patients were eligible for inclusion if they were aged 18-75 years, had moderate CKD (stages 3 and 4; estimated GFR [eGFR] 25-60 ml/min per 1.73 m^2), and had one or more uncontrolled yet modifiable cardiovascular risk factors that were: blood pressure (BP) exceeding target (>130/80 mmHg, or >120/75 mmHg for those with diabetes or proteinuria > 1 g/ 24 h); overweight (body mass index [BMI] >25 kg/m^2); poor diabetic control (haemoglobin A1c [HbA1c] >7%); or hyperlipidaemia (low-density lipoprotein [LDL-C] <2.5 or <2.0 mmol/L in those with diabetes or existing coronary heart disease). Exclusion criteria were: intervention for, or symptomatic, coronary artery disease (within 3 months); current heart failure (according to New York Heart Association class III and IV) or significant valvular heart disease; pregnant or planning to become pregnant; previous kidney transplant; and life expectancy or anticipated time to dialysis or transplant <6 months. Participants provided written informed consent and the study complied with the Declaration of Helsinki.

7.2.3 Outcomes

The primary outcomes of this sub-study were change in (Δ) systemic oxidative stress over 12 months, as measured by (IsoP, GPX and TAC). Secondary outcome was Δ kidney function over 12 months, as measured by eGFR.

7.2.4 Patient groups

7.2.4.1 Control group

The control group received standard nephrology care, which included review by a nephrologist, recommended lifestyle modification but no specific information or education, and referral to an allied health professional on an *ad hoc* basis.

7.2.4.2 Exercise training and lifestyle modification group

In addition to standard nephrologic care, cardiovascular risk factor management was provided by a multidisciplinary clinic, including a CKD nurse practitioner, dietician, exercise physiologist, diabetic educator, psychologist, and social worker to target risk factors to national guidelines (Johnson, 2007; NHF, 2010). The exercise-training component involved 150 min of moderate intensity exercise per week, with 8 weeks of training supervised by an accredited clinical exercise physiologist. Patients attended gym sessions two to three times per week. The sessions included a warm-up, 20-30 min of aerobic activity using a treadmill, stationary bike, or rowing ergometer, and whole body resistance training with machines and free weights. On completion of the gym-based training, patients began a home-based program and were provided a booklet depicting resistance exercise using Thera-Bands and a Swiss ball. Regular contact was maintained via telephone and email. Participants were questioned on their ability to maintain the prescribed exercise and, if they identified difficulty, they were encouraged to attend gym-based refresher visits. Patients performed exercise at a moderate intensity, with perceived exertion of 11-13 on a 20-point Borg scale (Borg, 1982), and which was tailored individually. Patients also underwent 4 weeks of group behaviour and lifestyle modification facilitated by a dietician and psychologist. The program focused on sustainable diet and behaviour change to assist with weight loss. The dietician therapy complied with the Evidence-Based Practice Guidelines for Nutritional Management of CKD for patients with eGFR between 25 and 60 ml/min per 1.73 m^2 (Ash *et al.*, 2006).

7.2.5 Outcome measures

7.2.5.1 Oxidative stress biomarkers

Full details of oxidative stress assays are described in Chapter 2 Sections 2.7.5-7. Briefly, IsoP was determined via negative chemical ionization gas chromatography-tandem mass spectroscopy from plasma (Briskey *et al.*, 2014). GPX was measured via a spectrophotometric assay based on the oxidation of NADPH to NADP+. TAC was measured via a spectrophotometric assay based on the inhibition of the absorbance of the radical cation $ABTS^{+}$.

7.2.5.2 Laboratory assessment

Venous blood and spot urine samples were collected from all patients following an overnight fast. Kidney function was determined as the eGFR using the Modified Diet in Renal Disease formula based on the isotype dilution mass spectroscopy standardized creatinine assay ($MDRD_{175}$) (Levey *et al.*, 1999). Blood urea, haemoglobin (Hb), HbA1c, homeostasis model assessment (HOMA), high density lipoprotein (HDL), low density lipoprotein (LDL), cholesterol and triglycerides were measured using standard automated laboratory techniques by Queensland Health Pathology.

Demographic data relating to co-morbidities and medication use was collected from patient histories.

7.2.6 Statistical analysis

Data were checked for normality using the Shapiro-Wilk test. Data that were not normally distributed were log transformed (as an expression of the natural logarithm Log_e.). Data that remained non-normally distributed after log transformation underwent non-parametric statistical tests to prevent assumptions of normality. Results are expressed as mean ± SD for normally distributed data, median (interquartile range) for non-normally distributed data, or total number (*n*) percentage (%) for categorical data. Baseline characteristics and change scores over 12-months (Δ 12-mo) were compared between groups using independent *t*-tests for normally distributed data, and Mann-Whitney U tests for non-normally distributed data. The full set of patient samples was separated into different batches to be assayed (for IsoP, GPX and TAC) on different days. Therefore a possible batch effect was tested using a one-way analysis of variance (ANOVA) comparing the differences between means of different batches. To investigate the effect of exercise training and lifestyle intervention on IsoP, GPX and TAC in stage 3-4 CKD patients, a linear mixed model was performed to test the main effect of patient group (standard care or lifestyle intervention), time (baseline or 12-mo), and the interaction between them. Patient group, time point, and their interaction were defined as fixed-effects for the model, whilst patient identification number was defined as a random effect to account for repeated measures. Batch number was defined as a random effect to adjust for a possible batch effect. Pearson's product-moment correlations and spearman's correlations were performed between changes in oxidative stress measures and other secondary measures. Data were analysed using standard commercially available statistical software (SPSS version 22, Chicago, IL). Statistical significance was defined as $p \leq 0.05$.

7.3 RESULTS

7.3.1 Patient characteristics

The effects of the exercise and lifestyle intervention on health and fitness outcomes have been previously reported (Howden *et al.*, 2013), with an 11 % improvement in maximal oxygen consumption (VO_2 max), 20 % improvement in diastolic tissue velocity (e'), and decreased body mass index (BMI). The baseline characteristics of this patient group are summarised in Table 7.1 and there were no significant group differences at baseline. Men comprised the majority of each group and mean BMI of each patient group was within the obese range. The prevalence of co-

morbidities was high with 96 % and 69 % of patients having hypertension or hyperlipidaemia, respectively. All patients were taking at least one medication.

7.3.2 Changes in oxidative stress biomarkers

Table 7.2 presents the results of Shapiro-Wilk tests for normal distribution on oxidative stress biomarkers (IsoP, GPX and TAC) and eGFR after log transformation. All data were log transformed prior to Shapiro-Wilk tests for normality. All data were normally distributed except for baseline eGFR ($p=0.033$), Δ12-mo eGFR ($p<0.0001$), and GPX Δ12-mo ($p=0.014$).

There was no statistically significant difference ($p>0.05$; independent samples t-test) between patient groups at baseline for each of the oxidative stress biomarkers (IsoP, GPX and TAC). There was a noticeable large range of variation in oxidative stress biomarkers which is indicated in the reported SD values. A significant batch effect was identified using a one-way analysis of variance (ANOVA) on batch data for IsoP ($p<0.01$) and GPX ($p<0.0005$), and a Kuskal-Wallis Test for TAC ($p<0.0005$). Batch means were also found to follow the trend of the quality control sample measures at the time of each batch. Therefore, the batches were taken into account as random effects in the linear mixed model to adjust the results for this effect

Table 7.1: Baseline Demographics		
	Standard Care (n=64)	Lifestyle Intervention (n=72)
Women	30 (40)	29 (41)
Age (yr)	58.8±11.9	61.1±9.3
Height (cm)	168.6±9.9	168.6±8.9
Weight (kg)	94±20	95.8±22.7
BMI (kg/m^2)	33±6	33.6±7.1
Clinical Markers		
eGFR (ml/min per 1.73 m^2)	38.8±8.5	40.6±8.9
Urea (mmol/L)	11.1±3.9	10.3±3.9
Hb (g/L)	131.7±16.4	132.1±13.8
HbA1c (%)	6.3±1.5	6.6±1.4
HOMA	9.9±21.9	9.3±14.1
HDL (mmol/L)	1.2±0.6	1.1±0.3
LDL (mmol/L)	2.6±0.8	2.3±0.9
Cholesterol (mmol/L)	4.4±0.9	4.5±1.2
Triglycerides (mmol/L)	1.6±0.9	2.2±2
Risk Factors		
Diabetes	32 (43)	28 (40)
Hyperlipidaemia	47 (63)	47 (67)
Myocardial Infarction	11 (15)	14 (20)
Heart Failure	3 (4)	2 (3)
Peripheral vascular disease	17 (23)	8 (11)
Hypertension	70 (95)	61 (87)
Stent	9 (12)	8 (11)
Coronary artery bypass graft	7 (9)	5 (7)
Medications		
ACEi	34 (45)	35 (50)
β-Blocker	23 (31)	31 (44)
Thiazide	13 (17)	16 (23)
Statin	47 (63)	42 (60)
Insulin	15 (20)	16 (23)
Allopurinol	9 (12)	13 (19)

Values are mean ± SD, or number (%) for categorical variables. Abbreviations: BMI, body mass index; eGFR, estimated glomerular filtration rate; HbA1c, Haemoglobin A1c; HOMA, homeostatic model assessment; Hb, Haemoglobin; HDL, high density lipoprotein; LDL, low density lipoprotein.

Table 7.2: Normal or non-normal distribution of baseline and change in oxidative stress biomarkers

	Standard Care Group		Lifestyle Intervention Group	
	Baseline	Δ12-month	Baseline	Δ12-month
IsoP	0.659	0.185	0.337	0.084
GPX	0.351	0.348	0.055	0.014*
TAC	0.958	0.487	0.395	0.686
eGFR	0.033*	0.257	0.281	<0.0001*

* p value from Shapiro-Wilk test of normality distribution. $p < 0.05$ rejects the null hypothesis of normal distribution

There was no statistically significant difference in mean IsoP Δ 12-mo (p=0.88) between patients undergoing standard care (35.2±117.8 pg/mL) and patients undergoing the lifestyle intervention (26.9±146.6 pg/mL) demonstrated in Figure 7.1A and Table 7.3. A linear mixed model found no interaction between patient group and time on IsoP levels (Table 7.4; p=0.893). Patients identified as having high IsoP at baseline (defined as > 250 pg/mL at baseline) had a mean decrease in IsoP following standard care (-38.1±81.6 pg/mL), and this was more pronounced in patients undergoing lifestyle intervention (-106.2±157.8 pg/mL). However, differences in mean Δ 12-mo IsoP between groups in patients with high IsoP was not statistically significant (p=0.064). The observed power of this relationship was 16 %. This is demonstrated in Figures 7.1B and C, and Table 7.3.

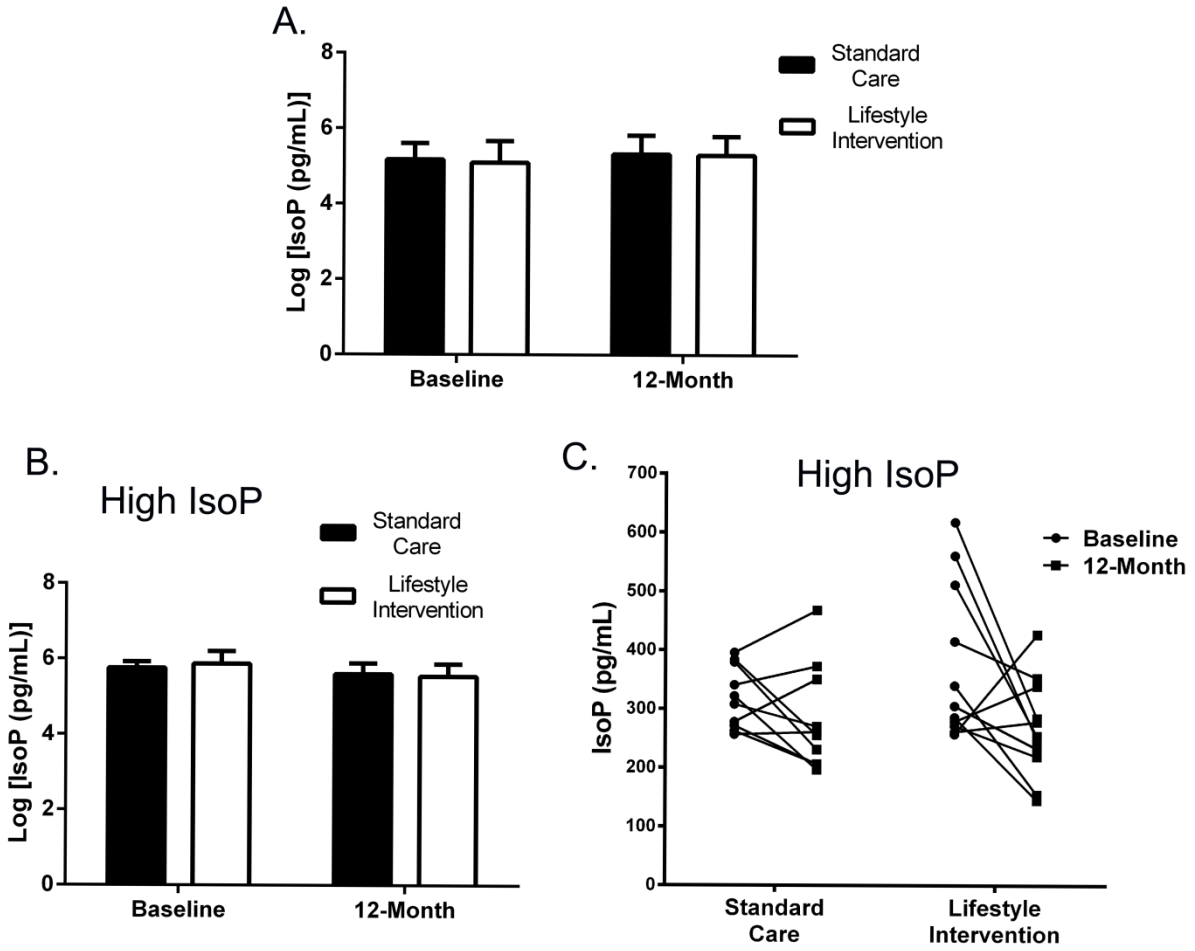

Figure 7.1: Changes in plasma isoprostanes over 12-months following exercise and lifestyle intervention

Values are mean ± SD of normally distributed data following log transformation – Log [IsoP (pg/mL)]. All CKD patient IsoP measures at baseline and over 12-months (A.) and CKD patient subgroups that had high (> 250 pg/mL) IsoP at baseline demonstrating no significant differences (B.). Repeated measures comparison demonstrates individual subject changes in IsoP over 12-months in patients receiving standard care or undergoing a lifestyle intervention (C.).

Table 7.3: Baseline and changes in plasma isoprostanes measures

	Standard Care Group		Lifestyle Intervention Group		p value*
	Baseline	Δ 12-month	Baseline	Δ 12-month	
IsoP (pg/mL)	192.0±80.3	35.2±117.8	187.0±115.4	26.9±146.6	0.88
High IsoP (pg/mL)	319.8±53.1	-38.1±81.6	373.3±132.1	-106.2±157.8	0.064

Values are mean ± SD for plasma isoprostanes (IsoP) measurements (pg/mL). Patients identified with >250 pg/mL IsoP at baseline have been allocated a subgroup (High Iso). *p value indicates parametric unpaired t-test performed on Δ 12-month log transformed IsoP data.

Table 7.4: Linear mixed model testing the effect of time and patient group of plasma isoprostanes

	F	df1	df2	p value
Corrected Model	0.696	3	226	0.555
Time-Point (Baseline and 12-month)	1.476	1	226	0.226
Patient Group (Standard care and lifestyle intervention)	0.525	1	226	0.469
Interaction (between time-point and patient group)	0.018	1	226	0.893

Linear mixed model incorporated the time-point, patient group, and the interaction between time-point and patient group as the main effects on plasma IsoP. Subject trial number to account for repeated measures, and sample batch data to account for the known batch effect were incorporated as random effects into the model. F, *F*-statistic of *F* distribution; df1, degrees of freedom of effect; df2, degrees of freedom of error; p Value, significant effect at ≤ 0.05. Linear mixed model was performed on log transformed IsoP data

There was no statistically significant difference in mean GPX Δ 12-mo (p=0.87) between patients undergoing standard care (5.0±4.1 U/L) and patients undergoing the lifestyle intervention (5.3±6.0 U/L), as demonstrated in Figure 7.2A and Table 7.5. Table 7.6 demonstrates the results of the linear-mixed model performed on the data. The main effect of time (12 months) was a significant effect on GPX activity in patients, regardless of whether they were receiving standard care or lifestyle intervention (95% CI, -0.3 to -0.1, t(-6.1)=-0.2, p<0.0001; Fig 7.2B). Yet there is no statistically significant interaction between patient group and time on GPX levels (p=0.787).

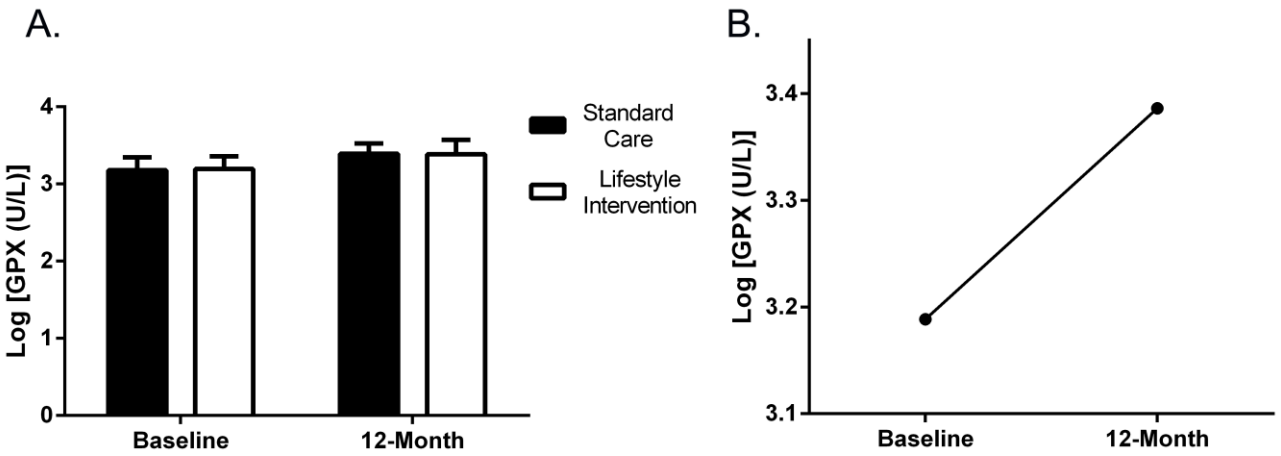

Figure 7.2: Changes in plasma glutathione peroxidase activity over 12-months following exercise and lifestyle intervention

Values are mean ± SD following log transformation – Log [GPX (U/L)] (A.). The main effect of time was a significant interaction on GPX activity which is identified in Table 7.5.

Table 7.5: Baseline and changes in plasma glutathione peroxidase activity

	Standard Care Group		Lifestyle Intervention Group		p value*
	Baseline	Δ 12-month	Baseline	Δ 12-month	
GPX (U/L)	24.3±4	5.0±4.1	24.7±4.3	5.3±6.0	0.87

Values are mean ± SD for plasma glutathione peroxidase (GPX) activity (U/L). *p value indicates non-parametric Mann-Whitney U Test performed on Δ 12-month log transformed GPX data.

Table 7.6: Linear mixed model testing effect of time and patient group on plasma glutathione peroxidase activity

	F	df1	df2	p value
Corrected Model	17.8	3	220	<0.0001*
Time-Point (Baseline and 12-month)	52.9	1	220	<0.0001*
Patient Group (Standard care and lifestyle intervention)	0.173	1	220	0.678
Interaction (between time-point and patient group)	0.073	1	220	0.787

				95% confidence interval		
	Coefficient	**Std. E**	**t**	**Lower**	**Upper**	**p value**
Intercept	3.383	0.028	122.521	3.33	3.438	<0.0001*
Time-Point	-0.202	0.033	-6.069	-0.268	-0.137	<0.0001*
Patient Group	0.005	0.032	0.167	-0.057	0.068	0.867
Interaction	0.010	0.037	0.271	-0.063	0.083	0.787

Linear mixed model incorporated the time-point, patient group, and the interaction between time-point and patient group as the main effects on plasma GPX. Subject trial number to account for repeated measures, and sample batch data to account for the known batch effect were incorporated as random effects into the model. F, *F*-statistic of *F* distribution; df1, degrees of freedom of effect; df2, degrees of freedom of error; t, *t*-statistic; p Value, significant effect at ≤ 0.05. Linear mixed model performed on log transformed GPX data.

There was no statistically significant difference in mean TAC Δ 12-mo (p=0.56) between patients undergoing standard care (-0.03±0.1 mmol/L) and patients undergoing the lifestyle intervention (-0.05±0.2 mmol/L), as demonstrated in Figure 7.3 and Table 7.7. A linear mixed model found no interaction between patient group and time on TAC levels (Table 7.8; p=0.926).

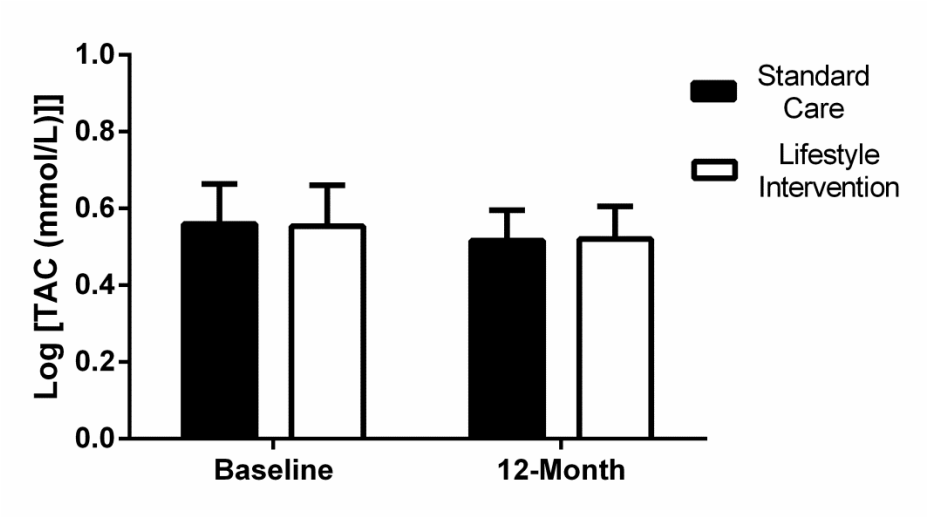

Figure 7.3: Changes in plasma total antioxidant capacity over 12-months following exercise and lifestyle intervention

Values are mean ± SD of normally distributed data following log transformation – Log [TAC (mmol/L)].

Table 7.7: Baseline and changes in plasma total antioxidant capacity measures

	Standard Care Group		Lifestyle Intervention Group		p value*
	Baseline	Δ 12-month	Baseline	Δ 12-month	
TAC (mmol/L)	1.8±0.2	-0.03±0.1	1.7±0.2	-0.05±0.2	0.56

Values are mean ± SD for plasma total antioxidant capacity (TAC) measurements (mmol/L). *p value indicates parametric unpaired t-test performed on Δ 12-month log transformed TAC data.

Table 7.8: Linear mixed model testing effect of time and patient group of plasma total antioxidant activity

	F	df1	df2	p value
Corrected Model	1.155	3	221	0.328
Time-Point (Baseline and 12-month)	3.300	1	221	0.071
Patient Group (Standard care and lifestyle intervention)	0.145	1	221	0.703
Interaction (between time-point and patient group)	0.009	1	221	0.926

Linear mixed model incorporated the time-point, patient group, and the interaction between time-point and patient group as the main effects on plasma TAC. Subject trial number to account for repeated measures, and sample batch data to account for the known batch effect were incorporated as random effects into the model. F, *F*-statistic of *F* distribution; df1, degrees of freedom of effect; df2, degrees of freedom of error; p Value, significant effect at ≤ 0.05. Linear mixed model performed on log transformed TAC data

Figure 7.4 and Table 7.9 demonstrate that there was no statistically significant difference in mean eGFR Δ 12-mo (p=0.33) between patients undergoing standard care (-0.2±7.8 mL/min/1.73m^2) and patients undergoing the lifestyle intervention (-1.6±6.7 mL/min/1.73m^2).

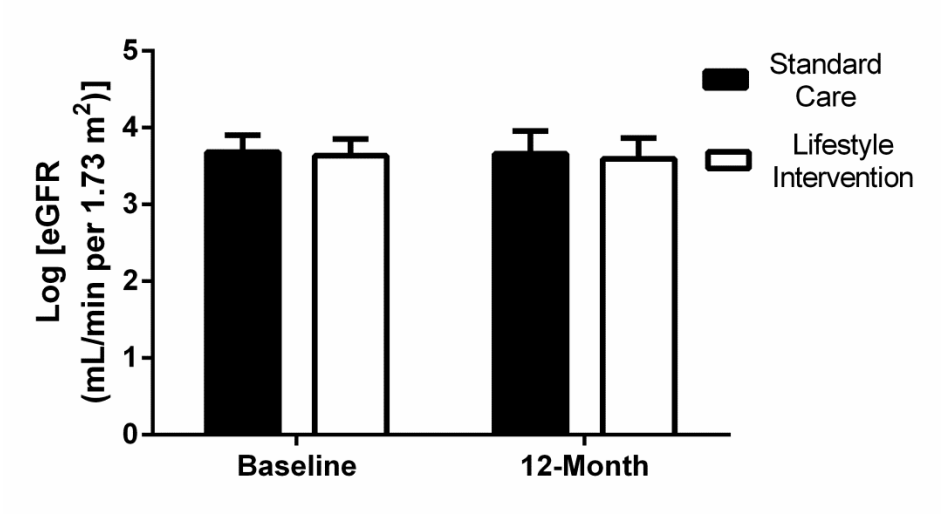

Figure 7.4: Changes in estimated glomerular filtration rate over 12-months following exercise and lifestyle intervention

Values are mean ± SD of data following log transformation – Log [eGFR (mL/min per 1.73 m^2)]

Table 7.9: Baseline and changes in estimated glomerular filtration rate

	Standard Care Group		Lifestyle Intervention Group		p value*
	Baseline	Δ 12-month	Baseline	Δ 12-month	
eGFR (mL/min/1.73m^2)	40.6±8.9	-0.2±7.8	38.8±8.5	-1.6±6.7	0.33

Values are mean ± SD for plasma estimated glomerular filtration rate (mL/min/1.73 m^2). *p value indicates non-parametric Mann-Whitney U Test performed on Δ 12-month log transformed eGFR data.

7.3.3 Clinical correlations to changes in oxidative stress biomarkers

Table 7.10 outlines clinical parameters that were associated with oxidative stress biomarkers regardless of patient allocation at baseline. There was a small positive correlation between IsoP and BMI (r_s=0.209, p=0.020), HDL (r_s=0.274, p=0.002), total cholesterol (r_s=0.333, p<0.001), and total triglycerides (r_s=0.272, p=0.002) at baseline. There was a small negative correlation between IsoP and Hb (r_s=-0.176, 0.048). There was a small positive correlation between GPX and eGFR (r_s=0.235, p=0.008), HbA1c (r_s=0.190, p=0.035), and HDL (r_s=0.193, p=0.033) at baseline. There was a small negative correlation between TAC and eGFR (r_s=-0.192, p=0.030) and a small positive correlation between TAC and Hb (r_s=0.220, p=0.012) at baseline.

Table 7.11 outlines clinical parameters that were associated with oxidative stress biomarkers at baseline in standard care and lifestyle intervention patient groups. There was a moderate positive correlation between IsoP and total cholesterol (r_s=0.434, p<0.001), IsoP and total triglycerides (r_s=0.344, p=0.008), and a small positive correlation between GPX and HbA1c (r_s=0.292, p=0.023) at baseline in the standard care group. In the lifestyle intervention group there was a small positive correlation between TAC and BMI (r_s=0.253, p=0.042), TAC and weight (r_s=0.261, p=0.036), and IsoP and HDL (r_s=0.373, p=0.003) at baseline.

Table 7.12 outlines changes in clinical parameters that were associated with changes in oxidative stress biomarkers in standard care and lifestyle intervention groups. There was a moderate positive correlation between change in IsoP and change in HDL (r_s=0.317, p=0.044), and a moderate negative correlation between change in TAC and change in total triglycerides (r_s=-0.305, p=0.039) over 12-months in the standard care group. In the lifestyle intervention group there was a small negative correlation between change in TAC and change in eGFR (r_s=-0.291, p=0.042) over 12-months.

Table 7.13 demonstrates selected categorical patient characteristics, co-morbidities and medications that were associated to changes in oxidative stress biomarkers in standard care and lifestyle intervention groups. Patients with hypertension receiving standard care had a statistically significant greater increase in GPX over 12-months, compared to patients without hypertension receiving standard care (5.3±3.8 U/L and 0.8±5.4 U/L respectively; p=0.011). Females had a statistically significant greater increase in GPX over 12-months compared to males (6.9±5.9 U/L and 4.3±6.0 U/L respectively; p=0.029) in the lifestyle intervention. Patients in the lifestyle intervention who did not have hypertension had a statistically significant greater increase in GPX over 12-months, compared to patients who had hypertension (11.4±5.3 U/L and 4.9±5.9 U/L, respectively; p=0.032). Patients taking a thiazide diuretic had a statistically significant greater increase in GPX over 12-months compared to patients who were not on such medication within the standard care group (7.1±3.9 U/L and 4.1±3.9 U/L, respectively; p=0.025) and in the lifestyle intervention group (8.1±5.4 U/L and 4.4±6.06 U/L, respectively; p=0.039). Patients on insulin therapy had a more pronounced decrease in TAC over 12-months compared to patients not on insulin therapy (-0.2±0.2 mmol/L and -0.01±0.2 mmol/L, respectively; p=0.018) within the intervention group. There was no significant influence of peripheral vascular disease, or allopurinol or ACEi medication use, on changes in biomarkers of oxidative stress over 12-months in patients receiving standard care or undergoing lifestyle modification.

Table 7.10: Correlation analysis between clinical parameters and oxidative stress biomarkers at baseline in all patients

Baseline	Baseline					
	IsoP (pg/mL)		GPX (U/L)		TAC (mmol/L)	
	r_s	p	r_s	p	r_s	p
Kidney Function						
eGFR (ml/min/1.73m^2)	-0.007	0.942	0.235**	0.008	-0.192*	0.030
Urea (mmol/L)	0.046	0.611	0.065	0.467	0.060	0.503
Body Parameters						
BMI (kg/m^2)	0.209*	0.020	-0.147	0.106	0.064	0.479
Weight (kg)	0.095	0.295	-0.135	0.136	0.101	0.260
Glycaemic Control						
HbA1c (%)	0.034	0.707	0.190*	0.035	-0.049	0.589
HOMA (mmol/L)	0.136	0.134	0.033	0.719	0.109	0.226
Blood Profile						
Hb (g/L)	-0.176*	0.048	-0.043	0.636	0.220*	0.012
HDL (mmol/L)	0.274**	0.002	0.193*	0.033	0.067	0.456
LDL (mmol/L)	0.129	0.168	0.094	0.318	0.054	0.564
Cholesterol (mmol/L)	0.333**	<0.001	0.092	0.311	-0.026	0.775
Triglycerides(mmol/L)	0.272**	0.002	-0.148	0.101	0.053	0.556

Spearman's correlation was performed on continuous clinical parameters and oxidative stress biomarkers to obtain a coefficient (r_s) and *p* value of the relationship. * p<0.05; **p<0.01. Shaded boxes indicate Pearson's correlation that was performed to confirm significant relationship on normally distributed data. All analysis was performed on log transformation data. Abbreviations: IsoP, isoprostanes; GPX, glutathione peroxidase; TAC, total antioxidant capacity eGFR, estimated glomerular filtration rate; BMI, body mass index; HbA1c, Haemoglobin A1c; HOMA, homeostatic model assessment; Hb, Haemoglobin; HDL, high density lipoprotein; LDL, low density lipoprotein.

Table 7.11: Correlation analysis between clinical parameters and oxidative stress biomarkers at baseline in patients randomised to standard care or lifestyle intervention.

	Standard Care (Baseline)						Lifestyle Intervention (Baseline)					
	IsoP (pg/mL)		GPX (U/L)		TAC (mmol/L)		IsoP (pg/mL)		GPX (U/L)		TAC (mmol/L)	
Baseline	r_s	p	r_s	p	r_s	p	r_s	p	r_s	p	r_s	p
Kidney Function												
eGFR (ml/min/1.73m^2)	0.002	0.985	0.242	0.061	-0.178	0.166	-0.027	0.832	0.242	0.052	-0.202	0.104
Urea (mmol/L)	0.100	0.444	0.112	0.391	0.119	0.357	0.040	0.751	0.024	0.847	-0.014	0.913
Body Parameters												
BMI (kg/m^2)	0.195	0.139	-0.136	0.303	-0.141	0.284	0.241	0.055	-0.149	0.241	0.253	0.042*
Weight (kg)	0.123	0.353	-0.149	0.261	-0.064	0.627	0.066	0.606	-0.125	0.325	0.261	0.036*
Glycaemic Control												
HbA1c (%)	0.056	0.671	0.292	0.023*	-0.050	0.702	0.006	0.964	0.091	0.478	-0.054	0.669
HOMA (mmol/L)	0.114	0.390	0.060	0.651	0.012	0.926	0.156	0.220	0.024	0.853	0.203	0.105
Blood Profile												
Hb (g/L)	-0.180	0.166	-0.195	0.133	0.211	0.100	-0.180	0.150	0.095	0.478	0.242	0.051
HDL (mmol/L)	0.179	0.184	0.239	0.070	0.006	0.926	0.373	0.003**	0.139	0.274	0.107	0.395
LDL (mmol/L)	0.214	0.132	0.160	0.263	-0.099	0.490	0.068	0.590	0.067	0.596	0.183	0.144
Cholesterol (mmol/L)	0.434	0.001**	0.014	0.915	-0.155	0.238	0.236	0.058	0.160	0.202	0.101	0.421
Triglycerides(mmol/L)	0.344	0.008**	-0.156	0.239	-0.119	0.364	0.207	0.097	-0.152	0.227	0.236	0.056

Spearman's correlation was performed on continuous clinical parameters and oxidative stress biomarkers to obtain a coefficient (r_s) and *p* value of the relationship. * p<0.05; **p<0.01. Shaded boxes indicate Pearson's correlation that was performed to confirm significant relationship on normally distributed data. All analysis was performed on log transformation data. Abbreviations: IsoP, isoprostanes; GPX, glutathione peroxidase; TAC, total antioxidant capacity eGFR, estimated glomerular filtration rate; BMI, body mass index; HbA1c, Haemoglobin A1c; HOMA, homeostatic model assessment; Hb, Haemoglobin; HDL, high density lipoprotein; LDL, low density lipoprotein.

Table 7.12: Correlation analysis between clinical parameters and oxidative stress biomarkers over 12-months in patients undergoing standard care or lifestyle intervention.

	Standard Care (Δ 12-Months)						Lifestyle Intervention (Δ 12-Months)					
	IsoP (pg/mL)		GPX (U/L)		TAC (mmol/L)		IsoP (pg/mL)		GPX (U/L)		TAC (mmol/L)	
Δ 12-Months	r_s	p	r_s	p	r_s	p	r_s	p	r_s	p	r_s	p
Kidney Function												
eGFR (ml/min/1.73m^2)	0.075	0.637	0.104	0.492	-0.001	0.994	0.257	0.088	0.081	0.586	-0.291	0.042*
Urea (mmol/L)	0.006	0.969	-0.074	0.623	0.133	0.374	-0.015	0.923	-0.104	0.481	0.275	0.055
Body Parameters												
BMI (kg/m^2)	0.110	0.489	0.076	0.613	-0.191	0.197	-0.046	0.764	-0.003	0.983	0.095	0.515
Weight (kg)	0.107	0.498	0.083	0.582	-0.184	0.217	-0.014	0.927	0.015	0.922	0.108	0.460
Glycaemic Control												
HbA1c (%)	0.192	0.229	0.192	0.205	0.003	0.983	0.071	0.651	0.029	0.847	-0.135	0.366
HOMA (mmol/L)	0.097	0.563	-0.157	0.322	0.218	0.161	-0.089	0.591	-0.052	0.727	0.114	0.440
Blood Profile												
Hb (g/L)	0.092	0.560	-0.116	0.444	0.170	0.253	0.083	0.586	-0.008	0.956	-0.105	0.478
HDL (mmol/L)	0.317	0.044*	0.269	0.074	-0.016	0.915	0.087	0.569	0.121	0.412	0.010	0.948
LDL (mmol/L)	-0.040	0.814	0.137	0.393	-0.046	0.774	0.082	0.591	0.111	0.459	-0.181	0.217
Cholesterol (mmol/L)	0.139	0.387	0.152	0.320	-0.122	0.420	-0.139	0.361	-0.146	0.323	0.147	0.312
Triglycerides(mmol/L)	0.293	0.063	0.002	0.991	-0.305	0.039*	0.077	0.616	-0.195	0.185	0.080	0.584

Spearman's correlation was performed on continuous clinical parameters and oxidative stress biomarkers to obtain a coefficient (r_s) and *p* value of the relationship. * denotes p<0.05. Shaded boxes indicate Pearson's correlation that was performed to confirm significant relationship on normally distributed data. All analysis was performed on log transformation data. Abbreviations: IsoP, isoprostanes; GPX, glutathione peroxidase; TAC, total antioxidant capacity eGFR, estimated glomerular filtration rate; BMI, body mass index; HbA1c, Haemoglobin A1c; HOMA, homeostatic model assessment; Hb, Haemoglobin; HDL, high density lipoprotein; LDL, low density lipoprotein.

Table 7.13: Influence of categorical patient characteristics on changes in oxidative stress biomarkers in patients undergoing standard care or lifestyle intervention

	Standard Care (Δ 12-Month)						Lifestyle Intervention (Δ 12-Month)					
	IsoP (pg/mL)		GPX (U/L)		TAC (mmol/L)		IsoP (pg/mL)		GPX (U/L)		TAC (mmol/L)	
	Mean	p	Mean	p	Mean	p	Mean	p	Mean	p	Mean	p
Gender												
Male	13.7±71.7	0.233	4.8±3.5	0.881	-0.02±0.1	0.506	22.9±151.9	0.196^	4.3±6.0	0.029	-0.02±0.2	0.128
Female	64.7±158.7		5.1±4.8		-0.05±0.2		32.8±141.9		6.9±5.9	*^	-0.10±0.2	
Diabetes												
Yes	26.3±123.8	0.215	6.4±3.2	0.044	-0.06±0.2	0.321	-9.33±143.5	0.059	4.5±6.5	0.511	-0.09±0.2	0.236
No	41.8±115.2	^	3.7±4.4		-0.01±0.1	^	55.6±145.0		6.1±.6	^	-0.02±0.2	
Hypertension												
Yes	34.0±116.3	0.482	5.3±3.8	0.011	-0.04±0.1	0.051	20.1±149.5	0.141	4.9±5.9	0.032	-0.07±0.2	0.092
No	47.6±151.7		0.8±5.4	*	0.1±0.01		108.2±74.2		11.4±5.3	*^	0.1±0.3	
PVD												
Yes	-29.0±57.6	0.069	3.9±3.0	0.471	-0.1±0.3	0.264	20.4±113.2	0.922	2.6±5.4	0.061	-0.1±0.2	0.378
No	45.1±121.9		5.1±4.3		-0.02±0.1		29.0±156.5		6.1±6.1	^	-0.04±0.21	
Allopurinol												
Yes	84.9±144.7	0.055	6.2±4.5	0.622	-0.03±0.2	0.940	117.5±233.3	0.091^	6.7±8.1	0.872	-0.1±0.2	0.194
No	21.1±107.1		4.6±4.0	^	-0.03±0.1		9.6±124.4		5.1±5.7	^	-0.03±0.2	
ACEi												
Yes	20.4±125.8	0.085	5.05±3.4	0.774	-0.03±0.2	0.972	5.0±182.1	0.263^	5.3±4.6	0.487	-0.04±0.2	0.715
No	53.7±107.1		4.8±5.1		-0.03±0.1		48.8±106.8		5.4±7.3		-0.06±0.2	
Thiazide												
Yes	16.9±105.4	0.809	7.1±3.9	0.025	-0.04±0.1	0.776	30.6±99.8	0.583	8.1±5.4	0.039	-0.1±0.2	0.345
No	42.7±123.3		4.1±3.9	*^	-0.03±0.1		25.7±163.1		4.4±6.06	*^	-0.03±0.2	
Insulin												
Yes	57.4±143.3	0.655	7.2±3.9	0.102	-0.1±0.2	0.261	-17.7±150.4	0.487	5.6±7.9	0.895	-0.2±0.2	0.018
No	28.9±111.1		4.2±4.0		-0.01±0.1		39. 4±148.6		5.3±5.5		-0.01±0.2	*

Mean or median oxidative stress Δ 12-month values between each patient characteristic (categorical) were compared by a unpaired t-test for normally distributed data or a Mann-Whitney U test for non-normally distributed data denoted by (^). * denotes $p < 0.05$ and is highlighted by shaded boxes. All tests were performed on log transformed data. Abbreviations: IsoP, isoprostanes; GPX, glutathione peroxidase; TAC, total antioxidant capacity; PVD, peripheral vascular disease; ACEi, angiotensin converting enzyme inhibitor.

7.4 DISCUSSION

The influence of metabolism and systemic redox homeostasis may underlie the proven benefits of physical exercise and lifestyle modification in general health and the burden of disease. This study sought to understand the role of exercise and lifestyle modification on systemic biomarkers of oxidative stress in the progression of moderate CKD. Improvements in cardiorespiratory fitness, body composition, and diastolic function of exercise and lifestyle intervention have been previously demonstrated within a smaller cohort of these patients (Howden *et al.*, 2013). We demonstrated that changes in systemic biomarkers of oxidative stress over 12-months in stage 3-4 CKD patients undergoing an exercise and lifestyle intervention were not different from patients receiving standard nephrology care. Secondly, changes in systemic biomarkers of oxidative stress were highly variable and associated with many clinical parameters within these moderate CKD patients.

Previous studies have demonstrated changes in systemic oxidative stress biomarkers in response to exercise and lifestyle intervention despite disease (Alessio and Goldfarb, 1988; Radak *et al.*, 2001). However, the majority of studies investigating exercise and lifestyle interventions within chronic disease populations commonly report improvements in functional parameters of disease, yet rarely report changes to oxidative stress biomarkers or mechanisms underlying the benefit (Wang *et al.*, 2013). In the haemodialysis CKD population, 4 months of intradialytic exercise training reduced plasma TBARS that was associated with a reduction in epicardial fat thickness (Wilund *et al.*, 2010). Chronic heart failure patients undergoing 6-month exercise therapy have been shown to increase skeletal muscle GPX and CAT while reducing lipid peroxidation (Linke *et al.*, 2005), whereas coronary artery disease patients, who demonstrate improved endothelial dysfunction, do so independent of changes in oxidative stress markers (Luk *et al.*, 2012). This variability of oxidative stress responses to different types of exercise, for different periods of time, and within different disease populations, highlights the complexities of adaptations to exercise. We would expect to observe significant differences in oxidative stress biomarkers, especially in the patient group randomised to the intervention, considering the noted impact exercise can have on the systemic redox environment. Failure to do so could indicate a resistance to exercise-induced redox adaptations within a uraemic CKD state, or alternately, the beneficial physical adaptations to exercise do not involve changes in oxidative stress in the CKD population. The latter is unlikely considering that patients, identified as having high systemic oxidative stress (> 250 pg/mL IsoP) at baseline, appeared to have an enhanced reduction in IsoP following 12-month of exercise and lifestyle intervention compared to patients receiving standard care. However, the power of this comparison is 16 %, indicating that there is an 84 % chance that this is a type 2 statistical error. A

sample size of 250 patients is necessary to achieve power of 95 % of this comparison to confirm a relationship. This finding suggests patients with high IsoPs may benefit from therapies aimed at reducing oxidative stress. A similar concept exists for vitamin D therapy, whereby vitamin D-deficient CKD patients were more responsive than those who are not (Marckmann *et al.*, 2012; Petchey *et al.*, 2013). Future work that follows these "responders" may demonstrate associated improvements in physiological function and burden of disease with sustain exercise and lifestyle modification.

GPX activity was highly responsive over the course of the trial. GPX activity over 12-months significantly increased in CKD patients, regardless of the intervention therapy, as well as being associated with various co-morbidities and medication use in this population. GPX is an intracellular endogenous antioxidant responsible for the scavenging of ROS, as well as a crucial regulator of intracellular glutathione homeostasis, which in itself is vital for maintaining the cellular redox environment (Raha *et al.*, 2000; Godoy *et al.*, 2011). Previous studies have demonstrated dampened GPX activity with decreased kidney function (eGFR) in mild-moderate CKD patients (El-Far *et al.*, 2005; Crawford *et al.*, 2011), which is consistent with the baseline data we report. Increased GPX activity over 12 months may indicate a greater ability to counter ROS and ensuing oxidative stress. However, this effect is not due to exercise and lifestyle modification in the current study. CKD is characteristically progressive, regardless of exercise or lifestyle habits. Increased GPX may indicate, more so, an increase in ROS and therefore increased adaptive ability to reduced ROS through GPX activity, which is demonstrated in unchanging levels of IsoP. Furthermore, eGFR levels did not change significantly within both patient groups, which may suggest that maintenance of kidney function is dependent on increased GPX activity. This is interesting considering that PTE cells are the main source of plasma GPX activity (Avissar *et al.*, 1994).

A high degree of variability in systemic oxidative stress biomarkers is evident, regarding cross-sectional differences, as well as change, over 12 months. This high degree of variation questions the reliability of plasma IsoP, GPX and TAC as valid biomarkers of systemic oxidative stress. IsoPs are generated from arachidonic acid through cyclooxygenase-independent pathways following free radical damage, and are considered a reliable marker primarily because they are stable (Roberts and Morrow, 2002). Despite IsoP being chemically stable and reliably assayed, the biological variation of IsoP remains uncharacterised and appears to be large, as our results suggest. There have been claims that IsoP levels vary with time of day, and from day to day, within samples taken from the same subjects at different times (Helmersson and Basu, 2001; Kanabrocki *et al.*, 2002). This is relevant considering that oxidative stress is a highly dynamic process that can change significantly

as a result of minor influences such as O_2 supply and metabolism (Tribble and Jones, 1990; Stincone *et al.*, 2014; Zorov *et al.*, 2014). Therefore it is essential that *systemic* biomarkers of oxidative stress take biological factors of variation into account (Strobel *et al.*, 2011). Within the current CKD population, this was difficult given complexity of co-morbid disorders, many of which have previously shown a relationship to oxidative stress, including peripheral vascular disease (Roller *et al.*, 2001), hypertension (Velayutham *et al.*, 2013), obesity (Matsuda and Shimomura, 2013), as well as medication use, such as allopurinol (Vina *et al.*, 2000) and ACEi/ARB (Nakamura *et al.*, 2013). Measuring oxidative stress systemically is an area of research that requires further characterisation considering the extensive use of oxidative stress biomarkers in clinical oxidative stress studies. This also supports site-specific measurements of oxidative stress rather than systemic assessments. An alternative means to gauge responses in oxidative stress would be to assess a functional reserve, whereby subjects would undergo a stress test, such as exercise, and oxidative stress markers would be analysed from plasma pre- and post-stress. The capacity to respond to this oxidative challenge, through changes in the activity of antioxidant enzymes and end-products of oxidative damage, may provide a more relevant assessment of oxidative stress and impart some control over complex patient variables. However, variability has still been shown following these measures (Mullins *et al.*, 2013). A kidney biopsy would provide a "gold" standard in kidney-specific changes in oxidative stress in this CKD population, however, this is unrealistic considering its invasive nature. Alternatively, a skeletal muscle biopsy that is less invasive may provide more relevant information, especially since skeletal muscle is known to be highly responsive to exercise therapy and oxidative stress (Radak *et al.*, 2013).

Plasma IsoPs in both patient groups correlated significantly with changes in blood lipid profiles. This is primarily because IsoP is a primary measure of lipid peroxidation. Specifically, HDL is the major lipoprotein carrier for IsoP (Proudfoot *et al.*, 2009) and is more susceptible to oxidation than LDL (Raveh *et al.*, 2000; Nagyova *et al.*, 2001), which is consistent with the observed positive correlation with IsoP in the standard care patient group over 12 months. Blood lipids may present a biological influence on plasma IsoP concentration, and therefore may need to be considered for the interpretation of oxidative stress.

Kidney function, measured by eGFR, did not change significantly over time or with respect to the intervention. Dramatic differences between changes in eGFR of both patient groups are unlikely over 12 months, even in the standard care group. Stage 3-4 CKD indicates existing kidney damage. Tubulointerstitial fibrosis has the strongest correlation to impaired kidney function (Rodriguez-Iturbe *et al.*, 2005), and represents irreversible kidney damage that most interventions would fail to

improve. However, improvements in eGFR, within the exercise and lifestyle intervention groups, may be off-set by increases in serum creatinine due to increased physical activity or lean body mass. eGFR was calculated using the serum creatinine-based MDRD formula (Levey *et al.*, 1999). Creatinine is a breakdown product of creatinine phosphate in muscle and is produced at a constant rate that is freely excreted by the kidneys during resting conditions. Baxmann *et al.* (2008) demonstrated that healthy individuals with moderate/intense physical activity have higher serum and urinary creatinine compared to sedentary individuals. Furthermore, creatinine clearance (measured by urine and serum creatinine) can return to resting levels 1 h after stopping physical exercise, however serum creatinine remains elevated (Poortmans *et al.*, 2013). Whether these changes apply to patients with established CKD remains unknown, however the biological possibility does exist. A recent in-depth review of GFR estimation noted increased accuracy of eGFR formulas that incorporate serum cystatin C (Levey *et al.*, 2014), namely, the 2012 CKD-EPI creatinine-cystatin C equation (Inker *et al.*, 2012). Cystatin C is a cysteine protease inhibitor that is produced by all nucleated cells and enters the blood, where it is freely filtered then reabsorbed and catabolized by tubules without re-entering the blood (Curhan, 2005). Therefore, it is unlikely physical activity would interfere with eGFR determination, and would be interesting to pursue in the current population.

There were relevant limitations to the present study. These include the open label design increasing the chance of observer and performance biases, the relatively short duration, and small sample size increasing the likelihood of type 2 statistical errors. The observed results may not be generalizable to other centres considering that this is a single centre study design. Proteinuria, as a marker of kidney damage, was not evaluated and therefore no association can be made between oxidative stress biomarkers and kidney damage in moderate CKD patients. Notably, there is a lack of consistent, robust associations of oxidative stress markers with clinical variables raising doubts about validity and possibility of type 1 statistical error.

In summary, this study has demonstrated that exercise training and lifestyle intervention in patients with stage 3-4 CKD does not produce changes in systemic biomarkers of oxidative stress. GPX activity is responsive to the progression of CKD independent of exercise and lifestyle changes. CKD patients identified with high systemic levels of oxidative stress are more responsive to exercise and lifestyle interventions, and may present an ideal population to treat with oxidative stress-targeted therapies. However, the accurate assessment of oxidative stress and/or alterations to the body's redox state is difficult, owing to vast biological variation and the dynamic nature of oxidative stress that is enhanced markedly in the CKD population. Future research into exercise and

lifestyle interventions longer than 12 months, and the association of oxidative stress biomarkers to the noted improvements in physical fitness, may prove more informative. One positive outcome of the study is that patients, randomised to undergo exercise and lifestyle intervention, now possess additional physical fitness, support, and knowledge, to improve general health and potentially reduce their disease burden, regardless of a known underlying mechanism.

CHAPTER 8

Conclusions and Future Directions

8.1 OVERVIEW

CKD is a common and serious problem to human health that is characterised by progressive failure of kidney function and structural damage. The pathophysiological mechanisms common to the progressive changes in kidney function and structure form a complex network of overlapping, cyclical, yet distinct processes: tubular epithelial cell death by apoptosis or autophagic cell death, and cell cycle arrest; intra-renal capillary loss causing parenchymal hypoxia; activation and proliferation of tubulointerstitial fibroblasts causing fibrosis;, and maladaptive repair. These combine to promote nephron loss. The resultant impact on the kidney is a sustained progression of CKD, eventually to ESKD.

Oxidative stress has been associated with the progression of CKD, as well as each cellular and molecular pathological mechanism common to CKD including apoptosis, senescence and fibrosis (Dounousi *et al.*, 2006; Percy *et al.*, 2009). Despite this, antioxidant trials continue to demonstrate a lack of benefit in preventing CKD progression (Bjelakovic *et al.*, 2012; Jun *et al.*, 2012). This paradox highlights the need to better understand and define oxidative stress. ROS have a tightly regulated role as effectors of intracellular signalling pathways, by the activation of downstream targets for the maintenance of healthy tissue functionality. Mitochondrial function is central to cell metabolism, ROS production, and oxidative stress. Mitochondrial dysfunction is both a contributor and target of oxidative stress in the kidney.

The hypotheses tested in this thesis were that: (1) oxidative stress impacts adversely on cellular bioenergetics in the kidney and leads to loss of functioning kidney tissue in chronic kidney pathologies; and (2) modulation of oxidative stress will minimise the development and progression of kidney cell injury. The aims were to: (1) determine how oxidative stress in PTE cells causes cell injury and to then determine whether exogenous antioxidants can prevent or reduce renal cell injury *in vitro*; (2) use molecular and metabolic imaging with an established model of oxidative stress-induced kidney injury and progression, to measure oxidative stress processes in association with structure and function, and to then determine whether antioxidant therapy modulated kidney disease pathology *in vivo*; and (3) explore the association of systemic biomarkers of oxidative stress in CKD patients undergoing standard nephrology care in addition to exercise therapy and lifestyle changes, and to determine if oxidative stress correlates to clinical markers of renal function.

The hypotheses were partially upheld. Oxidative stress does impact adversely on cellular bioenergetics in the kidney and leads to loss of functioning kidney tissue in chronic kidney

pathologies. However, a general antioxidant therapy does not minimise the development and progression of kidney cell injury. Rather, in the results presented here, kidney cell injury and progression of chronic kidney pathology could be enhanced by antioxidant therapy.

8.2 DISCUSSION OF MAJOR RESULTS

8.2.1 Oxidative stress involves more than an imbalance of oxidants and antioxidants

Oxidative stress was first defined by Sies in 1985 as "a disturbance in the pro-oxidant-antioxidant balance in favour of the former" (Sies, 1985; Sies and Cadenas, 1985). This thesis demonstrates that this definition is far too simple, and that vital intracellular signalling related to overall cell functionality is disrupted during oxidative stress in the kidney. These alterations account for the primary pathological consequences that result in whole organ dysfunction and failure.

In PTE cells, oxidative stress combined with senescence to induce the greatest renal cell loss and mitochondrial destabilisation. Senescent PTE cells further promoted oxidative stress and therefore mitochondrial dysfunction. PPARγ signalling is a specific intracellular pathway disrupted during, and contributing to, oxidative stress in PTE cells of the kidney. Oxidative stress induced-PPARγ *Ser112* phosphorylation of PTE cells resulted in mitochondrial destabilisation, and a failure to restore mitochondrial health due to defective activation of PPARγ-dependent biogenesis pathways. This mechanism was conserved *in vivo* following AKI and future development of chronic kidney pathology.

The role of ROS and endogenous antioxidants still has a pathological significance. However, the biological role of ROS in physiology is one that is highly conserved and of great importance, especially within highly metabolic tissue, such as the kidney. This is supported in this thesis, demonstrating enhanced chronic kidney pathology with antioxidant therapy. Correcting these imbalances is difficult given the dynamic and reactive nature of ROS. Therefore more focus should be aimed at correcting oxidative stress-induced altered cellular signalling, rather than simply ROS levels.

8.2.2 Mitochondrial preservation and restoration is vital

The ancestral origins of mitochondria highlight the importance of them for life. Countless studies have implicated mitochondrial dysfunction in a diverse range of diseases. This thesis has demonstrated the key role of mitochondria in the cellular redox environment, and its dysregulation, which often precedes pathological change in the kidney.

In vitro experiments demonstrated mitochondrial dysfunction during oxidative stress contributing to senescence and apoptosis in PTE cells. Mitochondrial homeostasis, indicated by specific mitophagy and biogenesis pathways, was significantly impaired following oxidative stress-induced alterations to PPARγ signalling, causing PTE cell death. Intravital imaging demonstrated conserved mitochondrial dysfunction in the tubular epithelium *in vivo*, and this was associated with altered metabolic substrate utilisation that triggered persistent mitochondrial dysfunction and oxidative stress in the chronically damaged kidney. SOD2 decreased and cytoplasmic localisation of 8-OHdG in tubular epithelial cells implicated mitochondrial damage as an event that preceded tubular cell death, senescence and atrophy. Remnant tubules within areas of focal fibrotic change displayed consistently impaired metabolism and mitochondrial health, and they were identified as a site of persistent ROS production.

It is important to note the differences of kidney damage in humans versus animal models when assessing mitochondrial dynamics. A recent detailed study of human kidney clamp ischaemia during partial nephrectomy surgery highlighted these differences. Biopsies were taken prior to clamping, at the end of clamping, and after 5 min reperfusion. Findings demonstrated less severe structural damage of PTE cells and rapid resolution of mitochondrial swelling, suggesting that human kidneys can safely tolerate 30-60 min of controlled ischaemia with only minor structural changes and transient yet mild acute functional loss at 24 h post IR (Parekh *et al.*, 2013).

8.2.3 General cell antioxidants can enhance progressive kidney pathology

Antioxidant therapy for CKD continues to show inconclusive results despite oxidative stress continually being associated to CKD progression. This thesis demonstrated that targeting oxidative stress using a general cell antioxidant, NAC, promoted the progression of chronic kidney pathology following AKI. NAC was the only antioxidant that showed benefit in vitro. NAC has also been used in human trials for preventing hospital acquired AKI (Kay *et al.*, 2003; Santana-Santos *et al.*, 2014).

Treatment of PTE cells *in vitro* with NAC during oxidative stress inhibited oxidative stress-induced apoptosis, senescence and restored the proliferative capacity of PTE cells. *In vivo*, the protective effects of NAC were maintained in the early response to IR-induced AKI, however proved deleterious long-term. NAC promoted chronic kidney pathology by altering the cellular redox environment, thereby promoting metabolic and mitochondrial dysfunction, and preventing conserved cytoprotective redox-signalling, such as Nrf2 activation. TGF-β1 protein expression

increased in mice on an NAC diet, and this was thought to enhance the progression of chronic injury in the kidney.

This general failure of non-specific antioxidant therapy supports the evidence that non-mitochondrial ROS have important physiological signalling roles in the kidney, especially following AKI. Therefore mitochondrial-derived ROS in the kidney present a crucial target. This is discussed in the ensuing paragraphs. More importantly, the lack of translation of *in vitro* antioxidant benefit to *in vivo* benefit in the kidney, highlights the need for careful interpretation of *in vitro* antioxidant studies. The results also highlight the susceptibility of kidney metabolism to alterations in the cellular redox environment.

8.2.4 Oxidative stress is an important *cellular* mechanism of kidney injury

The association of oxidative stress to CKD progression relies on the measurement of systemic end-products of oxidative damage. It is has been shown previously that end-products of oxidative damage vary significantly in different tissues within the same organism (Abarikwu, 2014; Guillot *et al.*, 2014). This thesis demonstrated dynamic alterations to cellular processes during oxidative stress-induced damage to cells of the kidney, yet no association was seen of systemic biomarkers of oxidative stress in association with the progression of CKD in human patients.

However, this does not exclude oxidative stress as a major contributor to kidney disease. Rather, it questions the methods and times of measurement of systemic oxidative stress in human disease populations. For example, IsoP is a measure of lipid peroxidation. Lipid peroxidation is an end-product of a single pathway of oxidative damage, and does not account for many cell-specific changes that occur as a result of oxidative stress, such as impaired PPARγ signalling, mitochondrial dysfunction, or Nrf2 activation. Accurate oxidative stress assessments in the CKD population remain a challenge given the high degree of biological variation, and multiple assays should always be incorporated.

8.3 FUTURE DIRECTIONS

Future directions of this thesis have been outlined in the discussion of results chapters. Major future directions are discussed here.

It is clear that targeting oxidative stress by preserving and restoring mitochondrial health may offer a better approach to prevent or slow the progression of CKD. The development of mitochondrial-

specific antioxidants has already made progress, however experimental evidence has largely occurred in models of AKI. More research is needed to determine the long-term use of mitochondrial-targeted therapies to prevent progression to chronic kidney pathology after AKI. An *in vivo* model similar to that used in this thesis may provide this information. It remains unknown whether eliminating mitochondrial-derived ROS would have a similar affect to that of general cell antioxidants in enhancing chronic kidney pathology long-term, as was demonstrated in this thesis. In the case of chronic kidney pathologies where mitochondrial dysfunction (specifically, a depolarised mitochondrial membrane potential) is already established, promise lies with mitochondrial-targeted antioxidants whose mechanism of action is not dependent on a positive charge. One such agent, Szeto-Schiller (SS)-31 peptide, has been shown to exert effects mediated, in part, by its interaction with cardiolipan and inhibition of Cyt C mediation of peroxidation on the IMM (Birk *et al.*, 2013). However, this has only been shown in IR-induced AKI and it remains to be determined if these beneficial effects are preserved long-term.

We have demonstrated chronic metabolic alterations within remnant tubules in focal fibrotic areas of the cortex in the chronically damaged kidney. Future work is needed to characterise these populations of cells and their role in either repair after injury, or their potential pathogenic role as a site for progressive damage. It is possible that these populations of cells stem from the dedifferentiation and proliferation of damaged PTE cells, rather than remnant tubules more resistant to damage. Sub-populations of these fully-differentiated PTE cells that can dedifferentiate have been previously demonstrated by cell lineage tracing in models of AKI (Kusaba *et al.*, 2014). However, considering that these populations of cells display impaired mitochondrial function and metabolic profiles following chronic damage, they present a promising target to restore the cellular bioenergetics and proliferative capacity.

Intravital MPM has provided valuable insights into the kidney over the past decade. Nevertheless, much more can be discovered using this technology. Intravital MPM has the potential to increase our understanding of mitochondrial biology *in vivo* which at present is limited and based primarily on extrapolation from *in vitro* experiments from isolated cells and organelles. We simply do not know the extent of ROS generation from mitochondria *in vivo*. The infusion of specific ROS detectors, and imaging with MPM during AKI and CKD animal models, will increase this knowledge. Real-time cell signalling interactions of oxidative stress-responsive proteins, such as PPARγ and Nrf2, could be investigated using genetic mouse models of conditional proximal tubule expression of fluorescent tags, coupled with MPM. Advances in imaging technology are currently restricted by the depths within the kidney cortex, but new developments will improve this

technology. Human *in vivo* MPM is a promising advance, however at present this is also limited to the cortex via endoscopic utilisation. Intravascular studies with a flexible microscope objective are still not possible due to the large size of the microscope objective compared with renal luminal vasculature.

8.4 SUMMARY

This thesis presents oxidative stress as a common and unifying concept of pathophysiological change in chronic kidney pathology at a cellular level. Oxidative stress actively promotes cell death and cell cycle arrest in PTE cells whilst enhancing the secretion of pro-fibrotic factors to increase tubulointerstitial fibrosis. Targeted approaches are required to correct oxidative stress and prevent its diverse range of damaging pathophysiological consequences. The difficulty of finding useful targeted therapies for CKD is that we still do not fully understand the complexity of the cellular, physiological, and systemic responses of the kidney to oxidative stress. Progress is being made on multiple fronts. However, we continue to be humbled by this insidious disease whose morbidity and mortality rates remain at epidemic proportions.

BIBLIOGRAPHY

Abarikwu SO. 2014. Protective effect of quercetin on atrazine-induced oxidative stress in the liver, kidney, brain, and heart of adult wistar rats. *Toxicol Int* **21**: 148-155.

ABS, 2012. Australian Health Survey: First Results 2011-12, In: Health (Ed.). Commmonwealth Government, Canberra.

ABS, 2013. Australian Health Survey: Biomedical Results for Chronic Diseases, 2011-12, In: ABS (Ed.). Commonwealth Government, Canberra, pp. 31-32.

Abulrob A, Brunette E, Slinn J, Baumann E, Stanimirovic D. 2007. In vivo time domain optical imaging of renal ischemia-reperfusion injury: discrimination based on fluorescence lifetime. *Mol Imaging* **6**: 304-314.

Agarwal R, Saha C, Battiwala M, Vasavada N, Curley T, Chase SD, Sachs N, Semret MH. 2005. A pilot randomized controlled trial of renal protection with pioglitazone in diabetic nephropathy. *Kidney Int* **68**: 285-292.

Ahmadian M, Suh JM, Hah N, Liddle C, Atkins AR, Downes M, Evans RM. 2013. PPARgamma signaling and metabolism: the good, the bad and the future. *Nat Med* **19**: 557-566.

Alessio HM, Goldfarb AH. 1988. Lipid peroxidation and scavenger enzymes during exercise: adaptive response to training. *J Appl Physiol (1985)* **64**: 1333-1336.

Allan LA, Clarke PR. 2009. Apoptosis and autophagy: Regulation of caspase-9 by phosphorylation. *FEBS J* **276**: 6063-6073.

Alonso A, Lau J, Jaber BL, Weintraub A, Sarnak MJ. 2004. Prevention of radiocontrast nephropathy with N-acetylcysteine in patients with chronic kidney disease: a meta-analysis of randomized, controlled trials. *Am J Kidney Dis* **43**: 1-9.

Aminzadeh MA, Nicholas SB, Norris KC, Vaziri ND. 2013. Role of impaired Nrf2 activation in the pathogenesis of oxidative stress and inflammation in chronic tubulo-interstitial nephropathy. *Nephrol Dial Transplant* **28**: 2038-2045.

An WS, Kim HJ, Cho KH, Vaziri ND. 2009. Omega-3 fatty acid supplementation attenuates oxidative stress, inflammation, and tubulointerstitial fibrosis in the remnant kidney. *Am J Physiol Renal Physiol* **297**: F895-903.

Andersen HR, Nielsen JB, Nielsen F, Grandjean P. 1997. Antioxidative enzyme activities in human erythrocytes. *Clin Chem* **43**: 562-568.

Angelotti ML, Ronconi E, Ballerini L, Peired A, Mazzinghi B, Sagrinati C, Parente E, Gacci M, Carini M, Rotondi M, Fogo AB, Lazzeri E, Lasagni L, Romagnani P. 2012. Characterization of renal progenitors committed toward tubular lineage and their regenerative potential in renal tubular injury. *Stem Cells* **30**: 1714-1725.

Angermuller S, Islinger M, Volkl A. 2009. Peroxisomes and reactive oxygen species, a lasting challenge. *Histochem Cell Biol* **131**: 459-463.

Arab K, Rossary A, Flourie F, Tourneur Y, Steghens JP. 2006. Docosahexaenoic acid enhances the antioxidant response of human fibroblasts by upregulating gamma-glutamyl-cysteinyl ligase and glutathione reductase. *Br J Nutr* **95**: 18-26.

Arany I, Faisal A, Clark JS, Vera T, Baliga R, Nagamine Y. 2010. $p66^{shc}$-mediated mitochondrial dysfunction in renal proximal tubule cells during oxidative injury. *Am J Physiol Renal Physiol* **298**: F1214-1221.

Ash S, Campbell K, Maclaughlin H, McCoy E, Chan M, Anderson K, Corke K, Dumont R, Lloyd L, Meade A, Montgomery-Johnson R, Tasker T, Thrift P, Trotter B. 2006. Evidence-based practice guidelines for the nutritional management of chronic kidney disease. *Nutr Diet* **63**: S35 - S45.

Atamer A, Kocyigit Y, Ecder SA, Selek S, Ilhan N, Ecder T, Atamer Y. 2008. Effect of oxidative stress on antioxidant enzyme activities, homocysteine and lipoproteins in chronic kidney disease. *J Nephrol* **21**: 924-930.

Atkinson SJ, Hosford MA, Molitoris BA. 2004. Mechanism of actin polymerization in cellular ATP depletion. *J Biol Chem* **279**: 5194-5199.

Auletta JJ, Alabran JL, Kim BG, Meyer CJ, Letterio JJ. 2010. The synthetic triterpenoid, CDDO-Me, modulates the proinflammatory response to in vivo lipopolysaccharide challenge. *J Interferon Cytokine Res* **30**: 497-508.

Avissar N, Ornt DB, Yagil Y, Horowitz S, Watkins RH, Kerl EA, Takahashi K, Palmer IS, Cohen HJ. 1994. Human kidney proximal tubules are the main source of plasma glutathione peroxidase. *Am J Physiol* **266**: C367-375.

Baar K. 2014. Nutrition and the adaptation to endurance training. *Sports Med* **44 Suppl 1**: S5-12.

Baar K, Wende AR, Jones TE, Marison M, Nolte LA, Chen M, Kelly DP, Holloszy JO. 2002. Adaptations of skeletal muscle to exercise: rapid increase in the transcriptional coactivator PGC-1. *FASEB J* **16**: 1879-1886.

Bachmanov AA, Reed DR, Beauchamp GK, Tordoff MG. 2002. Food intake, water intake, and drinking spout side preference of 28 mouse strains. *Behav Genet* **32**: 435-443.

Baeuerle PA, Henkel T. 1994. Function and activation of NF-kappa B in the immune system. *Annu Rev Immunol* **12**: 141-179.

Baggott JE. 2005. High-dosage vitamin E supplementation and all-cause mortality. *Ann Intern Med* **143**: 155-156; author reply 156-158.

Balaban RS, Mandel LJ. 1988. Metabolic substrate utilization by rabbit proximal tubule. An NADH fluorescence study. *Am J Physiol* **254**: F407-416.

Barish GD, Narkar VA, Evans RM. 2006. PPAR delta: a dagger in the heart of the metabolic syndrome. *J Clin Invest* **116**: 590-597.

Basile DP, Donohoe D, Roethe K, Osborn JL. 2001. Renal ischemic injury results in permanent damage to peritubular capillaries and influences long-term function. *Am J Physiol Renal Physiol* **281**: F887-899.

Baxmann AC, Ahmed MS, Marques NC, Menon VB, Pereira AB, Kirsztajn GM, Heilberg IP. 2008. Influence of muscle mass and physical activity on serum and urinary creatinine and serum cystatin C. *Clin J Am Soc Nephrol* **3**: 348-354.

Becker W. 2012. Fluorescence lifetime imaging--techniques and applications. *J Microsc* **247**: 119-136.

Beeson CC, Beeson GC, Schnellmann RG. 2010. A high-throughput respirometric assay for mitochondrial biogenesis and toxicity. *Anal Biochem* **404**: 75-81.

Belardinelli R, Georgiou D, Cianci G, Purcaro A. 2012. 10-year exercise training in chronic heart failure: a randomized controlled trial. *J Am Coll Cardiol* **60**: 1521-1528.

Berezin MY, Achilefu S. 2010. Fluorescence lifetime measurements and biological imaging. *Chem Rev* **110**: 2641-2684.

Bhagavan HN, Chopra RK. 2006. Coenzyme Q10: absorption, tissue uptake, metabolism and pharmacokinetics. *Free Radic Res* **40**: 445-453.

Bharakhada N, Yates T, Davies MJ, Wilmot EG, Edwardson C, Henson J, Webb D, Khunti K. 2012. Association of sitting time and physical activity with CKD: a cross-sectional study in family practices. *Am J Kidney Dis* **60**: 583-590.

Bhaskaran M, Reddy K, Radhakrishanan N, Franki N, Ding G, Singhal PC. 2003. Angiotensin II induces apoptosis in renal proximal tubular cells. *Am J Physiol Renal Physiol* **284**: F955-965.

Bhattacharya A, Lustgarten M, Shi Y, Liu Y, Jang YC, Pulliam D, Jernigan AL, Van Remmen H. 2011. Increased mitochondrial matrix-directed superoxide production by fatty acid hydroperoxides in skeletal muscle mitochondria. *Free Radic Biol Med* **50**: 592-601.

Bird DK, Yan L, Vrotsos KM, Eliceiri KW, Vaughan EM, Keely PJ, White JG, Ramanujam N. 2005. Metabolic mapping of MCF10A human breast cells via multiphoton fluorescence lifetime imaging of the coenzyme NADH. *Cancer Res* **65**: 8766-8773.

Birk AV, Liu S, Soong Y, Mills W, Singh P, Warren JD, Seshan SV, Pardee JD, Szeto HH. 2013. The mitochondrial-targeted compound SS-31 re-energizes ischemic mitochondria by interacting with cardiolipin. *J Am Soc Nephrol* **24**: 1250-1261.

Bjelakovic G, Nikolova D, Gluud LL, Simonetti RG, Gluud C. 2012. Antioxidant supplements for prevention of mortality in healthy participants and patients with various diseases. *Cochrane Database Syst Rev* **3**: CD007176.

Bjorkoy G, Lamark T, Brech A, Outzen H, Perander M, Overvatn A, Stenmark H, Johansen T. 2005. p62/SQSTM1 forms protein aggregates degraded by autophagy and has a protective effect on huntingtin-induced cell death. *J Cell Biol* **171**: 603-614.

Blanchetot C, Tertoolen LG, den Hertog J. 2002. Regulation of receptor protein-tyrosine phosphatase alpha by oxidative stress. *EMBO J* **21**: 493-503.

Blatt DH, Pryor WA. 2005. High-dosage vitamin E supplementation and all-cause mortality. *Ann Intern Med* **143**: 150-151; author reply 156-158.

Bloom DA, Jaiswal AK. 2003. Phosphorylation of Nrf2 at Ser40 by protein kinase C in response to antioxidants leads to the release of Nrf2 from INrf2, but is not required for Nrf2 stabilization/accumulation in the nucleus and transcriptional activation of antioxidant response element-mediated NAD(P)H:quinone oxidoreductase-1 gene expression. *J Biol Chem* **278**: 44675-44682.

Boaz M, Smetana S, Weinstein T, Matas Z, Gafter U, Iaina A, Knecht A, Weissgarten Y, Brunner D, Fainaru M, Green MS. 2000. Secondary prevention with antioxidants of cardiovascular disease in endstage renal disease (SPACE): randomised placebo-controlled trial. *Lancet* **356**: 1213-1218.

Bolisetty S, Traylor AM, Kim J, Joseph R, Ricart K, Landar A, Agarwal A. 2010. Heme oxygenase-1 inhibits renal tubular macroautophagy in acute kidney injury. *J Am Soc Nephrol* **21**: 1702-1712.

Bolton WK, Cattran DC, Williams ME, Adler SG, Appel GB, Cartwright K, Foiles PG, Freedman BI, Raskin P, Ratner RE, Spinowitz BS, Whittier FC, Wuerth JP. 2004. Randomized trial of an inhibitor of formation of advanced glycation end products in diabetic nephropathy. *Am J Nephrol* **24**: 32-40.

Bondi CD, Manickam N, Lee DY, Block K, Gorin Y, Abboud HE, Barnes JL. 2010. NAD(P)H oxidase mediates TGF-beta1-induced activation of kidney myofibroblasts. *J Am Soc Nephro* **21**: 93-102.

Bonventre JV, Yang L. 2011. Cellular pathophysiology of ischemic acute kidney injury. *J Clin Invest* **121**: 4210-4221.

Borg GA. 1982. Psychophysical bases of perceived exertion. *Med Sci Sports Exerc* **14**: 377-381.

Borkham-Kamphorst E, Meurer SK, Gressner AM, Weiskirchen R. 2005. Disruption of intermolecular disulfide bonds in PDGF-BB dimers by N-acetyl-L-cysteine does not prevent PDGF signaling in cultured hepatic stellate cells. *Biochem Biophys Res Commun* **338**: 1711-1718.

Bouzidi N, Mekki K, Boukaddoum A, Dida N, Kaddous A, Bouchenak M. 2010. Effects of omega-3 polyunsaturated fatty-acid supplementation on redox status in chronic renal failure patients with dyslipidemia. *J Ren Nutr* **20**: 321-328.

Boveris A, Chance B. 1973. The mitochondrial generation of hydrogen peroxide. General properties and effect of hyperbaric oxygen. *Biochem J* **134**: 707-716.

Brenner BM, Cooper ME, de Zeeuw D, Keane WF, Mitch WE, Parving HH, Remuzzi G, Snapinn SM, Zhang Z, Shahinfar S. 2001. Effects of losartan on renal and cardiovascular outcomes in patients with type 2 diabetes and nephropathy. *N Engl J Med* **345**: 861-869.

Briskey DR, Wilson GR, Fassett RG, Coombes JS. 2014. Optimized method for quantification of total F(2)-isoprostanes using gas chromatography-tandem mass spectrometry. *J Pharm Biomed Anal* **90**: 161-166.

Brownlee M. 2001. Biochemistry and molecular cell biology of diabetic complications. *Nature* **414**: 813-820.

Brunet J, Boily MJ, Cordeau S, Des RC. 1995. Effects of N-acetylcysteine in the rat heart reperfused after low-flow ischemia: evidence for a direct scavenging of hydroxyl radicals and a nitric oxide-dependent increase in coronary flow. *Free Radic Biol Med* **19**: 627-638.

Budiono BP, See HLE, Peart JN, Sabapathy S, Ashton KJ, Haseler LJ, Headrick JP. 2012. Voluntary running in mice beneficially modulates myocardial ischemic tolerance, signaling kinases, and gene expression patterns. *Am J Physiol Regul Integr Comp Physiol* **302**: R1091-1100.

Cachofeiro V, Goicochea M, de VSG, Oubina P, Lahera V, Luno J. 2008. Oxidative stress and inflammation, a link between chronic kidney disease and cardiovascular disease. *Kidney Int Suppl* **(111)**: S4-9.

Cadenas E, Boveris A, Ragan CI, Stoppani AO. 1977. Production of superoxide radicals and hydrogen peroxide by NADH-ubiquinone reductase and ubiquinol-cytochrome c reductase from beef-heart mitochondria. *Arch Biochem Biophys* **180**: 248-257.

Cadenas E, Davies KJ. 2000. Mitochondrial free radical generation, oxidative stress, and aging. *Free Radic Biol Med* **29**: 222-230.

Cai Q, Zakaria HM, Simone A, Sheng ZH. 2012. Spatial parkin translocation and degradation of damaged mitochondria via mitophagy in live cortical neurons. *Curr Biol* **22**: 545-552.

Calabrese V, Mancuso C, Sapienza M, Puleo E, Calafato S, Cornelius C, Finocchiaro M, Mangiameli A, Di Mauro M, Stella AM, Castellino P. 2007. Oxidative stress and cellular stress response in diabetic nephropathy. *Cell Stress Chaperones* **12**: 299-306.

Calderon-Salinas JV, Munoz-Reyes EG, Guerrero-Romero JF, Rodriguez-Moran M, Bracho-Riquelme RL, Carrera-Gracia MA, Quintanar-Escorza MA. 2011. Eryptosis and oxidative damage in type 2 diabetic mellitus patients with chronic kidney disease. *Mol Cell Biochem* **357**: 171-179.

Calkin AC, Giunti S, Jandeleit-Dahm KA, Allen TJ, Cooper ME, Thomas MC. 2006. PPAR-alpha and -gamma agonists attenuate diabetic kidney disease in the apolipoprotein E knockout mouse. *Nephrol Dial Transplant* **21**: 2399-2405.

Camp HS, Tafuri SR. 1997. Regulation of peroxisome proliferator-activated receptor gamma activity by mitogen-activated protein kinase. *J Biol Chem* **272**: 10811-10816.

Campisi J, d'Adda dFF. 2007. Cellular senescence: when bad things happen to good cells. *Nat Rev Mol Cell Biol* **8**: 729-740.

Canaud G, Bonventre JV. 2014. Cell cycle arrest and the evolution of chronic kidney disease from acute kidney injury. *Nephrol Dial Transplant* **Epub ahead of print**.

Capeillere-Blandin C, Gausson V, Descamps-Latscha B, Witko-Sarsat V. 2004. Biochemical and spectrophotometric significance of advanced oxidized protein products. *Biochim Biophys Acta* **1689**: 91-102.

Carnicer R, Crabtree MJ, Sivakumaran V, Casadei B, Kass DA. 2012. Nitric Oxide Synthases in Heart Failure. *Antioxid Redox Signal* **18**: 1078-1099.

Carter T. 2005. High-dosage vitamin E supplementation and all-cause mortality. *Ann Intern Med* **143**: 155; author reply 156-158.

Chacko BK, Reily C, Srivastava A, Johnson MS, Ye Y, Ulasova E, Agarwal A, Zinn KR, Murphy MP, Kalyanaraman B, Darley-Usmar V. 2010. Prevention of diabetic nephropathy in Ins2(+/)(AkitaJ) mice by the mitochondria-targeted therapy MitoQ. *Biochem J* **432**: 9-19.

Chance B, Cohen P, Jobsis F, Schoener B. 1962. Intracellular oxidation-reduction states in vivo. *Science* **137**: 499-508.

Chance B, Schoener B, Oshino R, Itshak F, Nakase Y. 1979a. Oxidation-reduction ratio studies of mitochondria in freeze-trapped samples. NADH and flavoprotein fluorescence signals. *J Biol Chem* **254**: 4764-4771.

Chance B, Sies H, Boveris A. 1979b. Hydroperoxide metabolism in mammalian organs. *Physiol Rev* **59**: 527-605.

Chawla A, Schwarz EJ, Dimaculangan DD, Lazar MA. 1994. Peroxisome proliferator-activated receptor (PPAR) gamma: adipose-predominant expression and induction early in adipocyte differentiation. *Endocrinology* **135**: 798-800.

Chawla LS, Amdur RL, Amodeo S, Kimmel PL, Palant CE. 2011. The severity of acute kidney injury predicts progression to chronic kidney disease. *Kidney Int* **79**: 1361-1369.

Chawla LS, Kimmel PL. 2012. Acute kidney injury and chronic kidney disease: an integrated clinical syndrome. *Kidney Int* **82**: 516-524.

Che R, Yuan Y, Huang S, Zhang A. 2014. Mitochondrial dysfunction in the pathophysiology of renal diseases. *Am J Physiol Renal Physiol* **306**: F367-378.

Chen Q, Ames BN. 1994. Senescence-like growth arrest induced by hydrogen peroxide in human diploid fibroblast F65 cells. *Proc Natl Acad Sci U S A* **91**: 4130-4134.

Chen S, Kapturczak MH, Wasserfall C, Glushakova OY, Campbell-Thompson M, Deshane JS, Joseph R, Cruz PE, Hauswirth WW, Madsen KM, Croker BP, Berns KI, Atkinson MA, Flotte TR, Tisher CC, Agarwal A. 2005. Interleukin 10 attenuates neointimal proliferation and inflammation in

aortic allografts by a heme oxygenase-dependent pathway. *Proc Natl Acad Sci U S A* **102**: 7251-7256.

Chen YC, Su CT, Wang ST, Lee HD, Lin SY. 2009. A preliminary investigation of the association between serum uric acid and impaired renal function. *Chang Gung Med J* **32**: 66-71.

Chen YT, Chang FC, Wu CF, Chou YH, Hsu HL, Chiang WC, Shen J, Chen YM, Wu KD, Tsai TJ, Duffield JS, Lin SL. 2011. Platelet-derived growth factor receptor signaling activates pericyte-myofibroblast transition in obstructive and post-ischemic kidney fibrosis. *Kidney Int* **80**: 1170-1181.

Chiang MC, Cheng YC, Lin KH, Yen CH. 2013. PPARgamma regulates the mitochondrial dysfunction in human neural stem cells with tumor necrosis factor alpha. *Neuroscience* **229**: 118-129.

Chien KL, Hsu HC, Lee YT, Chen MF. 2008. Renal function and metabolic syndrome components on cardiovascular and all-cause mortality. *Atherosclerosis* **197**: 860-867.

Childs A, Jacobs C, Kaminski T, Halliwell B, Leeuwenburgh C. 2001. Supplementation with vitamin C and N-acetyl-cysteine increases oxidative stress in humans after an acute muscle injury induced by eccentric exercise. *Free Radic Biol Med* **31**: 745-753.

Chin M, Lee CY, Chuang JC, Bumeister R, Wigley WC, Sonis ST, Ward KW, Meyer C. 2013. Bardoxolone methyl analogs RTA 405 and dh404 are well tolerated and exhibit efficacy in rodent models of Type 2 diabetes and obesity. *Am J Physiol Renal Physiol* **304**: F1438-1446.

Chipuk JE, Moldoveanu T, Llambi F, Parsons MJ, Green DR. 2010. The BCL-2 family reunion. *Mol Cell* **37**: 299-310.

Choi JH, Banks AS, Estall JL, Kajimura S, Bostrom P, Laznik D, Ruas JL, Chalmers MJ, Kamenecka TM, Bluher M, Griffin PR, Spiegelman BM. 2010. Anti-diabetic drugs inhibit obesity-linked phosphorylation of PPARgamma by Cdk5. *Nature* **466**: 451-456.

Choksi KB, Nuss JE, Boylston WH, Rabek JP, Papaconstantinou J. 2007. Age-related increases in oxidatively damaged proteins of mouse kidney mitochondrial electron transport chain complexes. *Free Radic Biol Med* **43**: 1423-1438.

Clark B. 2000. Biology of renal aging in humans. *Adv Ren Replace Ther* **7**: 11-21.

Clarkson MR, Friedwald JJ, Eustace H, Rabb H, 2008. Acute Kidney Injury, 8th ed. 943-986. Saunders Elsevier, Philadelphia, Pennsylvania, USA.

Close GL, Kayani AC, Ashton T, McArdle A, Jackson MJ. 2007. Release of superoxide from skeletal muscle of adult and old mice: an experimental test of the reductive hotspot hypothesis. *Aging Cell* **6**: 189-195.

Coca SG, Singanamala S, Parikh CR. 2012. Chronic kidney disease after acute kidney injury: a systematic review and meta-analysis. *Kidney Int* **81**: 442-448.

Cohen MG, Rossi JS, Garbarino J, Bowling R, Motsinger-Reif AA, Schuler C, Dupont AG, Gabriel D. 2011. Insights into the inhibition of platelet activation by omega-3 polyunsaturated fatty acids: Beyond aspirin and clopidogrel. *Thromb Res* **128**: 335-340.

Coling D, Kachar B. 2001. Principles and application of fluorescence microscopy. *Curr Protoc Mol Biol* **Chapter 14**: Unit 14 10.

Conesa EL, Valero F, Nadal JC, Fenoy FJ, Lopez B, Arregui B, Salom MG. 2001. N-acetyl-L-cysteine improves renal medullary hypoperfusion in acute renal failure. *Am J Physiol Regul Integr Comp Physiol* **281**: R730-737.

Cooper CE, Patel RP, Brookes PS, Darley-Usmar VM. 2002. Nanotransducers in cellular redox signaling: modification of thiols by reactive oxygen and nitrogen species. *Trends Biochem Sci* **27**: 489-492.

Coux G, Elias MM, Trumper L. 2009. Ischaemia/reperfusion in rat renal cortex: vesicle leakiness and Na+, K+-ATPase activity in membrane preparations. *Nephrol Dial Transplant* **24**: 3020-3024.

Crawford A, Fassett RG, Coombes JS, Kunde DA, Ahuja KD, Robertson IK, Ball MJ, Geraghty DP. 2011. Glutathione peroxidase, superoxide dismutase and catalase genotypes and activities and the progression of chronic kidney disease. *Nephrol Dial Transplant* **26**: 2806-2813.

Curhan G. 2005. Cystatin C: a marker of renal function or something more? *Clin Chem* **51**: 293-294.

Cuttle L, Zhang XJ, Endre ZH, Winterford C, Gobe GC. 2001. Bcl-X(L) translocation in renal tubular epithelial cells in vitro protects distal cells from oxidative stress. *Kidney Int* **59**: 1779-1788.

Das DK, Engelman RM, Clement R, Otani H, Prasad MR, Rao PS. 1987. Role of xanthine oxidase inhibitor as free radical scavenger: a novel mechanism of action of allopurinol and oxypurinol in myocardial salvage. *Biochem Biophys Res Commun* **148**: 314-319.

Davies KJ, Quintanilha AT, Brooks GA, Packer L. 1982. Free radicals and tissue damage produced by exercise. *Biochem Biophys Res Commun* **107**: 1198-1205.

de Grey AD. 2000. The reductive hotspot hypothesis: an update. *Arch Biochem Biophys* **373**: 295-301.

de Grey AD. 2002. The reductive hotspot hypothesis of mammalian aging: membrane metabolism magnifies mutant mitochondrial mischief. *Eur J Biochem* **269**: 2003-2009.

de ZD, Akizawa T, Audhya P, Bakris GL, Chin M, Christ-Schmidt H, Goldsberry A, Houser M, Krauth M, Lambers HHJ, McMurray JJ, Meyer CJ, Parving HH, Remuzzi G, Toto RD, Vaziri ND, Wanner C, Wittes J, Wrolstad D, Chertow GM. 2013. Bardoxolone methyl in type 2 diabetes and stage 4 chronic kidney disease. *N Engl J Med* **369**: 2492-2503.

Degenhardt K, Sundararajan R, Lindsten T, Thompson C, White E. 2002. Bax and Bak independently promote cytochrome C release from mitochondria. *J Biol Chem* **277**: 14127-14134.

Dendooven A, Ishola DA, Jr., Nguyen TQ, Van der Giezen DM, Kok RJ, Goldschmeding R, Joles JA. 2011. Oxidative stress in obstructive nephropathy. *Int J Exp Pathol* **92**: 202-210.

DeZee KJ, Shimeall W, Douglas K, Jackson JL. 2005. High-dosage vitamin E supplementation and all-cause mortality. *Ann Intern Med* **143**: 153-154; author reply 156-158.

Di LGA, Sweeney SM, Korkko J, Ala-Kokko L, San AJD. 2002. Mapping the ligand-binding sites and disease-associated mutations on the most abundant protein in the human, type I collagen. *J Biol Chem* **277**: 4223-4231.

Diaz Encarnacion MM, Warner GM, Cheng J, Gray CE, Nath KA, Grande JP. 2011. n-3 Fatty acids block TNF-alpha-stimulated MCP-1 expression in rat mesangial cells. *Am J Physiol Renal Physiol* **300**: F1142-1151.

Diers AR, Broniowska KA, Hogg N. 2013. Nitrosative stress and redox-cycling agents synergize to cause mitochondrial dysfunction and cell death in endothelial cells. *Redox Biol* **1**: 1-7.

Dijkers PF, Medema RH, Lammers JW, Koenderman L, Coffer PJ. 2000. Expression of the pro-apoptotic Bcl-2 family member Bim is regulated by the forkhead transcription factor FKHR-L1. *Curr Biol* **10**: 1201-1204.

Ding Y, Stidham RD, Bumeister R, Trevino I, Winters A, Sprouse M, Ding M, Ferguson DA, Meyer CJ, Wigley WC, Ma R. 2013. The synthetic triterpenoid, RTA 405, increases the glomerular filtration rate and reduces angiotensin II-induced contraction of glomerular mesangial cells. *Kidney Int* **83**: 845-854.

Dinkova-Kostova AT, Holtzclaw WD, Cole RN, Itoh K, Wakabayashi N, Katoh Y, Yamamoto M, Talalay P. 2002. Direct evidence that sulfhydryl groups of Keap1 are the sensors regulating induction of phase 2 enzymes that protect against carcinogens and oxidants. *Proc Natl Acad Sci U S A* **99**: 11908-11913.

Doi T, Vlassara H, Kirstein M, Yamada Y, Striker GE, Striker LJ. 1992. Receptor-specific increase in extracellular matrix production in mouse mesangial cells by advanced glycosylation end products is mediated via platelet-derived growth factor. *Proc Natl Acad Sci U S A* **89**: 2873-2877.

Dounousi E, Papavasiliou E, Makedou A, Ioannou K, Katododis K, Tselepis A, Siamopoulos K, Tsakiris D. 2006. Oxidative stress is progressively enhanced with advancing stages of chronic kidney disease. *Nephrol Dial Transplant* **21**: 385-385.

Du XL, Edelstein D, Dimmeler S, Ju Q, Sui C, Brownlee M. 2001. Hyperglycemia inhibits endothelial nitric oxide synthase activity by posttranslational modification at the Akt site. *J Clin Invest* **108**: 1341-1348.

Du XL, Edelstein D, Rossetti L, Fantus IG, Goldberg H, Ziyadeh F, Wu J, Brownlee M. 2000. Hyperglycemia-induced mitochondrial superoxide overproduction activates the hexosamine pathway and induces plasminogen activator inhibitor-1 expression by increasing Sp1 glycosylation. *Proc Natl Acad Sci U S A* **97**: 12222-12226.

Eckardt KU, Coresh J, Devuyst O, Johnson RJ, Kottgen A, Levey AS, Levin A. 2013. Evolving importance of kidney disease: from subspecialty to global health burden. *Lancet* **382**: 158-169.

Egan DF, Shackelford DB, Mihaylova MM, Gelino S, Kohnz RA, Mair W, Vasquez DS, Joshi A, Gwinn DM, Taylor R, Asara JM, Fitzpatrick J, Dillin A, Viollet B, Kundu M, Hansen M, Shaw RJ. 2011. Phosphorylation of ULK1 (hATG1) by AMP-activated protein kinase connects energy sensing to mitophagy. *Science* **331**: 456-461.

El-Far MA, Bakr MA, Farahat SE, Abd E-FEA. 2005. Glutathione peroxidase activity in patients with renal disorders. *Clin Exp Nephrol* **9**: 127-131.

El-Sheikh AA, van den Heuvel JJ, Koenderink JB, Russel FG. 2008. Effect of hypouricaemic and hyperuricaemic drugs on the renal urate efflux transporter, multidrug resistance protein 4. *Br J Pharmacol* **155**: 1066-1075.

Elson D, Requejo-Isidro J, Munro I, Reavell F, Siegel J, Suhling K, Tadrous P, Benninger R, Lanigan P, McGinty J, Talbot C, Treanor B, Webb S, Sandison A, Wallace A, Davis D, Lever J, Neil M, Phillips D, Stamp G, French P. 2004. Time-domain fluorescence lifetime imaging applied to biological tissue. *Photochem Photobiol Sci* **3**: 795-801.

Epstein FH, Agmon Y, Brezis M. 1994. Physiology of renal hypoxia. *Ann N Y Acad Sci* **718**: 72-81; discussion 81-72.

Eskiocak U, Kim SB, Roig AI, Kitten E, Batten K, Cornelius C, Zou YS, Wright WE, Shay JW. 2010. CDDO-Me protects against space radiation-induced transformation of human colon epithelial cells. *Radiat Res* **174**: 27-36.

Esposito C, Plati A, Mazzullo T, Fasoli G, De Mauri A, Grosjean F, Mangione F, Castoldi F, Serpieri N, Cornacchia F, Dal Canton A. 2007. Renal function and functional reserve in healthy elderly individuals. *J Nephrol* **20**: 617-625.

Eum HA, Lee SM. 2004. Effects of Trolox on the activity and gene expression of cytochrome P450 in hepatic ischemia/reperfusion. *Br J Pharmacol* **142**: 35-42.

Evans RM, Barish GD, Wang YX. 2004. PPARs and the complex journey to obesity. *Nat Med* **10**: 355-361.

Ezzati M, Riboli E. 2013. Behavioral and dietary risk factors for noncommunicable diseases. *N Engl J Med* **369**: 954-964.

Finkel T, Holbrook NJ. 2000. Oxidants, oxidative stress and the biology of ageing. *Nature* **408**: 239-247.

Flegal KM, Carroll MD, Ogden CL, Johnson CL. 2002. Prevalence and trends in obesity among US adults, 1999-2000. *JAMA* **288**: 1723-1727.

Forbes JM, Hewitson TD, Becker GJ, Jones CL. 2000. Ischemic acute renal failure: long-term histology of cell and matrix changes in the rat. *Kidney Int* **57**: 2375-2385.

Fourquet S, Guerois R, Biard D, Toledano MB. 2010. Activation of NRF2 by nitrosative agents and H2O2 involves KEAP1 disulfide formation. *J Biol Chem* **285**: 8463-8471.

Fox CS, Larson MG, Leip EP, Culleton B, Wilson PW, Levy D. 2004. Predictors of new-onset kidney disease in a community-based population. *JAMA* **291**: 844-850.

Frasier CR, Moukdar F, Patel HD, Sloan RC, Stewart LM, Alleman RJ, La FJD, Brown DA. 2013. Redox-dependent increases in glutathione reductase and exercise preconditioning: role of NADPH oxidase and mitochondria. *Cardiovasc Res* **98**: 47-55.

Frei B, Kim MC, Ames BN. 1990. Ubiquinol-10 is an effective lipid-soluble antioxidant at physiological concentrations. *Proc Natl Acad Sci U S A* **87**: 4879-4883.

Frippiat C, Chen QM, Zdanov S, Magalhaes JP, Remacle J, Toussaint O. 2001. Subcytotoxic H2O2 stress triggers a release of transforming growth factor-beta 1, which induces biomarkers of cellular senescence of human diploid fibroblasts. *J Biol Chem* **276**: 2531-2537.

Fuenzalida K, Quintanilla R, Ramos P, Piderit D, Fuentealba RA, Martinez G, Inestrosa NC, Bronfman M. 2007. Peroxisome proliferator-activated receptor gamma up-regulates the Bcl-2 anti-apoptotic protein in neurons and induces mitochondrial stabilization and protection against oxidative stress and apoptosis. *J Biol Chem* **282**: 37006-37015.

Fujisawa K, Nishikawa T, Kukidome D, Imoto K, Yamashiro T, Motoshima H, Matsumura T, Araki E. 2009. TZDs reduce mitochondrial ROS production and enhance mitochondrial biogenesis. *Biochem Biophys Res Commun* **379**: 43-48.

Fujisawa S, Ishihara M, Atsumi T, Kadoma Y. 2006. A quantitative approach to the free radical interaction between alpha-tocopherol or ascorbate and flavonoids. *In Vivo* **20**: 445-452.

Funk JA, Odejinmi S, Schnellmann RG. 2010. SRT1720 induces mitochondrial biogenesis and rescues mitochondrial function after oxidant injury in renal proximal tubule cells. *J Pharmacol Exp Ther* **333**: 593-601.

Galicia-Moreno M, Favari L, Muriel P. 2012. Antifibrotic and antioxidant effects of N-acetylcysteine in an experimental cholestatic model. *Eur J Gastroenterol Hepatol* **24**: 179-185.

Gane EJ, Weilert F, Orr DW, Keogh GF, Gibson M, Lockhart MM, Frampton CM, Taylor KM, Smith RA, Murphy MP. 2010. The mitochondria-targeted anti-oxidant mitoquinone decreases liver damage in a phase II study of hepatitis C patients. *Liver Int* **30**: 1019-1026.

Gao X, Deeb D, Danyluk A, Media J, Liu Y, Dulchavsky SA, Gautam SC. 2008. Immunomodulatory activity of synthetic triterpenoids: inhibition of lymphocyte proliferation, cell-mediated cytotoxicity, and cytokine gene expression through suppression of NF-kappaB. *Immunopharmacol Immunotoxicol* **30**: 581-600.

Geisler S, Holmstrom KM, Skujat D, Fiesel FC, Rothfuss OC, Kahle PJ, Springer W. 2010. PINK1/Parkin-mediated mitophagy is dependent on VDAC1 and p62/SQSTM1. *Nat Cell Biol* **12**: 119-131.

Gerard-Monnier D, Erdelmeier I, Regnard K, Moze-Henry N, Yadan JC, Chaudiere J. 1998. Reactions of 1-methyl-2-phenylindole with malondialdehyde and 4-hydroxyalkenals. Analytical applications to a colorimetric assay of lipid peroxidation. *Chem Res Toxicol* **11**: 1176-1183.

Ghiran IC. 2011. Introduction to fluorescence microscopy. *Methods Mol Biol* **689**: 93-136.

Giorgio M, Migliaccio E, Orsini F, Paolucci D, Moroni M, Contursi C, Pelliccia G, Luzi L, Minucci S, Marcaccio M, Pinton P, Rizzuto R, Bernardi P, Paolucci F, Pelicci PG. 2005. Electron transfer between cytochrome c and p66Shc generates reactive oxygen species that trigger mitochondrial apoptosis. *Cell* **122**: 221-233.

Giray B, Kan E, Bali M, Hincal F, Basaran N. 2003. The effect of vitamin E supplementation on antioxidant enzyme activities and lipid peroxidation levels in hemodialysis patients. *Clin Chim Acta* **338**: 91-98.

Glotin AL, Debacq-Chainiaux F, Brossas JY, Faussat AM, Treton J, Zubielewicz A, Toussaint O, Mascarelli F. 2008. Prematurely senescent ARPE-19 cells display features of age-related macular degeneration. *Free Radic Biol Med* **44**: 1348-1361.

Go AS, Chertow GM, Fan D, McCulloch CE, Hsu CY. 2004. Chronic kidney disease and the risks of death, cardiovascular events, and hospitalization. *N Engl J Med* **351**: 1296-1305.

Gobe G. 2009. Identification of apoptosis in kidney tissue sections. *Methods Mol Biol* **466**: 175-192.

Gobe GC, Axelsen RA. 1987. Genesis of renal tubular atrophy in experimental hydronephrosis in the rat. Role of apoptosis. *Lab Invest* **56**: 273-281.

Gobe GC, Axelsen RA, Searle JW. 1990. Cellular events in experimental unilateral ischemic renal atrophy and in regeneration after contralateral nephrectomy. *Lab Invest* **63**: 770-779.

Gobe GC, Bennett NC, West M, Colditz P, Brown L, Vesey DA, Johnson DW. 2014. Increased progression to kidney fibrosis after erythropoietin is used as a treatment for acute kidney injury. *Am J Physiol Renal Physiol* **306**: F681-692.

Godoy JR, Oesteritz S, Hanschmann EM, Ockenga W, Ackermann W, Lillig CH. 2011. Segment-specific overexpression of redoxins after renal ischemia and reperfusion: protective roles of glutaredoxin 2, peroxiredoxin 3, and peroxiredoxin 6. *Free Radic Biol Med* **51**: 552-561.

Goicoechea M, de Vinuesa SG, Verdalles U, Ruiz-Caro C, Ampuero J, Rincon A, Arroyo D, Luno J. 2010. Effect of allopurinol in chronic kidney disease progression and cardiovascular risk. *Clin J Am Soc Nephrol* **5**: 1388-1393.

Goldenthal MJ, Marin-Garcia J. 2004. Mitochondrial signaling pathways: a receiver/integrator organelle. *Mol Cell Biochem* **262**: 1-16.

Gomes AP, Price NL, Ling AJ, Moslehi JJ, Montgomery MK, Rajman L, White JP, Teodoro JS, Wrann CD, Hubbard BP, Mercken EM, Palmeira CM, de CR, Rolo AP, Turner N, Bell EL, Sinclair

DA. 2013. Declining NAD(+) induces a pseudohypoxic state disrupting nuclear-mitochondrial communication during aging. *Cell* **155**: 1624-1638.

Gomes P, Simao S, Silva E, Pinto V, Amaral JS, Afonso J, Serrao MP, Pinho MJ, Soares-da-Silva P. 2009. Aging increases oxidative stress and renal expression of oxidant and antioxidant enzymes that are associated with an increased trend in systolic blood pressure. *Oxid Med Cell Longev* **2**: 138-145.

Gomez-Cabrera MC, Domenech E, Romagnoli M, Arduini A, Borras C, Pallardo FV, Sastre J, Vina J. 2008. Oral administration of vitamin C decreases muscle mitochondrial biogenesis and hampers training-induced adaptations in endurance performance. *Am J Clin Nutr* **87**: 142-149.

Gonzalez-Pacheco FR, Caramelo C, Castilla MA, Deudero JJ, Arias J, Yague S, Jimenez S, Bragado R, Alvarez-Arroyo MV. 2002. Mechanism of vascular smooth muscle cells activation by hydrogen peroxide: role of phospholipase C gamma. *Nephrol Dial Transplant* **17**: 392-398.

Gounder SS, Kannan S, Devadoss D, Miller CJ, Whitehead KS, Odelberg SJ, Firpo MA, Paine R, 3rd, Hoidal JR, Abel ED, Rajasekaran NS. 2012. Impaired transcriptional activity of Nrf2 in age-related myocardial oxidative stress is reversible by moderate exercise training. *PLoS One* **7**: e45697.

Goyal VK. 1982. Changes with age in the human kidney. *Exp Gerontol* **17**: 321-331.

Graham D, Huynh NN, Hamilton CA, Beattie E, Smith RA, Cocheme HM, Murphy MP, Dominiczak AF. 2009. Mitochondria-targeted antioxidant MitoQ10 improves endothelial function and attenuates cardiac hypertrophy. *Hypertension* **54**: 322-328.

Granata S, Zaza G, Simone S, Villani G, Latorre D, Pontrelli P, Carella M, Schena FP, Grandaliano G, Pertosa G. 2009. Mitochondrial dysregulation and oxidative stress in patients with chronic kidney disease. *BMC Genomics* **10**: 388.

Greiber S, Muller B, Daemisch P, Pavenstadt H. 2002. Reactive oxygen species alter gene expression in podocytes: induction of granulocyte macrophage-colony-stimulating factor. *J Am Soc Nephrol* **13**: 86-95.

Guan Y, Breyer MD. 2001. Peroxisome proliferator-activated receptors (PPARs): novel therapeutic targets in renal disease. *Kidney Int* **60**: 14-30.

Guan Y, Zhang Y, Breyer MD. 2002. The Role of PPARs in the Transcriptional Control of Cellular Processes. *Drug News Perspect* **15**: 147-154.

Guarente L, Kenyon C. 2000. Genetic pathways that regulate ageing in model organisms. *Nature* **408**: 255-262.

Guillot M, Charles AL, Chamaraux-Tran TN, Bouitbir J, Meyer A, Zoll J, Schneider F, Geny B. 2014. Oxidative stress precedes skeletal muscle mitochondrial dysfunction during experimental aortic cross-clamping but is not associated with early lung, heart, brain, liver, or kidney mitochondrial impairment. *J Vasc Surg* **60**: 1043-1051 e1045.

Gunst J, Derese I, Aertgeerts A, Ververs EJ, Wauters A, Van dBG, Vanhorebeek I. 2013. Insufficient autophagy contributes to mitochondrial dysfunction, organ failure, and adverse outcome in an animal model of critical illness. *Crit Care Med* **41**: 182-194.

Guo Q, Packer L. 2000. Ascorbate-dependent recycling of the vitamin E homologue Trolox by dihydrolipoate and glutathione in murine skin homogenates. *Free Radic Biol Med* **29**: 368-374.

Halestrap AP. 2010. A pore way to die: the role of mitochondria in reperfusion injury and cardioprotection. *Biochem Soc Trans* **38**: 841-860.

Hall AM, Crawford C, Unwin RJ, Duchen MR, Peppiatt-Wildman CM. 2011. Multiphoton imaging of the functioning kidney. *J Am Soc Nephrol* **22**: 1297-1304.

Hall AM, Rhodes GJ, Sandoval RM, Corridon PR, Molitoris BA. 2013. In vivo multiphoton imaging of mitochondrial structure and function during acute kidney injury. *Kidney Int* **83**: 72-83.

Hall AM, Unwin RJ, Parker N, Duchen MR. 2009. Multiphoton imaging reveals differences in mitochondrial function between nephron segments. *J Am Soc Nephrol* **20**: 1293-1302.

Hall ME, do CJM, da SAA, Juncos LA, Wang Z, Hall JE. 2014. Obesity, hypertension, and chronic kidney disease. *Int J Nephrol Renovasc Dis* **7**: 75-88.

Hallan SI, Matsushita K, Sang Y, Mahmoodi BK, Black C, Ishani A, Kleefstra N, Naimark D, Roderick P, Tonelli M, Wetzels JF, Astor BC, Gansevoort RT, Levin A, Wen CP, Coresh J. 2012. Age and association of kidney measures with mortality and end-stage renal disease. *JAMA* **308**: 2349-2360.

Halliwell B, Whiteman M. 2004. Measuring reactive species and oxidative damage in vivo and in cell culture: how should you do it and what do the results mean? *Br J Pharmacol* **142**: 231-255.

Hanschmann EM, Lonn ME, Schutte LD, Funke M, Godoy JR, Eitner S, Hudemann C, Lillig CH. 2010. Both thioredoxin 2 and glutaredoxin 2 contribute to the reduction of the mitochondrial 2-Cys peroxiredoxin Prx3. *J Biol Chem* **285**: 40699-40705.

Harris WS. 1997. n-3 fatty acids and serum lipoproteins: human studies. *Am J Clin Nutr* **65**: 1645S-1654S.

Hauser S, Adelmant G, Sarraf P, Wright HM, Mueller E, Spiegelman BM. 2000. Degradation of the peroxisome proliferator-activated receptor gamma is linked to ligand-dependent activation. *J Biol Chem* **275**: 18527-18533.

Heiss WD. 2012. The ischemic penumbra: how does tissue injury evolve? *Ann N Y Acad Sci* **1268**: 26-34.

Hellsten Y, Ahlborg G, Jensen-Urstad M, Sjodin B. 1988. Indication of in vivo xanthine oxidase activity in human skeletal muscle during exercise. *Acta Physiol Scand* **134**: 159-160.

Helmersson J, Basu S. 2001. F(2)-isoprostane and prostaglandin F(2 alpha)metabolite excretion rate and day to day variation in healthy humans. *Prostaglandins Leukot Essent Fatty Acids* **65**: 99-102.

Hemila H. 2005. High-dosage vitamin E supplementation and all-cause mortality. *Ann Intern Med* **143**: 151-152; author reply 156-158.

Heyman SN, Rosenberger C, Rosen S. 2011. Acute kidney injury: lessons from experimental models. *Contrib Nephrol* **169**: 286-296.

Higashida K, Kim SH, Higuchi M, Holloszy JO, Han DH. 2011. Normal adaptations to exercise despite protection against oxidative stress. *Am J Physiol Endocrinol Metab* **301**: E779-784.

Higuchi M, Honda T, Proske RJ, Yeh ET. 1998. Regulation of reactive oxygen species-induced apoptosis and necrosis by caspase 3-like proteases. *Oncogene* **17**: 2753-2760.

Himmelfarb J, Ikizler TA, Ellis C, Wu P, Shintani A, Dalal S, Kaplan M, Chonchol M, Hakim RM. 2014. Provision of antioxidant therapy in hemodialysis (PATH): a randomized clinical trial. *J Am Soc Nephrol* **25**: 623-633.

Hock MB, Kralli A. 2009. Transcriptional control of mitochondrial biogenesis and function. *Annu Rev Physiol* **71**: 177-203.

Honda T, Yoshizawa H, Sundararajan C, David E, Lajoie MJ, Favaloro FG, Jr., Janosik T, Su X, Honda Y, Roebuck BD, Gribble GW. 2011. Tricyclic compounds containing nonenolizable cyano enones. A novel class of highly potent anti-inflammatory and cytoprotective agents. *J Med Chem* **54**: 1762-1778.

Hondares E, Mora O, Yubero P, Rodriguez dlCM, Iglesias R, Giralt M, Villarroya F. 2006. Thiazolidinediones and rexinoids induce peroxisome proliferator-activated receptor-coactivator (PGC)-1alpha gene transcription: an autoregulatory loop controls PGC-1alpha expression in adipocytes via peroxisome proliferator-activated receptor-gamma coactivation. *Endocrinology* **147**: 2829-2838.

Hoogwerf BJ. 2010. Renin-angiotensin system blockade and cardiovascular and renal protection. *Am J Cardiol* **105**: 30A-35A.

Howden EJ, Leano R, Petchey W, Coombes JS, Isbel NM, Marwick TH. 2013. Effects of exercise and lifestyle intervention on cardiovascular function in CKD. *Clin J Am Soc Nephrol* **8**: 1494-1501.

Hsu SP, Chiang CK, Yang SY, Chien CT. 2010. N-acetylcysteine for the management of anemia and oxidative stress in hemodialysis patients. *Nephron Clin Pract* **116**: c207-216.

Hsu TF, Huang MK, Yu SH, Yen DH, Kao WF, Chen YC, Huang MS. 2012. N-acetylcysteine for the prevention of contrast-induced nephropathy in the emergency department. *Intern Med* **51**: 2709-2714.

Hu E, Kim JB, Sarraf P, Spiegelman BM. 1996. Inhibition of adipogenesis through MAP kinase-mediated phosphorylation of PPARgamma. *Science* **274**: 2100-2103.

Huang HY, Appel LJ. 2003. Supplementation of diets with alpha-tocopherol reduces serum concentrations of gamma- and delta-tocopherol in humans. *J Nutr* **133**: 3137-3140.

Hughes J, Gobe G. 2007. Identification and quantification of apoptosis in the kidney using morphology, biochemical and molecular markers. *Nephrology (Carlton)* **12**: 452-458.

Hughson MD, Gobe GC, Hoy WE, Manning RD, Jr., Douglas-Denton R, Bertram JF. 2008. Associations of glomerular number and birth weight with clinicopathological features of African Americans and whites. *Am J Kidney Dis* **52**: 18-28.

Hybertson BM, Gao B, Bose SK, McCord JM. 2011. Oxidative stress in health and disease: the therapeutic potential of Nrf2 activation. *Mol Aspects Med* **32**: 234-246.

Iemitsu M, Maeda S, Jesmin S, Otsuki T, Kasuya Y, Miyauchi T. 2006. Activation pattern of MAPK signaling in the hearts of trained and untrained rats following a single bout of exercise. *J Appl Physiol (1985)* **101**: 151-163.

Inagami T. 2011. Mitochondrial Angiotensin receptors and aging. *Circ Res* **109**: 1323-1324.

Inker LA, Schmid CH, Tighiouart H, Eckfeldt JH, Feldman HI, Greene T, Kusek JW, Manzi J, Van LF, Zhang YL, Coresh J, Levey AS. 2012. Estimating glomerular filtration rate from serum creatinine and cystatin C. *N Engl J Med* **367**: 20-29.

Irita J, Okura T, Jotoku M, Nagao T, Enomoto D, Kurata M, Desilva VR, Miyoshi KI, Matsui Y, Uede T, Denhardt DT, Rittiling SR, Higaki J. 2011. Osteopontin deficiency protects against aldosterone-induced inflammation, oxidative stress, and interstitial fibrosis in the kidney. *Am J Physiol Renal Physiol* **301**: F833-844.

Ishani A, Xue JL, Himmelfarb J, Eggers PW, Kimmel PL, Molitoris BA, Collins AJ. 2009. Acute kidney injury increases risk of ESRD among elderly. *J Am Soc Nephrol* **20**: 223-228.

Ishihara M, Urushido M, Hamada K, Matsumoto T, Shimamura Y, Ogata K, Inoue K, Taniguchi Y, Horino T, Fujieda M, Fujimoto S, Terada Y. 2013. Sestrin-2 and BNIP3 regulate autophagy and mitophagy in renal tubular cells in acute kidney injury. *Am J Physiol Renal Physiol* **305**: F495-509.

Ishii N, Fujii M, Hartman PS, Tsuda M, Yasuda K, Senoo-Matsuda N, Yanase S, Ayusawa D, Suzuki K. 1998. A mutation in succinate dehydrogenase cytochrome b causes oxidative stress and ageing in nematodes. *Nature* **394**: 694-697.

Ishikawa A, Kawarazaki H, Ando K, Fujita M, Fujita T, Homma Y. 2011. Renal preservation effect of ubiquinol, the reduced form of coenzyme Q10. *Clin Exp Nephrol* **15**: 30-33.

Islam KN, O'Byrne D, Devaraj S, Palmer B, Grundy SM, Jialal I. 2000. Alpha-tocopherol supplementation decreases the oxidative susceptibility of LDL in renal failure patients on dialysis therapy. *Atherosclerosis* **150**: 217-224.

Islinger M, Li KW, Seitz J, Volkl A, Luers GH. 2009. Hitchhiking of Cu/Zn superoxide dismutase to peroxisomes-evidence for a natural piggyback import mechanism in mammals. *Traffic* **10**: 1711-1721.

James AM, Smith RA, Murphy MP. 2004. Antioxidant and prooxidant properties of mitochondrial Coenzyme Q. *Arch Biochem Biophys* **423**: 47-56.

Jha V, Garcia-Garcia G, Iseki K, Li Z, Naicker S, Plattner B, Saran R, Wang AY, Yang CW. 2013. Chronic kidney disease: global dimension and perspectives. *Lancet* **382**: 260-272.

Jia L, Huang XL, Zhao Y, Zhang XG, Wu K. 2010. Vitamin E succinate (VES) inhibits cell growth and induces apoptosis by mitochondrial-derived ROS in SGC-7901 cells. *Med Sci Monit* **16**: BR131-139.

Jiang D, Chen K, Lu X, Gao HJ, Qin ZH, Lin F. 2013. Exercise ameliorates the detrimental effect of chloroquine on skeletal muscles in mice via restoring autophagy flux. *Acta Pharmacol Sin*.

Jiao S, Meng F, Zhang J, Yang X, Zheng X, Wang L. 2012. STAT1 mediates cellular senescence induced by angiotensin II and H(2)O(2) in human glomerular mesangial cells. *Mol Cell Biochem* **365**: 9-17.

Jin YN, Yu YV, Gundemir S, Jo C, Cui M, Tieu K, Johnson GV. 2013. Impaired mitochondrial dynamics and Nrf2 signaling contribute to compromised responses to oxidative stress in striatal cells expressing full-length mutant huntingtin. *PLoS One* **8**: e57932.

Johnson DW. 2007. Prevention of progression of kidney disease - CARI guidelines. *Aust Fam Physician* **36**: 353.

Johnson DW, Armstrong K, Campbell SB, Mudge DW, Hawley CM, Coombes JS, Prins JB, Isbel NM. 2007. Metabolic syndrome in severe chronic kidney disease: Prevalence, predictors, prognostic significance and effects of risk factor modification. *Nephrology (Carlton)* **12**: 391-398.

Johnson DW, Atai E, Chan M, Phoon RK, Scott C, Toussaint ND, Turner GL, Usherwood T, Wiggins KJ. 2013. KHA-CARI guideline: Early chronic kidney disease: detection, prevention and management. *Nephrology (Carlton)* **18**: 340-350.

Johnson DW, Pat B, Vesey DA, Guan Z, Endre Z, Gobe GC. 2006. Delayed administration of darbepoetin or erythropoietin protects against ischemic acute renal injury and failure. *Kidney Int* **69**: 1806-1813.

Joshi G, Johnson JA. 2012. The Nrf2-ARE pathway: a valuable therapeutic target for the treatment of neurodegenerative diseases. *Recent Pat CNS Drug Discov* **7**: 218-229.

Jun M, Venkataraman V, Razavian M, Cooper B, Zoungas S, Ninomiya T, Webster AC, Perkovic V. 2012. Antioxidants for chronic kidney disease. *Cochrane Database Syst Rev* **10**: CD008176.

Kaasik A, Safiulina D, Zharkovsky A, Veksler V. 2007. Regulation of mitochondrial matrix volume. *Am J Physiol Cell Physiol* **292**: C157-163.

Kadkhodaee M, Hanson GR, Towner RA, Endre ZH. 1996. Detection of hydroxyl and carbon-centred radicals by EPR spectroscopy after ischaemia and reperfusion of the rat kidney. *Free Radic Res* **25**: 31-42.

Kadkhodaee M, Khastar H, Arab HA, Ghaznavi R, Zahmatkesh M, Mahdavi-Mazdeh M. 2007. Antioxidant vitamins preserve superoxide dismutase activities in gentamicin-induced nephrotoxicity. *Transplant Proc* **39**: 864-865.

Kagan V, Serbinova E, Packer L. 1990. Antioxidant effects of ubiquinones in microsomes and mitochondria are mediated by tocopherol recycling. *Biochem Biophys Res Commun* **169**: 851-857.

Kagan VE, Serbinova EA, Forte T, Scita G, Packer L. 1992. Recycling of vitamin E in human low density lipoproteins. *J Lipid Res* **33**: 385-397.

Kaisar OM, Johnson DW, Prins JB, Isbel N. 2008. The role of novel biomarkers of cardiovascular disease in chronic kidney disease: focus on adiponectin and leptin. *Curr Cardiol Rev* **4**: 287-292.

Kalaitzidis RG, Siamopoulos KC. 2011. The role of obesity in kidney disease: recent findings and potential mechanisms. *Int Urol Nephrol* **43**: 771-784.

Kanabrocki EL, Murray D, Hermida RC, Scott GS, Bremner WF, Ryan MD, Ayala DE, Third JL, Shirazi P, Nemchausky BA, Hooper DC. 2002. Circadian variation in oxidative stress markers in healthy and type II diabetic men. *Chronobiol Int* **19**: 423-439.

Kanbay M, Ozkara A, Selcoki Y, Isik B, Turgut F, Bavbek N, Uz E, Akcay A, Yigitoglu R, Covic A. 2007. Effect of treatment of hyperuricemia with allopurinol on blood pressure, creatinine clearence, and proteinuria in patients with normal renal functions. *Int Urol Nephrol* **39**: 1227-1233.

Kang C, O'Moore KM, Dickman JR, Ji LL. 2009. Exercise activation of muscle peroxisome proliferator-activated receptor-gamma coactivator-1alpha signaling is redox sensitive. *Free Radic Biol Med* **47**: 1394-1400.

Kang DH, Kanellis J, Hugo C, Truong L, Anderson S, Kerjaschki D, Schreiner GF, Johnson RJ. 2002. Role of the microvascular endothelium in progressive renal disease. *J Am Soc Nephrol* **13**: 806-816.

Kang KW, Cho MK, Lee CH, Kim SG. 2001. Activation of phosphatidylinositol 3-kinase and Akt by tert-butylhydroquinone is responsible for antioxidant response element-mediated rGSTA2 induction in H4IIE cells. *Mol Pharmacol* **59**: 1147-1156.

Kanjanabuch T, Ma LJ, Chen J, Pozzi A, Guan Y, Mundel P, Fogo AB. 2007. PPAR-gamma agonist protects podocytes from injury. *Kidney Int* **71**: 1232-1239.

Karamouzis I, Sarafidis PA, Karamouzis M, Iliadis S, Haidich AB, Sioulis A, Triantos A, Vavatsi-Christaki N, Grekas DM. 2008. Increase in oxidative stress but not in antioxidant capacity with advancing stages of chronic kidney disease. *Am J Nephrol* **28**: 397-404.

Kawai Y, Garduno L, Theodore M, Yang J, Arinze IJ. 2011. Acetylation-deacetylation of the transcription factor Nrf2 (nuclear factor erythroid 2-related factor 2) regulates its transcriptional activity and nucleocytoplasmic localization. *J Biol Chem* **286**: 7629-7640.

Kay J, Chow WH, Chan TM, Lo SK, Kwok OH, Yip A, Fan K, Lee CH, Lam WF. 2003. Acetylcysteine for prevention of acute deterioration of renal function following elective coronary angiography and intervention: a randomized controlled trial. *JAMA* **289**: 553-558.

Kensler TW, Wakabayashi N, Biswal S. 2007. Cell survival responses to environmental stresses via the Keap1-Nrf2-ARE pathway. *Annu Rev Pharmacol Toxicol* **47**: 89-116.

Kerr JF, Gobe GC, Winterford CM, Harmon BV. 1995. Anatomical methods in cell death. *Methods Cell Biol* **46**: 1-27.

Kerr JF, Wyllie AH, Currie AR. 1972. Apoptosis: a basic biological phenomenon with wide-ranging implications in tissue kinetics. *Br J Cancer* **26**: 239-257.

Kezic A, Thaiss F, Becker JU, Tsui TY, Bajcetic M. 2013. Effects of everolimus on oxidative stress in kidney model of ischemia/reperfusion injury. *Am J Nephrol* **37**: 291-301.

KHA. 2014. Pre-Budget Submission 2014-15 Federal Budget: Charting a Comprehensive Approach to Tackling Kidney Disease. *Kidney Health Australia*.

Kim HJ, Vaziri ND. 2010. Contribution of impaired Nrf2-Keap1 pathway to oxidative stress and inflammation in chronic renal failure. *Am J Physiol Renal Physiol* **298**: F662-671.

Kim KM, Jung BH, Paeng KJ, Kim I, Chung BC. 2004. Increased urinary F(2)-isoprostanes levels in the patients with Alzheimer's disease. *Brain Res Bull* **64**: 47-51.

Kim S, Lee HG, Park SA, Kundu JK, Keum YS, Cha YN, Na HK, Surh YJ. 2014. Keap1 cysteine 288 as a potential target for diallyl trisulfide-induced Nrf2 activation. *PLoS One* **9**: e85984.

Kim YJ, Chung HY. 2007. Antioxidative and anti-inflammatory actions of docosahexaenoic acid and eicosapentaenoic acid in renal epithelial cells and macrophages. *J Med Food* **10**: 225-231.

Kincaid-Smith P, Fairley KF, Farish S, Best JD, Proietto J. 2008. Reduction of proteinuria by rosiglitazone in non-diabetic renal disease. *Nephrology (Carlton)* **13**: 58-62.

Kirkin V, McEwan DG, Novak I, Dikic I. 2009. A role for ubiquitin in selective autophagy. *Mol Cell* **34**: 259-269.

Klein AS, Joh JW, Rangan U, Wang D, Bulkley GB. 1996. Allopurinol: discrimination of antioxidant from enzyme inhibitory activities. *Free Radic Biol Med* **21**: 713-717.

Klein EA, Thompson IM, Jr., Tangen CM, Crowley JJ, Lucia MS, Goodman PJ, Minasian LM, Ford LG, Parnes HL, Gaziano JM, Karp DD, Lieber MM, Walther PJ, Klotz L, Parsons JK, Chin JL, Darke AK, Lippman SM, Goodman GE, Meyskens FL, Jr., Baker LH. 2011. Vitamin E and the risk of prostate cancer: the Selenium and Vitamin E Cancer Prevention Trial (SELECT). *JAMA* **306**: 1549-1556.

Knight JA, Pieper RK, McClellan L. 1988. Specificity of the thiobarbituric acid reaction: its use in studies of lipid peroxidation. *Clin Chem* **34**: 2433-2438.

Kokoszka JE, Coskun P, Esposito LA, Wallace DC. 2001. Increased mitochondrial oxidative stress in the Sod2 (+/-) mouse results in the age-related decline of mitochondrial function culminating in increased apoptosis. *Proc Natl Acad Sci U S A* **98**: 2278-2283.

Koltai E, Hart N, Taylor AW, Goto S, Ngo JK, Davies KJ, Radak Z. 2012. Age-associated declines in mitochondrial biogenesis and protein quality control factors are minimized by exercise training. *Am J Physiol Regul Integr Comp Physiol* **303**: R127-134.

Komatsu M, Kageyama S, Ichimura Y. 2012. p62/SQSTM1/A170: physiology and pathology. *Pharmacol Res* **66**: 457-462.

Komatsu M, Kurokawa H, Waguri S, Taguchi K, Kobayashi A, Ichimura Y, Sou YS, Ueno I, Sakamoto A, Tong KI, Kim M, Nishito Y, Iemura S, Natsume T, Ueno T, Kominami E, Motohashi H, Tanaka K, Yamamoto M. 2010. The selective autophagy substrate p62 activates the stress responsive transcription factor Nrf2 through inactivation of Keap1. *Nat Cell Biol* **12**: 213-223.

Komatsu M, Waguri S, Koike M, Sou YS, Ueno T, Hara T, Mizushima N, Iwata J, Ezaki J, Murata S, Hamazaki J, Nishito Y, Iemura S, Natsume T, Yanagawa T, Uwayama J, Warabi E, Yoshida H, Ishii T, Kobayashi A, Yamamoto M, Yue Z, Uchiyama Y, Kominami E, Tanaka K. 2007. Homeostatic levels of p62 control cytoplasmic inclusion body formation in autophagy-deficient mice. *Cell* **131**: 1149-1163.

Kongkham S, Sriwong S, Tasanarong A. 2013. Protective effect of alpha tocopherol on contrast-induced nephropathy in rats. *Nefrologia* **33**: 116-123.

Kopp J, Seyhan H, Muller B, Lanczak J, Pausch E, Gressner AM, Dooley S, Horch RE. 2006. N-acetyl-L-cysteine abrogates fibrogenic properties of fibroblasts isolated from Dupuytren's disease by blunting TGF-beta signalling. *J Cell Mol Med* **10**: 157-165.

Kops GJ, Dansen TB, Polderman PE, Saarloos I, Wirtz KW, Coffer PJ, Huang TT, Bos JL, Medema RH, Burgering BM. 2002. Forkhead transcription factor FOXO3a protects quiescent cells from oxidative stress. *Nature* **419**: 316-321.

Kosugi T, Nakayama T, Heinig M, Zhang L, Yuzawa Y, Sanchez-Lozada LG, Roncal C, Johnson RJ, Nakagawa T. 2009. Effect of lowering uric acid on renal disease in the type 2 diabetic db/db mice. *Am J Physiol Renal Physiol* **297**: F481-488.

Krishnan K, Campbell S, Stone WL. 2005. High-dosage vitamin E supplementation and all-cause mortality. *Ann Intern Med* **143**: 151; author reply 156-158.

Kuchta A, Pacanis A, Kortas-Stempak B, Cwiklinska A, Zietkiewicz M, Renke M, Rutkowski B. 2011. Estimation of oxidative stress markers in chronic kidney disease. *Kidney Blood Press Res* **34**: 12-19.

Kung J, Henry RR. 2012. Thiazolidinedione safety. *Expert Opin Drug Saf* **11**: 565-579.

Kurz T, Terman A, Brunk UT. 2007. Autophagy, ageing and apoptosis: the role of oxidative stress and lysosomal iron. *Arch Biochem Biophys* **462**: 220-230.

Kusaba T, Lalli M, Kramann R, Kobayashi A, Humphreys BD. 2014. Differentiated kidney epithelial cells repair injured proximal tubule. *Proc Natl Acad Sci U S A* **111**: 1527-1532.

Kwong LK, Kamzalov S, Rebrin I, Bayne AC, Jana CK, Morris P, Forster MJ, Sohal RS. 2002. Effects of coenzyme Q(10) administration on its tissue concentrations, mitochondrial oxidant generation, and oxidative stress in the rat. *Free Radic Biol Med* **33**: 627-638.

Lafrance JP, Miller DR. 2010. Acute kidney injury associates with increased long-term mortality. *J Am Soc Nephrol* **21**: 345-352.

Lagoa R, Graziani I, Lopez-Sanchez C, Garcia-Martinez V, Gutierrez-Merino C. 2011. Complex I and cytochrome c are molecular targets of flavonoids that inhibit hydrogen peroxide production by mitochondria. *Biochim Biophys Acta* **1807**: 1562-1572.

Laisalmi-Kokki M, Pesonen E, Kokki H, Valta P, Pitkanen M, Teppo AM, Honkanen E, Lindgren L. 2009. Potentially detrimental effects of N-acetylcysteine on renal function in knee arthroplasty. *Free Radic Res* **43**: 691-696.

Lakowicz JR, Szmacinski H, Nowaczyk K, Johnson ML. 1992. Fluorescence lifetime imaging of free and protein-bound NADH. *Proc Natl Acad Sci U S A* **89**: 1271-1275.

Lash LH. 2009. Renal glutathione transport: Identification of carriers, physiological functions, and controversies. *Biofactors* **35**: 500-508.

Lash LH, Putt DA, Hueni SE, Cao W, Xu F, Kulidjian SJ, Horwitz JP. 2002. Cellular energetics and glutathione status in NRK-52E cells: toxicological implications. *Biochem Pharmacol* **64**: 1533-1546.

Lass A, Forster MJ, Sohal RS. 1999. Effects of coenzyme Q10 and alpha-tocopherol administration on their tissue levels in the mouse: elevation of mitochondrial alpha-tocopherol by coenzyme Q10. *Free Radic Biol Med* **26**: 1375-1382.

Lass A, Sohal RS. 1998. Electron transport-linked ubiquinone-dependent recycling of alpha-tocopherol inhibits autooxidation of mitochondrial membranes. *Arch Biochem Biophys* **352**: 229-236.

Lass A, Sohal RS. 2000. Effect of coenzyme Q(10) and alpha-tocopherol content of mitochondria on the production of superoxide anion radicals. *FASEB J* **14**: 87-94.

Lawler JM, Powers SK, Visser T, Van DH, Kordus MJ, Ji LL. 1993. Acute exercise and skeletal muscle antioxidant and metabolic enzymes: effects of fiber type and age. *Am J Physiol* **265**: R1344-1350.

Lee DH, Blomhoff R, Jacobs DR, Jr. 2004. Is serum gamma glutamyltransferase a marker of oxidative stress? *Free Radic Res* **38**: 535-539.

Lee JJ, Lee JH, Ko YG, Hong SI, Lee JS. 2010. Prevention of premature senescence requires JNK regulation of Bcl-2 and reactive oxygen species. *Oncogene* **29**: 561-575.

Leeuwenburgh C, Fiebig R, Chandwaney R, Ji LL. 1994. Aging and exercise training in skeletal muscle: responses of glutathione and antioxidant enzyme systems. *Am J Physiol* **267**: R439-445.

Leff T. 2003. AMP-activated protein kinase regulates gene expression by direct phosphorylation of nuclear proteins. *Biochem Soc Trans* **31**: 224-227.

Leite-Silva VR, Le LM, Sanchez WY, Liu DC, Sanchez WH, Morrow I, Martin D, Silva HD, Prow TW, Grice JE, Roberts MS. 2013. The effect of formulation on the penetration of coated and uncoated zinc oxide nanoparticles into the viable epidermis of human skin in vivo. *Eur J Pharm Biopharm* **84**: 297-308.

Lejay A, Meyer A, Schlagowski AI, Charles AL, Singh F, Bouitbir J, Pottecher J, Chakfe N, Zoll J, Geny B. 2014. Mitochondria: mitochondrial participation in ischemia-reperfusion injury in skeletal muscle. *Int J Biochem Cell Biol* **50**: 101-105.

Lenaz G. 2001. The mitochondrial production of reactive oxygen species: mechanisms and implications in human pathology. *IUBMB Life* **52**: 159-164.

Lepenies J, Hewison M, Stewart PM, Quinkler M. 2010. Renal PPARgamma mRNA expression increases with impairment of renal function in patients with chronic kidney disease. *Nephrology (Carlton)* **15**: 683-691.

Lesnefsky EJ, Minkler P, Hoppel CL. 2009. Enhanced modification of cardiolipin during ischemia in the aged heart. *J Mol Cell Cardiol* **46**: 1008-1015.

Levey AS, Bosch JP, Lewis JB, Greene T, Rogers N, Roth D. 1999. A more accurate method to estimate glomerular filtration rate from serum creatinine: a new prediction equation. Modification of Diet in Renal Disease Study Group. *Ann Intern Med* **130**: 461-470.

Levey AS, Coresh J. 2012. Chronic kidney disease. *Lancet* **379**: 165-180.

Levey AS, Coresh J, Greene T, Stevens LA, Zhang YL, Hendriksen S, Kusek JW, Van LF. 2006. Using standardized serum creatinine values in the modification of diet in renal disease study equation for estimating glomerular filtration rate. *Ann Intern Med* **145**: 247-254.

Levey AS, Inker LA, Coresh J. 2014. GFR estimation: from physiology to public health. *Am J Kidney Disease* **63**: 820-834.

Lewis EJ, Hunsicker LG, Clarke WR, Berl T, Pohl MA, Lewis JB, Ritz E, Atkins RC, Rohde R, Raz I. 2001. Renoprotective effect of the angiotensin-receptor antagonist irbesartan in patients with nephropathy due to type 2 diabetes. *N Engl J Med* **345**: 851-860.

Li H, Bergeron L, Cryns V, Pasternack MS, Zhu H, Shi L, Greenberg A, Yuan J. 1997. Activation of caspase-2 in apoptosis. *J Biol Chem* **272**: 21010-21017.

Li H, Ruan XZ, Powis SH, Fernando R, Mon WY, Wheeler DC, Moorhead JF, Varghese Z. 2005. EPA and DHA reduce LPS-induced inflammation responses in HK-2 cells: evidence for a PPAR-gamma-dependent mechanism. *Kidney Int* **67**: 867-874.

Li HY, Hou FF, Zhang X, Chen PY, Liu SX, Feng JX, Liu ZQ, Shan YX, Wang GB, Zhou ZM, Tian JW, Xie D. 2007. Advanced oxidation protein products accelerate renal fibrosis in a remnant kidney model. *J Am Soc Nephrol* **18**: 528-538.

Li M, Qureshi AR, Ellis E, Axelsson J. 2013. Impaired postprandial fibroblast growth factor (FGF)-19 response in patients with stage 5 chronic kidney diseases is ameliorated following antioxidative therapy. *Nephrol Dial Transplant* **28 Suppl 4**: iv212-219.

Li M, Sun K, Redelman D, Welniak LA, Murphy WJ. 2010. The triterpenoid CDDO-Me delays murine acute graft-versus-host disease with the preservation of graft-versus-tumor effects after allogeneic bone marrow transplantation. *Biol Blood Marrow Transplant* **16**: 739-750.

Li Y, Dash RK, Kim J, Saidel GM, Cabrera ME. 2009. Role of NADH/NAD+ transport activity and glycogen store on skeletal muscle energy metabolism during exercise: in silico studies. *Am J Physiol Cell Physiol* **296**: C25-46.

Liao CT, Chen YM, Shiao CC, Hu FC, Huang JW, Kao TW, Chuang HF, Hung KY, Wu KD, Tsai TJ. 2009. Rate of decline of residual renal function is associated with all-cause mortality and technique failure in patients on long-term peritoneal dialysis. *Nephrol Dial Transplant* **24**: 2909-2914.

Liby K, Risingsong R, Royce DB, Williams CR, Ma T, Yore MM, Sporn MB. 2009. Triterpenoids CDDO-methyl ester or CDDO-ethyl amide and rexinoids LG100268 or NRX194204 for prevention and treatment of lung cancer in mice. *Cancer Prev Res (Phila)* **2**: 1050-1058.

Liby K, Risingsong R, Royce DB, Williams CR, Yore MM, Honda T, Gribble GW, Lamph WW, Vannini N, Sogno I, Albini A, Sporn MB. 2008. Prevention and treatment of experimental estrogen receptor-negative mammary carcinogenesis by the synthetic triterpenoid CDDO-methyl Ester and the rexinoid LG100268. *Clin Cancer Res* **14**: 4556-4563.

Liby K, Royce DB, Williams CR, Risingsong R, Yore MM, Honda T, Gribble GW, Dmitrovsky E, Sporn TA, Sporn MB. 2007. The synthetic triterpenoids CDDO-methyl ester and CDDO-ethyl amide prevent lung cancer induced by vinyl carbamate in A/J mice. *Cancer Res* **67**: 2414-2419.

Liby KT, Royce DB, Risingsong R, Williams CR, Maitra A, Hruban RH, Sporn MB. 2010. Synthetic triterpenoids prolong survival in a transgenic mouse model of pancreatic cancer. *Cancer Prev Res (Phila)* **3**: 1427-1434.

Lillig CH, Holmgren A. 2007. Thioredoxin and related molecules--from biology to health and disease. *Antioxid Redox Signal* **9**: 25-47.

Lim JS, Yang JH, Chun BY, Kam S, Jacobs DR, Jr., Lee DH. 2004. Is serum gamma-glutamyltransferase inversely associated with serum antioxidants as a marker of oxidative stress? *Free Radic Biol Med* **37**: 1018-1023.

Lim WS, Liscic R, Xiong C, Morris JC. 2005. High-dosage vitamin E supplementation and all-cause mortality. *Ann Intern Med* **143**: 152; author reply 156-158.

Lin Q, Weis S, Yang G, Weng YH, Helston R, Rish K, Smith A, Bordner J, Polte T, Gaunitz F, Dennery PA. 2007a. Heme oxygenase-1 protein localizes to the nucleus and activates transcription factors important in oxidative stress. *J Biol Chem* **282**: 20621-20633.

Lin Q, Weis S, Yang G, Weng YH, Helston R, Rish K, Smith A, Bordner J, Polte T, Gaunitz F, Dennery PA. 2007b. Heme oxygenase-1 protein localizes to the nucleus and activates transcription factors important in oxidative stress. *J Biol Chem* **282**: 20621-20633.

Lindgren D, Bostrom AK, Nilsson K, Hansson J, Sjolund J, Moller C, Jirstrom K, Nilsson E, Landberg G, Axelson H, Johansson ME. 2011. Isolation and characterization of progenitor-like cells from human renal proximal tubules. *Am J Pathol* **178**: 828-837.

Lindsay J, Esposti MD, Gilmore AP. 2011. Bcl-2 proteins and mitochondria--specificity in membrane targeting for death. *Biochim Biophysica Acta* **1813**: 532-539.

Ling X, Konopleva M, Zeng Z, Ruvolo V, Stephens LC, Schober W, McQueen T, Dietrich M, Madden TL, Andreeff M. 2007. The novel triterpenoid C-28 methyl ester of 2-cyano-3, 12-dioxoolen-1, 9-dien-28-oic acid inhibits metastatic murine breast tumor growth through inactivation of STAT3 signaling. *Cancer Res* **67**: 4210-4218.

Linke A, Adams V, Schulze PC, Erbs S, Gielen S, Fiehn E, Mobius-Winkler S, Schubert A, Schuler G, Hambrecht R. 2005. Antioxidative effects of exercise training in patients with chronic heart failure: increase in radical scavenger enzyme activity in skeletal muscle. *Circulation* **111**: 1763-1770.

Linnane AW, Eastwood H. 2004. Cellular redox poise modulation; the role of coenzyme Q10, gene and metabolic regulation. *Mitochondrion* **4**: 779-789.

Linnane AW, Eastwood H. 2006. Cellular redox regulation and prooxidant signaling systems: a new perspective on the free radical theory of aging. *Ann N Y Acad Sci* **1067**: 47-55.

Linnane AW, Kios M, Vitetta L. 2007a. Coenzyme Q(10)--its role as a prooxidant in the formation of superoxide anion/hydrogen peroxide and the regulation of the metabolome. *Mitochondrion* **7 Suppl**: S51-61.

Linnane AW, Kios M, Vitetta L. 2007b. The essential requirement for superoxide radical and nitric oxide formation for normal physiological function and healthy aging. *Mitochondrion* **7**: 1-5.

Liu J, Yeo HC, Doniger SJ, Ames BN. 1997. Assay of aldehydes from lipid peroxidation: gas chromatography-mass spectrometry compared to thiobarbituric acid. *Anal Biochem* **245**: 161-166.

Liu LZ, Fang J, Zhou Q, Hu X, Shi X, Jiang BH. 2005. Apigenin inhibits expression of vascular endothelial growth factor and angiogenesis in human lung cancer cells: implication of chemoprevention of lung cancer. *Mol Pharmacol* **68**: 635-643.

Liu Y, Fiskum G, Schubert D. 2002. Generation of reactive oxygen species by the mitochondrial electron transport chain. *J Neurochem* **80**: 780-787.

Lonn ME, Hudemann C, Berndt C, Cherkasov V, Capani F, Holmgren A, Lillig CH. 2008. Expression pattern of human glutaredoxin 2 isoforms: identification and characterization of two testis/cancer cell-specific isoforms. *Antioxid Redox Signal* **10**: 547-557.

Loverre A, Capobianco C, Ditonno P, Battaglia M, Grandaliano G, Schena FP. 2008. Increase of proliferating renal progenitor cells in acute tubular necrosis underlying delayed graft function. *Transplantation* **85**: 1112-1119.

Lucio M, Nunes C, Gaspar D, Ferreira H, Lima JLFC, Reis S. 2009. Antioxidant Activity of Vitamin E and Trolox: Understanding of the Factors that Govern Lipid Peroxidation Studies In Vitro. *Food Biophys* **4**: 312-320.

Luk TH, Dai YL, Siu CW, Yiu KH, Chan HT, Lee SW, Li SW, Fong B, Wong WK, Tam S, Lau CP, Tse HF. 2012. Effect of exercise training on vascular endothelial function in patients with stable coronary artery disease: a randomized controlled trial. *Eur J Prev Cardiol* **19**: 830-839.

Lum H, Roebuck KA. 2001. Oxidant stress and endothelial cell dysfunction. *Am J Physiol Cell Physiol* **280**: C719-741.

Machlin LJ, Gabriel E. 1982. Kinetics of tissue alpha-tocopherol uptake and depletion following administration of high levels of vitamin E. *Ann N Y Acad Sci* **393**: 48-60.

Madesh M, Hajnoczky G. 2001. VDAC-dependent permeabilization of the outer mitochondrial membrane by superoxide induces rapid and massive cytochrome c release. *J Cell Biol* **155**: 1003-1015.

Malins DC, Hellstrom KE, Anderson KM, Johnson PM, Vinson MA. 2002. Antioxidant-induced changes in oxidized DNA. *Proc Natl acad Sci U S A* **99**: 5937-5941.

Mancuso M, Coppede F, Migliore L, Siciliano G, Murri L. 2006. Mitochondrial dysfunction, oxidative stress and neurodegeneration. *J Alzheimers Dis* **10**: 59-73.

Marckmann P, Agerskov H, Thineshkumar S, Bladbjerg EM, Sidelmann JJ, Jespersen J, Nybo M, Rasmussen LM, Hansen D, Scholze A. 2012. Randomized controlled trial of cholecalciferol supplementation in chronic kidney disease patients with hypovitaminosis D. *Nephrol Dial Transplant* **27**: 3523-3531.

Marras C, Lang AE, Oakes D, McDermott MP, Kieburtz K, Shoulson I, Tanner CM, Fahn S. 2005. High-dosage vitamin E supplementation and all-cause mortality. *Ann Intern Med* **143**: 152-153; author reply 156-158.

Marsh SA, Laursen PB, Coombes JS. 2006. Effects of antioxidant supplementation and exercise training on erythrocyte antioxidant enzymes. *Int J Vitam Nutr Res* **76**: 324-331.

Martin A, Perez-Giron JV, Hernanz R, Palacios R, Briones AM, Fortuno A, Zalba G, Salaices M, Alonso MJ. 2012. Peroxisome proliferator-activated receptor-gamma activation reduces cyclooxygenase-2 expression in vascular smooth muscle cells from hypertensive rats by interfering with oxidative stress. *J Hypertens* **30**: 315-326.

Martinon F, Petrilli V, Mayor A, Tardivel A, Tschopp J. 2006. Gout-associated uric acid crystals activate the NALP3 inflammasome. *Nature* **440**: 237-241.

Marton O, Koltai E, Takeda M, Koch LG, Britton SL, Davies KJ, Boldogh I, Radak Z. 2014. Mitochondrial biogenesis-associated factors underlie the magnitude of response to aerobic endurance training in rats. *Pflugers Arch* **Epub ahead of print**.

Masajtis-Zagajewska A, Nowicki M. 2009. Influence of dual blockade of the renin-angiotensin system on thirst in hemodialysis patients. *Nephron Clin Pract* **112**: c242-247.

Massy ZA, Guijarro C, O'Donnell MP, Kim Y, Kashtan CE, Egido J, Kasiske BL, Keane WF. 1999. The central role of nuclear factor-kappa B in mesangial cell activation. *Kidney Int Suppl* **71**: S76-79.

Mather M, Rottenberg H. 2000. Aging enhances the activation of the permeability transition pore in mitochondria. *Biochem Biophys Res Commun* **273**: 603-608.

Matsuda M, Shimomura I. 2013. Increased oxidative stress in obesity: implications for metabolic syndrome, diabetes, hypertension, dyslipidemia, atherosclerosis, and cancer. *Obes Res Clin Pract* **7**: e330-341.

Matsumoto T, Nakayama N, Ishida K, Kobayashi T, Kamata K. 2009. Eicosapentaenoic acid improves imbalance between vasodilator and vasoconstrictor actions of endothelium-derived factors in mesenteric arteries from rats at chronic stage of type 2 diabetes. *J Pharmacol Exp Ther* **329**: 324-334.

Matsushita K, Mahmoodi BK, Woodward M, Emberson JR, Jafar TH, Jee SH, Polkinghorne KR, Shankar A, Smith DH, Tonelli M, Warnock DG, Wen CP, Coresh J, Gansevoort RT, Hemmelgarn BR, Levey AS. 2012. Comparison of risk prediction using the CKD-EPI equation and the MDRD study equation for estimated glomerular filtration rate. *JAMA* **307**: 1941-1951.

Matthews DR, Hosker JP, Rudenski AS, Naylor BA, Treacher DF, Turner RC. 1985. Homeostasis model assessment: insulin resistance and beta-cell function from fasting plasma glucose and insulin concentrations in man. *Diabetologia* **28**: 412-419.

Mayer K, Meyer S, Reinholz-Muhly M, Maus U, Merfels M, Lohmeyer J, Grimminger F, Seeger W. 2003a. Short-time infusion of fish oil-based lipid emulsions, approved for parenteral nutrition, reduces monocyte proinflammatory cytokine generation and adhesive interaction with endothelium in humans. *J Immunol* **171**: 4837-4843.

Mayer RD, Wang X, Maines MD. 2003b. Nitric oxide inhibitor N omega -nitro-l-arginine methyl ester potentiates induction of heme oxygenase-1 in kidney ischemia/reperfusion model: a novel mechanism for regulation of the oxygenase. *J Pharmacol Exp Ther* **306**: 43-50.

McMahon M, Itoh K, Yamamoto M, Hayes JD. 2003. Keap1-dependent proteasomal degradation of transcription factor Nrf2 contributes to the negative regulation of antioxidant response element-driven gene expression. *J Biol Chem* **278**: 21592-21600.

Medina-Gomez G, Gray SL, Yetukuri L, Shimomura K, Virtue S, Campbell M, Curtis RK, Jimenez-Linan M, Blount M, Yeo GS, Lopez M, Seppanen-Laakso T, Ashcroft FM, Oresic M, Vidal-Puig A. 2007. PPAR gamma 2 prevents lipotoxicity by controlling adipose tissue expandability and peripheral lipid metabolism. *PLoS Genet* **3**: e64.

Melk A. 2003. Senescence of renal cells: molecular basis and clinical implications. *Nephrol Dial Transplant* **18**: 2474-2478.

Meng Q, Wong YT, Chen J, Ruan R. 2007. Age-related changes in mitochondrial function and antioxidative enzyme activity in fischer 344 rats. *Mech Ageing Dev* **128**: 286-292.

Meng TC, Fukada T, Tonks NK. 2002. Reversible oxidation and inactivation of protein tyrosine phosphatases in vivo. *Mol Cell* **9**: 387-399.

Menini S, Amadio L, Oddi G, Ricci C, Pesce C, Pugliese F, Giorgio M, Migliaccio E, Pelicci P, Iacobini C, Pugliese G. 2006. Deletion of p66Shc longevity gene protects against experimental diabetic glomerulopathy by preventing diabetes-induced oxidative stress. *Diabetes* **55**: 1642-1650.

Menini S, Iacobini C, Ricci C, Oddi G, Pesce C, Pugliese F, Block K, Abboud HE, Giorgio M, Migliaccio E, Pelicci PG, Pugliese G. 2007. Ablation of the gene encoding p66Shc protects mice against AGE-induced glomerulopathy by preventing oxidant-dependent tissue injury and further AGE accumulation. *Diabetologia* **50**: 1997-2007.

Merker MP, Audi SH, Lindemer BJ, Krenz GS, Bongard RD. 2007. Role of mitochondrial electron transport complex I in coenzyme Q1 reduction by intact pulmonary arterial endothelial cells and the effect of hyperoxia. *Am J Physiol Lung Cell Mol Physiol* **293**: L809-819.

Meurer SK, Lahme B, Tihaa L, Weiskirchen R, Gressner AM. 2005. N-acetyl-L-cysteine suppresses TGF-beta signaling at distinct molecular steps: the biochemical and biological efficacy of a multifunctional, antifibrotic drug. *Biochem Pharmacol* **70**: 1026-1034.

Meydani SN, Lau J, Dallal GE, Meydani M. 2005. High-dosage vitamin E supplementation and all-cause mortality. *Ann Intern Med* **143**: 153; author reply 156-158.

Mezzano D, Pais EO, Aranda E, Panes O, Downey P, Ortiz M, Tagle R, Gonzalez F, Quiroga T, Caceres MS, Leighton F, Pereira J. 2001. Inflammation, not hyperhomocysteinemia, is related to oxidative stress and hemostatic and endothelial dysfunction in uremia. *Kidney Int* **60**: 1844-1850.

Migliaccio E, Giorgio M, Mele S, Pelicci G, Reboldi P, Pandolfi PP, Lanfrancone L, Pelicci PG. 1999. The p66shc adaptor protein controls oxidative stress response and life span in mammals. *Nature* **402**: 309-313.

Miglio G, Rosa AC, Rattazzi L, Grange C, Camussi G, Fantozzi R. 2012. Protective effects of peroxisome proliferator-activated receptor agonists on human podocytes: proposed mechanisms of action. *Br J Pharmacol* **167**: 641-653.

Miller ER, 3rd, Pastor-Barriuso R, Dalal D, Riemersma RA, Appel LJ, Guallar E. 2005a. Meta-analysis: high-dosage vitamin E supplementation may increase all-cause mortality. *Ann Intern Med* **142**: 37-46.

Miller ER, 3rd, Pastor-Barriuso R, Dalal D, Riemersma RA, Appel LJ, Guallar E. 2005b. Meta-analysis: high-dosage vitamin E supplementation may increase all-cause mortality. *Ann Intern Med* **142**: 37-46.

Miller NJ, RiceEvans CA. 1996. Spectrophotometric determination of antioxidant activity. *Redox Report* **2**: 161-171.

Mironov SL, Richter DW. 2001. Oscillations and hypoxic changes of mitochondrial variables in neurons of the brainstem respiratory centre of mice. *J Physiol* **533**: 227-236.

Miyata T, Suzuki N, van YdSC. 2013. Diabetic nephropathy: are there new and potentially promising therapies targeting oxygen biology? *Kidney Int* **84**: 693-702.

Miyazawa M, Ishii T, Yasuda K, Noda S, Onouchi H, Hartman PS, Ishii N. 2009. The role of mitochondrial superoxide anion (O2(-)) on physiological aging in C57BL/6J mice. *J Radiat Res (Tokyo)* **50**: 73-83.

Moist L, Sontrop JM, Gallo K, Mainra R, Cutler M, Freeman D, House AA. 2010. Effect of N-acetylcysteine on serum creatinine and kidney function: results of a randomized controlled trial. *Am J Kidney Dis* **56**: 643-650.

Molitoris BA, Dahl R, Geerdes A. 1992. Cytoskeleton disruption and apical redistribution of proximal tubule Na(+)-K(+)-ATPase during ischemia. *Am J Physiol* **263**: F488-495.

Molnar Z, Shearer E, Lowe D. 1999. N-Acetylcysteine treatment to prevent the progression of multisystem organ failure: a prospective, randomized, placebo-controlled study. *Crit Care Med* **27**: 1100-1104.

Moorhouse PC, Grootveld M, Halliwell B, Quinlan JG, Gutteridge JM. 1987. Allopurinol and oxypurinol are hydroxyl radical scavengers. *FEBS Lett* **213**: 23-28.

Morigi M, Macconi D, Zoja C, Donadelli R, Buelli S, Zanchi C, Ghilardi M, Remuzzi G. 2002. Protein overload-induced NF-kappaB activation in proximal tubular cells requires H(2)O(2) through a PKC-dependent pathway. *J Am Soc Nephrol* **13**: 1179-1189.

Morrow JD, Roberts LJ, Daniel VC, Awad JA, Mirochnitchenko O, Swift LL, Burk RF. 1998. Comparison of formation of D2/E2-isoprostanes and F2-isoprostanes in vitro and in vivo--effects of oxygen tension and glutathione. *Arch Biochem Biophys* **353**: 160-171.

Mullins AL, van RSP, Briskey DR, Fassett RG, Wilson GR, Coombes JS. 2013. Variability in oxidative stress biomarkers following a maximal exercise test. *Biomarkers* **18**: 446-454.

Munusamy S, MacMillan-Crow LA. 2009. Mitochondrial superoxide plays a crucial role in the development of mitochondrial dysfunction during high glucose exposure in rat renal proximal tubular cells. *Free Radic Biol Med* **46**: 1149-1157.

Mussig K, Staiger H, Machicao F, Stancakova A, Kuusisto J, Laakso M, Thamer C, Machann J, Schick F, Claussen CD, Stefan N, Fritsche A, Haring HU. 2009. Association of common genetic variation in the FOXO1 gene with beta-cell dysfunction, impaired glucose tolerance, and type 2 diabetes. *J Clin Endocrinol Metab* **94**: 1353-1360.

Muthusamy VR, Kannan S, Sadhaasivam K, Gounder SS, Davidson CJ, Boeheme C, Hoidal JR, Wang L, Rajasekaran NS. 2012. Acute exercise stress activates Nrf2/ARE signaling and promotes antioxidant mechanisms in the myocardium. *Free Radic Biol Med* **52**: 366-376.

Nagaraj S, Youn JI, Weber H, Iclozan C, Lu L, Cotter MJ, Meyer C, Becerra CR, Fishman M, Antonia S, Sporn MB, Liby KT, Rawal B, Lee JH, Gabrilovich DI. 2010. Anti-inflammatory triterpenoid blocks immune suppressive function of MDSCs and improves immune response in cancer. *Clin Cancer Res* **16**: 1812-1823.

Nagyova A, Krajcovicova-Kudlackova M, Klvanova J. 2001. LDL and HDL oxidation and fatty acid composition in vegetarians. *Ann Nutr Metab* **45**: 148-151.

Nakamura A, Shikata K, Nakatou T, Kitamura T, Kajitani N, Ogawa D, Makino H. 2013. Combination therapy with an angiotensin-converting-enzyme inhibitor and an angiotensin II receptor antagonist ameliorates microinflammation and oxidative stress in patients with diabetic nephropathy. *J Diabetes Investig* **4**: 195-201.

Narendra D, Tanaka A, Suen DF, Youle RJ. 2008. Parkin is recruited selectively to impaired mitochondria and promotes their autophagy. *J Cell Biol* **183**: 795-803.

Nascimento MM, Suliman ME, Silva M, Chinaglia T, Marchioro J, Hayashi SY, Riella MC, Lindholm B, Anderstam B. 2010. Effect of oral N-acetylcysteine treatment on plasma inflammatory and oxidative stress markers in peritoneal dialysis patients: a placebo-controlled study. *Perit Dial Int* **30**: 336-342.

Nath KA. 1992. Tubulointerstitial changes as a major determinant in the progression of renal damage. *Am J Kidney Dis* **20**: 1-17.

Nath KA, Croatt AJ, Hostetter TH. 1990. Oxygen consumption and oxidant stress in surviving nephrons. *Am J Physiol* **258**: F1354-1362.

Navarro A, Gomez C, Lopez-Cepero JM, Boveris A. 2004. Beneficial effects of moderate exercise on mice aging: survival, behavior, oxidative stress, and mitochondrial electron transfer. *Am J Physiol Regul Integr Comp Physiol* **286**: R505-511.

Nemoto S, Finkel T. 2002. Redox regulation of forkhead proteins through a p66shc-dependent signaling pathway. *Science* **295**: 2450-2452.

Nemoto S, Takeda K, Yu ZX, Ferrans VJ, Finkel T. 2000. Role for mitochondrial oxidants as regulators of cellular metabolism. *Mol Cell Biol* **20**: 7311-7318.

Nethery D, Stofan D, Callahan L, DiMarco A, Supinski G. 1999. Formation of reactive oxygen species by the contracting diaphragm is PLA(2) dependent. *J Appl Physiol (1985)* **87**: 792-800.

Nguyen T, Sherratt PJ, Nioi P, Yang CS, Pickett CB. 2005. Nrf2 controls constitutive and inducible expression of ARE-driven genes through a dynamic pathway involving nucleocytoplasmic shuttling by Keap1. *J Biol Chem* **280**: 32485-32492.

NHF. 2010. Guide to Management of Hypertension: National Heart Foundation 2008. Sydney, Australia.

Niesner R, Peker B, Schlusche P, Gericke KH. 2004. Noniterative biexponential fluorescence lifetime imaging in the investigation of cellular metabolism by means of NAD(P)H autofluorescence. *Chemphyschem* **5**: 1141-1149.

Niizuma S, Nakamura S, Ishibashi-Ueda H, Yoshihara F, Kawano Y. 2011. Kidney function and histological damage in autopsy subjects with myocardial infarction. *Ren Fail* **33**: 847-852.

Noeman SA, Hamooda HE, Baalash AA. 2011. Biochemical study of oxidative stress markers in the liver, kidney and heart of high fat diet induced obesity in rats. *Diabetol Metab Syndr* **3**: 17.

Nohl H, Gille L, Kozlov AV. 1999. Critical aspects of the antioxidant function of coenzyme Q in biomembranes. *Biofactors* **9**: 155-161.

Nohl H, Hegner D. 1978. Do mitochondria produce oxygen radicals in vivo? *Eur J Biochem* **82**: 563-567.

Numazawa S, Ishikawa M, Yoshida A, Tanaka S, Yoshida T. 2003. Atypical protein kinase C mediates activation of NF-E2-related factor 2 in response to oxidative stress. *Am J Physiol Cell Physiol* **285**: C334-342.

O'Toole JF, Patel HV, Naples CJ, Fujioka H, Hoppel CL. 2010. Decreased cytochrome c mediates an age-related decline of oxidative phosphorylation in rat kidney mitochondria. *Biochem J* **427**: 105-112.

Oberg BP, McMenamin E, Lucas FL, McMonagle E, Morrow J, Ikizler TA, Himmelfarb J. 2004. Increased prevalence of oxidant stress and inflammation in patients with moderate to severe chronic kidney disease. *Kidney Int* **65**: 1009-1016.

Obermuller N, Kranzlin B, Verma R, Gretz N, Kriz W, Witzgall R. 1997. Renal osmotic stress-induced cotransporter: expression in the newborn, adult and post-ischemic rat kidney. *Kidney Int* **52**: 1584-1592.

Ohnishi T, Ohnishi ST, Shinzawa-Ito K, Yoshikawa S. 2008. Functional role of coenzyme Q in the energy coupling of NADH-CoQ oxidoreductase (Complex I): stabilization of the semiquinone state

with the application of inside-positive membrane potential to proteoliposomes. *Biofactors* **32**: 13-22.

Okada H, Kikuta T, Kobayashi T, Inoue T, Kanno Y, Takigawa M, Sugaya T, Kopp JB, Suzuki H. 2005. Connective tissue growth factor expressed in tubular epithelium plays a pivotal role in renal fibrogenesis. *J Am Soc Nephrol* **16**: 133-143.

Okamoto K, Kondo-Okamoto N, Ohsumi Y. 2009. Mitochondria-anchored receptor Atg32 mediates degradation of mitochondria via selective autophagy. *Dev Cell* **17**: 87-97.

Orsini F, Migliaccio E, Moroni M, Contursi C, Raker VA, Piccini D, Martin-Padura I, Pelliccia G, Trinei M, Bono M, Puri C, Tacchetti C, Ferrini M, Mannucci R, Nicoletti I, Lanfrancone L, Giorgio M, Pelicci PG. 2004. The life span determinant p66Shc localizes to mitochondria where it associates with mitochondrial heat shock protein 70 and regulates trans-membrane potential. *J Biol Chem* **279**: 25689-25695.

Ott M, Gogvadze V, Orrenius S, Zhivotovsky B. 2007. Mitochondria, oxidative stress and cell death. *Apoptosis* **12**: 913-922.

Pannarale G, Carbone R, Del Mastro G, Gallo C, Gattullo V, Natalicchio L, Navarra A, Tedesco A. 2010. The aging kidney: structural changes. *J Nephrol* **23 Suppl 15**: S37-40.

Parekh DJ, Weinberg JM, Ercole B, Torkko KC, Hilton W, Bennett M, Devarajan P, Venkatachalam MA. 2013. Tolerance of the human kidney to isolated controlled ischemia. *J Am Soc Nephrol* **24**: 506-517.

Park J, Lee J, Choi C. 2011. Mitochondrial Network Determines Intracellular ROS Dynamics and Sensitivity to Oxidative Stress through Switching Inter-Mitochondrial Messengers. *PLoS One* **6**: e23211.

Parra CT, Conejo GJR, Carballo AF, de AG. 2003. Antioxidant nutrients protect against cyclosporine A nephrotoxicity. *Toxicology* **189**: 99-111.

Passos JF, Von Zglinicki T. 2006. Oxygen free radicals in cell senescence: are they signal transducers? *Free Radic Res* **40**: 1277-1283.

Pat B, Yang T, Kong C, Watters D, Johnson DW, Gobe G. 2005. Activation of ERK in renal fibrosis after unilateral ureteral obstruction: modulation by antioxidants. *Kidney Int* **67**: 931-943.

Pattwell DM, McArdle A, Morgan JE, Patridge TA, Jackson MJ. 2004. Release of reactive oxygen and nitrogen species from contracting skeletal muscle cells. *Free Radic Biol Med* **37**: 1064-1072.

Peake JM, Gobe GC, Fassett RG, Coombes JS. 2011. The effects of dietary fish oil on inflammation, fibrosis and oxidative stress associated with obstructive renal injury in rats. *Mol Nutr Food Res* **55**: 400-410.

Peake SL, Moran JL, Leppard PI. 1996. N-acetyl-L-cysteine depresses cardiac performance in patients with septic shock. *Crit Care Med* **24**: 1302-1310.

Peerapanyasut W, Thamprasert K, Wongmekiat O. 2014. Ubiquinol supplementation protects against renal ischemia and reperfusion injury in rats. *Free Radic Res* **48**: 180-189.

Pena AM, Boulesteix T, Dartigalongue T, Schanne-Klein MC. 2005. Chiroptical effects in the second harmonic signal of collagens I and IV. *J Am Chem Soc* **127**: 10314-10322.

Pennington KN, Taylor JA, Bren GD, Paya CV. 2001. IkappaB kinase-dependent chronic activation of NF-kappaB is necessary for p21(WAF1/Cip1) inhibition of differentiation-induced apoptosis of monocytes. *Mol Cell Biol* **21**: 1930-1941.

Percy CJ, Brown L, Power DA, Johnson DW, Gobe GC. 2009. Obesity and hypertension have differing oxidant handling molecular pathways in age-related chronic kidney disease. *Mech Ageing Dev* **130**: 129-138.

Percy CJ, Power D, Gobe GC. 2008. Renal ageing: changes in the cellular mechanism of energy metabolism and oxidant handling. *Nephrology (Carlton)* **13**: 147-152.

Pergola PE, Krauth M, Huff JW, Ferguson DA, Ruiz S, Meyer CJ, Warnock DG. 2011a. Effect of bardoxolone methyl on kidney function in patients with T2D and Stage 3b-4 CKD. *Am J Nephrol* **33**: 469-476.

Pergola PE, Raskin P, Toto RD, Meyer CJ, Huff JW, Grossman EB, Krauth M, Ruiz S, Audhya P, Christ-Schmidt H, Wittes J, Warnock DG. 2011b. Bardoxolone methyl and kidney function in CKD with type 2 diabetes. *N Engl J Med* **365**: 327-336.

Petchey WG, Hickman IJ, Prins JB, Hawley CM, Johnson DW, Isbel NM, Duncan EL. 2013. Vitamin D does not improve the metabolic health of patients with chronic kidney disease stage 3-4: a randomized controlled trial. *Nephrology (Carlton)* **18**: 26-35.

Philp A, Chen A, Lan D, Meyer GA, Murphy AN, Knapp AE, Olfert IM, McCurdy CE, Marcotte GR, Hogan MC, Baar K, Schenk S. 2011. Sirtuin 1 (SIRT1) deacetylase activity is not required for mitochondrial biogenesis or peroxisome proliferator-activated receptor-gamma coactivator-1alpha (PGC-1alpha) deacetylation following endurance exercise. *J Biol Chem* **286**: 30561-30570.

Pias EK, Aw TY. 2002. Apoptosis in mitotic competent undifferentiated cells is induced by cellular redox imbalance independent of reactive oxygen species production. *FASEB J* **16**: 781-790.

Pinton P, Rimessi A, Marchi S, Orsini F, Migliaccio E, Giorgio M, Contursi C, Minucci S, Mantovani F, Wieckowski MR, Del Sal G, Pelicci PG, Rizzuto R. 2007. Protein kinase C beta and prolyl isomerase 1 regulate mitochondrial effects of the life-span determinant p66Shc. *Science* **315**: 659-663.

Pistrosch F, Herbrig K, Kindel B, Passauer J, Fischer S, Gross P. 2005. Rosiglitazone improves glomerular hyperfiltration, renal endothelial dysfunction, and microalbuminuria of incipient diabetic nephropathy in patients. *Diabetes* **54**: 2206-2211.

Piwowar A. 2010. Advanced oxidation protein products. Part I. Mechanism of the formation, characteristics and property. *Pol Merkur Lekarski* **28**: 166-169.

Plotnikov EY, Kazachenko AV, Vyssokikh MY, Vasileva AK, Tcvirkun DV, Isaev NK, Kirpatovsky VI, Zorov DB. 2007. The role of mitochondria in oxidative and nitrosative stress during ischemia/reperfusion in the rat kidney. *Kidney Int* **72**: 1493-1502.

Polesskaya O, Sun A, Salahura G, Silva JN, Dewhurst S, Kasischke K. 2012. Detection of microregional hypoxia in mouse cerebral cortex by two-photon imaging of endogenous NADH fluorescence. *J Vis Exp* **(60)**.

Poortmans JR, Gulbis B, De BE, Baudry S, Carpentier A. 2013. Limitations of serum values to estimate glomerular filtration rate during exercise. *Br J Sports Med* **47**: 1166-1170.

Portilla D, Dai G, McClure T, Bates L, Kurten R, Megyesi J, Price P, Li S. 2002. Alterations of PPARalpha and its coactivator PGC-1 in cisplatin-induced acute renal failure. *Kidney Int* **62**: 1208-1218.

Possolo AM. 2005. High-dosage vitamin E supplementation and all-cause mortality. *Ann Intern Med* **143**: 154; author reply 156-158.

Post JB, Jegede AB, Morin K, Spungen AM, Langhoff E, Sano M. 2010. Cognitive profile of chronic kidney disease and hemodialysis patients without dementia. *Nephron Clin Pract* **116**: c247-255.

Powers SK, Criswell D, Lawler J, Ji LL, Martin D, Herb RA, Dudley G. 1994. Influence of exercise and fiber type on antioxidant enzyme activity in rat skeletal muscle. *Am J Physiol* **266**: R375-380.

Proudfoot JM, Barden AE, Loke WM, Croft KD, Puddey IB, Mori TA. 2009. HDL is the major lipoprotein carrier of plasma F2-isoprostanes. *J Lipid Res* **50**: 716-722.

Puigserver P, Rhee J, Lin J, Wu Z, Yoon JC, Zhang CY, Krauss S, Mootha VK, Lowell BB, Spiegelman BM. 2001. Cytokine stimulation of energy expenditure through p38 MAP kinase activation of PPARgamma coactivator-1. *Mol Cell* **8**: 971-982.

Qiang L, Wang L, Kon N, Zhao W, Lee S, Zhang Y, Rosenbaum M, Zhao Y, Gu W, Farmer SR, Accili D. 2012. Brown remodeling of white adipose tissue by SirT1-dependent deacetylation of Ppargamma. *Cell* **150**: 620-632.

Qiao X, Chen X, Wu D, Ding R, Wang J, Hong Q, Shi S, Li J, Xie Y, Lu Y, Wang Z. 2005. Mitochondrial pathway is responsible for aging-related increase of tubular cell apoptosis in renal ischemia/reperfusion injury. *J Gerontol A Biol Sci Med Sci* **60**: 830-839.

Queisser N, Oteiza PI, Stopper H, Oli RG, Schupp N. 2011. Aldosterone induces oxidative stress, oxidative DNA damage and NF-kappaB-activation in kidney tubule cells. *Mol Carcinog* **50**: 123-135.

Quiroz Y, Ferrebuz A, Vaziri ND, Rodriguez-Iturbe B. 2009. Effect of chronic antioxidant therapy with superoxide dismutase-mimetic drug, tempol, on progression of renal disease in rats with renal mass reduction. *Nephron Exp Nephrol* **112**: e31-42.

Radak Z, Asano K, Inoue M, Kizaki T, Oh-Ishi S, Suzuki K, Taniguchi N, Ohno H. 1996. Superoxide dismutase derivative prevents oxidative damage in liver and kidney of rats induced by exhausting exercise. *Eur J Appl Physiol Occup Physiol* **72**: 189-194.

Radak Z, Chung HY, Goto S. 2008. Systemic adaptation to oxidative challenge induced by regular exercise. *Free Radic Biol Med* **44**: 153-159.

Radak Z, Chung HY, Naito H, Takahashi R, Jung KJ, Kim HJ, Goto S. 2004. Age-associated increase in oxidative stress and nuclear factor kappaB activation are attenuated in rat liver by regular exercise. *FASEB J* **18**: 749-750.

Radak Z, Taylor AW, Ohno H, Goto S. 2001. Adaptation to exercise-induced oxidative stress: from muscle to brain. *Exerc Immunol Rev* **7**: 90-107.

Radak Z, Zhao Z, Koltai E, Ohno H, Atalay M. 2013. Oxygen consumption and usage during physical exercise: the balance between oxidative stress and ROS-dependent adaptive signaling. *Antioxid Redox Signal* **18**: 1208-1246.

Radhakrishnan J, Remuzzi G, Saran R, Williams DE, Rios-Burrows N, Powe N, Bruck K, Wanner C, Stel VS, Venuthurupalli SK, Hoy WE, Healy HG, Salisbury A, Fassett RG, O'Donoghue D, Roderick P, Matsuo S, Hishida A, Imai E, Iimuro S. 2014. Taming the chronic kidney disease epidemic: a global view of surveillance efforts. *Kidney Int* **86**: 246-250.

Raha S, McEachern GE, Myint AT, Robinson BH. 2000. Superoxides from mitochondrial complex III: the role of manganese superoxide dismutase. *Free Radic Biol Med* **29**: 170-180.

Rao RK, Clayton LW. 2002. Regulation of protein phosphatase 2A by hydrogen peroxide and glutathionylation. *Biochem Biophys Res Commun* **293**: 610-616.

Rasbach KA, Schnellmann RG. 2007. Signaling of mitochondrial biogenesis following oxidant injury. *J Biol Chem* **282**: 2355-2362.

Raveh O, Pinchuk I, Schnitzer E, Fainaru M, Schaffer Z, Lichtenberg D. 2000. Kinetic analysis of copper-induced peroxidation of HDL, autoaccelerated and tocopherol-mediated peroxidation. *Free Radic Biol Med* **29**: 131-146.

Reiniger N, Lau K, McCalla D, Eby B, Cheng B, Lu Y, Qu W, Quadri N, Ananthakrishnan R, Furmansky M, Rosario R, Song F, Rai V, Weinberg A, Friedman R, Ramasamy R, D'Agati V, Schmidt AM. 2010. Deletion of the receptor for advanced glycation end products reduces glomerulosclerosis and preserves renal function in the diabetic OVE26 mouse. *Diabetes* **59**: 2043-2054.

Reisman SA, Chertow GM, Hebbar S, Vaziri ND, Ward KW, Meyer CJ. 2012. Bardoxolone methyl decreases megalin and activates nrf2 in the kidney. *J Am Soc Nephrol* **23**: 1663-1673.

Renke M, Tylicki L, Rutkowski P, Larczynski W, Aleksandrowicz E, Lysiak-Szydlowska W, Rutkowski B. 2008. The effect of N-acetylcysteine on proteinuria and markers of tubular injury in

non-diabetic patients with chronic kidney disease. A placebo-controlled, randomized, open, cross-over study. *Kidney Blood Press Res* **31**: 404-410.

Ribeiro G, Roehrs M, Bairros A, Moro A, Charao M, Araujo F, Valentini J, Arbo M, Brucker N, Moresco R, Leal M, Morsch V, Garcia SC. 2011. N-acetylcysteine on oxidative damage in diabetic rats. *Drug Chem Toxicol* **34**: 467-474.

Rice-Evans C, Miller NJ. 1994. Total antioxidant status in plasma and body fluids. *Methods Enzymol* **234**: 279-293.

Rieg T, Vallon V. 2009. ATP and adenosine in the local regulation of water transport and homeostasis by the kidney. *Am J Physiol Regul Integr Comp Physiol* **296**: R419-427.

Riegersperger M, Covic A, Goldsmith D. 2011. Allopurinol, uric acid, and oxidative stress in cardiorenal disease. *Int Urol Nephrol* **43**: 441-449.

Ristow M, Zarse K, Oberbach A, Kloting N, Birringer M, Kiehntopf M, Stumvoll M, Kahn CR, Bluher M. 2009. Antioxidants prevent health-promoting effects of physical exercise in humans. *Proc Natl Acad Sci U S A* **106**: 8665-8670.

Roberts LJ, 2nd, Morrow JD. 2002. Products of the isoprostane pathway: unique bioactive compounds and markers of lipid peroxidation. *Cell Mol Life Sci* **59**: 808-820.

Rodgers JT, Lerin C, Haas W, Gygi SP, Spiegelman BM, Puigserver P. 2005. Nutrient control of glucose homeostasis through a complex of PGC-1alpha and SIRT1. *Nature* **434**: 113-118.

Rodriguez-Cuenca S, Cocheme HM, Logan A, Abakumova I, Prime TA, Rose C, Vidal-Puig A, Smith AC, Rubinsztein DC, Fearnley IM, Jones BA, Pope S, Heales SJ, Lam BY, Neogi SG, McFarlane I, James AM, Smith RA, Murphy MP. 2010. Consequences of long-term oral administration of the mitochondria-targeted antioxidant MitoQ to wild-type mice. *Free Radic Biol Med* **48**: 161-172.

Rodriguez-Iturbe B, Johnson RJ, Herrera-Acosta J. 2005. Tubulointerstitial damage and progression of renal failure. *Kidney Int Suppl*: S82-86.

Roller RE, Renner W, Dorr A, Pilger E, Schnedl WJ. 2001. Oxidative stress and increase of vascular endothelial growth factor in plasma of patients with peripheral arterial occlusive disease. *Thromb Haemost* **85**: 368.

Ronco C, McCullough P, Anker SD, Anand I, Aspromonte N, Bagshaw SM, Bellomo R, Berl T, Bobek I, Cruz DN, Daliento L, Davenport A, Haapio M, Hillege H, House AA, Katz N, Maisel A, Mankad S, Zanco P, Mebazaa A, Palazzuoli A, Ronco F, Shaw A, Sheinfeld G, Soni S, Vescovo G, Zamperetti N, Ponikowski P. 2010. Cardio-renal syndromes: report from the consensus conference of the acute dialysis quality initiative. *Eur Heart J* **31**: 703-711.

Rubattu S, Mennuni S, Testa M, Mennuni M, Pierelli G, Pagliaro B, Gabriele E, Coluccia R, Autore C, Volpe M. 2013. Pathogenesis of chronic cardiorenal syndrome: is there a role for oxidative stress? *Int J Mol Sci* **14**: 23011-23032.

Rushmore TH, Morton MR, Pickett CB. 1991. The antioxidant responsive element. Activation by oxidative stress and identification of the DNA consensus sequence required for functional activity. *J Biol Chem* **266**: 11632-11639.

Ryan MJ, Johnson G, Kirk J, Fuerstenberg SM, Zager RA, Torok-Storb B. 1994. HK-2: an immortalized proximal tubule epithelial cell line from normal adult human kidney. *Kidney Int* **45**: 48-57.

Ryoo IG, Ha H, Kwak MK. 2014. Inhibitory role of the KEAP1-NRF2 pathway in TGFbeta1-stimulated renal epithelial transition to fibroblastic cells: a modulatory effect on SMAD signaling. *PLoS One* **9**: e93265.

Ryu SW, Woo JH, Kim YH, Lee YS, Park JW, Bae YS. 2006. Downregulation of protein kinase CKII is associated with cellular senescence. *FEBS Lett* **580**: 988-994.

Sachdeva MM, Cano M, Handa JT. 2014. Nrf2 signaling is impaired in the aging RPE given an oxidative insult. *Exp Eye Res* **119**: 111-114.

Sadi G, Bozan D, Yildiz HB. 2014. Redox regulation of antioxidant enzymes: post-translational modulation of catalase and glutathione peroxidase activity by resveratrol in diabetic rat liver. *Mol Cell Biochem* **393**: 111-122.

Saha PK, Reddy VT, Konopleva M, Andreeff M, Chan L. 2010. The triterpenoid 2-cyano-3,12-dioxooleana-1,9-dien-28-oic-acid methyl ester has potent anti-diabetic effects in diet-induced diabetic mice and Lepr(db/db) mice. *J Biol Chem* **285**: 40581-40592.

Sakamaki I, Inai K, Tsutani Y, Ueda T, Tsutani H. 2008. Binding of monosodium urate crystals with idiotype protein efficiently promote dendritic cells to induce cytotoxic T cells. *Cancer Sci* **99**: 2268-2273.

Sakellariou GK, Jackson MJ, Vasilaki A. 2014. Redefining the major contributors to superoxide production in contracting skeletal muscle. The role of NAD(P)H oxidases. *Free Radic Res* **48**: 12-29.

Sanchez-Lozada LG, Soto V, Tapia E, Avila-Casado C, Sautin YY, Nakagawa T, Franco M, Rodriguez-Iturbe B, Johnson RJ. 2008. Role of oxidative stress in the renal abnormalities induced by experimental hyperuricemia. *Am J Physiol Renal Physiol* **295**: F1134-1141.

Sanchez WY, Obispo C, Ryan E, Grice JE, Roberts MS. 2013. Changes in the redox state and endogenous fluorescence of in vivo human skin due to intrinsic and photo-aging, measured by multiphoton tomography with fluorescence lifetime imaging. *J Biomed Opt* **18**: 061217.

Sanchez WY, Prow TW, Sanchez WH, Grice JE, Roberts MS. 2010. Analysis of the metabolic deterioration of ex vivo skin from ischemic necrosis through the imaging of intracellular NAD(P)H by multiphoton tomography and fluorescence lifetime imaging microscopy. *J Biomed Opt* **15**: 046008.

Sanders SA, Eisenthal R, Harrison R. 1997. NADH oxidase activity of human xanthine oxidoreductase--generation of superoxide anion. *Eur J Biochem* **245**: 541-548.

Santana-Santos E, Gowdak LH, Gaiotto FA, Puig LB, Hajjar LA, Zeferino SP, Drager LF, Shimizu MH, Bortolotto LA, De LJJ. 2014. High dose of N-acetylcystein prevents acute kidney injury in chronic kidney disease patients undergoing myocardial revascularization. *Ann Thorac Surg* **97**: 1617-1623.

Sanz AB, Sanchez-Nino MD, Ramos AM, Moreno JA, Santamaria B, Ruiz-Ortega M, Egido J, Ortiz A. 2010. NF-kappaB in renal inflammation. *J Am Soc Nephrol* **21**: 1254-1262.

Sanz AB, Santamaria B, Ruiz-Ortega M, Egido J, Ortiz A. 2008. Mechanisms of renal apoptosis in health and disease. *J Am Soc Nephrol* **19**: 1634-1642.

Saran R, Hedgeman E, Huseini M, Stack A, Shahinian V. 2010. Surveillance of chronic kidney disease around the world: tracking and reining in a global problem. *Adv Chronic Kidney Dis* **17**: 271-281.

Sattelmair J, Pertman J, Ding EL, Kohl HW, 3rd, Haskell W, Lee IM. 2011. Dose response between physical activity and risk of coronary heart disease: a meta-analysis. *Circulation* **124**: 789-795.

Savickiene J, Treigyte G, Pivoriunas A, Navakauskiene R, Magnusson KE. 2004. Sp1 and NF-kappaB transcription factor activity in the regulation of the p21 and FasL promoters during promyelocytic leukemia cell monocytic differentiation and its associated apoptosis. *Ann N Y Acad Sci* **1030**: 569-577.

Schaaf GJ, Maas RF, de Groene EM, Fink-Gremmels J. 2002. Management of oxidative stress by heme oxygenase-1 in cisplatin-induced toxicity in renal tubular cells. *Free Radic Res* **36**: 835-843.

Sedighi O, Zargari M, Varshi G. 2014. Effect of selenium supplementation on glutathione peroxidase enzyme activity in patients with chronic kidney disease: a randomized clinical trial. *Nephrourol Mon* **6**: e17945.

Seguro AC, Poli dFLF, Shimizu MH. 2012. N-acetylcysteine (NAC) protects against acute kidney injury (AKI) following prolonged pneumoperitoneum in the rat. *J Surg Res* **175**: 312-315.

Sekhar KR, Rachakonda G, Freeman ML. 2010. Cysteine-based regulation of the CUL3 adaptor protein Keap1. *Toxicol Appl Pharmacol* **244**: 21-26.

Sen CK, Khanna S, Roy S, Packer L. 2000. Molecular basis of vitamin E action. Tocotrienol potently inhibits glutamate-induced pp60(c-Src) kinase activation and death of HT4 neuronal cells. *J Biol Chem* **275**: 13049-13055.

Serbinova E, Kagan V, Han D, Packer L. 1991. Free radical recycling and intramembrane mobility in the antioxidant properties of alpha-tocopherol and alpha-tocotrienol. *Free Radic Biol Med* **10**: 263-275.

Shan Y, Zhang Q, Liu Z, Hu X, Liu D. 2010. Prevalence and risk factors associated with chronic kidney disease in adults over 40 years: a population study from Central China. *Nephrology (Carlton)* **15**: 354-361.

Shao D, Liu J, Ni J, Wang Z, Shen Y, Zhou L, Huang Y, Wang J, Xue H, Zhang W, Lu L. 2013. Suppression of XBP1S mediates high glucose-induced oxidative stress and extracellular matrix synthesis in renal mesangial cell and kidney of diabetic rats. *PLoS One* **8**: e56124.

Sharfuddin AA, Molitoris BA. 2011. Pathophysiology of ischemic acute kidney injury. *Nat Rev Nephrol* **7**: 189-200.

Shelmadine B, Bowden RG, Wilson RL, Beavers D, Hartman J. 2009. The effects of lowering uric acid levels using allopurinol on markers of metabolic syndrome in end-stage renal disease patients: a pilot study. *Anadolu Kardiyol Derg* **9**: 385-389.

Shelton LM, Park BK, Copple IM. 2013. Role of Nrf2 in protection against acute kidney injury. *Kidney Int* **84**: 1090-1095.

Shimizu M, Yamashita D, Yamaguchi T, Hirose F, Osumi T. 2006. Aspects of the regulatory mechanisms of PPAR functions: analysis of a bidirectional response element and regulation by sumoylation. *Mol Cell Biochem* **286**: 33-42.

Shing CM, Adams MJ, Fassett RG, Coombes JS. 2011. Nutritional compounds influence tissue factor expression and inflammation of chronic kidney disease patients in vitro. *Nutrition* **27**: 967-972.

Shukla S, Gupta S. 2006. Molecular targets for apigenin-induced cell cycle arrest and apoptosis in prostate cancer cell xenograft. *Mol Cancer Ther* **5**: 843-852.

Sies H, 1985. Oxidative stress: introductory remarks. 1-8. Academic Press, London.

Sies H, Cadenas E. 1985. Oxidative stress: damage to intact cells and organs. *Philos Trans R Soc Lond B Biol Sci* **311**: 617-631.

Sim AS, Salonikas C, Naidoo D, Wilcken DE. 2003. Improved method for plasma malondialdehyde measurement by high-performance liquid chromatography using methyl malondialdehyde as an internal standard. *J Chromatogr B Analyt Technol Biomed Life Sci* **785**: 337-344.

Simmons EM, Langone A, Sezer MT, Vella JP, Recupero P, Morrow JD, Ikizler TA, Himmelfarb J. 2005. Effect of renal transplantation on biomarkers of inflammation and oxidative stress in end-stage renal disease patients. *Transplantation* **79**: 914-919.

Singh DK, Winocour P, Farrington K. 2011. Oxidative stress in early diabetic nephropathy: fueling the fire. *Nat Rev Endocrinol* **7**: 176-184.

Skala MC, Riching KM, Bird DK, Gendron-Fitzpatrick A, Eickhoff J, Eliceiri KW, Keely PJ, Ramanujam N. 2007a. In vivo multiphoton fluorescence lifetime imaging of protein-bound and free nicotinamide adenine dinucleotide in normal and precancerous epithelia. *J Biomed Opt* **12**: 024014.

Skala MC, Riching KM, Gendron-Fitzpatrick A, Eickhoff J, Eliceiri KW, White JG, Ramanujam N. 2007b. In vivo multiphoton microscopy of NADH and FAD redox states, fluorescence lifetimes, and cellular morphology in precancerous epithelia. *Proc Natl Acad Sci U S A* **104**: 19494-19499.

Small DM, Bennett NC, Roy S, Gabrielli BG, Johnson DW, Gobe GC. 2012a. Oxidative Stress and Cell Senescence Combine to Cause Maximal Renal Tubular Epithelial Cell Dysfunction and Loss in an in vitro Model of Kidney Disease. *Nephron Exp Nephrol* **122**: 123-130.

Small DM, Coombes JS, Bennett N, Johnson DW, Gobe GC. 2012b. Oxidative stress, anti-oxidant therapies and chronic kidney disease. *Nephrology (Carlton)* **17**: 311-321.

Small DM, Gobe GC. 2012. Cytochrome c: potential as a noninvasive biomarker of drug-induced acute kidney injury. *Expert Opin Drug Metab Toxicol* **8**: 655-664.

Small DM, Morais C, Coombes JS, Bennett NC, Johnson DW, Gobe GC. 2014a. Oxidative Stress-Induced Alterations in PPARgamma and Associated Mitochondrial Destabilisation Contribute to Kidney Cell Apoptosis. *Am J Physiol Renal Physiol* **307**: F814-822.

Small DM, Sanchez WY, Roy S, Hickey MJ, Gobe GC. 2014b. Multiphoton fluorescence microscopy of the live kidney in health and disease. *J Biomed Opt* **19**: 020901.

Snow BJ, Rolfe FL, Lockhart MM, Frampton CM, O'Sullivan JD, Fung V, Smith RA, Murphy MP, Taylor KM. 2010. A double-blind, placebo-controlled study to assess the mitochondria-targeted antioxidant MitoQ as a disease-modifying therapy in Parkinson's disease. *Mov Disord* **25**: 1670-1674.

Soderdahl T, Enoksson M, Lundberg M, Holmgren A, Ottersen OP, Orrenius S, Bolcsfoldi G, Cotgreave IA. 2003. Visualization of the compartmentalization of glutathione and protein-glutathione mixed disulfides in cultured cells. *FASEB J* **17**: 124-126.

Sohal RS, Kamzalov S, Sumien N, Ferguson M, Rebrin I, Heinrich KR, Forster MJ. 2006. Effect of coenzyme Q10 intake on endogenous coenzyme Q content, mitochondrial electron transport chain, antioxidative defenses, and life span of mice. *Free Radic Biol Med* **40**: 480-487.

Soubannier V, McBride HM. 2009. Positioning mitochondrial plasticity within cellular signaling cascades. *Biochim Biophys Acta* **1793**: 154-170.

Spapen HD, Diltoer MW, Nguyen DN, Hendrickx I, Huyghens LP. 2005. Effects of N-acetylcysteine on microalbuminuria and organ failure in acute severe sepsis: results of a pilot study. *Chest* **127**: 1413-1419.

Sperling RI, Benincaso AI, Knoell CT, Larkin JK, Austen KF, Robinson DR. 1993. Dietary omega-3 polyunsaturated fatty acids inhibit phosphoinositide formation and chemotaxis in neutrophils. *J Clin Invest* **91**: 651-660.

St-Pierre J, Buckingham JA, Roebuck SJ, Brand MD. 2002. Topology of superoxide production from different sites in the mitochondrial electron transport chain. *J Biol Chem* **277**: 44784-44790.

Stadtman ER, Levine RL. 2003. Free radical-mediated oxidation of free amino acids and amino acid residues in proteins. *Amino Acids* **25**: 207-218.

Stanton RC. 2011. Oxidative stress and diabetic kidney disease. *Curr Diab Rep* **11**: 330-336.

Stec DE, Drummond HA, Gousette MU, Storm MV, Abraham NG, Csongradi E. 2012. Expression of heme oxygenase-1 in thick ascending loop of henle attenuates angiotensin II-dependent hypertension. *J Am Soc Nephrol* **23**: 834-841.

Stein GH, Drullinger LF, Soulard A, Dulic V. 1999. Differential roles for cyclin-dependent kinase inhibitors p21 and p16 in the mechanisms of senescence and differentiation in human fibroblasts. *Mol Cell Biol* **19**: 2109-2117.

Stenvinkel P, Larsson TE. 2013. Chronic Kidney Disease: A Clinical Model of Premature Aging. *Am J Kidney Dis* **62**: 339-351.

Stincone A, Prigione A, Cramer T, Wamelink MM, Campbell K, Cheung E, Olin-Sandoval V, Gruening NM, Krueger A, Tauqeer AM, Keller MA, Breitenbach M, Brindle KM, Rabinowitz JD, Ralser M. 2014. The return of metabolism: biochemistry and physiology of the pentose phosphate pathway. *Biol Rev Camb Philos Soc* **Epub ahead of print**.

Stoyanovsky DA, Osipov AN, Quinn PJ, Kagan VE. 1995. Ubiquinone-dependent recycling of vitamin E radicals by superoxide. *Arch Biochem Biophys* **323**: 343-351.

Stratta P, Segoloni GP, Canavese C, Muzio G, Dogliani M, Serra A, Allemandi P, Salomone M, Caramellino C, Canuto R. 1994. Oxygen free radicals are not the main factor in experimental gentamicin nephrotoxicity. *Ren Fail* **16**: 445-455.

Strobel NA, Fassett RG, Marsh SA, Coombes JS. 2011. Importance of understanding pre-analytical variability in biomarker development. *Int J Cardiol* **150**: 223-224.

Sturtz LA, Diekert K, Jensen LT, Lill R, Culotta VC. 2001. A fraction of yeast Cu,Zn-superoxide dismutase and its metallochaperone, CCS, localize to the intermembrane space of mitochondria. A physiological role for SOD1 in guarding against mitochondrial oxidative damage. *J Biol Chem* **276**: 38084-38089.

Sun Y, Zhang J, Zhang JQ, Ramires FJ. 2000. Local angiotensin II and transforming growth factor-beta1 in renal fibrosis of rats. *Hypertension* **35**: 1078-1084.

Swartz HM, Khan N, Khramtsov VV. 2007. Use of electron paramagnetic resonance spectroscopy to evaluate the redox state in vivo. *Antioxid Redox Signal* **9**: 1757-1771.

Tan X, Zhang L, Jiang Y, Yang Y, Zhang W, Li Y, Zhang X. 2013. Postconditioning ameliorates mitochondrial DNA damage and deletion after renal ischemic injury. *Nephrol Dial Transplant* **28**: 2754-2765.

Tang SC, Chan LY, Leung JC, Cheng AS, Lin M, Lan HY, Lai KN. 2011. Differential effects of advanced glycation end-products on renal tubular cell inflammation. *Nephrology (Carlton)* **16**: 417-425.

Tayek JA, Kalantar-Zadeh K. 2013. The extinguished BEACON of bardoxolone: not a Monday morning quarterback story. *Am J Nephrol* **37**: 208-211.

Terrier-Lenglet A, Nollet A, Liabeuf S, Barreto DV, Brazier M, Lemke HD, Vanholder R, Choukroun G, Massy ZA. 2011. Plasma malondialdehyde may not predict mortality in patient with chronic kidney disease. *Nephrol Ther* **7**: 219-224.

Thorling CA, Liu X, Burczynski FJ, Fletcher LM, Gobe GC, Roberts MS. 2011. Multiphoton microscopy can visualize zonal damage and decreased cellular metabolic activity in hepatic ischemia-reperfusion injury in rats. *J Biomed Opt* **16**: 116011.

Thorling CA, Liu X, Burczynski FJ, Fletcher LM, Roberts MS, Sanchez WY. 2013. Intravital multiphoton microscopy can model uptake and excretion of fluorescein in hepatic ischemia-reperfusion injury. *J Biomed Opt* **18**: 101306.

Tontonoz P, Hu E, Graves RA, Budavari AI, Spiegelman BM. 1994. mPPAR gamma 2: tissue-specific regulator of an adipocyte enhancer. *Genes Dev* **8**: 1224-1234.

Tontonoz P, Spiegelman BM. 2008. Fat and beyond: the diverse biology of PPARgamma. *Annu Rev Biochem* **77**: 289-312.

Tribble DL, Jones DP. 1990. Oxygen dependence of oxidative stress. Rate of NADPH supply for maintaining the GSH pool during hypoxia. *Biochem Pharmacol* **39**: 729-736.

Tucker PS, Dalbo VJ, Han T, Kingsley MI. 2013. Clinical and research markers of oxidative stress in chronic kidney disease. *Biomarkers* **18**: 103-115.

Tumur Z, Shimizu H, Enomoto A, Miyazaki H, Niwa T. 2010. Indoxyl sulfate upregulates expression of ICAM-1 and MCP-1 by oxidative stress-induced NF-kappaB activation. *Am J Nephrol* **31**: 435-441.

Turrens JF. 2003. Mitochondrial formation of reactive oxygen species. *J Physiol* **552**: 335-344.

Turrens JF, Alexandre A, Lehninger AL. 1985. Ubisemiquinone is the electron donor for superoxide formation by complex III of heart mitochondria. *Arch Biochem Biophys* **237**: 408-414.

Turrens JF, Boveris A. 1980. Generation of superoxide anion by the NADH dehydrogenase of bovine heart mitochondria. *Biochem J* **191**: 421-427.

van der Horst A, Burgering BM. 2007. Stressing the role of FoxO proteins in lifespan and disease. *Nat Rev Mol Cell Biol* **8**: 440-450.

Vay L, Hernandez-SanMiguel E, Lobaton CD, Moreno A, Montero M, Alvarez J. 2009. Mitochondrial free [Ca2+] levels and the permeability transition. *Cell Calcium* **45**: 243-250.

Velayutham PK, Adhikary SD, Babu SK, Vedantam R, Korula G, Ramachandran A. 2013. Oxidative stress-associated hypertension in surgically induced brain injury patients: effects of beta-blocker and angiotensin-converting enzyme inhibitor. *J Surg Res* **179**: 125-131.

Venkatachalam MA, Bernard DB, Donohoe JF, Levinsky NG. 1978. Ischemic damage and repair in the rat proximal tubule: differences among the S1, S2, and S3 segments. *Kidney Int* **14**: 31-49.

Vesey DA, Cheung C, Pat B, Endre Z, Gobé G, Johnson DW. 2004. Erythropoietin protects against ischaemic acute renal injury. *Nephrol Dial Transplant* **19**: 348-355.

Vesey DA, Qi W, Chen X, Pollock CA, Johnson DW. 2009. Isolation and primary culture of human proximal tubule cells. *Methods Mol Biol* **466**: 19-24.

Vina J, Gomez-Cabrera MC, Lloret A, Marquez R, Minana JB, Pallardo FV, Sastre J. 2000. Free radicals in exhaustive physical exercise: mechanism of production, and protection by antioxidants. *IUBMB Life* **50**: 271-277.

Visarius TM, Putt DA, Schare JM, Pegouske DM, Lash LH. 1996. Pathways of glutathione metabolism and transport in isolated proximal tubular cells from rat kidney. *Biochem Pharmacol* **52**: 259-272.

Vlassara H, Brownlee M, Manogue KR, Dinarello CA, Pasagian A. 1988. Cachectin/TNF and IL-1 induced by glucose-modified proteins: role in normal tissue remodeling. *Science* **240**: 1546-1548.

Vogetseder A, Picard N, Gaspert A, Walch M, Kaissling B, Le Hir M. 2008a. Proliferation capacity of the renal proximal tubule involves the bulk of differentiated epithelial cells. *Am J Physiol Cell Physiol* **294**: C22-28.

Vogetseder A, Picard N, Gaspert A, Walch M, Kaissling B, Le HM. 2008b. Proliferation capacity of the renal proximal tubule involves the bulk of differentiated epithelial cells. *Am J Physiol Cell Physiol* **294**: C22-28.

Volonte D, Zhang K, Lisanti MP, Galbiati F. 2002. Expression of caveolin-1 induces premature cellular senescence in primary cultures of murine fibroblasts. *Mol Biol Cell* **13**: 2502-2517.

Vostalova J, Galandakova A, Svobodova AR, Orolinova E, Kajabova M, Schneiderka P, Zapletalova J, Strebl P, Zadrazil J. 2012. Time-course evaluation of oxidative stress-related biomarkers after renal transplantation. *Ren Fail* **34**: 413-419.

Wakabayashi N, Itoh K, Wakabayashi J, Motohashi H, Noda S, Takahashi S, Imakado S, Kotsuji T, Otsuka F, Roop DR, Harada T, Engel JD, Yamamoto M. 2003. Keap1-null mutation leads to postnatal lethality due to constitutive Nrf2 activation. *Nat Genet* **35**: 238-245.

Walsh J, Jenkins RE, Wong M, Olayanju A, Powell H, Copple I, O'Neill PM, Goldring CE, Kitteringham NR, Park BK. 2014. Identification and quantification of the basal and inducible Nrf2-dependent proteomes in mouse liver: Biochemical, pharmacological and toxicological implications. *J Proteomics* **108**: 171-187.

Wang F, Nguyen M, Qin FX, Tong Q. 2007. SIRT2 deacetylates FOXO3a in response to oxidative stress and caloric restriction. *Aging Cell* **6**: 505-514.

Wang HW, Gukassyan V, Chen CT, Wei YH, Guo HW, Yu JS, Kao FJ. 2008. Differentiation of apoptosis from necrosis by dynamic changes of reduced nicotinamide adenine dinucleotide fluorescence lifetime in live cells. *J Biomed Opt* **13**: 054011.

Wang X, Dai Y, Ding Z, Khaidakov M, Mercanti F, Mehta JL. 2013a. Regulation of autophagy and apoptosis in response to angiotensin II in HL-1 cardiomyocytes. *Biochem Biophys Res Commun* **440**: 696-700.

Wang X, McLennan SV, Twigg SM. 2011. CCN-2 is up-regulated by and mediates effects of matrix bound advanced glycated end-products in human renal mesangial cells. *J Cell Commun Signal* **5**: 193-200.

Wang XQ, Gabrielli BG, Milligan A, Dickinson JL, Antalis TM, Ellem KA. 1996. Accumulation of p16CDKN2A in response to ultraviolet irradiation correlates with late S-G(2)-phase cell cycle delay. *Cancer Res* **56**: 2510-2514.

Wang YL, Shu KH, Yang MF, Yang WC, Wu MJ, Lin TM, Chen CH. 2013b. The impact of body weight management in chronic kidney disease patients with obesity. *J Ren Nutr* **23**: 372-379.

Weinberg JM. 2011. Mitochondrial biogenesis in kidney disease. *J Am Soc Nephrol* **22**: 431-436.

Werner E, Werb Z. 2002. Integrins engage mitochondrial function for signal transduction by a mechanism dependent on Rho GTPases. *J Cell Biol* **158**: 357-368.

Wheeler CR, Salzman JA, Elsayed NM, Omaye ST, Korte DW, Jr. 1990. Automated assays for superoxide dismutase, catalase, glutathione peroxidase, and glutathione reductase activity. *Anal Biochem* **184**: 193-199.

White S, Chadban S. 2014. Diabetic Kidney Disease in Australia: Current Burden and Future Projections. *Nephrology (Carlton)* **19**: 450-458.

Whiteside C, Wang H, Xia L, Munk S, Goldberg HJ, Fantus IG. 2009. Rosiglitazone prevents high glucose-induced vascular endothelial growth factor and collagen IV expression in cultured mesangial cells. *Exp Diabetes Res* **2009**: 910783.

Wilkinson-Berka JL, Kelly DJ, Koerner SM, Jaworski K, Davis B, Thallas V, Cooper ME. 2002. ALT-946 and aminoguanidine, inhibitors of advanced glycation, improve severe nephropathy in the diabetic transgenic (mREN-2)27 rat. *Diabetes* **51**: 3283-3289.

Wilund KR, Tomayko EJ, Wu PT, Ryong CH, Vallurupalli S, Lakshminarayanan B, Fernhall B. 2010. Intradialytic exercise training reduces oxidative stress and epicardial fat: a pilot study. *Nephrol Dial Tranplant* **25**: 2695-2701.

Wiswedel I, Gardemann A, Storch A, Peter D, Schild L. 2010. Degradation of phospholipids by oxidative stress--exceptional significance of cardiolipin. *Free Radic Res* **44**: 135-145.

Witko-Sarsat V, Friedlander M, Capeillere-Blandin C, Nguyen-Khoa T, Nguyen AT, Zingraff J, Jungers P, Descamps-Latscha B. 1996. Advanced oxidation protein products as a novel marker of oxidative stress in uremia. *Kidney Int* **49**: 1304-1313.

Witko-Sarsat V, Friedlander M, Nguyen Khoa T, Capeillere-Blandin C, Nguyen AT, Canteloup S, Dayer JM, Jungers P, Drueke T, Descamps-Latscha B. 1998. Advanced oxidation protein products as novel mediators of inflammation and monocyte activation in chronic renal failure. *J Immunol* **161**: 2524-2532.

Witzgall R, Brown D, Schwarz C, Bonventre JV. 1994. Localization of proliferating cell nuclear antigen, vimentin, c-Fos, and clusterin in the postischemic kidney. Evidence for a heterogenous genetic response among nephron segments, and a large pool of mitotically active and dedifferentiated cells. *J Clin Invest* **93**: 2175-2188.

Wongmekiat O, Thamprasert K, Lumlertgul D. 2007. Renoprotective effect of trolox against ischaemia-reperfusion injury in rats. *Clin Exp Pharmacol Physiol* **34**: 753-759.

Woodman RJ, Mori TA, Burke V, Puddey IB, Watts GF, Beilin LJ. 2002. Effects of purified eicosapentaenoic and docosahexaenoic acids on glycemic control, blood pressure, and serum lipids in type 2 diabetic patients with treated hypertension. *Am J Clin Nutr* **76**: 1007-1015.

Wu JS, Lin TN, Wu KK. 2009. Rosiglitazone and PPAR-gamma overexpression protect mitochondrial membrane potential and prevent apoptosis by upregulating anti-apoptotic Bcl-2 family proteins. *J Cell Physiol* **220**: 58-71.

Wu QQ, Wang Y, Senitko M, Meyer C, Wigley WC, Ferguson DA, Grossman E, Chen J, Zhou XJ, Hartono J, Winterberg P, Chen B, Agarwal A, Lu CY. 2011. Bardoxolone methyl (BARD) ameliorates ischemic AKI and increases expression of protective genes Nrf2, PPARgamma, and HO-1. *Am J Physiol Renal Physiol* **300**: F1180-1192.

Xu Y, Ruan S, Wu X, Chen H, Zheng K, Fu B. 2013. Autophagy and apoptosis in tubular cells following unilateral ureteral obstruction are associated with mitochondrial oxidative stress. *Int J Mol Med* **31**: 628-636.

Yamamoto K, Wilson DR, Baumal R. 1984a. Blood supply and drainage of the outer medulla of the rat kidney: scanning electron microscopy of microvascular casts. *Anat Rec* **210**: 273-277.

Yamamoto K, Wilson DR, Baumal R. 1984b. Outer medullary circulatory defect in ischemic acute renal failure. *Am J Pathol* **116**: 253-261.

Yamamoto T, Suzuki T, Kobayashi A, Wakabayashi J, Maher J, Motohashi H, Yamamoto M. 2008. Physiological significance of reactive cysteine residues of Keap1 in determining Nrf2 activity. *Mol Cell Biol* **28**: 2758-2770.

Yan SD, Schmidt AM, Anderson GM, Zhang J, Brett J, Zou YS, Pinsky D, Stern D. 1994. Enhanced cellular oxidant stress by the interaction of advanced glycation end products with their receptors/binding proteins. *J Biol Chem* **269**: 9889-9897.

Yang H, Yang T, Baur JA, Perez E, Matsui T, Carmona JJ, Lamming DW, Souza-Pinto NC, Bohr VA, Rosenzweig A, de CR, Sauve AA, Sinclair DA. 2007a. Nutrient-sensitive mitochondrial NAD+ levels dictate cell survival. *Cell* **130**: 1095-1107.

Yang HC, Deleuze S, Zuo Y, Potthoff SA, Ma LJ, Fogo AB. 2009. The PPARgamma agonist pioglitazone ameliorates aging-related progressive renal injury. *J Am Soc Nephrol* **20**: 2380-2388.

Yang HC, Liu SJ, Fogo AB. 2014. Kidney regeneration in mammals. *Nephron Exp Nephrol* **126**: 50.

Yang HC, Ma LJ, Ma J, Fogo AB. 2006. Peroxisome proliferator-activated receptor-gamma agonist is protective in podocyte injury-associated sclerosis. *Kidney Int* **69**: 1756-1764.

Yang JJ, Tao H, Huang C, Li J. 2013. Nuclear erythroid 2-related factor 2: a novel potential therapeutic target for liver fibrosis. *Food Chem Toxicol* **59**: 421-427.

Yang L, Besschetnova TY, Brooks CR, Shah JV, Bonventre JV. 2010. Epithelial cell cycle arrest in G2/M mediates kidney fibrosis after injury. *Nat Med* **16**: 535-543, 531p following 143.

Yang L, Humphreys BD, Bonventre JV. 2011. Pathophysiology of acute kidney injury to chronic kidney disease: maladaptive repair. *Contrib Nephrol* **174**: 149-155.

Yang T, Vesey DA, Johnson DW, Wei MQ, Gobe GC. 2007b. Apoptosis of tubulointerstitial chronic inflammatory cells in progressive renal fibrosis after cancer therapies. *Transl Res* **150**: 40-50.

Ye J, Li J, Yu Y, Wei Q, Deng W, Yu L. 2010. L-carnitine attenuates oxidant injury in HK-2 cells via ROS-mitochondria pathway. *Regul Pept* **161**: 58-66.

Yoshida T, Ishikawa K, Sato M. 1991. Degradation of heme by a soluble peptide of heme oxygenase obtained from rat liver microsomes by mild trypsinization. *Eur J Biochem* **199**: 729-733.

Young PA, Clendenon SG, Byars JM, Decca RS, Dunn KW. 2011a. The effects of spherical aberration on multiphoton fluorescence excitation microscopy. *J Microsc* **242**: 157-165.

Young PA, Clendenon SG, Byars JM, Dunn KW. 2011b. The effects of refractive index heterogeneity within kidney tissue on multiphoton fluorescence excitation microscopy. *J Microsc* **242**: 148-156.

Yu JS, Guo HW, Wang CH, Wei YH, Wang HW. 2011. Increase of reduced nicotinamide adenine dinucleotide fluorescence lifetime precedes mitochondrial dysfunction in staurosporine-induced apoptosis of HeLa cells. *J Biomed Opt* **16**: 036008.

Yu Y, Lee AM, Wang H, Tang S, Zhao J, Lui H, Zeng H. 2012. Imaging-guided two-photon excitation-emission-matrix measurements of human skin tissues. *J Biomed Opt* **17**: 077004.

Yurchenco PD, Schittny JC. 1990. Molecular architecture of basement membranes. *FASEB J* **4**: 1577-1590.

Zafarullah M, Li WQ, Sylvester J, Ahmad M. 2003. Molecular mechanisms of N-acetylcysteine actions. *Cell Mol Life Sci* **60**: 6-20.

Zager RA, Johnson AC, Becker K. 2012. Plasma and urinary heme oxygenase-1 in AKI. *J Am Soc Nephrol* **23**: 1048-1057.

Zhan M, Brooks C, Liu F, Sun L, Dong Z. 2013. Mitochondrial dynamics: regulatory mechanisms and emerging role in renal pathophysiology. *Kidney Int* **83**: 568-581.

Zhang B, Berger J, Zhou G, Elbrecht A, Biswas S, White-Carrington S, Szalkowski D, Moller DE. 1996. Insulin- and mitogen-activated protein kinase-mediated phosphorylation and activation of peroxisome proliferator-activated receptor gamma. *J Biol Chem* **271**: 31771-31774.

Zhang DD, Hannink M. 2003. Distinct cysteine residues in Keap1 are required for Keap1-dependent ubiquitination of Nrf2 and for stabilization of Nrf2 by chemopreventive agents and oxidative stress. *Mol Cell Biol* **23**: 8137-8151.

Zhang DD, Lo SC, Cross JV, Templeton DJ, Hannink M. 2004. Keap1 is a redox-regulated substrate adaptor protein for a Cul3-dependent ubiquitin ligase complex. *Mol Cell Biol* **24**: 10941-10953.

Zhang F, Lau SS, Monks TJ. 2011. The cytoprotective effect of N-acetyl-L-cysteine against ROS-induced cytotoxicity is independent of its ability to enhance glutathione synthesis. *Toxicol Sci* **120**: 87-97.

Zhang W, Ji W, Yang L, Xu Y, Yang J, Zhuang Z. 2010. Epigenetic enhancement of p66Shc during cellular replicative or premature senescence. *Toxicology* **278**: 189-94.

Zhao CR, Gao ZH, Qu XJ. 2010. Nrf2-ARE signaling pathway and natural products for cancer chemoprevention. *Cancer Epidemiol* **34**: 523-533.

Zheng PW, Chiang LC, Lin CC. 2005. Apigenin induced apoptosis through p53-dependent pathway in human cervical carcinoma cells. *Life Sci* **76**: 1367-1379.

Zhong Q, Terlecky SR, Lash LH. 2009. Diabetes increases susceptibility of primary cultures of rat proximal tubular cells to chemically induced injury. *Toxicol Appl Pharmacol* **241**: 1-13.

Zhu C, Huang S, Yuan Y, Ding G, Chen R, Liu B, Yang T, Zhang A. 2011. Mitochondrial dysfunction mediates aldosterone-induced podocyte damage: a therapeutic target of PPARgamma. *Am J Pathol* **178**: 2020-2031.

Zhuang S, Yan Y, Daubert RA, Han J, Schnellmann RG. 2007. ERK promotes hydrogen peroxide-induced apoptosis through caspase-3 activation and inhibition of Akt in renal epithelial cells. *Am J Physiol Renal Physiol* **292**: F440-447.

Zipfel WR, Williams RM, Christie R, Nikitin AY, Hyman BT, Webb WW. 2003. Live tissue intrinsic emission microscopy using multiphoton-excited native fluorescence and second harmonic generation. *Proc Natl Acad Sci U S A* **100**: 7075-7080.

Zoccali C, Mallamaci F. 2011. Adiponectin and leptin in chronic kidney disease: causal factors or mere risk markers? *J Ren Nutr* **21**: 87-91.

Zoellner H, Siddiqui S, Kelly E, Medbury H. 2009. The anti-apoptotic activity of albumin for endothelium is inhibited by advanced glycation end products restricting intramolecular movement. *Cell Mol Biol Lett* **14**: 575-586.

Zoja C, Corna D, Nava V, Locatelli M, Abbate M, Gaspari F, Carrara F, Sangalli F, Remuzzi G, Benigni A. 2013. Analogs of bardoxolone methyl worsen diabetic nephropathy in rats with additional adverse effects. *Am J Physiol Renal Physiol* **304**: F808-819.

Zorov DB, Juhaszova M, Sollott SJ. 2014. Mitochondrial reactive oxygen species (ROS) and ROS-induced ROS release. *Physiol Rev* **94**: 909-950.

APPENDIX A

Published Papers Incorporated into this Thesis

NEPHROLOGY

Nephrology **17** (2012) 311–321

Review Article

Oxidative stress, anti-oxidant therapies and chronic kidney disease

DAVID M SMALL,[1] JEFF S COOMBES,[2] NIGEL BENNETT,[1] DAVID W JOHNSON[1,3] and GLENDA C GOBE[1]

[1]Centre for Kidney Disease Research, School of Medicine, [2]School of Human Movement Studies, The University of Queensland, and [3]Department of Nephrology, Princess Alexandra Hospital, Woolloongabba, Brisbane, Queensland, Australia

KEY WORDS:
ageing, anti-oxidant, chronic kidney disease, mitochondria, oxidative stress.

Correspondence:
Dr Glenda Gobe, Centre for Kidney Disease Research, School of Medicine, University of Queensland, Building 33 Princess Alexandra Hospital, Woolloongabba, Brisbane, Qld 4102, Australia. Email: g.gobe@uq.edu.au

Accepted for publication 17 January 2012.
Accepted manuscript online 31 January 2012.

doi:10.1111/j.1440-1797.2012.01572.x

SUMMARY AT A GLANCE

Oxidative stress is an important mechanism of injury in chronic kidney disease. Potential pathways of oxidative stress mediating kidney injury are discussed.

ABSTRACT:

Chronic kidney disease (CKD) is a common and serious problem that adversely affects human health, limits longevity and increases costs to health-care systems worldwide. Its increasing incidence cannot be fully explained by traditional risk factors. Oxidative stress is prevalent in CKD patients and is considered to be an important pathogenic mechanism. Oxidative stress develops from an imbalance between free radical production often increased through dysfunctional mitochondria formed with increasing age, type 2 diabetes mellitus, inflammation, and reduced anti-oxidant defences. Perturbations in cellular oxidant handling influence downstream cellular signalling and, in the kidney, promote renal cell apoptosis and senescence, decreased regenerative ability of cells, and fibrosis. These factors have a stochastic deleterious effect on kidney function. The majority of studies investigating anti-oxidant treatments in CKD patients show a reduction in oxidative stress and many show improved renal function. Despite heterogeneity in the oxidative stress levels in the CKD population, there has been little effort to measure patient oxidative stress levels before the use of any anti-oxidants therapies to optimize outcome. This review describes the development of oxidative stress, how it can be measured, the involvement of mitochondrial dysfunction and the molecular pathways that are altered, the role of oxidative stress in CKD pathogenesis and an update on the amelioration of CKD using anti-oxidant therapies.

One of the key functions of the kidneys is to filter waste products that build up in the blood. Renal failure determines that waste products are not removed completely or sufficiently. This can occur quickly (acute renal failure, or acute kidney injury) often as the result of ischaemia, toxins or mechanical trauma. More often, however, the development of renal failure is gradual and insidious, with resultant chronic kidney disease (CKD). It is often many years before noticeable loss of renal function occurs. People with CKD have a high risk of death from stroke or heart attack, and CKD may also progress to total and permanent renal failure (end-stage renal disease). Dialysis or transplantation is then necessary, with loss of quality of life, decreased individual life expectancy and increased costs to health-care systems. This review article focuses mainly on patients developing CKD.

Chronic kidney disease has increasing incidence and prevalence in developed and developing nations. The kidneys show the greatest age-associated chronic pathology compared with brain, liver and heart,[1] and one in six adults over 25 years of age has some degree of CKD,[2] with incidence increasing with age. A study of almost 20 000 ethnic Chinese men and women greater than 20 years of age demonstrated that changes in renal function could predict longevity.[3] The structural characteristics of CKD include increased tubular atrophy, interstitial fibrosis, glomerulosclerosis, renal vasculopathy and reduced renal regenerative capability. These characteristics may be caused, at least in part, by the gradual loss of renal energy through development of mitochondrial dysfunction and resultant, increasing, oxidative stress.

OXIDATIVE STRESS AND NORMAL KIDNEY METABOLISM

Oxidative stress may be defined as a disturbance in regular cellular and molecular function caused by an imbalance between production of reactive species and the natural anti-oxidant ability of our cells. Reactive oxygen species (ROS) and reactive nitrogen species often act together to create a state of oxidative stress. ROS are arguably the most

Table 1 Common physiological reactive species

	Free radicals†	Non-radical‡
Reactive oxygen species	Superoxide (O_2^-)	Hydrogen peroxide (H_2O_2)
	Hydroxyl (OH^-)	Organic peroxides (R-OOH) e.g. lipid peroxides
	Peroxyl ($R\text{-}O^-$)	Hypochlorous acid (HOCl)
Reactive nitrogen species	Nitric oxide (NO)	Peroxynitrite ($ONOO^-$)
	Nitrogen dioxide (NO_2)	

†A free radical is defined as any molecule that has an unpaired electron in its outer shell. ‡A non-radical does not contain unpaired electrons but is either an oxidizing agent or is easily converted to a free radical.

Table 2 Endogenous and exogenous sources of reactive species

Endogenous factors	Exogenous factors
Mitochondrial oxidative phosphorylation	Environmental pollutants and toxins
Xanthine oxidase, NADPH oxidase	Cigarette smoke
Inflammatory cells	Hypoxia
Endosome/lysosome degradation	Hyperoxia
Angiotensin II	Radiation (sunlight, UV radiation)
Fibroblasts	Infectious microbes
Endoplasmic reticulum	High calorie diet
Peroxisomes	Glucotoxicity

important of the free radicals in biological systems. A list of the common reactive species is found in Table 1. The main ROS are superoxide (O_2^-), the hydroxyl radical (OH^-) and hydrogen peroxide (H_2O_2). Examples of the endogenous and exogenous sources of reactive species are listed in Table 2.

Estimated levels of ROS within mitochondria are 5- to 10-fold higher than other cytosolic and nuclear compartments.[4] Other contributing sites of ROS generation include the endoplasmic reticulum, peroxisomes and lysosomes. One to three per cent of inspired molecular oxygen is converted to O_2^-, which is the most common of the ROS and a powerful precursor of H_2O_2.[5] Although cellular H_2O_2 is stable, it has the potential to interact with a variety of substrates to cause damage, especially in the presence of the reduced metal ion Fe^{2+}. This leads to H_2O_2 to break down and form the most reactive and damaging of the ROS, OH^-. In healthy cells, the production of the potentially harmful H_2O_2 is countered by the catalysing actions of mitochondrial or cytosolic catalase (CAT) or thiol peroxidases into H_2O and O_2. Figure 1 demonstrates pathways to, and natural anti-oxidant neutralization of, common ROS.

Given that ROS are likely to be highly damaging molecules to cells, why have the mitochondria not evolved more efficient systems that limit mitochondrial oxidants? One possible answer is that ROS have an essential role in oxidant metabolism where they are involved in highly conserved basic physiological processes as effectors of downstream pathways. Thus, to some, oxidative stress theories of disease pathogenesis must be intrinsically flawed.[6] Nonetheless, ROS are damaging molecules. Even when they are produced during normal respiration, they could cause cumulative damage that would eventually lead to loss of cell and tissue function and, ultimately, disease. Their production is known to increase, over natural anti-oxidant levels, during progressive disease and during ageing.[4]

The kidney is highly energetic and therefore relies heavily on aerobic metabolism for the production of ATP by oxidative phosphorylation. The reduction of molecular O_2 along the electron transport chain (ETC) within mitochondria is vital for renal cellular function, yet potentially devastating long-term. The ETC consists of five multi-enzyme complexes responsible for maintaining mitochondrial membrane potential and ATP generation. Each of these complexes presents a site of ROS generation; however, complexes I and III have been identified as primary sites of O_2^- generation.[7] Complex I, also known as nicotinamide adenine dinucleotide (NADH) dehydrogenase, or NADH-CoenzymeQ (NADH-CoQ) reductase, facilitates the transfer of electrons between NADH and CoQ10 (sometimes known as ubiquinone). Defects in oxidative phosphorylation may be due to the use of substrates in the respiratory chain, such as the reduced NADH and NADH oxidase, and not due to alterations in the proteins of the respiratory complexes. Thus, it is likely that altered respiratory complexes and substrates lead to an inefficiency of electron transport, and subsequent increased ROS, decreased ATP and a loss of the mitochondrial membrane potential. Oxidatively damaged proteins of the mitochondrial complexes increase with age in mice.[8] In CKD patients (stages 2–3) and haemodialysis patients, impaired mitochondrial respiration was recorded.[9] In this latter report, Granata and colleagues used a combined strategy based on high throughput genome-based microarray and classical molecular methodologies, to investigate the mechanisms underlying alterations in cell metabolism in CKD patients. In particular, oxidative phosphorylation system components were analysed. The results demonstrated clear deregulation of the mitochondrial respiratory machinery in CKD patients, closely associated with enhanced oxidative stress. These results may help explain other reports on CKD patients that indicate a subnormal energy metabolism in this population.

NATURAL DEFENCES: ENDOGENOUS ANTI-OXIDANTS

The production of ROS is usually in balance with the availability and cellular localization of anti-oxidant enzymes and thiols, such as superoxide dismutase (SOD), CAT, glutathione peroxidase (Gpx) and glutathione (GSH) (Fig. 2). GSH synthesis is dependent on ATP but the maintenance of its reducing power is dependent on NADPH and the pentose phosphate pathway.[10] *In vivo* studies have found accumulated oxidative damage occurs from decreased levels of these endogenous anti-oxidants rather than increased ROS pro-

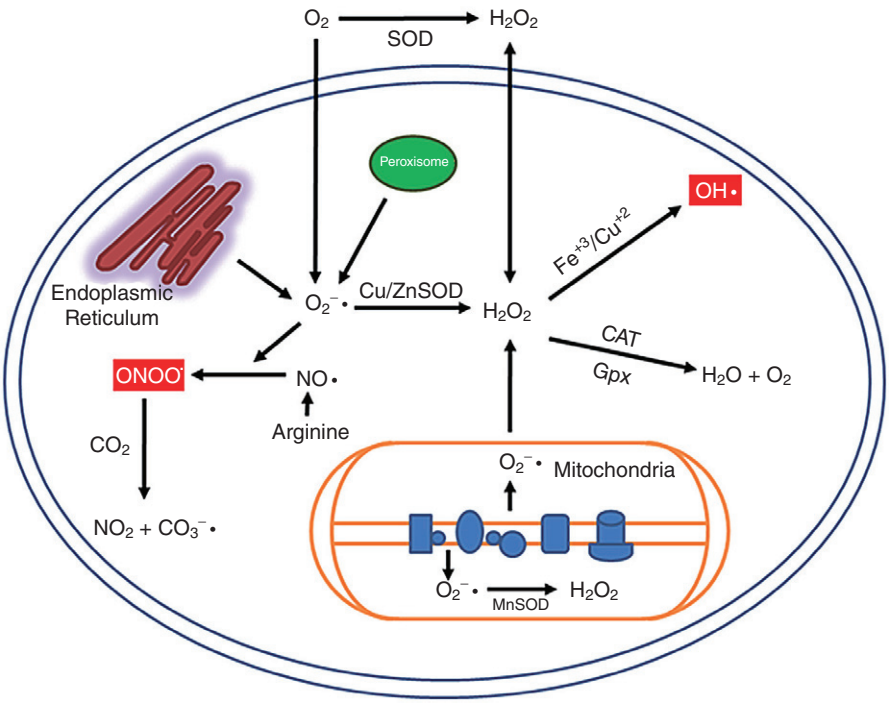

Fig. 1 Cellular sites of free radical generation and interactions. Mitochondria produce high levels of the superoxide anion (O_2^-•) as a by-product of oxidative phosphorylation. This is converted to the stable hydrogen peroxide (H_2O_2) by manganese superoxide dismutase (MnSOD). Protein assemblage by the endoplasmic reticulum and fatty acid breakdown by peroxisomes also account for O_2^-• generation, whereby conversion to H_2O_2 occurs due to copper/zinc superoxide dismutase (Cu/ZnSOD). Catalase (CAT) and glutathione peroxidase (Gpx) are able to neutralize H_2O_2 into water (H_2O) and oxygen (O_2). However, in the presence of high amounts of H_2O_2, heavy metals (Fe^{+3} or Cu^{+2}) can generate the highly reactive hydroxyl anion (OH•). Nitric oxide (NO•) and O_2^-• have the ability to form the highly reactive nitrogen species, peroxynitrite ($ONOO^-$), which in the presence of carbon dioxide (CO_2) forms nitrogen dioxide (NO_2) and the reactive carbonyl species, the carboxyl anion (CO_3^-•).

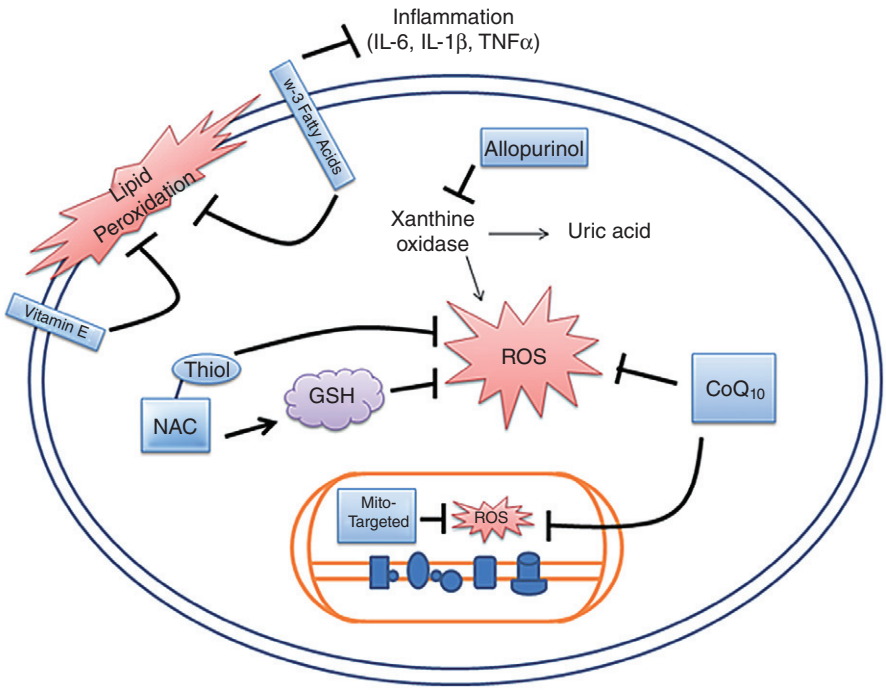

Fig. 2 Cellular sites of reducing oxidative stress by oxidant modifying compounds. Inflammation, lipid peroxidation and reactive oxygen species (ROS) from mitochondrial, cytoplasmic and extracellular sources contribute to oxidative stress. Vitamin E incorporates into the phospholipid bilayer of the cell membrane halting lipid peroxidation chain reactions. ω-3 fatty acids displace arachidonic acid in the cell membrane and thus reduce arachidonic-derived ROS, but also significantly reduce inflammation and subsequent fibrosis. The cysteine residue of N-acetyl-cysteine (NAC) is a precursor for glutathione (GSH) synthesis, and the thiol group is able to scavenge ROS directly. Allopurinol inhibits xanthine oxidase derived ROS and the damaging effects of uraemia. Coenzyme Q_{10} (CoQ_{10}) enhances the efficiency of electron transport in the mitochondria, thereby reducing mitochondrial derived ROS, and is also able to directly scavenge ROS. Mitochondrial (mito)-targeted anti-oxidants accumulate in the mitochondria, reducing mitochondrial-derived ROS.

duction.[11] However, adequate levels of both are likely to be vital for normal cell function. Mitochondria possess their own pool of anti-oxidants such as mitochondrial manganese-SOD (Mn-SOD) to counteract their generation of ROS. Mn-SOD or copper/zinc-SOD (Cu/Zn-SOD) converts O_2^- to H_2O_2, which is then decomposed to H_2O and O_2 by CAT and Gpx. Cu/Zn-SOD has been implicated in stabilizing O_2^- within other cellular compartments, especially peroxisomes, and must be considered in maintenance of the redox state of the whole cell. Limited anti-oxidant actions of Cu/Zn-SOD may also occur within the inter-membrane space of the mitochondria.

Among the various endogenous defences against ROS, glutathione homeostasis is critical for a cellular redox environment. Glutathione-linked enzymatic defences include Gpx, glutathione-S-transferase (GST), glutaredoxins (Grx), thioredoxins (Trx) and peroxiredoxins (Prx). Many of these proteins are known to interact with each other, forming networks that may be prone to dysfunction. Mitochondrial-specific isoforms of these proteins also exist,[12] and these may be more critical for cell survival compared with their cytosolic counterparts. Mitochondrial dysfunction, resulting in depleted ATP synthesis, has the potential to reduce the redox control of glutathione because the rate of glutathione synthesis is ATP-dependent. In the kidney, intracellular synthesis of glutathione from amino acid derivatives (glycine, glutamate and cysteine) accounts for the majority of cellular glutathione compared with, for example, the uptake of extracellular glutathione from the basolateral membrane in epithelial tubular cells of the renal nephron.[13] This characteristic may account for different segments of the nephron being differentially susceptible to the same insult, as proximal tubular epithelial cells lack the ability to synthesize glutathione, compared with other segments of the nephron, which have that ability.[14]

DYSFUNCTIONAL MITOCHONDRIA AND OXIDATIVE STRESS

Mitochondrial biogenesis and degradation (mitophagy) usually occur in balance within healthy cells, and their imbalance may be a major contributor to oxidative stress and cellular metabolic decline. Mitophagy is carried out by autophagy, a process that was originally thought to be a non-selective cell regulatory mechanism for the degradation of dysfunctional organelles within the cellular lysosome system. More recently, the discovery of the autophagy (*Atg*) genes has uncovered a highly selective process for removal of damaged mitochondria.[15] In particular, the mitochondrial transmembrane receptor gene *Atg32* directs autophagosome formation. This response is enhanced by a decrease in ATP production due to dysfunctional mitochondria, and is regulated by the intracellular energy sensor, adenosine monophosphate-activated protein kinase.[16] Should ATP reach critical levels through removal of too many dysfunctional mitochondria, autophagic cell death will be induced. Increasing mitochondrial biogenesis is an attractive target to reduce cellular metabolic injury. However, increasing the number of mitochondria could possibly worsen or induce tissue hypoxia due to increased oxygen consumption.

Oxidative stress also induces apoptosis,[17] a process central to functional tissue loss in CKD.[18] Oxidative stress-induced mitochondrial dysfunction and ROS generation may cause suppression of phosphorylation of the anti-apoptotic B-cell lymphoma-2 (Bcl-2) protein and loss of mitochondrial membrane potential. The intrinsic, mitochondrial-driven, pathway to apoptosis is of particular importance to age-related CKD.[19] Opening of the mitochondrial permeability transition pore releases the pro-apoptotic factor cytochrome C (CytC). CytC is bound to the inner mitochondrial membrane by an association with the anionic phospholipid, cardiolipan. Increased ROS result in dissociation of CytC from cardiolipan, and increased amounts of CytC in the cytosol. Pro-apoptotic proteases, known as caspases, also play essential roles in apoptosis. Cytoplasmic CytC forms an apoptosome with apoptotic peptidase activating factor-1 and caspase-9, leading to cleavage and activation of caspase-9 and caspase-3, and the structural changes of apoptosis. The translocation of the Bcl-2 family proteins, especially pro-apoptotic Bax (Bcl-2-associated x protein) and Bak (Bcl-2 antagonist killer), to the mitochondria of kidney cells is the precursor to opening of the mitochondrial permeability transition pore, release of CytC and resultant apoptosis.[20] These proteins can interact with the outer mitochondrial membrane, causing its permeabilization. Endogenous anti-apoptotic Bcl-XL (the Bcl-X long isoform) also translocates from the cytoplasm to the mitochondrial membrane, and is known to protect renal distal tubular epithelium against oxidative stress.[17]

OXIDATIVE STRESS IN CKD

During the pathogenesis of CKD, perturbations in cellular oxidant handling influence downstream cell signalling and, in the kidney, promote renal cell apoptosis and senescence, decreased regenerative ability of cells and fibrosis. The pathways are tightly controlled, with transcription often determined by specific transcription factors, and post-translational modifications that include phosphorylation, methylation, acetylation, ubiquitination and O-GlcNAylation to regulate outcomes. Several of these genes, which are regulated by oxidative stress and may act in the development of CKD, are reviewed in the following paragraph.

The Forkhead (FoxO) proteins are a family of transcription factors that play a critical role in the regulation of genes in ageing. They comprise FoxO1 to FoxO4 and FoxO6; however, FoxO1 has most association with CKD. FoxO1 has increased levels of phosphorylation in the kidneys of elderly overweight people with type 2 diabetes and CKD[21] and old hypertensive rats with CKD.[1] FoxOs induce apoptosis mainly by upregulation of pro-apoptotic genes such as Bax,[22] yet they can also detoxify harmful cellular oxidants like O_2^- and H_2O_2 and protect cells.[23] Their exact role in oxidative stress-induced CKD needs further investigation. Nuclear factor-kappa B (NF-κB) comprises a family of rapid-acting nuclear transcription factors that transcriptionally regulate a wide variety of genes involved in inflammation, immunity, apoptosis, cell proliferation and differentiation. In oxidative stress-induced kidney disease, NF-κB is activated by ROS and initiates signalling pathways involved in renal fibrosis.[24] It has been implicated in the transcriptional activation of the

cell cycle inhibitor p21,[25] linking this transcriptional regulator with renal cell senescence. The adapter protein $p66^{shc}$ is a mediator of mitochondrial dysfunction.[26] An isoform of the ShcA protein, $p66^{shc}$ antagonizes the cell proliferative actions of two other isoforms, $p46^{shc}$ and $p52^{shc}$. Oxidative stress induces the phosphorylation of serine 36 of $p66^{shc}$ before its translocation into the mitochondria. Here, it translates oxidative stress into Ca^{2+}-mediated mitochondrial damage and subsequent apoptosis.[27] Although the role of $p66^{shc}$ has been noted in glomerulopathies and diabetes,[28] and its differential expression has been demonstrated in ageing kidneys,[1] the functional significance of $p66^{shc}$ in the pathogenesis of CKD needs further investigation.

Uremic toxins may also be a source of oxidative stress in CKD patients. Uric acid is the hepatic end-product of purine metabolism in humans. It is synthesized by xanthine oxidoreductase, which catalyses the oxidation of hypoxanthine to xanthine and xanthine to uric acid. Resulting hyperuricaemia is associated with an increased risk for developing CKD and enhances its progression.[29] In addition, retention of uremic toxins promotes inflammation, and therefore oxidative stress, by priming polymorphonuclear lymphocytes, activating IL-1β and IL-8[30] and stimulating the innate immune response through CD8+ cells.[31] Uric acid synthesis can also promote oxidative stress directly through the activity of xanthine oxidoreductase. This enzyme is synthesized as xanthine dehydrogenase, which can be converted to xanthine oxidase by calcium-dependant proteolysis[32] or modification of cysteine residues.[33] In doing so, the enzyme loses its capacity to bind NADH by alterations in its catalytic site and, instead, transfers electrons to O_2, thereby generating $O_2^{-}\cdot$.[34] However, the role of uric acid in many conditions associated with oxidative stress is not clear and there are experimental and clinical data showing that uric acid also has a role *in vivo* as an anti-oxidant.[35]

MEASURING OXIDATIVE STRESS

Free radicals have extremely short half-lives, so that in most cases oxidative stress is measured by specific end-products of the process. Reactive species can be measured directly by electron paramagnetic resonance or various spin trapping methods, but these methods present some practical limitations, especially in humans. At present, they are costly, and their safety and efficacy have not been proven. Oxidative stress biomarkers are available, and it is their use that has indicated a positive correlation between increasing oxidative stress with increasing stages of CKD.[36] Assays for oxidative stress or anti-oxidant status and some of the popular biomarkers are shown in Table 3, which also indicates whether the end-product can be measured in urine, serum, tissue, cell culture or other biological products. Common and reliable assays for oxidative stress in CKD in humans are discussed specifically.

Isoprostanes

As with most oxidative stress biomarkers, the isoprostanes detect levels of specific end-products from free radical damage. They are considered by some researchers to be the best available biomarker of lipid peroxidation and have been investigated in the pathogenesis of CKD.[36–38] Studies have focused primarily on F_2-isoprostanes, which are formed by non-enzymatic peroxidation of arachidonyl lipids. Specifically, 8-isoprostane (8-*epi*-PGF2a) is measured. F_2-isoprostanes are best detected using mass spectroscopy, and urine and plasma are typically used.[39] One of their limitations as a biomarker of oxidative stress is that they are rapidly metabolized and, as a result, any increase in plasma isoprostane concentration may be due not only to their increased formation from lipid peroxidation, but also to a slower metabolism.[40,41] Measurements of F_2-isoprostanes also have relatively low reproducibility, for example, in the one healthy patient on a defined diet and exercise regimen, carried out at the same time of day on subsequent days.[42] A final, important, consideration is that the F_2-isoprostanes, like all end-product biomarkers, are a measure of whole-body oxidative stress rather than oxidative stress localized only to the kidney. Nevertheless, the use of isoprostanes has delivered important information on increased oxidative stress and related loss of kidney function,[36] early in the progression of CKD.[38]

Malondialdehyde

Malondialdehyde (MDA) is another end-product generated by lipid peroxidation and has been used to demonstrate increased oxidative stress during CKD.[43] Unlike F_2-isoprostanes, MDA has the ability to react further and possibly cause protein and DNA adducts, thus levels of MDA should be interpreted with caution. MDA, along with other lipid peroxidation products such as 4-hydroxyalkenals, is a thiobarbituric acid reactive substance (TBARS). Earlier investigations into oxidative stress commonly assayed TBARS; however, simple TBARS assays are unreliable measures of oxidative stress because most TBARS in human body fluids are formed non-specifically and artefactually, and are not specifically related to lipid peroxidation.[44] High-performance liquid chromatography extraction of MDA from plasma, with subsequent quantification, is considered a reliable measure of oxidative stress.[45] Improved methods derivatize MDA with 2,4-dinitrophenylhydrazine, which forms specific hydrazones for MDA that can be separated by high-performance liquid chromatography and quantified using methyl-MDA as an internal standard.[46] Urinary MDA as a measure of impaired kidney function in patients can be difficult to interpret given that renal clearance of MDA possibly provides an adaptive mechanism to prevent lipid peroxidation accumulating within kidney tubular cells.[47]

Table 3 Markers and assays of oxidative stress

Marker type or method	Samples				
	Blood	Urine	Tissue	Culture	Other
Lipid peroxidation					
F_2-isoprostanes	✓	✓	✓	✓	
Malondialdehyde	✓	✓	✓	✓	
Thiobarbituric acid reactive substances	✓	✓	✓	✓	
Aldehydes					Breath
Lipid hydroperoxides	✓		✓	✓	
Protein oxidation or nitration					
Protein carbonyls	✓	✓	✓	✓	
3-nitrotyrosine	✓	✓	✓	✓	
Advanced glycation end-products	✓	✓	✓	✓	Skin
Advanced oxidation protein products	✓		✓	✓	
Kidney injury molecule-1 (KIM-1)		✓	✓	✓	
Oxidized low-density lipoproteins	✓		✓	✓	
Reactive oxygen species					
Intracellular ROS (fluorescence)				✓	
Hydrogen peroxide	✓	✓	✓	✓	Breath
Electron spin resonance for ROS			✓	✓	
DNA or RNA damage					
8-hydroxy deoxyguanosine (8-OHdG)	✓	✓	✓	✓	
Double strand breaks (ApopTag)			✓	✓	
Comet assay for general DNA damage			✓	✓	
Anti-oxidants					
Catalase	✓		✓	✓	
Glutathione	✓	✓	✓	✓	
Reduced-oxidized glutathione (GSH : GSSH)	✓		✓	✓	
Glutathione peroxidase	✓	✓	✓	✓	
Superoxide dismutase (Mn-SOD and Cu/Zn-SOD)	✓	✓	✓	✓	
Oxygen radical anti-oxidant capacity (ORAC)	✓	✓	✓		Food samples
Hydroxyl radical anti-oxidant capacity (HORAC)	✓	✓	✓		Food samples
Ferric reducing ability of plasma (FRAP)	✓				
Total anti-oxidant capacity (TAC)	✓	✓	✓	✓	Food samples

Other common assays or biomarkers of oxidative stress in CKD patients

Advanced oxidation protein products (AOPP) accumulate in the serum of CKD patients, especially those with uraemia and diabetes,[48] contributing to the pathogenesis of CKD.[49] AOPP are primarily derived from serum albumin following hypochlorous acid free radical attack[50] and they provide a valuable indicator of oxidation-mediated protein damage. The prevalence of albuminuria/proteinuria in CKD and its impact on AOPP has not yet been investigated. Protein carbonyl assays quantify the carbonyl groups associated with oxidant-damaged proteins. Protein carbonyls are not specific for oxidative stress as they also measure glycated proteins and bound aldehydes.[51] An increase in protein carbonyls was demonstrated in CKD patients in stages 3–5, yet no correlation was found between protein carbonyl levels and decreased GFR.[38] The pathogenesis of type 2 diabetes includes oxidative stress as a mechanism.[52] Protein carbonyls are increased in plasma and lymphocytes of diabetes patients compared with healthy control.[39] γ-Glutamyl transpeptidase (GGT) has been trialled as a biomarker of CKD onset through the mechanism of oxidative stress. Extracellular GGT is required to metabolize extracellular-reduced glutathione, allowing for the intracellular synthesis of glutathione. Serum anti-oxidant levels had an inverse relationship to serum GGT, indicating a redox-regulating role.[53] The relationship between plasma and extracellular GGT is not fully defined, but it does appear that serum GGT presents a favourable biomarker of oxidative stress. It is stable, quick and inexpensive to test, and provides an indication of whole-body oxidative stress compared with specific oxidative damage to lipids, DNA or proteins. In an excellent review of measures of oxidative stress, Halliwell and colleagues discuss more broadly the different measures of oxidative stress, including reasons leading to poor correspondence between markers, like the rapid metabolism of isoprostanes compared with the slower metabolism of oxidized proteins.[51]

COMBATING CKD BY TARGETING OXIDATIVE STRESS

Two major goals for controlling development of CKD are early detection and slowing progression to end-stage renal

disease. Using oxidative stress biomarkers in a panel of biomarkers of processes known to impact on CKD development may allow early detection. Slowing its development is more problematic. Traditionally, inhibition of the renin-angiotensin-aldosterone system has been used to slow the progression of CKD,[54] with established therapies relying on pharmacologic blockade of the renin-angiotensin-aldosterone system with angiotensin-converting enzyme inhibitors and angiotensin II receptor blockers. However, decline of GFR and elevated serum creatinine have continued in treated patients,[55,56] and the need for novel treatments and interventions continues. Although the prophylactic use of anti-oxidant therapies in the treatment and amelioration of CKD is still in dispute, oxidant dysregulation occurs with age and age is one of the greatest risk factors for CKD. Some modifiable pathways and anti-oxidant treatments are summarized in Figure 2. There are many anti-oxidants that might be mentioned here, but we have selected some that have some demonstrated benefits in CKD.

Vitamin E

Vitamin E comprises a family of eight different lipid-soluble tocopherols and tocotrienols that scavenge free radicals by incorporating into the plasma membrane of cells, thus halting lipid peroxidation chain reactions.[57] Vitamin E foodstuffs primarily consist of α-tocotrienol, which has a higher anti-oxidant efficacy; however, α-tocopherol has higher bioavailability *in vivo* than the other seven compounds and so the focus has been on its usage. The basis of vitamin E supplementation is to enhance α-tocopherol levels in cell plasma membranes to prevent lipid peroxidation and resultant oxidative stress. Vitamin E is often delivered with vitamin C in an attempt to boost the anti-oxidant efficacy, as vitamin C has been shown to assist in recycling vitamin E. One drawback of α-tocopherol is that it takes several days of pretreatment to exhibit anti-oxidant effects.[58] Trolox (±-6-hydroxy-2,5,7,8-tetramethylchromane-2-carboxylic acid), is an analogue of α-tocopherol that has shown far better free radical scavenging properties owing to its water solubility. The majority of *in vivo* studies using Trolox have reported beneficial effects in acute cases of renal injury such as ischaemia reperfusion, due to rapid solubility and increased potency.[59] A combination supplement containing both α-tocopherol and Trolox may offer greater efficacy due to the fast-acting activities of Trolox combined with the sustained scavenging actions of α-tocopherol.

Patients with progressive CKD display the largest decrease in serum α-tocopherol levels, indicating an increased need for α-tocopherol in the CKD population.[37] Supplementation of α-tocopherol in an end-stage kidney disease dialysis population reduced the risk of associated cardiovascular disease, decreased oxidative stress and increased erythrocyte anti-oxidants SOD, Gpx and CAT.[60] However, in a meta-analysis by Miller and colleagues,[61] based on the combination of several studies, an increase in all-cause mortality was found with high-dose vitamin E (≥400 IU/day) in patients with chronic diseases.[62] Furthermore, the SELECT trial demonstrated that dietary supplementation with vitamin E significantly increased the risk of prostate cancer among healthy men.[63] Future trials should determine the cause of these risks as well as focus on γ- and δ-tocopherol supplementation.

Omega-3 polyunsaturated fatty acids

Although considered more an anti-inflammatory[64] than anti-oxidant treatment, long chain omega(ω)-3 polyunsaturated fatty acids, including docosahexanoic acid and eicosapentanoic acid, have been investigated in a large range of *in vitro* and *in vivo* CKD models. They were found to enhance endogenous anti-oxidant defence systems such as γ-glutamylcysteinyl ligase and glutathione reductase.[65] In models of progressive renal fibrosis, kidney function and structure were improved using eicosapentanoic acid and docosahexanoic acid supplementation, with reduced oxidative stress, inflammation and tubulointerstitial fibrosis.[66] Use of ω-3 polyunsaturated fatty acids in human CKD patients is under multicentre trials and the anti-oxidant status of the patients will, hopefully, be recorded in these trials.

N-acetyl cysteine

N-acetyl cysteine (NAC) is an essential precursor to many endogenous anti-oxidants involved in the decomposition of peroxides. It attenuates oxidative stress from various underlying causes by replenishing intracellular glutathione stores. The limiting precursor to glutathione biosynthesis is L-cysteine. This amino acid is not readily available in the human diet and this was the primary basis for NAC supplementation – to replenish cysteine levels. However, the sulfhydryl-thiol group of L-cysteine is also able to exert direct anti-oxidant effects by scavenging free radicals. The results of NAC supplementation in kidney disease have been variable. NAC pretreatment reduced endothelial dysfunction caused by uremic toxins by reducing ROS-dependent expression of NF-κB.[67] NAC reduced kidney MDA levels in a mouse model of diabetic nephropathy.[68] The treatment of CKD patients with NAC has been largely disappointing,[69] but in end-stage kidney disease patients receiving either haemodialysis or peritoneal dialysis, NAC reduced serum 8-isoprostane and the inflammatory cytokine IL-6.[70,71]

Allopurinol

Allopurinol and its metabolite, oxypurinol, are xanthine oxidoreductase inhibitors that lower serum uric acid levels. Treatment with allopurinol blocks uric acid reabsorption by urate transporters in the proximal tubule, facilitating enhanced uric acid excretion.[72] Allopurinol has a protective effect in diseases involving oxidative stress in their pathogen-

esis. Allopurinol treatment of diabetic mice attenuated hyperuricaemia, albuminuria, and tubulo-interstitial injury.[73] Several studies in human CKD patients have shown the benefit of treatment with allopurinol. For example, Kao *et al*. reported that allopurinol ameliorated endothelial dysfunction and prevented increased left ventricular mass in patients with CKD,[74] and Siu *et al*. reported that allopurinol slowed progression of CKD through its ability to lower serum uric acid levels.[75]

Coenzyme Q_{10} and mitochondrial-targeted anti-oxidants

The kidneys contain the highest endogenous levels of CoQ_9 and CoQ_{10} compared with all other organs.[76] This is likely due to the reliance of the kidney on aerobic metabolism and high density of mitochondria. It is imperative that endogenous CoQ_{10} levels are maintained to ensure mitochondrial health, and this forms the rationale for CoQ_{10} therapy. CoQ_{10} has three well-characterized functions: (i) the transfer of electrons from complexes I and II to complex III along the ETC of the inner mitochondrial membrane and subsequent membrane polarization and ATP generation;[77] (ii) the pro-oxidant generation of O_2^- and H_2O_2;[78] and (iii) the anti-oxidant quenching of free radicals.[79] The major direct anti-oxidant role of CoQ_{10} is prevention of lipid peroxidation, and it also acts indirectly through its interactions with α-tocopherol.[80] Although results regarding its benefit are disparate, Ishikawa and colleagues[81] demonstrated a decrease in kidney O_2^- levels and improved renal function in hemi-nephrectomized rats on a CoQ_{10} supplemented diet. There is a general lack of human studies investigating CoQ_{10} therapy for the treatment and/or prevention of CKD, but CoQ_{10} levels decrease with age[82] and identification of patients with low CoQ_{10} levels may allow for targeted therapy with beneficial outcome.

Mitochondrial-targeted compounds have created much interest for their application in reducing oxidative stress. One of the most tested is the mitochondrial-targeted derivative of endogenous CoQ_{10}, termed MitoQ (mitoquinone mesylate). This compound and those alike, such as mitochondrial-targeted vitamin E (MitoVitE), are prepared by covalently attaching a lipophilic cation to an alkyltriphenylphosphonium, allowing rapid accumulation into the mitochondria driven by the large negative value of the mitochondrial membrane potential. Administration of MitoQ in a rat model of diabetic nephropathy decreased mesangial expansion and tubulointerstitial fibrosis, thereby improving renal function.[83] Human trials have shown that MitoQ can decrease biomarkers of liver inflammation in hepatitis C patients.[84] However, a larger scale, double-blinded, placebo-controlled study found that MitoQ did not slow the progression of untreated Parkinson's disease, a disease associated with mitochondrial oxidative stress.[85] The effect may be tissue specific, and early intervention with MitoQ in CKD patients could prove fruitful given that oxidative stress is evident early in CKD progression (stages 1–3).

SUMMARY

The transcriptional networks that maintain oxidant balance in the mature kidney provide promising entry points for future therapeutic interventions, including for CKD. The use of anti-oxidants targeted to specific pathways that are altered in CKD may prove beneficial, but it is likely that several anti-oxidants will be needed as a multi-drug therapy to target oxidant modifying pathways during the development of CKD. These include lipid peroxidation, which can be improved by α-tocopherol; glutathione redox regulation, which can be restored by NAC; uremic toxins, which can be reduced by allopurinol; inflammation, which can be attenuated by ω-3 polyunsaturated fatty acids; and finally, mitochondrial dysfunction, which may be improved by CoQ_{10}. Mosca and colleagues[86] found that healthy individuals taking a combination of α-tocopherol, α-lipoic acid, CoQ_{10}, carnitines and selenomethionine increased plasma anti-oxidant status, decreased lymphocyte apoptosis and decreased mitochondrial-derived ROS. In the CKD population, identification of patients who would benefit from anti-oxidant therapy is first needed, and then a multifaceted anti-oxidant approach may be necessary for successful treatment of CKD.

REFERENCES

1. Percy CJ, Brown L, Power DA, Johnson DW, Gobe GC. Obesity and hypertension have differing oxidant handling molecular pathways in age-related chronic kidney disease. *Mech. Ageing Dev.* 2009; **130**: 129–38.
2. Chadban SJ, Briganti EM, Kerr PG *et al*. Prevalence of kidney damage in Australian adults: The AusDiab kidney study. *J. Am. Soc. Nephrol.* 2003; **14**: S131–8.
3. Chien KL, Hsu HC, Lee YT, Chen MF. Renal function and metabolic syndrome components on cardiovascular and all-cause mortality. *Atherosclerosis* 2008; **197**: 860–67.
4. Cadenas E, Davies KJ. Mitochondrial free radical generation, oxidative stress, and aging. *Free Radic. Biol. Med.* 2000; **29**: 222–30.
5. Nohl H, Hegner D. Do mitochondria produce oxygen radicals in vivo? *Eur. J. Biochem.* 1978; **82**: 563–7.
6. Linnane AW, Eastwood H. Cellular redox regulation and prooxidant signaling systems: A new perspective on the free radical theory of aging. *Ann. N. Y. Acad. Sci.* 2006; **1067**: 47–55.
7. Liu Y, Fiskum G, Schubert D. Generation of reactive oxygen species by the mitochondrial electron transport chain. *J. Neurochem.* 2002; **80**: 780–87.
8. Choksi KB, Nuss JE, Boylston WH, Rabek JP, Papaconstantinou J. Age-related increases in oxidatively damaged proteins of mouse kidney mitochondrial electron transport chain complexes. *Free Radic. Biol. Med.* 2007; **43**: 1423–38.
9. Granata S, Zaza G, Simone S *et al*. Mitochondrial dysregulation and oxidative stress in patients with chronic kidney disease. *BMC Genomics* 2009; **10**: 388.
10. Lu SC. Regulation of glutathione synthesis. *Mol. Aspects Med.* 2009; **30**: 42–59.

11. Meng Q, Wong YT, Chen J, Ruan R. Age-related changes in mitochondrial function and antioxidative enzyme activity in fischer 344 rats. *Mech. Ageing Dev.* 2007; **128**: 286–92.
12. Hanschmann EM, Lonn ME, Schutte LD *et al*. Both thioredoxin 2 and glutaredoxin 2 contribute to the reduction of the mitochondrial 2-Cys peroxiredoxin Prx3. *J. Biol. Chem.* 2010; **285**: 40699–705.
13. Visarius TM, Putt DA, Schare JM, Pegouske DM, Lash LH. Pathways of glutathione metabolism and transport in isolated proximal tubular cells from rat kidney. *Biochem. Pharmacol.* 1996; **52**: 259–72.
14. Hall AM, Unwin RJ, Parker N, Duchen MR. Multiphoton imaging reveals differences in mitochondrial function between nephron segments. *J. Am. Soc. Nephrol.* 2009; **20**: 1293–302.
15. Okamoto K, Kondo-Okamoto N, Ohsumi Y. Mitochondria-anchored receptor Atg32 mediates degradation of mitochondria via selective autophagy. *Dev. Cell* 2009; **17**: 87–97.
16. Egan DF, Shackelford DB, Mihaylova MM *et al*. Phosphorylation of ULK1 (hATG1) by AMP-activated protein kinase connects energy sensing to mitophagy. *Science* 2011; **331**: 456–61.
17. Cuttle L, Zhang XJ, Endre ZH, Winterford C, Gobe GC. Bcl-X(L) translocation in renal tubular epithelial cells in vitro protects distal cells from oxidative stress. *Kidney Int.* 2001; **59**: 1779–88.
18. Yang T, Vesey DA, Johnson DW, Wei MQ, Gobe GC. Apoptosis of tubulointerstitial chronic inflammatory cells in progressive renal fibrosis after cancer therapies. *Transl. Res.* 2007; **150**: 40–50.
19. Madesh M, Hajnoczky G. VDAC-dependent permeabilization of the outer mitochondrial membrane by superoxide induces rapid and massive cytochrome c release. *J. Cell Biol.* 2001; **155**: 1003–15.
20. Degenhardt K, Sundararajan R, Lindsten T, Thompson C, White E. Bax and Bak independently promote cytochrome C release from mitochondria. *J. Biol. Chem.* 2002; **277**: 14127–34.
21. Mussig K, Staiger H, Machicao F *et al*. Association of common genetic variation in the FOXO1 gene with beta-cell dysfunction, impaired glucose tolerance, and type 2 diabetes. *J. Clin. Endocrinol. Metab.* 2009; **94**: 1353–60.
22. Dijkers PF, Medema RH, Lammers JW, Koenderman L, Coffer PJ. Expression of the pro-apoptotic Bcl-2 family member Bim is regulated by the forkhead transcription factor FKHR-L1. *Curr. Biol.* 2000; **10**: 1201–4.
23. Kops GJ, Dansen TB, Polderman PE *et al*. Forkhead transcription factor FOXO3a protects quiescent cells from oxidative stress. *Nature* 2002; **419**: 316–21.
24. Greiber S, Muller B, Daemisch P, Pavenstadt H. Reactive oxygen species alter gene expression in podocytes: Induction of granulocyte macrophage-colony-stimulating factor. *J. Am. Soc. Nephrol.* 2002; **13**: 86–95.
25. Savickiene J, Treigyte G, Pivoriunas A, Navakauskiene R, Magnusson KE. Sp1 and NF-kappaB transcription factor activity in the regulation of the p21 and FasL promoters during promyelocytic leukemia cell monocytic differentiation and its associated apoptosis. *Ann. N. Y. Acad. Sci.* 2004; **1030**: 569–77.
26. Migliaccio E, Giorgio M, Mele S *et al*. The p66shc adaptor protein controls oxidative stress response and life span in mammals. *Nature* 1999; **402**: 309–13.
27. Arany I, Faisal A, Clark JS, Vera T, Baliga R, Nagamine Y. $p66^{shc}$-mediated mitochondrial dysfunction in renal proximal tubule cells during oxidative injury. *Am. J. Physiol. Renal Physiol.* 2010; **298**: F1214–21.
28. Menini S, Iacobini C, Ricci C *et al*. Ablation of the gene encoding p66Shc protects mice against AGE-induced glomerulopathy by preventing oxidant-dependent tissue injury and further AGE accumulation. *Diabetologia* 2007; **50**: 1997–2007.
29. Shan Y, Zhang Q, Liu Z, Hu X, Liu D. Prevalence and risk factors associated with chronic kidney disease in adults over 40 years: A population study from Central China. *Nephrology (Carlton)* 2010; **15**: 354–61.
30. Martinon F, Petrilli V, Mayor A, Tardivel A, Tschopp J. Gout-associated uric acid crystals activate the NALP3 inflammasome. *Nature* 2006; **440**: 237–41.
31. Sanchez-Lozada LG, Soto V, Tapia E *et al*. Role of oxidative stress in the renal abnormalities induced by experimental hyperuricemia. *Am. J. Physiol. Renal Physiol.* 2008; **295**: F1134–41.
32. Amaya Y, Yamazaki K, Sato M, Noda K, Nishino T. Proteolytic conversion of xanthine dehydrogenase from the NAD-dependent type to the O2-dependent type. Amino acid sequence of rat liver xanthine dehydrogenase and identification of the cleavage sites of the enzyme protein during irreversible conversion by trypsin. *J. Biol. Chem.* 1990; **265**: 14170–75.
33. Nishino T, Okamoto K, Kawaguchi Y *et al*. Mechanism of the conversion of xanthine dehydrogenase to xanthine oxidase: Identification of the two cysteine disulfide bonds and crystal structure of a non-convertible rat liver xanthine dehydrogenase mutant. *J. Biol. Chem.* 2005; **280**: 24888–94.
34. Maia L, Duarte RO, Ponces-Freire A, Moura JJ, Mira L. NADH oxidase activity of rat and human liver xanthine oxidoreductase: Potential role in superoxide production. *J. Biol. Inorg. Chem.* 2007; **12**: 777–87.
35. Miller NJ, RiceEvans CA. Spectrophotometric determination of antioxidant activity. *Redox Rep.* 1996; **2**: 161–71.
36. Dounousi E, Papavasiliou E, Makedou A *et al*. Oxidative stress is progressively enhanced with advancing stages of chronic kidney disease. *Nephrol. Dial. Transplant.* 2006; **21**: 385–85.
37. Karamouzis I, Sarafidis PA, Karamouzis M *et al*. Increase in oxidative stress but not in antioxidant capacity with advancing stages of chronic kidney disease. *Am. J. Nephrol.* 2008; **28**: 397–404.
38. Oberg BP, McMenamin E, Lucas FL *et al*. Increased prevalence of oxidant stress and inflammation in patients with moderate to severe chronic kidney disease. *Kidney Int.* 2004; **65**: 1009–16.
39. Calabrese V, Mancuso C, Sapienza M *et al*. Oxidative stress and cellular stress response in diabetic nephropathy. *Cell Stress Chaperones* 2007; **12**: 299–306.
40. Basu S. Isoprostanes: Novel bioactive products of lipid peroxidation. *Free Radic. Res.* 2004; **38**: 105–22.
41. Roberts LJ 2nd, Morrow JD. Products of the isoprostane pathway: Unique bioactive compounds and markers of lipid peroxidation. *Cell. Mol. Life Sci.* 2002; **59**: 808–20.
42. Nourooz-Zadeh J. Key issues in F2-isoprostane analysis. *Biochem. Soc. Trans.* 2008; **36**: 1060–65.
43. Atamer A, Kocyigit Y, Ecder SA *et al*. Effect of oxidative stress on antioxidant enzyme activities, homocysteine and lipoproteins in chronic kidney disease. *J. Nephrol.* 2008; **21**: 924–30.
44. Knight JA, Pieper RK, McClellan L. Specificity of the thiobarbituric acid reaction: Its use in studies of lipid peroxidation. *Clin. Chem.* 1988; **34**: 2433–8.
45. Johnson DW, Armstrong K, Campbell SB *et al*. Metabolic syndrome in severe chronic kidney disease: Prevalence, predictors, prognostic significance and effects of risk factor modification. *Nephrology (Carlton)* 2007; **12**: 391–8.
46. Sim AS, Salonikas C, Naidoo D, Wilcken DE. Improved method for plasma malondialdehyde measurement by high-performance liquid chromatography using methyl malondialdehyde as an internal

standard. *J. Chromatogr. B Analyt. Technol. Biomed. Life Sci.* 2003; **785**: 337–44.
47. Nath KA, Croatt AJ, Hostetter TH. Oxygen consumption and oxidant stress in surviving nephrons. *Am. J. Physiol.* 1990; **258**: F1354–62.
48. Mezzano D, Pais EO, Aranda E *et al*. Inflammation, not hyperhomocysteinemia, is related to oxidative stress and hemostatic and endothelial dysfunction in uremia. *Kidney Int.* 2001; **60**: 1844–50.
49. Li HY, Hou FF, Zhang X *et al*. Advanced oxidation protein products accelerate renal fibrosis in a remnant kidney model. *J. Am. Soc. Nephrol.* 2007; **18**: 528–38.
50. Capeillere-Blandin C, Gausson V, Descamps-Latscha B, Witko-Sarsat V. Biochemical and spectrophotometric significance of advanced oxidized protein products. *Biochim. Biophys. Acta* 2004; **1689**: 91–102.
51. Halliwell B, Whiteman M. Measuring reactive species and oxidative damage in vivo and in cell culture: How should you do it and what do the results mean? *Br. J. Pharmacol.* 2004; **142**: 231–55.
52. Forbes S, Robinson S, Dungu J *et al*. Sustained endogenous glucose production, diminished lipolysis and non-esterified fatty acid appearance and oxidation in non-obese women at high risk of type 2 diabetes. *Eur. J. Endocrinol.* 2006; **155**: 469–76.
53. Lim JS, Yang JH, Chun BY, Kam S, Jacobs DR Jr, Lee DH. Is serum gamma-glutamyltransferase inversely associated with serum antioxidants as a marker of oxidative stress? *Free Radic. Biol. Med.* 2004; **37**: 1018–23.
54. Hoogwerf BJ. Renin-angiotensin system blockade and cardiovascular and renal protection. *Am. J. Cardiol.* 2010; **105**: 30A–35A.
55. Brenner BM, Cooper ME, de Zeeuw D *et al*. Effects of losartan on renal and cardiovascular outcomes in patients with type 2 diabetes and nephropathy. *N. Engl. J. Med.* 2001; **345**: 861–9.
56. Lewis EJ, Hunsicker LG, Clarke WR *et al*. Renoprotective effect of the angiotensin-receptor antagonist irbesartan in patients with nephropathy due to type 2 diabetes. *N. Engl. J. Med.* 2001; **345**: 851–60.
57. Serbinova E, Kagan V, Han D, Packer L. Free radical recycling and intramembrane mobility in the antioxidant properties of alpha-tocopherol and alpha-tocotrienol. *Free Radic. Biol. Med.* 1991; **10**: 263–75.
58. Machlin LJ, Gabriel E. Kinetics of tissue alpha-tocopherol uptake and depletion following administration of high levels of vitamin E. *Ann. N. Y. Acad. Sci.* 1982; **393**: 48–60.
59. Wongmekiat O, Thamprasert K, Lumlertgul D. Renoprotective effect of trolox against ischaemia-reperfusion injury in rats. *Clin. Exp. Pharmacol. Physiol.* 2007; **34**: 753–9.
60. Giray B, Kan E, Bali M, Hincal F, Basaran N. The effect of vitamin E supplementation on antioxidant enzyme activities and lipid peroxidation levels in hemodialysis patients. *Clin. Chim. Acta* 2003; **338**: 91–8.
61. Miller ER 3rd, Pastor-Barriuso R, Dalal D, Riemersma RA, Appel LJ, Guallar E. Meta-analysis: High-dosage vitamin E supplementation may increase all-cause mortality. *Ann. Intern. Med.* 2005; **142**: 37–46.
62. Huang HY, Appel LJ. Supplementation of diets with alpha-tocopherol reduces serum concentrations of gamma- and delta-tocopherol in humans. *J. Nutr.* 2003; **133**: 3137–40.
63. Klein EA, Thompson IM Jr, Tangen CM *et al*. Vitamin E and the risk of prostate cancer: The Selenium and Vitamin E Cancer Prevention Trial (SELECT). *JAMA* 2011; **306**: 1549–56.
64. Shing CM, Adams MJ, Fassett RG, Coombes JS. Nutritional compounds influence tissue factor expression and inflammation of chronic kidney disease patients in vitro. *Nutrition* 2011; **27**: 967–72.
65. Arab K, Rossary A, Flourie F, Tourneur Y, Steghens JP. Docosahexaenoic acid enhances the antioxidant response of human fibroblasts by upregulating gamma-glutamyl-cysteinyl ligase and glutathione reductase. *Br. J. Nutr.* 2006; **95**: 18–26.
66. Peake JM, Gobe GC, Fassett RG, Coombes JS. The effects of dietary fish oil on inflammation, fibrosis and oxidative stress associated with obstructive renal injury in rats. *Mol. Nutr. Food Res.* 2011; **55**: 400–10.
67. Tumur Z, Shimizu H, Enomoto A, Miyazaki H, Niwa T. Indoxyl sulfate upregulates expression of ICAM-1 and MCP-1 by oxidative stress-induced NF-kappaB activation. *Am. J. Nephrol.* 2010; **31**: 435–41.
68. Ribeiro G, Roehrs M, Bairros A *et al*. N-acetylcysteine on oxidative damage in diabetic rats. *Drug Chem. Toxicol.* 2011; **34**: 467–74.
69. Renke M, Tylicki L, Rutkowski P *et al*. The effect of N-acetylcysteine on proteinuria and markers of tubular injury in non-diabetic patients with chronic kidney disease. A placebo-controlled, randomized, open, cross-over study. *Kidney Blood Press. Res.* 2008; **31**: 404–10.
70. Hsu SP, Chiang CK, Yang SY, Chien CT. N-acetylcysteine for the management of anemia and oxidative stress in hemodialysis patients. *Nephron Clin. Pract.* 2010; **116**: c207–16.
71. Nascimento MM, Suliman ME, Silva M *et al*. Effect of oral N-acetylcysteine treatment on plasma inflammatory and oxidative stress markers in peritoneal dialysis patients: A placebo-controlled study. *Perit. Dial. Int.* 2010; **30**: 336–42.
72. El-Sheikh AA, van den Heuvel JJ, Koenderink JB, Russel FG. Effect of hypouricaemic and hyperuricaemic drugs on the renal urate efflux transporter, multidrug resistance protein 4. *Br. J. Pharmacol.* 2008; **155**: 1066–75.
73. Kosugi T, Nakayama T, Heinig M *et al*. Effect of lowering uric acid on renal disease in the type 2 diabetic db/db mice. *Am. J. Physiol. Renal Physiol.* 2009; **297**: F481–8.
74. Kao MP, Ang DS, Gandy SJ *et al*. Allopurinol benefits left ventricular mass and endothelial dysfunction in chronic kidney disease. *J. Am. Soc. Nephrol.* 2011; **22**: 1382–9.
75. Siu YP, Leung KT, Tong MK, Kwan TH. Use of allopurinol in slowing the progression of renal disease through its ability to lower serum uric acid level. *Am. J. Kidney Dis.* 2006; **47**: 51–9.
76. Lass A, Forster MJ, Sohal RS. Effects of coenzyme Q10 and alpha-tocopherol administration on their tissue levels in the mouse: Elevation of mitochondrial alpha-tocopherol by coenzyme Q10. *Free Radic. Biol. Med.* 1999; **26**: 1375–82.
77. Ohnishi T, Ohnishi ST, Shinzawa-Ito K, Yoshikawa S. Functional role of coenzyme Q in the energy coupling of NADH-CoQ oxidoreductase (Complex I): Stabilization of the semiquinone state with the application of inside-positive membrane potential to proteoliposomes. *Biofactors* 2008; **32**: 13–22.
78. James AM, Smith RA, Murphy MP. Antioxidant and prooxidant properties of mitochondrial Coenzyme Q. *Arch. Biochem. Biophys.* 2004; **423**: 47–56.
79. Nohl H, Gille L, Kozlov AV. Critical aspects of the antioxidant function of coenzyme Q in biomembranes. *Biofactors* 1999; **9**: 155–61.
80. Frei B, Kim MC, Ames BN. Ubiquinol-10 is an effective lipid-soluble antioxidant at physiological concentrations. *Proc. Natl. Acad. Sci. U.S.A.* 1990; **87**: 4879–83.

81. Ishikawa A, Kawarazaki H, Ando K, Fujita M, Fujita T, Homma Y. Renal preservation effect of ubiquinol, the reduced form of coenzyme Q10. *Clin. Exp. Nephrol.* 2011; **15**: 30–33.
82. Wada H, Goto H, Hagiwara S, Yamamoto Y. Redox status of coenzyme Q10 is associated with chronological age. *J. Am. Geriatr. Soc.* 2007; **55**: 1141–2.
83. Chacko BK, Reily C, Srivastava A *et al*. Prevention of diabetic nephropathy in Ins2(+/)(AkitaJ) mice by the mitochondria-targeted therapy MitoQ. *Biochem. J.* 2010; **432**: 9–19.
84. Gane EJ, Weilert F, Orr DW *et al*. The mitochondria-targeted anti-oxidant mitoquinone decreases liver damage in a phase II study of hepatitis C patients. *Liver Int.* 2010; **30**: 1019–26.
85. Snow BJ, Rolfe FL, Lockhart MM *et al*. A double-blind, placebo-controlled study to assess the mitochondria-targeted antioxidant MitoQ as a disease-modifying therapy in Parkinson's disease. *Mov. Disord.* 2010; **25**: 1670–74.
86. Mosca L, Marcellini S, Perluigi M *et al*. Modulation of apoptosis and improved redox metabolism with the use of a new antioxidant formula. *Biochem. Pharmacol.* 2002; **63**: 1305–14.

Original Paper

nephron
Experimental
Nephrology

Nephron Exp Nephrol 2012;122:123–130
DOI: 10.1159/000350726

Received: October 10, 2012
Accepted: March 8, 2013
Published online: June 1, 2013

Oxidative Stress and Cell Senescence Combine to Cause Maximal Renal Tubular Epithelial Cell Dysfunction and Loss in an in vitro Model of Kidney Disease

David M. Small[a] Nigel C. Bennett[a] Sandrine Roy[b] Brian G. Gabrielli[b]
David W. Johnson[a, c] Glenda C. Gobe[a]

[a]Centre for Kidney Disease Research, School of Medicine and [b]Diamantina Institute, The University of Queensland, Princess Alexandra Hospital, and [c]Department of Nephrology, Princess Alexandra Hospital, Brisbane, Qld., Australia

Key Words
Chronic kidney disease · Cell senescence · Oxidative stress · Apoptosis · Mitochondria

Abstract

Background:
The incidence and cost of chronic kidney disease (CKD) are increasing. Renal tubular epithelial cell dysfunction and attrition, involving increased apoptosis and cell senescence, are central to the pathogenesis of CKD. The aim here was to use an in vitro model to investigate the separate and cumulative effects of oxidative stress, mitochondrial dysfunction and cell senescence in promoting loss of renal mass. ***Methods:*** Human kidney tubular epithelial cells (HK2) were treated with moderate hydrogen peroxide (H_2O_2) for oxidative stress, with or without cell cycle inhibition (apigenin, API) for cell senescence. Adenosine triphosphate (ATP) and oxidative stress were measured by ATP assay, lipid peroxidation, total antioxidant capacity, mitochondrial function with confocal microscopy, MitoTracker Red CMXRos and live cell imaging with JC-1. In parallel, cell death and injury (i.e. apoptosis and Bax/Bcl-X_L expression, lactate dehydrogenase), cell senescence (SA-β-galactosidase) and renal regenerative ability (cell proliferation), and their modulation with the antioxidant N-acetyl-cysteine (NAC) were investigated. ***Results:*** H_2O_2 and API, separately, increased oxidative stress and mitochondrial dysfunction, apoptosis and cell senescence. Although API caused cell senescence, it also induced oxidative stress at levels similar to H_2O_2 treatment alone, indicating that senescence and oxidative stress may be intrinsically linked. When H_2O_2 and API were delivered concurrently, their detrimental effects on renal cell loss were compounded. The antioxidant NAC attenuated apoptosis and senescence, and restored regenerative potential to the kidney. ***Conclusion:*** Oxidative stress and cell senescence both cause mitochondrial destabilization and cell loss and contribute to the development of the cellular characteristics of CKD.

Introduction

Chronic kidney disease (CKD) affects approximately 10–15% of the adult population in industrialised countries. The incidence of CKD and its associated end-stage disease are increasing. Although diabetes and hypertension are known causes of CKD, aging alone causes a gradual loss of kidney function independent of any other pathology [1]. Oxidative stress increases with aging [2], and

KARGER

1660–2129/12/1224–0123$38.00/0

E-Mail karger@karger.com
www.karger.com/nee

Assoc. Prof. Glenda Gobe
Centre for Kidney Disease Research, School of Medicine
The University of Queensland, Translational Research Institute
Woolloongabba, Brisbane, QLD 4102 (Australia)
E-Mail g.gobe@uq.edu.au

it has been described in the pathogenesis of diabetes [3] and hypertension [4]. Nonetheless, oxidative stress as a significant cause of CKD and the associated loss of functioning renal mass are still being debated. Mitochondria are increasingly being recognised as key participants in renal cellular metabolism [5] including the generation of energy in the form of adenosine triphosphate (ATP) and the regulation of calcium homeostasis [6], tissue O_2 gradients, apoptosis [7] and cell signalling [8]. However, their contribution to CKD is largely unknown.

The kidney is a highly metabolic organ that relies heavily on oxidative phosphorylation, accounting for approximately 10% of the O_2 consumption of the whole body. Mitochondrial energy generates 95% of required ATP for the kidney [9]. The proximal tubular epithelial cells, most often atrophic in CKD, contain many large active mitochondria [10]. A decrease in mitochondrial efficiency and subsequent cell function could have a significant impact on CKD development and renal failure. Mitochondria are also a major cellular producer of reactive oxygen species (ROS) and are themselves targets of ROS-mediated damage [11]. Along the respiratory chain complexes of the inner mitochondrial membrane, reduction in molecular O_2 yields ROS mainly in the forms of the superoxide anion ($O_2^{\cdot-}$) and hydrogen peroxide (H_2O_2). Defining mitochondrial dysfunction in the highly metabolic proximal tubular epithelium may hold a key to explaining how oxidative stress contributes to the pathogenesis of diseases like CKD.

Cell senescence is commonly observed in CKD with increased levels of senescence-associated β-galactosidase (SA-β-gal) and lipofuscin granules predominately in tubular cells [12], and to a lesser extent in glomerular mesangial cells [13]. Senescent kidney cells can die or persist in a damaged form, showing little function and an inability to proliferate [14]. Persisting senescent cells can compromise the healthy functioning of the kidney and reduce the ability of the aging nephron to cope with disease stresses, since it is the tissue in its whole form that accounts for function rather than the individual cells. Senescent cells have been shown to secrete multiple pro-inflammatory growth factors, cytokines and chemokines [15] and therefore promote inflammation, and also present promising targets to inhibit the many co-morbid conditions associated with inflammation in CKD. Oxidative stress itself can induce premature senescence in non-renal cells: in fibroblast cultures [16] and in retinal epithelium during macular degeneration [17]. Senescing cells undergo irreversible cell cycle arrest, mainly in the G1 phase, have increased SA-β-gal activity and up-regulation of cyclin-dependent kinase inhibitors, like $p16^{ink4a}$ [18]. Oxidative stress may cause premature senescence of kidney cells in CKD. However, the mechanisms underlying mitochondrial dysfunction and subsequent oxidative stress-induced premature senescence in the kidney remain largely undefined. We demonstrated previously that protecting the mitochondria in renal proximal tubular epithelium protects these cells from increasing apoptosis [5]. The aim of this study was, therefore, to use an in vitro model to investigate the separate and cumulative effects of oxidative stress, mitochondrial dysfunction and cell senescence in promoting loss of renal tubular epithelium.

Material and Methods

Experimental Design

The human renal proximal tubular epithelial cell line HK2 (ATCC, Rockville, Mass., USA) was cultured in Dulbecco's modified Eagle's medium/Ham's F12 containing 10% fetal bovine serum and antibiotics using published methods [5]. After dose-response studies (unpublished data), they were grown to 80–90% confluence and then treated for 18–24 h with 0.4 mM H_2O_2 for oxidative stress, and 100 μM apigenin (API) to induce renal cell senescence [19]. DMSO as a vehicle control was <1% in growth medium). N-acetyl-cysteine (NAC), a general renal cell antioxidant [20], was used at 10 mM (n = 3 replicates).

Determination of ATP, Oxidative Stress and Cytotoxicity

ATP levels (luciferase-based bioluminescence assay, Promega, Sydney, N.S.W., Australia), lipid peroxidation with malondialdehyde (MDA) (Bioxytech LPO-586 Assay, OxisResearch Products, Percipio Biosciences Inc., Calif., USA) and total antioxidant capacity (TAC; OxiSelect™ TAC assay kit, Cell Biolabs, San Diego, Calif., USA) was measured according to the manufacturers' protocols and with appropriate controls. Lactate dehydrogenase was measured as a % of its maximal release from cells treated with 5 mM H_2O_2 (Cytotoxicity Detection Kit^{PLUS}, Roche Diagnostics, Castle Hill, N.S.W., Australia).

Mitochondrial Function

MitoTracker Red CMXRos (Invitrogen Australia) localises to mitochondria with healthy membrane potential, and fades as mitochondria lose membrane potential. HK2 cells were incubated for 30 min with 100 nM MitoTracker Red before being fixed (4% paraformaldehyde) and mounted for microscopy (Vectashield antifade, Vecta Laboratories, East Brisbane, Qld., Australia). DAPI (4′,6-diamidino-2-phenylindole) was used to label nuclei. A Zeiss 510 Meta confocal fluorescence microscope with Zen 2008 software (×63 oil lens; 579 nm) was used. Mean fluorescence intensity was analysed (Nikon FN-S2N fluorescence microscope, NIS Image software, ×63 objective).

JC-1 is a fluorophore that has mitochondrial membrane potential-dependent accumulation in mitochondria. A decrease in red fluorescence and an increase in green fluorescence indicate mitochondrial membrane depolarisation. JC-1 (3 μM) was applied 30 min preceding H_2O_2 exposure and then for 1 h of 0.4 or 1 mM H_2O_2

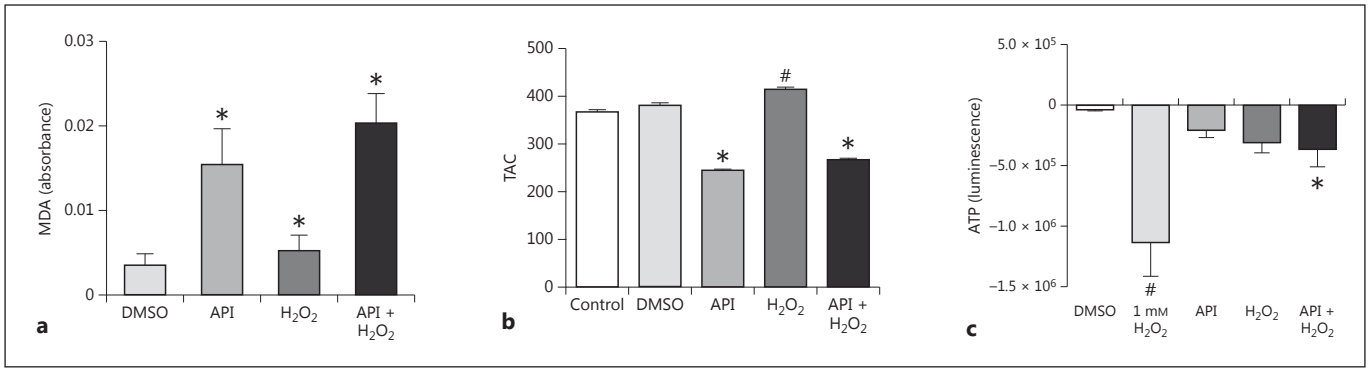

Fig. 1. Lipid peroxidation, TAC and ATP generation following oxidative stress and cell senescence. **a** Lipid peroxidation was measured by MDA assay. Cells exposed to API, H_2O_2 or API + H_2O_2 had a significant increase in MDA compared to DMSO vehicle controls (* $p < 0.05$ compared to DMSO). **b** TAC was measured by colorimetric assay. Cells exposed to API or API + H_2O_2 had a significant reduction in TAC compared to DMSO controls. H_2O_2 induced a small but significant increase in TAC (* $p < 0.05$ compared to DMSO and # $p < 0.05$ compared to untreated controls). **c** ATP generation was measured by luminescence assay; 1 mM H_2O_2 was used to demonstrate maximal ATP loss. Compared with untreated controls, API + H_2O_2 caused the greatest ATP loss (* $p < 0.05$ compared to DMSO and # $p < 0.05$ compared to all).

(as high oxidative stress as control) treatments. Cells were fixed (4% paraformaldehyde) before being mounted (Vectashield mounting medium with DAPI) and visualised at 590 nm (red), 529 nm (green) and 460 nm (blue) using confocal florescence microscopy (×63 oil lens). For live-cell imaging, HK2 cells were seeded onto MatTek Corp (Ashland, Mass., USA) glass bottom dishes before JC-1 incubation. Cultures were placed in a live-cell imaging chamber at 37°C and 5% CO_2 in air. A representative field was then visualised to assess background laser-induced fluorescence leaching. H_2O_2 treatment was then added to the cells and the same field photographed over 25 min at consecutive 5-min intervals.

Light and Fluorescence Microscopy

Cells were fixed in 4% buffered paraformaldehyde or 100% ice-cold methanol for 30 min at 4°C for haematoxylin and eosin (HE) staining or fluorescence microscopy. HE-stained cells were assessed using the Aperio ScanScope XT system (Aperio Technologies, Vista, Calif., USA) for % apoptosis, mitosis and cell senescence by counting ten frames of cells (×200) for each treatment [21]. The ApopTag® peroxidase in situ apoptosis detection kit (Merck-Millipore Pty Ltd, Kilsyth, Vic., Australia) was used for identifying apoptosis according to our published methods [21]. Ki67 (Santa Cruz Biotechnology Inc., Santa Cruz, Calif., USA; 1:100) immunocytochemistry was used to assess proliferative activity. Senescent cell morphology and SA-β-gal immunofluorescence (Cell Signalling Technologies, Danvers, Mass., USA; 1:500) for cell senescence were used in parallel. Senescent cells had reduced staining saturation [22] and were 3–4 times the diameter of control cells.

Western Immunoblotting for Bax, Bcl-X_L and p16^{Ink4a}

Protein was extracted by lysing HK2 cells in RIPA buffer according to our published protocols [5, 20]. Protein concentration was determined (Pierce BCA assay) and 40 μg of each protein separated (10% SDS-polyacrylamide gel electrophoresis). Immunoblotting was performed against Bax (1:1,000, Santa Cruz Biotechnology), Bcl-X_L (1:1,000, Zymed), GAPDH (1:1,000; Sigma) and p16^{Ink4a} (1:100; [23]). HRP-conjugated secondary antibodies were used. Protein bands were visualised using enhanced chemiluminescence. Scion Image software Alpha 4.0.3.2 was used for densitometry. GAPDH immunoblots were used to normalise densitometry.

Statistical Analysis

Values reported are mean ± SEM. Data were analysed using one-way analysis of variance (ANOVA) and Tukey's post hoc analysis, two-way ANOVA and Bonferroni's post hoc test, or Student's t test where appropriate, with statistical significance at $p < 0.05$.

Results

ATP, Lipid Peroxidation and TAC Assays Indicate Oxidative Stress with All Treatments

API, alone or in combination with H_2O_2, significantly increased MDA ($p < 0.05$; fig. 1a) and reduced TAC ($p < 0.05$; fig. 1b). Both API and H_2O_2 resulted in loss of ATP; however, both treatments were necessary for a significant loss (fig. 1c).

Confocal Fluorescence Microscopy and Live Cell Imaging Indicate Loss of Mitochondrial Function with All Treatments

MitoTracker Red fluorescence was significantly reduced following API and/or H_2O_2 exposure (fig. 2a–e; $p < 0.05$). There was no additive effect when H_2O_2 was delivered with API. Live-cell imaging captured the loss of

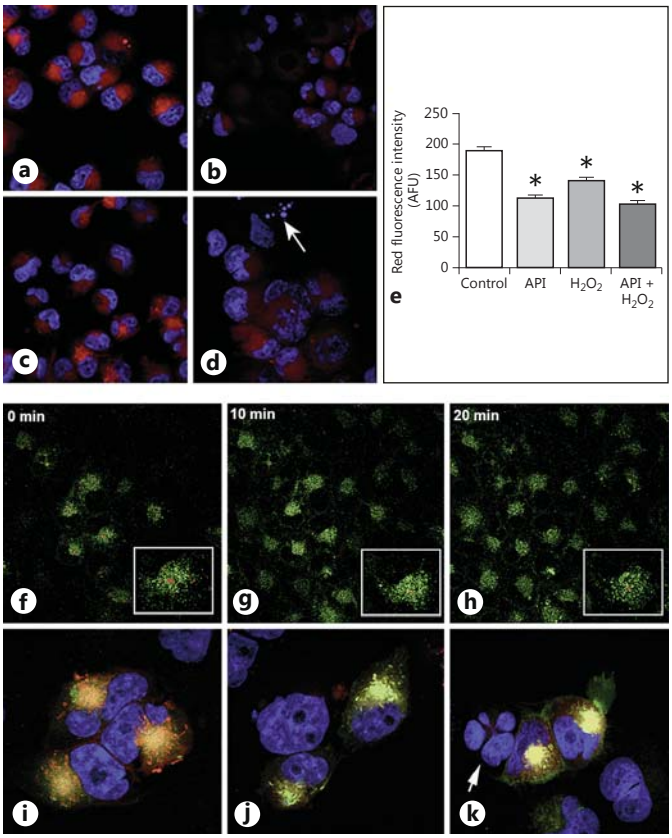

Fig. 2. Live- and fixed-cell imaging verified mitochondrial dysfunction with oxidative stress and cell senescence. **a–d** MitoTracker Red CMXRos confocal fluorescence microscopy is demonstrated. **e** Fluorimetry is presented graphically as arbitrary fluorescence units (AFU). Compared with control cultures (**a**), all treatments (**b** API, **c** H_2O_2 and **d** API + H_2O_2) had decreased MitoTracker Red. **e** AFU were significantly decreased in all treatments (* $p < 0.05$ compared to untreated controls). **f–h** Confocal fluorescence microscopy using live-cell imaging and JC-1 labelling. **f** Control cells during 20-min exposure to H_2O_2. **g**, **h** Mitochondrial membrane depolarisation during 20-min exposure to H_2O_2. There was a gradual decrease in red fluorescence (polarised mitochondria, approx. 590 nm) to predominantly green fluorescence (depolarised mitochondria, approx. 525 nm). **i–k** Mitochondrial depolarisation was also demonstrated by JC-1 pre-treatment, oxidative stress, and then fixing the cells before confocal microscopy. **i** Control cells have red fluorescing mitochondria. **j**, **k** The predominance of green fluorescence after exposure to H_2O_2, again demonstrating mitochondrial membrane depolarisation. **k** Apoptosis is also seen (DAPI-stained nuclear condensation and fragmentation, arrow).

mitochondrial membrane permeability in the kidney cells with oxidative stress (H_2O_2). Results of time-lapse photography (fig. 2f–h) using JC-1 demonstrated healthy polarised mitochondrial membrane (red fluorescence) transitioning to green fluorescence and dysfunctional mitochondria. Fixed cells (JC-1, fig. 2i–k) also showed mitochondrial depolarisation in response to oxidative stress. Concomitant apoptosis is indicated (arrow, fig. 2k).

Oxidative Stress as a Mechanism Unifies Outcomes of Increased Renal Cell Apoptosis, Decreased Mitosis and Cell Senescence

Apoptosis was increased and mitosis decreased by all treatments. API in association with H_2O_2 produced greatest effect (fig. 3a; $p < 0.05$). These results were supported by the cytotoxicity assay (fig. 3b). Representative photomicrographs of morphological characteristics of apoptosis, mitosis and senescence are demonstrated in figure 3c (control) and 3d (API + H_2O_2). ApopTag labelling is demonstrated in figure 3e–g. Ki67 immunocytochemistry is demonstrated in figure 3h–j. Representative Western immunoblots of Bax and Bcl-X_L (fig. 4a) and densitometry (fig. 4b) demonstrated increased Bax and decreased Bcl-X_L, with a pro-apoptotic ratio of Bax:Bcl-X_L increased, with all treatments. The greatest increase was observed with API + H_2O_2 (all $p < 0.05$).

Senescent cell morphology (fig. 5b) and SA-β-gal immunofluorescence (fig. 5a) are presented. API and API + H_2O_2 produced significant morphological senescence changes ($p < 0.001$ compared to DMSO), but all treatments caused increased SA-β-gal immunofluorescence ($p < 0.05$ compared to DMSO). Examples of immunofluorescence demonstrated little SA-β-gal in controls (fig. 5c) versus extensive punctuate green cytoplasmic fluorescence in figure 5d (API treatment). Expression of the cell cycle regulator $p16^{Ink4a}$ (fig. 6a–c) did not change with API or H_2O_2 treatments after 2 h of exposure. However, a significant increase was demonstrated at 24 h after H_2O_2 treatment.

The Antioxidant NAC Protects Renal Cells from Oxidative Stress and Senescence

NAC significantly modulated apoptosis for all treatments, restored the mitotic potential of H_2O_2-treated cells and decreased senescence morphology induced by API and H_2O_2 (fig. 7a–c; $p < 0.05$).

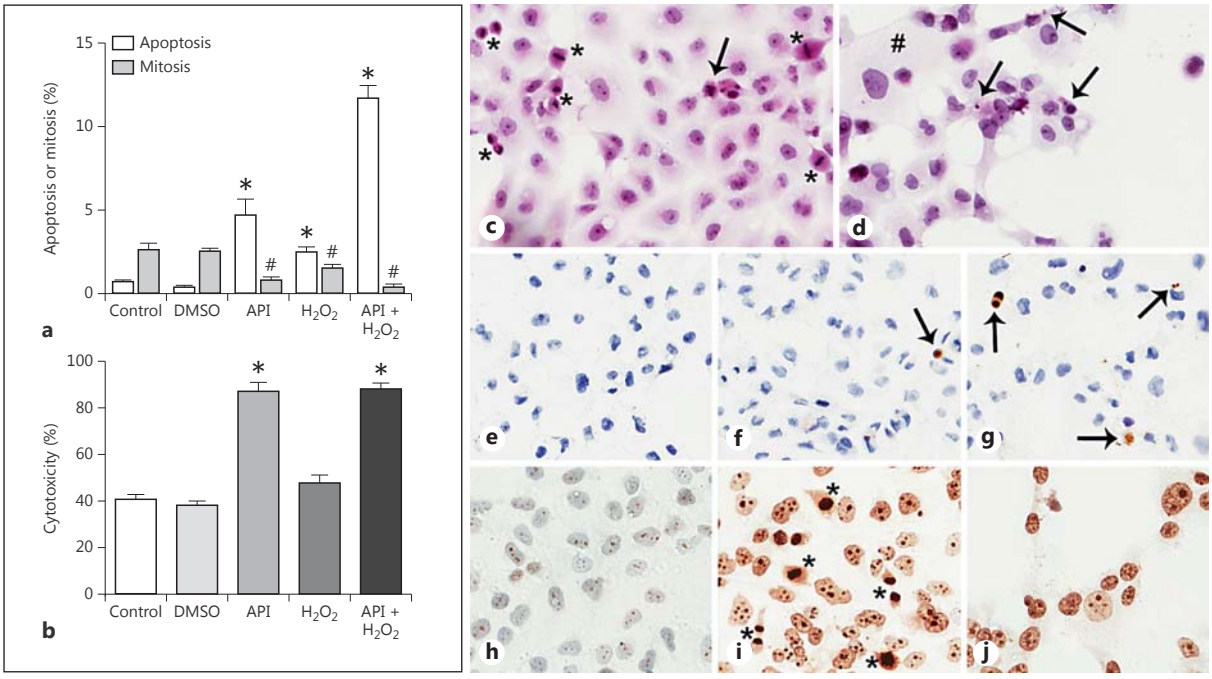

Fig. 3. Increased apoptosis and decreased mitosis occur with oxidative stress and senescence. **a** The mean ± SEM of % apoptosis and mitosis. Apoptosis increased significantly with all treatments compared with control or DMSO but was greater than the addition of counts for API and H_2O_2 in the API + H_2O_2 treatment, indicating a synergistic effect of the treatments (* $p < 0.05$ compared to control). Mitosis decreased in all treatments compared to control and DMSO (# $p < 0.05$ compared to control). **b** The mean ± SEM of lactate dehydrogenase (as % maximal cytotoxicity of HK2 cells exposed to 5 mM of H_2O_2). API and API + H_2O_2 produced the greatest % cytotoxicity compared with untreated cells and DMSO controls (* $p < 0.05$ compared to untreated control). **c–j** Representative histology. The morphological characteristics of apoptosis (arrows), mitosis (*) and senescence (#) are shown in HE-stained cells (**c** control and **d** API treatment as an example). **e–g** Verification of apoptosis with ApopTag (brown nuclei, arrows; colours refer to the online version only). **e** Negative control. **f** ApopTag in untreated controls. **g** ApopTag in H_2O_2 treatment as an example. **h–j** Proliferative activity was identified using Ki67 immunocytochemistry (* positive nuclei as intense brown). **h** Negative control for Ki67. **i** Untreated controls where mitosis was high. **j** API + H_2O_2 as an example where mitosis was negated.

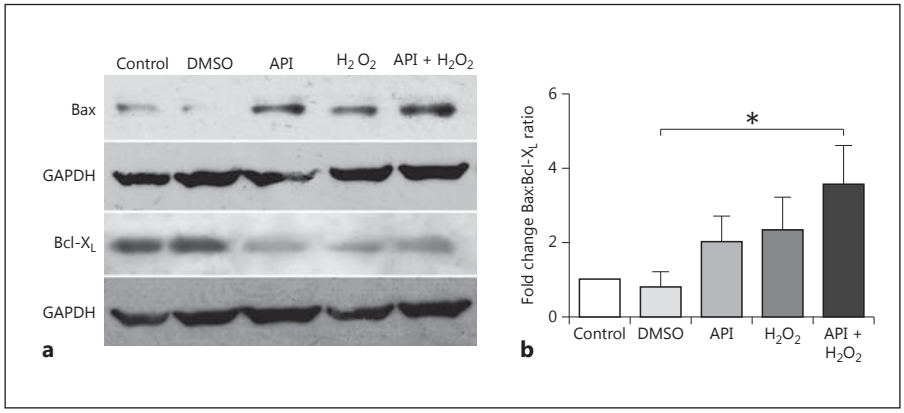

Fig. 4. Western immunoblot and densitometry for Bax and Bcl-X_L expression. **a** Representative examples of Western immunoblots for pro-apoptotic Bax and anti-apoptotic Bcl-X_L plus the GAPDH loading controls for these blots. All treatments resulted in increased Bax and decreased Bcl-X_L. **b** Relative densitometry was normalised to GAPDH, calculated as a fold-change of controls and presented graphically as a ratio of Bax:Bcl-X_L. The pro-apoptotic ratio of Bax:Bcl-X_L increased with all treatments compared with DMSO with the greatest increase observed in the API + H_2O_2 treatment (* $p < 0.05$).

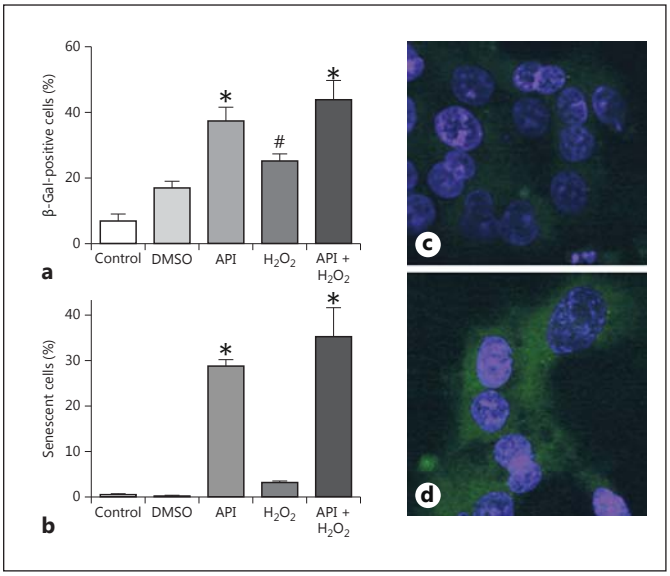

Fig. 5. Induction of senescence in HK2 cells. **a**, **b** Senescence was identified and quantified using morphology (enlarged cells with reduced staining saturation). **c**, **d** Senescence was identified and quantified using immunofluorescence of SA-β-gal. **b** API and API + H_2O_2 produced significant changes in senescence morphology (* $p < 0.05$ compared with controls); however, SA-β-gal (**a**) was significantly increased by all treatments (* $p < 0.05$ compared to DMSO and # $p < 0.05$ compared to untreated controls). **c**, **d** Immunofluorescence for controls (**c**) had little labelling versus extensive punctuate green fluorescence in the cytoplasm of API-treated cells (**d**). DAPI-stained nuclei are blue.

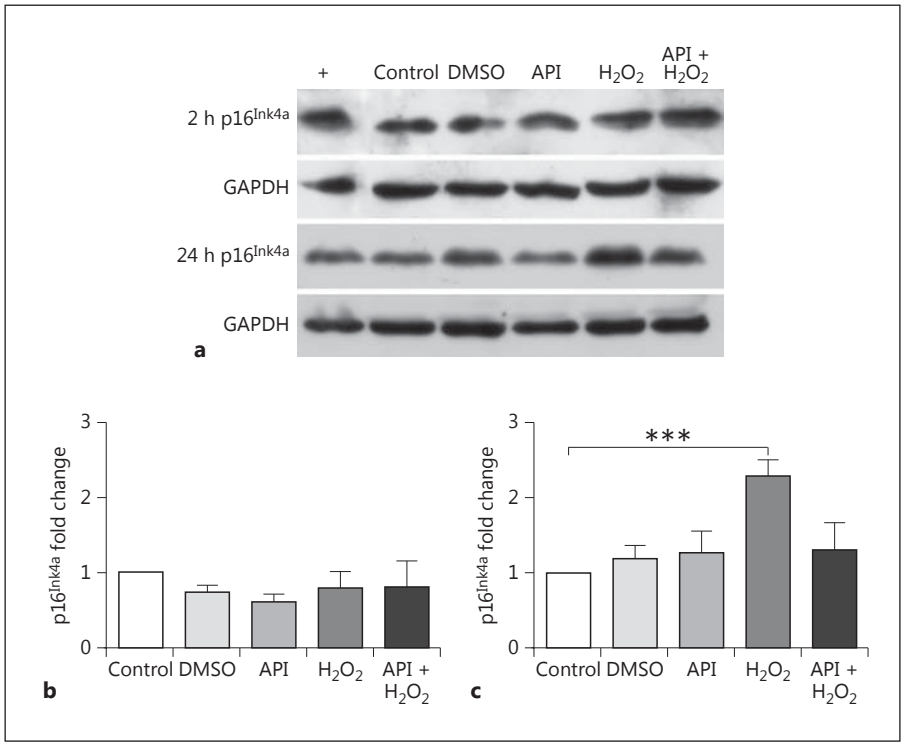

Fig. 6. Western immunoblot and densitometry for $p16^{Ink4a}$. **a** Western immunoblots for the cell cycle regulator $p16^{Ink4a}$ at 2 h (**b**) and 24 h (**c**) after treatment, plus the GAPDH loading controls. Suberohydroxamic acid (+) was used as a positive control for induction of $p16^{Ink4a}$ expression. Blots and densitometry are labelled with control, DMSO vehicle, API, H_2O_2 or API + H_2O_2. $p16^{Ink4a}$ expression did not change significantly at 2 h following all treatments; however, after 24-hour exposure to H_2O_2 there was significantly increased $p16^{Ink4a}$ expression (*** $p < 0.05$ compared to controls).

Discussion

Although oxidative stress and cell senescence may contribute to renal cell dysfunction and attrition in CKD, the involvement of the mitochondria and their health or dysfunction in the pathogenesis of CKD has not yet been well defined. This study used an in vitro kidney disease model with oxidative stress and cell senescence to investigate mitochondria involvement in the loss of renal tubular epithelial cells, as a cell culture model of oxidative stress in CKD. The results have provided evidence that oxidative stress and cell senescence combine to cause most renal cell

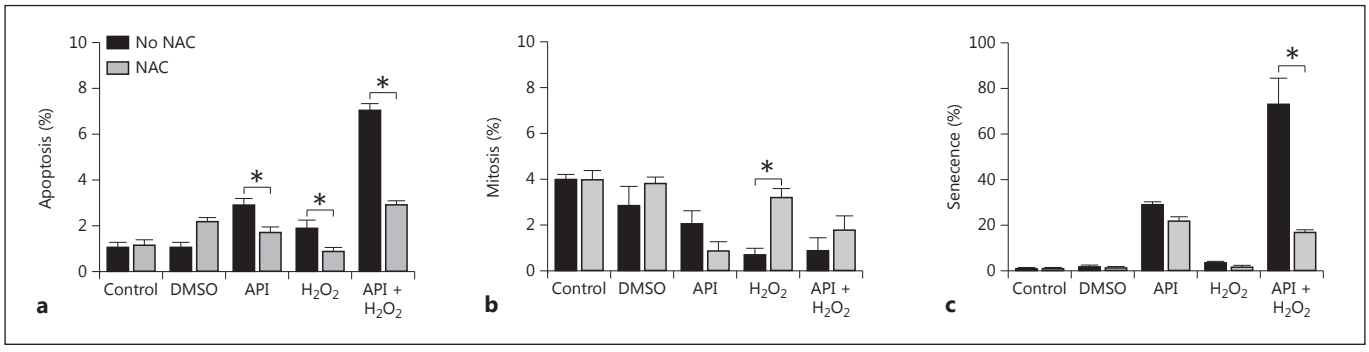

Fig. 7. The antioxidant NAC ameliorates effects of oxidative stress and senescence. Percentage apoptosis (**a**), mitosis (**b**) and senescence (**c**) are shown. Cells were pre-treated with NAC (10 mM), or with vehicle control, for 2 h prior to the treatments. Significant changes are indicated by an asterisk ($p < 0.05$). NAC significantly modulated apoptosis for all treatments, restored the mitotic potential of H_2O_2-treated cells and decreased senescence induced by API + H_2O_2.

loss as well as decrease the proliferative activity of renal cells; both involve mitochondrial destabilization.

One of the unusual outcomes was that the flavonoid API, used successfully here and elsewhere [19] to induce renal cell senescence, also caused increased lipid peroxidation (increased MDA), decreased TAC and the greatest mitochondrial dysfunction with or without concurrent H_2O_2. Lagoa et al. [24] recently reported, using mitochondria isolated from rat brain and heart, that API (10 μM) inhibited the activity of Complex I of the electron transport chain by affecting the binding of the coenzyme substrate. Increased reliance on Complex I–III electron transfer reduces the efficiency of oxidative phosphorylation, perhaps leading to mitochondrial dysfunction. These results and our own suggest that the oxidative stress produced by API may exhaust antioxidant stores. In our study, API did not alter the expression of the cell cycle regulator $p16^{Ink4a}$ after 2 or 24 h, indicating that API-induced kidney cell senescence occurs via $p16^{Ink4a}$-independent mechanisms. The apparent lack of $p16^{Ink4a}$ activity may indicate a protective mechanism, thereby ceasing their progression to transcription. Transcriptional regulation by API may need to be investigated, such as was published by Liu et al. [25] for the inhibitory action of API on vascular endothelial growth factor and angiogenesis.

Apoptosis and mitosis contribute to renal homeostasis by ensuring adequate cell numbers for healthy renal function. Loss of functioning renal cells (increased apoptosis), decreased mitosis and increased cell senescence reflect a decreased ability for the kidney to metabolise and repair in CKD [26, 27]. All of these characteristics featured in the current experiments. API and H_2O_2 were pro-apoptotic, notably with a synergistic effect seen on renal cell apoptosis when the treatments were combined. The pro-apoptotic effect of API has been recorded previously, but mostly in investigations of cancer treatments, where it caused apoptosis in cervical and prostate cancer cell lines when trialled as a therapy against cancer growth [28, 29].

Apoptosis, as a result of oxidative damage, is well recognised. In CKD, apoptosis may initially act as a cellular adaptive response to oxidative stress to eliminate dysfunctional cells. The outcome for the whole kidney, however, is likely to be renal atrophy with loss of renal function. The Bcl-2 family proteins, including pro-apoptotic Bax and anti-apoptotic $Bcl\text{-}X_L$, regulate the intrinsic, mitochondrial-dependent pathway of apoptosis [7, 30]. Changes in the ratio of pro-apoptotic Bax to anti-apoptotic $Bcl\text{-}X_L$ following oxidative insult have been seen previously in renal epithelium [5, 31]. In the current experiments, there was a similar pro-apoptotic change with all treatments.

NAC is a free-radical scavenger that has been used successfully to reduce injury in a variety of nephrotoxic and ischemic experimental and clinical renal models, and has had some success in CKD patients [32]. When it was used concurrently with API and/or H_2O_2, it significantly reduced apoptosis and senescence and also restored the regenerative capacity of the kidney. However, antioxidant therapy is sometimes disappointing in models of CKD [33] and more studies are now being completed comparing multiple antioxidants.

In conclusion, the cellular and biomolecular alterations in the kidney during CKD are undoubtedly very complex, but our investigation provides evidence that oxidative stress and cell senescence together produce the greatest renal cell loss and mitochondrial destabilisation. The antioxidant NAC attenuated many of the character-

istics that likely contribute to CKD. A more targeted approach to antioxidant therapy in CKD may limit mitochondrial dysfunction, with an improved outcome for CKD patients. The model may serve as a baseline to test the role of mitochondria after various putative causes of CKD, and to further analyse the benefits of antioxidants in ameliorating mitochondrial dysfunction in CKD.

Acknowledgements

D.M.S. received an Australian Postgraduate Award PhD Scholarship and a National Health and Medical Research Foundation of Australia Top-Up Grant from the Australian Government.

References

1 Inagami T: Mitochondrial angiotensin receptors and aging. Circ Res 2011;109:1323–1324.
2 Finkel T, Holbrook NJ: Oxidants, oxidative stress and the biology of ageing. Nature 2000; 408:239–247.
3 Singh DK, Winocour P, Farrington K: Oxidative stress in early diabetic nephropathy: fueling the fire. Nat Rev Endocrinol 2011;7:176–184.
4 Carnicer R, Crabtree MJ, Sivakumaran V, Casadei B, Kass DA: Nitric oxide synthases in heart failure. Antioxid Redox Signal 2012, E-pub ahead of print.
5 Cuttle L, Zhang XJ, Endre ZH, Winterford C, Gobe GC: Bcl-x(l) translocation in renal tubular epithelial cells in vitro protects distal cells from oxidative stress. Kidney Int 2001; 59:1779–1788.
6 Vay L, Hernandez-SanMiguel E, Lobaton CD, Moreno A, Montero M, Alvarez J: Mitochondrial free [Ca2+] levels and the permeability transition. Cell Calcium 2009;45:243–250.
7 Madesh M, Hajnoczky G: VDAC-dependent permeabilization of the outer mitochondrial membrane by superoxide induces rapid and massive cytochrome c release. J Cell Biol 2001; 155:1003–1015.
8 Soubannier V, McBride HM: Positioning mitochondrial plasticity within cellular signaling cascades. Biochim Biophys Acta 2009; 1793:154–170.
9 Rieg T, Vallon V: ATP and adenosine in the local regulation of water transport and homeostasis by the kidney. Am J Physiol Regul Integr Comp Physiol 2009;296:R419–R427.
10 Hall AM, Unwin RJ, Parker N, Duchen MR: Multiphoton imaging reveals differences in mitochondrial function between nephron segments. J Am Soc Nephrol 2009;20:1293–1302.
11 St-Pierre J, Buckingham JA, Roebuck SJ, Brand MD: Topology of superoxide production from different sites in the mitochondrial electron transport chain. J Biol Chem 2002; 277:44784–44790.
12 Melk A: Senescence of renal cells: molecular basis and clinical implications. Nephrol Dial Transplant 2003;18:2474–2478.
13 Jiao S, Meng F, Zhang J, Yang X, Zheng X, Wang L: Stat1 mediates cellular senescence induced by angiotensin II and H_2O_2 in human glomerular mesangial cells. Mol Cell Biochem 2012;365:9–17.
14 Stenvinkel P, Larsson TE: Chronic kidney disease: a clinical model of premature aging. Am J Kidney Dis 2013, E-pub ahead of print.
15 Campisi J, d'Adda FF: Cellular senescence: when bad things happen to good cells. Nat Rev Mol Cell Biol 2007;8:729–740.
16 Frippiat C, Chen QM, Zdanov S, Magalhaes JP, Remacle J, Toussaint O: Subcytotoxic H_2O_2 stress triggers a release of transforming growth factor-beta 1, which induces biomarkers of cellular senescence of human diploid fibroblasts. J Biol Chem 2001;276:2531–2537.
17 Glotin AL, Debacq-Chainiaux F, Brossas JY, Faussat AM, Treton J, Zubielewicz A, Toussaint O, Mascarelli F: Prematurely senescent ARPE-19 cells display features of age-related macular degeneration. Free Radic Biol Med 2008;44:1348–1361.
18 Stein GH, Drullinger LF, Soulard A, Dulic V: Differential roles for cyclin-dependent kinase inhibitors p21 and p16 in the mechanisms of senescence and differentiation in human fibroblasts. Mol Cell Biol 1999;19:2109–2117.
19 Ryu SW, Woo JH, Kim YH, Lee YS, Park JW, Bae YS: Downregulation of protein kinase CKII is associated with cellular senescence. FEBS Lett 2006;580:988–994.
20 Pat BK, Cuttle L, Watters D, Yang T, Johnson DW, Gobe GC: Fibrogenic stresses activate different mitogen-activated protein kinase pathways in renal epithelial, endothelial or fibroblast cell populations. Nephrology (Carlton) 2003;8:196–204.
21 Hughes J, Gobe G: Identification and quantification of apoptosis in the kidney using morphology, biochemical and molecular markers. Nephrology (Carlton) 2007;12:452–458.
22 Chen Q, Ames BN: Senescence-like growth arrest induced by hydrogen peroxide in human diploid fibroblast F65 cells. Proc Natl Acad Sci USA 1994;91:4130–4134.
23 Wang XQ, Gabrielli BG, Milligan A, Dickinson JL, Antalis TM, Ellem KA: Accumulation of p16CDKN2A in response to ultraviolet irradiation correlates with late S-G(2)-phase cell cycle delay. Cancer Res 1996;56:2510–2514.
24 Lagoa R, Graziani I, Lopez-Sanchez C, Garcia-Martinez V, Gutierrez-Merino C: Complex I and cytochrome c are molecular targets of flavonoids that inhibit hydrogen peroxide production by mitochondria. Biochim Biophys Acta 2011;1807:1562–1572.
25 Liu LZ, Fang J, Zhou Q, Hu X, Shi X, Jiang BH: Apigenin inhibits expression of vascular endothelial growth factor and angiogenesis in human lung cancer cells: implication of chemoprevention of lung cancer. Mol Pharmacol 2005;68:635–643.
26 Percy CJ, Brown L, Power DA, Johnson DW, Gobe GC: Obesity and hypertension have differing oxidant handling molecular pathways in age-related chronic kidney disease. Mech Ageing Dev 2009;130:129–138.
27 Vogetseder A, Picard N, Gaspert A, Walch M, Kaissling B, Le Hir M: Proliferation capacity of the renal proximal tubule involves the bulk of differentiated epithelial cells. Am J Physiol Cell Physiol 2008;294:C22–C28.
28 Zheng PW, Chiang LC, Lin CC: Apigenin induced apoptosis through p53-dependent pathway in human cervical carcinoma cells. Life Sci 2005;76:1367–1379.
29 Shukla S, Gupta S: Molecular targets for apigenin-induced cell cycle arrest and apoptosis in prostate cancer cell xenograft. Mol Cancer Ther 2006;5:843–852.
30 Chipuk JE, Moldoveanu T, Llambi F, Parsons MJ, Green DR: The bcl-2 family reunion. Mol Cell 2010;37:299–310.
31 Ye J, Li J, Yu Y, Wei Q, Deng W, Yu L: L-carnitine attenuates oxidant injury in HK-2 cells via ROS-mitochondria pathway. Regul Pept 2010;161:58–66.
32 Alonso A, Lau J, Jaber BL, Weintraub A, Sarnak MJ: Prevention of radiocontrast nephropathy with N-acetylcysteine in patients with chronic kidney disease: a meta-analysis of randomized, controlled trials. Am J Kidney Dis 2004;43:1–9.
33 Quiroz Y, Ferrebuz A, Vaziri ND, Rodriguez-Iturbe B: Effect of chronic antioxidant therapy with superoxide dismutase-mimetic drug, tempol, on progression of renal disease in rats with renal mass reduction. Nephron Exp Nephrol 2009;112:e31–e42.

Am J Physiol Renal Physiol 307: F814–F822, 2014.
First published August 13, 2014; doi:10.1152/ajprenal.00205.2014.

Oxidative stress-induced alterations in PPAR-γ and associated mitochondrial destabilization contribute to kidney cell apoptosis

David M. Small,[1] Christudas Morais,[1] Jeff S. Coombes,[1,2] Nigel C. Bennett,[1,3] David W. Johnson,[1,4] and Glenda C. Gobe[1]

[1]*Centre for Kidney Disease Research, School of Medicine, The University of Queensland, Translational Research Institute, Brisbane, Queensland, Australia;* [2]*School of Human Movement Studies, The University of Queensland, Brisbane, Queensland, Australia;* [3]*UQ Centre for Clinical Research, The University of Queensland, Brisbane, Queensland, Australia; and* [4]*Department of Nephrology, Princess Alexandra Hospital, Brisbane, Queensland, Australia*

Submitted 15 April 2014; accepted in final form 6 August 2014

Small DM, Morais C, Coombes JS, Bennett NC, Johnson DW, Gobe GC. Oxidative stress-induced alterations in PPAR-γ and associated mitochondrial destabilization contribute to kidney cell apoptosis. *Am J Physiol Renal Physiol* 307: F814–F822, 2014. First published August 13, 2014; doi:10.1152/ajprenal.00205.2014.—The mechanism(s) underlying renoprotection by peroxisome proliferator-activated receptor (PPAR)-γ agonists in diabetic and nondiabetic kidney disease are not well understood. Mitochondrial dysfunction and oxidative stress contribute to kidney disease. PPAR-γ upregulates proteins required for mitochondrial biogenesis. Our aim was to determine whether PPAR-γ has a role in protecting the kidney proximal tubular epithelium (PTE) against mitochondrial destabilisation and oxidative stress. HK-2 PTE cells were subjected to oxidative stress (0.2–1.0 mM H_2O_2) for 2 and 18 h and compared with untreated cells for apoptosis, mitosis (morphology/biomarkers), cell viability (MTT), superoxide (dihydroethidium), mitochondrial function (MitoTracker red and JC-1), ATP (luminescence), and mitochondrial ultrastructure. PPAR-γ, phospho-PPAR-γ, PPAR-γ coactivator (PGC)-1α, Parkin (Park2), p62, and light chain (LC)3β were investigated using Western blots. PPAR-γ was modulated using the agonists rosiglitazone, pioglitazone, and troglitazone. Mitochondrial destabilization increased with H_2O_2 concentration, ATP decreased (2 and 18 h; $P < 0.05$), Mitotracker red and JC-1 fluorescence indicated loss of mitochondrial membrane potential, and superoxide increased (18 h, $P < 0.05$). Electron microscopy indicated sparse mitochondria, with disrupted cristae. Mitophagy was evident at 2 h (Park2 and LC3β increased; p62 decreased). Impaired mitophagy was indicated by p62 accumulation at 18 h ($P < 0.05$). PPAR-γ expression decreased, phospho-PPAR-γ increased, and PGC-1α decreased (2 h), indicating aberrant PPAR-γ activation and reduced mitochondrial biogenesis. Cell viability decreased (2 and 18 h, $P < 0.05$). PPAR-γ agonists promoted further apoptosis. In summary, oxidative stress promoted mitochondrial destabilisation in kidney PTE, in association with increased PPAR-γ phosphorylation. PPAR-γ agonists failed to protect PTE. Despite positive effects in other tissues, PPAR-γ activation appears to be detrimental to kidney PTE health when oxidative stress induces damage.

peroxisome proliferator-activated receptor-γ; thiozolidinediones; mitochondria; oxidative stress

ALTERATIONS IN THE BIOENERGETIC CONTROLS of kidney cells can lead to a failure in oxidant handling, leading to a state of oxidative stress in kidney disease. The causes are multiple, from high glucose in diabetes to ischemia-reperfusion, toxins, and acute kidney injury to the long-term effects of aging and the development of chronic kidney disease (CKD). Kidney tubular atrophy, mainly due to tubular cell apoptosis of the proximal tubule, is a common characteristic of these diseases and therefore presents a crucial target to preserve kidney health (36, 37). Oxidative stress is a mediating factor in mitochondrial dysfunction and subsequent cell dysregulation and death during kidney disease (16, 41, 47). The importance of mitochondrial dysregulation comes from the large number of mitochondria in proximal tubular epithelial (PTE) cells and their heavy reliance on oxidative phosphorylation for ATP-dependent active solute transport in the nephron (19). Identifying oxidant-handling pathways that are perturbed in the kidney during oxidative stress is necessary for the development of reliable therapies.

Peroxisome proliferator-activated receptor (PPAR)-γ is a member of the highly conserved nuclear hormone receptor superfamily of ligand-dependent transcription factors that play central roles in lipid metabolism, glucose homeostasis, cell proliferation, and inflammation (1). Ligand binding induces heterodimer formation with the retinoic acid receptor and complex binding to the peroxisome proliferator response element within the promoter region of target genes (18). Phosphorylation may modulate the activity of PPAR-γ through activating multiple kinase signaling pathways, including ERK and AMP-activated protein kinase (AMPK). However, PPAR-γ phosphorylation does not always indicate the activation of PPAR-γ (5, 23, 51). Its inhibition may also be important for the overall outcome, which largely depends on tissue type and the mode of PPAR-γ modulation.

The family of thiozolidinediones (TZDs) consists of potent pharmacological agonists of PPAR-γ, commonly used in the treatment of type 2 diabetes. The targeting of PPAR-γ, however, is not limited to diabetes and its effect or dependence on insulin. For example, PPAR-γ mRNA expression is increased in kidney biopsies of CKD patients of diverse etiologies (32) raising the possibility of mechanisms not dependent on insulin; the TZD rosiglitazone attenuated kidney structural and functional damage in a mouse model of diabetes, yet no change was observed in glucose, insulin, or lipid levels (4), and a reduction in proteinuria was achieved in patients with nondiabetic kidney disease of various etiologies after 4 mo of rosiglitazone treatment (27). A possible explanation for the diverse outcomes from PPAR-γ agonist success is that PPAR-γ also positively regulates mitochondrial biogenesis through the activation of PPAR-γ coactivator (PGC)-1α. Thus, PPAR-γ may influence mitochondrial function (6, 12). This is important given the vital

Address for reprint requests and other correspondence: G. C. Gobe, Centre for Kidney Disease Research, School of Medicine, Univ. of Queensland, Translational Research Institute, 37 Kent St., Woolloongabba, Brisbane, QLD 4102, Australia (e-mail: g.gobe@uq.edu.au).

role mitochondria play in regulating the intracellular redox environment (50). Healthy mitochondrial function relies on the degradation of defective mitochondria via the activation of selective autophagy pathways (mitophagy) and upregulation of mitochondrial biogenesis pathways to restore a healthy pool of functioning mitochondria (44). PPAR-α, an alternate isoform of PPAR, also plays a role in mitochondrial biogenesis, but is more widely expressed in the skeletal muscle and liver (17) than in the kidney.

Several molecular pathways may be involved for the influence of PPAR-γ on mitochondrial function. A major pathway for injury-induced mitochondrial degradation is the phosphate and tensin homology-induced kinase-Parkin 2 (Park2) pathway. Park2 is an E3 ubiquitin ligase that translocates to mitochondria and mediates mitochondrial degradation (3, 35). The adaptor protein p62 facilitates selective autophagy into the light chain (LC)3β-regulated machinery for lysosomal degradation (2, 13). p62 is not required for Park2 translocation to damaged mitochondria but is essential for final autophagic clearance (13). PGC-1α is a nuclear transcription factor that has been shown to mediate almost all aspects of mitochondrial biogenesis and is therefore considered a master regulator of biogenesis (21). Failure to restore mitochondrial homeostasis and function can lead to a progressive increase in ROS and ensuing oxidative stress. Therefore, PGC-1α activation presents a crucial target for mitochondrial preservation. Previous studies (22, 39) have demonstrated TZD induction of mitochondrial biogenesis.

This study sought to *1*) investigate the role of PPAR-γ in oxidative stress and mitochondrial destabilization in damage and loss of human kidney proximal tubular cells and *2*) determine whether PPAR-γ modulation can protect human kidney PTE cells from oxidative stress-induced damage by preserving mitochondrial function.

METHODS AND MATERIALS

Experimental design. HK-2 PTE cells were maintained in DMEM-F-12 Ham's medium containing 10% FBS and 1% penicillin-streptomycin. Cells were grown at 37°C in a humidified atmosphere of 95% O_2 and 5% CO_2, in 25- or 75-cm^2 flasks. Cells were treated with H_2O_2 (0.2–1.0 mM) for 2 and 18 h to induce oxidative stress. In some treatments, the PPAR-γ agonists troglitazone, rosiglitazone, and pioglitazone were used as treatments for 2 h before and during H_2O_2 exposure. Troglitazone (T2573) and pioglitazone (E6910) were purchased from Sigma-Aldrich (Castle Hill, NSW, Australia); rosiglitazone (no. 71740) was purchased from Cayman Chemical (Ann Arbor, MI). All agonists were dissolved as stock solutions in DMSO and stored frozen as small aliquots. A vehicle control was always used for these experiments.

Western blot analysis. Western blots were performed from whole cell lysates dissociated in lysis buffer (0.15M sodium chloride, 0.025M sodium fluoride, 0.5M EDTA, 0.1% SDS, and 1.0% Igepal in 50 mM Tris·Cl, pH 7.5) containing phosphatase and protease inhibitors (10 μg/ml aprotinin, 10 μg/ml leupeptin, 1 mM sodium orthovanidate, and 100 μg/ml phenylmethylsulfonyl chloride). Protein was separated by SDS-PAGE on 10% acrylamide gel and electrophoretically transferred onto polyvinyldodecylfluoride membranes. Membranes were blotted using antibodies against PPAR-γ, phosphorylated (p-)PPAR-γ (phosphorylation site: Ser^{112}), PPAR-α, PGC-1α, Park2, p62, LC3β, and GAPDH as a loading control. Ponceau S was also used as a dye on the polyvinyldodecylfluoride membrane to indicate even loading of protein. Appropriate secondary antibodies were used and visualised using chemiluminescent enhancer and X-ray film. Scion software (Release Alpha 4.0.3.2) was used to quantify bands for densitometry, which was normalized to GAPDH.

Light and fluorescence microscopy. Cells were grown to ~70% confluence on 12-mm glass coverslips. Immunofluorescence and cytochemistry were used to assess p62 cellular localization. The primary antibody for p62 (1:500, Santa Cruz Biotechnologies, Santa Cruz, CA) was used with a secondary anti-rabbit Alexa fluor green fluorescence conjugate (1:300, Cell Signaling Technologies, Danvers, MA). Apoptosis and mitosis were assessed using morphology (14) after hematoxylin and eosin staining and digital scanning using Aperio ImageScope histology software. Data were obtained by counting 10 frames (×200) of cells for each treatment and calculating the percentage of apoptotic or mitotic cells. The morphological characteristics for apoptosis were *1*) shrunken eosinophilic cells with condensed, marginated nuclear chromatin and an intact cell membrane; *2*) discrete apoptotic bodies compromising large, dense, pyknotic nuclear fragments surrounded by a narrow eosinophilic cytoplasm; and *3*) clusters of small apoptotic bodies (assessed as a single apoptotic occurrence) (14). The morphological characteristics used to distinguish mitosis were *1*) the formation of mitotic spindles occurring during metaphase and remaining visible in anaphase or *2*) cells in the later stages of mitosis, telophase, or undergoing cytokinesis. Morphological verification of quantification has been confirmed in a similar experimental protocol using molecular biomarkers for apoptosis (ApopTag) and mitosis (proliferating cell nuclear antigen) in parallel with morphology (41).

Oxidative stress and mitochondrial function. Oxidative stress was determined and quantified using microfluorimetry detection of the oxidation of dihydroethidium (DHE) to ethidium. Superoxide selectively oxidizes this reaction and is an essential precursor to harmful cellular oxidants, such as the hydroxyl radical and peroxynitrite. Cells were cultured in black 96-well plates and treated as previously described. The growth medium was then replaced with 5μM DHE in serum-free DMEM-F-12 and incubated for 30 min. Fluorescence intensity was measured at 536-nm excitation and 610-nm emission (Synergy Mx Multi-Mode Microplate reader, BioTek, Winooski, VT). Fluorescence values were normalized to protein content for the corresponding wells and expressed as DHE fluorescence per microgram of protein. JC-1 is a cationic fluorophore that possesses a mitochondrial membrane-dependent accumulation in mitochondria and was quantified using the same technique. A decrease in red fluorescence (JC-1 aggregate uptake into healthy mitochondria) and increase in green fluorescence (JC-1 in the cytoplasm) indicates mitochondrial membrane depolarization. JC-1 (3 μM) was used posttreatment, and fluorescence intensity was measured at 525-nm excitation and 590-nm emission (red) and 490-nm excitation and 530-nm emission (green) and normalized to protein content. ATP production was measured using a luciferase-based luminescence assay (Promega). Cells were seeded into white opaque 96-well plates and treated as previously described. Chemiluminescent reagent was added, and cell lysis was induced before luminescence was measured at an integration time of 0.5 s using a Titertek-Berthold Luminometer (Titertek-Berthold Detection Systems, Pforzheim, Germany).

Mitochondrial viability. MitoTracker red CMXRos (Invitrogen) and confocal fluorescence microscopy were used to determine mitochondrial density. MitoTracker localizes to mitochondria with a healthy mitochondrial membrane potential. Cells were grown on glass coverslips and exposed to 100 nm MitoTracker red CMXRos for 30 min after treatments as previously described. Coverslips were mounted after fixation in 4% paraformaldehyde and 4′,6-diamidino-2-phenylindole nuclear staining. Cells were observed at ×63 with a Zeiss 510 Meta confocal fluorescence microscope using Zen 2008 software. Transmission electron microscopy was used to visualize the ultrastructure of mitochondria. Briefly, cells were grown on sapphire disks in growth media and exposed to treatments. High-pressure freezing fixation was performed, and samples were imaged with a Jeol 1010 transmission electron microscope.

Cell viability. Cell viability was measured using the assay based on the reduction 3-(4,5-dimethylthiazol-2-yl)-2,5-diphenyltetrazolium bromide (MTT; Sigma). Briefly, cells were treated as previously described in 96-well plates, and 100μl MTT solution was prepared in DMEM-F-12 solution (0.5 mg/ml), added to wells, and incubated for 90 min at 37°C. MTT culture media were removed, and formazan crystals that had formed during the assay were dissolved in 200 μl DMSO. Absorbance was measured in a microplate reader at 570 nm with background collection at 690 nm.

Statistical analysis. Values are reported as means ± SE. Data were analyzed using one-way ANOVA and Tukey's post hoc analysis, two-way ANOVA and Bonferroni's post hoc test, or Student's *t*-test where appropriate. Significance was established at $P < 0.05$.

RESULTS

Oxidative stress decreased PPAR-γ expression and increased PPAR-γ Ser^{112} phosphorylation. HK-2 cells displayed a dose-dependent significant increase in apoptosis and dose-dependent decrease in mitosis after oxidative stress at both 2 and 18 h (Fig. 1, *A* and *B*). This was associated with a decrease in PPAR-γ protein levels ($P < 0.001$ starting at 0.4 mM H_2O_2; Fig. 2*A*) and a dose-dependent increase in p-PPAR-γ levels ($P < 0.001$ starting at 0.4 mM H_2O_2; Fig. 2*A*) after 2 h of exposure to H_2O_2. After 18 h of H_2O_2 exposure (Fig. 2*B*), PPAR-γ and p-PPAR-γ returned to basal levels, indicating that oxidative stress promotes the phosphorylation of PPAR-γ as an early response. Conversely, PPAR-α expression decreased in a dose-dependent manner after 2 h of exposure to H_2O_2 ($P < 0.05$ starting at 0.4 mM H_2O_2; Fig. 2*A*) and returned to control levels after 18 h of H_2O_2 exposure (Fig. 2*B*).

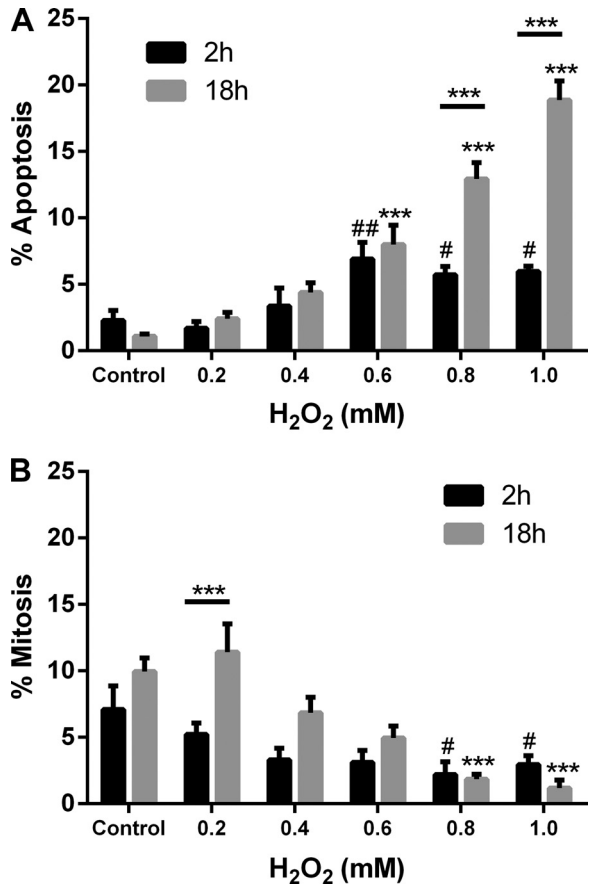

Fig. 1. Oxidative stress promotes apoptosis and impairs mitosis in HK-2 cells. HK-2 cells were exposed to H_2O_2 at concentrations ranging from 0.2 to 1.0 mM. Percentages of apoptotic and mitotic cells were imaged at ×200 and quantified using morphology after hematoxylin and eosin staining. Apoptosis significantly increased in a dose-dependent manner after H_2O_2 exposure at both 2 and 18 h (*A*). Mitosis significantly decreased in a dose-dependent manner after H_2O_2 exposure at both 2 and 18 h (*B*). Results are expressed as means ± SE. ***$P < 0.001$ compared with 18-h controls; #$P < 0.05$ and ##$P < 0.01$ compared with 2-h controls.

Oxidative stress induced mitochondrial dysfunction. Mitochondrial function was significantly reduced after exposure to H_2O_2 for both 2 and 18 h (Fig. 3). H_2O_2 (0.6 mM) significantly increased DHE fluorescence, indicating enhanced levels of superoxide production and confirming an intracellular state of oxidative stress ($P < 0.05$; Fig. 3*A*). The mitochondrial membrane potential significantly decreased, as indicated by a decrease in JC-1 red fluorescence intensity ($P < 0.01$ starting at 0.4 mM H_2O_2; Fig. 3*B*) and an increase in JC-1 green fluorescence intensity ($P < 0.01$ starting at 0.4 mM H_2O_2; Fig. 3*C*). Confocal microscopy revealed that, compared with untreated HK-2 cells (Fig. 3*H*), uptake of MitoTracker red CMXRos fluorescence was impaired after H_2O_2 exposure at both 2 h (Fig. 3*I*) and 18 h (Fig. 3*J*). Mitochondrial ultrastructure (Fig. 3, *D–G*) revealed abundant elongated mitochondria with clear cristae in untreated HK-2 cells (Fig. 3, *D* and *E*) compared with segmented and swollen mitochondria (Fig. 3*F*) and absent cristae (Fig. 3*G*) after H_2O_2 exposure. These changes relate to a significant dose-dependent decrease in ATP production by mitochondria after H_2O_2 exposure at both 2 h ($P < 0.001$ at 0.4 mM H_2O_2; Fig. 4*A*) and 18 h ($P < 0.001$ at 0.4 mM H_2O_2; Fig. 4*B*), indicating impaired oxidative phosphorylation.

Oxidative stress-induced PPAR-γ dysregulation impaired mitochondrial autophagy (mitophagy) and biogenesis. After oxidative stress and the initial insult affecting mitochondrial function (Figs. 3 and 4), the cellular autophagy machinery needed for selective mitochondrial clearance was upregulated. These results are shown in Fig. 5. Two hours of H_2O_2 exposure significantly increased Park2 expression ($P < 0.01$ at 0.4 mM H_2O_2; Fig. 5*A*), indicating effective tagging of defective/damaged mitochondria for autophagic clearance. Simultaneously, expression of the adapter protein p62 was significantly downregulated ($P < 0.05$ at 0.4 mM H_2O_2; Fig. 5*B*), and a significant increase was seen in LC3β protein levels ($P < 0.01$ at 0.6 mM H_2O_2; Fig. 5*C*), demonstrating early selective autophagy of mitochondria (mitophagy). Park2 expression was not significantly altered after extended (18 h) H_2O_2 exposure (Fig. 5*D*), yet there was a significant increase in p62 and LC3β protein levels, indicating impaired p62 degradation with intracellular accumulation. Altered p62 expression, as seen by Western immunoblot analysis and assumed intracellular accumulation, was verified using confocal microscopy (Fig. 5, *G–I*). There was a decrease in the PPAR-γ coactivator and mitochondrial biogenesis marker PGC-1α after 2 h of H_2O_2 exposure ($P < 0.05$ at 0.4 mM H_2O_2; Fig. 6*A*) that corresponded with the changes in Park2, p62, and LC3β. The cumulative results demonstrate impaired PPAR-γ-dependent mitochondrial biogenesis.

PPAR-γ activation does not protect kidney proximal tubular cells from oxidative stress-induced damage. PPAR-γ expression and phosphorylation changes with selective PPAR-γ TZD agonists were tested to determine whether this protected cells

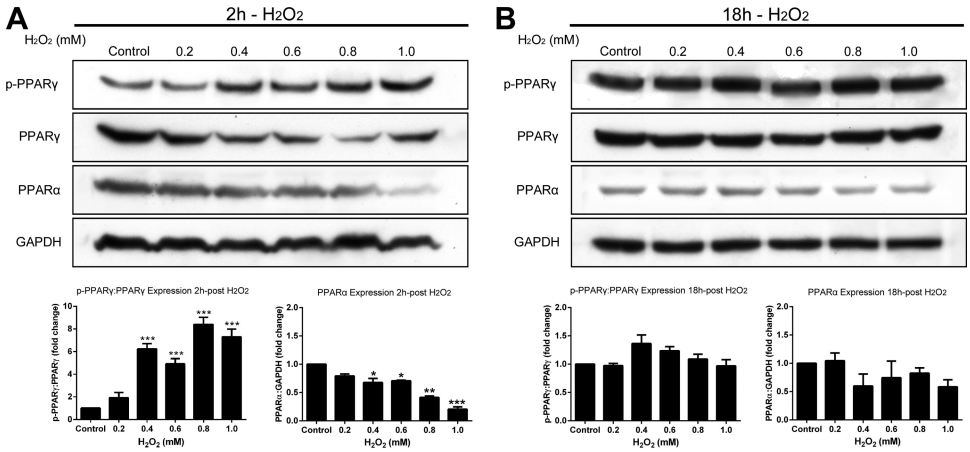

Fig. 2. Peroxisome proliferator-activated receptor (PPAR)-γ and PPAR-α respond early (2 h) after oxidative stress. HK-2 cells were exposed to a range of H_2O_2 concentrations (0.2–1.0 mM) for 2 and 18 h. *A*: representative Western blots. There was a dose-dependent significant increase in PPAR-γ phosphorylation [phosphorylated (p-)PPAR-γ] after 2 h of H_2O_2 exposure that corresponded to a decrease in PPAR-γ expression. PPAR-α significantly increased in a dose-dependent manner after 2 h of H_2O_2 exposure. *B*: results for 18 h. H_2O_2 exposure for 18 h did not significantly alter PPAR-γ phosphorylation or PPAR-α expression. p-PPAR-γ and PPAR-γ are expressed as a ratio, and PPAR-α protein expression was normalized to GAPDH expression. Results are expressed as means ± SE. $*P < 0.05$, $**P < 0.01$, and $***P < 0.001$ compared with controls.

from oxidative stress. The TZD agonists were delivered 2 h before H_2O_2 (0.6 mM) exposure and during the 2- and 18-h H_2O_2 treatment periods. Concentrations of the TZD agonists (rosiglitazone and troglitazone at 10 μM and pioglitazone at 1 μM) were chosen from our preliminary data (not shown) and were consistent with concentrations used in similar previous studies (6, 11, 22, 33, 34). Expression of p-PPAR-γ was calculated as a ratio of PPAR, and the fold change compared with control cells was then compared for each of the TZDs at 2 h (Fig. 7, *A–C*) and 18 h (Fig. 7, *G–I*). H_2O_2 exposure alone caused a significant increase in Ser^{112} phosphorylation of PPAR-γ at both 2 and 18 h ($P < 0.05$, Fig. 7, *A–C*; and $P < 0.001$, Fig. 7, *G–I*). This occurred in conjunction with a significant decrease in cell viability compared with control cells at 2 and 18 h ($P < 0.001$, Fig. 7, *D–F*; and $P < 0.001$, Fig. 7, *J–L*). Cell viability was not improved above H_2O_2 levels when each of the PPAR-γ agonists was used in combination with H_2O_2 for 2 h (Fig. 7, *D–F*). Thus, these results demonstrate a lack of protection by TZDs against oxidative stress-induced loss of viability at a time when the p-PPAR-γ-to-PPAR ratio was significantly increased. After extended exposure to PPAR-γ agonists and H_2O_2 (18 h), cell viability levels remained significantly low ($P < 0.001$; Fig. 7, *J–L*), with the cell viability of the dual TZD and H_2O_2 treatment showing a further significant reduction with rosiglitazone and troglitazone ($P < 0.05$; Fig. 7, *J* and *K*). Expression of the p-PPAR-γ-to-

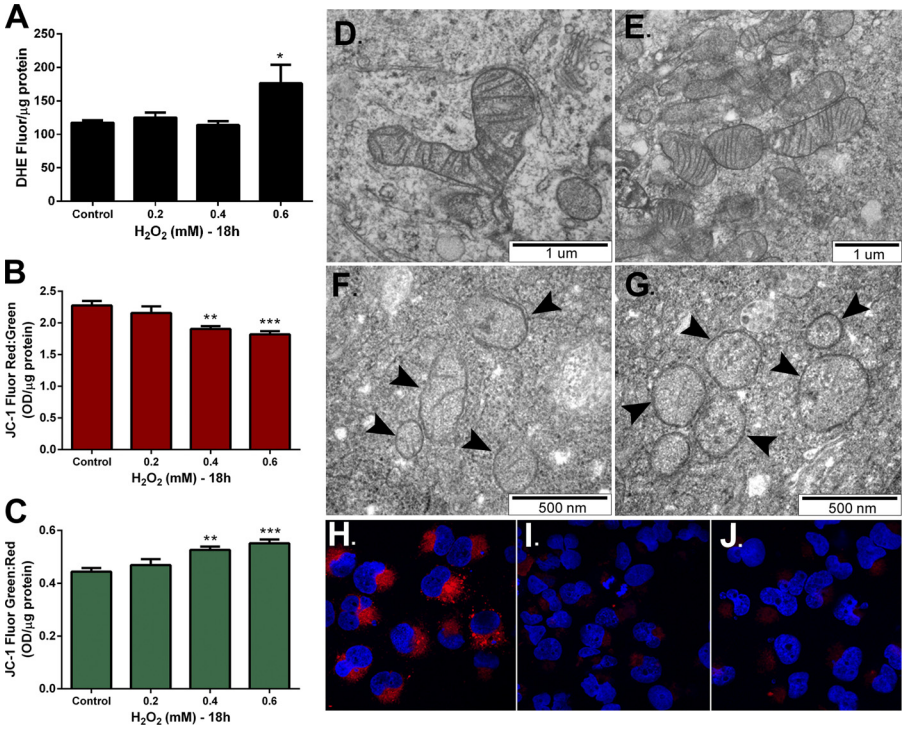

Fig. 3. Oxidative stress induces mitochondrial dysfunction. HK-2 cells were exposed to a range of H_2O_2 concentrations (0.2–0.6 mM) for 2 and 18 h. Dihydroethidium (DHE) and JC-1 fluorescence was quantified by fluorimetry at 18 h. *A*: DHE fluorescence significantly increased after 0.6 mM H_2O_2 exposure, demonstrating ROS generation at 18 h. *B* and *C*: JC-1 red fluorescence significantly decreased in a dose-dependent manner (*B*) while increasing in green fluorescence (*C*), indicating mitochondrial membrane depolarization at 18 h. *D–G*: transmission electron microscopy revealed elongated morphologically healthy mitochondria with cristae in untreated HK-2 cells (*D* and *E*) and segmented, swollen mitochondria (*F*) often with absent cristae (*G*) in 0.6 mM H_2O_2-treated HK-2 cells at 18h (arrow heads). *H–J*: MitoTracker red CMXRos uptake was visualized with confocal microscopy and shown to decline after both 2 h (*I*) and 18 h (*J*) of 0.6 mM H_2O_2 exposure compared with untreated HK-2 cells (*H*). Results are expressed as means ± SE. $*P < 0.05$, $**P < 0.01$, and $***P < 0.001$ compared with controls.

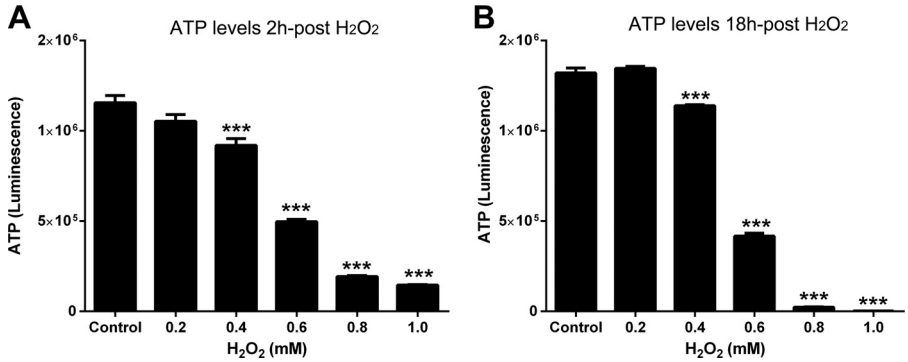

Fig. 4. Oxidative stress impaired cellular ATP production. HK-2 cells were exposed to a range of H_2O_2 concentrations (0.2–1.0 mM) for 2 and 18 h. An ATP assay was performed based on luminescence. ATP levels significantly decreased in a dose-dependent manner after H_2O_2 exposure for both 2 h (*A*) and 18 h (*B*). Results are expressed as means ± SE. $***P < 0.001$ compared with controls.

PPAR-γ ratio remained significantly increased at 18 h for rosiglitazone combined with H_2O_2 ($P < 0.001$; Fig. 7*G*), whereas the ratio returned to that observed in untreated controls after troglitazone cotreatment (Fig. 7*H*) and was lower than untreated controls with pioglitazone cotreatment ($P < 0.01$; Fig. 7*I*). Extended exposure of TZD agonists for 18 h before H_2O_2 exposure also demonstrated no protection to cell viability (data not shown).

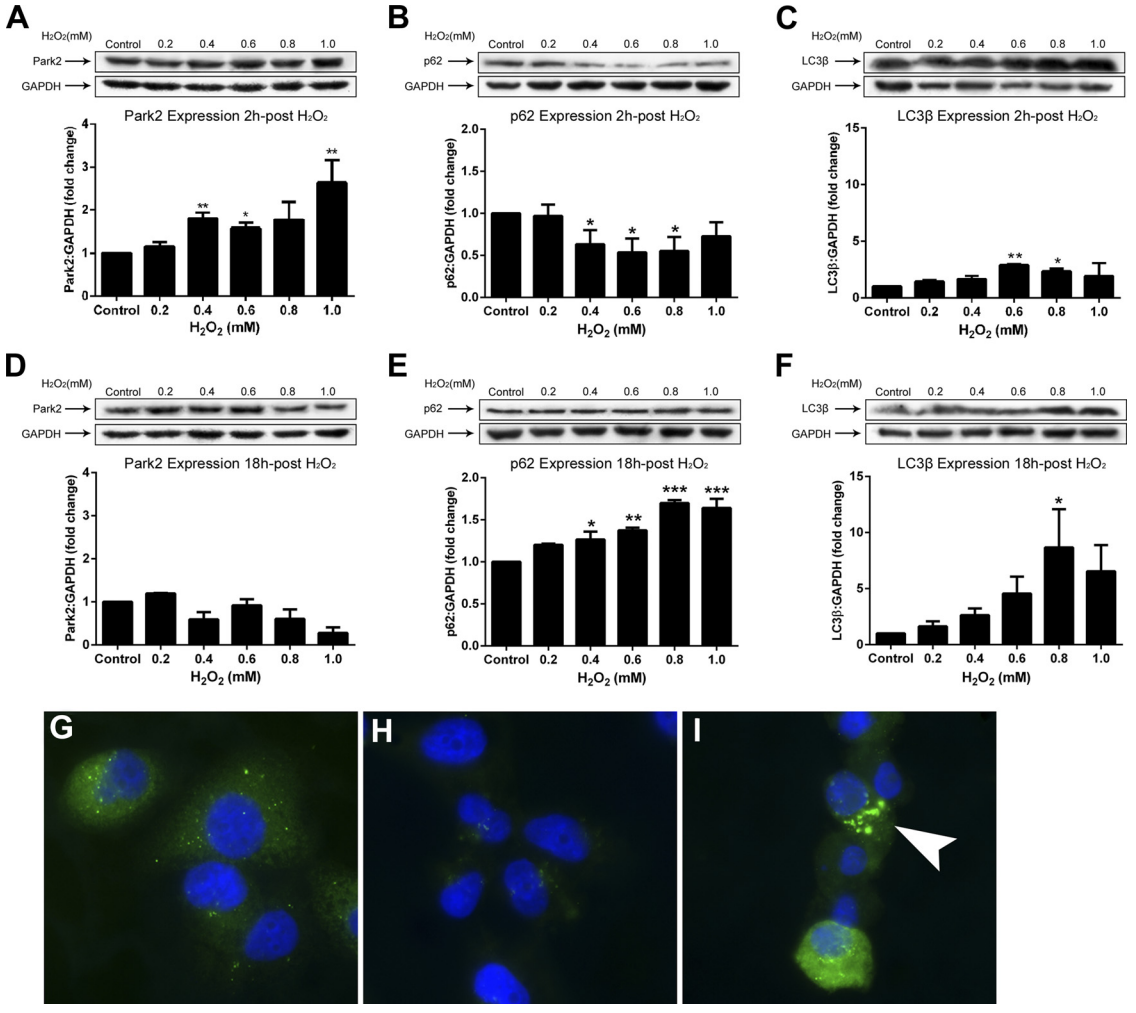

Fig. 5. Oxidative stress promotes selective mitochondrial autophagy (mitophagy). HK-2 cells were exposed to a range of H_2O_2 concentrations (0.2–1.0 mM) for 2 and 18 h. Cells were lysed, and Western blot analysis was performed. Immunofluorescence of p62 was performed (anti-p62 is green fluorescence and nuclear 4′,6-diamidino-2-phenylindole is blue). Protein levels of Parkin (Park2; *A*) and p62 (*B*) significantly increased and decreased, respectively, in a dose-dependent manner, whereas light chain (LC)3β (*C*) significantly increased after 2 h of H_2O_2 exposure. Park2 protein levels returned to control levels after 18 h of H_2O_2 (*D*), whereas p62 (*E*) and LC3β (*F*) expression significantly increased in a dose-dependent manner. Immunofluorescence revealed decreased cytoplasmic localisation of p62 after 2 h of H_2O_2 (*H*) compared with untreated HK-2 cells (*G*), which increased after 18 h of H_2O_2 (*I*) to show a punctate perinuclear cytoplasmic pattern (white arrowhead). Protein expression was normalized to GAPDH expression. Results are expressed as means ± SE. $*P < 0.05$, $**P < 0.01$, and $***P < 0.001$, compared with controls.

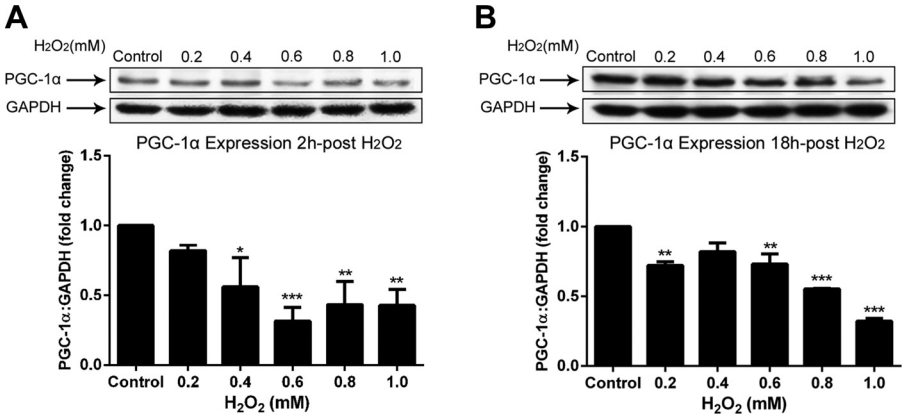

Fig. 6. Oxidative stress impairs PPAR-γ coactivator (PGC)-1α-dependent mitochondrial biogenesis that persists long term. HK-2 cells were exposed to a range of H_2O_2 concentrations (0.2–1.0 mM) for 2 and 18 h. Cells were lysed, and Western blot analysis was performed. Protein levels of PGC-1α significantly decreased in a dose-dependent manner after both 2 h (*A*) and 18 h (*B*) of H_2O_2 exposure. Protein expression was normalized to GAPDH expression. Results are expressed as means ± SE. $*P < 0.05$, $**P < 0.01$, and $***P < 0.001$ compared with controls.

DISCUSSION

Oxidative stress and mitochondrial dysfunction have been implicated in the pathogenesis of kidney disease of diverse causes, including diabetes and CKD, two diseases of increasing incidence (8, 15, 16). However, the molecular mechanisms are still unclear. Here, oxidative stress-induced PPAR-γ alterations were associated with mitochondrial destabilization and a failure to restore mitochondrial health due to defective activation of PPAR-γ-dependent biogenesis pathways. Furthermore, selective PPAR-γ activation enhanced oxidative stress-mediated tubular cell damage that was associated with PPAR-γ Ser^{112} phosphorylation. The results suggest that, despite positive benefits in other tissues, PPAR-γ activation may be detrimental to kidney PTE cells in the scenario of oxidative stress-induced injury.

Our results demonstrate that PPAR-γ is present in kidney PTE cells and is responsive early in oxidative stress-induced injury. The associated increase in Ser^{112}-phosphorylation of PPAR-γ (p-PPAR-γ) was not beneficial to cellular outcome in these cells. The increase in the p-PPAR-γ-to-PPAR-γ ratio may be injurious to cells via the development of mitochondrial dysfunction. However, at 18 h of exposure to oxidative stress, the p-PPAR-γ-to-PPAR-γ ratio was not elevated, perhaps demonstrating that early stress-induced PPAR-γ dysregulation stimulates a series of persistent negative cellular events, primarily targeting mitochondrial homeostasis.

Oxidative stress-induced posttranslational modifications to PPAR-γ, including phosphorylation, have had little study in kidney PTE cells. In adipocytes, MAPK-induced phosphorylation of PPAR-γ at Ser^{112} was linked to decreased transcriptional activity of PPAR-γ by inhibition of ligand binding and cofactor recruitment (5, 23, 51). In addition, PPAR-γ phosphorylation at Ser^{87} by AMP kinase in baby hamster kidney cells repressed the transactivating function of the receptor (31). Our data, demonstrating a decrease in PPAR-γ transcriptional activity along with a failure to upregulate PGC-1α and mitochondrial biogenesis, at a time of increased Ser^{112} PPAR-γ phosphorylation in human kidney PTE cells, agree with those reports. The decrease in total functional PPAR-γ is likely due to phosphorylation. Similar results have been shown in kidney mesangial cells exposed to a high-glucose environment (45), a mechanism of kidney injury involving increased oxidative stress (40, 42).

PTE cells of the kidney have a high density of mitochondria (20). It is likely, therefore, that the relationship between PPAR-γ and mitochondrial function will be especially important. Yang and colleagues (48) have previously shown, in an in vivo rat model of aging, that PPAR-γ activation attenuates age-related mitochondrial injury in the kidney by maintaining the integrity of the mitochondrial membrane potential. However, these results represent an outcome from the heterogeneous renal cell population and not specifically mitochondria from PTE cells. The majority of in vitro studies that have demonstrated protective actions of PPAR-γ have done so in glomerular cell types, namely, podocytes and mesangial cells (26, 34, 49). Our results demonstrate oxidative stress-induced PTE cell mitochondrial dysfunction that is associated with a decreased p-PPAR-γ-to-PPAR-γ ratio. This alteration is persistent, indicating that PPAR-γ induces negative downstream effects. We hypothesized that PPAR-γ phosphorylation induced disruptions to the mitochondrial homeostatic machinery and was responsible for this persistent cumulative dysfunction.

Autophagy is a highly conserved protective response to eliminate damaged cellular components. Mitochondrial homeostasis relies on the degradation of defective mitochondria and upregulation of mitochondrial biogenesis to restore a healthy pool of functioning mitochondria (9). Our results demonstrate significant perturbation to these pathways during oxidative stress. The induction of selective mitophagy mediated by the Park2-p62-LC3β pathway is evident after the initial (2 h) response to oxidative stress. However, long-term (18 h) oxidative stress facilitates significant impairments to this system, as indicated by p62 aggregation. Park2 upregulation after 2 h of oxidative stress demonstrates labeling and translocation of the E3 ligase Parkin to depolarized mitochondria and the initiation of polyubiquination to signal p62 binding (13). p62 degradation has been shown to be a consistent marker of selective autophagy due to its clearance within the autophagosome (25, 28, 29, 43), and our results further confirm this with enhanced LC3β expression. Mitophagy has received little study in the kidney, with Parkin-mediated mitophagy previously shown to be dependent upon p62 in HeLa and neuroblastoma cell lines (13). Recently, Ishikawa and colleagues (24) used rat acute kidney injury models to demonstrate that increased mitophagy in the kidney was highly influenced by ROS. The results of the present investigation show an increase in p62 after 18 h of oxidative stress, demonstrating impaired selective turnover and accumulation of p62. A previous study (30) has demonstrated liver injury accompanied by the formation of p62-positive inclusions and that the removal of p62

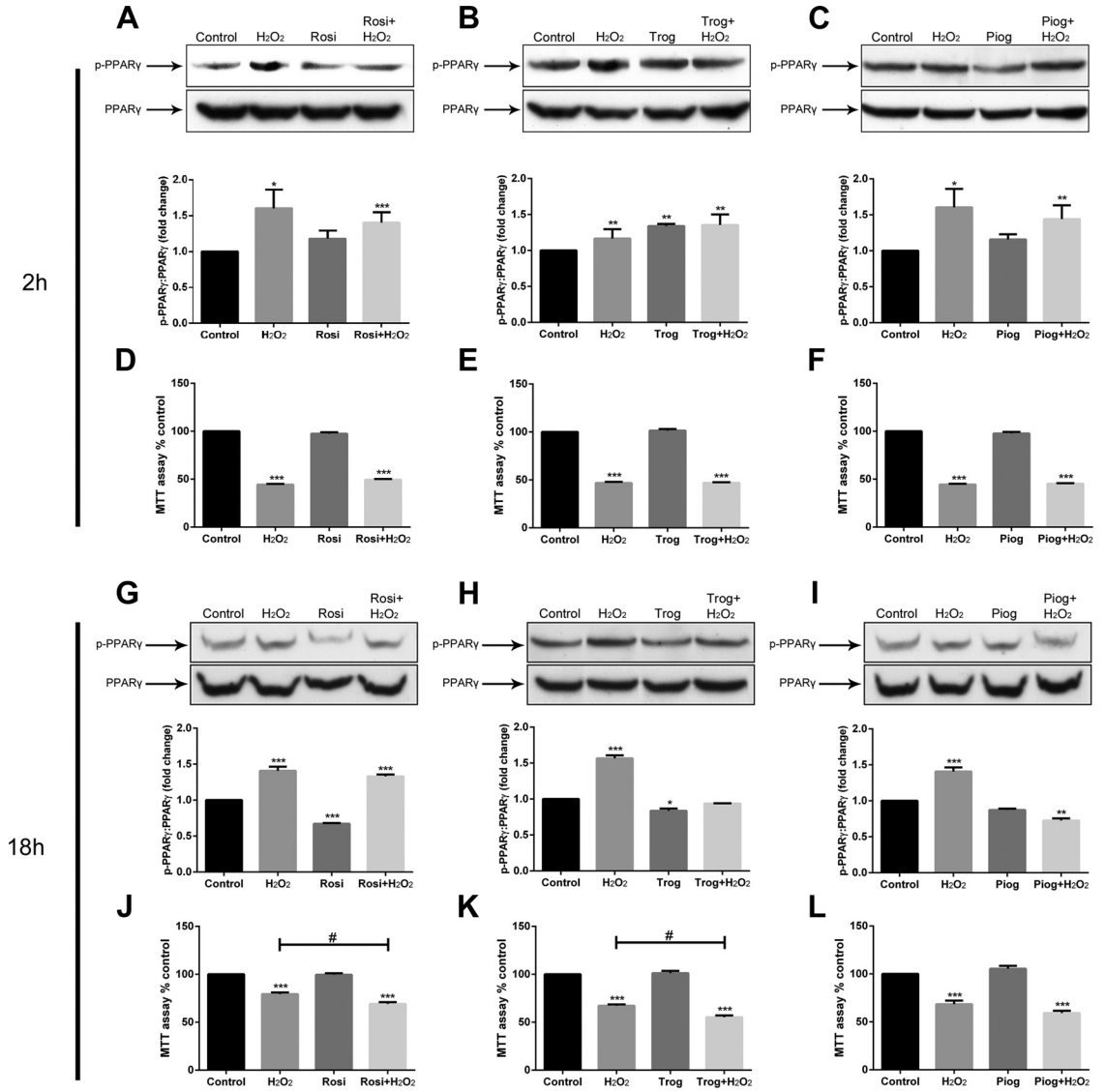

Fig. 7. PPAR-γ activation does not protect HK-2 cells against oxidative stress-induced injury. HK-2 cells were exposed for 2h with either rosiglitazone (Rosi; 10μM), troglitazone (Trog; 10 μM), or pioglitazone (Piog; 1 μM) followed by 2 h of exposure to H_2O_2 (0.6 mM) in combination with Rosi, Trog, or Piog. Western blot analysis and MTT assay were performed. At 2 h, H_2O_2 alone and in combination with Rosi significantly increased the fold difference in the p-PPAR-γ-to-PPAR-γ ratio compared with controls (*A*). H_2O_2 and Trog treatment alone or in combination significantly increased the p-PPAR-γ-to-PPAR-γ ratio (*B*). H_2O_2 treatment alone or in combination with Piog significantly increased the p-PPAR-γ-to-PPAR-γ ratio (*C*). Cell viability significantly decreased after H_2O_2 treatment alone and in combination with Rosi (*D*), Trog (*E*), or Piog (*F*). At 18 h, H_2O_2 exposure alone and in combination with Rosi significantly increased the p-PPAR-γ-to-PPAR-γ ratio, whereas Rosi treatment alone significantly decreased the p-PPAR-γ-to-PPAR-γ ratio (*G*). H_2O_2 exposure alone significantly increased, whereas Trog treatment alone significantly decreased, the p-PPAR-γ-to-PPAR-γ ratio (*H*). H_2O_2 treatment alone significantly increased the p-PPAR-γ-to-PPAR-γ ratio, which was significantly decreased when H_2O_2 was used in combination with Piog (*I*). Cell viability was significantly decreased after H_2O_2 exposure alone, and this was significantly enhanced when combined with Rosi (*J*) or Trog (*K*). Piog treatment in combination with H_2O_2 significantly decreased cell viability compared with control (*L*). Results are expressed as means ± SE. $*P < 0.05$, $**P < 0.01$, and $***P < 0.001$ compared with controls; $\#P < 0.05$ compared as indicated.

attenuated this injury. Impaired selective mitochondrial autophagy caused by persistent ROS production and ensuing oxidative damage results in p62 accumulation, which further contributes to cellular dysfunction. This result was compounded by the failure of PPAR-γ to activate PGC-1α to stimulate mitochondrial biogenesis and restore the cellular redox environment. This change would have provided a continuation of negatively regulating intracellular signaling, with persistent oxidative stress and reduced mitochondria-dependent ATP production. This demonstrates early, persistent, and indirect mitochondrial dysfunction resulting from a failure of PGC-1α activity after oxidative stress.

PPAR-γ agonist treatment has previously been shown to protect against mitochondrial dysfunction in other cell types, including neuronal cells (10, 46) and endothelial cells (11). In the kidney, disparate results have been previously described and largely depend on the cell type and insult used (26, 45, 46). Important to note is that PPAR-γ Ser^{112} phosphorylation has been shown to modify PPAR-γ activity rather than act as a marker of PPAR-γ activation. PPAR-γ agonists can inhibit

obesity-linked Ser^{273} phosphorylation of PPAR-γ by cyclin-dependent kinase 5 in adipose tissue (7). Our results show an inability of rosiglitazone to inhibit PPAR-γ Ser^{112} phosphorylation during oxidative stress, therefore preventing classical downstream actions of PPAR-γ, primarily the upregulation of PGC-1α and maintenance of mitochondrial homeostasis (21, 39). This finding appears to be unique to kidney tubular cells. Of note is that PPAR-α is an alternate inducer of PGC-1α-dependent mitochondrial biogenesis (38, 44), and its down-regulation in response to oxidative stress further impairs the restoration of mitochondrial homeostasis. The ability of rosiglitazone and troglitazone to decrease PTE cell viability after extended oxidative stress is a novel finding and may result from the inability to prevent PPAR-γ phosphorylation, not only at Ser^{112} but on other sites of phosphorylation, including Ser^{273} and Ser^{82}, that were not studied here.

In summary, our findings describe oxidative stress-induced PPAR-γ alterations and resulting mitochondrial destabilization and a failure to restore mitochondrial health due to defective activation of PPAR-γ-dependent biogenesis pathways. These changes may contribute to the pathogenesis of diverse kidney disease, including CKD. A novel finding is that activation of PPAR-γ by TZD enhances oxidative stress-mediated tubular cell damage that is associated with PPAR-γ Ser^{112} phosphorylation. This may account for the tubular damage and a lack of therapeutic benefit of TZDs seen in some human trials.

ACKNOWLEDGMENTS

The authors thank Dr. Sandrine Roy (Translational Research Institute microscopy core facility) for expert assistance with confocal microscopy and Dr. Robyn Webb and Dr. Richard Webb (Australian Institute of Biotechnology and Nanotechnology, Centre for Advanced Imaging) for expert assistance with transmission electron microscopy.

DISCLOSURES

D. W. Johnson has received consultancy fees, research funds, speaking honoraria, and travel sponsorships from Jannsen-Cilag, Amgen, Pfizer, and Roche. All other authors have no conflicts of interest.

AUTHOR CONTRIBUTIONS

Author contributions: D.M.S., J.S.C., and G.C.G. conception and design of research; D.M.S. and N.C.B. performed experiments; D.M.S. and G.C.G. analyzed data; D.M.S., C.M., J.S.C., D.W.J., and G.C.G. interpreted results of experiments; D.M.S. prepared figures; D.M.S. drafted manuscript; D.M.S., C.M., N.C.B., D.W.J., and G.C.G. edited and revised manuscript; D.M.S. and G.C.G. approved final version of manuscript.

REFERENCES

1. **Ahmadian M, Suh JM, Hah N, Liddle C, Atkins AR, Downes M, Evans RM.** PPARγ signaling and metabolism: the good, the bad and the future. *Nat Med* 19: 557–566, 2013.
2. **Bjorkoy G, Lamark T, Brech A, Outzen H, Perander M, Overvatn A, Stenmark H, Johansen T.** p62/SQSTM1 forms protein aggregates degraded by autophagy and has a protective effect on huntingtin-induced cell death. *J Cell Biol* 171: 603–614, 2005.
3. **Cai Q, Zakaria HM, Simone A, Sheng ZH.** Spatial parkin translocation and degradation of damaged mitochondria via mitophagy in live cortical neurons. *Curr Biol* 22: 545–552, 2012.
4. **Calkin AC, Giunti S, Jandeleit-Dahm KA, Allen TJ, Cooper ME, Thomas MC.** PPAR-α and -γ agonists attenuate diabetic kidney disease in the apolipoprotein E knockout mouse. *Nephrol Dial Transplant* 21: 2399–2405, 2006.
5. **Camp HS, Tafuri SR.** Regulation of peroxisome proliferator-activated receptor gamma activity by mitogen-activated protein kinase. *J Biol Chem* 272: 10811–10816, 1997.
6. **Chiang MC, Cheng YC, Lin KH, Yen CH.** PPARγ regulates the mitochondrial dysfunction in human neural stem cells with tumor necrosis factor α. *Neuroscience* 229: 118–129, 2013.
7. **Choi JH, Banks AS, Estall JL, Kajimura S, Bostrom P, Laznik D, Ruas JL, Chalmers MJ, Kamenecka TM, Bluher M, Griffin PR, Spiegelman BM.** Anti-diabetic drugs inhibit obesity-linked phosphorylation of PPARγ by Cdk5. *Nature* 466: 451–456, 2010.
8. **Dounousi E, Papavasiliou E, Makedou A, Ioannou K, Katododis K, Tselepis A, Siamopoulos K, Tsakiris D.** Oxidative stress is progressively enhanced with advancing stages of chronic kidney disease. *Nephrol Dial Transplant* 21: 385–385, 2006.
9. **Egan DF, Shackelford DB, Mihaylova MM, Gelino S, Kohnz RA, Mair W, Vasquez DS, Joshi A, Gwinn DM, Taylor R, Asara JM, Fitzpatrick J, Dillin A, Viollet B, Kundu M, Hansen M, Shaw RJ.** Phosphorylation of ULK1 (hATG1) by AMP-activated protein kinase connects energy sensing to mitophagy. *Science* 331: 456–461, 2011.
10. **Fuenzalida K, Quintanilla R, Ramos P, Piderit D, Fuentealba RA, Martinez G, Inestrosa NC, Bronfman M.** Peroxisome proliferator-activated receptor γ up-regulates the Bcl-2 anti-apoptotic protein in neurons and induces mitochondrial stabilization and protection against oxidative stress and apoptosis. *J Biol Chem* 282: 37006–37015, 2007.
11. **Fujisawa K, Nishikawa T, Kukidome D, Imoto K, Yamashiro T, Motoshima H, Matsumura T, Araki E.** TZDs reduce mitochondrial ROS production and enhance mitochondrial biogenesis. *Biochem Biophys Res Commun* 379: 43–48, 2009.
12. **Funk JA, Odejinmi S, Schnellmann RG.** SRT1720 induces mitochondrial biogenesis and rescues mitochondrial function after oxidant injury in renal proximal tubule cells. *J Pharmacol Exp Ther* 333: 593–601, 2010.
13. **Geisler S, Holmstrom KM, Skujat D, Fiesel FC, Rothfuss OC, Kahle PJ, Springer W.** PINK1/Parkin-mediated mitophagy is dependent on VDAC1 and p62/SQSTM1. *Nat Cell Biol* 12: 119–131, 2010.
14. **Gobe G.** Identification of apoptosis in kidney tissue sections. *Methods Mol Biol* 466: 175–192, 2009.
15. **Gomes P, Simao S, Silva E, Pinto V, Amaral JS, Afonso J, Serrao MP, Pinho MJ, Soares-da-Silva P.** Aging increases oxidative stress and renal expression of oxidant and antioxidant enzymes that are associated with an increased trend in systolic blood pressure. *Oxid Med Cell Longev* 2: 138–145, 2009.
16. **Granata S, Zaza G, Simone S, Villani G, Latorre D, Pontrelli P, Carella M, Schena FP, Grandaliano G, Pertosa G.** Mitochondrial dysregulation and oxidative stress in patients with chronic kidney disease. *BMC Genomics* 10: 388, 2009.
17. **Guan Y, Breyer MD.** Peroxisome proliferator-activated receptors (PPARs): novel therapeutic targets in renal disease. *Kidney Int* 60: 14–30, 2001.
18. **Guan Y, Zhang Y, Breyer MD.** The role of PPARs in the transcriptional control of cellular processes. *Drug News Perspect* 15: 147–154, 2002.
19. **Hall AM, Crawford C, Unwin RJ, Duchen MR, Peppiatt-Wildman CM.** Multiphoton imaging of the functioning kidney. *J Am Soc Nephrol* 22: 1297–1304, 2011.
20. **Hall AM, Unwin RJ, Parker N, Duchen MR.** Multiphoton imaging reveals differences in mitochondrial function between nephron segments. *J Am Soc Nephrol* 20: 1293–1302, 2009.
21. **Hock MB, Kralli A.** Transcriptional control of mitochondrial biogenesis and function. *Annu Rev Physiol* 71: 177–203, 2009.
22. **Hondares E, Mora O, Yubero P, Rodriguez dlCM, Iglesias R, Giralt M, Villarroya F.** Thiazolidinediones and rexinoids induce peroxisome proliferator-activated receptor-coactivator (PGC)-1α gene transcription: an autoregulatory loop controls PGC-1α expression in adipocytes via peroxisome proliferator-activated receptor-γ coactivation. *Endocrinology* 147: 2829–2838, 2006.
23. **Hu E, Kim JB, Sarraf P, Spiegelman BM.** Inhibition of adipogenesis through MAP kinase-mediated phosphorylation of PPARγ. *Science* 274: 2100–2103, 1996.
24. **Ishihara M, Urushido M, Hamada K, Matsumoto T, Shimamura Y, Ogata K, Inoue K, Taniguchi Y, Horino T, Fujieda M, Fujimoto S, Terada Y.** Sestrin-2 and BNIP3 regulate autophagy and mitophagy in renal tubular cells in acute kidney injury. *Am J Physiol Renal Physiol* 305: F495–F509, 2013.
25. **Jiang D, Chen K, Lu X, Gao HJ, Qin ZH, Lin F.** Exercise ameliorates the detrimental effect of chloroquine on skeletal muscles in mice via restoring autophagy flux. *Acta Pharmacol Sin* 35: 135–142, 2014.

26. **Kanjanabuch T, Ma LJ, Chen J, Pozzi A, Guan Y, Mundel P, Fogo AB.** PPAR-γ agonist protects podocytes from injury. *Kidney Int* 71: 1232–1239, 2007.
27. **Kincaid-Smith P, Fairley KF, Farish S, Best JD, Proietto J.** Reduction of proteinuria by rosiglitazone in non-diabetic renal disease. *Nephrology (Carlton)* 13: 58–62, 2008.
28. **Komatsu M, Kageyama S, Ichimura Y.** p62/SQSTM1/A170: physiology and pathology. *Pharmacol Res* 66: 457–462, 2012.
29. **Komatsu M, Kurokawa H, Waguri S, Taguchi K, Kobayashi A, Ichimura Y, Sou YS, Ueno I, Sakamoto A, Tong KI, Kim M, Nishito Y, Iemura S, Natsume T, Ueno T, Kominami E, Motohashi H, Tanaka K, Yamamoto M.** The selective autophagy substrate p62 activates the stress responsive transcription factor Nrf2 through inactivation of Keap1. *Nat Cell Biol* 12: 213–223, 2010.
30. **Komatsu M, Waguri S, Koike M, Sou YS, Ueno T, Hara T, Mizushima N, Iwata J, Ezaki J, Murata S, Hamazaki J, Nishito Y, Iemura S, Natsume T, Yanagawa T, Uwayama J, Warabi E, Yoshida H, Ishii T, Kobayashi A, Yamamoto M, Yue Z, Uchiyama Y, Kominami E, Tanaka K.** Homeostatic levels of p62 control cytoplasmic inclusion body formation in autophagy-deficient mice. *Cell* 131: 1149–1163, 2007.
31. **Leff T.** AMP-activated protein kinase regulates gene expression by direct phosphorylation of nuclear proteins. *Biochem Soc Trans* 31: 224–227, 2003.
32. **Lepenies J, Hewison M, Stewart PM, Quinkler M.** Renal PPARγ mRNA expression increases with impairment of renal function in patients with chronic kidney disease. *Nephrology (Carlton)* 15: 683–691, 2010.
33. **Martin A, Perez-Giron JV, Hernanz R, Palacios R, Briones AM, Fortuno A, Zalba G, Salaices M, Alonso MJ.** Peroxisome proliferator-activated receptor-γ activation reduces cyclooxygenase-2 expression in vascular smooth muscle cells from hypertensive rats by interfering with oxidative stress. *J Hypertens* 30: 315–326, 2012.
34. **Miglio G, Rosa AC, Rattazzi L, Grange C, Camussi G, Fantozzi R.** Protective effects of peroxisome proliferator-activated receptor agonists on human podocytes: proposed mechanisms of action. *Br J Pharmacol* 167: 641–653, 2012.
35. **Narendra D, Tanaka A, Suen DF, Youle RJ.** Parkin is recruited selectively to impaired mitochondria and promotes their autophagy. *J Cell Biol* 183: 795–803, 2008.
36. **Nath KA.** Tubulointerstitial changes as a major determinant in the progression of renal damage. *Am J Kidney Dis* 20: 1–17, 1992.
37. **Niizuma S, Nakamura S, Ishibashi-Ueda H, Yoshihara F, Kawano Y.** Kidney function and histological damage in autopsy subjects with myocardial infarction. *Ren Fail* 33: 847–852, 2011.
38. **Portilla D, Dai G, McClure T, Bates L, Kurten R, Megyesi J, Price P, Li S.** Alterations of PPARα and its coactivator PGC-1 in cisplatin-induced acute renal failure. *Kidney Int* 62: 1208–1218, 2002.
39. **Rasbach KA, Schnellmann RG.** Signaling of mitochondrial biogenesis following oxidant injury. *J Biol Chem* 282: 2355–2362, 2007.
40. **Shao D, Liu J, Ni J, Wang Z, Shen Y, Zhou L, Huang Y, Wang J, Xue H, Zhang W, Lu L.** Suppression of XBP1S mediates high glucose-induced oxidative stress and extracellular matrix synthesis in renal mesangial cell and kidney of diabetic rats. *PLOS ONE* 8: e56124, 2013.
41. **Small DM, Bennett NC, Roy S, Gabrielli BG, Johnson DW, Gobe GC.** Oxidative stress and cell senescence combine to cause maximal renal tubular epithelial cell dysfunction and loss in an in vitro model of kidney disease. *Nephron Exp Nephrol* 122: 123–130, 2012.
42. **Stanton RC.** Oxidative stress and diabetic kidney disease. *Curr Diab Rep* 11: 330–336, 2011.
43. **Wang X, Dai Y, Ding Z, Khaidakov M, Mercanti F, Mehta JL.** Regulation of autophagy and apoptosis in response to angiotensin II in HL-1 cardiomyocytes. *Biochem Biophys Res Commun* 440: 696–700, 2013.
44. **Weinberg JM.** Mitochondrial biogenesis in kidney disease. *J Am Soc Nephrol* 22: 431–436, 2011.
45. **Whiteside C, Wang H, Xia L, Munk S, Goldberg HJ, Fantus IG.** Rosiglitazone prevents high glucose-induced vascular endothelial growth factor and collagen IV expression in cultured mesangial cells. *Exp Diabetes Res* 2009: 910783, 2009.
46. **Wu JS, Lin TN, Wu KK.** Rosiglitazone and PPAR-γ overexpression protect mitochondrial membrane potential and prevent apoptosis by up-regulating anti-apoptotic Bcl-2 family proteins. *J Cell Physiol* 220: 58–71, 2009.
47. **Xu Y, Ruan S, Wu X, Chen H, Zheng K, Fu B.** Autophagy and apoptosis in tubular cells following unilateral ureteral obstruction are associated with mitochondrial oxidative stress. *Int J Mol Med* 31: 628–636, 2013.
48. **Yang HC, Deleuze S, Zuo Y, Potthoff SA, Ma LJ, Fogo AB.** The PPARγ agonist pioglitazone ameliorates aging-related progressive renal injury. *J Am Soc Nephrol* 20: 2380–2388, 2009.
49. **Yang HC, Ma LJ, Ma J, Fogo AB.** Peroxisome proliferator-activated receptor-γ agonist is protective in podocyte injury-associated sclerosis. *Kidney Int* 69: 1756–1764, 2006.
50. **Zhan M, Brooks C, Liu F, Sun L, Dong Z.** Mitochondrial dynamics: regulatory mechanisms and emerging role in renal pathophysiology. *Kidney Int* 83: 568–581, 2013.
51. **Zhang B, Berger J, Zhou G, Elbrecht A, Biswas S, White-Carrington S, Szalkowski D, Moller DE.** Insulin- and mitogen-activated protein kinase-mediated phosphorylation and activation of peroxisome proliferator-activated receptor gamma. *J Biol Chem* 271: 31771–31774, 1996.

Journal of Biomedical Optics

SPIEDigitalLibrary.org/jbo

Multiphoton fluorescence microscopy of the live kidney in health and disease

David M. Small
Washington Y. Sanchez
Sandrine Roy
Michael J. Hickey
Glenda C. Gobe

SPIE

Journal of Biomedical Optics 19(2), 020901 (February 2014)

REVIEW

Multiphoton fluorescence microscopy of the live kidney in health and disease

David M. Small,[a] Washington Y. Sanchez,[b] Sandrine Roy,[c] Michael J. Hickey,[d] and Glenda C. Gobe[a,*]
[a]University of Queensland, Translational Research Institute, Centre for Kidney Disease Research, Brisbane 4102, Australia
[b]University of Queensland, Translational Research Institute, Therapeutics Research Centre, School of Medicine, Brisbane 4102, Australia
[c]University of Queensland, Translational Research Institute, Diamantina Institute, Brisbane 4102, Australia
[d]Monash University, Department of Medicine, Monash Medical Centre, Centre for Inflammatory Diseases, Clayton, Victoria 3168, Australia

Abstract. The structural and functional heterogeneity of the kidney ensures a diversity of response in health and disease. Multiphoton microscopy has improved our understanding of kidney physiology and pathophysiology by enabling the visualization of the living kidney in comparison with the static view of previous technologies. The use of multiphoton microscopy with rodent models in conjunction with endogenous fluorescence and exogenous infused dyes permits the measurement of renal processes, such as glomerular permeability, juxtaglomerular apparatus function, tubulointerstitial function, tubulovascular interactions, vascular flow rate, and the intrarenal renin-angiotensin-aldosterone system. Subcellular processes, including mitochondrial dynamics, reactive oxygen species production, cytosolic ion concentrations, and death processes apoptosis and necrosis, can also be measured by multiphoton microscopy. This has allowed valuable insight into the pathophysiology of diabetic nephropathy, renal ischemia-reperfusion injury, hypertensive nephropathy, as well as inflammatory responses of the kidney. The current review presents an overview of multiphoton microscopy with a focus on techniques for imaging the kidney and gives examples of instances where multiphoton microscopy has been utilized to study renal pathophysiology in the living kidney. With continued advancements in the field of biological optics and increased adoption in experimental nephrology, multiphoton microscopy will undoubtedly continue to create new paradigms in kidney disease. [DOI: 10.1117/1.JBO.19.2.020901]

Keywords: kidney; multiphoton microscopy; fluorescence lifetime imaging; pathophysiology.

Paper 130645VRR received Sep. 6, 2013; revised manuscript received Dec. 18, 2013; accepted for publication Dec. 20, 2013; published online Feb. 13, 2014.

1 Introduction

Over the past decade, fluorescence microscopy has provided visual insight into the temporal and spatial interactions of molecules at a cellular and subcellular level. Continuing advancements into fluorescence microscopy have led to imaging that is less damaging to biological material, thus enabling visualization of living tissues at a greater penetration depth. Multiphoton microscopy (MPM) is such a technology. It has brought the visualization and localization of cellular interactions, typically seen only in cell culture models, to living animals. Conventional confocal microscopy relies on a stream of single photons to procure two- and three-dimensional (3-D) images, whereas MPM uses rapidly pulsed photons at half of the single photon energy required to excite the fluorophore. MPM is sometimes referred to as two-photon excitation microscopy or two-photon fluorescence. The simultaneous absorption of two lower-energy photons excites the fluorophore, reduces background fluorescence due to a narrow focal volume, and minimizes toxicity to the biological material due to photo bleaching. The use of lower-energy photons together with infrared lasers increases the effective tissue depth of imaging. MPM imaging has been used to study the structure and function in numerous systems, including liver,[1–3] skin,[4–8] cornea,[9,10] thymus,[11,12] and kidney.[13–16]

The kidney has a complex internal three-dimensional structure and a heterogeneous cell population, with glomeruli, tubules, interstitial space, and vasculature interacting in the vital kidney, an organ that is ideal for imaging with MPM. The renal interstitium, situated between the basement membranes of nephrons and the vessels, contains interstitial fibroblasts, dendritic cells, and occasional macrophages that quickly react to stress and damage of the intrinsic functioning tissues of the kidney. Developments in image reconstruction and analysis software have provided additional advancement to bring MPM imaging to its potential for analyzing the kidney in health and disease. This review will present an overview of the principles of MPM, MPM techniques for imaging the kidney, and examples of instances where MPM has been able to explain novel aspects of renal pathophysiology.

2 Principles and Advantages of Multiphoton Microscopy

The basic principles of fluorescence apply to MPM imaging. Fluorescence occurs by the absorption of a photon by a fluorophore that brings an electron from the fluorophore to an excited state. The electron returning to its ground state causes the release of a photon (fluorescence emission photon), which is then efficiently detected.[17,18] The initial excitation photon is typically of a high energy. This is known as single-photon fluorescence. MPM fluorescence is based on the simultaneous absorption of two low-energy, near-infrared wavelength photons by a fluorophore, and hence, the alternative name two-photon fluorescence (Fig. 1). Three-photon excitation and second harmonic

*Address all correspondence to: Glenda C. Gobe, E-mail: g.gobe@uq.edu.au

generation work on similar principles and can also be used to visualize fluorescent optical sections.[19]

Although the energy of either of these photons is too low to raise an electron to an excited state, it is the combination of the two energies that is sufficient to excite and thus release a fluorescence emission photon. However, the two photons must meet the fluorophore at exactly the same time, within approximately an attosecond (10^{-18} s) of one another. During the early stages of development of MPM, this was difficult to achieve since simultaneous electronic stimulation at a single specified point was very unlikely. It was not until the development of higher-powered lasers (~10 mW) that could produce the necessary photon flux,[21,22] as well as ultrashort pulsed laser systems[22] that greatly reduced the power, that MPM became possible with biological material.

A further advantage of using near-infrared wavelengths, instead of ultraviolet light, for fluorescence excitation was the reduction of scattering and increase in imaging penetration depth in the sample (from ~20 to 500 to 600 μm). Additionally, single-photon microscopy uses a pinhole detection device to remove out-of-focus and out-of-plane light. Removal of the pinhole allows fluorescence emission detectors to be placed closer to the microscope objective to optimize collection of scattered light, as well as enhance imaging depth.

3 Techniques for Imaging the Kidney

Various MPM approaches have been utilized to analyze the functioning kidney at the subcellular level. These include *in vitro* imaging,[23,24] imaging of live isolated microperfused preparations of tubules, vessels, and glomeruli,[25,26] and live perfused kidney slice preparations.[27] Although MPM can produce significant information from *in vitro* experimental models, it is the whole live kidney where MPM techniques are used to their full potential. The interplay between segments of the nephron (glomeruli, tubule segments), the vasculature, and its contents, and the interstitium can be observed in detail.

The choice of animal, microscope settings, surgical or pharmacological methods, autofluorescence and fluorescent dyes are all important considerations for the application of MPM to normal and diseased kidney. Limitations that have been discovered in other tissues apply equally in kidney research, and in some cases, the kidney presents its own set of problems. For example, early studies in neural tissue had demonstrated that the maximal tissue depth for two-photon excitation was 500 to 600 μm.[28,29] The main problem of MPM in the kidney was that the depth was limited to a maximum of 150 to 200 μm. This is primarily due to substantial scattering of emission photons from the high refractive index and heterogeneity of kidney tissue. In addition, the ability of cytochrome c oxidase and hemoglobin to absorb light, and the spherical aberration (a deviation of rays of light through a spherical lens from the expected focal point) seen in the kidney, all contributed to a reduction in the maximal excitation depth.[30,31] Another important consideration of intravital MPM is the possibility of photodamage and cytotoxicity due to extended periods of excitation, and adequate controls need to be included.

The limitation in maximal excitation depth is important since glomerular depth from the renal capsule differs among rodents. For example, the kidneys of Munich-Wistar rats possess superficial glomeruli that are easily imaged with MPM. The afferent and efferent capillaries and Bowman's space, as well as the contiguous S1 segment of the proximal tubule, can be seen in this model.[32] In comparison, imaging of mouse kidneys is usually restricted to tubular and vascular structures because of the depth of their glomeruli. A quantitative analysis of glomerular depths from 10 commonly used mouse strains was performed by Schiessl and colleagues,[33] who found that the BALB/c and C57Bl6 mouse strains contained the most superficial glomeruli at both 4 and 10 weeks of age, regardless of sex. However, it still remains challenging to visualize glomeruli in mice, and the use

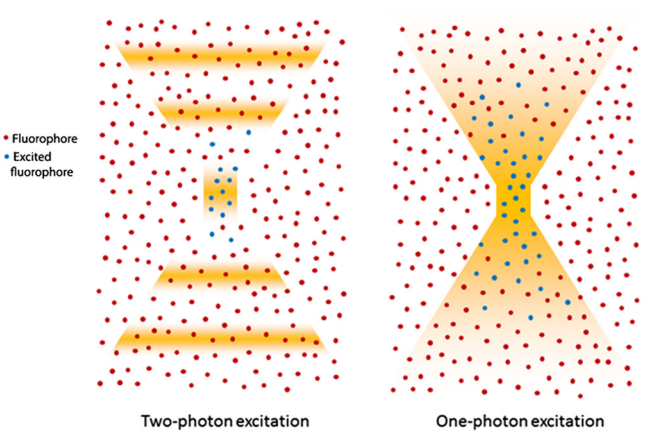

Fig. 1 Pictorial representation of one-photon and two-photon fluorescence. Two-photon excitation demonstrates simultaneous absorption of infrared laser pulses at a single point compared to one-photon excitation, which uses visible or ultraviolet light lasers that excite photons throughout the biological material. Adapted from Ref. 20.

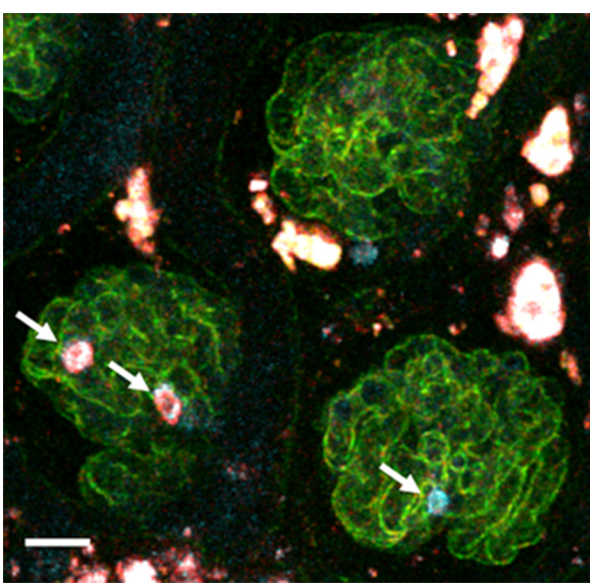

Fig. 2 Close-to-surface glomeruli from hydronephrotic mouse kidneys. Capillary endothelium is stained with isolectin B4-conjugated to Alexa Fluor 488 (green), neutrophils are stained using anti-Gr1-conjugated to phycoerythrin (arrows—orange/red), and surface myeloperoxidase (MPO) is stained with polyclonal anti-MPO-conjugated to Alexa-647 (arrow—blue) demonstrating activated neutrophils. Bright autofluorescence from remnants of the tubulointerstitium can be seen outside of glomeruli. Excitation wavelength was 810 nm and emitted signal was collected by three nondescanned detectors: 500 to 550 nm (Alexa 488), 575 to 605 nm (phycoerythrin), and 625 to 675 nm (Alexa 647). A 20× 1.0 NA water immersion objective (Leica) was used. Scale bar represents 30 μm. Methods of glomerular preparation have been described within text and in detail elsewhere.[35]

of MPM for studying the functional significance of certain glomerular genes or proteins, in specific gene knock-in and knockout strains of mice, is limited. Khoury and colleagues[34] demonstrated podocyte biology in female nephrin knockout/green fluorescent protein (GFP) knock-in heterozygote ($Nps1^{tm1Rkl}$/J) mice using superficially located glomeruli. Close-to-surface glomeruli have also been imaged using MPM in C57Bl6 mice;[35] however, this was only possible in three- to four-week-old mice of ~12 g weight. These mice have smaller kidneys and some glomeruli are sufficiently superficial in the cortex to be visualized via MPM. Another approach for visualizing glomeruli in mice is to use the posthydronephrosis model.[36] In this model, one kidney undergoes ureteric ligation for 12 weeks to allow dilatation of the renal pelvis and marked tubulointerstitial atrophy. The remaining thin rim of transparent cortical tissue has clear glomeruli, and these can be visualized by both transmission and confocal microscopy. This approach also allows assessment of numerous glomeruli in the same animal and is particularly amendable for assessment of leukocyte recruitment during models of glomerular inflammation[2–4]

Table 1 Types of fluorescent probes, their characteristics, and functions.

Probe	Characteristic	Function	References
Hoecsht 33342	Labels cell nuclei blue	Nuclear change (apoptosis, mitosis)	23, 32, 39 to 50
Propidium iodide	Labels cell nuclei red, membrane-impermeable	Necrotic change of nuclei	32, 51, 52
Octadecyl rhodamine B chloride R-18	Labels cell membrane	Single cell size and structure	23, 42, 48, 49
Calcein-acetoxymethyl (AM)	Labels cytosol of tubular and endothelial cells	Cell viability	27, 40
Quinacrine	Loads preferentially into brush border and subapical vesicles	Endo- and exocytosis, and apical shedding. Renin granules in the juxta-glomerular apparatus	16, 23 to 25, 39 to 41, 48 to 50, 53, 54
Tetramethyl rhodamine methyl ester	Mitochondrial membrane-dependent dye	Mitochondrial density and health that loads well into proximal and distal tubules, and glomeruli	14, 27, 40
Monochlorobimane	Forms a fluorescent adduct in the presence of glutathione	Indicates levels of intracellular glutathione	14, 27, 40
Rhod-2 AM	Calcium-sensitive dye that is generally localized to the mitochondria	Indicates levels of intracellular calcium	40 to 42, 55
Seminaphthorhodafluor (SNARF)-1 AM	pH-sensitive dye	Indicated changes in pH levels	42
Dihydroethidium	Superoxide-sensitive dye that fluoresces red and binds to DNA	Indicates levels of reactive oxygen species production	14, 27, 35
Rhodamine-123	Mitochondrial membrane-dependent dye	Mitochondrial density and health that loads preferentially into the proximal tubule	14
Rhodamine B hexyl ester	Endothelial cell mitochondrial membrane-dependant dye	Labels metabolically active endothelial cells	32
Lucifer yellow	Stains endothelium yellow, endocytosed from the plasma	Indicates endocytosis	15, 25, 41, 42, 49
Fura-red AM	Calcium-sensitive dye	Fluorescence intensity decreases on calcium binding	23, 54 to 56
Fluo-4 AM	Calcium-sensitive dye	Fluorescence intensity increases on calcium binding	23, 54 to 56
ANNINE-6	Voltage-sensitive dye	Vascular smooth muscle cell selective (afferent arteriole)	38, 41
Sulfonefluorescein	Organic ion secreted by proximal tubules	Marker of proximal tubule derived renal cysts	57, 58
3000 to 4000-Da dextran-fluorophore conjugate	Freely filtered by the glomerulus	Indicates glomerular permeability and proximal tubule endocytosis	15, 32, 42, 45, 59
10,000-Da dextran-fluorophore conjugate	Freely filtered by the glomerulus and somewhat permeant in the vasculature	Indicates glomerular permeability, proximal tubule endocytosis, and vascular permeability	32, 40
40,000-Da dextran-fluorophore conjugate	Slowly filtered by the kidney, and largely impermeant in the vasculature	Indicates glomerular permeability, vascular flow, and vascular permeability	32, 45, 59
7000 to 500,000-Da dextran fluorophore conjugate	Not filtered by the kidney, but retained in the vasculature	Indicates glomerular permeability, vascular flow, and vascular permeability	15, 16, 25, 32, 34, 39 to 41, 45, 48 to 50, 54, 59

(Fig. 2). We have found that glomeruli in the C57Bl6 mouse kidney, made atrophic and fibrotic after ischemia-reperfusion injury (IRI), may be located superficially and visualized using MPM because of the atrophy of the tubulointerstitium (unpublished data). Thus, MPM offers enhanced knowledge of kidney pathophysiology from experimental studies, especially where modulation of mouse genetics is also used.

The infusion of fluorescent, or fluorescence-conjugated, probes for live cell imaging allows differentiation of structures in the kidney, as well as study of the function at the single nephron level. Table 1 identifies common MPM probes that will be discussed here. The spatial organization of the nucleus in the cell is paramount not only as a point of reference for cellular subcompartments, but also for detailed information on internal kidney structure when used in conjunction with endogenous autofluorescence. Hoechst 33342 is a membrane permeable dye that may be used to stain nuclei blue. Gene delivery with adenovirus-cDNA constructs containing GFP have been microinfused successfully into the tubule or vascular space of the rat kidney and visualized with MPM imaging.[37] Although this approach has not had wide application, it offers a unique way to study the behavior of any fluorescently tagged protein in the kidney. Intrarenal blood flow, both glomerular and peritubular, has an intimate relationship with tubular function and glomerular filtration. The renal microvasculature can now be imaged at greater depth in real time with MPM. This technique relies on performing a line scan along the central axis of a vessel of interest in conjunction with a high molecular weight nonfilterable fluorescent dextran (70 kDa).[32] Red blood cells do not take up fluorescent dye and, therefore, present apparent dark areas for which movement can be measured through time. This technique has been utilized to study the electronic vascular signal conduction with nephron synchronization.[38] Furthermore, Kang and colleagues[39] have confirmed a significantly higher flow rate occurs in intraglomerular capillaries compared with peritubular capillaries with similar diameters and the same systolic blood pressure. The measured red blood cell speed in the kidney was found to be higher than in most other vascular beds, which is consistent with the higher blood flow to the kidneys.[28]

3.1 *Practical Considerations of In Vivo MPM*

The commercialization of MPM has provided a greater degree of automation compared to earlier models that were based on a conventional confocal microscope equipped with a secondary laser. Current systems can be either inverted or upright. Upright systems need to employ a stabilization device, such as a kidney cup, to prevent respiratory movement distorting live images. Inverted systems limit the need for kidney stabilization devices, however, these devices may still be necessary. Two excellent step-by-step protocols provide a detailed description of effective preparation of the rat kidney and microscope stage for MPM imaging.[32,60] The first decision is whether to image using objectives in the inverted or conventional mode. Subsequently, high-quality image acquisition and data reproducibility of kidney imaging require two important considerations: (1) the size of the inner muscle layer incision and (2) the implementation of a kidney stabilization device. Three layers must be incised to reach the peritoneal cavity to externalize the kidney in both the rat and mouse: skin, thin outer muscle layer, and thick inner muscle layer. The incision of the inner muscle layer should be smaller than the length of the kidney, so that externalization of the kidney through the incision stabilizes the kidney without stretching the renal pedicle and reducing renal perfusion. In some cases (for example, with the objective set to image from below the animal), a kidney stabilization device may not be needed because the body weight of the animal effectively stabilizes the kidney. However, where the body weight of the animal is small, as for a mouse, stabilization devices may still be needed. The devices can range in complexity from a simple cue-tip cotton bud placed near the renal pedicle to a custom-made kidney cup (for example, for imaging from above the kidney). Suturing the kidney capsule to a fixed point has also been used to stabilize the kidney. Effective temperature control devices are also essential for real-time imaging of anaesthetized

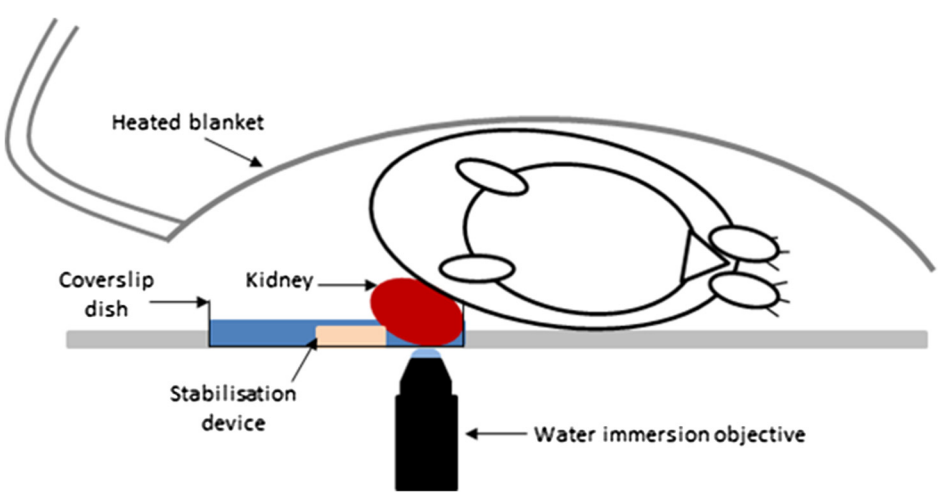

Fig. 3 Schematic diagram showing a common setup for intravital imaging of a mouse or rat kidney. The animal is placed on its side with the exposed kidney lying in a shallow coverslip dish. Appropriate stabilization devices may need to be employed (depicted here are small pieces of autoclave tap stacked upon each other). The coverslip dish is filled with warm physiological saline, and a heated blanket is placed over the animal to maintain physiological temperature. Further temperature control devices may be employed, such as heating pads underneath the animal's torso and hind limbs and around the microscope objective. Adapted from Ref. 60.

animals. Figure 3 gives an example of a setup for intravital MPM, visualizing from below the kidney and employing a coverslip-bottom dish to stabilize the kidney.

3.2 *Quantifying Kidney Function*

MPM provides an alternate technique to quantify kidney function during physiological and diseased states. An important measure of kidney function is its ability to filter molecules, which may also provide information regarding the site of damage. Quantifying renal permeability of any macromolecule with intravital MPM requires conjugation of a fluorphore to a known molecule and identification of kidney microstructure compartments. Two excellent descriptions of methods are available: ratiometric determination of glomerular filtration rate (GFR) was applied during physiological and acute kidney injury conditions,[61] and similar use has been made of the glomerular sieving coefficient (GSC).[60] When quantiying changes in fluorescence from specific compartments, it is important to compensate for background fluorescence for each image by subtracting the average fluorescence intensity within the compartment of interest prior to injection of fluorescent biomarkers from the average intensity from the same region taken after infusion.

The fundamental principle for assessing GFR using intravital MPM is to monitor the decay of a fluorescent reporter molecule from the vascular lumen or extracellular space over time following a bolus injection, and not neccesarily only from within the glomerulus and Bowman's space. The procedure relies on the use of one compartment, and one reporter molecule, and is known as a one-compartent model. The process is greatly enhanced by incorporating a second, larger (kDa), species of fluorescently labeled conjugate infused into the aminal at the same time, thereby having the larger-size conjugate confined to the vascular space and the other freely filterable by the kidney. Measuring the fluorescence ratio of the larger to the smaller molecule, rather than purely relying on measuring the fluorescence only from the freely filterable smaller molecule, significantly enhances the accuracy of GFR measurment by reducing the fluctuation of the signal caused by movement of the focal point.[62] Using this method, GFR may be rapidly quantified; however, a large number of data points are needed to assess the kinetics of conjugated molecules adequately. GFR values obtained via this method using fluorescein isothiocyanate (FITC)-inulin (reporter) and 500-kDa Texas Red-dextran (large molecule) were found to have a Pearson correlation coefficient of 0.85 when compared to GFR values obtained via standard inulin clearance from blood and urine.[61]

Determining the GSC is another useful quantitative measure based on the fundamental concept of fluorescence decay between compartments. This method requires 3-D data sets acquired from glomeruli, and localization of glomerular capillary loops, Bowman's space, and the S1 segment of the proximal tubule. Serum albumin, conjugated to Texas Red, has been used extensively to quantify the GSC of albumin in rats, and preparation of the conjugated fluorphore has been described.[60] During rat intravital MPM preparations, prior to infusion of reporter molecules, glomeruli appear as dark circular spaces surrounded by autofluorescent proximal tubules, and these should be demarcated *in situ* to allow ease of transition between glomeruli. Following infusion of the fluorescent reporter, an appropriate time is allowed for systemic distribution of the fluorophore before aquiring 3-D volumes of selected glomeruli at $\sim$1-μm intervals. 3-D data image analysis software (for example, MetaMorph Microscopy Automation and Image Analysis Software; Volocity 3D Image Analysis Software; and Imaris Scientific 3D/4D Processing and Analysis Software) is available and often free, and facilitates export of 3-D volumetric data. To obtain the volumetric data, the capillary loop containing the fluorescent marker and the empty space (Bowman's space) between its margins and Bowman's capsule need to be identified, taking note of the average intensity reading within the capillary loop and the average intensity reading in Bowman's space from the same focal plane. Adequate background readings prior to fluorescence marker infusion are necessary. The GSC can then be determined using the equation

$$\mathrm{GSC} = \frac{(\text{raw Bowman's space intensity} - \text{background Bowman's space intensity})}{(\text{raw capillary loop intensity} - \text{background capillary loop intensity})}.$$

Similar principles can be applied to the reabsorption of the fluorescent marker within the S1 segment of the proximal tubule.

Four-dimensional cell tracking over time, combined with MPM, has also produced novel data in the field of immunology and immune cell tracing,[5,63,64] and has been used in the kidney to describe a new paradigm of leukocyte recruitment in the glomerulus.[35] A detailed methodology for the data acquisition and analysis is available.[65] The possibility of the visualization and quantitation of kidney myofibroblast proliferation during profibrotic processes in the kidney presents an interesting opportunity that remains untapped.

3.3 *Significance of Endogenous Fluorescence*

Autofluorescence is commonly a hindrance of routine fluorescence microscopy, yet it is used to advantage in MPM. The reduced form of nicotinamide adenine dinucleotide (NADH) is a useful and plentiful endogenous fluorophore in the kidney due to the high density of mitochondria of which NADH is a metabolic substrate.[27] Images captured without the infusion of fluorescent dyes can rely on this signal for basic information of tubular structure. As the fluorescence excitation, emission, and fluorescence lifetime of NADH and NADPH overlap, these two molecules are measured together and referred to as NAD(P)H.[66] Hall and colleagues[40] have demonstrated that the mitochondrial membrane-dependent fluorophore tetremethyl rhodamine methyl ester (TMRM) colocalizes with the endogenous fluorescence pattern of NAD(P)H. Changes in the intensity of NAD(P)H fluorescence can provide valuable information regarding cell metabolism, given that the oxidized form (NAD^+) is nonfluorescent (see Fig. 4, comparing the healthy kidney with ischemia-reperfused kidney; our data). NAD(P)H is a respiratory substrate for complex I of the mitochondrial electron transport chain. The total emitted fluorescence is, therefore, equal to the total NAD pool in a reduced state. A quantitative measure of this fluorescence provides information of the mitochondrial redox state,

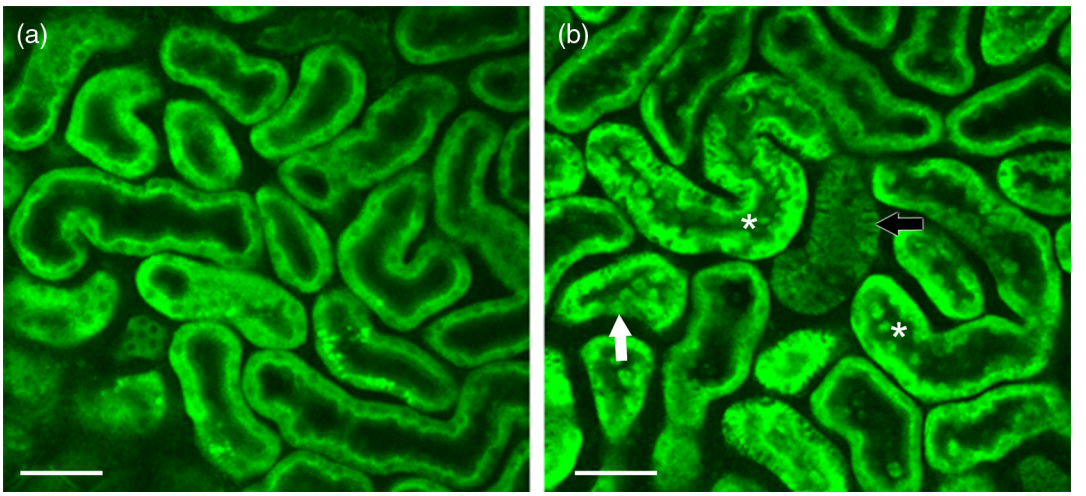

Fig. 4 Endogenous fluorescence of NAD(P)H excited at 740 nm (green) in the healthy (a) and ischemia-reperfused mouse kidney (b). Seven-week-old C57Bl6 mice were anesthetized, a lateral flank incision made, and 20 min ischemia-reperfusion performed. Images were captured using a Lavision Biotec Nikon multiphoton microscope to a depth of 71 μm from the kidney capsule. Imaris 7.6.0 software was used to adjust images to normalized fluorescence. 740-nm two-photon excitation clearly demonstrates the cortical tubular network with distal tubules, proximal tubules with associated brush border, and interstitial space (a). In (b), tubular pathology during the 20 min following renal ischemia demonstrates tubular cell effacement (white arrow), formation of cast material (*), and epithelial cell striations (black arrow). Excitation wavelength was 740 nm and emission was detected using three nondescanned filters: 447 to 460 nm (blue), 485 to 550 nm (green), and 593 to 600 nm (red). A 20× 0.95 NA water immersion objective (Olympus) was used. Scale bar represents 50 μm.

which is dependent on factors such as substrate supply and mitochondrial respiratory chain function. Detailed measurements can also be made using fluorescence lifetime imaging (FLIM) techniques, which are discussed in more detail below. Flavins, which only fluoresce in their oxidative state, can provide further information of the cellular redox state. The autofluorescent properties of NAD(P)H can also be a problem when using MPM, especially in proximal tubules, as it can interfere with quantitative analysis when using some fluorophores that have overlapping excitation/emission.

Functional autofluorescent markers have also been used to detect accumulation of the so-called aging or wear and tear pigment, lipofuscin, in retinal pigment epithelial cells and the brain.[67,68] To our knowledge, this has not been carried out in the kidney, despite the presence of lipofuscin in the atrophic kidney. In addition, aberrant indoleamines, such as serotonin (5-HT) and melatonin, under conditions of oxidative stress can form dimerized indolamine oxidation products producing intrinsic fluorescence that can be detected by three-photon excitation. This approach has been used to image 5-HT granules induced in mucosal mast cells by oxidative stress.[19]

3.4 *Multiphoton Microscopy and FLIM*

The fluorescence lifetime of a fluorophore is the mean time a fluorophore remains in an excited state before emitting a photon (fluorescence) and returning to the initial ground state. The fluorescence lifetime of a fluorophore, either endogenous or synthetic, depends on the type of molecule, its conformation, and the way the molecule interacts with the surrounding microenvironment.[69] FLIM constructs a spatial distribution map of fluorescence lifetimes of a sample imaged by confocal, multiphoton, endoscopic, or wide-field microscopy.[70] Importantly, FLIM microscopy can be used to measure molecular environmental parameters, the metabolic state of cells and tissues via endogenous autofluorescence, drug distribution and interactions, and protein-interactions by fluorescence resonance energy transfer (FRET).

There are two major approaches used to measure the fluorescence lifetime of a sample: time-domain and frequency-domain. For time-domain FLIM, the fluorescence of a sample is acquired by time-correlated single-photon counting (TCSPC) to generate a lifetime decay curve. The lifetime curve is generated by repeatedly measuring the appearance of an emitted photon following an excitation pulse from the confocal or multiphoton laser source. This approach allows for the direct measurement of the decay curve, which is modeled to an exponential function according to the number of estimated components (i.e., independent physiochemical states of one or more fluorophores). The advantages of time-domain FLIM include the direct measurement of the decay curve, calculation of fluorescence lifetimes of the major components (typically a maximum of three to four), and relatively simple analysis compared to frequency-domain FLIM. Time-domain FLIM in multiphoton microscopy may require longer acquisition times compared to frequency-domain in order to generate an accurate decay curve. However, time-domain FLIM by TCSPC delivers excellent signal-to-noise ratio for weak signal samples.[70,71]

For frequency-domain FLIM, the intensity of the excitation light source is modulated sinusoidally at a radio frequency. The resulting emission fluorescence has the same frequency as the excitation light, but demonstrates changes in phase and amplitude (demodulation) relative to the incident light depending on the fluorescence lifetime.[72] For multiphoton frequency-domain FLIM, an image intensifier is used to modulate the gain of the detector at the same frequency as the incidence light. Ideally, the fluorescence lifetime of a single molecule with one physiochemical state will be identical to both the phase and modulation

lifetimes.[71,72] The advantage of the frequency-domain FLIM is comparatively better signal-to-noise ratio than time-domain FLIM via TCSPC for complex systems with multiple fluorophores.

3.5 *Multiphoton FLIM Applications*

A useful application of FLIM in conjunction with MPM in the kidney is measuring the fluorescence lifetime of NAD(P)H. NAD(P)H lifetime measurements are widely used for metabolic and redox imaging *in vitro* and *in vivo*.[2,7,73–76] The lifetime of NAD(P)H is resolved as a two-component system with the short (~0.3 to 4 ns) and long (~2.3 ns) lifetimes represented as the free and protein-bound conformations, respectively.[72,77,78]

As previously mentioned, the reduced form of NADH, NAD+, is not fluorescent and the ratio of NADH:NAD+ has been used previously as a measure of the redox state of the cell. Bird and colleagues demonstrated that the free-to-bound ratio of NAD(P)H, represented by the ratio of the amplitude coefficients for the short and long lifetimes (i.e., α_1/α_2), is related to the NADH/NAD+ ratio and can be used as an indicator for redox changes within the cell.[73] While the free-to-bound ratio of NAD(P)H can be used to measure redox changes within the cells, this ratio should not be confused with the widely used redox ratio that is calculated by measuring the ratio of flavin adenine dinucleotide (FAD) to NADH intensity.[79]

FAD is also examined routinely by FLIM for intracellular metabolic and redox analysis. While FAD can be found in a free and protein-bound conformation, the former has a significantly higher quantum yield with a lifetime of 2.91 ns.[72] In contrast to NAD(P)H, only the oxidized form of FAD is fluorescent and is used to measure changes in the redox state of the cell in combination with NADH.[79]

Figure 5 shows a depth- and spectrally resolved stack of multiphoton FLIM images and corresponding lifetime histograms measured from a healthy mouse kidney. TCSPC was used to generate the lifetime decay curve for each image (depth range: 120 μm) and fit to a two-component exponential function. Two spectral windows were used to simultaneously isolate the fluorescence lifetimes of NAD(P)H (350 to 450 nm) and FAD (515 to 620 nm). The data show a relatively consistent average lifetime of NAD(P)H as the imaging depth increases. Similarly, the FAD lifetime shows a tendency for a minimal decrease in average lifetime with depth. As expected, the total fluorescence intensity decreased with depth. This figure demonstrates that multiphoton FLIM yields consistent lifetime data, which can be used to assess changes in the metabolic and redox states of the tissue, with increasing depth imaging of the kidney.

Cellular autofluorescence lifetime has also been used to distinguish between normal, dysplastic, and cancerous tissues, including oral,[74] breast,[80] basal cell carcinoma,[81] and head and neck squamous cell carcinoma.[82] In addition, FLIM was used to characterize morphological features of basal cell carcinoma within *in vivo* human skin.[83,84] The fluorescence lifetime properties of FAD and porphyrin were used to distinguish between normal kidney and renal cell carcinoma within the living rat kidney.[85] The fluorescence lifetime of NAD(P)H and FAD is a viable indicator of IRI within the liver[1,2] and kidney[86] *in vivo*. The fluorescence lifetime changes associated with necrosis[76] and apoptosis[87,88] have also been described and can be used to measure tissue responses to drug treatments and disease states[89] within the kidney.

FRET describes the energy transfer from a donor to an acceptor fluorophore with overlapping emission and excitation spectra, respectively.[90] However, the two substrates must be within a critical distance of each other so that the donor energy is quenched by the acceptor.[91] Therefore, measuring the fluorescence lifetime of the donor substrate can provide quantitation of protein–protein proximity and interactions.[92,93] This technique has been harnessed in conjunction with MPM and FLIM in studies of renin synthesis in the kidney: by utilizing fluorescence-based fluorogenic renin substrates, the direct visualization of the enzyme activity of renin *in vivo*, rather than only the granular content, has been seen.[24,41] These fluorogenic renin substrates contain donor and acceptor fluorophores connected by a sequence of rodent angiotensinogen, which includes the renin cleavage site. In the absence of renin activity, the donor fluorescence is quenched by the acceptor molecule due to its close proximity and FRET. In the presence of renin and subsequent cleavage of angiotensinogen producing separation of the donor and acceptor, fluorescence is recovered and can be visualized. This technology potentially offers unique insight into disease models of altered renin-angiotensin-aldosterone system (RAAS) activation. More recently, Baird and coworkers have developed a quantitative FRET system using MPM to investigate the interaction of NF-E2 p45-related factor 2 (Nrf2) and its inhibitor Kelch-like erythroid-cell-derived protein with CNC homology [ECH]-associated protein 1 (Keap1).[94] The Nrf2/Keap1 complex is a master regulator of cytoprotective genes[95] and has been shown to play a role in both acute and chronic kidney pathologies.[96–98]

4 Utilization of Multiphoton Fluorescence Microscopy in the Kidney

4.1 *Multiphoton Microscopy and Renal Physiology*

The ability of MPM to provide high-resolution real-time optical sections that can produce 3-D images has led to significant improvements in our understanding of kidney physiology. Interactions between hormones, tubular cells, and vessels can all be observed. In particular, our understanding of the functions of the juxtaglomerular apparatus (JGA), tubular transport, and glomerular filtration have all improved. Powerful studies have utilized single nephrons to demonstrate tubulovascular interactions, the intrarenal RAAS, renal vascular flow rate, and permeability. Subsequently, this has uncovered subcellular processes that can also be visualized and include apoptosis, necrosis, mitochondrial dynamics, reactive oxygen species (ROS) production, cytosolic ion concentrations, pH, signal propagation, and protein expression.[32,42]

Some of the first insights into kidney function using MPM were found after imaging of the JGA.[26] The JGA is a critical structure that regulates renal blood flow and glomerular filtration for a single nephron, and the multiple cell types of the JGA make real-time MPM 3-D reconstruction of living kidney preparations an ideal tool for studying the structure. The cell types include mesangial cells, secretory granular epithelioid cells, vascular smooth muscle cells, vascular endothelium, and macula densa tubular epithelial cells. Macula densa cells in the thick ascending limb detect changes in fluid osmolality and/or NaCl concentration via specific transport mechanisms and send signals through mesangial cells to the glomerulus (tubuloglomerular feedback), resulting in vascular resistance and renin release by granular mesangial cells.[99]

Initial MPM approaches utilized *in situ* isolation of glomeruli with attached afferent and efferent arterioles, S1 segments of the

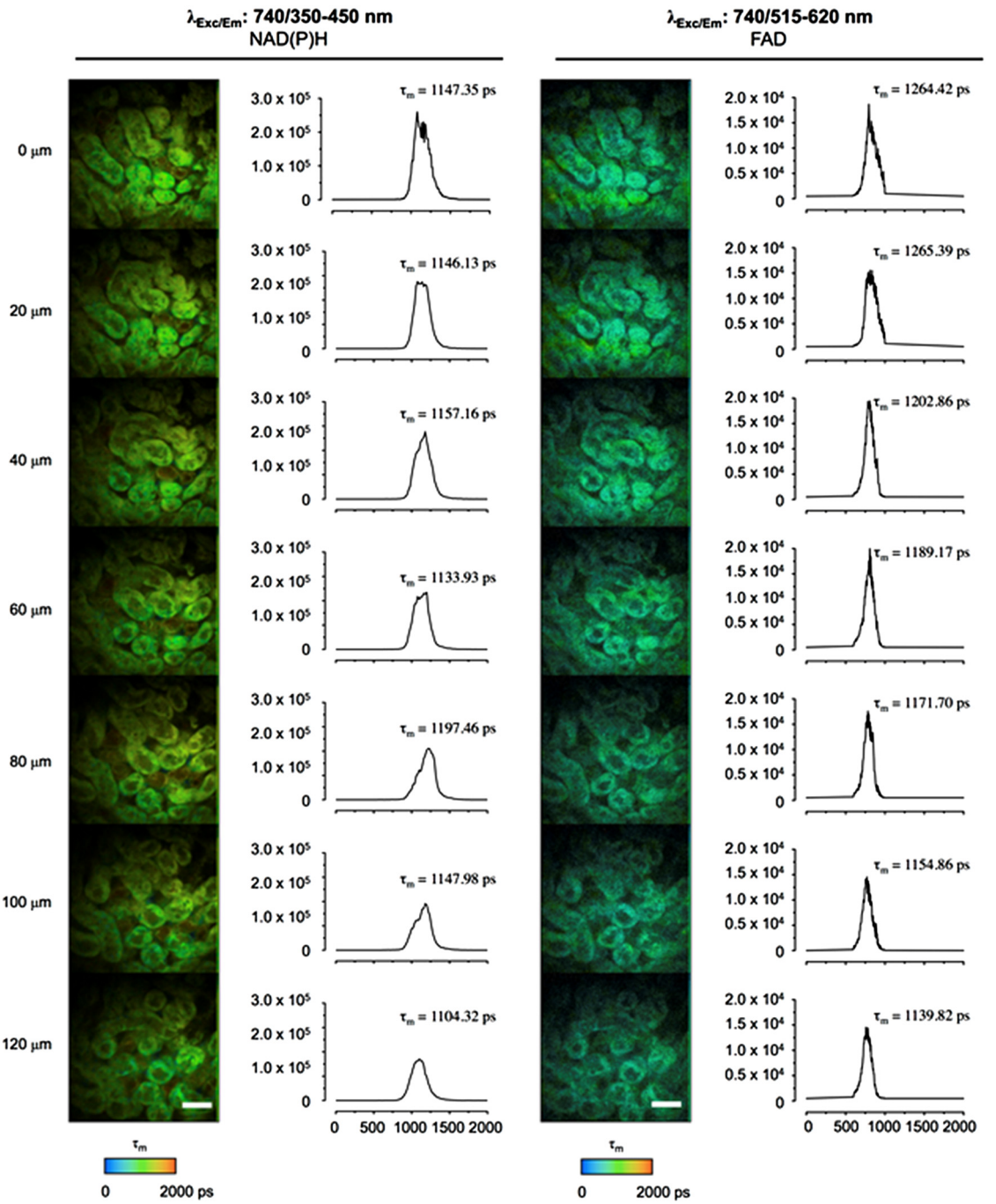

Fig. 5 Fluorescence lifetime imaging (FLIM) of (a) NAD(P)H and (b) flavin adenine dinucleotide (FAD) in healthy mouse kidney. Seven-week-old C57Bl6 mice were sacrificed and the kidney excised prior to multiphoton FLIM imaging on the JenLab DermaInspect microscope at an excitation wavelength of 740 nm. Endogenous fluorescence was separated into two emission channels, (a) 350 to 450 nm and (b) 515 to 620 nm, corresponding to NAD(P)H and FAD, respectively. Z-stack FLIM images were taken from a depth of ~20 μm below the kidney surface and are pseudo-colored according to average weighted τ_m lifetime (0 to 2000 ps; blue-green-red). Scale bare represents 40 μm.

proximal tubule, and the cortical thick ascending limb of the loops of Henle. By increasing the osmolality and NaCl concentration of tubular perfusate, this approach allowed direct visualization of the tubuloglomerular feedback mechanism. It was noted that macula densa cells swelled significantly, most likely due to increased NaCl transport, and that membrane blebbing of the apical membrane of the macula densa also occurred, resulting in afferent arteriole constriction.[26] The inclusion of angiotensin II (AngII) in the perfusate also decreased the glomerular capillary diameter and increased the calcium concentration in cells of the JGA.[26] Liu and Persson[100] then demonstrated that macula densa cells could regulate their volume and that calcium elevation, due to decreased tubular NaCl and osmolarity, was not dependent on cell volume. Furthermore, physiological

increases in luminal NaCl concentration and osmolality could result in macula densa cell shrinkage, a change that may have implications for cell signaling.[101]

Studies using MPM fully show the integrated nature of cell-to-cell communication in the kidney. MPM on live kidney tissue and confocal microscopy on fixed kidney tissue have combined to give a novel understanding of JGA physiology. MPM allowed the visualization of endothelial fenestrations of the JGA portion of the afferent arteriole for the first time.[25] The release of renin into the JGA interstitium, a common and integral component for endocrine function, was therefore demonstrated. Using techniques similar to that of MPM, standard confocal microscopy has highlighted that tubuloglomerular feedback relies on a calcium-dependent vasoconstriction caused by extracellular ATP and gap junction communication in the JGA.[56] Electronic vascular signal propagation in isolated JGA preparations has also been visualized with a fluorescent voltage-sensitive dye loaded into tubular-vascular preparations highlighting nephron synchronization.[38] Recently, Peppiatt-Wildman and colleagues[55] have taken a subcellular approach to calcium handling in the kidney to complement these studies. Using calcium-sensitive fluorophores and transgenic mice expressing the GCaMP2-calcium sensor, they were able to record calcium dynamics from endothelial, glomerular, and tubular origins.

Another primary role of JGA cells is to release renin into the vasculature to activate the RAAS, which maintains body salt and water balance. Renin release is slow and, therefore, is the rate-limiting step of the RAAS pathway. As such, the temporal information that MPM provides adds value onto more conventional methods of analysis. Specific labeling of JGA granular cells containing renin with acidotrophic fluorophores that are highly membrane-permeant, therefore accumulating in acidic cellular organelles, allows temporal and spatial tracking of renin activity at a cellular level. The JGA is the classic anatomical site of renin synthesis and its biosynthetic precursor prorenin; however, significant amounts of renin have been found in the principal cells of the connecting tubule as well as the cortical and medullary collecting ducts.[16,102,103] The study of renin dynamics using acidotrophic fluorophores, such as quinacrine and Lyso Tracker-Red, must be interpreted with caution given that these studies rely on surrogate molecules being observed rather than renin itself.

4.2 *New Paradigms in Renal Physiology*

The postglomerular uptake of selected glomerular filtrates contributes to the complex process of urine production. The simultaneous visualization of tubular uptake and glomerular filtration provided by MPM has allowed direct quantification of single nephron filtration. These measurements utilize dextrans of varying molecular weights conjugated to fluorophores. The approach has already challenged our understanding of the etiology of albuminuria. Russo and colleagues[43] used a puromycin aminonucleoside nephrosis rodent model. They administered fluorescent serum albumin to rats and demonstrated that the glomeruli filter albumin at nephrotic levels in both controls and rats with nephrosis (albumin excretion rate >300 mg/day); however, a rapid retrieval of almost all albumin occurred at the epithelium of the S1 segment of the proximal tubule in control rats, but not nephrotic rats. This result is in direct contrast with previous studies that measured glomerular-tubular filtration using micropuncture techniques.[104,105]

The proximal tubule apical endocytotic machinery megalin, vacuolar H+-ATPase A subunit, and clathrin were shown to decrease in expression in nephrotic rats, and this provides a possible mechanism for albuminuria.[43,106] Quantitative MPM studies were performed to validate the result, with some finding the GSC of albumin much lower than reported.[44,53,107] However, the issue remains controversial,[108–111] with debate on the ability of MPM to identify multiple factors that influence glomerular albumin permeability, including the depth of image acquisition, the selection of fluorophore, genetic strain of rat, and dietary status.[53,112] The generalized polarity concept, whereby the intensity difference between two fluorescent molecules is normalized to the total intensity of the two dyes, has revealed further differences in proximal tubule uptake following glomerular filtration. Specifically, negatively charged 40-kDa dextran is more readily absorbed in the proximal tubule than neutral 40-kDa dextran.[45]

4.3 *Multiphoton Microscopy and Renal Pathophysiology*

Significant advancements have been achieved using MPM in experimental models of kidney disease. Possibly, the most valuable aspect of the utilization of MPM in models of kidney pathophysiology is the temporal and spatial imaging of subcellular processes, such as apoptosis, necrosis, and mitochondrial dynamics. Renal IRI,[14,27,40,113,114] kidney cyst development,[57] diabetic nephropathy,[16,39,44,115] renal inflammation,[35,116,117] and gentamicin toxicity[14] have been investigated using MPM.

Renal IRI is the most common form of acute kidney injury and has been studied extensively. As an experimental model, this has a translational focus for transplant nephrology and is a useful model to study cellular responses to IRI. IRI is characterized by tubular swelling, cell death (apoptosis and necrosis), mitochondrial dysfunction, inflammatory responses, and deregulated vascular function.[46] Microvascular and tubular components of the kidney have mutual, as well as unique, responses to IRI, which contribute to decreased kidney function. Given that IRI is potentially reversible, MPM can be used to image these cellular processes and then determine the success, or failure, of novel interventions. Recently, Hall and colleagues[14] have used MPM to demonstrate the role of redox alterations occurring as a result of IRI. By using endogenous NADH fluorescence, mitochondrial selective probes (TMRM), ROS-sensitive dyes [dihydroethidium (DHE)], and glutathione indicators, they have shown that IRI mainly affects the distribution of mitochondria in the proximal tubular epithelium, with increased superoxide levels. Although increased ROS have been implicated in the pathophysiology of IRI before, MPM has allowed direct visualization of ROS in conjunction with cell damage. MPM image analysis of IRI during two models of kidney transplantation has revealed cast formation in the tubular profiles, mainly from increased tubular injury, necrosis, and apoptosis.[51] This study also assessed the efficacy of p53 siRNA during rodent kidney transplantation and found that it significantly improved kidney function and decreased cast formation, perhaps by increasing blood flow through the vasculature.

Inflammation within the kidney may be reparative or profibrotic; however, the underlying mechanisms remain poorly understood. Routine histological analysis, of necessity at a single point in time, often fails to uncover important cellular interactions given the high motility of circulating inflammatory cells in a time-dependent manner. Recently, MPM revealed a new

leukocyte recruitment paradigm in the glomerulus of the inflamed kidney.[35] This has implications for glomerular basement membrane disease and other forms of immune cell-mediated glomerulonephritis, common causes of end-stage kidney disease, associated with inflammatory cell recruitment to the glomerulus. Devi et al.[35] used MPM of glomeruli in mice in combination with fluorescence-based approaches for labeling leukocytes to demonstrate that even in the absence of inflammation, neutrophils and monocytes undergo transient (~5 min) periods of retention and migration in the glomerular capillaries before returning to the bloodstream. In addition, in three separate models of glomerular inflammation, neutrophils increased their dwell time in the glomerulus in response to inflammation. This model also spatially tracked neutrophils and monocytes, separating them into static and crawling groups. In addition, ~30% of intravascular neutrophils in the inflamed glomeruli generated ROS that were detected by DHE, which also displayed increased dwell time.[35]

The manipulability of mouse genetics combined with intravital microscopy is especially useful in the field of renal immunology. Soos and colleagues[118] used conventional intravital confocal microscopy in the $CX_3CR1^{GFP/+}$ mouse in the normal kidney to examine interstitial macrophages and dendritic cells in the normal kidney. This demonstrated the contiguous network and probing dendritic behavior throughout the entire kidney. Using a robust model of kidney inflammation and fibrosis [unilateral ureteral obstruction (UUO)] and MPM, renal dentritic cells identified via endogenous expression of yellow fluorescent protein (YFP) in CD11c-YFP mice were seen to adapt to a proinflammatory phenotype to activate T-cells. However, following dentritic cell depletion, UUO mice continued to develop fibrosis, indicating that these cells do not directly contribute to fibrosis.[116] Fluorescently labeled *Escherichia Coli* has been used in a model of upper urinary tract infection and visualized using MPM. This study revealed the initial stages of neutrophil infiltration with the Hoechst 33342 fluorophore and morphology as well as vascular, tubular, and lymphatic structural interactions.[117] The use of GFP-labeled immune components in these murine models, as well as fluorophore-conjugated antibodies, have fully utilized immunological analyses using MPM.

Diabetic nephropathy is the leading cause of chronic kidney disease worldwide and comprises a large proportion of nephrology research. The progressive nature of diabetes-induced kidney damage, coupled with the quantitative aspects of MPM image acquisition and analysis, allows structural and functional relationships to be explored. The previously mentioned controversy of the nonglomerular origin of albuminuria has been further supported in models of streptozotocin-induced diabetes in rats.[44,115] The GSC of albumin was found to be unaltered in 12-week-old diabetic rats compared to controls. Infusion of a 69-kDa FITC-dextran (which has the same GSC as albumin) in control rats was not retained in the plasma following 24 h; however, albumin-Alexa568 (used to image albumin with MPM) was well retained in the plasma.[44] This supported the theory that filtered albumin was reabsorbed by the proximal tubule epithelium and returned to the circulation. This system of reabsorption appears to be disturbed early in diabetes within the proximal tubular cells captured *in vivo* using MPM, showing a marked reduction in intracellular uptake of albumin-Alexa568. However, despite albuminuria being an outcome in diabetic nephropathy, the question still remains as to what causes a disruption of the proximal tubule endocytosis machinery. Studies have shown that proximal tubule albumin uptake relies on clathrin- and receptor-mediated mechanisms.[119,120] Proximal tubule endocytosis is modulated by AngII through AngII (type 2) receptor mediated protein kinase B activation and may present a target for albuminuria.[121]

Diabetes also increases collecting duct prorenin levels, observed by quinacrine-labeled renin/prorenin granules and MPM, suggesting that prorenin content and release from collecting duct cells may be more important than the JGA when regulating levels of AngII in diabetes.[16] This alternate pattern of AngII renin stimulation makes MPM an ideal tool, compared with fixed whole kidney or cortex preparations, and provides a theoretical pathway for inhibiting proximal tubular albumin endocytosis early in diabetes. Using the same rodent model of diabetes (streptozotocin-induced diabetic rat), Satoh and colleagues[115] demonstrated early morphological changes in glomeruli at four and eight weeks, including glomerular hypertrophy and an increased diameter ratio of afferent and efferent arterioles, which correlated to hyperfiltration of a 40-kDa dextran fluorophore. However, the hyperfiltration of the glomeruli had already occurred before the diabetic rats developed albuminuria. A novel finding relating to established proteinuric kidney disease has shown significant alterations to endothelial surface layer of the glomerulus.[122] This endothelial glycocalyx composed of glycosaminoglycans, proteoglycans, absorbed plasma components, and a loose matrix is significantly reduced in old spontaneously proteinuric kidney disease rats. This technique utilized MPM in conjunction with various fluorochrome-conjugated lectins to specifically label the glomerular glycocalyx in conjunction with physiological microvascular permeability measurements.

Polycystic kidney disease is an autosomal dominant genetic disorder that often leads to destructive renal cyst development. Studies into the pathophysiology of autosomal dominant polycystic kidney disease (ADPKD) using MPM are limited, yet provide an untapped opportunity, given that the tubule-derived cysts often lack important transport functions. Sulfonefluorescein, which is a fluorescent organic anion that has been shown to be secreted from kidney proximal tubular cells,[58] provides a useful tool to study tubule-derived cysts. Tanner and colleagues[57] have demonstrated in heterozygous Han:SPRD rat with ADPKD that sulfonefluorescein accumulation in proximal tubules was diminished compared with control proximal tubules in control rats. However, the proximal tubule epithelial cells of cysts were variable in accumulating sulfonefluorescein, suggesting a broad deficiency in transport functions.

5 Conclusion: Future Advances in Multiphoton Microscopy in the Kidney

The use of MPM imaging has rapidly increased over the past decade and with this comes an unprecedented possibility for advancements in our knowledge in live cell physiology and pathophysiology. A major limitation to current MPM technologies in the kidney is the limitation of imaging depth in the cortex. Continuing efforts toward imaging at greater depths, possibly into the medulla, are needed. New infrared dyes with longer wavelengths that penetrate deeper due to less absorption and scattering appear to be the next step. Researchers are also continuing to find new applications for MPM technology. The use of a compact and flexible microendoscope utilizing multiphoton excitation has been used to visualize rodent colon, kidney, and liver *in vivo*.[123] This opens the possibility of *in vivo* imaging in human organs. MPM has already been applied in

a clinical setting to assess skin diseases[124] and gastric cancer.[125] Peti-Peterdi and colleagues[42] have now demonstrated the unconventional use of multiphoton lasers as micromanipulators in the kidney. By focusing the multiphoton excitation laser beam at a small site, such as the capillary wall in the glomerulus, the local tissue damage can cause a disruption and may help to study the local effects of this damage. Recently, Corridon and colleagues[126] developed a method to facilitate and monitor the expression of exogenous genes in the rat kidney using plasmid and viral vectors, which can be visualized with MPM.

In conclusion, the ability to visualize and quantify cellular and intracellular processes in multiple dimensions in living animals offers endless rewards in experimental nephrology research. MPM provides an avenue to answer some unknown kidney processes both in terms of physiology and pathophysiology.

References

1. C. A. Thorling et al., "Multiphoton microscopy can visualize zonal damage and decreased cellular metabolic activity in hepatic ischemia-reperfusion injury in rats," *J. Biomed. Opt.* **16**(11), 116011 (2011).
2. C. A. Thorling et al., "Intravital multiphoton microscopy can model uptake and excretion of fluorescein in hepatic ischemia-reperfusion injury," *J. Biomed. Opt.* **18**(10), 101306 (2013).
3. M. Honda et al., "Intravital imaging of neutrophil recruitment in hepatic ischemia-reperfusion injury in mice," *Transplantation* **95**(4), 551–558 (2013).
4. M. Yuryev and L. Khiroug, "Dynamic longitudinal investigation of individual nerve endings in the skin of anesthetized mice using in vivo two-photon microscopy," *J. Biomed. Opt.* **17**(4), 046007 (2012).
5. J. L. Li et al., "Intravital multiphoton imaging of immune responses in the mouse ear skin," *Nat. Protoc.* **7**(2), 221–234 (2012).
6. W. Y. Sanchez et al., "Changes in the redox state and endogenous fluorescence of in vivo human skin due to intrinsic and photo-aging, measured by multiphoton tomography with fluorescence lifetime imaging," *J. Biomed. Opt.* **18**(6), 061217 (2013).
7. V. R. Leite-Silva et al., "The effect of formulation on the penetration of coated and uncoated zinc oxide nanoparticles into the viable epidermis of human skin in vivo," *Eur. J. Pharm. Biopharm.* **84**(2), 297–308 (2013).
8. W. Y. Sanchez et al., "Dichloroacetate inhibits aerobic glycolysis in multiple myeloma cells and increases sensitivity to bortezomib," *Br. J. Cancer* **108**(8), 1624–1633 (2013).
9. W. Lo et al., "Fast Fourier transform-based analysis of second-harmonic generation image in keratoconic cornea," *Invest. Ophthalmol. Vis. Sci.* **53**(7), 3501–3507 (2012).
10. U. Gehlsen et al., "Two-photon fluorescence lifetime imaging monitors metabolic changes during wound healing of corneal epithelial cells in vitro," *Graefes. Arch. Clin. Exp. Ophthalmol.* **250**(9), 1293–1302 (2012).
11. Y. Chen et al., "Automated 5-D analysis of cell migration and interaction in the thymic cortex from time-lapse sequences of 3-D multi-channel multi-photon images," *J. Immunol. Methods* **340**(1), 65–80 (2009).
12. S. S. Caetano, T. Teixeira, and C. E. Tadokoro, "Intravital imaging of the mouse thymus using 2-photon microscopy," *J. Vis. Exp.* **59**, e3504 (2012).
13. B. A. Molitoris, R. Sandoval, and T. A. Sutton, "Endothelial injury and dysfunction in ischemic acute renal failure," *Crit. Care Med.* **30**(Suppl. 5), S235–240 (2002).
14. A. M. Hall et al., "In vivo multiphoton imaging of mitochondrial structure and function during acute kidney injury," *Kidney Int.* **83**(1), 72–83 (2013).
15. J. Peti-Peterdi and A. Sipos, "A high-powered view of the filtration barrier," *J. Am. Soc. Nephrol.* **21**(11), 1835–1841 (2010).
16. J. J. Kang et al., "The collecting duct is the major source of prorenin in diabetes," *Hypertension* **51**(6), 1597–1604 (2008).
17. I. C. Ghiran, *Introduction to Fluorescence Microscopy*, Methods in Molecular Biology, Vol. 689, pp. 93–136, Humana Press, New York, NY (2011).
18. D. Coling and B. Kachar, "Principles and application of fluorescence microscopy," *Current Protocols in Molecular Biology* Chapter 14 Unit 14 10, John Wiley & Sons Inc., Hoboken, NJ (2001).
19. W. R. Zipfel et al., "Live tissue intrinsic emission microscopy using multiphoton-excited native fluorescence and second harmonic generation," *Proc. Natl. Acad. Sci. U S A* **100**(12), 7075–7080 (2003).
20. K. W. Dunn and P. A. Young, "Principles of multiphoton microscopy," *Nephron Exp. Nephrol.* **103**(2), e33–40 (2006).
21. W. Kaiser and C. G. B. Garrett, "2-photon excitation in $CaF_2 - Eu^{2+}$," *Phys. Rev. Lett.* **7**(6), 229–231 (1961).
22. W. Denk, J. H. Strickler, and W. W. Webb, "Two-photon laser scanning fluorescence microscopy," *Science* **248**(4951), 73–76 (1990).
23. J. Peti-Peterdi, "Multiphoton imaging of renal tissues in vitro," *Am. J. Physiol. Renal Physiol.* **288**(6), F1079–1083 (2005).
24. J. Peti-Peterdi et al., "Real-time imaging of renin release in vitro," *Am. J. Physiol. Renal Physiol.* **287**(2), F329–335 (2004).
25. L. Rosivall et al., "Fluid flow in the juxtaglomerular interstitium visualized in vivo," *Am. J. Physiol. Renal Physiol.* **291**(6), F1241–1247 (2006).
26. J. Peti-Peterdi et al., "Two-photon excitation fluorescence imaging of the living juxtaglomerular apparatus," *Am. J. Physiol. Renal Physiol.* **283**(1), F197–201 (2002).
27. A. M. Hall et al., "Multiphoton imaging reveals differences in mitochondrial function between nephron segments," *J. Am. Soc. Nephrol.* **20**(6), 1293–1302 (2009).
28. D. Kleinfeld et al., "Fluctuations and stimulus-induced changes in blood flow observed in individual capillaries in layers 2 through 4 of rat neocortex," *Proc. Natl. Acad. Sci. U S A* **95**(26), 15741–15746 (1998).
29. F. Helmchen et al., "In vivo dendritic calcium dynamics in deep-layer cortical pyramidal neurons," *Nat. Neurosci.* **2**(11), 989–996 (1999).
30. P. A. Young et al., "The effects of spherical aberration on multiphoton fluorescence excitation microscopy," *J. Microsc.* **242**(2), 157–165 (2011).
31. P. A. Young et al., "The effects of refractive index heterogeneity within kidney tissue on multiphoton fluorescence excitation microscopy," *J. Microsc.* **242**(2), 148–156 (2011).
32. K. W. Dunn, T. A. Sutton, and R. M. Sandoval, "Live-animal imaging of renal function by multiphoton microscopy," *Current Protocols in Cytometry* Chapter 14 Unit12 19, John Wiley & Sons Inc., Hoboken, NJ (2012).
33. I. M. Schiessl, S. Bardehle, and H. Castrop, "Superficial nephrons in BALB/c and C57BL/6 mice facilitate in vivo multiphoton microscopy of the kidney," *PLoS One* **8**(1), e52499 (2013).
34. C. C. Khoury et al., "Visualizing the mouse podocyte with multiphoton microscopy," *Biochem. Biophys. Res. Commun.* **427**(3), 525–530 (2012).
35. S. Devi et al., "Multiphoton imaging reveals a new leukocyte recruitment paradigm in the glomerulus," *Nat. Med.* **19**(1), 107–112 (2013).
36. M. Steinhausen et al., "Hydronephrosis: a new method to visualize vas afferens, efferens, and glomerular network," *Kidney Int.* **23**(6), 794–806 (1983).
37. G. A. Tanner et al., "Micropuncture gene delivery and intravital two-photon visualization of protein expression in rat kidney," *Am. J. Physiol. Renal Physiol.* **289**(3), F638–643 (2005).
38. D. J. Marsh et al., "Electrotonic vascular signal conduction and nephron synchronization," *Am. J. Physiol. Renal Physiol.* **296**(4), F751–761 (2009).
39. J. J. Kang et al., "Quantitative imaging of basic functions in renal (patho) physiology," *Am. J. Physiol. Renal Physiol.* **291**(2), F495–502 (2006).
40. A. M. Hall et al., "Multiphoton imaging of the functioning kidney," *J. Am. Soc. Nephrol.* **22**(7), 1297–1304 (2011).
41. J. Peti-Peterdi et al., "Multiphoton imaging of renal regulatory mechanisms," *Physiology (Bethesda)* **24**(2), 88–96 (2009).
42. J. Peti-Peterdi, J. L. Burford, and M. J. Hackl, "The first decade of using multiphoton microscopy for high-power kidney imaging," *Am. J. Physiol. Renal Physiol.* **302**(2), F227–233 (2012).
43. L. M. Russo et al., "The normal kidney filters nephrotic levels of albumin retrieved by proximal tubule cells: retrieval is disrupted in nephrotic states," *Kidney Int.* **71**(6), 504–513 (2007).
44. L. M. Russo et al., "Impaired tubular uptake explains albuminuria in early diabetic nephropathy," *J. Am. Soc. Nephrol.* **20**(3), 489–494 (2009).
45. W. Yu, R. M. Sandoval, and B. A. Molitoris, "Quantitative intravital microscopy using a generalized polarity concept for kidney studies," *Am. J. Physiol. Cell Physiol.* **289**(5), C1197–1208 (2005).

46. J. V. Bonventre and J. M. Weinberg, "Recent advances in the pathophysiology of ischemic acute renal failure," *J. Am. Soc. Nephrol.* **14**(8), 2199–2210 (2003).
47. G. Camirand et al., "Multiphoton intravital microscopy of the transplanted mouse kidney," *Am. J. Transplant.* **11**(10), 2067–2074 (2011).
48. I. Toma, J. J. Kang, and J. Peti-Peterdi, "Imaging renin content and release in the living kidney," *Nephron Physiol.* **103**(2), p71–74 (2006).
49. J. J. Kang et al., "Imaging the renin-angiotensin system: an important target of anti-hypertensive therapy," *Adv. Drug Deliv. Rev.* **58**(7), 824–833 (2006).
50. A. Prokai and J. Peti-Peterdi, "Recent advances in tissue (pro)renin imaging," *Front. Biosci. (Elite Ed).* **E2**(4), 1227–1233 (2010).
51. R. Imamura et al., "Intravital two-photon microscopy assessment of renal protection efficacy of siRNA for p53 in experimental rat kidney transplantation models," *Cell Transplant.* **19**(12), 1659–1670 (2010).
52. K. W. Dunn et al., "Functional studies of the kidney of living animals using multicolor two-photon microscopy," *Am. J. Physiol. Cell Physiol.* **283**(3), C905–916 (2002).
53. J. Peti-Peterdi, "Independent two-photon measurements of albumin GSC give low values," *Am. J. Physiol. Renal Physiol.* **296**(6), F1255–1257 (2009).
54. A. Sipos et al., "Advances in renal (patho)physiology using multiphoton microscopy," *Kidney Int.* **72**(10), 1188–1191 (2007).
55. C. M. Peppiatt-Wildman, C. Crawford, and A. M. Hall, "Fluorescence imaging of intracellular calcium signals in intact kidney tissue," *Nephron Exp. Nephrol.* **121**(1–2), e49–58 (2012).
56. J. Peti-Peterdi, "Calcium wave of tubuloglomerular feedback," *Am. J. Physiol. Renal Physiol.* **291**(2), F473–480 (2006).
57. G. A. Tanner, R. M. Sandoval, and K. W. Dunn, "Two-photon in vivo microscopy of sulfonefluorescein secretion in normal and cystic rat kidneys," *Am. J. Physiol. Renal Physiol.* **286**(1), F152–160 (2004).
58. G. A. Tanner et al., "Organic anion secretion in polycystic kidney disease," *J. Am. Soc. Nephrol.* **8**(8), 1222–1231 (1997).
59. S. L. Ashworth et al., "Two-photon microscopy: visualization of kidney dynamics," *Kidney Int.* **72**(4), 416–421 (2007).
60. R. M. Sandoval and B. A. Molitoris, "Quantifying glomerular permeability of fluorescent macromolecules using 2-photon microscopy in Munich Wistar rats," *J. Vis. Exp.* **74** (2013).
61. E. Wang et al., "Rapid diagnosis and quantification of acute kidney injury using fluorescent ratio-metric determination of glomerular filtration rate in the rat," *Am. J. Physiol. Renal Physiol.* **299**(5), F1048–1055 (2010).
62. W. Yu, R. M. Sandoval, and B. A. Molitoris, "Rapid determination of renal filtration function using an optical ratiometric imaging approach," *Am. J. Physiol. Renal Physiol.* **292**(6), F1873–1880 (2007).
63. M. J. Miller et al., "Two-photon imaging of lymphocyte motility and antigen response in intact lymph node," *Science* **296**(5574), 1869–1873 (2002).
64. M. J. Miller et al., "Autonomous T cell trafficking examined in vivo with intravital two-photon microscopy," *Proc. Natl. Acad. Sci. U. S. A.* **100**(5), 2604–2609 (2003).
65. M. Kitano and T. Okada, "Four-dimensional tracking of lymphocyte migration and interactions in lymph nodes by two-photon microscopy," *Methods in Enzymology* Vol. 506, pp. 437–454, Academic Press, Amsterdam, Netherlands (2012).
66. S. Huang, A. A. Heikal, and W. W. Webb, "Two-photon fluorescence spectroscopy and microscopy of NAD(P)H and flavoprotein," *Biophys. J.* **82**(5), 2811–2825 (2002).
67. S. O. La and J. F. Bille, "High-speed two-photon excited autofluorescence imaging of ex vivo human retinal pigment epithelial cells toward age-related macular degeneration diagnostic," *J. Biomed. Opt.* **13**(6), 064008 (2008).
68. G. Eichhoff, M. A. Busche, and O. Garaschuk, "In vivo calcium imaging of the aging and diseased brain," *Eur. J. Nucl. Med. Mol. Imaging* **35**(Suppl. 1), S99–106 (2008).
69. W. Becker, "Fluorescence lifetime imaging—techniques and applications," *J. Microsc.* **247**(2), 119–136 (2012).
70. D. Elson et al., "Time-domain fluorescence lifetime imaging applied to biological tissue," *Photochem. Photobiol. Sci.* **3**(8), 795–801 (2004).
71. E. Gratton et al., "Fluorescence lifetime imaging for the two-photon microscope: time-domain and frequency-domain methods," *J. Biomed. Opt.* **8**(3), 381–390 (2003).
72. M. Y. Berezin and S. Achilefu, "Fluorescence lifetime measurements and biological imaging," *Chem. Rev.* **110**(5), 2641–2684 (2010).
73. D. K. Bird et al., "Metabolic mapping of MCF10A human breast cells via multiphoton fluorescence lifetime imaging of the coenzyme NADH," *Cancer Res.* **65**(19), 8766–8773 (2005).
74. M. C. Skala et al., "In vivo multiphoton fluorescence lifetime imaging of protein-bound and free nicotinamide adenine dinucleotide in normal and precancerous epithelia," *J. Biomed. Opt.* **12**(2), 024014 (2007).
75. M. C. Skala et al., "In vivo multiphoton microscopy of NADH and FAD redox states, fluorescence lifetimes, and cellular morphology in precancerous epithelia," *Proc. Natl. Acad. Sci. U. S. A.* **104**(49), 19494–19499 (2007).
76. W. Y. Sanchez et al., "Analysis of the metabolic deterioration of ex vivo skin from ischemic necrosis through the imaging of intracellular NAD(P)H by multiphoton tomography and fluorescence lifetime imaging microscopy," *J. Biomed. Opt.* **15**(4), 046008 (2010).
77. R. Niesner et al., "Noniterative biexponential fluorescence lifetime imaging in the investigation of cellular metabolism by means of NAD(P)H autofluorescence," *Chemphyschem.* **5**(8), 1141–1149 (2004).
78. J. R. Lakowicz et al., "Fluorescence lifetime imaging of free and protein-bound NADH," *Proc. Natl. Acad. Sci. U. S. A.* **89**(4), 1271–1275 (1992).
79. B. Chance et al., "Oxidation-reduction ratio studies of mitochondria in freeze-trapped samples. NADH and flavoprotein fluorescence signals," *J. Biol. Chem.* **254**(11), 4764–4771 (1979).
80. M. W. Conklin et al., "Fluorescence lifetime imaging of endogenous fluorophores in histopathology sections reveals differences between normal and tumor epithelium in carcinoma in situ of the breast," *Cell Biochem. Biophys.* **53**(3), 145–157 (2009).
81. N. P. Galletly et al., "Fluorescence lifetime imaging distinguishes basal cell carcinoma from surrounding uninvolved skin," *Br. J. Dermatol.* **159**(1), 152–161 (2008).
82. Y. Sun et al., "Endoscopic fluorescence lifetime imaging for in vivo intraoperative diagnosis of oral carcinoma," *Microsc. Microanal.* **19**(4), 791–798 (2013).
83. M. Manfredini et al., "High-resolution imaging of basal cell carcinoma: a comparison between multiphoton microscopy with fluorescence lifetime imaging and reflectance confocal microscopy," *Skin Res. Technol.* **19**(1), e433–443 (2013).
84. S. Seidenari et al., "Multiphoton laser tomography and fluorescence lifetime imaging of basal cell carcinoma: morphologic features for non-invasive diagnostics," *Exp. Dermatol.* **21**(11), 831–836 (2012).
85. D. B. Tata et al., "Fluorescence polarization spectroscopy and time-resolved fluorescence kinetics of native cancerous and normal rat kidney tissues," *Biophys. J.* **50**(3), 463–469 (1986).
86. A. Abulrob et al., "In vivo time domain optical imaging of renal ischemia-reperfusion injury: discrimination based on fluorescence lifetime," *Mol. Imaging* **6**(5), 304–314 (2007).
87. J. S. Yu et al., "Increase of reduced nicotinamide adenine dinucleotide fluorescence lifetime precedes mitochondrial dysfunction in staurosporine-induced apoptosis of HeLa cells," *J. Biomed. Opt.* **16**(3), 036008 (2011).
88. H. W. Wang et al., "Differentiation of apoptosis from necrosis by dynamic changes of reduced nicotinamide adenine dinucleotide fluorescence lifetime in live cells," *J. Biomed. Opt.* **13**(5), 054011 (2008).
89. Q. Yu and A. A. Heikal, "Two-photon autofluorescence dynamics imaging reveals sensitivity of intracellular NADH concentration and conformation to cell physiology at the single-cell level," *J. Photochem. Photobiol. B* **95**(1), 46–57 (2009).
90. R. R. Duncan et al., "Multi-dimensional time-correlated single photon counting (TCSPC) fluorescence lifetime imaging microscopy (FLIM) to detect FRET in cells," *J. Microsc.* **215**(1), 1–12 (2004).
91. G. H. Patterson, D. W. Piston, and B. G. Barisas, "Forster distances between green fluorescent protein pairs," *Anal. Biochem.* **284**(2), 438–440 (2000).
92. G. W. Gordon et al., "Quantitative fluorescence resonance energy transfer measurements using fluorescence microscopy," *Biophys. J.* **74**(5), 2702–2713 (1998).
93. A. Periasamy and R. N. Day, "Visualizing protein interactions in living cells using digitized GFP imaging and FRET microscopy," *Methods in Cell Biology*, Vol. 58, pp. 293–314, Elsevier, Amsterdam, Netherlands (1999).

94. L. Baird et al., "Regulatory flexibility in the Nrf2-mediated stress response is conferred by conformational cycling of the Keap1-Nrf2 protein complex," *Proc. Natl. Acad. Sci. U. S. A.* **110**(38), 15259–15264 (2013).
95. T. Nguyen, P. Nioi, and C. B. Pickett, "The Nrf2-antioxidant response element signaling pathway and its activation by oxidative stress," *J. Biol. Chem.* **284**(20), 13291–13295 (2009).
96. A. Wilmes et al., "Identification and dissection of the Nrf2 mediated oxidative stress pathway in human renal proximal tubule toxicity," *Toxicol. In Vitro* **25**(3), 613–622 (2011).
97. B. M. Hybertson et al., "Oxidative stress in health and disease: the therapeutic potential of Nrf2 activation," *Mol. Aspects Med.* **32**(4–6), 234–246 (2011).
98. P. E. Pergola et al., "Bardoxolone methyl and kidney function in CKD with type 2 diabetes," *N. Engl. J. Med.* **365**(4), 327–336 (2011).
99. P. D. Bell and J. Y. Lapointe, "Characteristics of membrane transport processes of macula densa cells," *Clin. Exp. Pharmacol. Physiol.* **24**(7), 541–547 (1997).
100. R. Liu and A. E. Persson, "Simultaneous changes of cell volume and cytosolic calcium concentration in macula densa cells caused by alterations of luminal NaCl concentration," *J. Physiol.* **563**(3), 895–901 (2005).
101. P. Komlosi, A. Fintha, and P. D. Bell, "Unraveling the relationship between macula densa cell volume and luminal solute concentration/osmolality," *Kidney Int.* **70**(5), 865–871 (2006).
102. M. C. Prieto-Carrasquero et al., "Collecting duct renin is upregulated in both kidneys of 2-kidney, 1-clip goldblatt hypertensive rats," *Hypertension* **51**(6), 1590–1596 (2008).
103. A. Rohrwasser et al., "Renin and kallikrein in connecting tubule of mouse," *Kidney Int.* **64**(6), 2155–2162 (2003).
104. A. Tojo and H. Endou, "Intrarenal handling of proteins in rats using fractional micropuncture technique," *Am. J. Physiol.* **263**(4 Pt 2), F601–F606 (1992).
105. D. E. Oken and W. Flamenbaum, "Micropuncture studies of proximal tubule albumin concentrations in normal and nephrotic rats," *J. Clin. Invest.* **50**(7), 1498–1505 (1971).
106. A. Hurtado-Lorenzo et al., "V-ATPase interacts with ARNO and Arf6 in early endosomes and regulates the protein degradative pathway," *Nat. Cell Biol.* **8**(2), 124–136 (2006).
107. G. A. Tanner, "Glomerular sieving coefficient of serum albumin in the rat: a two-photon microscopy study," *Am. J. Physiol. Renal Physiol.* **296**(6), F1258–1265 (2009).
108. E. I. Christensen et al., "Controversies in nephrology: renal albumin handling, facts, and artifacts!," *Kidney Int.* **72**(10), 1192–1194 (2007).
109. W. D. Comper, B. Haraldsson, and W. M. Deen, "Resolved: normal glomeruli filter nephrotic levels of albumin," *J. Am. Soc. Nephrol.* **19**(3), 427–432 (2008).
110. M. Gekle, "Renal albumin handling: a look at the dark side of the filter," *Kidney Int.* **71**(6), 479–481 (2007).
111. A. Remuzzi et al., "Albumin concentration in the Bowman's capsule: multiphoton microscopy vs micropuncture technique," *Kidney Int.* **72**(11), 1410–1411 (2007).
112. R. M. Sandoval et al., "Multiple factors influence glomerular albumin permeability in rats," *J. Am. Soc. Nephrol.* **23**(3), 447–457 (2012).
113. A. A. Sharfuddin et al., "Soluble thrombomodulin protects ischemic kidneys," *J. Am. Soc. Nephrol.* **20**(3), 524–534 (2009).
114. D. P. Basile et al., "Impaired endothelial proliferation and mesenchymal transition contribute to vascular rarefaction following acute kidney injury," *Am. J. Physiol. Renal Physiol.* **300**(3), F721–733 (2011).
115. M. Satoh et al., "In vivo visualization of glomerular microcirculation and hyperfiltration in streptozotocin-induced diabetic rats," *Microcirculation* **17**(2), 103–112 (2010).
116. S. L. Snelgrove et al., "Renal dendritic cells adopt a pro-inflammatory phenotype in obstructive uropathy to activate T cells but do not directly contribute to fibrosis," *Am. J. Pathol.* **180**(1), 91–103 (2012).
117. F. X. Choong et al., "Multiphoton microscopy applied for real-time intravital imaging of bacterial infections in vivo," *Methods in Enzymology* Vol. 506, pp. 35–61, Academic Press, Amsterdam, Netherlands (2012).
118. T. J. Soos et al., "CX3CR1+ interstitial dendritic cells form a contiguous network throughout the entire kidney," *Kidney Int.* **70**(3), 591–596 (2006).
119. K. Koral and E. Erkan, "PKB/Akt partners with Dab2 in albumin endocytosis," *Am. J. Physiol. Renal Physiol.* **302**(8), F1013–1024 (2012).
120. K. Weyer et al., "Mouse model of proximal tubule endocytic dysfunction," *Nephrol. Dial. Transplant.* **26**(11), 3446–3451 (2011).
121. C. Caruso-Neves, S. H. Kwon, and W. B. Guggino, "Albumin endocytosis in proximal tubule cells is modulated by angiotensin II through an AT2 receptor-mediated protein kinase B activation," *Proc. Natl. Acad. Sci. U. S. A.* **102**(48), 17513–17518 (2005).
122. A. H. Salmon et al., "Loss of the endothelial glycocalyx links albuminuria and vascular dysfunction," *J. Am. Soc. Nephrol.* **23**(8), 1339–1350 (2012).
123. C. M. Brown et al., "In vivo imaging of unstained tissues using a compact and flexible multiphoton microendoscope," *J. Biomed. Opt.* **17**(4), 040505 (2012).
124. M. J. Koehler et al., "Clinical application of multiphoton tomography in combination with confocal laser scanning microscopy for in vivo evaluation of skin diseases," *Exp. Dermatol.* **20**(7), 589–594 (2011).
125. J. Yan et al., "A pilot study of using multiphoton microscopy to diagnose gastric cancer," *Surg. Endosc.* **25**(5), 1425–1430 (2011).
126. P. R. Corridon et al., "A method to facilitate and monitor expression of exogenous genes in the rat kidney using plasmid and viral vectors," *Am. J. Physiol. Renal Physiol.* **304**(9), F1217–1229 (2013).

David M. Small is a PhD scholar with the Centre for Kidney Disease Research, University of Queensland at the Translational Research Institute. His main research interests are in understanding the role of oxidative stress in acute and chronic kidney pathologies and how alterations in mitochondrial dynamics influence nephron function. These research interests involve the application of multiphoton imaging of the healthy and diseased kidney.

Washington Y. Sanchez is a postdoctoral research scientist for the Therapeutics Research Centre, University of Queensland, which is led by Professor Michael Roberts. He investigated steroid transport/delivery in prostate cancer for his PhD and performed postdoctoral research in metabolic-targeting therapeutics for multiple myeloma. Currently, he specializes in measuring drug penetration and distribution into human skin, liver, and other tissues, along with cellular metabolic changes associated with drug therapy.

Sandrine Roy manages the Core Microscopy Facility of the Translational Research Institute (TRI), Brisbane, Australia, and supports the LaVision Biotek Multiphoton system. Her background is in cell biology, with postdoctoral experience at Washington University as well as the University of Queensland in Australia. During that time, she gained experience on many imaging platforms, with extensive animal work experience. She is now developing novel imaging techniques as well as expanding the facility at TRI.

Michael J. Hickey is a National Health & Medical Research Council senior research fellow at Monash University. He received his PhD from the University of Melbourne and undertook postdoctoral training at the University of Calgary in Canada. His expertise lies in the analysis of the actions of leukocytes during inflammation. His laboratory uses various forms of advanced *in vivo* imaging to image organs undergoing inflammatory responses.

Glenda C. Gobe heads the Translational Research Laboratories of the Centre for Kidney Disease Research University of Queensland at the new Translational Research Institute located near Princess Alexandra Hospital, Brisbane, Australia. She is known for her research into molecular pathways controlling apoptosis, particularly in the kidney, and her experimental and translational research into molecular strategies aimed at improving patient outcome in acute and chronic kidney disease. Australian and overseas postgraduate students take part in her research programs.

APPENDIX B

General Reagents and Solutions

B.1 Trypsin / Versene

10x Versene (500 mL)	10x PBS (1 L)
NaCl 40 g	NaCl 80 g
KCL 1 g	KCl 2 g
NaHPO4.12H2O 14.14 g	NaHPO4 14.4 g
KH2PO4 1 g	KH2PO4 2.4 g
EDTA 10 g	

- In a 1 L beaker:
  10 mL of 10x versene (above)
  100 mL of 10x PBS (above)
- Make up to 1 L with MilliQ water and pour into a 2 L bottle.
- Autoclave and leave to cool.
- Add 20 mL of 2.5 % trypsin (10x) liquid (Gibco, Catalogue no. 15090) at 37 ºC to versene/PBS solution pre-cooled to room temperature.
- Aliquot into 50 mL falcon tubes and store at -20 ºC.

B.2 1 x PBS

- In a 1 mL beaker: 100 mL of 10x PBS (above)
- Make up to 1 L with MilliQ water.
- Autoclave for sterility if required.

B.3 1 x TBST (high salt)

TBST - High Salt (4 L)	
Tris	9.69 g
NaCl	116.88 g
10% Tween 20	20 mL
pH 7.4 – 7.5 using HCl	

B.4 4% buffered paraformaldehyde (PF) in sodium phosphate buffer

4 % PF (2 L)	
Paraformaldehyde pellets	80 g
NaH2PO4	6.2 g
Na2H PO4	28.5 g
Barnstead water	1600 mL

- In a beaker, add reagents as stated above.
- In a fume hood, heat at 60 ºC while stirring. Do not let the temperature of the solution roise above 80 ºC. Add approximately 15-20 NaOH pellets to assist dissolving solids.
- pH the solution to 7.2.
- Make the total volume up to 2 L using MilliQ water.
- Filter the solution with a 0.2 µm filter and aliquot into 50 mL falcon tubes and store at -20 ºC. Defrost in refrigerator before use.

B.5 Radioimmuno precipitation (RIPA) buffer

- Prepare 50 mM Tris-Cl (pH 7.5) by dissolving 6.06 g of Tris in 900 mL of sterile water, adjusting the pH to 7.5 and making up to 1 L. Autoclave and store at room temperature.
- Add the following to 200 mL of 50 mM Tris-Cl (pH 7.5):

RIPA buffer (200 mL in 50 mM Tris-Cl, pH 7.5)	
NaCl (150 mM)	1.75 g
NaF (25 mM)	0.21 g
EDTA (0.5 mM)	0.037 g
SDS (0.1 % w/v)	0.2 g
Sodium deoxycholate (0.5 % w/v)	1.0 g
IGEPAL CA-630 (1 %)	2 mL

- Prior to use, add the following proteinase and phosphatase inhibitors to 10 mL of RIPA buffer and mix well (vortex):

RIPA additives prior to use	
Phenylmethylsulfonyl fluoride (PMSF) (100 µg/mL)	200 µL
Leupeptin (10 mg/mL)	10 µL
Aprotinin (10 mg/mL)	10 µL
Sodium orthovanadate (Na3VO4) (200 mM)	50 µL

B.6 SDS-PAGE buffer solutions and gel recipes

- *Resolving gel buffer* – 48 mL 1M HCl + 36.33 g Tris base per 100 mL (pH 8.9). Store at room temperature.
- *12% ammonium persulfate* – (w/v), store in dark at 4 ˚C.
- *Spacer gel buffer* – 6.055 g Tris base (pH 6.7) per 100 mL, store at 4 ˚C.
- *Running buffer* – 3 g Tris base + 14.4 g glycine + 10 mL 10 % SDS per 1 L of H_2O
- *4X Sample buffer* – 1.25 mL spacer gel buffer + 1 mL 10 % SDS + 1.5 mL glycerol + 0.1 mL β-mercaptoethanol + 1.15 mL H_2O + 0.25 g bromophenol blue to colour the solution.
- *Transfer buffer* – 3 g Tris base +14.4 g glycine + 10-20 % methanol per 1 L of H_2O.

B.7.1 Resolving Gel (25 mL)

Resolving Gel (25 mL – 4 Gels)					
% Gel	**8**	**10**	**12**	**15**	**20**
30% acrylamide	6.664 mL	8.33 mL	9.996 mL	12.495 mL	16.66 mL
H_2O	14.806 mL	13.14 mL	11.474 mL	8.975 mL	4.81 mL
Resolving gel buffer	3.13 mL	3.13 mL	3.13 mL	3.13 mL	3.13 mL
10% SDS	250 µL	250 µL	250 µL	250 µL	250 µL
12% ammonium persulphate	143 µL	143 µL	143 µL	143 µL	143 µL
TEMED	12 µL	12 µL	12 µL	12 µL	12 µL

B.7.2 Spacer Gel (10 mL)

Spacer Gel (10 mL – 4 Gels)		
% Gel	4	7
30% acrylamide	1.33mL	2.3275mL
H_2O	6.115mL	5.1175mL
Spacer gel buffer	2.4mL	2.4mL
10% SDS	75µL	75µL
12% ammonium persulphate	75µL	75µL
TEMED	5µL	5µL

APPENDIX C

Dose-Response Validation

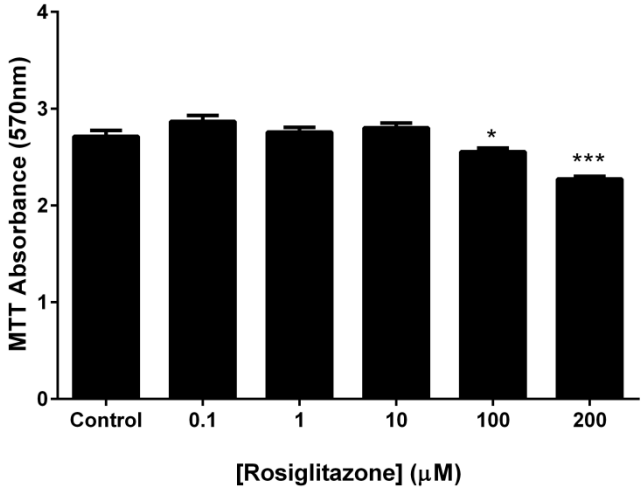
MTT Absorbance (570nm)
0
1
2
3
4
*
***
Control
0.1
1
10
100
200
[Rosiglitazone] (μM)

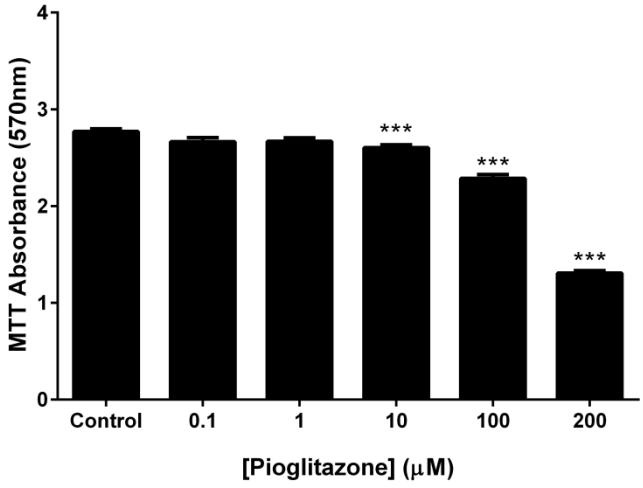
MTT Absorbance (570nm)
0
1
2
3
4
***
***
***
Control
0.1
1
10
100
200
[Pioglitazone] (μM)

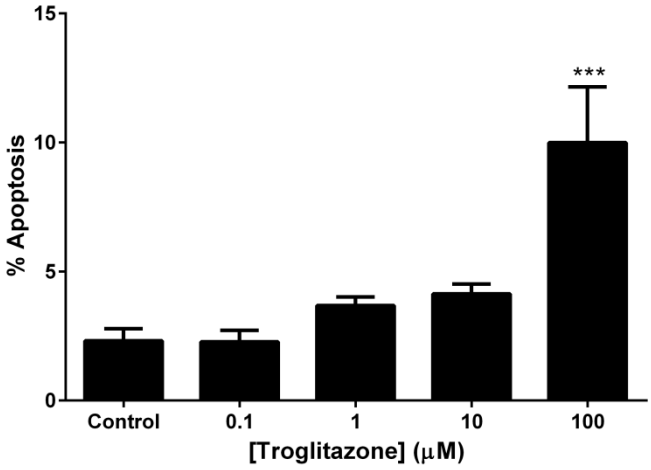
% Apoptosis
0
5
10
15
***
Control
0.1
1
10
100
[Troglitazone] (μM)